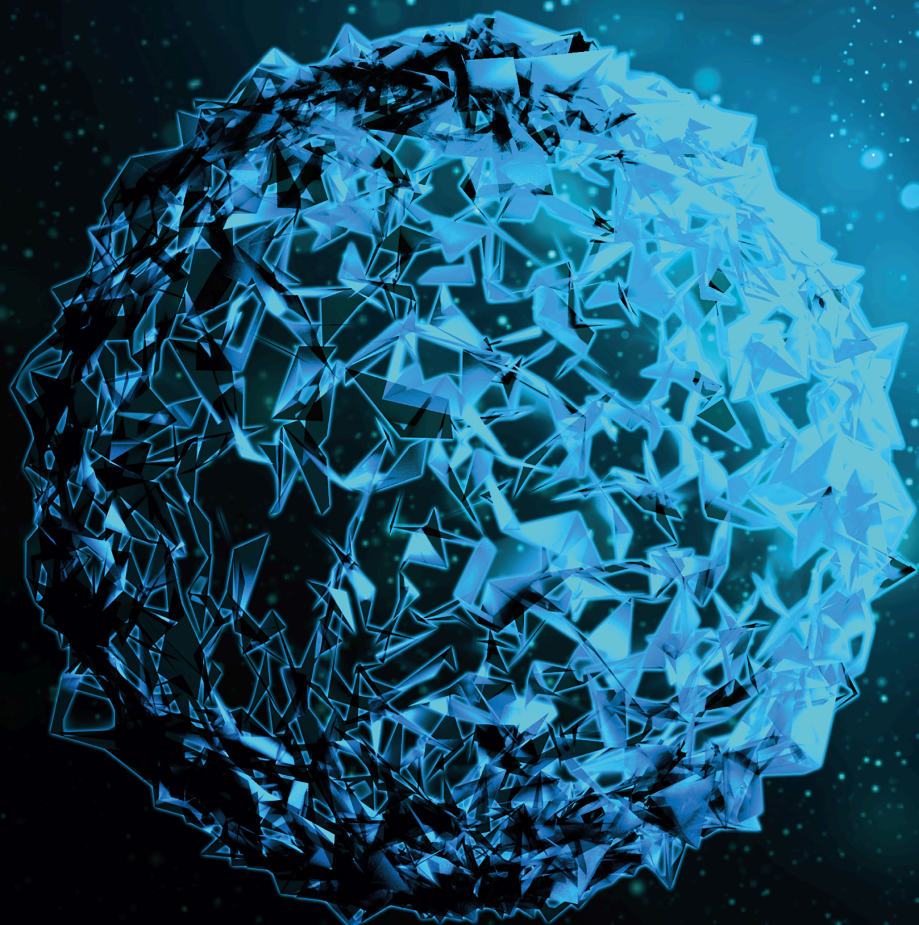# Natural Compounds-Based Strategy in Treatment of Malignancies

Lead Guest Editor: Yue Gu
Guest Editors: Lei Song, Chunling Dai, and Ling Chen

Natural Compounds-Based Strategy in Treatment of Malignancies

Natural Compounds-Based Strategy in Treatment of Malignancies

Lead Guest Editor: Yue Gu
Guest Editors: Lei Song, Chunling Dai, and Ling Chen

Eugenio Zoni ⓘD, Switzerland

Contents

Contents

Hindawi

Retraction

Retracted: Gene Differential Expression and Interaction Networks Illustrate the Biomarkers and Molecular Biological Mechanisms of Unsaponifiable Matter in Kanglaite Injection for Pancreatic Ductal Adenocarcinoma

BioMed Research International

This article has been retracted by Hindawi following an investigation undertaken by the publisher [1]. This investigation has uncovered evidence of one or more of the following indicators of systematic manipulation of the publication process:

(1) Discrepancies in scope

(2) Discrepancies in the description of the research reported

(3) Discrepancies between the availability of data and the research described

(4) Inappropriate citations

(5) Incoherent, meaningless and/or irrelevant content included in the article

(6) Manipulated or compromised peer review

The presence of these indicators undermines our confidence in the integrity of the article's content and we cannot, therefore, vouch for its reliability. Please note that this notice is intended solely to alert readers that the content of this article is unreliable. We have not investigated whether authors were aware of or involved in the systematic manipulation of the publication process.

Wiley and Hindawi regrets that the usual quality checks did not identify these issues before publication and have since put additional measures in place to safeguard research integrity.

We wish to credit our own Research Integrity and Research Publishing teams and anonymous and named external researchers and research integrity experts for contributing to this investigation.

The corresponding author, as the representative of all authors, has been given the opportunity to register their agreement or disagreement to this retraction. We have kept a record of any response received.

References

[1] B. Xu, W. Dan, X. Zhang et al., "Gene Differential Expression and Interaction Networks Illustrate the Biomarkers and Molecular Biological Mechanisms of Unsaponifiable Matter in Kanglaite Injection for Pancreatic Ductal Adenocarcinoma," *BioMed Research International*, vol. 2022, Article ID 6229462, 19 pages, 2022.

Retraction

Retracted: SPOCK2 Promotes the Malignant Behavior of Ovarian Cancer via Regulation of the Wnt/β-Catenin Signaling Pathway

BioMed Research International

This article has been retracted by Hindawi following an investigation undertaken by the publisher [1]. This investigation has uncovered evidence of one or more of the following indicators of systematic manipulation of the publication process:

(1) Discrepancies in scope

(2) Discrepancies in the description of the research reported

(3) Discrepancies between the availability of data and the research described

(4) Inappropriate citations

(5) Incoherent, meaningless and/or irrelevant content included in the article

(6) Manipulated or compromised peer review

The presence of these indicators undermines our confidence in the integrity of the article's content and we cannot, therefore, vouch for its reliability. Please note that this notice is intended solely to alert readers that the content of this article is unreliable. We have not investigated whether authors were aware of or involved in the systematic manipulation of the publication process.

Wiley and Hindawi regrets that the usual quality checks did not identify these issues before publication and have since put additional measures in place to safeguard research integrity.

We wish to credit our own Research Integrity and Research Publishing teams and anonymous and named external researchers and research integrity experts for contributing to this investigation.

The corresponding author, as the representative of all authors, has been given the opportunity to register their agreement or disagreement to this retraction. We have kept a record of any response received.

References

[1] S. Zhao, H. Liu, and M. Fan, "SPOCK2 Promotes the Malignant Behavior of Ovarian Cancer via Regulation of the Wnt/β-Catenin Signaling Pathway," *BioMed Research International*, vol. 2022, Article ID 9223954, 10 pages, 2022.

Retraction

Retracted: The Value of m5C-Related lncRNAs in the Prognostic Assessment and Immunotherapy of Stomach Adenocarcinoma

BioMed Research International

This article has been retracted by Hindawi following an investigation undertaken by the publisher [1]. This investigation has uncovered evidence of one or more of the following indicators of systematic manipulation of the publication process:

(1) Discrepancies in scope

(2) Discrepancies in the description of the research reported

(3) Discrepancies between the availability of data and the research described

(4) Inappropriate citations

(5) Incoherent, meaningless and/or irrelevant content included in the article

(6) Peer-review manipulation

The presence of these indicators undermines our confidence in the integrity of the article's content and we cannot, therefore, vouch for its reliability. Please note that this notice is intended solely to alert readers that the content of this article is unreliable. We have not investigated whether authors were aware of or involved in the systematic manipulation of the publication process.

Wiley and Hindawi regrets that the usual quality checks did not identify these issues before publication and have since put additional measures in place to safeguard research integrity.

We wish to credit our own Research Integrity and Research Publishing teams and anonymous and named external researchers and research integrity experts for contributing to this investigation.

The corresponding author, as the representative of all authors, has been given the opportunity to register their agreement or disagreement to this retraction. We have kept a record of any response received.

References

[1] C. He, X. Zhu, F. Kong et al., "The Value of m5C-Related lncRNAs in the Prognostic Assessment and Immunotherapy of Stomach Adenocarcinoma," *BioMed Research International*, vol. 2022, Article ID 2747799, 26 pages, 2022.

Retraction

Retracted: lncRNA FOXD2-AS1 Promotes the Retinoblastoma Cell Viability and Migration by Sponging miR-31

BioMed Research International

This article has been retracted by Hindawi following an investigation undertaken by the publisher [1]. This investigation has uncovered evidence of one or more of the following indicators of systematic manipulation of the publication process:

(1) Discrepancies in scope

(2) Discrepancies in the description of the research reported

(3) Discrepancies between the availability of data and the research described

(4) Inappropriate citations

(5) Incoherent, meaningless and/or irrelevant content included in the article

(6) Peer-review manipulation

The presence of these indicators undermines our confidence in the integrity of the article's content and we cannot, therefore, vouch for its reliability. Please note that this notice is intended solely to alert readers that the content of this article is unreliable. We have not investigated whether authors were aware of or involved in the systematic manipulation of the publication process.

In addition, our investigation has also shown that one or more of the following human-subject reporting requirements has not been met in this article: ethical approval by an Institutional Review Board (IRB) committee or equivalent, patient/participant consent to participate, and/or agreement to publish patient/participant details (where relevant).

Wiley and Hindawi regrets that the usual quality checks did not identify these issues before publication and have since put additional measures in place to safeguard research integrity.

We wish to credit our own Research Integrity and Research Publishing teams and anonymous and named external researchers and research integrity experts for contributing to this investigation.

The corresponding author, as the representative of all authors, has been given the opportunity to register their agreement or disagreement to this retraction. We have kept a record of any response received.

References

[1] Y. Liang, H. Wang, R. Song, and X. Yin, "lncRNA FOXD2-AS1 Promotes the Retinoblastoma Cell Viability and Migration by Sponging miR-31," *BioMed Research International*, vol. 2022, Article ID 7723425, 11 pages, 2022.

Research Article

In Vitro Antimitotic and Hypoglycemic Effect Study and Acute Toxicity Assessment of the Aqueous and Organic Extracts of *Chamaerops humilis* L. var. argentea Andre

Nacima Lachkar [ID]**, Fatima Lamchouri** [ID]**, and Hamid Toufik** [ID]

Laboratory of Natural Substances, Pharmacology, Environment, Modeling, Health & Quality of Life (SNAMOPEQ), Polydisciplinary Faculty of Taza (FPT), Sidi Mohamed Ben Abdellah University (USMBA) of Fez, B.P.: 1223 Taza-Gare, Taza, Morocco

Correspondence should be addressed to Fatima Lamchouri; fatima.lamchouri@usmba.ac.ma

Background. Chamaerops humilis L. var. argentea Andre is a plant widely spread in the region of Taza (North-East of Morocco); it is used in traditional phytotherapy against cancer, diabetes, inflammations, cardiovascular and respiratory diseases, and for the treatment of digestive disorders. *Objective and Methods.* The objective of our work is to contribute firstly, to the study of the *in vitro* antimitotic potential by the phytotest of *Lepidium sativum* and the evaluation of the *in vitro* antidiabetic activity of three enzymes (α-amylase, α-glucosidase, and β-galactosidase) on nine aqueous and organic extracts prepared from the leaves of *Chamaerops humilis*. In addition, a correlation study was carried out on the chemical composition and the antimitotic and antidiabetic activities of *Chamaerops humilis* leaves. Then, we tested the acute toxicity of the decocted extract and the ethanolic extract. *Results.* The results of the antimitotic activity showed that the decocted extract showed a higher inhibitory activity than the other aqueous extracts ($IC_{50} = 9.624 \times 10^3 \pm 95.97\,\mu g/mL$); for the organic extracts, the ethanolic extract and ethanolic macerated expressed the highest values for the cell growth inhibition test with an IC_{50} of $5.638 \times 10^3 \pm 22.61$ and $5.599 \times 10^3 \pm 45.51\,\mu g/mL$ with statistically nonsignificant difference. Regarding the antidiabetic activity, the decocted showed a higher inhibitory activity than the other aqueous extracts for α-amylase ($IC_{50} = 1.781 \cdot 10^5 \pm 358.30\,\mu g/mL$), α-glucosidase ($2.540 \times 10^2 \pm 3.14\,\mu g/mL$), and β-galactosidase ($7.118 \times 10^2 \pm 16.13\,\mu g/mL$); the ethanolic extract also revealed the highest inhibitory activity for α-amylase ($IC_{50} = 8.902 \times 10^3 \pm 57.81\,\mu g/mL$), α-glucosidase ($2.216 \times 10^2 \pm 1.39\,\mu g/mL$), and β-galactosidase ($2.003 \times 10^2 \pm 7.41\,\mu g/mL$). A strong correlation was recorded between the antimitic activity and the inhibitory capacity of β-galactosidase and between these two activities and the chemical composition of *Chamaerops humilis* leaves. The acute toxicity study showed that the decocted and the ethanolic extract are weakly toxic with an LD_{50} greater than or equal to 5000 mg/kg. *Conclusion. Chamaerops humilis* could become a good source in traditional herbal medicine.

1. Introduction

The cancer represents one of the major causes of death in the world. In 2020, cancer was responsible for 10 million deaths worldwide [1]. In Morocco, tumors are the 2nd cause of mortality with a percentage of 13.4% of deaths, after the cardiovascular diseases [2].

Chemotherapy is an important treatment modality in oncology alongside other treatments [3]; however, the major problem with chemotherapy is that it is a nonspecific therapy; chemotherapeutic agents attack both the cancerous cells of the tumor and normal healthy cells, which can lead to multiple disorders in different organs; chemotherapy treatment leads to numerous changes in cell structure and function, resulting in progressive, continuous and often irreversible toxic side effects. In addition, chemotherapy is associated with various side effects, including cardiocytotoxicity, nephrotoxicity, myelosuppression, neurotoxicity, hepatotoxicity,

gastrointestinal toxicity, mucositis, and alopecia, which severely affect the quality of life of patients with cancer [4]. Therefore, it is essential to carry out experimental research to find new anticancer agents that are more effective and less harmful.

Diabetes in its turn constitutes a real public health problem on a worldwide scale. In 2021, diabetes was responsible for 6.7 million deaths worldwide with 1 death every 5 seconds and 796.000 deaths in the Middle East and North Africa [5]. In Morocco, this disease causes more than 24.000 deaths per year [6]. Diabetes can cause multiple complications that require follow-up by health professionals, and this makes its management costly in terms of the expenses required to care for the diabetic person.

In fact, there is a strong association between cancer and diabetes; people with diabetes have a high risk of developing cancer. Indeed, numerous studies have demonstrated the relationship between diabetes and the occurrence of cancer. Diabetes and insulin resistance could be the consequence of an early, undiagnosed cancer, but, in addition, diabetes could also be related to the precancerous state of the pancreas that affects its insulin-secreting capacity [7]. Insulin resistance and its associated inflammatory disturbances also contribute to the carcinogenic potential of NASH (nonalcoholic steatohepatitis). In addition, it has been shown that for every 1 mmol/l increase in blood glucose, and there is a 10-20% increase in cancer risk (incidence/mortality) in men and women [8]. Indeed, in noninsulin-dependent diabetes, there is insulin sensitivity, which leads to hyperinsulinism and elevated circulating levels of insulin-like growth factors (IGFs) that are capable of stimulating cell proliferation in many organs, in particular the liver, pancreas, colon, ovary, and breast [7, 9, 10]. In addition, cancer is among the major causes of death in type 2 diabetes [11, 12].

Faced with this situation, the treatment of cancer and diabetes in Morocco is based mainly on the use of modern protocols and drugs, which can be costly for poor people who find it difficult to access modern health care. In this regard, traditional phytotherapy is widely used due to its availability and accessibility for the treatment of several pathologies [13–15].

Moroccan flora constitutes a real resource of natural molecules because of its richness and phytodiversity, which classifies Morocco among the countries that have a long medical tradition and traditional know-how based on medicinal plants [16]. For its part, the region of Taza (North Eastern Morocco) is distinguished by the diversity and richness of its natural environment and has one of the main and oldest national parks in Morocco, the Tazekka Park, which is characterized by a diverse natural abundance of aromatic and medicinal plants [17, 18]. Among these plants we mention, *Chamaerops humilis* L. var. argentea Andre is widely distributed and used by the local population in basketry for the manufacture of the doum basket, the palm heart is consumed as a seasonal fruit, and the leaves are used to feed the livestock [15, 18]. *C. humilis* is also used in traditional medicine to treat various pathologies including cancer [15, 19, 20] and diabetes [15, 21–24] and for the treatment of digestive disorders [15, 19]. Additionally, *Chamaerops humilis* is naturally abundant in the chemical compounds including gallic tannins, steroids and terponoids, saponins, and reducing sugars [19]. Furthermore, according to a mineralogical and phythochemical study that we have recently conducted [15], the leaves of *Chamaerops humilis* L. var. argentea are rich in minerals such as iron (82395.00 mg kg^{-1}), potassium (9354.90 mg kg^{-1}), phosphorus (1828.62 mg kg^{-1}), magnesium (1312.47 mg kg^{-1}), sodium (627.03 mg kg^{-1}), copper (542.64 mg kg^{-1}), calcium (92.19 mg kg^{-1}), zinc (66.15 mg kg^{-1}), and selenium and strontium (3.00 mg kg^{-1}). In addition, the aqueous and organic extracts of this part of the plant contains catechic tannins, flavonoids, saponins, sterols, and free quinones. In addition, the aqueous and organic extracts of this part of the plant contains catechic tannins, flavonoids, saponins, sterols, and free quinones. The quantitative study also revealed that the aqueous and organic extracts of the leaves of *Chamaerops humilis* have high contents of phenolic compounds; the ethanolic extract and the ethanolic macerated have the highest values of total polyphenols, respectively, 96.99 ± 0.82 and 100.27 ± 1.95 mg EAG/gE, catechic tannins, respectively, 50.27 ± 0.99 and 52.11 ± 1.02 mg EC/gE with a statistically nonsignificant difference between these two extracts.

In Morocco, the strong progression of phytotherapy in recent years can pose risks for the consumers. Indeed, we have noticed that countless products and recipes based on plants or mixtures of plants are marketed on social networks and internet sites by unqualified people, which raises questions about the dose contained in these products and its conditions of extraction, manufacture, conservation, and possible interactions between the constituents of the product mixture or traditional recipe used. Ignorance of the use of medicinal plants can result in financial and human costs that will affect the national economy through the harmful toxic effects of the plants used [25, 26].

In view of these findings and as a continuation of the work carried out on *Chamaerops humilis* L. var. argentea Andre [15, 18], in the present work, we are interested in pursuing the validation of the therapeutic use of dwarf palm in traditional medicine through the *in vitro* study of its antimitotic and antihyperglycemic potentials of aqueous and organic extracts and the evaluation of its acute oral toxicity.

2. Material and Methods

2.1. Chemicals and Reagents. Colchicine, α-amylase from *Aspergillus oryzae*, starch, sodium phosphate buffer, dinitrosalicylic acid (DNS), acarbose, 4-p-nitrophenyl-α-D-glucopyranoside (pNPG), sodium carbonate (Na_2CO_3), α-glucosidase from *Saccharomyces cerevisiae*, β-galactosidase from *Escherichia coli*, 2-nitrophenyl β-D-galactopyranoside, quercetin, ethanol, chloroform, n-hexane, and dimethyl sulfoxide (DMSO) were used. These chemicals were purchased from Sigma Aldrich (Saint Louis, Missouri, USA).

2.2. Plant Material. The leaves of *Chamaerops humilis* L. var. argentea Andre used in the present study were collected in February 2017, in Bab Boudir located at 46 km from the city of Taza (Figure 1). The identification of the plant was carried

Figure 1: *Chamaerops humilis* L. var. argentea Andre (pictures taken in Bab Boudir, located 46 km from the city of Taza (North-East of Morocco). Geographical coordinates: N 34˚24.904″, W 004˚02.635″, Altitude: 1460 m).

out by Dr. Abdelmajid Khabbach, a reference sample "SB2017" was deposited in the herbarium of the laboratory Natural Substances, Pharmacology, Environment, Modelling, Health and Quality of Life (SNAMOPEQ), Polydisciplinary Faculty of Taza (FPT), Sidi Mohamed Ben Abdellah University (USMBA) [15].

2.3. Phytochemical Study. The collected leaves of *Chamaerops humilis* L. var. argentea Andre were dried and subjected to two types of extraction: aqueous extraction and organic extraction; the extraction procedure has been described in previous works of our laboratory [15, 27–30].

2.3.1. Preparation of the Aqueous Extracts. Three aqueous extraction methods were applied: decoction, infusion, and maceration. The extraction by the three modalities was done separately. For each aqueous extraction modality, 10 g of *C. humilis* leaves was extracted with 100 mL of distilled water. After filtration, the solutions obtained were concentrated using a freeze-dryer (Heto PowerDry LL3000). The recovered residues were stored in amber glass vials at 4˚C [15].

2.3.2. Preparation of Organic Extracts. The organic extraction was carried out in two ways: hot with the soxhlet and cold by maceration with solvents of different polarities (ethanol, chloroform, and n-hexane). The organic extraction was

performed separately for each solvent and modality used, in total 6 aqueous extracts were prepared (the ethanolic extract, the ethanolic macerated, the chloroformic extract, the chloroformic macerated, the hexanic extract, and the hexanic macerated). For each extraction, 40 g of plant material was used in a solvent volume of 400 mL. A rotary evaporator (Buchi R-210) was used at 40–50˚C to remove the solvent and concentrate the organic extract into residues. These were stored in the dark at 4˚C [15].

2.4. Cell Growth Inhibitory Activity of Aqueous and Organic Extracts of Chamaerops humilis L. var. argentea Andre: Phytotest Lepidium sativum. The phytotest *Lepidium sativum* is a biotest for the evaluation of antimitotic capacity based on the measurement of the length of the rootlet of a germinated seed of *Lepidium sativum* deposited in a medium containing the extract to be tested. In our study, we applied this test to evaluate the antimitotic capacity of aqueous and organic extracts prepared from the leaves of *C. humilis* following the method of [31]. To realize the test, 10 seeds of *Lepidium sativum* were germinated in petri dishes (55 mm) containing filter paper soaked with 1 mL of distilled water for 24 hours; then, 1 mL of the extract or reference standard to be tested was added at different concentrations to each dish, after which the dishes were incubated at 25˚C. The results were read after 24 hours of incubation.

For the reference drug, we used colchicine and the negative control was made by distilled water. During this test, we performed three replicates for each concentration tested. The percentage of cell growth inhibition was estimated by comparing the test batch with a control lot according to the formula below:

$$\% \text{of inhibition} = \frac{\text{LT} - \text{LC}^*}{\text{LT}} \, 100, \quad (1)$$

where LT is the length of control rootlets and LC is the length of rootlets treated with the extract or the reference drug.

2.5. In Vitro Study of Antidiabetic Activity

2.5.1. Inhibitory Activity of the Enzyme α-Amylase. The α-amylase inhibition test was performed using the procedure reported by [32], and the protocol followed is detailed in previous studies [15, 27, 29, 30, 33]. With a mixture containing 200 μL of sample and 200 μL of α-amylase enzyme (10 U/mL) prepared in 0.02 M sodium phosphate buffer (pH = 6.9), it was incubated for 10 min at 30°C. Subsequently, we added 200 μL of the 1% starch solution to the reaction mixture. A second incubation was performed 3 min at 30°C. Then, we added 1 mL of the solution (DNS) and the reaction mixture was incubated again at 90°C for 10 min.

The reaction mixture was then diluted with 5 mL of distilled water. The absorbance value was measured at 540 nm by spectrophotometer (SPECUVIS2 UV/Vis, no.: HF1309003). Acarbose was used as a positive control. The percentage inhibition of α-amylase was calculated with the following formula:

$$\% \text{of inhibition} = \left[\frac{((\text{Ac}^+ - \text{Acb}^-) - (\text{As} - \text{Ab}))}{(\text{Ac}^+ - \text{Acb}^-)} \right] * 100, \quad (2)$$

where Ac^+ is the absorbance of control with enzyme, Ac^- is the absorbance of control without enzyme, As is the absorbance of sample with enzyme, and Ab is the absorbance of sample without enzyme.

2.5.2. Inhibitory Activity of the Enzyme α-Glucosidase. The inhibitory activity of aqueous and organic extracts of C. humilis leaves towards α-glucosidase was determined according to the protocol of Lordan and collaborators [34], detailed in our previous work [15, 27–30].

150 μL of the sample at different concentrations was added to 100 μL of α-glucosidase enzyme solution (0.1 U/mL) prepared in 0.1 M sodium phosphate buffer (pH = 6.7); the mixture was incubated at 37°C for 10 min. After this, we added 200 μL of pNPG solution (1 mM). The reaction mixtures were incubated again at 37°C for 30 min. At the end, 1 mL Na$_2$CO$_3$ (0.1 M) was added to the reaction mixture. The absorbance was measured at 405 nm using a spectrophotometer (SPECUVIS2 UV/Vis, no.: HF1309003). The inhibitory capacity of α-glucosidase was expressed as percentage inhibition, and the median inhibitory concentra-

tions (IC$_{50}$) were calculated. Acarbose was used as a positive control.

2.5.3. Inhibitory Activity of the Enzyme β-Galactosidase. The evaluation of the inhibitory power of β-galactosidase of aqueous and organic extracts from the leaves of C. humilis was carried out according to the method of [35], and the protocol was described in our previous work [15, 27, 29, 30, 33]; 150 μL of different extracts or the reference drug was added to 100 μL of β-galactosidase enzyme solution (1 U/mL) prepared in sodium phosphate buffer (0.1 M) at pH = 7.6. The mixture was incubated at 37°C for 10 min. Subsequently, a volume of 200 μL of the substrate 2-nitrophenyl beta-D-galactopyranoside (1 mM) was added. The reaction mixture was incubated again at 37°C for 30 min. At the end of the protocol, we added 1 mL of Na$_2$CO$_3$ to stop the reaction and measured the absorbance at 410 nm using a spectrophotometer (SPECUVIS2 UV/Vis, no.: HF1309003). Quercetin was used as a positive control.

2.6. Acute Toxicity Assessment.
Acute in vivo toxicity was performed on the decocted and ethanolic extract of C. humilis leaves. These extracts were chosen as they were found to be the most active in vitro among the other extracts. The acute oral toxicity test was performed according to the Organisation for Economic Cooperation and Development (OECD) guideline 423 [36].

2.6.1. Animal Material. The in vivo toxicity study was performed on healthy, nulliparous, nonpregnant adult female Swiss mice weighing 25-30 g. The mice were provided by the animal facility of the Polydisciplinary Faculty of Taza, Sidi Mohamed Ben Abdellah University (USMBA) of Fez, Morocco. Mice were maintained, with free access to standard food and water, under standard conditions (12 h light/12 h dark at 23 ± 1°C). The mice were treated according to international guidelines for the care and use of animals in research [37].

2.6.2. Acute Toxicity. The assessment of acute toxicity was carried out according to the recommendations of the Organisation for Economic Co-operation and Development guideline no. 423 [36]; the protocol followed has been described in detail in a previous work of our laboratory [38]. The decocted extract and the ethanolic extract of the leaves of C. humilis were tested at a dose of 2000 mg/kg with a volume of 0.5 mL/20 g body weight of the mouse. The experiment is carried out at each stage on three female Swiss mice for each product tested. This test was performed in two independent experiments in order to estimate the LD$_{50}$. Therefore, 18 female mice were used. The first stage required a number of 9 mice for each stage which were fasted for a period of 4 h with free access to water; they were divided into 3 groups of three (3) mice each; the first and second groups were treated with the decocted and ethanolic extracts, respectively, and the last control group received distilled water. A behavioral observation was performed during the first 30 minutes and regularly during the first 24 hours after oral administration of the test products. According to the

OECD guideline 423, the absence or the occurrence of substance-related mortality in a group dosed at a given stage specifies the next stage, either by stopping the experiment, administering the same dose to three more animals, or administering an immediately higher or lower dose to three more animals [36]. The mice were observed for a period of 14 days for changes in weight, mortality rate, animal behavior, and signs of toxicity. In addition, hydration and feeding were carried out on a daily basis.

2.7. Statistical Study and Principal Component Analysis (PCA). GraphPad Prism 5 software was used to perform the statistical analysis of the data obtained using ANOVA variance followed by Tukey's test. When the p value is ≤0.05, the difference is considered statistically significant. Results are expressed as mean ± SEM.

For the correlation study between the content of total polyphenols, flavonoids, and catechic tannins in the aqueous and organic extracts determined in our previous work [15] and the results of the *Lepidium sativum* phytotest in the present study, we used Pearson's correlation analysis and principal component analysis (PCA) by Addinsoft XLSTAT software version 14.

3. Results

3.1. Cell Growth Inhibitory Activity of Aqueous and Organic Extracts of C. humilis Leaves: Phytotest Lepidium sativum. The results obtained on the inhibitory action of aqueous and organic extracts of *C. humilis* leaves on the cell growth of *Lepidium sativum* seeds are elucidated in the Figures 2–4.

From Figures 2 and 3, we notice that all aqueous and organic extracts have a cell growth inhibition capacity; this activity is proportional to the concentration tested. Firstly, the aqueous extracts expressed a maximum inhibitory effect at the concentration of $2 \times 10^5 \, \mu g/mL$: 75.76% for the decocted, 69.52% for the infused, and 75.93 for the macerated (Figure 2). Regarding the organic extracts at the concentration of $1.5 \times 10^4 \, \mu g/mL$; ethanolic extract and ethanolic macerated exerted a strong inhibition of cell growth with percentages of 89.86 and 90.68%, respectively, followed by chloroformic extract (71.15%), hexanic extract (65.32%), chloroformic macerated (61.57), and lastly hexanic macerated (59.57%) (Figure 3). In addition, colchicine also caused a high inhibition of 92.92% at the concentration $5 \times 10^3 \, \mu g/mL$ (Figure 4).

In order to make a comparison between all the extracts tested, we calculated the IC_{50} of each extract and that of colchicine (Table 1).

The cell growth inhibitory action is higher for the organic extracts than for the aqueous extracts; indeed, the decocted and infused showed a higher inhibitory activity than the aqueous macerated with an IC_{50} of $9.624 \times 10^3 \pm 95.97$, $9.642 \times 10^3 \pm 67.49$, and $2.547 \times 10^4 \pm 212.98 \, \mu g/mL$, respectively, with a nonsignificant statistical difference between the decocted and infused. Concerning the organic extracts, we found that ethanolic extract and ethanolic macerated expressed the highest values for the cell growth inhibition test with IC_{50} of $5.638 \times 10^3 \pm 22.61$ and
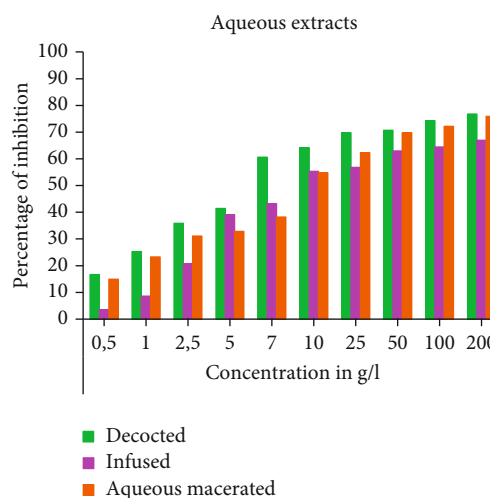
FIGURE 2: Cell growth inhibitory activity of aqueous extracts of *C. humilis* leaves.

$5.599 \times 10^3 \pm 45.51 \, \mu g/mL$ with a statistically insignificant difference, followed by chloroformic macerated ($IC_{50} = 7.770 \times 10^3 \pm 76.32 \, \mu g/mL$), hexanic macerated ($IC_{50} = 9.599 \times 10^3 \pm 69.90 \, \mu g/mL$), and chloroformic extract ($IC_{50} = 1.054 \times 10^4 \pm 93.12 \, \mu g/mL$). The analysis of variance showed a statistically insignificant difference between the hexanic extract and the hexanic macerated. In addition, colchicine showed a strong inhibitory activity expressed by the lowest IC_{50} ($IC_{50} = 4.746 \times 10^2 \pm 1.76 \, \mu g/mL$) with a statistically significant difference between all tested extracts.

3.2. In Vitro Study of Antidiabetic Activity. The study of the *in vitro* antidiabetic power of the aqueous and organic extracts prepared from the leaves of *C. humilis* was carried out by three tests for the inhibition of the enzymes α-amylase, α-glucosidase, and β-galactosidase. The expression of the results was done by calculating the IC_{50} (Table 2).

The tested aqueous and organic extracts showed an inhibitory activity of α-amylase with $IC_{50} = 8.902 \times 10^3 \pm 57.81 \, \mu g/mL$ to $3.463 \times 10^5 \pm 211.02 \, \mu g/mL$. For the aqueous extracts the decocted showed inhibitory activity: $IC_{50} = 1.781 \times 10^5 \pm 358.30 \, \mu g/mL$, followed, respectively, by the infused ($IC_{50} = 2.579 \times 10^5 \pm 690.80 \, \mu g/mL$) and the aqueous macerated ($IC_{50} = 2.781 \times 10^5 \pm 396.48 \, \mu g/mL$) with a statistically significant difference between the three extracts. Concerning the organic extracts, the ethanolic extract shows an inhibitory activity ($IC_{50} = 8.902 \times 10^3 \pm 57.81 \, \mu g/mL$), followed, respectively, by the chloroformic macerated ($IC_{50} = 1.604 \times 10^5 \pm 240.83 \, \mu g/mL$), the ethanolic macerated ($IC_{50} = 1.754 \times 10^5 \pm 107.08 \, \mu g/mL$) chloroformic extract ($IC_{50} = 2.114 \times 10^5 \pm 113.77 \, \mu g/mL$), hexanic extract ($IC_{50} = 2.401 \times 10^5 \pm 677.48 \, \mu g/mL$), and in the last place hexanic macerated extract ($IC_{50} = 3.463 \times 10^5 \pm 211.02 \, \mu g/mL$) with a statistically significant difference between all organic extracts. Acarbose shows high α-amylase inhibitory activity ($IC_{50} = 6.160 \, 10^2 \pm 5.00 \, \mu g/mL$). The evaluation of the inhibitory power of α-glucosidase *in vitro* shows that

FIGURE 3: Cell growth inhibitory activity of organic extracts from *C. humilis* leaves.

FIGURE 4: Cell growth inhibitory activity of colchicine.

TABLE 1: The median inhibitory concentrations (IC_{50}) of the cell growth inhibitory effect of aqueous and organic extracts of *C. humilis* leaves.

Extracts	IC_{50} (μg/mL)
Aqueous	
Decocted	$9.624 \times 10^3 \pm 95.97$[a]
Infused	$9.642 \times 10^3 \pm 67.49$[a,b]
Macerated	$2.547 \times 10^4 \pm 212.98$[c]
Organics	
Ethanolic extract	$5.638 \times 10^3 \pm 22.61$[d]
Ethanolic macerated	$5.599 \times 10^3 \pm 45.51$[d]
Chloroformic extract	$1.054 \times 10^4 \pm 93.12$[e]
Chloroformic macerated	$7.770 \times 10^3 \pm 76.32$[f]
Hexanic extract	$9.750 \times 10^3 \pm 73.61$[a,b,g]
Hexanic macerated	$9.599 \times 10^3 \pm 69.90$[a,b,g]
Colchicine	$4.746 \times 10^2 \pm 1.76$[h]

The results are expressed as the mean of three individual replicates ($n = 3 \pm$ SEM). Values with the same superscript letters in the same column are not significantly different ($p < 0.05$).

tory power ($IC_{50} = 1.950 \times 10^2 \pm 6.12 \mu$g/mL); the activity of acarbose is statistically insignificant with that of ethanolic extract and ethanolic macerated.

The aqueous and organic extracts also showed an inhibitory effect on β-galactosidase; for the aqueous extracts, the decocted recorded higher β-galactosidase inhibitory activity than the infused and aqueous macerated with IC_{50} values of $7.118 \times 10^2 \pm 16.13$, $9.050 \times 10^2 \pm 9.33$, and $8.544 \times 10^2 \pm 13.66 \mu$g/mL, respectively. The analysis of variance (ANOVA) showed that there is a nonsignificant difference between the decocted and the other two aqueous extracts (infused and aqueous macerated). Regarding the organic extracts, ethanolic extract showed the most powerful inhibitory action ($IC_{50} = 2.003 \times 10^2 \pm 7.41 \mu$g/mL) followed by hexanic extract ($IC_{50} = 2.593 \times 10^2 \pm 19.13 \mu$g/mL), hexanic macerated ($IC_{50} = 3.186 \times 10^2 \pm 6.19 \mu$g/mL), chloroformic extract ($IC_{50} = 3.598 \times 10^2 \pm 7.29 \mu$g/mL), ethanolic macerated ($IC_{50} = 4.792 \times 10^2 \pm 13.43 \mu$g/mL), and chloroformic macerated ($IC_{50} = 5.671 \times 10^2 \pm 3.29 \mu$g/mL); analysis of variance revealed a nonsignificant difference between chloroformic extract and hexanolic macerated and between ethanolic extract and quercetin ($IC_{50} = 1.711 \times 10^2 \pm 5.00 \mu$g/mL).

3.3. Correlation Study between Chemical Composition and Cell Growth Inhibiting Effect of C. humilis Leaf Extracts.
The correlation analysis between the chemical composition (total polyphenols, flavonoids, and catechic tannins) of the aqueous and organic extracts of *C. humilis* leaves and their antidiabetic and phytotoxic potencies was carried out on the basis of the results of the chemical content of the different extracts prepared in our previous work [15].

3.3.1. Correlation Matrix.
Principal component analysis (PCA) helped us to highlight possible correlations between

all the extracts present a remarkable inhibitory activity. Concerning the aqueous extracts, we found that the decocted has an inhibitory activity of $IC_{50} = 2.540 \times 10^2 \pm 3.14 \mu$g/mL followed by the infused ($IC_{50} = 3.653 \times 10^2 \pm 2.06 \mu$g/mL) with a statistically significant difference and the aqueous macerated comes last with a statistically nonsignificant difference with the infused ($IC_{50} = 4.212 \times 10^2 \pm 21.20 \mu$g/mL). Regarding the organic extracts, we found that ethanolic extract, ethanolic macerated extract, and chloroformic extract show relative IC_{50} inhibitory activity of $2.216 \times 10^2 \pm 1.39$, $2.352 \times 10^2 \pm 1.13$, and $2.804 \times 10^2 \pm 0.75 \mu$g/mL, respectively; these three extracts show statistically insignificant difference between them. Chloroformic macerated recorded an α-glucosidase inhibition value equal to $4.293 \times 10^2 \pm 2.65 \mu$g/mL, followed by hexanic extract ($IC_{50} = 5.194 \times 10^2 \pm 22.86 \mu$g/mL) and hexanic macerated ($IC_{50} = 5.286 \times 10^2 \pm 20.65 \mu$g/mL) with statistically nonsignificant difference between hexanic extract and hexanic macerated. Acarbose also showed high α-glucosidase inhibi-

TABLE 2: Median inhibitory concentrations (IC_{50}) in (μg/mL) of α-amylase, α-glucosidase, and β-galactosidase inhibitory activity of aqueous and organic extracts of *C. humilis* leaves.

Extracts	α-Amylase	α-Glucosidase	β-Galactosidase
Decocted	$1.781 \times 10^5 \pm 358.30^a$	$2.540 \times 10^2 \pm 3.14^a$	$7.118 \times 10^2 \pm 16.13^a$
Infused	$2.579 \times 10^5 \pm 690.80^b$	$3.653 \times 10^2 \pm 2.06^b$	$9.050 \times 10^2 \pm 9.33^b$
Aqueous macerated	$2.781 \times 10^5 \pm 396.48^c$	$4.212 \times 10^2 \pm 21.20^{b,c}$	$8.544 \times 10^2 \pm 13.66^b$
Ethanolic extract	$8.902 \times 10^3 \pm 57.81^d$	$2.216 \times 10^2 \pm 1.39^{a,d}$	$2.003 \times 10^2 \pm 7.41^c$
Ethanolic macerated	$1.754 \times 10^5 \pm 107.08^e$	$2.352 \times 10^2 \pm 1.13^{a,d}$	$4.792 \times 10^2 \pm 13.43^d$
Chloroformic extract	$2.114 \times 10^5 \pm 113.77^f$	$2.804 \times 10^2 \pm 0.75^{a,d}$	$3.598 \times 10^2 \pm 7.29^e$
Chloroformic macerated	$1.604 \times 10^5 \pm 240.83^g$	$4.293 \times 10^2 \pm 2.65^c$	$5.671 \times 10^2 \pm 3.29^f$
Hexanic extract	$2.401 \times 10^5 \pm 677.48^h$	$5.194 \times 10^2 \pm 22.86^e$	$2.593 \times 10^2 \pm 19.13^g$
Hexanic macerated	$3.463 \times 10^5 \pm 211.02^i$	$5.286 \times 10^2 \pm 20.65^e$	$3.186 \times 10^2 \pm 6.19^e$
Acarbose	$6.160 \times 10^2 \pm 5.00^j$	$1.950 \times 10^2 \pm 6.12^d$	—
Quercetin	—	—	$1.711 \times 10^2 \pm 5.00^c$

The results are expressed as the mean of three individual replicates ($n = 3 \pm$ SEM). Values with the same superscript letters in the same column are not significantly different ($p < 0.05$).

the chemical content and the antidiabetic and phytotoxic activity of *C. humilis* leaves (Table 3).

3.3.2. Graphical Representation of the Principal Component Analysis (PCA).
According to the PCA the two axes F1 and F2 present 86.73% of the total variance of the observations, which means that the interpretations will be highly significant, this analysis allowed us to define 3 groups (Figure 5):

(i) Group 1: consisting of ethanolic extract and ethanolic macerated which have high polyphenol contents and also express an antidiabetic effect for the enzymes α-amylase and α-glucosidase

(ii) Group 2: includes chloroformic extract, chloroformic macerated extract, hexanic extract and hexanic macerated extract, which are rich in catechic tannins and flavonoids. These extracts show antidiabetic activity for the enzyme β-galactosidase and cytotoxic capacity via the phytotest *Lepidium sativum*

(iii) Group 3: includes the aqueous extracts (decocted, infused, and macerated) which are characterized, according to this analysis, by a low chemical composition in total polyphenols, flavonoids, and catechic tannins; this group also presents low antidiabetic and antimitotic activities

3.4. Acute Toxicity

3.4.1. Mortality and Signs of Acute Toxicity.
Single-dose administration (2000 mg/kg) of the decocted and ethanolic extract did not cause any deaths in treated mice; however, a lack of appetite was observed on the first day of treatment. In addition, mice treated with ethanolic extract showed reduced mobility for 72 hours after treatment; however, mice from the control batch did not show any abnormal signs (Table 4).

3.4.2. The Evolution of the Body Weight of Mice.
The weight evolution of each animal was measured during the 14 days after the single administration of the two extracts: decocted and ethanolic extract; the weight of the groups treated with decocted and ethanolic extract showed no remarkable difference; however, the weight of the control group increased during the observation period with an average of 15.66% (Figure 6).

3.4.3. Determination of the LD_{50}.
The determination of the LD_{50} was performed according to the OECD acute toxicity assessment method code no. 423; during the treatment period no deaths were observed, this indicates that the LD_{50} is greater than or equal to 5000 mg/kg. Furthermore, according to the Global System of Classification of Chemical Substances (GHS), both tested extracts belong to toxicity class 5 or not classified. Both extracts are thus considered to be mixtures with relatively low acute toxicity, but which may under certain conditions be hazardous to susceptible individuals [36].

4. Discussion

4.1. Phytotest Lepidium sativum.
The *Lepidium sativum* test showed that the inhibitory effect on the growth of *Lepidium sativum* seed rootlets by the tested aqueous and organic extracts is dose dependent. Regarding the aqueous extracts, we found that the decocted and infused show better inhibitory activity presented by values of $9.624 \times 10^3 \pm 95.97$ and $9.642 \times 10^3 \pm 67.49\,\mu$g/mL, respectively, with a statistically nonsignificant difference. For the organic extracts, we found that the high *in vitro* antimitotic activity was presented by the ethanolic extract ($IC_{50} = 5.638 \times 10^3 \pm 22.61\,\mu$g/mL) and the ethanolic macerated ($IC_{50} = 5.599 \times 10^3 \pm 45.51\,\mu$g/mL) with a statistically nonsignificant difference between the two extracts. We can remark that the best results obtained via the *Lepidium sativum* phytotest are expressed by high polarity extracts prepared at high temperature (decocted, infused, and ethanolic extract) or by cold

TABLE 3: Correlation matrix between the chemical profile (total polyphenols, total flavonoids, and catechic tannins) and the antidiabetic antimitotic action of aqueous and organic extracts of *C. humilis* leaves.

Variables	Total polyphenols	Total flavonoids	Catechic tannins	α-Amylase	α-Glucosidase	β-Galactosidase	*Lepidium sativum* phytotest
Total polyphenols	1						
Total flavonoids	0.7556	1					
Catechic tannins	0.8924	0.9507	1				
α-Amylase	0.6638	0.4055	0.5189	1			
α-Glucosidase	0.5788	0.1613	0.3756	0.5970	1		
β-Galactosidase	0.5712	0.6345	0.7092	0.5363	0.0596	1	
Lepidium sativum Phytotest	0.7612	0.9153	0.9370	0.4456	0.1036	0.8592	1
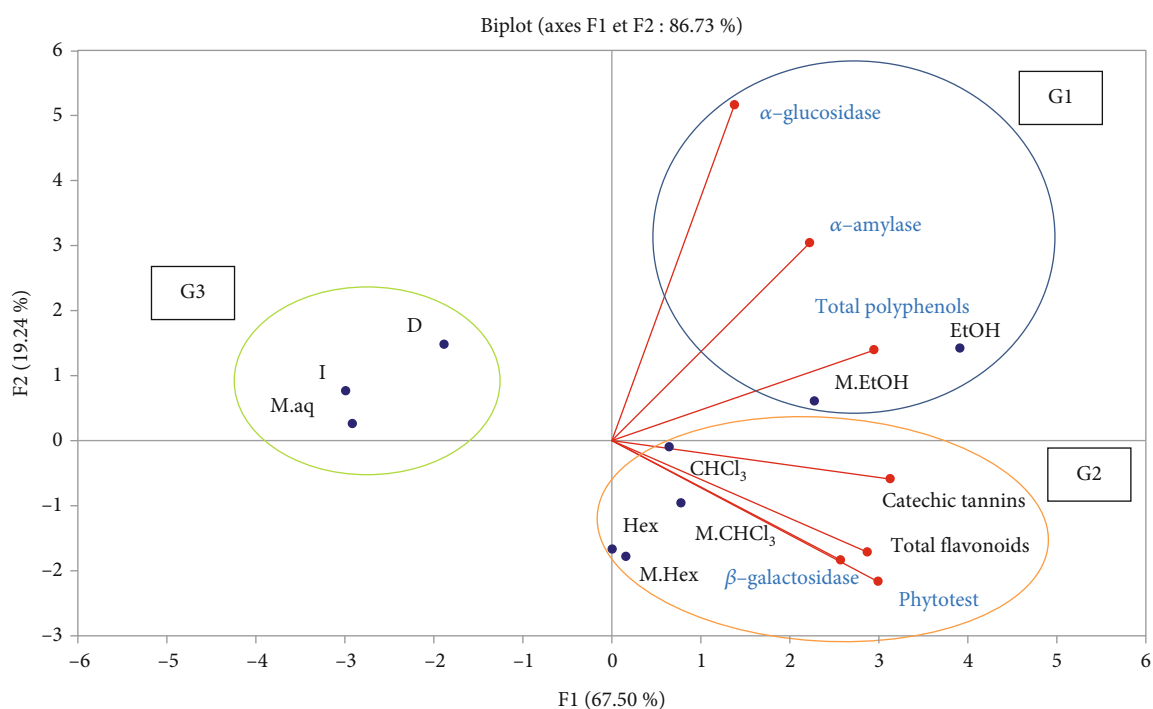
FIGURE 5: Principal component analysis (PCA) of the chemical composition and antidiabetic activity of aqueous and organic extracts of *C. humilis* leaves. D: decocted; I: infused; M.aq: aqueous macerated; E_tOH: ethanolic extract; $M.E_tOH$: ethanolic macerated; $CHCl_3$: chloroformic extract; $M.CHCl_3$: chloroformic macerated; Hex: hexanic extract; M.Hex: hexanic macerated; G1: group 1; G2: group 2; G3: group 3; TP: total polyphenols; TF: total flavonoids; CT: catechic tannins.

TABLE 4: Mortality and clinical signs recorded in the acute toxicity study of ethanolic extract and decocted of *C. humilis* leaves.

	Ethanolic extract	Signs of acute toxicity	Decocted	Signs of acute toxicity	Control	Signs of acute toxicity
		Step 1 (dose: 2000 mg/kg)				
Number of mice	3	(i) Anorexia	3	(i) Anorexia	3	
Number of deaths	0	(ii) Reduced mobility	0	(ii) Reduced mobility	0	—
		Step 2 (dose: 2000 mg/kg)				
Number of mice	3	(i) Anorexia	3	(i) Anorexia	3	
Number of deaths	0	(ii) Reduced mobility	0	(ii) Reduced mobility	0	—
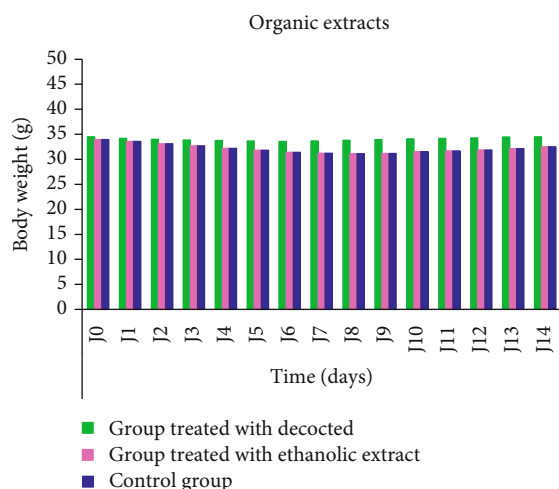
FIGURE 6: Weight evolution of the groups treated with decocted and ethanolic extract of *C. humilis* leaves and of the control group over 14 days.

extraction by maceration with a long contact time between the plant material and the solvent (ethanolic macerated). This suggests that the active ingredients responsible for the antimitotic activity are better extracted with these extraction modalities. In addition, the cell growth inhibition or antimitotic effect could also be due to the chemical composition. Indeed, our recent study confirmed the richness of *C. humilis* leaves in total polyphenols, flavonoids, and catechic tannins [15]. Another study showed that the presence of phenolic compounds, alkaloids, and flavonoids are responsible for the antimitotic activity of the aqueous extract of *Ficus benghalensis* [39]. Studies conducted under the same operating conditions as ours found that both hamaline and harmalol alkaloids have high inhibitory activity on *Lepidium sativum* rootlet growth with an IC_{50} of 134.15 and 239.43 μg/mL, respectively [40]. In addition, the methanolic extract and methanolic macerated of *Ajuga iva* had a strong antimitotic activity represented by an IC_{50} of 320.43 ± 8.96 and 375.77 ± 17.53 μg/mL, respectively [38]. The antimitotic effect of *C. humilis* extracts could also be due to the mineral richness of the plant: iron (Fe): 82395.00, potassium (K): 9354.90, phosphorus (P): 1828.62, magnesium (Mg): 1312.47, sodium (Na): 627.03; copper (Cu): 542.64, calcium (Ca): 92.19, zinc (Zn): 66.15, selenium (Se): 3.00, and strontium (Sr):3.00 mg/kg [15]. These mineral elements can be a means to fight or prevent the occurrence of cancer; several studies show that Zn deficiency leads to DNA oxidation and DNA breaks and chromosomal damage associated with increased cancer risk [41, 42]. Indeed, Zn plays a crucial role in DNA metabolism, and a deficiency in this element can induce important chromosomal mutations that increase the risk of cancer [43–45]. Selenium is another essential trace element that is vital for various cellular processes and is also frequently used to prevent the occurrence of cancer [46, 47]. In addition, both selenium and zinc play a role in the efficient progression of the DNA repair system, thereby mitigating DNA damage that could lead to cancer development [47, 48]. Magnesium (Mg) and potassium (K) may also

play a protective role significantly against the development of colorectal cancer (CRC) [49, 50].

4.2. *In Vitro Study of Antidiabetic Activity.* The results of the α-amylase, α-glucosidase, and β-galactosidase enzymatic inhibition tests showed that all aqueous and organic extracts of *C. humilis* leaves show antidiabetic capacity *in vitro*. Firstly, the decocted showed a high inhibitory power for all three enzymes; this activity is higher than that of the infused and aqueous macerated, and this could be explained by the ability of the high temperature to extract better the molecules that have antihyperglycemic activity [15]. For the α-amylase and β-galactosidase enzymes, we found that ethanolic extract presented the best inhibitory activity compared to other organic extracts with $IC_{50} = 8.902 \times 10^3 \pm 57.81$ and $IC_{50} = 2.003 \times 10^2 \pm 7.41$ μg/mL values, respectively. In addition, ethanolic extract and ethanolic macerated had remarkable α-glucosidase inhibitory power compared to other organic extracts presented by IC_{50} values of $2.216 \times 10^2 \pm 1.39$ and $2.352 \times 10^2 \pm 1.13$ μg/mL, respectively, with statistically insignificant difference between them and with acarbose $(1.950 \times 10^2 \pm 6.12$ μg/mL). This suggests that polar solvent extraction at high temperature for 6-8 hours and maceration extraction for a longer period of 48 hours are capable of extracting the active ingredients responsible for this activity. These results can be explained by the results of the study of the chemical composition of the same extracts of the leaves of *Chamaerops humilis* [15], which showed that the ethanolic extract and the ethanolic macerated have high contents of total polyphenols of 96.99 ± 0.82 and 100.27 ± 0.66 μg EAG/mE, respectively. Both of these extracts also showed a high content of flavonoids with values of 457.98 ± 5.18 and 468.25 ± 9.07 μg TE/mgE, respectively, and of catechic tannins with 50.27 ± 0.99 and 52.11 μg TE/mgE, respectively. ANOVA analysis proved that the statistical difference between ethanolic extract and ethanolic macerated is not significant [15]. Moreover, a recent study proved that polar extracts of *G. senegalensis* show better inhibitory activity on α-glucosidase [51]. The antihyperglycemic effect of all the extracts studied is also variable with respect to the three enzymes used which could be explained by the structural variation related to the origin of these enzymes [52]. The hypoglycemic effect of *Chamaerops humilis* could also be due to its mineralogical content; in our previous study, we found that the leaves of *C. humils* are rich in iron (82395.00 mg/kg), potassium (9354.90 mg/ kg), phosphorus (1828.62 mg/kg), magnesium (1312.47 mg/ kg), sodium (627.03 mg/kg), copper (542.64 mg/kg), calcium (92.19 mg/kg), and zinc (66.15 mg/kg) [15]. Firstly, potassium, zinc, and calcium play an important role in improving glucose tolerance and indirectly contribute in the management of type 2 diabetes; in addition, calcium also plays an important role in insulin release from islet β-cells [53, 54]. Mg supplementation may also be useful to resolve the phenomenon of insulin resistance [54, 55].

Our results are in agreement with an *in vivo* study conducted by Gaamoussi and collaborators, which demonstrated that plasma glucose levels in obese rats with hyperglycemia and hyperlipidemia decreased significantly

with daily administration of *Chamaerops humilis* decocted from 12.04 ± 0.94 mmol/L to 6.10 ± 0.27 mmol/L after 15 days and to 4.84 ± 0.22 mmol/L after 30 days of treatment [22].

Studies conducted under the same experimental conditions in our laboratory on plants from the same region as our *Chamaerops humilis* plant found that the methanolic macerated of *Atractylis gummifera* recorded high inhibitory activity against the three enzymes α-amylase, α-glucosidase, and β-galactosidase with an IC_{50} of 557 ± 0.013, 743 ± 0.017, and 2443 ± 0.071 μg/mL, respectively. Similarly, *Juglans regia* acetone macerated showed high inhibitory activity for α-amylase ($IC_{50} = 5445.33 \pm 82 : 58$ μg/mL), α-glucosidase ($IC_{50} = 323 : 7 \pm 1.71$ μg/mL), and β-galactosidase ($IC_{50} = 811.2 \pm 8.32$ μg/mL). *Ajuga iva* metanolic macerated showed a potent antidiabetic effect for β-galactosidase ($IC_{50} = 146.47 \pm 33.05$ μg/mL). The methanolic extract of *Haloxylon scoparium* also had a strong α-glucosidase inhibitory capacity ($IC_{50} = 193.4 \pm 8.57$ μg/mL) [28–30, 56].

4.3. Correlation between the Chemical Composition (Total Phenols, Total Flavonoids, and Catechic Tannins) and the Cell Growth Inhibitory and Antihyperglycemic Activity of Aqueous and Organic Extracts of C. humilis Leaves.

According to the results of the principal component analysis (PCA), polyphenol content correlated well with antihyperglycemic activity for α-amylase ($r = 0.6638$) and moderately correlated with α-glucosidase ($r = 0.5788$) and β-galactosidase ($r = 0.5712$). In contrast, the inhibitory activity by β-galactosidase was better correlated with the content of catechic tannins ($r = 0.7092$) and flavonoids ($r = 0.6345$). According to these results, the hypoglycemic activity could be attributed to the active ingredients of different chemical nature, this activity could also be variable depending on the enzyme used. According to Sales and collaborators, the action of polyphenols and flavonoids in inhibiting α-amylase is explained by the formation of hydrogen bonds between its hydroxyl groups and the residues of the enzyme binding site [57]. The hypoglycemic effect of *Chamaerops humilis* leaves could also be due to the catechic tannins; according to Hosoyama and coworkers, tannins and ellagic acid derivatives from banaba (*Lagerstroemia speciosa* L.) are potent inhibitors of α-amylase [58]. In addition, a study indicated a strong correlation between phenolic compounds of *Gymnema montanum* leaves and the inhibitory effect of α-glucosidase and α-amylase activity $r^2 = 0.92$ and $r^2 = 0.97$, respectively [59].

Regarding the results obtained via the *Lepidium sativum* phyotest, a strong correlation was noticed between the *in vitro* antimitotic activity and the content of catechic tannins ($r = 0.9370$), flavonoids ($r = 0.9153$), and total polyphenols ($r = 0.7612$), which means that the *in vitro* cytotoxic activity might be due to several chemical families. This is in concordance with the study conducted by Zhao and collaborators who reported that phenolic compounds can influence hormone production and inhibit aromatase and therefore prevent cancer development [60]; flavonoids may also be effective in the cancer inhibition mechanism [61]. In addition, Stanisavljević and collaborators have shown

strong correlations between the intensity of *in vitro* cytotoxic activity of *Pisum sativum* extracts and epigallocatechin and luteolin contents [62].

The present study clearly shows that *Chamaerops humilis* leaves possess both antimitotic and hypoglycemic effect; in the same sense, many studies have indicated the association between cancer and hyperglycemia; diabetes and insulin resistance could be the consequence of an as yet undiagnosed initial state of cancer; diabetes could also be related to the precancerous state of the pancreas which affects its insulin-secreting capacity [7]. Insulin resistance is associated with an inflammatory state that also promotes hepatic carcinogenesis. In addition, cancer is one of the most common causes of mortality in type 2 diabetes [11, 12]. According to Stocks and collaborators, for every 1 mmol/l increase in blood glucose, there is a 10-20% increase in cancer risk for both men and women [8]. Indeed, in the genesis of type 2 of diabetes, the existence of insulin sensitivity induces high blood levels of insulin and an increase in circulating levels of insulin-like growth factors (IGF). The IGFs stimulate cell proliferation in many organs, in particular the liver, pancreas, colon, ovary, and breast [7, 9, 10].

4.4. Acute Toxicity of Chamaerops humilis Leaves.

During the observation period (14 days) following the administration of the decocted and the ethanolic extract at a dose of 2000 mg/kg, no deaths were recorded in the treated animals.

According to the method for determining the lethal dose (LD_{50}) described by the European OECD guideline code no. 423, the tested extracts have a lethal dose (LD_{50}) which is estimated to be ≥ 5000 mg/kg by the oral route. In addition, the Globally Harmonised System of Classification (GHS) allowed us to classify the decocted and the ethanolic extract in category V or unclassified [36], which means that these two extracts are considered to be a mixture with a proportionally low acute toxicity, but which may under certain conditions be hazardous to vulnerable persons [36].

During the observation period, we noted that mice treated with the decocted and ethanolic extract showed some clinical signs such as loss of appetite and reduced mobility during the first hours after administration. The mice returned to their normal state after 72 hours. However, the control group did not show any behavioral changes. These clinical signs could explain the weight evolution, which showed a slight decrease in body weight in the treated mice during the first 6 days and an increase in weight in the control group. A subacute toxicity study conducted in the rat animal model of *Haloxylon scoparium* decocted recorded a gain in body weight in rats treated with 500, 1000, and 2000 mg/kg. This growth was lower than that of the control group, 11.87%, 9.32%, and 8.59%, respectively, compared to the control group (18.67%) [63].

5. Conclusion

The present work focused on the search for new anticancer and antidiabetic agents via tests dedicated to the evaluation of the antimitotic and antihyperglycemic effects *in vitro* of three aqueous extracts and nine organic extracts of the leaves

of *Chamaerops humilis* L. var. argentea Andre as well as the *in vivo* evaluation of the acute toxicity of the extracts which proved to be the most active *in vitro*, namely, that of the decocted and the ethanolic extract.

Our results show that all aqueous and organic extracts had antimitotic and antihyperglycemic effect *in vitro* with a variable degree with a better activity revealed mainly for ethanolic extract and ethanolic macerated for organic extracts and decocted for aqueous extracts. The mentioned extracts could constitute a natural source of anticancer and antidiabetic molecules for pharmaceutical applications.

The principal component analysis (PCA) showed that polyphenol content correlated better with antihyperglycemic activity for α-amylase ($r = 0.6638$). In addition, α-glucosidase inhibitory activity was better correlated with the content of catechic tannins ($r = 0.7092$) and with flavonoids ($r = 0.6345$). Concerning the *Lepidium sativum* phyotest, PCA showed that a strong correlation was observed between *in vitro* antimitotic activity and the content of catechic tannins ($r = 0.9370$), flavonoids ($r = 0.9153$), and total polyphenols ($r = 0.7612$). These results could lead to the conclusion that the antidiabetic activity and the antimitotic activity *in vitro* could be attributed to the active compounds that have different chemical natures.

Regarding the *in vivo* acute toxicity study, administration of a single dose of 2000 mg/kg of decocted and ethanolic extract did not cause any deaths; therefore, the LD_{50} is estimated to be ≥ 5000 mg/mL according to OECD and the tested extracts belong to class V or not classified according to the Globally Harmonised System of Classification (GHS).

Abbreviations

C. humilis:	*Chamaerops humilis* L. var. argentea Andre
DNS:	Dinitrosalicylic acid
pNPG:	4-p-Nitrophenyl-α-D-glucopyranoside
OECD:	Organisation for Economic Co-operation and Development
PCA:	Principal component analysis
IC_{50}:	The median inhibitory concentrations
GHS:	Global system of classification of chemical substances
LD_{50}:	Lethal dose.

Data Availability

The data generated or analyzed during this study are included in this article in form of tables and figures.

Ethical Approval

The procedures used to perform the *in vivo* study are in agreement with the international guidelines used for the use of laboratory animals and for animal care (OECD Guideline no. 423). The authors made a great effort to reduce the suffering of the animals and to minimize the number of animals used.

Conflicts of Interest

The authors declare no conflict of interest associated with this publication.

Authors' Contributions

Nacima Lachkar (NL) carried out the experiential studies and manuscript preparation. Fatima Lamchouri (FL) designed the experiments, provided consistent guidance, analyzed the data, prepared and reviewed the manuscript, and edited the final version and submitted it for publication. Hamid Toufik (HT) designed the experiments, provided consistent guidance, and reviewed the manuscript. All authors read, reviewed, and approved the final manuscript.

Acknowledgments

References

[1] World Health Organization (WHO), A, "Global Health Observatory," *Cancer*, 2022, August 2022, https://www.who.int/news-room/fact-sheets/detail/cancer.

[2] R. Bekkali, M. Bennani, Y. Chami Khazraji, L. Belakhel, and L. Abousselham, "Plan National de Prévention et de Contrôle du Cancer 2020-2029 (PNPCC)," *Ministry of Health of Morocco & Foundation Lalla Salma for Cancer Prevention and Treatment*, 2020, July 2022, https://www.sante.gov.ma/Documents/2021/03/Plan_National_de_Prevention_et_de_Controle_du_Cancer_2020-2029_VF.pdf?csf=1&e=ejDjaj.

[3] P. Nygren, "What is cancer chemotherapy?," *Acta Oncologica*, vol. 40, no. 2-3, pp. 166–174, 2001, https://www.tandfonline.com/doi/pdf/10.1080/02841860151116204.

[4] Y. Q. Liu, X. L. Wang, D. H. He, and Y. X. Cheng, "Protection against chemotherapy- and radiotherapy-induced side effects: a review based on the mechanisms and therapeutic opportunities of phytochemicals," *Phytomedicine*, vol. 80, article 153402, 2021.

[5] International Diabetes Federation, "IDF Diabetes Atlas 10th ed," 2021, https://diabetesatlas.org/idfawp/resourcefiles/2021/07/IDF_Atlas_10th_Edition_2021.pdf / https://diabetesatlas.org/.

[6] M. Belhadj, H. Lhassani, and I. Khochtali, "Management of type 2 diabetes in the Maghreb: current state," *Médecine Des Maladies Métaboliques*, vol. 13, p. eS4-eS7, 2019.

[7] D. Simon, "Relation entre cancer et diabète: l'hyperglycémie joue t-elle un rôle?," *Obésité*, vol. 9, no. 3, pp. 197–204, 2014.

[8] T. Stocks, K. Rapp, T. Bjørge et al., "Blood glucose and risk of incident and fatal cancer in the metabolic syndrome and cancer project (me-can): analysis of six prospective cohorts," *PLoS Medicine*, vol. 6, no. 12, article e1000201, 2009.

[9] H. M. Khandwala, I. E. McCutcheon, A. Flyvbjerg, and K. E. Friend, "The effects of insulin-like growth factors on tumorigenesis and neoplastic growth," *Endocrine Reviews*, vol. 21, no. 3, pp. 215–244, 2000.

[10] I. Wolf, S. Sadetzki, R. Catane, A. Karasik, and B. Kaufman, "Diabetes mellitus and breast cancer," *The Lancet Oncology*, vol. 6, no. 2, pp. 103–111, 2005.

[11] J. L. Schlienger, "Type 2 diabetes complications," *La Presse Médicale*, vol. 42, no. 5, pp. 839–848, 2013.

[12] P. Stattin, O. Bjor, P. Ferrari et al., "Prospective study of hyperglycemia and cancer risk," *Diabetes Care*, vol. 30, no. 3, pp. 561–567, 2007.

[13] M. Bourhia, A. A. Shahat, O. M. Almarfadi et al., "Ethnopharmacological survey of herbal remedies used for the treatment of cancer in the greater Casablanca-Morocco," *Evidence-based Complementary and Alternative Medicine*, vol. 2019, Article ID 1613457, 9 pages, 2019.

[14] N. Chaachouay, H. Orch, and L. Zidane, "Cystitis treatment with phytotherapy within the Rif, Northern Morocco," *Future Journal of Pharmaceutical Sciences*, vol. 7, no. 1, pp. 1–9, 2021.

[15] N. Lachkar, F. Lamchouri, and H. Toufik, "Ethnopharmacological survey, mineral and chemical content, in vitro antioxidant, and antibacterial activities of aqueous and organic extracts of *Chamaerops humilis* L. var. argentea Andre leaves," *BioMed Research International*, vol. 2022, article 1091247 1–27, 2022.

[16] A. M. Scherrer, R. Motti, and C. S. Weckerle, "Traditional plant use in the areas of Monte Vesole and Ascea, Cilento National Park (Campania, Southern Italy)," *Journal of Ethnopharmacology*, vol. 97, no. 1, pp. 129–143, 2005.

[17] M. Boulfia, F. Lamchouri, A. Khabbach, A. Zalaghi, N. Assem, and H. Toufik, "An ethnopharmacological evaluation of Moroccan medicinal plants of the middle atlas and pre-rif of the province of Taza," *Journal of Chemical and Pharmaceutical Research*, vol. 10, pp. 156–173, 2018.

[18] N. Lachkar, F. Lamchouri, and H. Toufik, "Socioeconomic position of *Chamaerops humilis* L. var. argentea Andre in the province of Taza (North East Morocco) and impact of the new Moroccan law n° 77-15 (Moroccan Official Bulletin N° 6422) on the preservation of the environment," *Ethnobotany Research and Applications*, vol. 20, pp. 1–14, 2020.

[19] H. Benmehdi, O. Hasnaoui, O. Benali, and F. Salhi, "Phytochemical investigation of leaves and fruits extracts of *Chamaerops humilis* L," *Journal of Materials and Environmental Science*, vol. 3, pp. 320–337, 2012.

[20] G. Fekkar, F. Yousfi, H. Elmsellem et al., "Eco-friendly *Chamaerops humilis* L. fruit extract corrosion inhibitor for mild steel in 1 M HCl," *International Journal of Corrosion and Scale Inhibition*, vol. 9, no. 2, pp. 446–459, 2020.

[21] J. El-Hilaly, M. Hmammouchi, and B. Lyoussi, "Ethnobotanical studies and economic evaluation of medicinal plants in Taounate province (Northern Morocco)," *Journal of Ethnopharmacology*, vol. 86, no. 2-3, pp. 149–158, 2003.

[22] F. Gaamoussi, Z. H. Israili, and B. Lyoussi, "Hypoglycemic and hypolipidemic effects of an aqueous extract of *Chamaerops humilis* leaves in obese, hyperglycemic and hyperlipidemic Meriones shawi rats," *Pakistan Journal of Pharmaceutical Sciences*, vol. 23, no. 2, pp. 212–219, 2010.

[23] A. Chetoui, K. Kaoutar, K. Boutahar et al., "Herbal medicine use among Moroccan type 2 diabetes patients in the Beni Mellal-Khenifra region," *Journal of Herbal Medicine*, vol. 29, article 100480, 2021.

[24] E. Idm'hand, F. Msanda, and K. Cherifi, "Ethnopharmacological review of medicinal plants used to manage diabetes in Morocco," *Clinical Phytoscience*, vol. 6, no. 1, pp. 1–32, 2020.

[25] E. K. Sumaili, J. M. Krzesinski, E. P. Cohen, and N. M. Nseka, "Epidemiology of chronic kidney disease in the Democratic Republic of Congo: review of cross-sectional studies from Kinshasa, the capital," *Néphrologie & Thérapeutique*, vol. 6, no. 4, pp. 232–239, 2010.

[26] E. Mills, C. Cooper, D. Seely, and I. Kanfer, "African herbal medicines in the treatment of HIV: Hypoxis and Sutherlandia. An overview of evidence and pharmacology," *Nutrition Journal*, vol. 4, no. 1, pp. 1–6, 2005.

[27] K. Bouabid, F. Lamchouri, H. Toufik, and M. E. A. Faouzi, "Phytochemical investigation, in vitro and in vivo antioxidant properties of aqueous and organic extracts of toxic plant: Atractylis gummifera L," *Journal of Ethnopharmacology*, vol. 253, article 112640, 2020.

[28] M. Boulfia, F. Lamchouri, S. Senhaji, N. Lachkar, K. Bouabid, and H. Toufik, "Mineral content, chemical analysis, in vitro antidiabetic and antioxidant activities, and antibacterial power of aqueous and organic extracts of Moroccan *Leopoldia comosa* (L.) Parl. Bulbs," vol. 2021, 2021.

[29] S. Senhaji, F. Lamchouri, M. Boulfia, N. Lachkar, K. Bouabid, and H. Toufik, "Mineral composition, in vitro inhibitory effects of α-amylase, α-glucosidase, β-galactosidase enzymes and antibacterial activity of *Ajuga iva* subsp. Pseudoiva (DC.) Bric," *Biointerface Research in Applied Chemistry*, vol. 12, pp. 2373–2391, 2021.

[30] N. Lachkar, F. Lamchouri, K. Bouabid et al., "Mineral composition, phenolic content, and in vitro antidiabetic and antioxidant properties of aqueous and organic extracts of *Haloxylon scoparium* aerial parts," *Evidence-Based Complementary and Alternative Medicine*, vol. 2021, Article ID 9011168, pp. 1–20, 2021.

[31] F. Gagiu, C. Nistor, F. Danciu et al., "Mitodepressive substances. a new biotest and its application to several alpha-alkyl-phenyl acetic derivatives," *Annales Pharmaceutiques Francaises*, vol. 31, no. 5, pp. 363–367, 1973.

[32] M. N. Wickramaratne, J. C. Punchihewa, and D. B. M. Wickramaratne, "In-vitro alpha amylase inhibitory activity of the leaf extracts of Adenanthera pavonina," *BMC Complementary and Alternative Medicine*, vol. 16, no. 1, p. 466, 2016.

[33] M. Boulfia, F. Lamchouri, and H. Toufik, "Mineral analysis, In Vitro Evaluation of Alpha-Amylase, Alpha-Glucosidase, and Beta-Galactosidase Inhibition, and Antibacterial Activities of Juglans regia L. Bark Extracts," *BioMed Research International*, vol. 2021, Article ID 1585692, pp. 1–14, 2021b.

[34] S. Lordan, T. J. Smyth, A. Soler-Vila, C. Stanton, and R. P. Ross, "The α-amylase and α-glucosidase inhibitory effects of Irish seaweed extracts," *Food Chemistry*, vol. 141, no. 3, pp. 2170–2176, 2013.

[35] D. Maruhn, "Rapid colorimetric assay of β-galactosidase and N-acetyl-β-glucosaminidase in human urine," *Clinica Chimica Acta*, vol. 73, no. 3, pp. 453–461, 1976.

[36] OECD, "OECD guideline for testing of chemicals: test no 423: acute oral toxicity - acute toxic class method," *The Organisation for Economic Co-operation and Development*, pp. 1–14, 2001.

[37] E. D. Olfert, B. M. Cross, and A. A. McWilliam, "Standards for experimental animal surgery. Canadian council on animal care guide to the care and use of experimental animals, 1," 1993, April 2020, https://www.ccac.ca/Documents/Standards/Guidelines/Experimental_Animals_Vol1.pdf.

[38] S. Senhaji, F. Lamchouri, M. Boulfia et al., "Cell growth inhibition, toxicity assessment, and correlation between chemical

composition of aqueous and organic extracts of Ajuga iva subsp. Pseudoiva (DC.) Bric. and their biological activities," *Biointerface Research in Applied Chemistry*, vol. 13, 2023.

[39] R. Ahirrao, B. Jain, P. Jaiswal, and A. Kabra, "Effect of aqueous extract on total phenolic content and antimitotic activity of *Ficus benghalensis* root on *allium Cepa* root meristamatic cells," *Archives in Biomedical Engineering & Biotechnology (ABEB)*, vol. 4, no. 4, p. 4, 2020.

[40] T. Akabli, F. Lamchouri, S. Senhaji, and H. Toufik, "Molecular docking, ADME/Tox prediction, and *in vitro* study of the cell growth inhibitory activity of five β-carboline alkaloids," *Structural Chemistry*, vol. 30, no. 4, pp. 1495–1504, 2019.

[41] M. F. Fenech, "Nutriomes and personalised nutrition for DNA damage prevention, telomere integrity maintenance and cancer growth control," *Advances in Nutrition and Cancer*, vol. 159, 2014.

[42] F. Maffei, J. M. Zolezzi Moraga, S. Angelini et al., "Micronucleus frequency in human peripheral blood lymphocytes as a biomarker for the early detection of colorectal cancer risk," *Mutagenesis*, vol. 29, no. 3, pp. 221–225, 2014.

[43] R. Sharif, P. Thomas, P. Zalewski, and M. Fenech, "The role of zinc in genomic stability," *Mutation Research/Fundamental and Molecular Mechanisms of Mutagenesis*, vol. 733, no. 1-2, pp. 111–121, 2012.

[44] I. E. Dreosti, "Zinc and the gene," *Mutation Research/Fundamental and Molecular Mechanisms of Mutagenesis*, vol. 475, no. 1-2, pp. 161–167, 2001.

[45] E. Ho, "Zinc deficiency, DNA damage and cancer risk," *The Journal of Nutritional Biochemistry*, vol. 15, no. 10, pp. 572–578, 2004.

[46] M. P. Rayman, "Selenium in cancer prevention: a review of the evidence and mechanism of action," *Proceedings of the Nutrition Society*, vol. 64, no. 4, pp. 527–542, 2005.

[47] A. Yildiz, Y. Kaya, and O. Tanriverdi, "Effect of the interaction between selenium and zinc on DNA repair in association with cancer prevention," *Cancer Prevention*, vol. 24, no. 3, pp. 146–154, 2019.

[48] P. Erkekoglu, B. Giray, W. Rachidi et al., "Effects of di(2-ethylhexyl)phthalate on testicular oxidant/antioxidant status in selenium-deficient and selenium-supplemented rats," *Environmental Toxicology*, vol. 29, no. 1, pp. 98–107, 2014.

[49] G. A. Kune, S. Kune, and L. F. Watson, "Dietary sodium and potassium intake and colorectal cancer risk," *Nutrition and Cancer*, vol. 12, no. 4, pp. 351–359, 1989.

[50] N. Hou, D. Huo, and J. J. Dignam, "Prevention of colorectal cancer and dietary management," *Chinese Clinical Oncology*, vol. 2, no. 2, p. 13, 2013.

[51] A. I. Dirar, D. H. M. Alsaadi, M. Wada, M. A. Mohamed, T. Watanabe, and H. P. Devkota, "Effects of extraction solvents on total phenolic and flavonoid contents and biological activities of extracts from Sudanese medicinal plants," *South African Journal of Botany*, vol. 120, pp. 261–267, 2019.

[52] S. Chiba, "Molecular mechanism in α-glucosidase and glucoamylase," *Bioscience, Biotechnology, and Biochemistry*, vol. 61, no. 8, pp. 1233–1239, 1997.

[53] A. Kar, B. K. Choudhary, and N. G. Bandyopadhyay, "Preliminary studies on the inorganic constituents of some indigenous hypoglycaemic herbs on oral glucose tolerance test," *Journal of Ethnopharmacology*, vol. 64, no. 2, pp. 179–184, 1999.

[54] P. K. Rai, D. Jaiswal, N. K. Rai, S. Pandhija, A. K. Rai, and G. Watal, "Role of glycemic elements of *Cynodon dactylon*

and *Musa paradisiaca* in diabetes management," *Lasers in Medical Science*, vol. 24, no. 5, pp. 761–768, 2009.

[55] R. Lopez-Ridaura, W. C. Willett, E. B. Rimm et al., "Magnesium intake and risk of type 2 diabetes in men and women," *Diabetes Care*, vol. 27, no. 1, pp. 134–140, 2004.

[56] K. Bouabid, F. Lamchouri, H. Toufik, K. Sayah, Y. Cherrah, and M. E. A. Faouzi, "Phytochemical screening and *in vitro* evaluation of alpha amylase, alpha glucosidase and beta galactosidase inhibition by aqueous and organic *Atractylis gummifera* L. extracts," *Plant Science Today*, vol. 5, no. 3, pp. 103–112, 2018.

[57] P. M. Sales, P. M. Souza, L. A. Simeoni, P. O. Magalhães, and D. Silveira, "α-Amylase inhibitors: a review of raw material and isolated compounds from plant source," *Journal of Pharmacy & Pharmaceutical Sciences*, vol. 15, no. 1, pp. 141–183, 2012.

[58] H. Hosoyama, A. Sugimoto, Y. Suzuki, I. Sakane, and T. Kakud, "Isolation and quantitative analysis of the α-amylase inhibitor in *Lagerstroemia speciosa* (L.) Pers. (Banaba)," *Journal of the Pharmaceutical Society of Japan*, vol. 123, no. 7, pp. 599–605, 2003.

[59] K. M. Ramkumar, B. Thayumanavan, T. Palvannan, and P. Rajaguru, "Inhibitory effect of *Gymnema montanum* leaves on α-glucosidase activity and α-amylase activity and their relationship with polyphenolic content," *Medicinal Chemistry Research*, vol. 19, no. 8, pp. 948–961, 2010.

[60] M. Zhao, B. Yang, J. Wang, Y. Liu, L. Yu, and Y. Jiang, "Immunomodulatory and anticancer activities of flavonoids extracted from litchi (Litchi chinensis Sonn.) pericarp," *International Immunopharmacology*, vol. 7, no. 2, pp. 162–166, 2007.

[61] S. Zhang, X. Yang, R. A. Coburn, and M. E. Morris, "Structure activity relationships and quantitative structure activity relationships for the flavonoid-mediated inhibition of breast cancer resistance protein," *Biochemical Pharmacology*, vol. 70, no. 4, pp. 627–639, 2005.

[62] N. S. Stanisavljević, M. D. Ilić, I. Z. Matić et al., "Identification of phenolic compounds from seed coats of differently colored European varieties of pea (*Pisum sativum* L.) and characterization of their antioxidant and *In Vitro* anticancer activities," *Nutrition and Cancer*, vol. 68, no. 6, pp. 988–1000, 2016.

[63] L. Kharchoufa, M. Bouhrim, N. Bencheikh et al., "Acute and subacute toxicity studies of the aqueous extract from *Haloxylon scoparium* Pomel (*Hammada scoparia* (Pomel)) by oral administration in rodents," *BioMed Research International*, vol. 2020, Article ID 4020647, 11 pages, 2020.

Retraction

Retracted: SPOCK2 Promotes the Malignant Behavior of Ovarian Cancer via Regulation of the Wnt/β-Catenin Signaling Pathway

BioMed Research International

This article has been retracted by Hindawi following an investigation undertaken by the publisher [1]. This investigation has uncovered evidence of one or more of the following indicators of systematic manipulation of the publication process:

(1) Discrepancies in scope

(2) Discrepancies in the description of the research reported

(3) Discrepancies between the availability of data and the research described

(4) Inappropriate citations

(5) Incoherent, meaningless and/or irrelevant content included in the article

(6) Manipulated or compromised peer review

The presence of these indicators undermines our confidence in the integrity of the article's content and we cannot, therefore, vouch for its reliability. Please note that this notice is intended solely to alert readers that the content of this article is unreliable. We have not investigated whether authors were aware of or involved in the systematic manipulation of the publication process.

Wiley and Hindawi regrets that the usual quality checks did not identify these issues before publication and have since put additional measures in place to safeguard research integrity.

We wish to credit our own Research Integrity and Research Publishing teams and anonymous and named external researchers and research integrity experts for contributing to this investigation.

The corresponding author, as the representative of all authors, has been given the opportunity to register their agreement or disagreement to this retraction. We have kept a record of any response received.

References

[1] S. Zhao, H. Liu, and M. Fan, "SPOCK2 Promotes the Malignant Behavior of Ovarian Cancer via Regulation of the Wnt/β-Catenin Signaling Pathway," *BioMed Research International*, vol. 2022, Article ID 9223954, 10 pages, 2022.

Research Article

SPOCK2 Promotes the Malignant Behavior of Ovarian Cancer via Regulation of the Wnt/β-Catenin Signaling Pathway

Shanshan Zhao ⓘ,[1] Haiyan Liu ⓘ,[2] and Mingying Fan ⓘ[3]

[1]*Obstetrical Department, Taian City Central Hospital, Taian, China*
[2]*Ultrasonic Diagnosis and Treatment Center, Taian City Central Hospital, Taian, China*
[3]*Gynecology Department, The Second Affiliated Hospital of Shandong First Medical University, Taian, China*

Correspondence should be addressed to Mingying Fan; fanmingying@sdfmu.net.cn

Background. Ovarian cancer (OC) is a common clinical gynecological disease, which seriously threatens women's health and life. We investigated the roles of SPOCK2 in OC and its associated molecular mechanism in the current study. *Methods.* The expressions and prognostic value of SPOCK2 in OC were identified using the clinical data and data from the GEPIA database. Then, SPOCK2 silence was implemented to search functions of SPOCK2 in OC cells. CCK-8 was used to examine cell proliferation. Cell apoptosis was detected by flow cytometry. The OC cell invasion and migration were evaluated by transwell assays. *Results.* Overexpressed SPOCK2 was identified in OC, which was correlated with poor prognosis and a shorter survival rate. SPOCK2 downregulation significantly suppressed OC cell proliferation, migration, and invasion, and cell apoptosis was markedly promoted by SPOCK2 silence. Meanwhile, SPOCK2 knockdown could effectively suppress Wnt/β-catenin. *Conclusion.* SPOCK2 exerted crucial functions in OC progression and could serve as a promising candidate for OC targeted therapy.

1. Introduction

Ovarian cancer (OC) is one of the common malignancies of the female reproductive system [1]. A recent study showed that ovarian cancer accounts for 3.4% of the 9.2 million new cancer cases in women worldwide in 2020, as well as 4.4 million female cancer deaths, of which ovarian cancer accounts for 4.7% [2]. OC is the eighth leading cause of malignancy incidence and death in women [3]. Most OC patients are at advanced stages when detected due to the insidious onset of OC and the lack of early diagnosis and effective screening methods, so the prognosis is still poor [4]. Currently, the treatment of ovarian cancer is mainly based on surgery combined with chemotherapy, and most ovarian cancer patients are sensitive to platinum-based chemotherapy, but some patients still have recurrence after complete remission with first-line treatment [5]. Moreover, with the increase in chemotherapy cycles, the time interval of recurrence gradually shortens, and the dose-limiting toxicity

of chemotherapeutic drugs increases, eventually leading to the decrease in patients' sensitivity to drugs, leading to treatment failure and death of ovarian cancer patients [6]. This is the main reason for treatment failures and deaths of OC patients. The development of drug resistance is an important cause of recurrence and death, but there is no effective treatment for platinum-resistant patients. The recurrence rate of OC patients after surgery is as high as 70% [7]. The recurrence and treatment failure of OC are closely related to the resistance to chemotherapy drugs. Therefore, finding new therapies for OC treatment is significant to reduce the death rate and prolong the survival time of OC patients.

SPOCK family proteins are proteoglycans of the vertebrate extracellular matrix (ECM) [8]. SPOCK-encoded proteins are capable of participating in a variety of physiological and pathological cellular processes, including tumor progression [9], epithelial-mesenchymal transition [10], and Alzheimer's disease [11], which are hallmarks of both pathological processes such as cancer cell invasion and
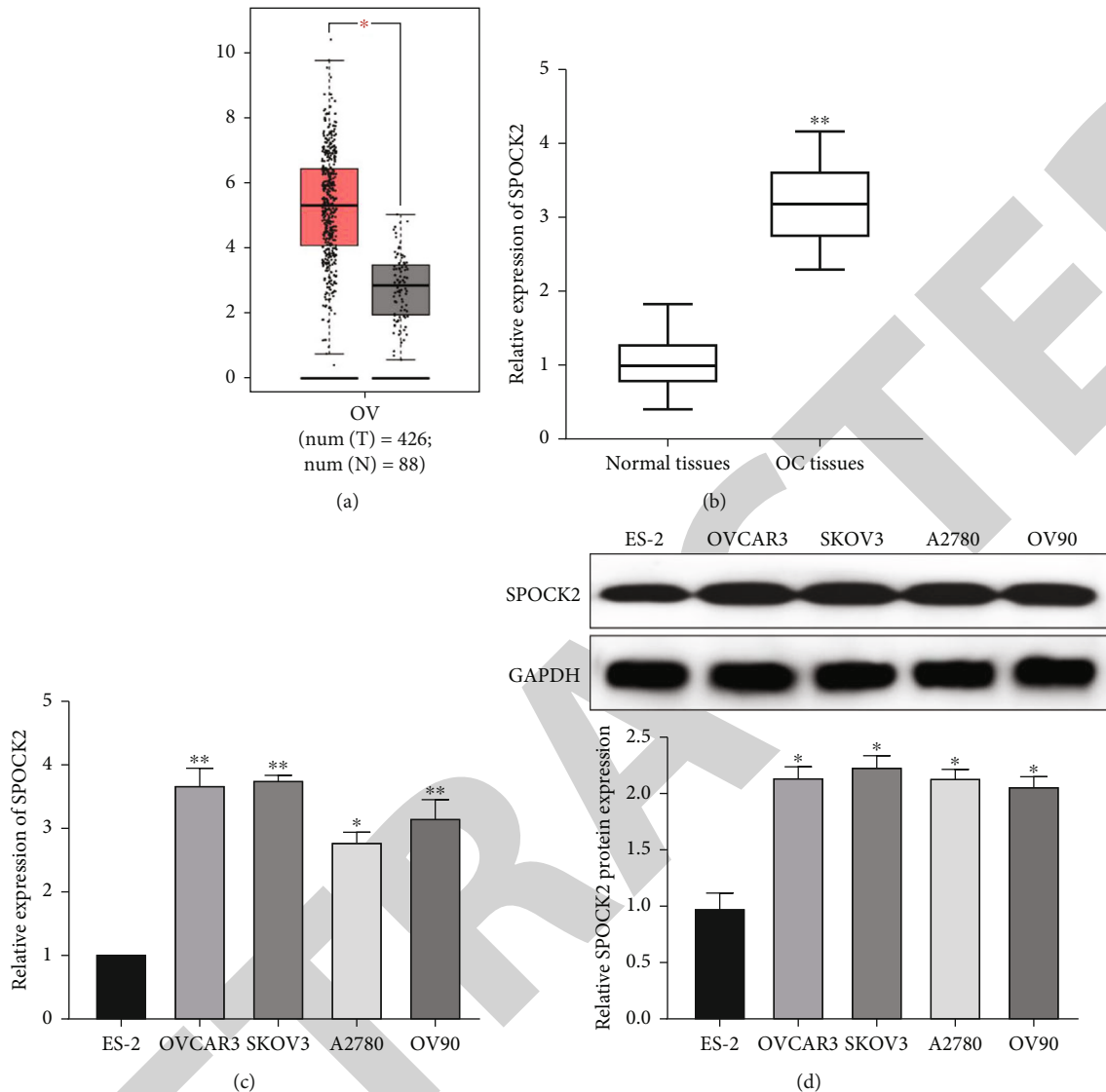
Figure 1: SPOCK2 was upregulated in OC tissues and cells. (a) The expression patterns of SPOCK2 in OC tumors and normal OC tissues from the GEPIA database. (b) The mRNA expressions of SPOCK2 in OC tissues and adjacent normal tissues. (c and d) The mRNA and protein expressions of SPOCK2 in OC cells.

normal physiological processes such as morphogenesis and differentiation. SPOCK2, also known as Testin-2, is a member of the SPOCK family. Abnormal expression of this gene has been associated with the development of several diseases, and SPOCK2 has been found to be abnormally expressed in lung adenocarcinoma [12], breast [13], and Endometrial cancers [14]. In this study, we examined the role of the SPCOK2 gene in ovarian cancer and preliminarily investigated the relevance of the SPOCK2 gene to the development of ovarian cancer.

2. Materials and Methods

2.1. Clinical Specimens. 54 OC Patients Who Underwent Tumor Resection from January 2015 to January 2017 at Our Hospital Were Selected. All Specimens Taken from the Adjacent Normal Tissues and the Cancer Tissues Were Stored at -80°C for Further Experiments

2.2. Cell Lines. OVCAR3, SKOV3, A2780, OV90, and ES-2 were cultured in DMEM medium (Invitrogen, Carlsbad, CA, USA) containing 10% FBS (Invitrogen) and stored in a humidified incubator at 37°C with 5% CO_2.

2.3. Clinical Prognosis Analysis from a Public Database. The online tool GEPIA (http://gepia.cancer-pku.cn/) was used to analyze the SPOCK2 levels between OC tissues and normal tissues. Additionally, OS and DFS analyses of OC patients in the database were downloaded from the website.

2.4. Plasmid Construction and Cell Transfection. Cell transfection with si-SPOCK2 or control siRNA was performed with

Table 1: Correlation of SPOCK2 expression with the clinicopathological characteristics of ovarian cancer patients.

Clinicopathological features	Cases (n = 54)	SPOCK2[a] expression		P value
		High (n = 27)	Low (n = 27)	
Age (years)				0.785
>60	29	14	15	
≤60	25	13	12	
Family history of cancer				0.102
Yes	26	10	16	
No	28	17	11	
Tumor size (cm)				0.112
≥5.0	26	12	17	
<5.0	28	15	10	
TNM stage				0.003*
I-II	29	9	20	
III	25	18	7	
Lymph-node metastasis				0.014*
Yes	25	17	8	
No	29	10	19	
Pausimenia				0.413
Yes	25	11	14	
No	29	16	13	
FIGO stage				0.013*
I-II	31	11	20	
III-IV	23	16	7	
Distant metastasis				0.029*
Yes	28	18	10	
No	26	9	17	
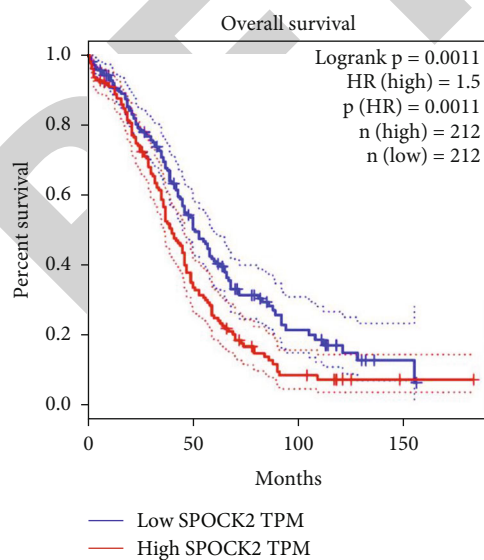
Figure 2: SPOCK2 overexpression indicated a shorter survival rate for OC patients.

Lipofectamine 2000 (Invitrogen). SPOCK2 overexpression was achieved by transfection of SPOCK2 expression plasmids.

2.5. qRT-PCR. Total RNA was isolated with Trizol reagent (Invitrogen), and cDNA was synthesized with a reverse transcription Kit (TaKaRa, Dalian, China). The qRT-PCR assay was performed using SYBR Green (Takara) on an ABI 7500 system. GAPDH was an internal control.

2.6. CCK-8 Assay. Cells transfected with corresponding vectors were cultured at densities of 2×10^3 cells/well. CCK-8 was added into the wells at the indicated time (24, 48, 72, and 96 h) and incubated for 2 h. The OD_{450} was estimated using a microplate reader.

2.7. Western Blotting. After measuring protein concentrations using a BCA assay (Beyotime Biotechnology, Jiangsu, China), the samples were separated on SDS-PAGE gels and transferred onto PVDF membranes (Millipore, Billerica, USA). The membranes were blocked with 5% skim milk and then incubated with primary antibodies at 4°C overnight. The antibodies included antibodies for SPOCK2, cleaved caspase-3, procaspase-3, β-catenin, c-Myc, cyclin D1, E-cadherin, N-cadherin, Vimentin, and GAPDH (1 : 1000, Abcam). Following 3 washes with TBST, the membranes were incubated with HRP-conjugated secondary antibodies for 1 h at room temperature. GAPDH was an internal control.

2.8. Cell Apoptosis Assay. Cell apoptosis was detected by Annexin V-FITC kit (BD Biosciences, USA). The cells were incubated with Annexin V-FITC and PI at room temperature and protected from light for 30 minutes.

2.9. Transwell Assay. For cell invasion assays, cells in serum-free DMEM were added into the upper chamber with matrigel on the filter membrane. After incubation for 24 h in 5% CO_2 at 37°C, the cells that had adhered to the lower membrane were fixed and stained with 20% methanol and 0.1% crystal violet. The cells were counted under an inverted light microscope (Olympus Corporation, Tokyo, Japan). For migration assay, the transwell chamber was not coated with matrigel.

2.10. Statistical Analysis. The data were analyzed using SPSS 18.0. The difference was analyzed by Student's t-test or by one-way analysis of variance (ANOVA) between two groups or in more than two groups. χ^2 analysis was used to analyze the correlation between JARID2 expressions and clinicopathologic features. $P < 0.05$ was considered statistically significant.

3. Results

3.1. Expression of SPOCK2 Was Upregulated in Human OC. To confirm the functions of SPOCK2 in OC progression, we examined the expressions of SPOCK2 in OC tissues and cells. The comparison of the expressions of SPOCK2 in OC and normal tissues based on the GEPIA database indicated that SPOCK2 expressions were increased in OC tumors (Figure 1(a)). Similarly, the results of this study also
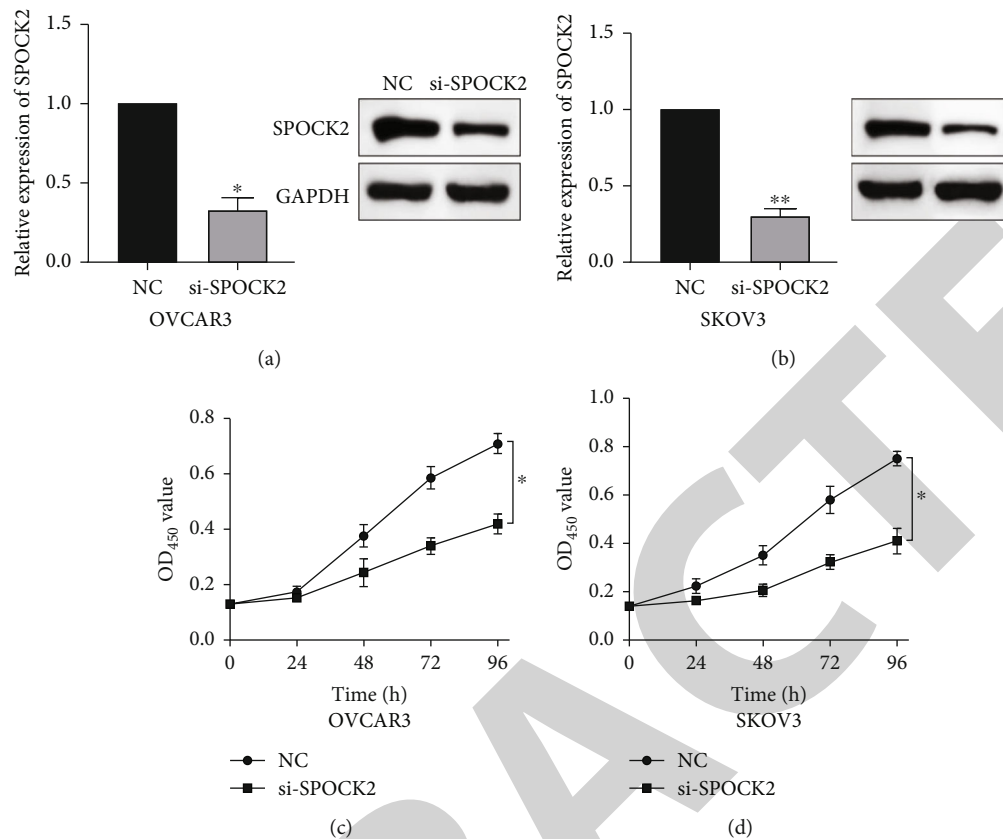
Figure 3: Knockdown of SPOCK2 suppressed OC cell viability. (a and b) SPOCK2 was silenced in OC cells. (C, D) SPOCK2 downregulation suppressed OC cell viability.

demonstrated the upregulated expressions of SPOCK2 in OC tissues (Figure 1(b)). To further confirm the results, the SPOCK2 expressions in OC cells were examined. Similarly, significantly high SPOCK2 expressions were also identified in OC cells (Figures 1(c) and 1(d)).

3.2. SPOCK2 Overexpression Predicted a Poor Prognosis of OC. To further evaluate the clinical significance of SPOCK2 in OC, we analyzed the relationship between SPOCK2 expressions and clinicopathological characteristics of OC patients. We found significant correlations between SPOCK2 overexpression and TNM stage, lymphoid metastasis, distant metastasis, and FIGO stage (Table 1). No evident correlation was observed between SPOCK2 levels and other clinicopathological features. Furthermore, the prognosis analysis of SPOCK2 in OC patients from the TCGA database also showed that the survival rate of OC patients was markedly decreased in patients with high SPOCK2 expression (Figure 2).

3.3. Knockdown of SPOCK2 Suppressed OC Cell Viability. To further determine the functions of SPOCK2 in OC progression, SPOCK2 was silenced by si-SPOCK2 in OC cells. The successful knockdown of SPOCK2 in OC cells was confirmed by RT-qPCR and western blot (Figures 3(a) and 3(b)). CCK-8 assay was used to verify the effect of SPOCK2

in OC cells. The results indicated that the proliferation of OVCAR3 and SKOV3 cells was significantly restrained after SPOCK2 knockdown (Figures 3(c) and 3(d)).

3.4. SPOCK2 Downregulation Increased OC Cell Apoptosis. Apoptosis plays a key role in tumor regression, and cell apoptosis was assessed to confirm whether SPOCK2 was involved in OC cell apoptosis. Results of flow cytometric analysis demonstrated that SPOCK2 silence significantly increased the apoptosis rates of OC cells (Figures 4(a) and 4(b)). Furthermore, to elucidate the apoptotic mechanisms of SPOCK2 in OC cells, we detected the levels of caspase-3. Significant upregulation of cleaved caspase-3 was observed in SPOCK2-silenced OC cells, but there were no notable changes in total caspase-3 (Figure 4(c)). These results showed that SPOCK2 downregulation induced OC cell apoptosis through regulation of apoptosis-related proteins.

3.5. Downregulation of SPOCK2 Restrained OC Cell Migration and Invasion. To verify the functions of SPOCK2 in OC cells, we performed transwell assays to determine whether SPOCK2 could affect OC cell migration and invasion. As shown in Figure 5(a), migration and invasion of OVCAR3 cells were significantly suppressed, when SPOCK2 was silenced. Similar results were found in SKOV3 cells with SPOCK2 silence (Figure 5(b)). All the above data suggested
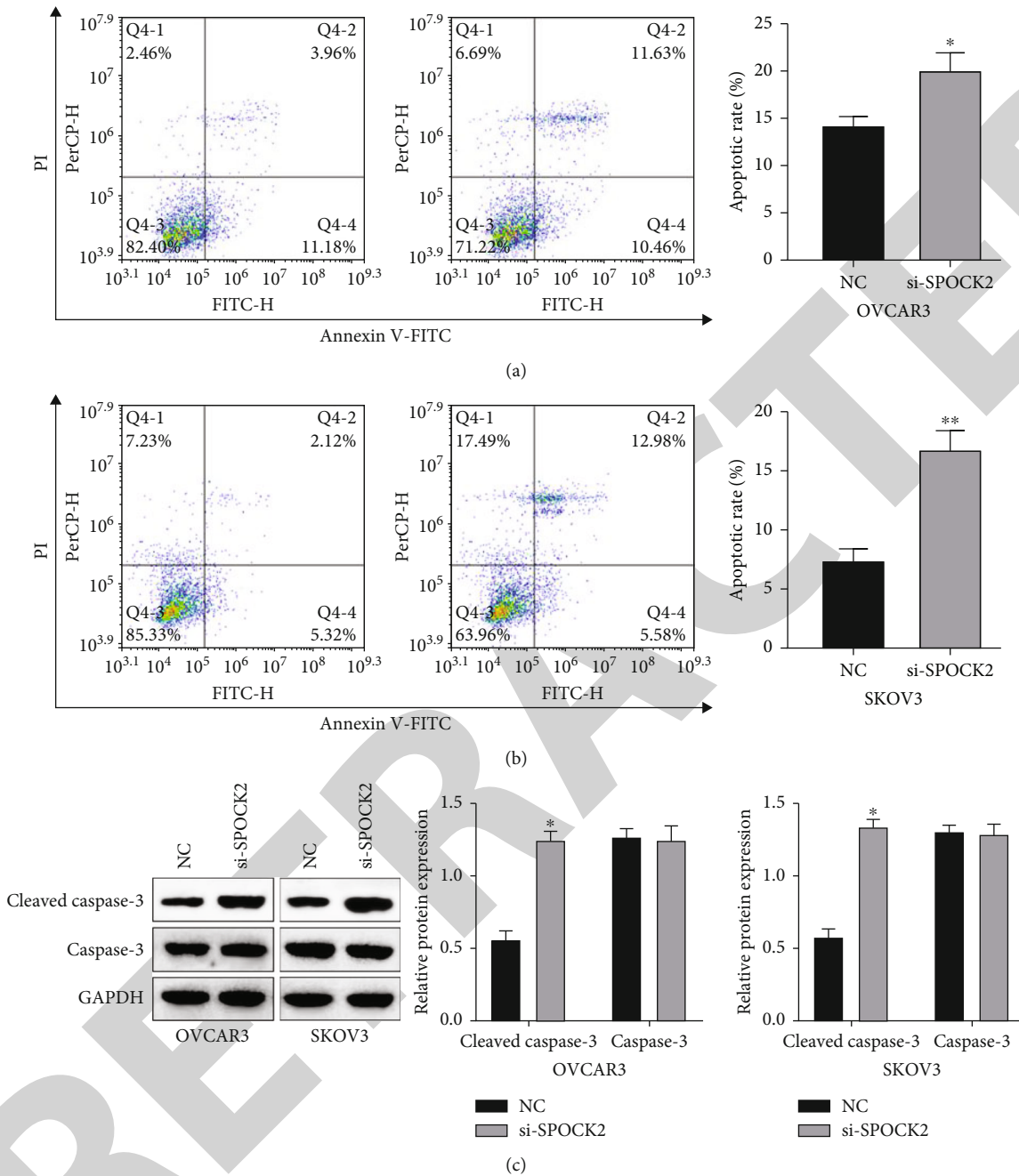
Figure 4: SPOCK2 downregulation increased OC cell apoptosis. (a and b) SPOCK2 silence significantly increased the apoptosis rates of OVCAR3 and SKOV3 cells. (c) Significant upregulation of cleaved caspase-3 was observed in SPOCK2 silenced OC cells.

that SPOCK2 promoted the invasion and metastasis of OC cells.

3.6. Upregulation of SPOCK2 Promoted OC Cell Proliferation, Invasion, and Migration. To further confirm the functions of SPOCK2 in OC progression, the SPOCK2 was upregulated in A2780 cells. As shown in Figure 6(a), the successful overexpression of SPOCK2 in A2780 cells was confirmed by RT-qPCR. Then, the proliferation of A2780 cells was examined by CCK-8 assays. Results showed that SPOCK2 upregulation significantly accelerated the proliferation of A2780 cells (Figure 6(b)). Similarly, the func-

tions of SPOCK2 upregulation in A2780 invasion and migration were also detected by transwell assays. We found that A2780 cell invasion and migration were markedly promoted by SPOCK2 overexpression (Figures 6(c) and 6(d)).

3.7. SPOCK2 Promoted OC via Wnt/β-Catenin Signaling. To elucidate the potential mechanism of SPOCK2 in OC progression, we analyzed whether the Wnt/β-catenin pathway was crucial for OC development. The expressions of activated β-catenin, cyclin D1, and c-Myc in OVCAR3 cells were determined, when SPOCK2 was silenced or overexpressed. As shown in Figure 7(a), activated β-catenin, cyclin

(a)

(b)
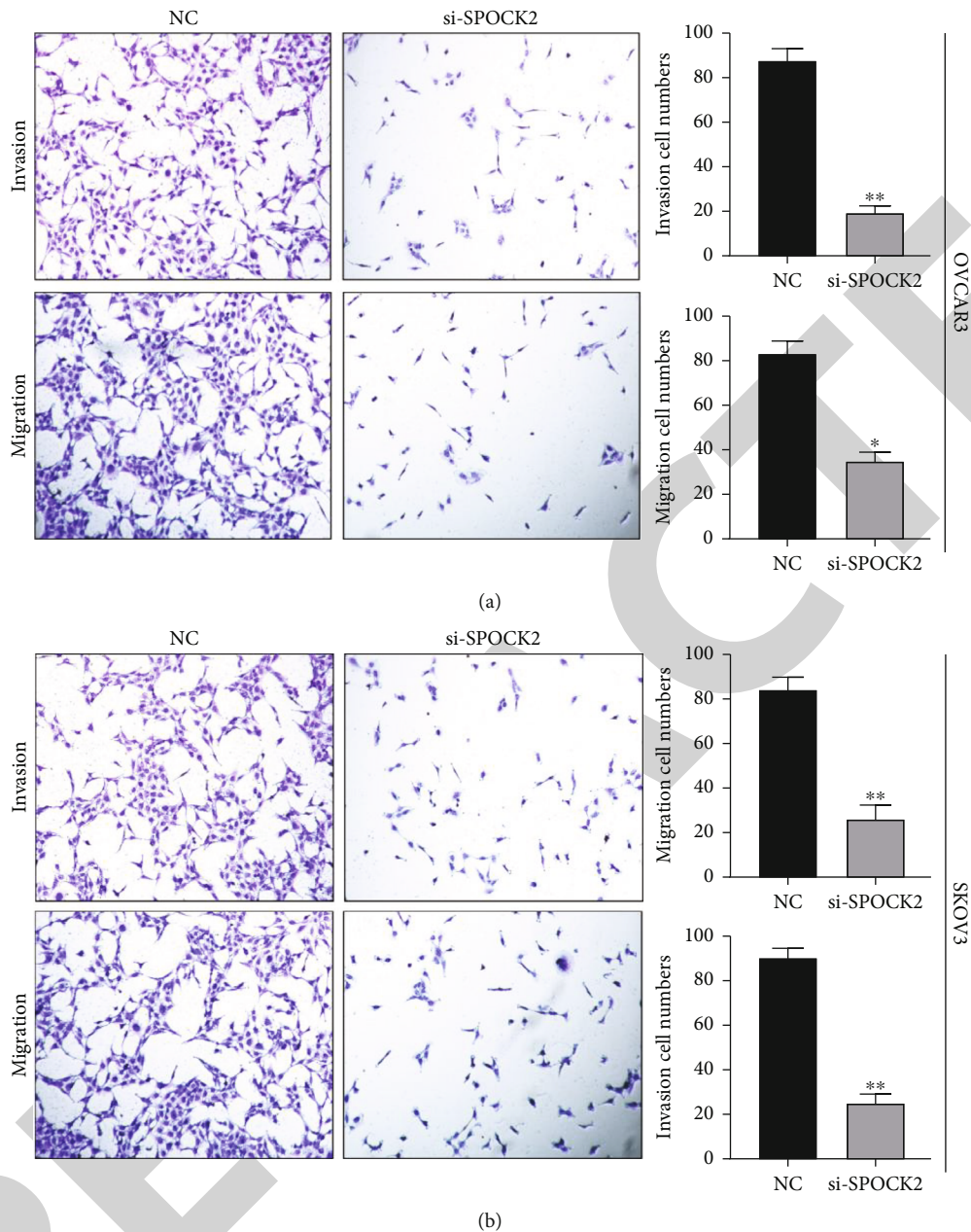
Figure 5: Downregulation of SPOCK2 restrained OC cell migration and invasion. (a and b) OVCAR3 and SKOV3 cell migration and invasion were significantly suppressed, when SPOCK2 was silenced.

D1, and c-Myc were significantly upregulated by SPOCK2 overexpression and decreased by SPOCK2 knockdown. Furthermore, we also detected the changes in the biological behaviors of OVCAR3 cells transfected with the SPOCK2 vector in the absence or presence of XAV-939, a specific inhibitor of Wnt/β-catenin signaling. Results showed that SPOCK2 overexpression remarkably promoted OC cell proliferation, invasion, and migration; the above effects of SPOCK2 were partially eliminated by XAV-939 (Figures 7(b) to 7(d)). These findings indicated that SPOCK2 activated the Wnt/β-catenin pathway, finally regulating OC progression.

4. Discussion

The incidence of ovarian malignancies has gradually increased in recent years, ranking third among gynecologic tumors, but its mortality rate ranks first among gynecologic tumors [15]. Unless significant progress has been made in ovarian cancer, the prognosis remains poor [16]. Therefore, it is significant to explore new therapies for OC to improve survival. Targeted therapy is a new therapy developed in recent years for the treatment of malignant tumors, which refers to the design of corresponding drugs against well-defined oncogenic protein molecules or gene fragments
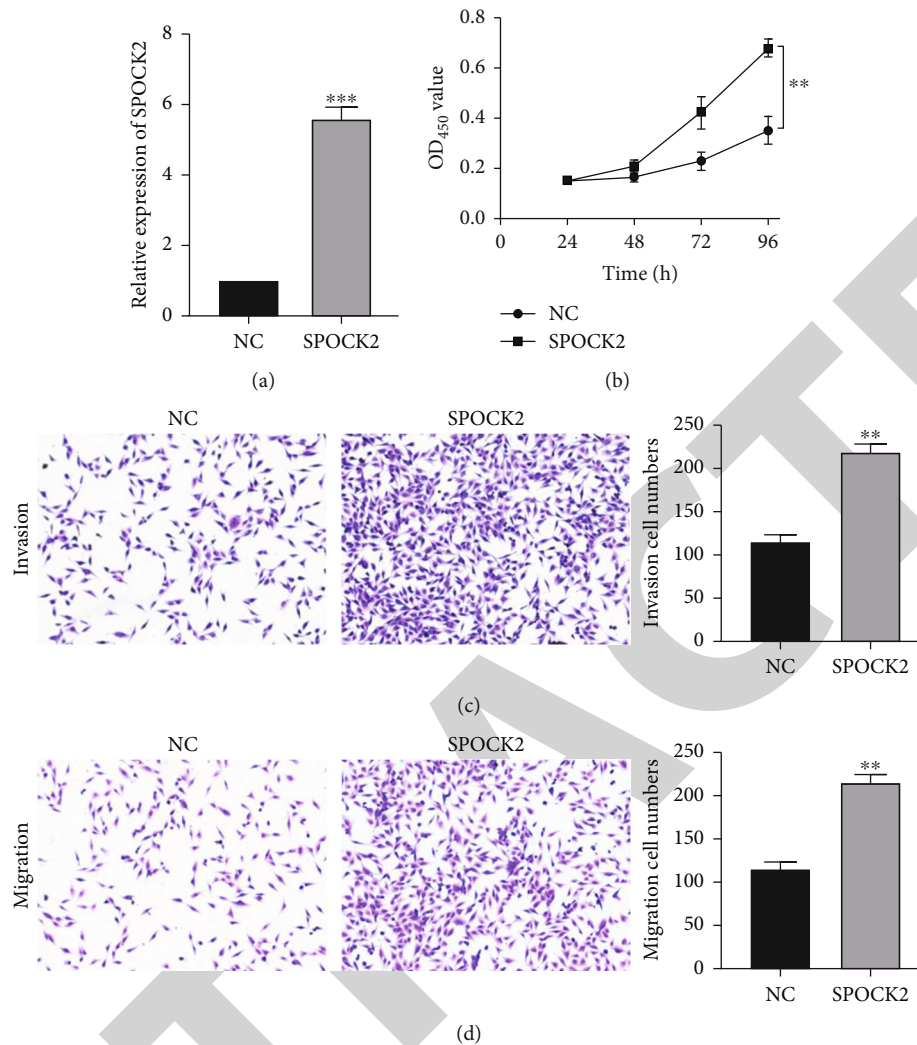
Figure 6: Upregulation of SPOCK2 promoted OC cell proliferation, invasion, and migration. (a) SPOCK2 was overexpressed in A2780 cells. (b–d) SPOCK2 overexpression promoted A2780 cell proliferation, invasion, and migration.

[17]. Targeted therapy causes specific death of cancer cells by binding targeted drugs to specific cancer sites without affecting surrounding normal tissue cells [18]. Currently, targeted therapeutic agents that have been used in ovarian cancer include olaparib and niraparib, VEGF inhibitors, and the antiangiogenesis inhibitor bevacizumab, but the above-targeted agents are less used in clinical practice because of their narrow indications, high prices, and certain adverse effects [19–21]. Exploring the molecular mechanisms associated with ovarian cancer progression is the basis for developing novel diagnostic and therapeutic approaches for ovarian cancer.

Previous studies showed that SPOCK presented high plasma levels in multiple cancers and could promote tumor growth, metastasis, and invasion through PI3K/Akt, Wnt/β-catenin, and other pathways, and increase cancer cell resistance to chemotherapeutic drugs [22, 23]. In contrast, the role of SPOCK2 in tumors has been less studied. The oligonucleotide polymorphisms of the SPOCK2 gene were associated with chromosome 16q deletion in breast cancer [24]. Sambuudash et al. found that the prevalence of SPOCK2

methylation was markedly increased in colon carcinoma than in normal mucosal tissues, suggesting that methylation of this gene may be associated with colon cancer development [25]. In addition, another study has shown that SPOCK2 plays a crucial role in prostate cancer development by inhibiting the invasion and metastasis of prostate cancer cells [26].

Our previous imaging genomics findings suggested that SPOCK2 was aberrantly expressed in OC. In this study, the expressions of SPOCK2 in OC tissues were significantly higher than that of normal controls, suggesting that this gene may be associated with the development of OC. This result was consistent with our imaging genomics findings. Moreover, we also find that the higher the level of SPOCK2 expression, the more malignant the OC was. Furthermore, the prognosis analysis of SPOCK2 in OC patients from the TCGA database also showed that the survival rate of OC patients markedly declined in patients with high SPOCK2 expressions. To further explore the roles and mechanism of SPOCK2 in OC progression, we knocked down SPOCK2 in OC cells and examined the proliferation, migration, and
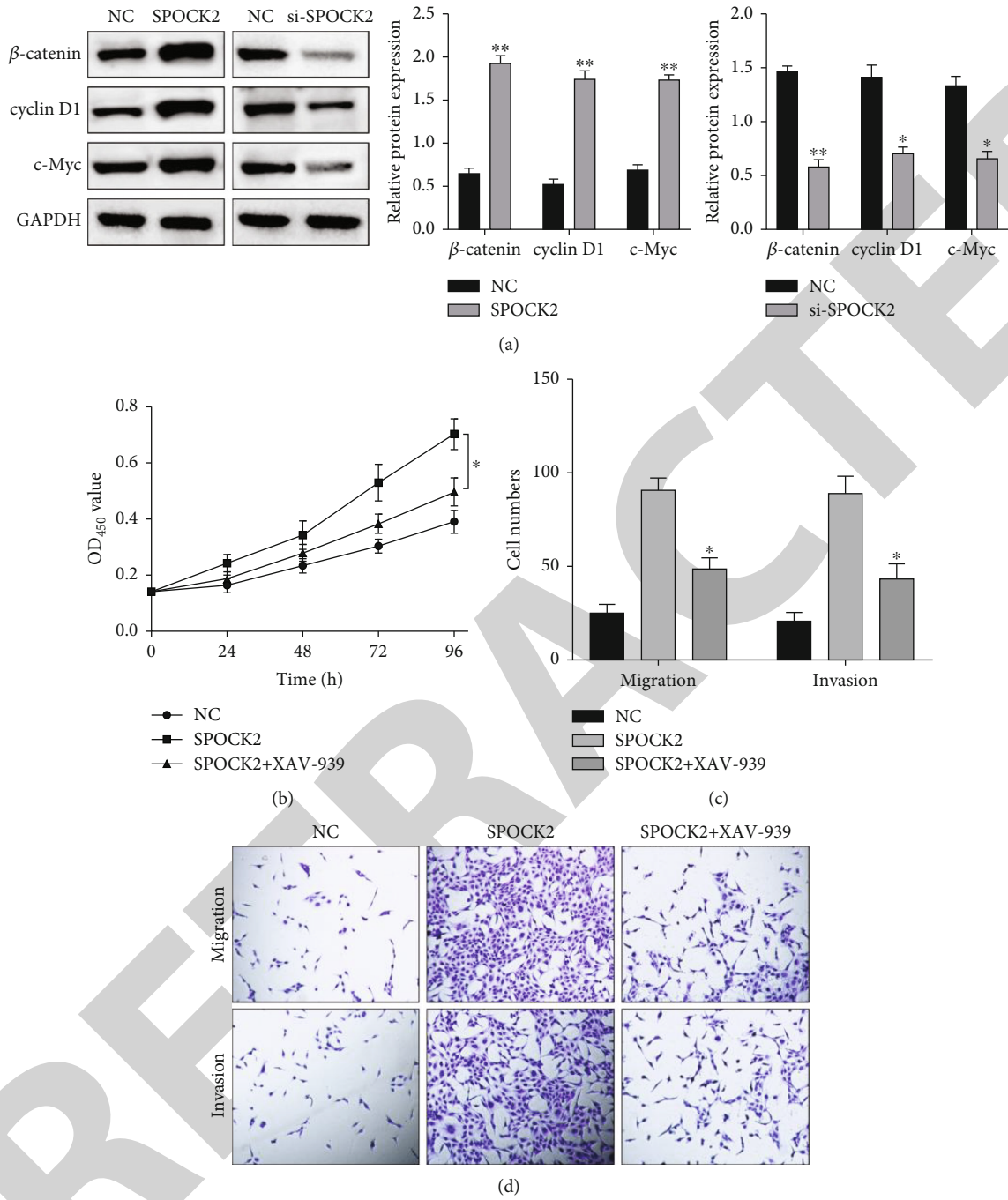
Figure 7: SPOCK2 promoted OC via the Wnt/β-catenin signaling pathway. (a) Expression of Wnt/β-catenin signaling-related proteins in SPOCK2-overexpressed or -silenced OC cells. (b–d) Wnt/β-catenin signaling was involved in the functions of SPOCK2 in OC proliferation, migration, and invasion.

invasion abilities. Results indicated that downregulation of SPOCK2 could promote cell apoptosis, and inhibit cell proliferation, migration and invasion. Moreover, activated β-catenin, cyclin D1, and c-Myc proteins were reduced after knockdown of SPOCK2, which suggested that SPOCK2 could affect the EMT of OC through Wnt/β-catenin, and thus affect the invasion and metastasis of OC. However, the mechanistic studies in the current study are insufficient, such as the functions of SPOCK2 *in vivo*, and whether SPOCK2 exerted functions in OC through regulation of certain downstream molecules, which deserves further exploration.

In conclusion, upregulated SPOCK2 in OC tissues was identified, which was related to poor OC prognosis. Silencing SPOCK2 may inhibit OC cell progression by inactivating Wnt/β-catenin, which may provide a reference for the clinical diagnosis and treatment of OC.

Data Availability

The datasets used during the current study are available from the corresponding author on reasonable request.

Conflicts of Interest

The authors declare that they have no conflicts of interest.

Authors' Contributions

Shanshan Zhao and Haiyan Liu contributed equally to this work.

References

[1] L. A. Torre, B. Trabert, C. E. DeSantis et al., "Ovarian cancer statistics, 2018," *CA: A Cancer Journal for Clinicians*, vol. 68, no. 4, pp. 284–296, 2018.

[2] H. Sung, J. Ferlay, R. L. Siegel et al., "GLOBOCAN Estimates of incidence and mortality worldwide for 36 cancers in 185 countries," *Global Cancer Statistics*, vol. 71, no. 3, pp. 209–249, 2021.

[3] W. Cao, H. D. Chen, Y. W. Yu, N. Li, and W. Q. Chen, "Changing profiles of cancer burden worldwide and in China: a secondary analysis of the global cancer statistics," *Chinese Medical Journal*, vol. 134, no. 7, pp. 783–791, 2021.

[4] Y. Huang, X. Ming, B. Li, and Z. Li, "Histological characteristics and early-stage diagnosis are associated with better survival in young patients with epithelial ovarian cancer: a retrospective analysis based on surveillance epidemiology and end results database," *Frontiers in Oncology*, vol. 10, 2020.

[5] L. Xin, W. Xiao, L. Che et al., "Label-free assessment of the drug resistance of eithelial ovarian cancer cells in a microfluidic holographic flow cytometer boosted through machine learning," *ACS Omega*, vol. 6, no. 46, pp. 31046–31057, 2021.

[6] W. Xie, H. Sun, X. Li, F. Lin, Z. Wang, and X. Wang, "Ovarian cancer: epigenetics, drug resistance, and progression," *Cancer Cell International*, vol. 21, no. 1, p. 434, 2021.

[7] X. Ju, H. Yu, D. Liang et al., "LDR reverses DDP resistance in ovarian cancer cells by affecting ERCC-1, Bcl-2, survivin and caspase-3 expressions," *Biomedicine Pharmacother*, vol. 102, pp. 549–554, 2018.

[8] J. K. Mouw, G. Ou, and V. M. Weaver, "Extracellular matrix assembly: a multiscale deconstruction," *Nature Reviews Molecular Cell Biology*, vol. 15, no. 12, pp. 771–785, 2014.

[9] L. Vancza, K. Karaszi, B. Peterfia et al., "SPOCK1 promotes the development of hepatocellular carcinoma," *Frontiers in Oncology*, vol. 12, p. 819883, 2022.

[10] X. Cui, Y. Wang, W. Lan et al., "SPOCK1 promotes metastasis in pancreatic cancer via NF-kappaB-dependent epithelial-mesenchymal transition by interacting with IkappaB-alpha," *Cellular Oncology*, vol. 45, no. 1, pp. 69–84, 2022.

[11] A. Barrera-Ocampo, S. Arlt, J. Matschke et al., "Amyloid-beta precursor protein modulates the sorting of testican-1 and contributes to its accumulation in brain tissue and cerebrospinal fluid from patients with alzheimer disease," *Journal of Neuropathology & Experimental Neurology*, vol. 75, no. 9, pp. 903–916, 2016.

[12] J. Zhao, M. Cheng, J. Gai, R. Zhang, T. Du, and Q. Li, "SPOCK2 serves as a potential prognostic marker and correlates with immune infiltration in lung adenocarcinoma," *Frontiers in Genetics*, vol. 11, p. 588499, 2020.

[13] R. Pedrosa, L. V. Wismans, R. Sinke et al., "Differential expression of BOC, SPOCK2, and GJD3 is associated with brain metastasis of ER-negative breast cancers," *Cancers (Basel)*, vol. 13, no. 12, 2021.

[14] F. Ren, D. Wang, Y. Wang, P. Chen, and C. Guo, "SPOCK2 affects the biological behavior of endometrial cancer cells by regulation of MT1-MMP and MMP2," *Reproductive Sciences*, vol. 27, pp. 1391–1399, 2020.

[15] B. Slomovitz, C. Gourley, M. S. Carey et al., "Low-grade serous ovarian cancer: state of the science," *Gynecologic Oncology*, vol. 156, no. 3, pp. 715–725, 2020.

[16] F. Rodel, S. Zhou, B. Gyorffy et al., "The prognostic relevance of the proliferation markers Ki-67 and Plk1 in early-stage ovarian cancer patients with serous, low-grade carcinoma based on mRNA and protein expression," *Frontiers in Oncology*, vol. 10, 2020.

[17] Y. T. Lee, Y. J. Tan, and C. E. Oon, "Molecular targeted therapy: treating cancer with specificity," *European Journal Of Pharmacology*, vol. 834, pp. 188–196, 2018.

[18] F. Chen and J. Fang, "Benefits of targeted molecular therapy to immune infiltration and immune-related genes predicting signature in breast cancer," *Frontiers of Oncology*, vol. 12, p. 824166, 2022.

[19] A. Pagkali, I. Mamais, A. Michalinos, and A. P. Agouridis, "Safety profile of niraparib as maintenance therapy for ovarian cancer: a systematic review and meta-analysis," *Current Oncology*, vol. 29, no. 1, pp. 321–336, 2022.

[20] K. Cottrell, C. L. Clark, and R. T. Penson, "An update on the safety of olaparib for treating ovarian cancer," *Expert Opinion on Drug Safety*, vol. 21, no. 4, pp. 447–451, 2022.

[21] S. Mukherjee, M. Abdalla, M. Yadav et al., "Structure-based virtual screening, molecular docking, and molecular dynamics simulation of VEGF inhibitors for the clinical treatment of ovarian cancer," *Journal of Molecular Modeling*, vol. 28, no. 4, p. 100, 2022.

[22] J. Yang, Q. Yang, J. Yu, X. Li, S. Yu, and X. Zhang, "SPOCK1 promotes the proliferation, migration and invasion of glioma cells through PI3K/AKT and Wnt/beta-catenin signaling

Hindawi

Research Article

Studying the Anticancer Effects of Thymoquinone on Breast Cancer Cells through Natural Killer Cell Activity

Huda F. Alshaibi [iD],[1,2] Nouf A. Aldarmahi,[1] Nuha A. Alkhattabi [iD],[1] Hadeil M. Alsufiani [iD],[1,3] and Nesrin I. Tarbiah [iD][1]

[1]*Biochemistry Department, Faculty of Sciences, King Abdulaziz University, Jeddah, Saudi Arabia*
[2]*Embryonic Stem Cell Unit, King Fahd Medical Research Center, King Abdulaziz University, Jeddah, Saudi Arabia*
[3]*Experimental Biochemistry Unit, King Fahd Medical Research Center, King Abdulaziz University, Jeddah, Saudi Arabia*

Correspondence should be addressed to Huda F. Alshaibi; halshaibi@kau.edu.sa

Cancer immunotherapy is quickly growing and can now be viewed as the "fifth column" of cancer treatment. In addition, cancer immunotherapy has shown promising results with different kinds of cancers and may be used as a complementary therapy with various types of treatments. Thus, "immuno-oncology" is showing astounding advantages. However, one of the main challenges that face this type of therapy is that cancer cells can evade immune system elimination through different mechanisms. Many studies were done to overcome this issue including adding immune stimulants to generate synergistic effects or by genetically modifying NK cells themselves to be stronger and more resistant. *Nigella sativa*, also known as black cumin, is a well-known example of a widely applicable herbal medicine. It can effectively treat a variety of diseases, such as hypertension, diabetes, bronchitis, gastrointestinal upset, and cancer. The anticancer qualities of *Nigella sativa* appear to be mediated by an immune-modulatory effect that stimulates human natural killer (NK) cells. These are a type of lymphocyte and first line of defense against pathogens. *Objectives*. In this study, we investigated the therapeutic effect of thymoquinone, a major component of *Nigella sativa*, on the cytotoxic pathways of NK cells. *Methods*. NK cells were cultured with breast cancer cell line Michigan Cancer Foundation-7 (MCF-7); and were treated with Thymoquinone. The cytotoxicity of NK cells on cancer cells was measured. The cultured media were then collected and measured via enzyme-linked immunosorbent assay (ELISA) for concentrations of perforin, granzyme B and interferon-α (IFN-α). *Results*. The cytotoxic effect of NK cells on tumor cells was increased in the presence of thymoquinone, with an increased release of perforin, granzyme B, and IFN-α. *Conclusion*. Thymoquinone promotes the cytotoxic activity of NK cells against breast cancer MCF-7 cells.

1. INTRODUCTION

Breast cancer is one of the main causes of death in women according to the world health organization [1]. It is a metastatic and commonly spreads from its origin to distant organs of the body, with the most common sites of distant metastases being bone, liver, lungs, and brain [2]. Breast cancer is a heterogeneous disease [3] at the histological and biological levels due to genetic, epigenetic, and transcriptome changes. This phenotypic difference influences breast cancer diagnosis, treatment, and thus prognosis. Thus, initially treatment of breast cancer was depending on tumor characteristics

such as its clinical stage, histopathologic features, and biomarker profiling. However, in the last few decades, our understanding of its biological and molecular characteristics has improved [4]. We can now classify breast cancer to five subtypes according to molecular profiling, hormone indicators, and growth factor expressions. These subtypes are luminal A and B, human epidermal growth factor receptor 2 (HER2) enriched, triple-negative or basal-like (BL), and normal-like BC. Luminal A subtype is characterized by high expression of luminal gene and hormone receptors genes including estrogen receptor (ER) and progesterone receptors (PR). Luminal B subtype is characterized by expressing

luminal gene and moderate to low expression of both ER/PR genes. HER2 subgroup is characterized by high expression of HER2 and low expression of ER and related genes. Triple negative or BL are characterized by high expression of basal epithelial genes and basal cytokeratins, low expression of ER and related genes, and low expression of HER2 [4, 5] . The luminal A subtype presents a greater prognosis and higher survival rate than the luminal B subtype [6–8] . While on the other hand, it has been indicated that the HER2 subtype, characterised by positivity for HER2, is linked with aggressive histological characters, poor prognosis, and unresponsiveness to normal treatments and decreased in survival rate [9, 10]. This outcome may change dramatically when chemotherapy is used in combination with anti-HER2 monoclonal antibodies and tyrosine kinase inhibitor [11, 12]. Thus ER, PR, and HER2 are well established breast cancer biomarkers that aid in the diagnoses and treatment prognosis [4, 5]. Recently, some studies suggested the involvement of matrix metalloproteinase 2 (MMP-2) and matrix metalloproteinase 9 (MMP-9), also known as gelatinase A and gelatinase B, respectively, in breast cancer initiation and growth throughout complex interactions with the key oncogenes and tumor-suppressor genes which are involved in the initial stage of tumorigenesis. Consequently, several authors have proposed MMP-2 and MMP-9 as promising prognostic markers that may be used in early detection and treatment [13, 14].

Cancer immunotherapy [15] is quickly progressing and can now be viewed as the "fifth column" of cancer treatment, joining medical surgery, cytotoxic chemotherapy, radiation, and targeted treatment [16]. In addition, Cancer Immunotherapy (CI) has shown promising results with different kinds of malignancies and may be used in combination with various treatments. Thus, "immuno-oncology" is showing astounding advantages [17, 18].

NK cells are a type of lymphocyte that plays a central role in the innate immune response against pathogens and tumors [19–21]. These cells can rapidly identify and attack infected and malignant cells [22, 23]. CD56 and CD16 cells constitute around 90% of the circulating NK cell population, inducing cell lyses via cytolytic granules containing perforin and granzyme. These work synergistically with interferon-α (IFN-α) to induce apoptosis in target cells [24, 25]. NK cells have also been found to enhance antibody-mediated cytotoxicity, where NK triggers the release of specific antibodies in the immune system that recognize certain antigens in the invading pathogens [26]. NK cells instantly target pathogens or foreign materials via different mechanisms, one of the most important mechanisms is the perforin/granzyme apoptotic pathway, and other mechanism is tumor necrosis factor, as mediated by the interaction between the FAS ligands on NK cells with the death receptors (FAS/CD95) on target cells [27].

According to the literature, NK cell–based immunotherapy is a promising treatment strategy that can be used in adjuvant chemotherapy for both solid and hematologic tumors. This treatment protocol could combine surgery, chemotherapy, radiation, and monoclonal antibodies (mAb) [28]. However, many studies showed that NK cell

activity decreases during the progression of many tumors including breast cancer especially those with functional estrogen receptors. Estrogen suppress NK cell activity by inhibiting NK cells activating receptors such as CD69, NKp46, NKG2D, and CD244, thus inhibiting NK cell activation and reducing the secretion of granzyme B, as well as FasL [29, 30].

Nigella sativa, also known as black cumin, it is a dicotyledon of the Ranunculaceae family, and has been used for two millennia as an appetizer, flavoring agent, and nourishing and nutraceutical substance in various societies in Asia, Africa, and Europe. Interestingly, *Nigella sativa* is a well-known example of a widely applicable herbal medicine [31]. Thymoquinone is a major active component of *Nigella sativa* [32]. As a heavenly panacea, *Nigella sativa* L. (Ranunculaceae) has attracted attention in traditional medication, as well as in present-day therapeutic exploration [33]. Research found that *Nigella sativa has* anticancer effects through mediated an immune-modulatory effect, which stimulates human natural killer (NK) cells [34].

Further investigations are still needed to understand the role of *Nigella sativa* in adjuvant chemotherapy at the molecular level [28]. However, its role in treating malignant cancer specifically is quite complicated, which can be ascribed to its multiple suppressive effects on proliferative cells, free radicals, mutagens and metastasis [15]. In this study, we examined the effect of thymoquinone, a component making up 30% of *Nigella sativa* [35], on cytotoxic pathways and the behavior and activity of NK cells. This may help in understanding the possible therapeutic role of thymoquinone on NK cell activity.

2. Methods

2.1. NK Isolation from PBMCs. Blood samples were collected from healthy volunteers in ethylene diamine tetra-acetic acid (EDTA) tubes (Xinlehj, India). The study was approved by the ethical committee of the Faculty of Medicine, King Abdulaziz University (ref. no. 640-20). Peripheral blood mononuclear cells (PBMCs) from healthy individuals are isolated by Ficoll density gradient centrifugation of peripheral venous blood (Sigma-Aldrich). NK cells are purified by positive selection of CD56 cells (CD56 MicroBeads, human, 130-050-401, Miltenyi biotec) and MACS column (130-042-201, Miltenyi biotec, USA) was used. In brief, the magnetically labelled CD56 + are retained within the column, the unlabeled cells run through; this cell fraction is thus depleted of CD56+ cells. After removing the column from the magnetic field, the magnetically retained CD56 + cells can be eluted as the positive selected cell. The purity of NK cells was 95.9% as assessed by flow cytometric analysis of cells stained with CD56-PE (DAKO, USA) (Novocyte Flow Cytometer; King Faisal Specialist Hospital & Research Centre, Jeddah, Saudi Arabia) Figure S1.

2.2. Thymoquinone Preparation. Thymoquinone (274666-1G, Sigma-Aldrich, USA) was prepared by dissolving 0.4926% thymoquinone crystal in 1% dimethyl sulfoxide anhydrous, ≥99.9% (276855, Sigma -Aldrich, USA) and

99.9% NK media (130-092-657, Miltenyi biotec, USA). Two dilutions of the extract, 25 and 50 μM, were prepared and stored at 2–8°C.

2.3. *Cell Lines and Tissue Culture.* Human breast cancer MCF-7 (Michigan Cancer Foundation-7; King Faisal Specialist Hospital & Research Centre, Jeddah, Saudi Arabia) is an epithelial invasive breast ductal carcinoma cell line that is oestrogen–and progesterone receptor–positive. MCF-7 cells were cultured in RPMI1640 (2242279, Gibco, USA) and supplemented with 10% penicillin-streptomycin (10,000 U/mL; 15140122, Sigma-Aldrich, USA). The NK cells were cultured in an NK MACS medium (Miltenyi Biotec, USA) and supplemented with 20% Fetal Bovine Serum FBS (12103C, Sigma-Aldrich, USA), 0.1 mM β-mercaptoethanol (Sigma-Aldrich, USA), Interleukin 2 IL-2 human animal-component-free recombinant expressed in E. coli, ≥98% SDS-PAGE and ≥98% HPLC (Sigma-Aldrich, USA) suitable for cell cultures. All cell lines were consistently maintained in a humidified incubator at 37°C and 5% CO2.

2.4. *Thymoquinone Cell Cytotoxicity on Tumor and NK Cells.* Thymoquinone cell cytotoxicity was analyzed with a CyQUANT LDH Cytotoxicity Assay kit (C20301, Invitrogen, USA). MCF-7 cells were seeded at a density of 15×10^3 cells per well in a 96-well flat-bottom plate and incubated overnight. Then, NK cells were cocultured at an effector cell/target cell (E/T) ratio of 1 : 2 in the presence of different thymoquinone concentrations (25 and 50 μM) for 5 h. A CytoTox 96 lysis buffer was added and incubated for 45 min in an incubator. CytoTox 96 reagent was added to each well and incubated for 30 min at room temperature in the dark, and then, a stop solution was added. Absorbance was measured at 680 and 490 nm. LDH activity was measured by subtracting the 680 nm absorbance value (background) from 490 nm absorbance [36]. Cytotoxicity % was calculated by using the formula:

$$\frac{\text{compound\_treated LDH activity} - \text{spontaneous LDH activity}}{\text{maximum LDH activity} - \text{spontaneous LDH activity}} \times 100.$$

(1)

2.5. *NK cell activity determination.* MCF-7 and NK cells were cocultured in the presence of thymoquinone for 5 h. Cell-free supernatants were harvested to measure the production of IFN-α (244304-026, Invitrogen, USA) granzyme B (E0899Hu, BT lab, UK), and perforin/pore-forming proteins (E0070Hu, BT lab, UK) using a human enzyme–linked immunosorbent assay kit. Absorbance was measured at 450 nm using a microplate reader (Multiskan G0 1.00.40, Thermo, serial no. 1510-03131C) [37]. The concentrations of the unknowns were calculated from standard curves Figure S2.

2.6. *Statistical Analyses.* The data were processed using GraphPad Prism 9 and the results were presented as the mean ± SD of three independent experiments. Statistical significance was tested using one-way analysis of variance (ANOVA) and Tukey's multiple comparison test to identify significant differences between groups, with $P < 0.05$ considered significant.

3. Results

3.1. *Cytotoxic Effect of Thymoquinone on NK Cells against MCF-7 Cells.* The target NK cell cytotoxicity was evaluated in a coculture with MCF-7 cells. The effector (NK cells) and target (MCF-7 cells) ratio was 1 : 2 and different concentrations of thymoquinone (25 and 50 μM) were added to the cultures. In the presence of thymoquinone, there was a significant increase in NK cell cytotoxicity. In particular, 50 μM thymoquinone increased NK cell cytotoxicity in MCF-7 cells to the maximum effect of 283.244%, as compared with the control NK cells cocultured with tumor cells (NK + TC) at 77.69% (one-way ANOVA, $n = 3$, $P < 0.04$). Cell cytotoxicity was also significantly increased in tumour cells treated with both 25 μM and 50 μM thymoquinone in the presence of NK cells, as compared to tumor cells treated with the same thymoquinone concentrations in the absence of NK cells (one-way ANOVA, $n = 3$, $P < 0.0064$, and $P < 0.0251$, respectively). In addition, there was a significant increase in NK cell cytotoxicity between the two doses of thymoquinone (25 and 50 μM; one-way ANOVA, $n = 3$, and $P < 0.04$), as seen in Figure 1.

3.2. *Effect of Thymoquinone on NK Cell Activity.* Thymoquinone enhances the release of perforin, granzyme B, and IFN-α, the major secreted cytokines of NK cells. In accordance with this understanding, the NK cells cocultured with MCF-7 cells and treated with 50 μM thymoquinone had significantly stimulated perforin production compared with the control NK cells cocultured with tumor cells (one-way ANOVA, $n = 3$, $P < 0.0041$, Tukey's). The higher 50-μM thymoquinone dose significantly enhanced the NK cells' perforin production over the lower 25-μM dose (one-way ANOVA, $n = 3$, $P < 0.0019$, Tukey's), as seen in Figure 2(a). In turn, the NK cells' granzyme B production was significantly increased in the presence of 25 and 50 μM thymoquinone compared with the control tumor cells in the presence of NK cells alone (one-way ANOVA, $n = 3$, $P = 0.0001$, and $P < 0.0001$, respectively, Tukeys), as seen in Figure 2(b). IFN-α production also significantly increased in tumor cells treated with 50 μM thymoquinone compared with control tumor cells and in tumor cells treated with 25 μM thymoquinone in the presence of NK cells (one-way ANOVA, $n = 3$, $P < 0.007$, and $P < 0.04$, respectively, Tukey's), as seen in Figure 2(c).

The correlation between individual cytokines and NK cytotoxicity was analyzed using Spearman correlation coefficient. There was no significant correlation between any of the cytokines and NK cytotoxicity although perforin production was the highest among them as seen in Figure 3.

4. Discussion

Many studies report the immunomodulatory effect of thymoquinone on NK cells [38–41]. The effect of thymoquinone on various immune cells is well-investigated, since
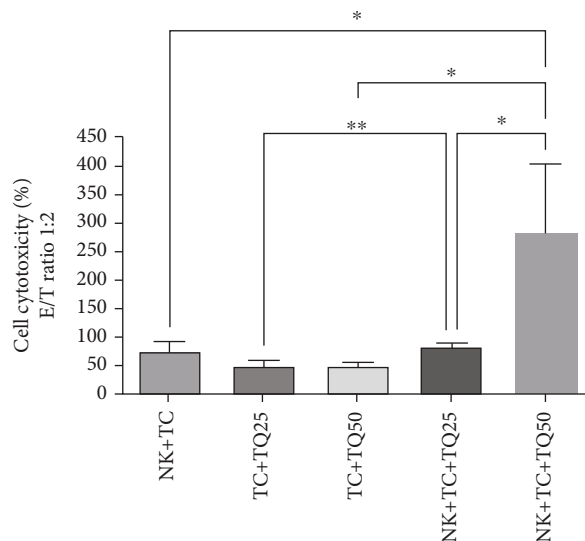
FIGURE 1: NK cell cytotoxicity against MCF-7 cells in the presence or absence of thymoquinone. Fifty μM of thymoquinone upregulated NK cell cytotoxicity in MCF-7 cells significantly compared to the control cells (NK + TC) at P < 0.04 (one-way ANOVA, Tukey's test). Cell cytotoxicity significantly increased in TC + TQ25 + NK and TC + TQ50 + NK compared to TC25 and TC + TQ50 at P < 0.0064 and P < 0.0251, respectively (one-way ANOVA, Tukey's test). There was a significant increase in NK cell cytotoxicity between the two doses of thymoquinone (25 and 50 μM) at P < 0.04 (one-way ANOVA, Tukey's test). All data are expressed as mean ± SD of three independent experiments.

inflammatory immune cells, such as NK cells, are considered part of the complex microenvironment that forms both primary and metastatic tumors [42]. Despite this, the mechanism that triggers thymoquinone's effect on cancer cells is not well-known. Moreover, it is not yet determined whether the anticancer effect of this active compound acts on the cancer cells itself or enhances NK cell anticancer activity.

In this study, we investigated the effect of two concentrations of thymoquinone on the cytotoxicity of NK cells and its anticancer activity using the MCF-7 breast cancer cell line. The results demonstrate that treating cancer cells with a high dose of thymoquinone in the presence of NK cells enhanced NK cell cytotoxicity more than NK cells cocultured with cancer cells alone or in cells with a lower dose of thymoquinone. In addition, NK cell cytotoxicity was significantly higher when used to treat cancer cells cocultured with either thymoquinone concentration compared to cancer cells treated with thymoquinone alone. This indicates that thymoquinone's antitumor effect is associated with its stimulation of NK cell function. This finding is similar to a study done by Shabsoug et al. who conclude that using an aqueous extract of Nigella sativa significantly enhanced the cytotoxic activity of NK cells isolated from human blood against a lymphoblast cell line (K-562) in vitro [43]. Our findings are also similar to an in vivo study done on mice with lymphoma, which were given an oral aqueous extract of Nigella sativa for 1 week. These results show that Nigella sativa caused a significant increase in splenic NK cell numbers, as associated with increased cytotoxic activity against Lymphoma YAC-1 tumor cells [44]. These findings are in an agreement with another in vitro study on the treatment of the same YAC-1 cell line with fresh aqueous Nigella sativa extract [45]. In addition, Majdalawieh et al. reported that treating YAC-1 cells with different concentrations of aqueous Nigella sativa extract significantly enhanced YAC-1 cell death upon amplifying NK cell cytotoxic activity, rather than the direct cytotoxic effect on the cancer cells themselves. This is also evidenced by our findings, suggesting that thymoquinone has no direct cytotoxic effect on MCF-7 cancer cells in the absence of NK cells [46].

The enhancement of the cytotoxic potential of NK cells against cancer cells is at least one proposed mechanism reported by other researchers using other plant extracts to examine their antitumour actions [46]. Our results show that thymoquinone stimulated the production of perforin, granzyme B and interferons in NK cells. These findings explain the enhanced cytotoxic potential of NK cells and its antitumour activity [43]. As mentioned earlier, our results are in line with Shabsoug, who report an increase in the production of interferons and granzyme B in NK cells after treating them with different concentrations of an aqueous Nigella sativa extract; as such, K-562 cancer cell death was significantly improved. In general, NK cells may eliminate different types of cancer cells through various cytotoxic mechanisms [43]. NK cells secrete many cytotoxic granules containing perforin and granzymes, which cause cell lysis. They also release sufficient amounts of cytokines, including IFN-α, thus increasing their cytotoxicity [47]. Moreover, NK cells express tumor necrosis factor–related, apoptosis-inducing ligand family TRAIL, and FAS ligand (FASL), which interact with TRAIL receptors and FAS ligands in cancer cells, respectively. This interaction results in cell death, signaling complex stimulating apoptosis [47]. The final mechanism involves the presence of CD16-activating receptors on NK cells, which recognize Fc on human IgG1 antibodies and trigger ADCC [48].

However, many tumors develop mechanisms to escape NK cell immunoresponses by modifying their cell surface

(a)

(b)

(c)
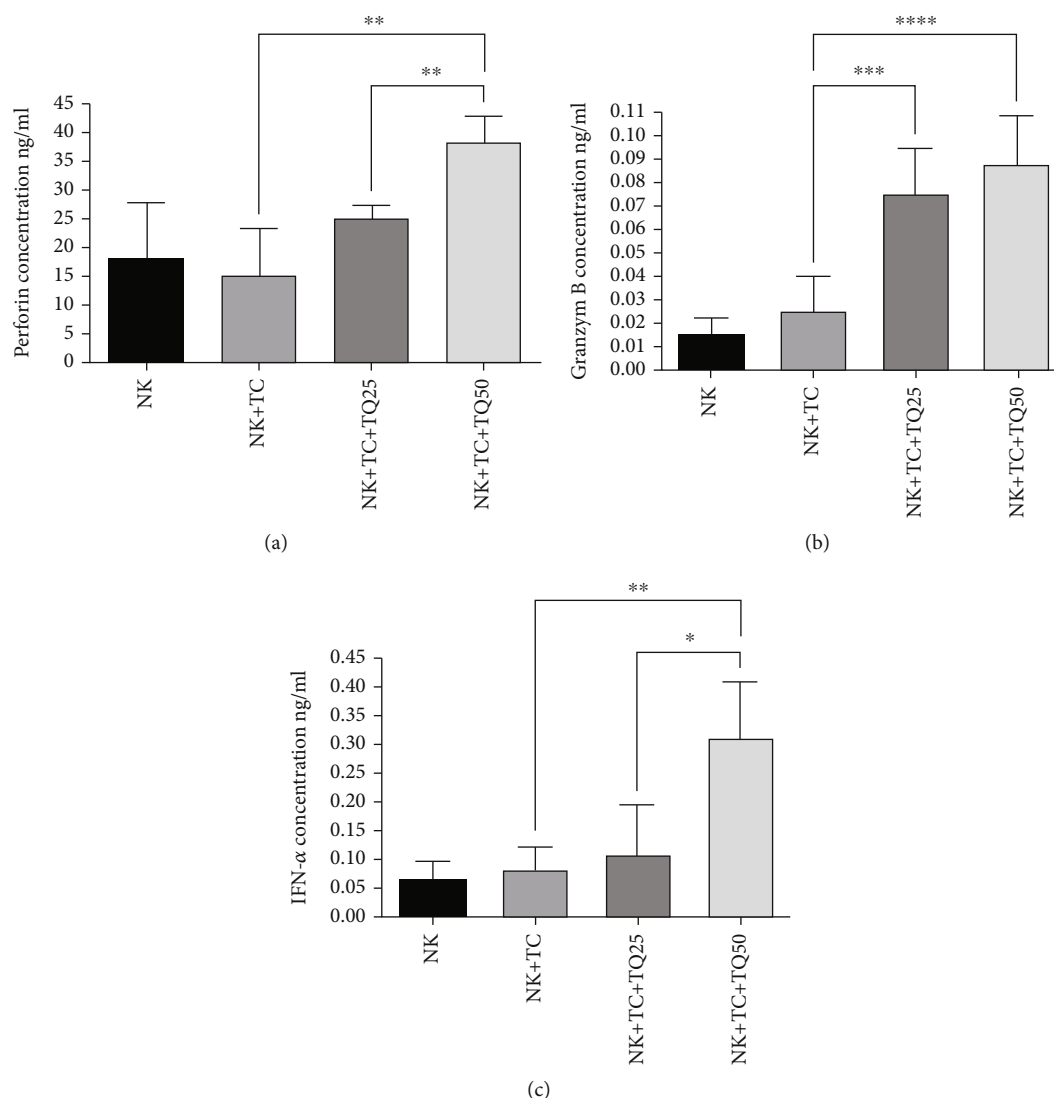
FIGURE 2: Major cytokines against MCF-7 cells, as produced by NK cells affected by thymoquinone. (a) The increased production of perforin from NK cells when cocultured with tumor MCF-7 cells treated with 50 μM thymoquinone compared to both the control (NK + TC) and NK cells cocultured with tumor cells treated with 25 μM (P < 0.0041 and P < 0.0019, respectively; one-way ANOVA, Tukey's test). (b) The enhanced production of granzyme B from NK cells cocultured with tumor cells treated with both thymoquinone concentrations (50 and 25 μM) compared to the control (NK + TC; P = 0.0001 and P < 0.0001, respectively; one-way ANOVA, Tukey's test). (c) illustrate the increased production of interferons in NK cells cocultured with tumor cells treated with 50 μM thymoquinone compared to both the control and NK cells cocultured with tumor cells treated with 25 μM (P < 0.007 and P < 0.04, respectively; one-way ANOVA, Tukey's test). All data are expressed as mean ± SD of three independent experiments.

molecules, which are involved in the recognition and release of the soluble factors that cause immunosuppressive reactions, such as TGF-β, prostaglandin E2 (PGE2), and IL-10 [49]. NK cell function can also be suppressed by tumor-associated fibroblasts (TAFs), the most abundant cell type within the stroma of many cancer types [50–52]. TAF/NK cell cross-talk results in inhibited NK cell activity through the release of PGE2, which in turn downregulates the expression of NKG2D, NKp30 and NKp44, and decreases NK cells' perforin/granzyme B production [53–55]. Therefore, the aim of much research has been to find therapeutic approaches to post/restore NK cell activity against cancer [56]. This research, together with other in vitro and in vivo studies, suggests that thymoquinone, the active component of Nigella sativa, may act as an immunomodulatory agent that enhances anticancer immune activity. It is worth mentioning that several investigations reveal that TQ may also act as a complementary therapy together with chemotherapy and radiation, thus enhancing treatment outcomes and minimizing their side effects [57–59]. This study confirmed the growth inhibitory effect of thymoquinone on human breast carcinoma MCF-7 cells, which is in agreement with previous studies. We also observed that thymoquinone treatment directly activates the cytolytic activity of NK cells against MCF-7 human breast cancer.

Our results provide strong evidence for the direct immune-stimulating effect of thymoquinone on NK cells. Even though some of the signaling molecules involved in
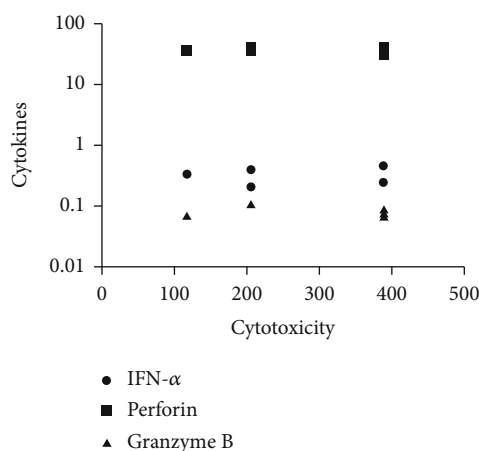
FIGURE 3: The plot of the Spearman correlation coefficient (2-tailed) between perforin, IFN-α and granzyme B cytokines and NK cytotoxicity. There was no significant correlation between perforin, IFN-α and granzyme B and NK cytotoxicity.

mediating thymoquinone immunostimulatory effect in NK cells have been identified, the exact signaling pathways and molecular targets in them are still unknown. Future in vitro and in vivo studies are thus required to identify the target receptors and intracellular and extracellular factors that play certain roles in the signal transduction pathways that TQ modifies in NK cells.

5. Conclusion

In summary, our study showed that thymoquinone promotes the cytotoxic activity of NK cells against breast cancer MCF-7 cells. Furthermore, thymoquinone's activation of perforin, granzyme B, and interferon proteins appears to be responsible for the NK cells enhanced anticancer activity, which resulted in killing MCF-7 cells.

Future studies should focus on finding the connection between the anticancer effect of Nigella sativa extracts and preclinical and clinical tumor inhibition/therapy and the molecular mechanisms involved in NK activation. NK cell memory could assist in developing good NK cell anticancer protocol, since it could prove advantageous for treatments.

Data Availability

No additional data are available.

Ethical Approval

This research was approved by unit of biomedical ethics research committee at King Abdulaziz University Faculty of Medicine. Reference No640-20 in 14/12/2020.

Conflicts of Interest

All authors declare that they have no conflicts of interest.

Authors' Contributions

NIT and NAA work the study design. NAA conducts the study. NAA, HFA, and HMA work on data analysis. NIT, NAA, and HFA work on data interpretation. HFA and NAA work on manuscript drafting, NIT, NAA, HMA, HFA, and NAA work on manuscript revision. All authors have critically reviewed and approved the final draft and are responsible for the content and similarity index of the manuscript.

Acknowledgments

Supplementary Materials

Supplementary 1. Figure S1: NK cells were isolated using CD56+ selection and the purity of NK cells was assessed by flow cytometric analysis of cells stained with CD56-PE

Supplementary 2. Figure S2: NK dot plot before treatment and indicating the purity of NK cells to be 95%. IFN-α, granzyme B and perforin cytokines were measured by using a human enzyme–linked immunosorbent assay kit and the concentration of these cytokines were calculated using standard curve.

References

[1] J. Ferlay, M. Colombet, I. Soerjomataram et al., "Cancer statistics for the year 2020: an overview," International Journal of Cancer, vol. 149, no. 4, pp. 778–789, 2021.

[2] F. Bray, J. Ferlay, I. Soerjomataram, R. L. Siegel, L. A. Torre, and A. Jemal, "Global cancer statistics 2018: GLOBOCAN estimates of incidence and mortality worldwide for 36 cancers in 185 countries," CA: a Cancer Journal for Clinicians, vol. 68, no. 6, pp. 394–424, 2018.

[3] A. C. Antoniou and D. F. Easton, "Models of genetic susceptibility to breast cancer," *Oncogene*, vol. 25, no. 43, pp. 5898–5905, 2006.

[4] M. Zubair, S. Wang, and N. Ali, "Advanced approaches to breast cancer classification and diagnosis," *Frontiers in Pharmacology*, vol. 11, article 632079, 2021.

[5] N. Patani, L.-A. Martin, and M. Dowsett, "Biomarkers for the clinical management of breast cancer: international perspective," *International Journal of Cancer*, vol. 133, no. 1, pp. 1–13, 2013.

[6] V. J. Bardou, G. Arpino, R. M. Elledge, C. K. Osborne, and G. M. Clark, "Progesterone receptor status significantly improves outcome prediction over estrogen receptor status alone for adjuvant endocrine therapy in two large breast cancer databases," *Journal of Clinical Oncology*, vol. 21, no. 10, pp. 1973–1979, 2003.

[7] C. J. Creighton, C. Kent Osborne, M. J. van de Vijver et al., "Molecular profiles of progesterone receptor loss in human breast tumors," *Breast Cancer Research and Treatment*, vol. 114, no. 2, pp. 287–299, 2009.

[8] C. J. Creighton, X. Fu, B. T. Hennessy et al., "Proteomic and transcriptomic profiling reveals a link between the PI3K pathway and lower estrogen-receptor (ER) levels and activity in ER + breast cancer," *Breast Cancer Research*, vol. 12, no. 3, p. R40, 2010.

[9] S. Banerjee and I. E. Smith, "Management of small HER2-positive breast cancers," *The Lancet Oncology*, vol. 11, no. 12, pp. 1193–1199, 2010.

[10] S. Radenkovic, G. Konjevic, A. Isakovic, P. Stevanovic, K. Gopcevic, and V. Jurisic, "HER2-positive breast cancer patients: correlation between mammographic and pathological findings," *Radiation Protection Dosimetry*, vol. 162, no. 1-2, pp. 125–128, 2014.

[11] M. J. Piccart-Gebhart, M. Procter, B. Leyland-Jones et al., "Trastuzumab after adjuvant chemotherapy in HER2-positive breast cancer," *New England Journal of Medicine*, vol. 353, no. 16, pp. 1659–1672, 2005.

[12] J. Cuzick, M. Dowsett, S. Pineda et al., "Prognostic value of a combined estrogen receptor, progesterone receptor, Ki-67, and human epidermal growth factor receptor 2 immunohistochemical score and comparison with the Genomic Health recurrence score in early breast cancer," *Journal of Clinical Oncology*, vol. 29, no. 32, pp. 4273–4278, 2011.

[13] S. Solanki and S. Menka, "Diagnostic importance of MATRIX metalloproteinase 2 and 9 as additional biomarkers in the sera of breast cancer patients," *International Journal of Advanced Research*, vol. 7, no. 9, pp. 167–177, 2019.

[14] S. Stankovic, G. Konjevic, K. Gopcevic, V. Jovic, M. Inic, and V. Jurisic, "Activity of MMP-2 and MMP-9 in sera of breast cancer patients," *Pathology, Research and Practice*, vol. 206, no. 4, pp. 241–247, 2010.

[15] R. Gomathinayagam, J. H. Ha, M. Jayaraman, Y. S. Song, C. Isidoro, and D. N. Dhanasekaran, "Chemopreventive and anticancer effects of Thymoquinone: cellular and molecular targets," *Journal of Cancer Prevention*, vol. 25, no. 3, pp. 136–151, 2020.

[16] S. J. Oiseth and M. S. Aziz, "Cancer immunotherapy: a brief review of the history, possibilities, and challenges ahead," *Journal of Cancer Metastasis and Treatment*, vol. 3, no. 10, pp. 250–261, 2017.

[17] C. J. Langer, S. M. Gadgeel, H. Borghaei et al., "Carboplatin and pemetrexed with or without pembrolizumab for advanced, non- squamous non-small-cell lung cancer: a randomised, phase 2 cohort of the open- label KEYNOTE-021 study," *The Lancet Oncology*, vol. 17, no. 11, pp. 1497–1508, 2016.

[18] S. H. Patel, A. Rimner, and R. B. Cohen, "Combining immunotherapy and radiation therapy for small cell lung cancer and thymic tumors," *Translational Lung Cancer Research*, vol. 6, no. 2, pp. 186–195, 2017.

[19] J. S. Orange and Z. K. Ballas, "Natural killer cells in human health and disease," *Clinical Immunology*, vol. 118, no. 1, pp. 1–10, 2006.

[20] E. Vivier, E. Tomasello, M. Baratin, T. Walzer, and S. Ugolini, "Functions of natural killer cells," *Nature Immunology*, vol. 9, no. 5, pp. 503–510, 2008.

[21] G. Konjevic, V. Jurisic, V. Jovic et al., "Investigation of NK cell function and their modulation in different malignancies," *Immunologic Research*, vol. 52, no. 1-2, pp. 139–156, 2012.

[22] D. G. Doherty and C. O'Farrelly, "Innate and adaptive lymphoid cells in the human liver," *Immunological Reviews*, vol. 174, no. 1, pp. 5–20, 2000.

[23] J. A. Joyce and J. W. Pollard, "Microenvironmental regulation of metastasis," *Nature Reviews. Cancer*, vol. 9, no. 4, pp. 239–252, 2009.

[24] G. Ferlazzo, M. Pack, D. Thomas et al., "Distinct roles of IL-12 and IL-15 in human natural killer cell activation by dendritic cells from secondary lymphoid organs," *Proceedings of the National Academy of Sciences of the United States of America*, vol. 101, no. 47, pp. 16606–16611, 2004.

[25] C. Romagnani, K. Juelke, M. Falco et al., "CD56^{bright}CD16-killer Ig-like receptor- NK cells display longer telomeres and acquire features of CD56^{dim} NK cells upon activation," *Journal of Immunology*, vol. 178, no. 8, pp. 4947–4955, 2007.

[26] M. A. Cooper, T. A. Fehniger, and M. A. Caligiuri, "The biology of human natural killer-cell subsets," *Trends in Immunology*, vol. 22, no. 11, pp. 633–640, 2001.

[27] M. Cheng, Y. Chen, W. Xiao, R. Sun, and Z. Tian, "NK cell-based immunotherapy for malignant diseases," *Cellular & Molecular Immunology*, vol. 10, no. 3, pp. 230–252, 2013.

[28] D. Cho, S.-K. Kim, and W. E. Carson 3rd., "NK cell-based immunotherapy for treating cancer: will it be promising?," *The Korean Journal of Hematology*, vol. 46, no. 1, pp. 3–5, 2011.

[29] G. Konjević, V. Jurišić, and I. Spuzić, "Association of NK cell dysfunction with changes in LDH characteristics of peripheral blood lymphocytes (PBL) in breast cancer patients," *Breast Cancer Research and Treatment*, vol. 66, no. 3, pp. 255–263, 2001.

[30] S. Hao, J. Zhao, J. Zhou, S. Zhao, Y. Hu, and Y. Hou, "Modulation of 17β-estradiol on the number and cytotoxicity of NK cells *in vivo* related to MCM and activating receptors," *International Immunopharmacology*, vol. 7, no. 13, pp. 1765–1775, 2007.

[31] E. Z. Dajani, T. G. Shahwan, and N. E. Dajani, "Overview of the preclinical pharmacological properties of Nigella sativa (black seeds): a complementary drug with historical and clinical significance," *Journal of Physiology and Pharmacology*, vol. 67, no. 6, pp. 801–817, 2016.

[32] A. Tavakkoli, V. Mahdian, B. M. Razavi, and H. Hosseinzadeh, "Review on clinical trials of black seed (*Nigella sativa*) and its

active Constituent, Thymoquinone," *Journal of Pharmacopuncture*, vol. 20, no. 3, pp. 179–193, 2017.

[33] M. F. Ramadan, "Nutritional value, functional properties and nutraceutical applications of black cumin (*Nigella sativa* L.): an overview," *International Journal of Food Science & Technology*, vol. 42, no. 10, pp. 1208–1218, 2007.

[34] A. F. Majdalawieh and M. W. Fayyad, "Recent advances on the anti-cancer properties of *Nigella sativa*, a widely used food additive," *Journal of Ayurveda and Integrative Medicine*, vol. 7, no. 3, pp. 173–180, 2016.

[35] E. A. Aboutabl, A. A. El-Azzouny, and F. J. Hammerschmidt, "Aroma volatiles of Nigella Sativa L. seeds," *Progress in essential oil research*, vol. 16, pp. 49–55, 1986.

[36] V. Jurisić, I. Spuzić, and G. Konjević, "A comparison of the NK cell cytotoxicity with effects of TNF- α against K-562 cells, determined by LDH release assay," *Cancer Letters*, vol. 138, no. 1-2, pp. 67–72, 1999.

[37] V. Jurisic, "Multiomic analysis of cytokines in immuno-oncology," *Expert Review of Proteomics*, vol. 17, no. 9, pp. 663–674, 2020.

[38] P. J. Beresford, M. Jaju, R. S. Friedman, M. J. Yoon, and J. Lieberman, "A role for heat shock protein 27 in CTL-mediated cell death," *Journal of Immunology*, vol. 161, no. 1, pp. 161–167, 1998.

[39] K. Ebnet, M. Hausmann, F. Lehmann-Grube et al., "Granzyme A-deficient mice retain potent cell-mediated cytotoxicity," *The EMBO Journal*, vol. 14, no. 17, pp. 4230–4239, 1995.

[40] P. J. Beresford, Z. Xia, A. H. Greenberg, and J. Lieberman, "Granzyme a loading induces rapid cytolysis and a novel form of DNA damage independently of caspase activation," *Immunity*, vol. 10, no. 5, pp. 585–595, 1999.

[41] M. S. Butt and M. T. Sultan, "*Nigella sativa*: reduces the risk of various maladies," *Critical Reviews in Food Science and Nutrition*, vol. 50, no. 7, pp. 654–665, 2010.

[42] L. M. Coussens and Z. Werb, "Inflammation and cancer," *Nature*, vol. 420, no. 6917, pp. 860–867, 2002.

[43] B. Shabsoug, R. Khalil, and N. Abuharfeil, "Enhancement of natural killer cell activity in vitro against human tumor cells by some plants from Jordan," *Journal of Immunotoxicology*, vol. 5, no. 3, pp. 279–285, 2008.

[44] N. M. Abuharfeil, M. Salim, and S. Von Kleist, "Augmentation of natural killer cell activity in vivo against tumour cells by some wild plants from Jordan," *Phytotherapy Research*, vol. 15, no. 2, pp. 109–113, 2001.

[45] N. M. Abuharfeil, A. Maraqa, and S. Von Kleist, "Augmentation of natural killer cell activity in vitro against tumor cells by wild plants from Jordan," *Journal of Ethnopharmacology*, vol. 71, no. 1-2, pp. 55–63, 2000.

[46] A. F. Majdalawieh, R. Hmaidan, and R. I. Carr, "*Nigella sativa* modulates splenocyte proliferation, Th1/Th2 cytokine profile, macrophage function and NK anti-tumor activity," *Journal of Ethnopharmacology*, vol. 131, no. 2, pp. 268–275, 2010.

[47] B. Martín-Antonio, G. Suñe, L. Perez-Amill, M. Castella, and A. Urbano-Ispizua, "Natural killer cells: angels and devils for immunotherapy," *International Journal of Molecular Sciences*, vol. 18, no. 9, p. 1868, 2017.

[48] L. L. Lanier, "NK cell recognition," *Annual Review of Immunology*, vol. 23, no. 1, pp. 225–274, 2005.

[49] J. Baginska, E. Viry, J. Paggetti et al., "The critical role of the tumor microenvironment in shaping natural killer cell-mediated anti-tumor immunity," *Frontiers in Immunology*, vol. 4, p. 490, 2013.

[50] G. S. Karagiannis, T. Poutahidis, S. E. Erdman, R. Kirsch, R. H. Riddell, and E. P. Diamandis, "Cancer-associated fibroblasts drive the progression of metastasis through both paracrine and mechanical pressure on cancer tissue," *Molecular Cancer Research*, vol. 10, no. 11, pp. 1403–1418, 2012.

[51] D. F. Quail and J. A. Joyce, "Microenvironmental regulation of tumor progression and metastasis," *Nature Medicine*, vol. 19, no. 11, pp. 1423–1437, 2013.

[52] L. Tao, G. Huang, H. Song, Y. Chen, and L. Chen, "Cancer associated fibroblasts: an essential role in the tumor microenvironment," *Oncology Letters*, vol. 14, no. 3, pp. 2611–2620, 2017.

[53] M. Balsamo, F. Scordamaglia, G. Pietra et al., "Melanoma-associated fibroblasts modulate NK cell phenotype and antitumor cytotoxicity," *Proceedings of the National Academy of Sciences of the United States of America*, vol. 106, no. 49, pp. 20847–20852, 2009.

[54] T. Li, S. Yi, W. Liu et al., "Colorectal carcinoma-derived fibroblasts modulate natural killer cell phenotype and antitumor cytotoxicity," *Medical Oncology*, vol. 30, no. 3, p. 663, 2013.

[55] L. Ziani, S. Chouaib, and J. Thiery, "Alteration of the antitumor immune response by cancer-associated fibroblasts," *Frontiers in Immunology*, vol. 9, p. 414, 2018.

[56] B. Bassani, D. Baci, M. Gallazzi, A. Poggi, A. Bruno, and L. Mortara, "Natural killer cells as key players of tumor progression and angiogenesis: old and novel tools to divert their pro-tumor activities into potent anti-tumor effects," *Cancers*, vol. 11, no. 4, p. 461, 2019.

[57] M. N. Nagi and M. A. Mansour, "Protective effect of thymoquinone against doxorubicin-induced cardiotoxicity in rats: a possible mechanism of protection," *Pharmacological Research*, vol. 41, no. 3, pp. 283–289, 2000.

[58] O. A. Al-Shabanah, O. A. Badary, M. N. Nagi, N. M. Al-Gharably, A. C. Al-Rikabi, and A. M. Al-Bekairi, "Thymoquinone protects against doxorubicin-induced cardiotoxicity without compromising its antitumor activity," *Journal of Experimental & Clinical Cancer Research*, vol. 17, no. 2, pp. 193–198, 1998.

[59] R. Velho-Pereira, A. Kumar, B. N. Pandey, A. G. Jagtap, and K. P. Mishra, "Radiosensitization in human breast carcinoma cells by thymoquinone: role of cell cycle and apoptosis," *Cell Biology International*, vol. 35, no. 10, pp. 1025–1029, 2011.

Hindawi

Research Article

Xiaotan Sanjie Decoction Inhibits Gastric Cancer Cell Proliferation, Migration, and Invasion through lncRNA-ATB and miR-200A

Zhe Zhou,[1,2,3] **Jiabin Chen,**[1,2,3] **Mingqian Li** iD**,**[2,3] **Liping Cao,**[1,2,3] **Miao Chen,**[2,3] **Qingqian Zhang,**[2,3] **Zhihong Yu** iD**,**[1,2,3] **and Kequn Chai** iD[1,2,3]

[1]*The Second Clinical Medical College, Zhejiang Chinese Medicine University, Hangzhou 310053, Zhejiang Province, China*
[2]*Cancer Institute of Integrated Tradition Chinese and Western Medicine, Zhejiang Academy of Traditional Chinese Medicine, Tongde Hospital of Zhejiang Province, Hangzhou 310012, Zhejiang Province, China*
[3]*Zhejiang Provincial Key Laboratory of Cancer Prevention and Treatment Technology of Integrated Traditional Chinese and Western Medicine, Hangzhou 310012, Zhejiang Province, China*

Correspondence should be addressed to Zhihong Yu; yzhmed@163.com and Kequn Chai; ckq_official@163.com

This study is aimed at exploring whether Xiaotan Sanjie decoction (XTSJ) inhibits gastric cancer (GC) proliferation and metastasis by regulating lncRNA-ATB expression. qRT-PCR and Western blot were used to analyze lncRNA-ATB and downstream-regulated genes/proteins in human GC cells. CCK8, Edu, and flow cytometry assays were used to detect the inhibitory effect of XTSJ on cell proliferation and apoptosis. Moreover, transwell and wound healing assays were used to detect the inhibitory effect of XTSJ on migration and invasion. qRT-PCR and Western blot were used to detect regulated genes and proteins levels. The HGC-27 cell line was used for follow-up analysis due to the high level of lncRNA-ATB and cell characteristics. XTSJ inhibited the proliferation and metastasis of HGC-27 in a dose-dependent manner. Further research found that XTSJ downregulated lncRNA-ATB, Vimentin, and N-cadherin, while it upregulated miR-200a and E-cadherin in a dose-dependent manner. XTSJ also upregulated Caspase 3, Caspase 9, Bax, and downregulated Bcl-2. Furthermore, XTSJ inhibited tumor growth *in vivo* and downregulated EMT signaling pathways. These results indicate that XTSJ may affect EMT and Bcl-2 signaling pathways by regulating lncRNA-ATB and miR-200a, thus inhibiting proliferation, migration, and invasion of HGC-27 cells. Therefore, XTSJ may be an effective treatment for the high levels of lncRNA-ATB in GC.

1. Introduction

Gastric cancer (GC) has a poor prognosis and is the leading cause of cancer-related deaths [1]. Research has shown that traditional Chinese medicine can treat cancer [2, 3]. Therefore, studying the molecular pathways of traditional Chinese medicine can effectively enhance GC treatment.

lncRNAs are long-chain noncoding RNAs regulating gene transcription and downstream biological signals in tumors [4, 5]. Preliminarily studies have shown that lncRNAs acts as "sponge" to modulate downstream biological signals by competitively binding or chelating microRNAs [6]. TGF-β-activated lncRNA-ATB can enhance epithelial-mesenchymal transition(EMT)-related metastasis and proliferation by competitively binding to the miR-200

family in certain malignant tumors [7, 8]. Recent research showed that lncRNA-ATB upregulation in GC enhances vascular infiltration and overall survival while lncRNA-ATB silencing inhibits cell proliferation [9]. Therefore, lncRNA-ATB and miR-200a are potential therapeutic targets for GC treatment.

Xiaotan Sanjie decoction (XTSJ) can effectively prolong the survival of GC patients, decrease TGF-β and IL-8 levels, and inhibit the expression of fibroblast activation protein (FAP) [10, 11]. This research aimed to assess whether XTSJ prevents GC proliferation and metastasis by regulating lncRNA-ATB and miR-200a.

2. Material and Methods

2.1. Cell Culture. MKN-45, SNU-1, HGC-27, AGS, and MGC-803 were obtained from the Institute of Biochemistry and Cell Biology at the Chinese Academy of Sciences. The cells were cultured in RPMI-1640 medium with 10% fetal bovine serum (ExCell bio, Shanghai, China).

2.2. Preparation of Drugs. Prof. Wei Pinkang provided the XTSJ. XTSJ components have been described in previous papers. Its active components have been analyzed via HPLC [12]. The 5-fluorouracil (5-Fu) was obtained from Lilly France (Suzhou, China).

2.3. CCK-8 Assay. The GC cells (5×10^3 cells/well) were reinoculated and treated with XTSJ for 24, 48, and 72 hours. An appropriate amount of CCK-8 solution was added to the sample, then incubated for 2 hours. A SpectraMax i3 microplate reader (Molecular Devices, CA, USA) was used to measure absorbance.

2.4. Ethynyl-2-Deoxyuridine (EdU) Assay. The HGC-27 cells (5×10^3 cells/well) were reinoculated and treated with XTSJ for 24 hours. EdU ($100 \mu L$; $50 \mu m$) was then added to the sample then co-cultured for 2 hours. Hoechst3342 ($5 \mu g$/ml) was stained at room temperature for 20 minutes. An Olympus TH4-200 fluorescence microscope (Olympus, Tokyo, Japan) was used to obtain images.

2.5. Flow Cytometry Assay. The HGC-27 cells (4×10^5 cells/well) were treated with Annexin V-fluorescein isothiocyanate and propidium iodide (Procell, Wuhan, China) for 15 minutes under a shading environment. BD FACSCanto™ II Flow Cytometry System (BD Biosciences, NJ, USA) was used to detect cell apoptosis.

2.6. Transwell Migration and Invasion Assays. The HGC-27 cells (4×10^4 cells/well) were reinoculated into the upper chamber coated with Matrigel for invasion assay. For the migration assay, HGC-27 cells (4×10^4 cells/well) were reinoculated into the upper chamber (4×10^4 cells/well) without Matrigel. The upper chamber was filled with serum-free medium, while the lower chamber was filled with medium containing 10% FBS. The transwell chambers were fixed with a 4.0% paraformaldehyde solution for 15 minutes, then stained with a 0.1% crystal violet solution for 10 minutes. A

TABLE 1: Primer sets used in the real-time PCR and qPCR.

Gene name	Primer
lncRNA-ATB	F: TCTGGCTGAGGCTGGTTGAC
	R: ATCTCTGGGTGCTGGTGAAGG
Vimentin	F: AATCCAAGTTTGCTGACCTCTCTGA
	R: GACTGCACCTGTCTCCGGTACTC
E-cadherin	F: GGGGTCTGTCATGGAAGGTGC
	R: GTAAGCGATGGCGGCATTGTA
N-cadherin	F: CATCATCATCCTGCTTATCCTGT
	R: GCTCTTCTTCTCCTCCACCTTCTT
GAPDH	F: ACACCCACTCCTCCACCTTT
	R: TTACTCCTTGGAGGCCATGT
miR-200a	F: CCTACGCCACAATTAACAAGCC
	R: GCCGTCTAACACTGTCTGGTA
U6	F: CTCGCTTCGGCAGCACA
	R: AACGCTTCACGAATTTGCGT

Leica DMi1 inverted microscope (Leica, Wetzlar, Germany) was used to obtain images.

2.7. Wound-Healing Assay. The HGC-27 cells (4×10^5 cells/well) were reinoculated until they reached 90% confluence. A $200 \mu l$ sterile pipette tip was then used to scratch the center of each well. A Leica DMi1 inverted microscope was then used to assess the wound after 0, 24, and 48 hours.

2.8. Western Blot. Total protein was extracted from the HGC-27 cells (3×10^6 cells/well) cells using cell lysate buffer after 24 hours. BCA protein quantitative Kit (Sangon Biotech, Shanghai, China) was used for protein quantitation. Protein concentration was adjusted before protein denaturation. Electrophoresis of the protein sample was conducted on SDS-polyacrylamide gels at 60 V for 3-5 hours. The samples were then transferred onto polyvinylidene difluoride film (Bio-Rad, Hercules, CA, USA) at 300 mA for 90 minutes. The film was blocked with a 5% BSA solution for 90 minutes, then incubated with primary antibodies (E-cadherin (20874-1-AP), Vimentin (60330-1-lg), N-cadherin (22018-1-AP), ZEB-1 (21544-1-AP), Bcl-2 (26593-1-AP), Bax (50599-2-Ig), Caspase 3 (19677-1-AP), Caspase 9 (10380-1-AP), and β-actin (66009-1-lg)) at 4°C overnight. The films were then incubated with secondary antibodies (HRP-conjugated Affinipure Goat Anti-mouse IgG (H + L) (SA00001-1) and HRP-conjugated Affinipure Goat Anti-rabbit IgG (H + L) (SA00001-2)) at room temperature for 60 minutes. These antibodies were obtained from Proteintech™ (Wuhan, China). The proteins were visualized using chemiluminescence. Grayscale analysis of Western blot images was conducted using ImageJ.

2.9. Real-Time Quantitative Reverse Transcription PCR (qRT-PCR). Total RNA was obtained from the HGC-27 (3×10^6 cells/well) cells using Trizol reagent after 24 hours.

(a)

(b)

(c)
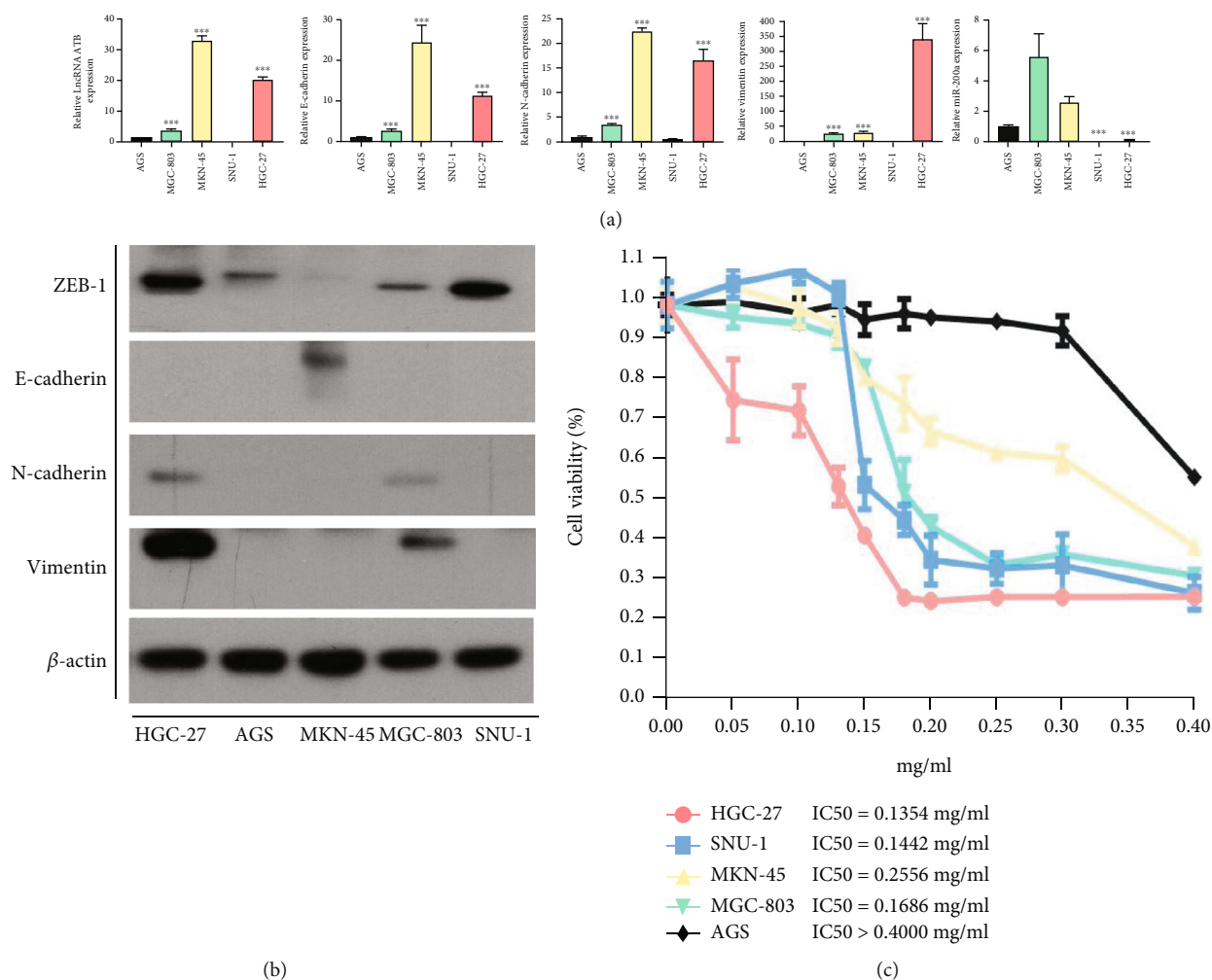
Figure 1: |Expression of related genes and protein expression in human gastric cancer cells. (a) qRT-PCR analysis of lncRNA-ATB, Vimentin, E-cadherin, N-cadherin, and miR-200a in 5 gastric cancer cells. (b) Western blotting based detection of ZEB-1, Vimentin, E-cadherin, and N-cadherin in 5 gastric cancer cells. (c) Effect of different concentrations of XTSJ on the cell viability in 5 gastric cancer cell lines. $*P < 0.05$; $**P < 0.01$; $***P < 0.001$.

The RNAs were reverse transcribed using the reverse aid first-strand cDNA synthesis Kit (Thermo Fisher Scientific, Ma, USA) to obtain cDNA. A LightCycler® 480 Real-Time PCR System (Roche, Basel, Switzerland) was used for qRT-PCR analysis. Each sample had three replicates. The primer sequences used for amplification are shown in Table 1. Quantitative analysis of each sample was conducted using the $2^{-\triangle\triangle Ct}$ method.

2.10. In Vivo Experiment. BALB/c nude mice (6-week-old, female) were reared in a sterile environment. The animal experiment was approved by the Ethics Committee of the Tongde Hospital of Zhejiang Province. The tumor model was established by subcutaneously inoculating the HGC-27 cells (1×10^6 cells/well) into the right side of mouse back. The mice were treated using intragastric of XTSJ (1 g/kg for low-dose and 2 g/kg for high-dose) or intraperitoneal injection of 5-FU (30 mg/kg) every day.

The mice were euthanized after seven days. The tumor tissues were dissected and collected. Pathological examination and SABER-FISH were used to assess the expression of EMT related antibodies and the location of lncRNA-ATB in tissues [13, 14].

2.11. Statistical Analysis. Quantitative data are expressed as mean ± SD. The normally distributed data were analyzed using students' t-test analyzed. Mann–Whitney U-test was used to analyze the nonnormally distributed data. Graph-Pad Prism8. 0 software was used for data analysis and drawing charts. $P < 0.05$, $P < 0.01$, and $P < 0.001$ represent significant differences.

3. Results

3.1. HGC27 Cell Line as a Model for Drug Intervention of lncRNA-ATB In Vitro. lncRNA-ATB and EMT signal pathway-related genes and proteins in five GC cells were

(a)

(b)

(c)

Figure 2: Continued.

(d)

(e)
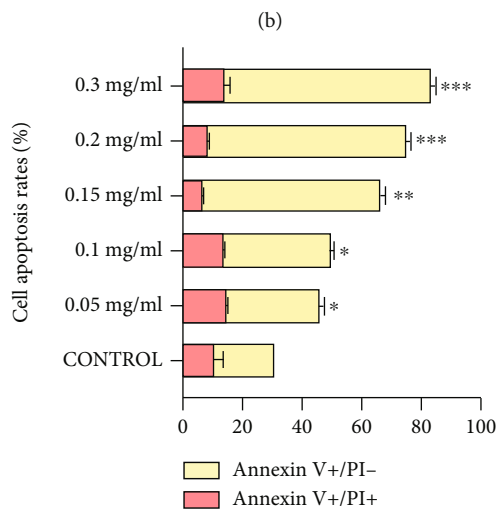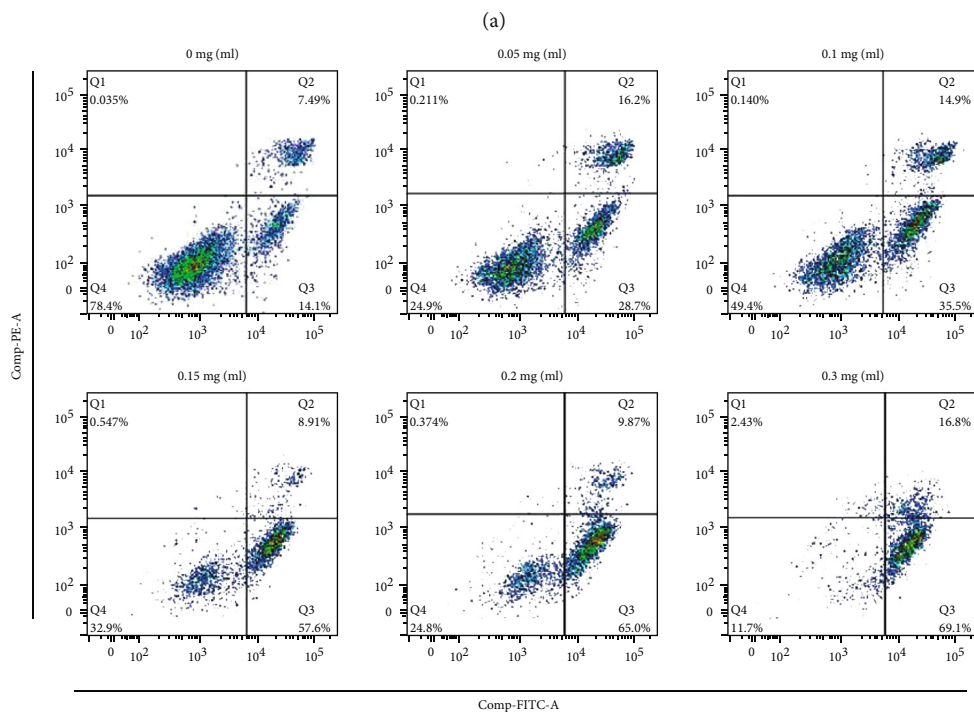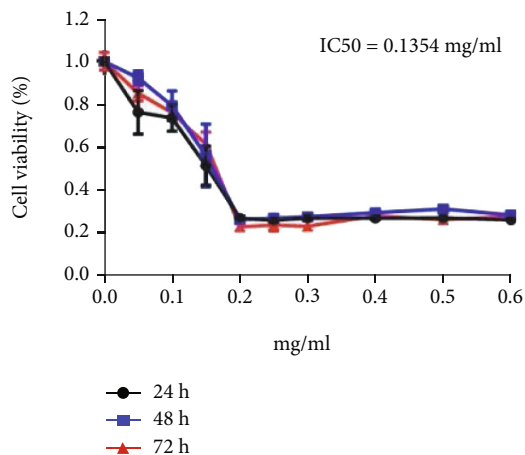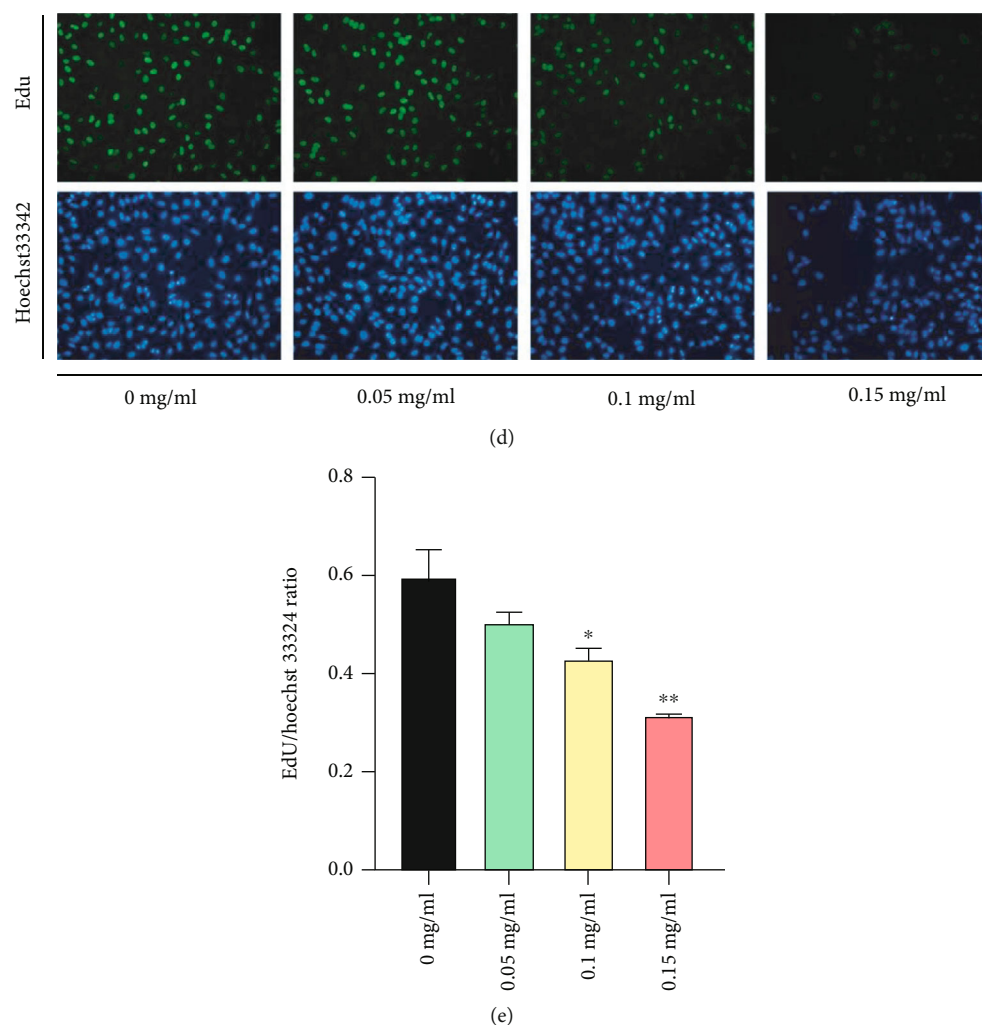
FIGURE 2: Effects of XTSJ on HGC-27 cells proliferation and apoptosis. (a) Effect of different concentrations of XTSJ in the viability of HGC-27 cells. (b) Effects of XTSJ on cells apoptosis were detected by flow cytometry, and (c) the cell apoptosis rate was quantified. (d) EdU assay was performed to observe cell proliferation intervened by XTSJ; blue-labeled (Hoechst 33324) is the nucleus, green-labeled implies the cells undergoing the proliferation process; and (e) the EdU/Hoechst 33324 ratio was quantified. $^{*}P < 0.05$; $^{**}P < 0.01$; $^{***}P < 0.001$.

analyzed to find a suitable cell model for *in vitro* drug intervention of lncRNA-ATB. lncRNA-ATB, Vimentin, and N-cadherin were upregulated in HGC-27 and MKN-45, while miR-200a and E-cadherin were downregulated (Figure 1(a)). Western blot also revealed that ZEB-1, Vimentin, and N-cadherin were upregulated in HGC-27 while E-cadherin was downregulated (Figure 1(b)). However, ZEB-1, Vimentin, and N-cadherin protein levels were relatively low in MKN-45 (a semisuspended cell), while E-cadherin level was relatively high (Figure 1(b)). Moreover, the viability of cells was detected using CCK8. HGC-27 had the lowest IC50 concentration (0.1354 mg/ml), indicating it was the most sensitive to drugs (Figure 1(c)). As a result, HGC-27 was selected as a model for drug intervention *in vitro*.

3.2. XTSJ Inhibits Proliferation and Promotes Apoptosis in HGC-27 Cells. Flow cytometry assays showed that apoptosis

increased with increasing drug concentration (0 mg/ml, 30.56%; 0.05 mg/ml, 46.23%; 0.1 mg/ml, 50.23%; 0.15 mg/ml, 67.41%; 0.2 mg/ml, 76.16%; 0.3 mg/ml, 83.83%), especially in early apoptosis (Figures 2(b) and 2(c)). EdU assays indicated that the ratio of EdU/Hoechst33342 decreased with increasing XTSJ concentration (0 mg/ml, 59.60%; 0.05 mg/ml, 50.48%; 0.1 mg/ml, 43.93%; 0.15 mg/ml, 31.89%), thus inhibiting proliferation. CCK8 assay showed that XTSJ had an inhibitory effect in a concentration dependent manner (IC50 = 0.1354 mg/ml) and not time-dependent (Figure 2(a)) (Figures 2(d) and 2(e)). These results suggest that XTSJ can inhibit HGC-27 cell proliferation and promote apoptosis.

3.3. XTSJ Inhibits Migration and Invasion in HGC-27 Cells. Transwell assays demonstrated that XTSJ significantly reduced cell number in the migration assays at high concentrations (0.15 mg/ml). XTSJ also significantly reduced

(a)

(b)

(c)

(d)
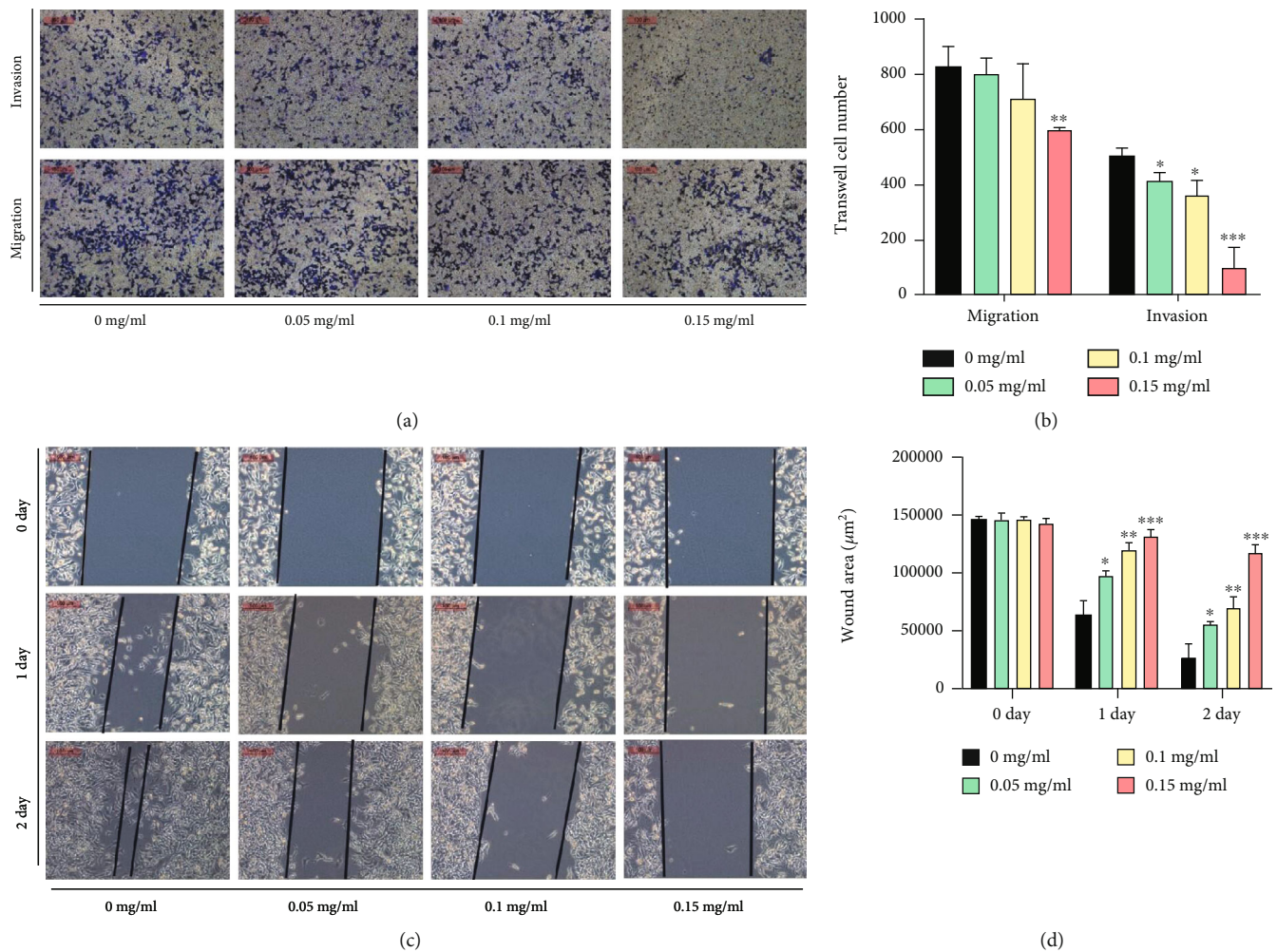
FIGURE 3: Effects of XTSJ on HGC-27 cell migration and invasion. (a) Effects of XTSJ on the migration and invasion were detected by Transwell assays, and (b) the Transwell cell number was quantified. (c) Wound healing assays detected effects of different concentrations of XTSJ on the cell migration, and (d) the wound area was quantified. $^{*}P < 0.05$; $^{**}P < 0.01$; $^{***}P < 0.001$.

cell number in the invasion assays in a dose-dependent effect (Figures 3(a) and 3(b)). Wound healing assays found that XTSJ effectively maintained the wound healing range and inhibited cell invasion (Figures 3(c) and 3(d)). These results suggest that XTSJ can effectively inhibit HGC-27 metastasis.

3.4. XTSJ Inhibits the Expression of lncRNA and Related EMT and Bcl-2 Signaling Pathways. lncRNA-ATB and downstream-regulated genes and proteins were analyzed using qRT-PCR and Western blotting to reveal how XTSJ inhibits the proliferation and metastasis of HGC-27. qRT-PCR showed that XTSJ reduced the levels of lncRNA-ATB, Vimentin, and N-cadherin while increasing miR-200a and E-cadherin levels in a dose-dependent effect (Figure 4(a)). Similarly, Western blot assays showed that XTSJ reduced ZEB-1, Vimentin, and N-cadherin levels while increasing E-cadherin levels (Figures 4(b) and 4(c)). Western blot also showed that

XTSJ reduced Bcl-2 level while it increased Caspase 3, Caspase 9, and Bax levels (Figures 4(d) and 4(e)). These results suggest that XTSJ affects EMT and Bcl-2 signal pathways by downregulating lncRNA-ATB and upregulating miR-200a.

3.5. The Effect of XTSJ on GC In Vivo. Pharmacodynamic analysis was conducted using HGC-27 transplanted tumor nude mice model. XTSJ inhibited the transplanted tumors in mice, similar to chemotherapeutic drugs (5-FU) (Figures 5(a) and 5(b)). SABER-FISH results showed that lncRNA-ATB was upregulated in the model group while it was downregulated in XTSJ group (Figure 5(c)). Immuno-histochemical (IHC) analysis showed that XTSJ reduced the levels of antibodies, such as Ki67, Vimentin, and N-cad-herin, while it increased E-cadherin levels (Figure 5(d)). These results indicate that XTSJ can affect EMT signaling pathway in vivo (Figure 6).

(a)

(b)

(c)

Figure 4: Continued.

(d)

(e)
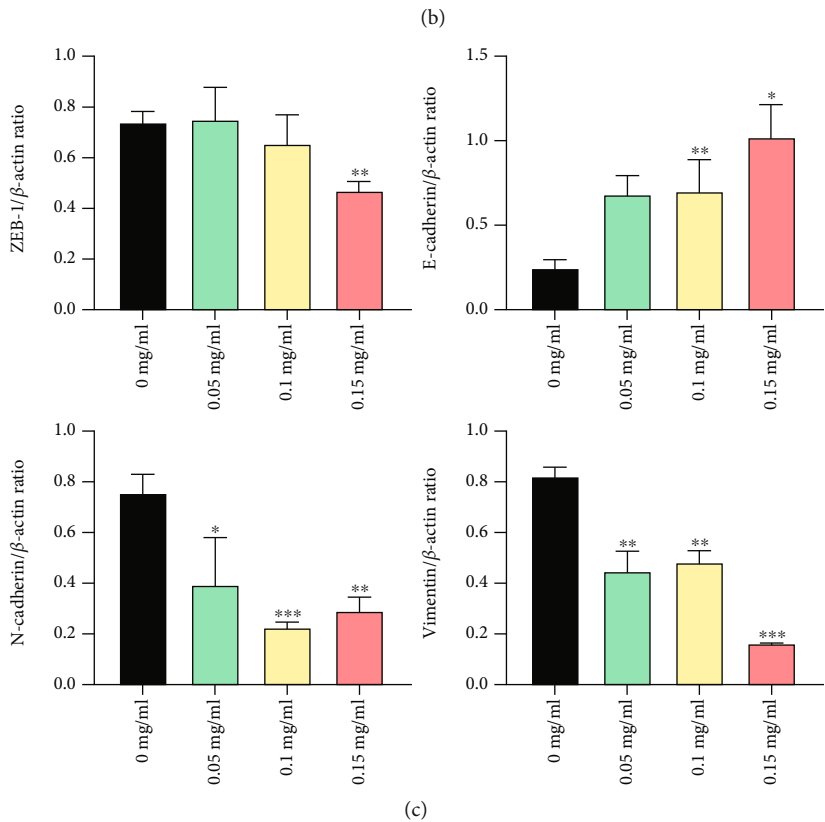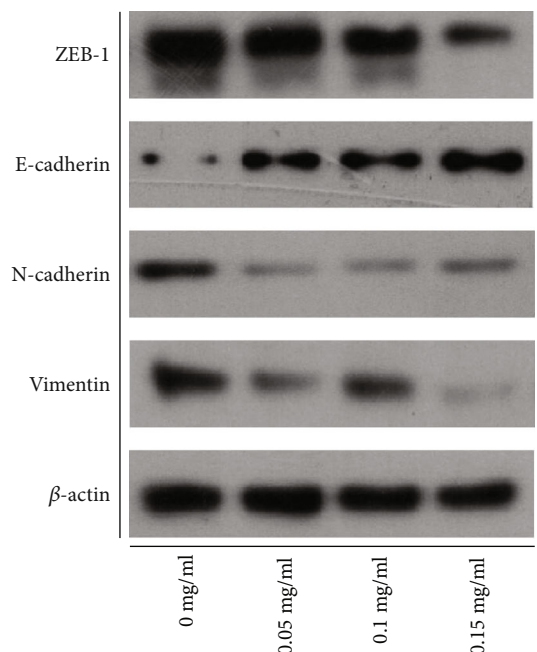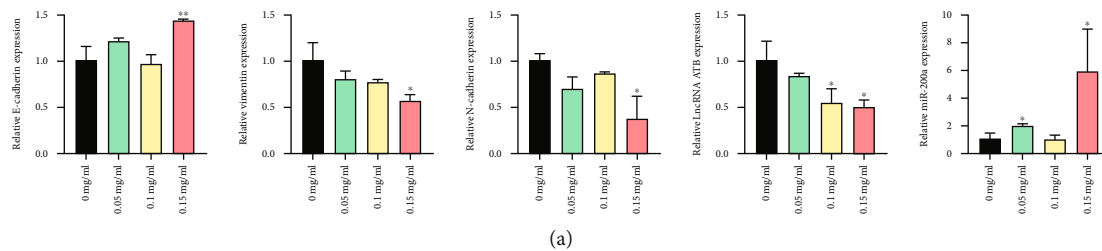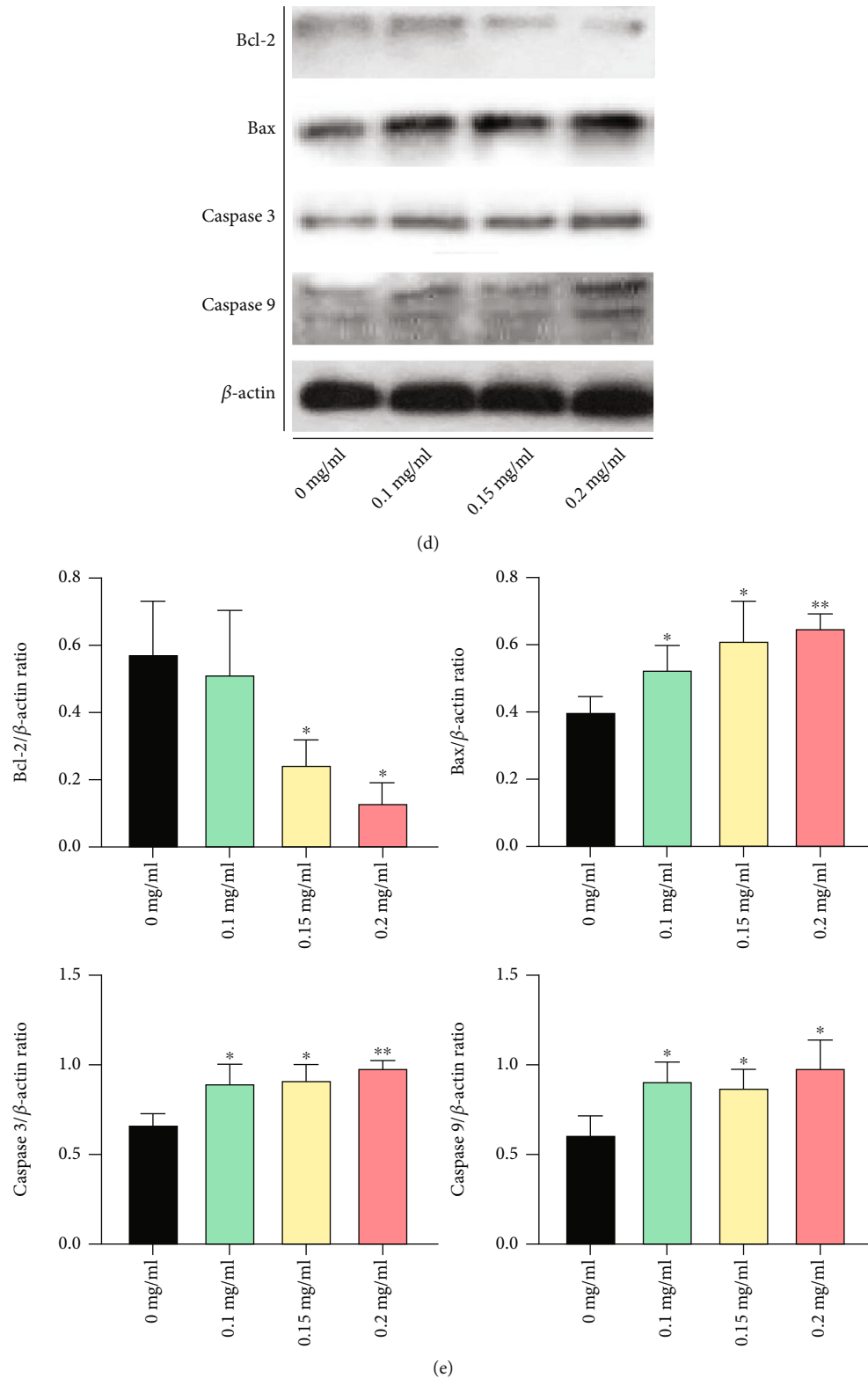
FIGURE 4: Effects of XTSJ on gastric cancer-related mRNA and protein expression. (a) qRT-PCR analysis of lncRNA-ATB, Vimentin, E-cadherin, N-cadherin, and miR-200a after intervention with XTSJ. (b) Western blotting based on detection of ZEB-1, Vimentin, E-cadherin, and N-cadherin after intervention with XTSJ. (c) The relative protein was carried out with β-actin as an internal reference. (d) Western blotting based on detection of Bcl-2, Bax, Caspase 3, and Caspase 9 after intervention with XTSJ. (e) The relative protein was carried out with β-actin as an internal reference. $^{*}P < 0.05$; $^{**}P < 0.01$; $^{***}P < 0.001$.

(a)

(b)

LncRNA ATB × 40

(c)

H&E × 40   Ki67 × 40   Vimentin × 40   E-cadherin × 40   N-cadherin × 40

(d)
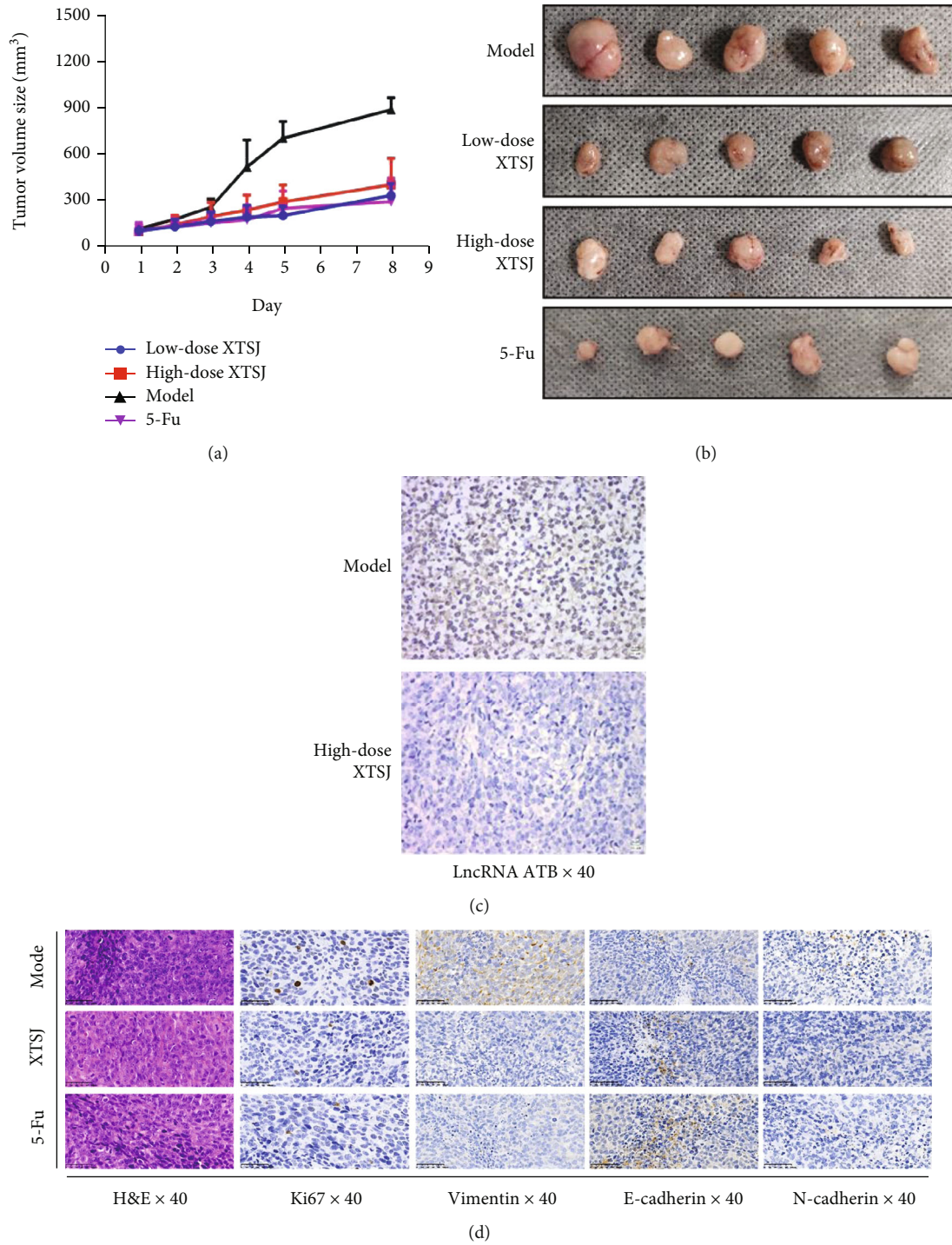
FIGURE 5: Effects of XTSJ on gastric cancer in vivo. (a) The tumor volume sizes after subcutaneous inoculation of HGC-27 cells in each group. (b) Tumors were dissected from each group. (c) The expression of SABER-FISH lncRNA-ATB was detected by SABER-FISH. (d) The expression of Ki67, Vimentin, E-cadherin, and N-cadherin in tumor tissues was analyzed by IHC analysis. $^{*}P < 0.05$; $^{**}P < 0.01$; $^{***}P < 0.001$.
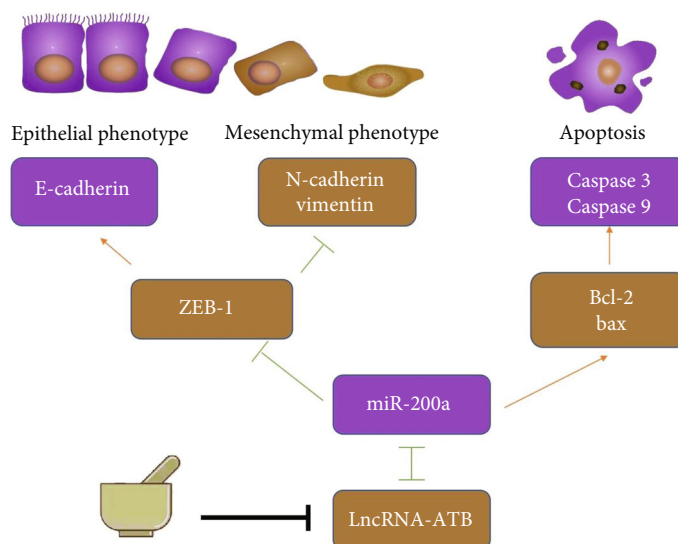
FIGURE 6: Molecular mechanism of XTSJ. The corresponding mechanism may be related to XTSJ reducing LncRNA-ATB and increasing miR-200a competing with it to reduce the expression of downstream ZEB-1 and reverse EMT. The process of reversing EMT showed decreased expression of Vimentin and N-cadherin associated with mesenchymal phenotype and increased E-cadherin expression associated with an epithelial phenotype. In addition, XTSJ could reduce Bcl-2, increase Bax, Caspase 3, and Caspase 9 to induce apoptosis.

4. Discussion and Conclusion

Gastric cancer (GC) has a poor prognosis, especially GC cells at low to medium differentiation stages that easily undergo proliferation, migration, invasion, and tumorigenesis [15]. Therefore, studies should assess the biological mechanism of proliferation and metastasis in GC.

lncRNA-ATB (TGF-β activated long-chain non-coding RNA) >200 nucleotides is located on chromosome 14, and it is related to the occurrence and progression of tumors [16]. lncRNA-ATB is improperly expressed in several cancers, particularly liver cancer [17], colon cancer [18, 19], pancreatic cancer [20], lung cancer [21, 22], breast cancer [23], and ovarian cancer [24, 25], based on research incorporating clinical correlation. Moreover, lncRNA-ATB is related to the prognosis of malignant tumors, including tumor stage, invasion, and metastasis, which directly or indirectly affect the recurrence and overall survival[26]. lncRNA-ATB is also a promising diagnostic index or an index related to drug resistance in some tumors [26–29].

Similarly, lncRNA-ATB was remarkably expressed in GC cells than in adjacent tissues. Increased lncRNA-ATB increases the infiltration depth, distant metastasis, and late tumor lymph node metastasis, affecting the overall survival of GC patients [30]. lncRNAs may act as sponges by competitively binding to microRNAs (miRNAs), thereby inhibiting the active functions [31]. Moreover, lncRNA-ATB silencing can upregulate miR-200 family and induce apoptosis through Bcl-2/caspase 3 pathway in lung cancer and prostate cancer [7, 21]. lncRNA-ATB can also upregulate ZEB1 and ZEB2 by competitively binding to miR-200 family in various tumors [32, 33], resulting in proliferation, migration, and invasion. However, lncRNA-ATB silencing can significantly inhibit ZEB1 and ZEB2 expression, thus inhibiting cell migration and invasion [17, 34]. These results indicate that lncRNA-ATB can affect EMT by competitively binding with miR-200a, thus promoting tumor metastasis in GC [35, 36]. Type I cadherin (epithelial cadherin and E-cadherin) is transformed into N-cadherin and Vimentin (mainly expressed in mesenchymal cells) during EMT [37]. In this study, HGC-27 was selected for follow-up experiments because it had lower E-cadherin and miR-200a levels and higher lncRNA-ATB, Vimentin, N-cadherin, and ZEB-1 levels. XTSJ has been proven in previous research to suppress proliferation, angiogenesis, invasion, and migration [10, 12, 38, 39]. This might be due to the fact that XTSJ lowers lncRNA-ATB and promotes competitive binding to miR-200a, lowering ZEB-1-mediated EMT and Bcl-2-mediated apoptosis. Reduced levels of Vimentin and N-cadherin associated with a mesenchymal phenotype and increasing levels of E-cadherin associated with an epithelial phenotype defined EMT reversal. However, more research should be conducted to identify the major target and effector chemicals of XTSJ that inhibit lncRNA-ATB expression. Furthermore, no research has demonstrated XTSJ's therapeutic effectiveness or associated biomolecular signals in human GC.

In conclusion, XTSJ may affect EMT and Bcl-2 signaling pathways by regulating lncRNA-ATB and miR-200a, thus inhibiting proliferation, migration, and invasion of HGC-27 cells. Therefore, XTSJ may be an effective treatment for the high level of lncRNA-ATB in GC.

Data Availability

The data used to support the findings of this study are included within the article.

Conflicts of Interest

The authors declare that they have no conflicts of interest.

Authors' Contributions

Cai KQ, Yu ZH, and Zhou Z designed this research. Zhou Z, Chen JB, Li MQ, Cao LP, Chen M, and Zhang QQ participated in the implementation of the experiment. Zhou Z, Li MQ, Yu ZH, and Cai KQ wrote and proofread manuscript. Zhou Z and Chen JB contributed equally to this work.

Acknowledgments

References

[1] J. Machlowska, J. Baj, M. Sitarz, R. Maciejewski, and R. Sitarz, "Gastric cancer: epidemiology, risk factors, classification, genomic characteristics and treatment strategies," *International Journal of Molecular Sciences*, vol. 21, no. 11, 2020.

[2] K. Wang, Q. Chen, Y. Shao et al., "Anticancer activities of TCM and their active components against tumor metastasis," *Biomedicine & Pharmacotherapy*, vol. 133, article 111044, 2021.

[3] L. Yang, J. Li, Z. Hu et al., "A systematic review of the mechanisms underlying treatment of gastric precancerous lesions by traditional Chinese medicine," *Evidence-Based Complementary and Alternative Medicine*, vol. 2020, Article ID 9154738, 12 pages, 2020.

[4] N. G. Lintner and J. H. D. Cate, "Regulating the ribosome: a spotlight on RNA dark matter," *Molecular Cell*, vol. 54, no. 1, pp. 1-2, 2014.

[5] C. P. Ponting, P. L. Oliver, and W. Reik, "Evolution and functions of long noncoding RNAs," *Cell*, vol. 136, no. 4, pp. 629–641, 2009.

[6] M. Cesana, D. Cacchiarelli, I. Legnini et al., "A long noncoding RNA controls muscle differentiation by functioning as a competing endogenous RNA," *Cell*, vol. 147, no. 2, pp. 358–369, 2011.

[7] H. Lin, L. Yang, F. Tian et al., "Up-regulated lncRNA-ATB regulates the growth and metastasis of cholangiocarcinoma via miR-200c signals," *OncoTargets and Therapy*, vol. 12, pp. 7561–7571, 2019.

[8] J. H. Yuan, F. Yang, F. Wang et al., "A long noncoding RNA activated by TGF-beta promotes the invasion-metastasis cascade in hepatocellular carcinoma," *Cancer Cell*, vol. 25, no. 5, pp. 666–681, 2014.

[9] Y. Chen, G. Wei, H. Xia, Q. Tang, and F. Bi, "Long noncoding RNAATB promotes cell proliferation, migration and invasion in gastric cancer," *Molecular Medicine Reports*, vol. 17, no. 1, pp. 1940–1946, 2018.

[10] J. Shi and P. K. Wei, "Xiaotan Sanjie decoction inhibits interleukin-8-induced metastatic potency in gastric cancer," *World Journal of Gastroenterology: WJG*, vol. 21, no. 5, pp. 1479–1487, 2015.

[11] M. Ye, D. Z. Sun, and P. K. Wei, "Inhibitory effect of Xiaotan Sanjie recipe on the microsatellite instability of orthotopic transplantation tumor in MKN-45 human gastric cancer nude mice," *Zhongguo Zhong Xi Yi Jie He Za Zhi Zhongguo Zhongxiyi Jiehe Zazhi= Chinese Journal of Integrated Traditional and Western Medicine*, vol. 34, no. 5, pp. 592–596, 2014.

[12] B. Yan, L. Liu, Y. Zhao et al., "Xiaotan Sanjie decoction attenuates tumor angiogenesis by manipulating Notch-1-regulated proliferation of gastric cancer stem-like cells," *World Journal of Gastroenterology: WJG*, vol. 20, no. 36, pp. 13105–13118, 2014.

[13] J. Y. Kishi, S. W. Lapan, B. J. Beliveau et al., "SABER amplifies FISH: enhanced multiplexed imaging of RNA and DNA in cells and tissues," *Nature Methods*, vol. 16, no. 6, pp. 533–544, 2019.

[14] M. Lai, L. Liu, L. Zhu et al., "Triptolide reverses epithelial-mesenchymal transition in glioma cells via inducing autophagy," *Annals of Translational Medicine*, vol. 9, no. 16, p. 1304, 2021.

[15] G. L. Sun, Z. Li, W. Z. Wang et al., "miR-324-3p promotes gastric cancer development by activating Smad4-mediated Wnt/beta-catenin signaling pathway," *Journal of Gastroenterology*, vol. 53, no. 6, pp. 725–739, 2018.

[16] J. C. Wang, Z. Buser, D. E. Fish et al., "Intraoperative death during cervical spinal surgery: a retrospective multicenter study," *Global Spine Journal*, vol. 7, Supplement 1, pp. 127S–131S, 2017.

[17] F. Chen, Y. Li, Y. Feng, X. He, and L. Wang, "Evaluation of antimetastatic effect of lncRNA-ATB siRNA delivered using ultrasound-targeted microbubble destruction," *DNA and Cell Biology*, vol. 35, no. 8, pp. 393–397, 2016.

[18] T. Iguchi, R. Uchi, S. Nambara et al., "A long noncoding RNA, lncRNA-ATB, is involved in the progression and prognosis of colorectal cancer," *Anticancer Research*, vol. 35, no. 3, pp. 1385–1388, 2015.

[19] B. Yue, S. Qiu, S. Zhao et al., "LncRNA-ATB mediated E-cadherin repression promotes the progression of colon cancer and predicts poor prognosis," *Journal of Gastroenterology and Hepatology*, vol. 31, no. 3, pp. 595–603, 2016.

[20] S. Qu, X. Yang, W. Song et al., "Downregulation of lncRNA-ATB correlates with clinical progression and unfavorable prognosis in pancreatic cancer," *Tumor Biology*, vol. 37, no. 3, pp. 3933–3938, 2016.

[21] T. Wang, X. Tang, and Y. Liu, "LncRNA-ATB promotes apoptosis of non-small cell lung cancer cells through miR-200a/beta-catenin," *Journal of BUON*, vol. 24, no. 6, pp. 2280–2286, 2019.

[22] L. Wei, T. Wu, P. He, J. L. Zhang, and W. Wu, "LncRNA ATB promotes the proliferation and metastasis of lung cancer via activation of the p38 signaling pathway," *Oncology Letters*, vol. 16, no. 3, pp. 3907–3912, 2018.

[23] Y. Zhang, J. Li, S. Jia, Y. Wang, Y. Kang, and W. Zhang, "Down-regulation of lncRNA-ATB inhibits epithelial-mesenchymal transition of breast cancer cells by increasing miR-141-3p expression," *Biochemistry and Cell Biology*, vol. 97, no. 2, pp. 193–200, 2019.

[24] D. Yuan, H. Qian, T. Guo et al., "LncRNA-ATB promotes the tumorigenesis of ovarian cancer via targeting miR-204-3p," *OncoTargets and Therapy*, vol. 13, pp. 573–583, 2020.

[25] D. Yuan, X. Zhang, Y. Zhao et al., "Role of lncRNA-ATB in ovarian cancer and its mechanisms of action," *Experimental and Therapeutic Medicine*, vol. 19, no. 2, pp. 965–971, 2020.

[26] F. Tang, Y. Xu, H. Wang, E. Bian, and B. Zhao, "LncRNA-ATB in cancers: what do we know so far?," *Molecular Biology Reports*, vol. 47, no. 5, pp. 4077–4086, 2020.

[27] N. E. El-Ashmawy, F. Z. Hussien, O. A. El-Feky, S. M. Hamouda, and G. M. Al-Ashmawy, "Serum LncRNA-ATB and FAM83H-AS1 as diagnostic/prognostic non-invasive biomarkers for breast cancer," *Life Sciences*, vol. 259, article 118193, 2020.

[28] S. J. Shi, L. J. Wang, B. Yu, Y. H. Li, Y. Jin, and X. Z. Bai, "Lncrna-ATB promotes trastuzumab resistance and invasion-metastasis cascade in breast cancer," *Oncotarget*, vol. 6, no. 13, pp. 11652–11663, 2015.

[29] W. Tang, X. Yu, R. Zeng, and L. Chen, "lncRNA-ATB promotes cisplatin resistance in lung adenocarcinoma cells by targeting the miR-200a/beta-catenin pathway," *Cancer Management and Research*, vol. 12, p. 2001, 2020.

[30] T. Saito, J. Kurashige, S. Nambara et al., "A long non-coding RNA activated by transforming growth Factor-β is an independent prognostic marker of gastric cancer," *Annals of Surgical Oncology*, vol. 22, Supplement 3, pp. S915–S922, 2015.

[31] C. L. Chen, Y. W. Tseng, J. C. Wu et al., "Suppression of hepatocellular carcinoma by baculovirus-mediated expression of long non-coding RNA PTENP1 and MicroRNA regulation," *Biomaterials*, vol. 44, pp. 71–81, 2015.

[32] U. Burk, J. Schubert, U. Wellner et al., "A reciprocal repression between ZEB1 and members of the miR-200 family promotes EMT and invasion in cancer cells," *EMBO Reports*, vol. 9, no. 6, pp. 582–589, 2008.

[33] C. C. Ma, Z. Xiong, G. N. Zhu et al., "Long non-coding RNA ATB promotes glioma malignancy by negatively regulating miR-200a," *Journal of Experimental & Clinical Cancer Research*, vol. 35, no. 1, p. 90, 2016.

[34] C. P. Bracken, P. A. Gregory, N. Kolesnikoff et al., "A double-negative feedback loop between ZEB1-SIP1 and the microRNA-200 family regulates epithelial-mesenchymal transition," *Cancer Research*, vol. 68, no. 19, pp. 7846–7854, 2008.

[35] J. Kozak, A. Forma, M. Czeczelewski et al., "Inhibition or reversal of the epithelial-mesenchymal transition in gastric cancer: pharmacological approaches," *International Journal of Molecular Sciences*, vol. 22, no. 1, 2020.

[36] H. Zhao, H. Hu, B. Chen et al., "Overview on the role of E-cadherin in gastric cancer: dysregulation and clinical implications," *Frontiers in Molecular Biosciences*, vol. 8, article 689139, 2021.

[37] J. Li, B. Yang, Q. Zhou et al., "Autophagy promotes hepatocellular carcinoma cell invasion through activation of epithelial-mesenchymal transition," *Carcinogenesis*, vol. 34, no. 6, pp. 1343–1351, 2013.

[38] C. J. Li, P. K. Wei, and B. L. Yue, "Study on the mechanism of Xiaotan Sanjie recipe for inhibiting proliferation of gastric cancer cells," *Journal of Traditional Chinese Medicine*, vol. 30, no. 4, pp. 249–253, 2010.

[39] J. Shi, Y. Lu, and P. Wei, "Xiaotan Sanjie decoction inhibits angiogenesis in gastric cancer through Interleukin-8-linked regulation of the vascular endothelial growth factor pathway," *Journal of Ethnopharmacology*, vol. 189, pp. 230–237, 2016.

Review Article
Antineoplastic Effects of Ankaferd Hemostat

Umit Yavuz Malkan [ID] **and Ibrahim Celalettin Haznedaroglu** [ID]

Hacettepe University, Faculty of Medicine, Department of Hematology, Ankara, Turkey

Correspondence should be addressed to Umit Yavuz Malkan; umitmalkan@hotmail.com

Objective. Ankaferd hemostat (ABS; Ankaferd Blood Stopper®) contains standardized plant extracts comprising Alpinia officinarum, Glycyrrhiza glabra, Thymus vulgaris, Urtica dioica, and Vitis vinifera. ABS especially was recognized for its hemostatic effect; however, antineoplastic role of ABS was identified during the last decade. The aim of this paper is to review the molecular basis and associated clinical implications of the ABS as a topical antineoplastic agent. *Materials and Methods*. Up to June 2022, literature searches were performed using the internet search engines Medline, Google Scholar, and Embase: Ankaferd. PRISMA flow diagram described the Ankaferd search. *Results*. ABS have important effects in several cellular processes, like control of the cell cycle, apoptosis, angiogenesis, signal transduction, inflammation, immunologic, and metabolic mechanisms. The molecular basis of antineoplastic roles of ABS depends on its proteomics, metabolomics, and transcriptomics features. ABS has antineoplastic effects on solid tumors like colon, bladder, breast, and osteosarcoma cancer cells. Also, ABS effects renal tubular apoptosis and has antitumoral roles on malign melanoma cells. ABS inhibits hematological tumors like myeloma and lymphoid cells. ABS induces apoptosis in retinal cells and has inhibitory effects on mesenchymal stem cells. It has an antiproliferative role on gastrointestinal tumors like hepatocellular carcinoma cells. Moreover, ABS has a treatment supportive role in cancer since it can prevent oxidative DNA damage and decrease the intestinal damage in necrotizing enterocolitis. Furthermore, it has chemopreventive and hepatoprotective features and can be used for prophylaxis and treatment of oral mucositis. *Conclusion*. ABS alters cell metabolism and cell cycle. ABS has antineoplastic role on cancer cells. The expanding context of ABS compromises anti-infective, antineoplastic, and wound healing features. ABS may also be used for the palliative, adjuvant, neoadjuvant, or supportive use by interventional radiology procedures for the treatment of solid tumors. Future controlled studies are necessary to clarify the pleiotropic role of ABS like antineoplastic, antithrombotic, anti-inflammatory, anti-infective, antifungal, and antioxidative effects.

1. Introduction

Ankaferd hemostat (ABS; Ankaferd Blood Stopper®) contains standardized plant extracts comprising Alpinia officinarum, Glycyrrhiza glabra, Thymus vulgaris, Urtica dioica, and Vitis vinifera [1]. These plant extracts have unique roles on the endothelium, blood cells, angiogenesis, cell growth, and cell mediators [2–4]. ABS especially was recognized for its hemostatic effect. ABS induces the creation of a protein network that has relationship between ABS and blood proteins, particularly with fibrinogen-gamma. Protein agglutination and erythroid aggregation are the two main mechanisms of ABS stimulated protein network. Spectrin,

ankyrin, and actin are unique proteins which are controlled by ABS throughout erythroid aggregation course [5]. On the other hand, antineoplastic role of ABS was identified during the last decade. The aim of this paper is to review the molecular basis and associated clinical implications of the ABS as a topical antineoplastic agent.

2. Materials and Methods

Up to June 2022, literature searches were performed using the internet search engines Medline, Google Scholar, and Embase: Ankaferd. Only articles written in English were taken in the search. All abstracts were scanned. The studies

that were found to be methodologically weak and not related with antineoplastic effects of Ankaferd were excluded. Articles in full text were assessed for eligibility and quality.Then, the qualitative synthesis included the following studies (Figure 1).

3. Molecular Basis of Antineoplastic Roles of Ankaferd Hemostat: Proteomics, Metabolomics, and Transcriptomics

ABS increases the level of various types of proteins and factors acting on cellular effects such as protein-2 (AP2), androgen receptor (AR), cyclic AMP response element or stimulating transcription factor-1 (CREATF1), cyclic AMP response element binding protein (CREB), E2F1–5, E2F6, EGR, interferon- (IFN-) stimulated response element (ISRE), Myc-Max, nuclear factor-1 (NF-1), protein53 (p53), SMAD2/3, peroxisome proliferator-activated receptor (PPAR), and Yin-Yang (YY1). These factors have important effects in several cellular processes, like control of the cell cycle, apoptosis, angiogenesis, signal transduction, inflammation, immunologic, and metabolic mechanisms [2].

Apoptosis seems to be the primary mechanism of action underlying antineoplastic effects of ABS. ABS can stimulate apoptosis in leukemia cells. Endothelial cell protein C receptor (EPCR) belongs to the activated protein C anticoagulant pathway. EPCR effect has not been completely clarified in various cell types where EPCR is known to be present, for example, hematopoietic cells and cerebral smooth muscle cells [6]. Protease-activated receptor 1 (PAR1) belongs to proteinase-activated receptor (PARs) family that present in seven transmembrane G-protein-coupled receptors group [7]. Stimulated PAR1 controls intracellular signaling by coupling G proteins. ABS modifies PAR1 and EPCR expression in K-562 and Jurkat cells in a time- and dose-dependent way. The role of PAR1 and p21 in this apoptotic mechanism was detected in Jurkat cells. ABS results in apoptosis via controlling PAR1- and p53-independent p21 involvement in apoptosis stimulation in leukemia cells, related with the concentration and duration of the application [8]. PAR1 has critical roles in hemostasis, inflammation, infection, apoptosis, and tumorigenesis. The effects of ABS on PAR-1 in the human umbilical vein endothelial cell (HUVEC) model and in relation to the "lipopolysaccharides- (LPS-) challenge" to endothelium were analyzed in a previous study [9]. In this study, ABS $10 \mu L$ and $100 \mu L$ had been given to HUVEC within the time periods of 5 minutes (min), 25 min, 50 min, 6 hours (h), and 24 h. The authors found dose-related reversible PAR1 decrease controlled via ABS inside the human umbilical vein endothelial cells. ABS-stimulated continuous PAR1 decreases with LPS. ABS is suggested as a topical biological response controller by altering PAR1 at the vascular endothelial and cellular level [9].

ABS has effects on colon cancer cells. The mechanism of antineoplastic effect of ABS over the Caco-2 colon cancer cells has been evaluated (Figures 2 and 3) [10]. ABS found to change glucose, fatty acids, and protein metabolisms. Also, ABS found to effect the cell cycle machinery. Besides, ABS stimulated critical cancer target and suppressor proteins such as carboxyl-terminal hydrolase 1, 60S ribosomal protein L5, Tumor protein D52-like2, karyopherin alpha 2, and protein deglycase DJ-1 were identified [10]. ABS has different effects on cancer targets and inhibitory proteins. ABS alters the cell metabolism and cell cycle in Caco-2 cells.

ABS has effects on renal tubular apoptosis. The effect of ABS, on renal tubular apoptosis and on expressions of endothelial nitric oxide synthase (eNOS), inducible nitric oxide synthase (iNOS), and apoptosis protease-activating factor-1 (Apaf-1) in the ipsilateral kidney was investigated [11]. ABS found to have a dual biphasic de novo effects on apoptosis. The challenge of severe hemorrhage in the renal tubular cellular microenvironment leads to ABS-stimulated decrease of the apoptotic molecules, suggesting that ABS can have role as a topical biological response controller.

ABS suggested to be a promising hemostatic agent in otology. Mucosal trauma stimulated apoptosis in guinea pig middle ear was investigated by comparing the hemostatic agents, absorbable gelatin sponge (AGS), microporous polysaccharide hemospheres (MPH), and ABS [12]. ABS and AGS groups showed lower epithelial thickness, inflammation, and capillary dilatation than did the control group. A reduction in Bcl-xl staining was detected in the middle ears of animals that were given MPH. Caspase 3 expression increased in the ABS and AGS groups than in the control group. Light microscopy clarified that ABS and AGS generate less inflammation and stimulated caspase expression that likely stimulate inflammatory cell apoptosis [12].

The resistance against chemotherapeutic drugs is a major problem in therapy of cancer. ABS has suggested to inhibit the development of melanoma cells, but mechanism is not yet fully clarified. ABS found to transfer some melanoma cell lines such as A2058 more sensitive to etoposide by changing the genes that have role in oxidative phosphorylation (OXPHOS) pathway [13]. ABS increases the sensitivity of A2058 against etoposide and has no effect against SK-MEL-5. The majority of the genes among oxidoreductase cluster found to take role in oxidative phosphorylation and electron transport chain [13]. The administration of ABS before etoposide may stimulate the response of melanoma cell lines because of the change of OXPHOS genes [13].

The antitumor effect of ABS on the MCF-7 breast cancer cell line was investigated [14]. The change of the levels of cancer-associated proteins of MCF-7 is upon application of ABS. Proteomic analysis clarified that ABS leads to an alteration in the levels of certain proteins including chaperones, p97, ATP5B, SELENBP1, PDIA6, and RPS10P5 [14]. ABS target certain proteins that were aberrantly expressed in breast cancer, especially the ER+ subtype [14].

ABS has effects on DNA, and it can prevent oxidative DNA damage [15]. In a previous study, the role of ABS on 8-hydroxy-2′-deoxyguanosine (8-OHdG), superoxide dismutase (SOD), and myeloperoxidase (MPO) levels over pleural adhesions in rabbits with pulmonary parenchymal damage was investigated [15]. The 8-OHdG levels were found to be lower in the ABS study group, and the differences between study and control groups were statistically
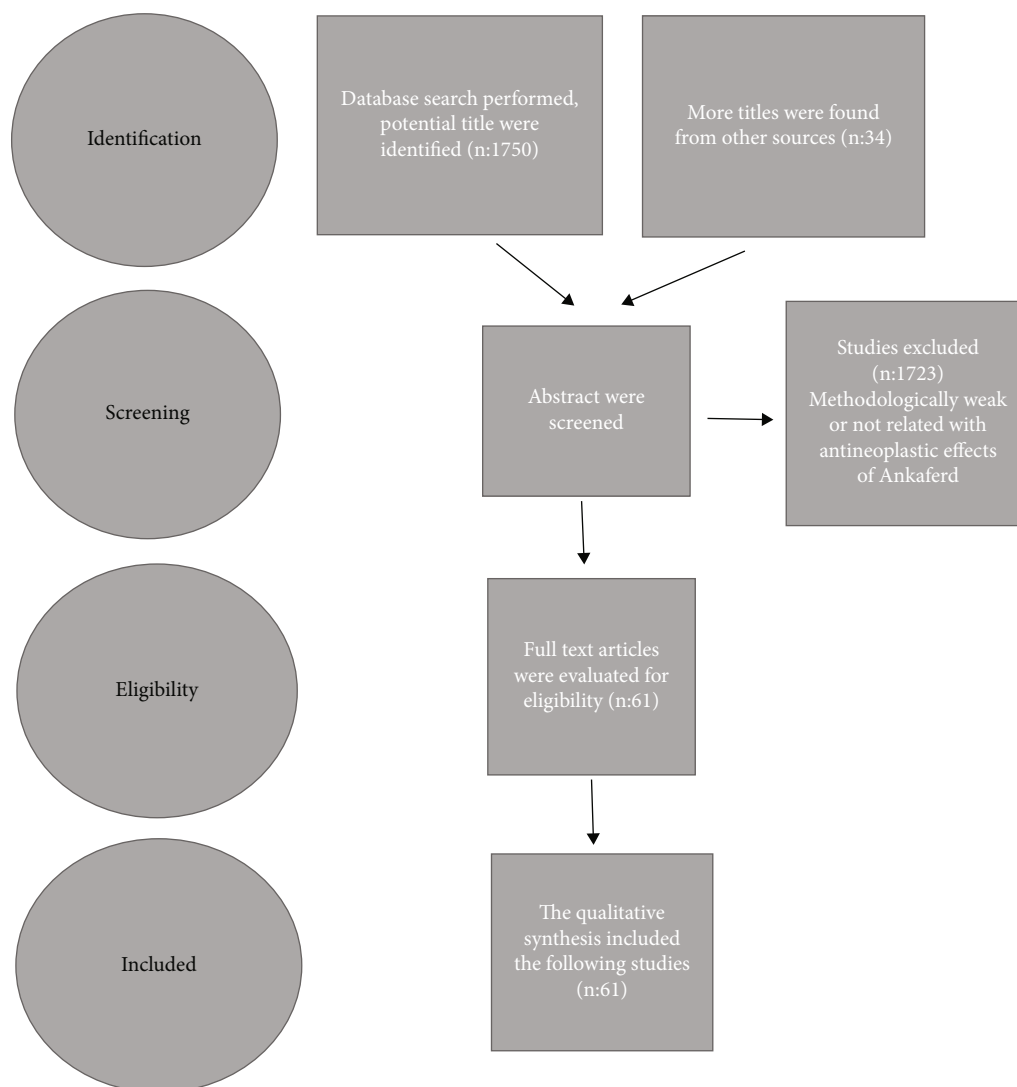
Figure 1: The PRISMA flow diagram for the Ankaferd search.

significant ($p < 0.001$). The difference of SOD and MPO levels is not statistically significant between the groups [15]. The prevention of oxidative DNA damage by ABS was proven.

ABS effects apoptosis on retinal cells [16]. In a previous analysis, the cellular apoptotic roles of ABS on rabbit retina tissues were investigated. ABS was given into the vitreous of right eye of five rabbits. Oxidative injury, apoptosis, protein carbonylation, and DNA breakup were analyzed. In the ABS given eyes, sodium dodecyl sulphate polyacrylamide gel electrophoresis pattern of protein bands was stimulated; however, the other bands were decreased. Apoptosis was postponed, clarified by the morphological methods and caspase activity in the ABS administrated eyes. ABS stimulates protein carbonyle generation and DNA breakup were showed in the rabbit retina [16]. ABS showed to have an important role on apoptosis. ABS-related reductions of apoptosis in the retinal microenvironment showed that ABS may have a role as a topical biological response controller.

The antioxidant and antimutagenic features of ABS were investigated in a previous study [17]. The antioxidant effects were investigated using 2,2-diphenyl-1-picrylhydrazyl (DPPH) radical-scavenging and β-carotene-linoleic acid tests. The antimutagenic role was detected using the Ames Salmonella/microsome mutagenicity test with the bacterial mutant strains Salmonella typhimurium TA98 and TA100. ABS showed no free-radical-scavenging effects in DPPH assays at the analyzed concentrations; however, β-carotene-linoleic acid analysis revealed that ABS has total antioxidant activity rate of $47.06 \pm 4.41\%$. Antimutagenic activity was found on TA100 at plate concentrations of 5%, 0.5%, and 0.05%, and on TA98 only at a plate concentration of 5%. ABS was proven to have antioxidant and antimutagenic features [17].

The proteomics, metabolomics, and transcriptomic of ABS are important to understand the molecular basis of antineoplastic effects of ABS. ABS has showed several pleiotropic roles, like antineoplastic and antimicrobial effects and tissue-healing features. Ankaferd's individual ingredients were clarified by the proteomic and chemical tests. ABS stimulates transcription of some transcription factors that is shown with transcriptomic analysis. ABS has showed
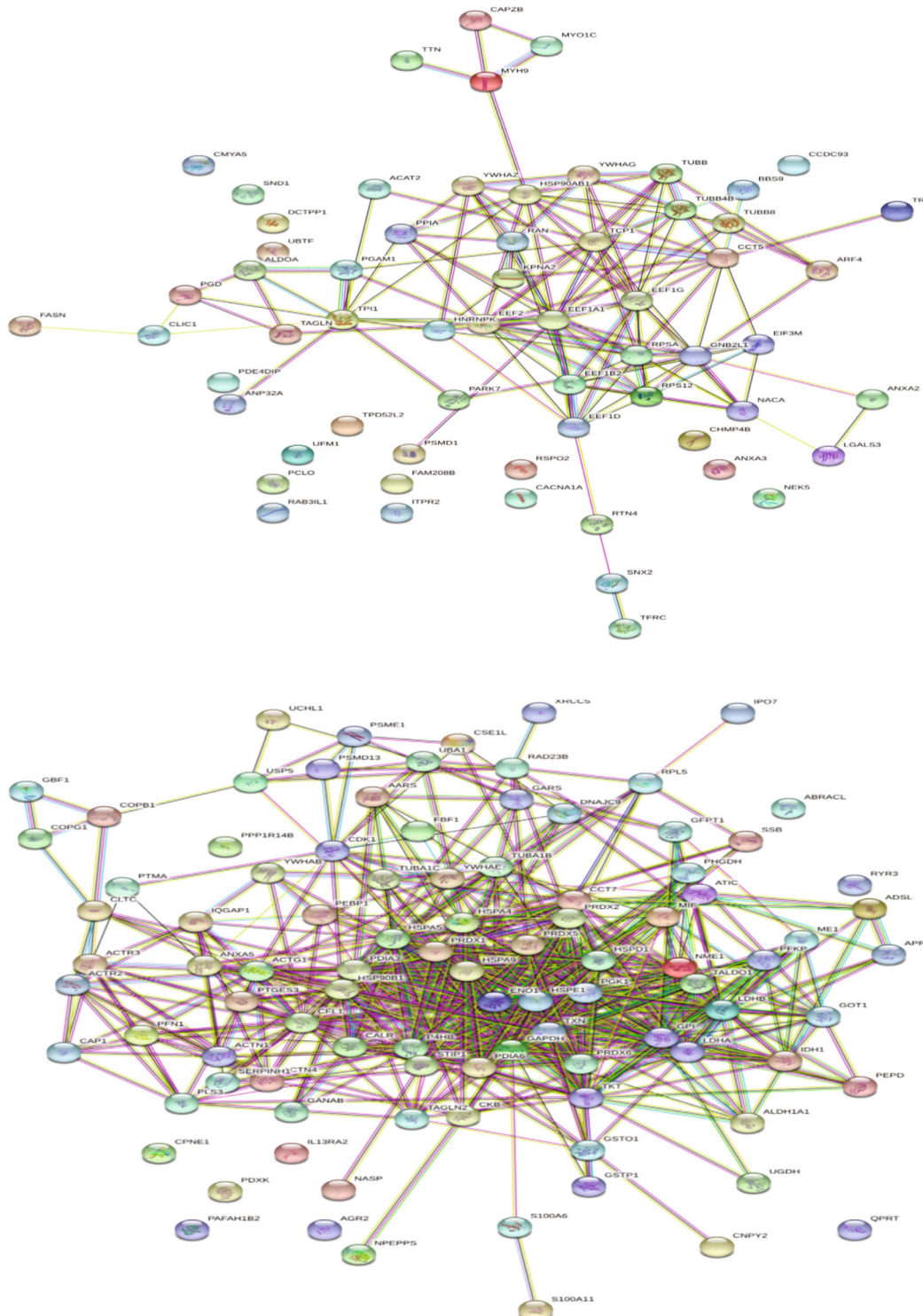
Figure 2: The scheme of downregulated (a) and upregulated (b) proteins after Ankaferd hemostat (ABS) given on the human colon cancer cell line, CACO-2 (reproduced with the open access policy of the Journal; Bio Med Res (https://www.hindawi.com/journals/bmri/2019/5268031/fig 4/).

cytotoxicity against human erythrocytes and tumoral cells in multiple myeloma, chronic myelogenous leukemia, and lymphoma [18–20]. Cyclic AMP response element-binding protein (CREB)/ATF BZIP transcription factor (CREBZF), PIAS-2, hepatocyte nuclear factor (HNF-4a), malic enzyme

(ME-1), P18INK4C, and Midkine are the possible associated ingredients of ABS for this effect. ABS has shown to stimulate the expression of CREBZF resulting to the stimulation of the antineoplastic protein p53 [21]. HNF-4a has antineoplastic effects, and it is a component of ABS and might be
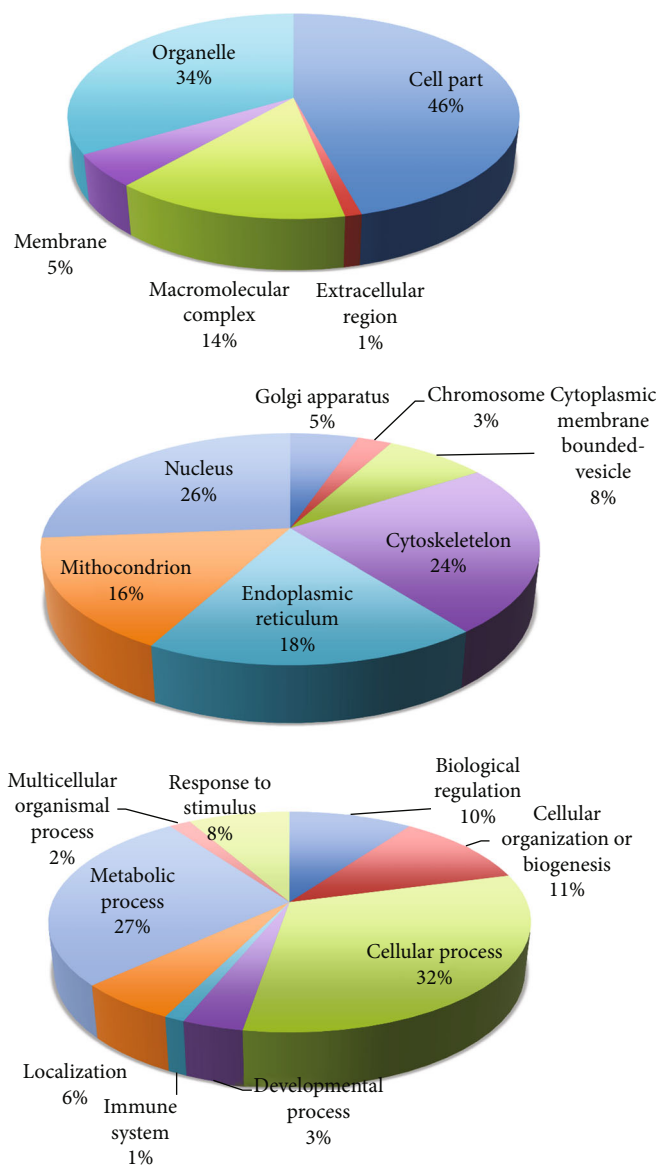
FIGURE 3: The classification of upregulated proteins in cellular component (a), in organelles (b), and in cellular processes (c) after Ankaferd hemostat (ABS) given on the human colon cancer cell line, CACO-2 (reproduced with the open access policy of the Journal; Bio Med Res (https://www.hindawi.com/journals/bmri/2019/5268031/fig 3/).

partially responsible for its antitumorigenic effects [22]. ME-1 is an intracellular cytosolic protein, and it converts malic acid to pyruvic acid, creating nicotinamide adenine dinucleotide phosphate (NAPDH) [23, 24]. ME-1 has significant effects on cancer metabolism because NADPH is necessary for anaerobic respiration, and ME-1 level is found to be high in some cancers. ME-1 is also found in ABS. Midkine is a heparin-binding protein that has significant effect in tumoral angiogenesis, and its blockade can inhibit tumor growth [25, 26]. Protein inhibitor of activated signal transducer and activator of transcription- (PIAS-) 2 belong to the PIAS family, whose members inhibit the activity of the STAT proteins [27]. JAK-STAT signaling is an important pathway which has role in human carcinogenesis [28]. Cyclin-dependent kinase (CDK) inhibitor P18INK4C decreases tumorigenesis [29].

Its deficiency may cause tumor growth [30, 31]. CDKs are serine/threonine kinases which control the cell cycle. P18INK4C may have a role in the tumor-suppressor activity of ABS by suppressing CDKs. ABS has effects on the targets on cancer therapy like SND1, KPNA2, and PARK7. ABS upregulates the tumor suppressor proteins UCHL1 and RPL5. RPL5 stimulates the p53 apoptotic mechanism and leads to apoptosis [32].

ABS has several roles on transcriptomic also. ABS stimulates the transcription factors of AP2, AR, CREATF1, CREB, E2F1-5, E2F6, EGR, GATA, HNF1, ISRE, Myc-Max, NF1, NF-κB, p53, PPAR, SMAD2/3, SP1, TRE/AP1, and YY1. These transcription factors control several biological mechanisms, like hemostasis, infection, cellular growth, and inflammation [33]. GATA controls erythroid differentiation and increases the erythroid proteins like spectin.
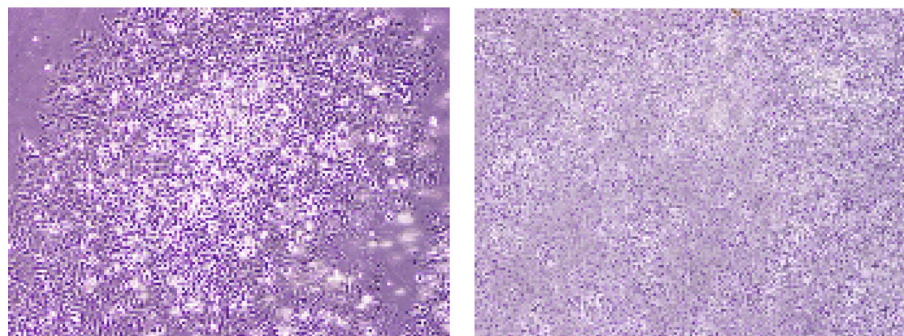
FIGURE 4: The inhibitory effect of Ankaferd Hemostat (ABS) on the Saos-2 cells. (a) The control group without ABS (10× magnification). (b) $10\,\mu$L ABS given Saos-2 cells (10× magnification) at the seventeenth day.

GATA is found to be increased after ABS administration [33]. ABS increases the following transcription factors; AP2, AR, CRE-ATF1, CREB, E2F1-5, E2F6, EGR, ISRE, Myc-Max, NF1, NF-κB, p53, PPAR, SMAD2/3, SP1, TRE/AP1, and YY1. These molecules have role in several stages of cellular growth, like control of cell cycle, signal transduction, angiogenesis, apoptosis, inflammation, acute phase reaction, immunity, and various metabolic molecular mechanisms [33].

4. Ankaferd Hemostat in Hematological Tumors

ABS has antineoplastic and cellular differentiation effects on the lymphoid cells [18]. ABS interacts tumor associated transcription factors. Effects of ABS on lymphoid neoplastic cells investigated in a previous study. ABS-treated B-CLL cells (at doses 0.5, 1 and 2μg/mL) stopped inflating, and more than half of tumor cells were died compared to 0.1 and 0.25μg/mL doses. Moreover, transformation of B-CLL cells to the blastic aggressive lymphoid forms was inhibited by ABS. ABS has antineoplastic effects at higher doses (>0.5μg/mL), and it stimulates the cellular differentiation at lower doses (<0.5μg/mL).

The role of ABS against myeloma cells in vitro and plasmocytoma generation in Balb/c mice was analyzed in vitro. The antineoplastic effect of ABS to the myeloma cells was detected by the 3-(4,5-dimethylthiazol-2-yl)-2,5-diphenyltetrazolium bromide-dye reduction assay [19].

5. Ankaferd Hemostat in Malign Melanoma

There is an unmet need for novel therapeutic and/or complementary methods in malign melanoma because the 5-year survival duration of metastatic melanoma patients is under 25% [34]. Plant extracts can have antineoplastic effects and can work synergistically with the conventional chemotherapeutics [35]. Melanocytes secrete "melanin" pigment. Melanocytes may transform into melanoma if their DNA injures [36]. The treatment response of nonmelanoma skin cancers to medical treatment is higher than melanoma. Melanoma cases have been rising nowadays, and nearly 53,000 people die annually worldwide because of melanoma [37]. ABS has antitumor effect on the primary melanoma

cells and cell lines. In a recent study, the effect of ABS on dissimilar melanoma cell lines and primary cells was analyzed [35]. SK-MEL-10 (CVCL_6020), SK-MEL-9 (CVCL_U934), A2058 (ATCC® CRL-11147™), and MeWo (ATCC HTB-65™) melanoma cell lines were used in the study. These cells were given various amounts of ABS to detect the role of various dosages. An important reduction in cell viability against the control groups was detected in the cells that were treated with ABS. Also, increasing the concentration of ABS and the incubation during had a negative effect on cell viability. As a result, the antineoplastic effect of ABS on various melanoma cells has been proven [35].

In another study, cytotoxic, genotoxic, apoptotic, and reactive oxygen generating (ROS) effects of ABS were analyzed in the melanoma and normal cell lines. The cells were exposed to various concentrations of ABS (0.125 to 2%) for twenty-four hours. ABS was found to stimulate DNA injury, apoptosis, and ROS levels in both melanoma and normal cells in a dose-related way [38]. Moreover, these activities were considerably greater in melanoma cells than in normal cells.

6. Ankaferd Hemostat in Solid Tumors

ABS has antineoplastic effects on solid tumors [39]. The antineoplastic effects of ABS on osteosarcoma cell line (SAOS-2) survival and growth were investigated previously (Figure 4) [40]. Saos-2 which is generally used in drug resistance analyses was cultured in RPMI media containing 10% FCS, 1% pen/strep, and 1% sodium pyruvate. Then, cells were moved into 12-well tissue plates, in which 2, 4, 6, 8, and 10μL/mL concentrations of ABS solution were given to the stimulate medium. A control group was prepared in a fresh growth medium without ABS. Increase of the Saos-2 cells was followed-up for the 17 days during which yellow and opaque-like aggregates were detected in cultures increasing with ABS. A dose-dependent decrease was detected in cell proliferation, and a significant decrease was found in the survival of Saos-2 cells. Aggregate formation augmented after higher doses of ABS, and dose-related decrease was found in cell invasion [2]. ABS given Saos-2 osteosarcoma cells were detected to lose adhesion in vitro. A dose-related blockade in cell growth and an important
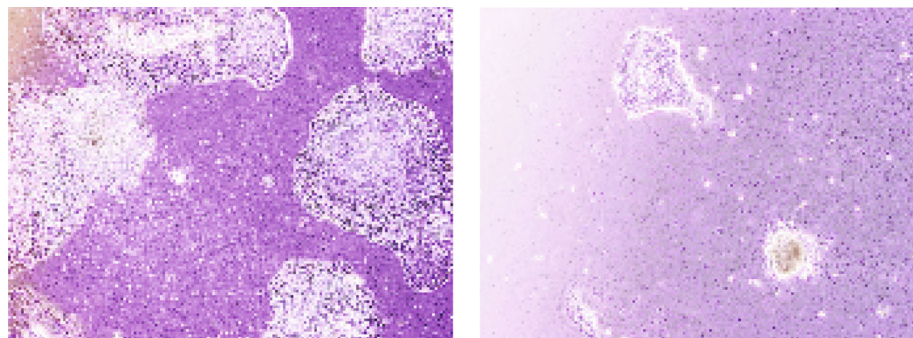
Figure 5: The inhibitory effect of Ankaferd Hemostat (ABS) on the CaCo-2 cells. (a) The control group without ABS (10× magnification). (b) 10 μL ABS given CaCo-2 cells (10× magnification) at the sixteenth day.

decrease were found in the survival of SAOS-2 cells with ABS.

ABS has anticancer role also in colon cancer [10]. Currently, alcohol, N-butyl-2-cyanoacrylate, and caustic materials are utilized as tumor embolizers. In colon cancer liver metastases and hepatocellular cancer cases, ABS may be utilized for the palliative, adjuvant, neoadjuvant, or supportive role via interventional radiology methods for the treatment of solid tumors [41]. In a different study, the antineoplastic role of ABS on the colon cancer cells was identified [42]. After the administration of ABS to the culture medium, the decrease of cellular reproduction and loss in the viabilities of the human colon CaCo-2 cells were detected. The cultures were cultivated independently in 12-well tissue-culture containers where ABS with 2, 4, 6, 8, and 10 μL/mL amounts was given to the culture medium. Cultivated cells without ABS in culture medium were prepared as a control group. The increase of CaCo-2 cells was followed-up for 16 days. ABS administration to culture medium leads to an increase in yellow and cloudy aggregates, together with enlarged amount of ABS. As a result, the inhibition of cellular reproduction and loss in the viabilities of the human colon CaCo-2 cells were associated with ABS concentrations in vitro (Figure 5) [42]. Another study regarding the Caco-2 cell also focused on the antineoplastic effects of ABS. The LC/MS-based proteomics technique was performed to analyze the role of ABS at the protein level [43]. The results were assessed with gene ontology, protein interaction, and pathway analysis. As a result of the study, ABS was found to alter glucose, fatty acids, and protein metabolism. Also, ABS has role in the cell cycle machinery. Furthermore, ABS was found to stimulate critical cancer target and suppressor proteins such as carboxyl-terminal hydrolase 1, 60S ribosomal protein L5, Tumor protein D52-like2, karyopherin alpha 2, and protein deglycase DJ-1 [43]. The proteomics results show that ABS affects various cancer targets and suppressor proteins. ABS has role on the cell metabolism and cell cycle in Caco-2 cells and indicates that ABS may be used as an antineoplastic treatment agent.

In a previous analysis, the molecular role of ABS on colon cancer was investigated. In the study, comparative analyses were performed with transcriptomic, proteomic, and metabolomic techniques on cancerous cells and untreated cancer cells in which antineoplastic effect was detected. As a result of this study, ABS was found to affect the biochemical processes happening in the cell with definite pathways. The levels of proteins such as Vinculin, Ezrin and HMGB1, that have roles in the mechanism of cancer, are altered by ABS and quantities of metabolites such as glutathione [44]. ABS affects several biological mechanisms as well as antioxidant activity and particularly cancer cell defense mechanisms.

ABS has also antineoplastic effects on bladder cancer. A previous study was conducted to analyze the antineoplastic role of ABS on bladder carcinoma in ex vivo patient tumor samples [45]. According to the results in the study, viability of cells decrease and the death rates of cells increased in statistically significant manner in bladder cancer cell cultures with ABS. Moreover, one of the main symptom of bladder cancer is bleeding. Therefore, the intravesical use of ABS may be beneficial, that has both haemorrhagic and antineoplastic features, in the control of patients with haematuria or postoperative bleeding after transurethral bladder resection. In the study, minimum 0.5 cm parts of fresh frozen tumor samples from patients with bladder tumor from 2015 to 2017 were collected. Primary bladder cancer cultures were collected from the frozen tumor samples. Two various doses of ABS were given on tumor cell cultures. Viability tests of each cell cultures were conducted. Flow cytometry was performed for the testing of apoptosis and necroptosis. Decreased cancer cell viability ratio in each ABS group compared with their own controls was found. Necroptosis was detected in the great majority of ABS groups, and necroptosis and apoptosis were found in some cell cultures [45]. The cytotoxic effect of ABS on bladder cancer cells was shown in the study. ABS may have potential for intravesical treatment agent for bladder cancer.

The role of ABS on breast cancer is also investigated in another study. Reduced cancer cell viability ratio in each ABS group against with their own controls was detected in a study [46]. Necroptosis was found in majority of ABS groups, and necroptosis and apoptosis were observed in breast cell cultures. The cytotoxic effect of ABS on breast cancer cells was well-demonstrated [46].

Being easily multiplication in vitro and having clinical usage potential in many fields primarily like hematopoietic stem cell transplants, regenerative medicine, tissue engineering, and gene therapy, mesenchymal stem cells pull
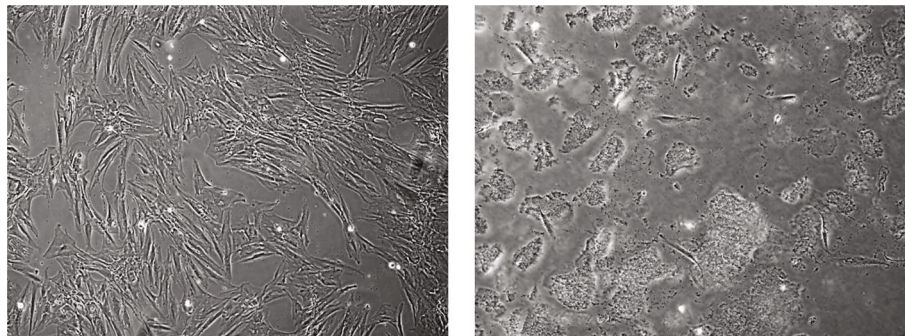
FIGURE 6: In vitro proliferation of the MSCs was negatively affected by Ankaferd Hemostat (ABS) due to intense aggregation. (a) The control group without ABS (10× magnification). (b) 10 μL ABS given mesenchymal stem cells (10× magnification) at the fourteenth day.

attention. In a previous study, the contribution of stromal oriented mesenchymal stem cells (MSC) to the bleed stopping and wound healing effects of ABS is investigated in in vitro environment [47]. MSCs had been described by flow cytometry according to their differentiation potentials and surface antigen properties. Those MSC obtained from healthy bone marrow transplant donors grown in the DMEM-LG media having 10% fetal calf serum and 1% pen/strep. In the first group, ABS solution in 2, 4, 6, 8, 10, 25, 50, and 100 μL/mL concentrations was added to the MSC cell groups which were confluent and grown in 12 pit tissue culture dishes. As a control group, cells to which medicine was not added and growing media were used. In the second group, by adding ABS solution to DMEM-LG having no serum, its effect to cells growth was investigated. Cells were followed for a period of 14 days. When liquid and homogenous ABS is added to the MSC growing media, aggregate formation was observed. It was observed that granule formation in cells showing adhesion or cells not sticking to culture dishes and aggregation was increased depending upon the ratio of ABS added to culture media. Since the cells have separated from the medium and have adhered to each other, further development steps could not be observed. Consequently, it is determined that ABS, when used in these ratios, affects culture media negatively on in vitro proliferation of MSCs due to intense aggregation (Figure 6) [47]. The effects of ABS in vitro in lower concentrations and its in vivo effects over cancer stem cell and in vivo stem cell dynamic need to be clarified.

7. Ankaferd Hemostat in Gastrointestinal Tumors

ABS has antineoplastic activity in hepatocellular carcinoma. In a previous analysis, HEPG2 hepatocellular carcinoma cells were given 8 μL/mL of ABS for 24 hours, and the alterations were analyzed on both proteomic and genomic manners [48]. ABS did not decrease cell viability subsequent to 24 hours of the therapy but, and ABS inhibited cell viability after 72 hours. On the other hand, at the 24 hours of therapy with ABS, genomic and oncoproteomic tests showed diversification. Protein processing networks in endoplasmic reticulum that control protein folding, relocation, and degradation were altered by ABS. Moreover, mitochondrial apoptotic

pathway can be stimulated by the hnRNP F-p53 interaction with the elongation of the ABS exposure period. ABS did not lead to P-glycoprotein-dependent drug resistance differently from several other used chemotherapeutics; therefore, ABS may also be used as combination treatment [48].

8. Ankaferd Hemostat as a Supportive Treatment of Cancer

ABS has chemopreventive, antioxidant, and supportive effects [49]. The chemopreventive role of ABS in 7,12-dimethylbenz[a]anthracene- (DMBA-) induced oral epithelial dysplasia is investigated in a previous study [49]. The buccal pouches of animals exposed to DMBA alone showed severe dysplasia; however, only mild or no dysplasia was found in DMBA + ABS group. ABS was also given to animals, and the control group revealed no dysplasia or other oral lesions [49]. The chemopreventive effect of ABS against DMBA-induced oral epithelial dysplasia was proven.

ABS is also beneficial in prophylaxis and treatment of oral mucositis [50]. In a previous study, the role of ABS in the prophylaxis and therapy of oral mucositis in patients who were given chemotherapy in childhood was investigated. In the study, citrulline which is a biochemical marker for mucosal barrier damage was analyzed, and the role of ABS treatment in mucositis was related to quantitative data along with the clinical findings. There was no important difference between the chemotherapy courses given with standard oral care (SOC) and with ABS plus SOC before chemotherapy, but an important difference was found between these courses after chemotherapy about stages of oral mucositis. The extent of the reduction in serum citrulline levels was found to be higher in the chemotherapy courses with SOC than in those with SOC plus ABS. As a result, ABS was considered as an effective agent for the prophylaxis and therapy of oral mucositis secondary to chemotherapy in childhood cancers [50].

On the other hand, ABS is also effective in chemotherapy-induced oral mucositis in adult population [51]. Oral mucositis is one of the most severe complications of anticancer therapy that affects 40-80% of cancer patients. The safety and efficacy of ABS in the management of chemotherapy-related oral mucositis in patients with hematological malignancies are analyzed previously. ABS was administrated to the patients

with grade 3-4 mucositis. After the patients' mouthwash and swallow the five milliliters of ABS, the healing time was calculated. Median healing time was found as 6.6 days [51]. As a result, ABS can play an important role in the therapy of chemotherapy-associated severe oral mucositis in patients with hematological malignancies.

In another study, the chemopreventive role of ABS in 7,12-dimethylbenz[a]anthracene (DMBA) is related oral epithelial dysplasia. The buccal pouches of animals given DMBA alone showed up dysplasia while only moderate or no dysplasia was found in DMBA + ABS group [49].

Necrotizing enterocolitis (NEC) is an important health problem that leads to morbidity and mortality. Risk factors for NEC include prematurity, oxidative stress, inflammation, and apoptosis. Whether treatment with ABS decreased the severity of NEC in rat pups in an experimental NEC model is investigated. Total oxidant status, oxidative stress index, tumor necrosis factor α and interleukin-1β levels, lipid, protein, and deoxyribonucleic acid oxidation products were lower in the NEC + ABS group compared to NEC + saline group while total antioxidant status, glutathione, and superoxide dismutase levels were higher in the NEC + ABS group. ABS found to decrease the intestinal damage in NEC due to its antioxidant, anti-inflammatory, and antiapoptotic features [52].

ABS also has hepatoprotective features [53, 54]. In previous studies on the trace element and vitamin content of ABS, Akar et al. analyzed the Fe (III), Cu (II), Zn (II), and Ag (I) ions in ABS. Concentrations were 2163 ± 7, 2.56, 9.2, and 45.0 ppm, respectively, which indicates an association between high iron levels and the hemostatic action of ABS [55]. The absence of Pb (II), Ni (II), Cr (IV), Co (II), and Cd (II) ions in ABS was also shown [55]. Koluman et al. found various antioxidant molecules in ABS, such as vitamin E [56]. Akişin and Akar found the zinc content of ABS and the association between high zinc levels and the wound healing action of ABS [57]. Because of the antioxidative and hepatoprotective roles of the trace elements and vitamins like magnesium, calcium, vitamin D, vitamin B12, vitamin B9, vitamin A, and vitamin E [58–61]; antioxidative, antiinflammatory, and hepatoprotective roles of ABS may be related with its trace elements and vitamins.

9. Future Perspectives on Ankaferd Hemostat as a Topical Biological Response Modifier

ABS has hemostatic roles in bleedings and has several pleiotropic effects. The quick generation of a protein network, most importantly fibrinogen gamma, with the erythrocyte aggregation is responsible for the hemostatic role of ABS. The whole mechanism involves ABS-stimulated generation of the protein network by vital erythrocyte aggregation. Vital erythrocyte aggregation happens with the help of spectrin, ankyrin, and actin proteins on the membrane of the erythrocytes. ABS most importantly alters cell metabolism and cell cycle. ABS has antineoplastic role on cancer cells. The expanding context of ABS compromises anti-infective, antineoplastic, and wound healing features. ABS is generally used for to provide hemostasis and stimulate wound healing.

However, ABS may also be used for the palliative, adjuvant, neoadjuvant, or supportive use by interventional radiology procedures for the treatment of solid tumors. This theory may be analyzed in future clinical studies. Furthermore, future controlled studies are necessary to clarify the pleiotropic role of ABS like antineoplastic, antithrombotic, anti-inflammatory, anti-infective, antifungal, and antioxidative effects.

Data Availability

The data supporting this systematic review are from previously reported studies and datasets, which have been cited. The processed data are available from the corresponding author upon request.

Conflicts of Interest

The authors declare that there is no conflicts of interest regarding the publication of this article.

References

[1] Y. Beyazit, M. Kurt, M. Kekilli, H. Goker, and I. C. Haznedaroglu, "Evaluation of hemostatic effects of Ankaferd as an alternative medicine," *Alternative Medicine Review*, vol. 15, no. 4, pp. 329–336, 2010.

[2] B. Z. Haznedaroglu, Y. Beyazit, S. L. Walker, and I. C. Haznedaroglu, "Pleiotropic cellular, hemostatic, and biological actions of Ankaferd hemostat," *Critical Reviews in Oncology/Hematology*, vol. 83, no. 1, pp. 21–34, 2012.

[3] M. L. Sheela, M. K. Ramakrishna, and B. P. Salimath, "Angiogenic and proliferative effects of the cytokine VEGF in Ehrlich ascites tumor cells is inhibited by *Glycyrrhiza glabra*," *International Immunopharmacology*, vol. 6, no. 3, pp. 494–498, 2006.

[4] D. Ö. Demiralp, I. C. Haznedaroglu, and N. Akar, "Functional proteomic analysis of Ankaferd (R) Blood Stopper," *Turkish Journal of Hematology*, vol. 27, 2010.

[5] D. Ozel-Demiralp, N. Igci, B. Ayhan, Y. Egin, I. C. Haznedaroglu, and N. Akar, "Prohemostatic and antithrombin activities of Ankaferd hemostat are linked to fibrinogen gamma chain and prothrombin by functional proteomic analyses," *Clinical and Applied Thrombosis/Hemostasis*, vol. 18, no. 6, pp. 604–610, 2012.

[6] K. Fukudome and C. T. Esmon, "Identification, cloning, and regulation of a novel endothelial cell protein C/activated protein C receptor," *The Journal of Biological Chemistry*, vol. 269, no. 42, pp. 26486–26491, 1994.

[7] S. R. Macfarlane, M. J. Seatter, T. Kanke, G. D. Hunter, and R. Plevin, "Proteinase-activated receptors," *Pharmacological Reviews*, vol. 53, no. 2, pp. 245–282, 2001.

[8] M. Mumcuoglu, D. F. Akin, U. Ezer, and N. Akar, "Ankaferd blood stopper induces apoptosis and regulates PAR1 and EPCR expression in human leukemia cells," *Egyptian Journal of Medical Human Genetics*, vol. 16, no. 1, pp. 19–27, 2015.

[9] A. Karabiyik, S. Güleç, E. Yilmaz, I. Haznedaroglu, and N. Akar, "Reversible protease-activated receptor 1 downregulation mediated by Ankaferd blood stopper inducible with lipopolysaccharides inside the human umbilical vein endothelial cells," *Clinical and Applied Thrombosis/Hemostasis*, vol. 17, no. 6, pp. E165–E170, 2011.

[10] E. Koçak, M. Çelebier, I. C. Haznedaroglu, and S. Altınöz, "Analysis of the antiproliferative effect of Ankaferd hemostat on Caco-2 colon cancer cells via LC/MS shotgun proteomics approach," *BioMed Research International*, vol. 2019, Article ID 5268031, 11 pages, 2019.

[11] E. Huri, I. C. Haznedaroglu, T. Akgul, M. Astarci, H. Ustun, and C. Germiyanoulu, "Biphasic effects of ankaferd blood stopper on renal tubular apoptosis in the rat partial nephrectomy model representing distinct levels of hemorrhage," *Saudi Medical Journal*, vol. 31, no. 8, pp. 864–868, 2010.

[12] E. Eren, M. S. Başoğlu, E. Kulduk, F. Şimsek, and S. İnan, "Mucosal trauma induced apoptosis in Guinea pig middle ear: comparision of hemostatic agents," *International Journal of Pediatric Otorhinolaryngology*, vol. 78, no. 12, pp. 2222–2228, 2014.

[13] M. Ghasemi, M. Okay, U. Y. Malkan et al., *Ankaferd hemostat affects etoposide resistance of the malignant melanoma cells*, DSpace Software, 2020.

[14] Ö. C. Zeki, M. Nenni, M. Çelebier et al., "Antitumor activity of Ankaferd Blood Stopper® on MCF-7 breast cancer: a proteomic approach to ascertain the mechanism of the action," *Journal of Herbal Medicine*, vol. 28, article 100449, 2021.

[15] B. Metin, E. Menevse, A. Sivrikaya, T. Altinoks, and H. Arıkoglu, "The effects of ankaferd blood stopper on DNA damage and enzymes with paranchymal damaged rabbits," *Medicine*, vol. 6, no. 1, pp. 5–10, 2017.

[16] M. Çitirik, N. Dilsiz, I. Haznedaroğlu, and K. Sönmez, "Effects of Ankaferd Hemostat on Retinal Apoptosis in an Experimental Rabbit Retinal Model," *Turkiye Klinikleri Journal of Medical Sciences*, vol. 33, no. 3, pp. 836–844, 2013.

[17] A. Uğur, N. Saraç, D. A. Çankal, and M. Özle, "The antioxidant and antimutagenic activities of Ankaferd blood stopper, a natural hemostatic agent used in dentistry," *Turkish Journal of Medical Sciences*, vol. 46, no. 3, pp. 657–663, 2016.

[18] I. Akalın, F. V. Okur, İ. C. Haznedaroglu et al., "Acute In Vitro Effects of ABS (Ankaferd Hemostat) on the Lymphoid Neoplastic Cells (B-CLL and RAJI Tumor Cell Lines)," *International Journal of Hematology and Oncology*, vol. 24, pp. 253–259, 2014.

[19] F. Avcu, M. Guner, M. Misirci et al., "Evaluation of antineoplastic effects of a new hemostatic agent Ankaferd blood stopper on myeloma cell line and plasmocytoma development in Balb/c mice: results of the first in vitro and in vivo study," *Blood*, vol. 124, no. 21, p. 5728, 2014.

[20] A. Mihmanli, Z. Ulker, L. Alpsoy, and S. Ezirganli, "Evaluation of cytotoxicity of a new hemostatic agent Ankaferd Blood Stopper® using different assays," *Human & Experimental Toxicology*, vol. 31, no. 8, pp. 780–787, 2012.

[21] I. López-Mateo, M. Á. Villaronga, S. Llanos, and B. Belandia, "The transcription factor CREBZF is a novel positive regulator of p53," *Cell Cycle*, vol. 11, no. 20, pp. 3887–3895, 2012.

[22] C. Walesky and U. Apte, "Role of hepatocyte nuclear factor 4α (HNF4α) in cell proliferation and cancer," *Gene Expression*, vol. 16, no. 3, pp. 101–108, 2015.

[23] F.-J. Zheng, H.-B. Ye, M.-S. Wu, Y.-F. Lian, C.-N. Qian, and Y.-X. Zeng, "Repressing malic enzyme 1 redirects glucose metabolism, unbalances the redox state, and attenuates migratory and invasive abilities in nasopharyngeal carcinoma cell lines," *Chinese Journal of Cancer*, vol. 31, no. 11, pp. 519–531, 2012.

[24] D. Wen, D. Liu, J. Tang et al., "Malic enzyme 1 induces epithelial–mesenchymal transition and indicates poor prognosis in hepatocellular carcinoma," *Tumor Biology*, vol. 36, no. 8, pp. 6211–6221, 2015.

[25] E. H. van der Horst, B. T. Frank, L. Chinn et al., "The growth factor midkine antagonizes VEGF signaling in vitro and in vivo," *Neoplasia*, vol. 10, no. 4, p. 340-IN3, 2008.

[26] H.-L. Huang, J.-F. Shen, L.-S. Min, J.-L. Ping, Y.-L. Lu, and L.-C. Dai, "Inhibitory effect of midkine-binding peptide on tumor proliferation and migration," *International Journal of Clinical and Experimental Pathology*, vol. 8, no. 5, pp. 5387–5394, 2015.

[27] Y. Zheng, L. Zhang, X. Jia, H. Wang, and Y. Hu, "Interaction of protein inhibitor of activated STAT 2 (PIAS2) with receptor of activated C kinase 1, RACK1," *FEBS Letters*, vol. 586, no. 2, pp. 122–126, 2012.

[28] J. J. O'Shea, D. M. Schwartz, A. V. Villarino, M. Gadina, I. B. McInnes, and A. Laurence, "The JAK-STAT pathway: impact on human disease and therapeutic intervention," *Annual Review of Medicine*, vol. 66, no. 1, pp. 311–328, 2015.

[29] T. Eguchi, T. Itadani, T. Shimomura, N. Kawanishi, H. Hirai, and H. Kotani, "Expression levels of p18INK4C modify the cellular efficacy of cyclin-dependent kinase inhibitors via regulation of Mcl-1 expression in tumor cell lines," *Molecular Cancer Therapeutics*, vol. 8, no. 6, pp. 1460–1472, 2009.

[30] Y. Matsuzaki, Y. Takaoka, T. Hitomi, H. Nishino, and T. Sakai, "Activation of protein kinase C promotes human cancer cell growth through downregulation of p18INK4c," *Oncogene*, vol. 23, no. 31, pp. 5409–5414, 2004.

[31] S. Gagrica, S. Brookes, E. Anderton, J. Rowe, and G. Peters, "Contrasting behavior of the p18INK4c and p16INK4a tumor suppressors in both replicative and oncogene-induced senescence," *Cancer Research*, vol. 72, no. 1, pp. 165–175, 2012.

[32] M. B. Ataman, M. N. Bucak, and K. Çoyan, "Esterified glucomannan improves aflatoxin-induced damage of sperm parameters during liquid storage of ram semen at 5 C," *Cryobiology*, vol. 68, no. 3, pp. 405–410, 2014.

[33] E. Yilmaz, S. Gulec, D. Torun, I. C. Haznedaroglu, and N. Akar, "The effects of Ankaferd (R) Blood Stopper on transcription factors in HUVEC and the erythrocyte protein profile," *Turkish Journal of Hematology*, vol. 28, pp. 276–285, 2011.

[34] O. K. Serrano, N. L. Parrow, P. C. Violet et al., "Antitumor effect of pharmacologic ascorbate in the B16 murine melanoma model," *Free Radical Biology & Medicine*, vol. 87, pp. 193–203, 2015.

[35] S. Turk, U. Y. Malkan, M. Ghasemi et al., "Growth inhibitory activity of Ankaferd hemostat on primary melanoma cells and cell lines," *SAGE Open Medicine*, vol. 5, 2017.

[36] G. P. Pfeifer and A. Besaratinia, "UV wavelength-dependent DNA damage and human non-melanoma and melanoma skin cancer," *Photochemical & Photobiological Sciences*, vol. 11, no. 1, pp. 90–97, 2012.

[37] C. Fellner, "Ipilimumab (yervoy) prolongs survival in advanced melanoma: serious side effects and a hefty price tag may limit its use," *Pharmacy and Therapeutics*, vol. 37, no. 9, pp. 503–530, 2012.

[38] A. Kocyigit, E. M. Guler, I. C. Haznedaroglu, and U. Y. Malkan, "Ankaferd hemostat induces DNA damage, apoptosis and cytotoxic activity by generating reactive oxygen species in melanoma and normal cell lines," *International Journal of*

Clinical and Experimental Medicine, vol. 10, no. 2, pp. 2116–2126, 2017.

[39] R. Ciftciler, A. E. Ciftciler, U. Y. Malkan, and I. C. Haznedaroglu, "Pharmacobiological management of hemostasis within clinical backgrounds via Ankaferd hemostat (Ankaferd blood stopper)," *SAGE Open Medicine*, vol. 8, 2020.

[40] H. Goker, D. Cetinkaya, E. Kilic, I. Haznedaroglu, S. Kirazli, and H. Firat, "Anti-cancer activity of ankaferd blood stopper on osteosarcom (SAOS-2) cell lines in vitro. Ankaferd: scientific perspectives and basic-clinical data Istanbul," *Naviga Publications*, vol. 109, 2008.

[41] R. Ciftciler and İ. C. Haznedaroğlu, "Ankaferd hemostat: from molecules to medicine," *Turkish Journal of Medical Sciences*, vol. 50, no. 7, pp. 1739–1750, 2020.

[42] H. Goker, E. Kilic, D. Cetinkaya et al., "Anti-cancer activity of Ankaferd on human colon cancer (CACO-2) in vitro. Ankaferd: scientific perspectives and basic-clinical data Istanbul," *Naviga Publications*, vol. 108, 2008.

[43] M. Nenni, M. Celebier, I. Süslü, and I. C. Haznedaroğlu, *Proteomic Investigation of In-Vitro Antineoplastic Effect of Ankaferd Hemostat with 2D Gel Electrophoresis and MALDI-TOF/TOF-MS in HepG2, Caco-2 and HT-29 Cancer Cells*, The International Society on Thrombosis and Hemostasis (ISTH), 2019.

[44] İ. C. Haznedaroğlu, İ. Süslü, Ö. Tacal, and S. Altinöz, *Ankaferd® Bloodstopper Kanama Durdurucu'nun Kolon Kanseri Üzerine İyileştirici Etkisinin Moleküler Düzeyde İncelenmesi*, Tübitak Ulakbim Ulusal Akademik Ağ ve Bilgi Merkezi Cahit Arf Bilgi Merkezi, 2017.

[45] H. Sarı, S. Çelik, F. Çağlar et al., "A candidate antineoplastic herbal agent for bladder cancer: Ankaferd blood stopper," *International Journal of Clinical Practice*, vol. 75, no. 11, article e14789, 2021.

[46] F. Çiğdem, *Ankaferd bloodstopper kanama durdurucunun in vitro meme kanseri hücrelerinin çoğalmalari üzerine olan etkisi, [M.S. thesis]*, Trakya Üniversitesi Sağlik Bilimleri Enstitüsü, 2018.

[47] E. Kılıç, D. Çetinkaya, İ. Haznedaroglu et al., *Ankaferd bloodstopper'in (ABS) in vitro ortamda mezenkimal kök hücre gelisimi üzerine etkisi. 34*, Ulusal Hematoloji Kongresi Bildiri Özet Kitabı, P065 no'lu bildiri, İzmir, 2008.

[48] M. Nenni, S. Öncül, A. Ercan, M. Çelebier, İ. Süslü, and İ. C. Haznedaroğlu, "Exposure of hepatocellular carcinoma cells to Ankaferd Blood Stopper® alters cell death signaling networks confirmed by oncoproteomic and genomic profiling studies," *Current Traditional Medicine*, vol. 7, no. 2, pp. 246–258, 2021.

[49] M. Ozle, D. A. Uğar Çankal, M. Ilhan, H. Keleş, and A. E. Küpeli, "Evaluation of the chemopreventive effects of ankaferd bloodstopper in 7, 12-dimethylbenz [a] anthracene-induced oral epithelial dysplasia," *Clinical Oral Investigations*, vol. 22, no. 9, pp. 3091–3096, 2018.

[50] T. Patıroğlu, N. E. Şahin, E. Ünal, M. Kendirci, M. Karakükcü, and M. A. Özdemir, "Effectiveness of ankaferd bloodstopper in prophylaxis and treatment of oral mucositis in childhood cancers evaluated with plasma citrulline levels," *Turkish Journal of Hematology*, vol. 35, no. 1, pp. 85-86, 2018.

[51] M. H. Atay, N. A. Arslan, S. Aktimur et al., "Safety and Efficacy of Ankaferd Hemostat (ABS) in the Chemotherapy-Induced Oral Mucositis," *International Journal of Hematology and Oncology*, vol. 25, no. 3, pp. 166–171, 2015.

[52] M. Buyuktiryaki, C. Tayman, I. Koyuncu et al., "Therapeutic and preventative effects of ankaferd blood stopper in an experimental necrotizing enterocolitis model," *Biomedicine & Pharmacotherapy*, vol. 110, pp. 105–110, 2019.

[53] B. Güneş, N. Y. A. Akişin, and M. N. Akar, "Trace element & vitamin content of Ankaferd hemostat and hepatoprotective effect," *Turkish Journal of Medical Sciences*, vol. 51, no. 6, pp. 3136-3137, 2021.

[54] K. Koşmaz, A. Durhan, M. Süleyman et al., "The effect of Ankaferd blood stopper on liver damage in experimental obstructive jaundice," *Turkish Journal of Medical Sciences*, vol. 51, no. 3, pp. 1472–1480, 2021.

[55] N. Akar, Y. Ardçoglu, Z. Öktem, N. Erduran, and I. C. Haznedaroglu, "High iron content of Ankaferd hemostat as a clue for its hemostatic action of red blood cell origin," *Blood Coagulation & Fibrinolysis*, vol. 26, no. 2, pp. 233-234, 2015.

[56] A. Koluman, N. Akar, U. Y. Malkan, and I. C. Haznedaroglu, "Qualitative/chemical analyses of Ankaferd hemostat and its antioxidant content in synthetic gastric fluids," *BioMed Research International*, vol. 2016, Article ID 8957820, 8 pages, 2016.

[57] N. Y. A. Akişin and M. N. Akar, "High zinc content of ankaferd hemostat and wound healing effect," *Turkish Journal of Medical Sciences*, vol. 51, no. 5, p. 2798, 2021.

[58] J. Dabak, S. Gazuwa, and G. Ubom, "Hepatoprotective potential of calcium and magnesium against cadmium and lead induced hepatotoxicity in Wistar rats," *Asian Journal of Biotechnology*, vol. 1, no. 1, pp. 12–19, 2008.

[59] A. E. T. Alaa El Den, N. I. Hussien, M. M. Allam, and D. A. Mohammed, "The potential effect of vitamin D on rats with fatty liver induced by a choline-deficient diet," *Benha Medical Journal*, vol. 35, no. 1, p. 67, 2018.

[60] O. O. Sinbad, A. A. Folorunsho, O. L. Olabisi, O. A. Ayoola, and E. J. Temitope, "Vitamins as antioxidants," *Journal of Food Science and Nutrition Research*, vol. 2, no. 3, pp. 214–235, 2019.

[61] F. E. Uboh, P. E. Ebong, and I. B. Umoh, "Comparative hepatoprotective effect of vitamins A and E against gasoline vapor toxicity in male and female rats," *Gastroenterology Research*, vol. 2, no. 5, p. 295, 2009.

Hindawi

Research Article

Dose-Dependent Variation in Anticancer Activity of Hexane and Chloroform Extracts of Field Horsetail Plant on Human Hepatocarcinoma Cells

Hadeel A. Almasoud, Daoud Ali, Khadijah N. Yaseen, Hanouf Almukhlafi, Norah S. Alothman, Bader Almutairi [ID], Rafa Almeer, Nouf Alyami, Saad Alkahtani [ID], and Saud Alarifi [ID]

Department of Zoology, College of Science, King Saud University, P. O. Box 2455, Riyadh 11451, Saudi Arabia

Correspondence should be addressed to Saud Alarifi; salarifi@ksu.edu.sa

Horsetail fern plant is botanically known as Equisetum arvense L., and it is a good source of phenolic flavonoids, phenolic acids, and compounds. Anticancer properties of hexane and chloroform extracts of the horsetail fern plant and their mechanisms involved in the anticancer activity on human hepatocarcinoma (HuH-7) cells were examined. Cytotoxicity was evaluated by using MTT (3-(4,5-dimethylthiazol-2-yl)-2,5-diphenyltetrazolium bromide) and NRU (neutral red uptake) assays. Other parameters such as oxidative stress and apoptosis in pretreated hexane and chloroform extracts of the horsetail fern plant were examined in HuH-7 cells. The observation showed that hexane and chloroform extract of the horsetail fern plant exhibited cytotoxicity against HuH-7 cells. The value of IC_{50}-24 h of hexane and chloroform extract of the horsetail fern plant was determined as 199.0 μg/ml and 161.90 0 μg/ml for HuH-7 cells, respectively, and on the basis of IC_{50} value, three acute concentrations, viz., 75% of IC_{50}, 50% of IC_{50}, and 25% of IC_{50}, were determined for further study. The lower dose of extracts hexane and chloroform extract of the horsetail fern plant did not show significant toxicity. Higher concentrations of extract induced significant antioxidant effects as well as apoptosis effects. However, exposure to hexane and chloroform extract of the horsetail fern plant upregulated the expression of Bax and p53 in HuH-7 cells. These data suggest that hexane and chloroform extract of the horsetail fern plant plays a significant role in the induction of toxicity via the regulation of oxidative stress in HuH-7 cells. This work may be useful for cancer chemotherapy.

1. Introduction

Cancer is one of the most dreadful diseases globally, and it appears to be due to extreme free radical damage, which eventually causes damage to the DNA, lipids, and protein. The horsetail plant scientifically called as *Equisetum arvense* L. (belongs to the Equisetaceae family) is a perennial fern (Figure 1). The horsetail plant has a green-branched sterile stem and grows during the late autumn seasons [1]. The horsetail plant has a medicinal value which was described in European Pharmacopoeia [1]. Extract of the horsetail plant has a gorgeous source of flavonoids, phenolic compounds, and phenolic acid with reducing and antioxidant properties [2, 3] have reported that some Chinese medicinal plant extract was able to detect immunological disorder during tumor disease. Some researchers had reported antioxidant, antifungal, anti-inflammatory, and neuro- and cardio-protective of horsetail plant [4].

(a)

(b)

(c)
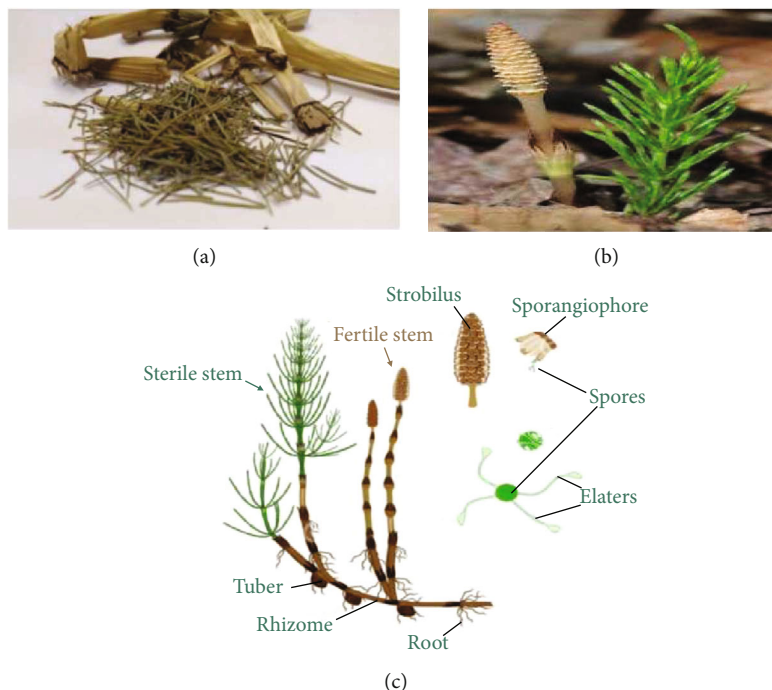
Figure 1: (a–c) *Equisetum arvense*.

A high concentration of extract horsetail plant had induced apoptosis and preoxidant and reduced secretion of IL-6 enzymes [4]. We experimented to confirm the toxicity of extracts of *Equisetum arvense* L. on HuH-7 cells. Aljarba et al. [5] reported that isolated alkaloid and sterol compounds of different medicinal plants induced synergistic anticancer effect on young Swiss albino mice. Reactive oxygen species (ROS) produced by mitochondria not only takes part in signaling of stress in normal cells but also contributes to the initiation of nuclear or mitochondrial DNA mutations that promote neoplastic transformation. Damaging of DNA generates activation of arrest cell growth, and the p53 gene stimulates apoptosis, as per the level of the ratio of oxidative stress [6]). Excessive production of ROS in cells leads to degeneration of mitochondrial membrane potential [7, 8]. have reported that induction of apoptosis is correlated with the generation of ROS. Hegedűs et al., [1] have reported that extract of horsetail plant has shown a preventive effect on oxidative stress and cardiovascular disease in diabetic rats. To my knowledge, there are no studies that have been reported on the toxic nature of hexane and chloroform extracts of the *E. arvense* on HuH-7 cells. In this study, we determined the role of oxidative stress in the toxicity of hexane and chloroform extracts of the *E. arvense* on HuH-7 cells.

2. Materials and Methods

2.1. Chemical and Reagents. MTT [3-(4, 5-dimethylthiazol-2-yl)-2, 5-diphenyltetrazolium bromide], H2-DCFH-DA), DMSO, Annexin V FITC, and PI dye were bought from Sigma-Aldrich (St. Louis, Missouri, United States). DMEM,

fetal bovine serum (FBS), and antibiotics were bought from Gibco, USA.

2.2. Plant Material Collection and Preparation of Plant Extracts. In this study, we used *E. arvense*, and it was purchased from the local market in Riyadh, Saudi Arabia (Figures 1(a)–1(c)). The plant was identified by Dr. Jacob Thomas, Taxonomist, Department of Botany and Microbiology at King Saud University, Riyadh, Saudi Arabia. The leaves and stems of the plant have been dried and ground using an electric mill. The plant powder (50 g) was weighed and then placed in a thimble in the Soxhlet extraction apparatus. The extraction process was performed for 24 h using two types of different solvents such as hexane and chloroform [9, 10]) to obtain the most significant number of secondary metabolic compounds in the plant. The extracts were collected, centrifuged at 5000 rpm for 10 min, and concentrated using a rotary evaporator (Heidolph, Germany) at 45°C. The concentrated extracts were stored in glass vials at 4°C until use. All extracts were dissolved in dimethyl sulfoxide (DMSO) (Sigma) at 50 mg/ml stock (European Medicines Agency, 2016).

2.3. Cell Culture and Plant Extract Exposure. Human hepatocarcinoma (HuH-7) cells were bought from American Type Culture Collection (ATCC), USA. HuH-7cells were subcultured in DMEM with 10% FBS and 10000 U/ml antibiotics at 5% CO_2 incubator at 37°C.

HuH-7 cells were subcultured for 24 h before treatment with hexane and chloroform extracts of the *E. arvense*. Stock solution of extract was prepared in DMSO at 50 mg extract/ml DMSO and diluted according to the experimental concentration (0-200 μg/ml).

2.4. MTT Assay. Cytotoxicity of HuH-7 cells due to coexposure of hexane and chloroform extracts of the E. arvense was performed by using the MTT test [11]). In brief, HuH-7 cells (2×10^4) were seeded/well in 96-well plates and kept in the 5% CO_2 incubator for 24 h at 37°C before experiments for the proper growth of the cells. After incubation, the cells were exposed to various concentrations of hexane and chloroform extracts of the E. arvense (0, 20, 50, 100, 150, 200, and 500 μg/ml) and incubated in a CO_2 incubator at 37°C for 24 h. At exposure, the culture medium was replaced with a new medium containing MTT solution (0.5 mg/ml) and incubated for 4 hours at in a CO_2 incubator at 37°C. The produced formazan crystals were dissolved in dimethyl sulfoxide. Then, the plate was read at 570 nm using a multiwell microplate reader (Synergy Fluostar, Germany). Untreated cell set was under identical conditions and served as controls.

2.5. NRU Assay. The NRU (neutral red uptake) test was done to quantify the viability of cells (Borenfreund and Puerner, [12]). In brief, HuH-7 cells (2×10^4) were seeded per well in 96-well plates and kept in the 5% CO_2 incubator for 24 h at 37°C before experiments for the proper growth of the cells. After incubation, HuH-7 cells were treated with a concentration of hexane and chloroform extracts of the E. arvense (0, 20, 50, 100, 150, and 200 μg/ml), and the exposed culture plate was incubated in a CO_2 incubator at 37°C for 24 h. After incubation, the cells were allowed to incubate for 3 h in a complete medium containing neutral red dye (50 μg/ml). Thereafter, the cells were washed with a washing solution to remove the excess dye. To extract the neutral red dye, a mixture of ethanol (50%) and acetic acid (1%) was filled into each well and kept for 20 min on a shaker. The absorbance was measured at 540 nm by using a multiwell microplate reader (Synergy Fluostar, Germany). Untreated cell set was under identical conditions and served as controls.

2.6. Determination of IC_{50} Value 24 h for Extracts of the E. Arvense. The effect of the hexane and chloroform extracts of the E. arvense on cells was measured by counting viable cells by calculating the concentration that inhibits 50% of cell line growth (IC_{50}) determined by the dose-response curve graph using the program (OrigenPro 8.5) after repeating the experiment three times [13].

2.7. LDH Assay. Cytotoxicity induced by hexane and chloroform extracts of the E. arvense was assessed by lactate dehydrogenase (LDH) leakage into the culture medium as per LDH cytotoxicity assay kit (Cayman chemical 601170 kit). Briefly, HuH-7 cells were seeded in 96-wells with 100 μl of culture medium for 24 h. Then, the culture medium was removed, and the plant extracts were added (per well) with 200 μl of medium, and 200 μl of medium only (without cells) was added to the three wells (background control), and 20 μg/ml of 10% Triton X-100 solution was added to the three wells (total release), and 20 μg/ml of assay buffer was added to the three wells (Spontaneous release) for 24 h. After incubation, they were centrifuged at 1000 rpm for 5 min.

100 μl of cell supernatant was transferred to a new 96-well plate, and a reaction solution was added 100 μl to each well. The plates were incubated with gentle shaking on an orbital shaker for 30 min at 37°C. Absorbance was read at 490 nm with a plate reader (Synergy Fluostar, Germany).

2.8. Catalase Activity. Measurement of catalase activity was based on the peroxidative function of catalase. Briefly, the cells were collected and sonicated in buffer (50 mM potassium phosphate, pH 7.0, containing 1 mM EDTA) followed by centrifugation at $10,000 \times g$ for 15 min at 4°C. The supernatant was then assayed for catalase activity using the manufacturer's protocol, and absorbance was monitored at 540 nm by using a plate reader (Synergy Fluostar, Germany). The activity was represented as n mole/(min ml).

2.9. Superoxide Dismutase (SOD) Activity. SOD estimation was done in cells collected by centrifugation at $1000 \times g$ for 10 min at 4°C. Cell pellets were lysed in cold 20 mM HEPES buffer, pH 7.2, containing 1 mM ethylene glycol tetra-acetic acid, 210 mM mannitol, and 70 mM sucrose. The cells were then centrifuged at $1500 \times g$ for 5 min at 4°C. Cell extracts were finally incubated with xanthine oxidase for 20 min according to the manufacturer's protocol, and absorbance of the reaction mixture was measured at 450 nm by using a plate reader (Synergy Fluostar, Germany).

2.10. Western Blotting. For western blotting, 20 mg of protein was applied to the lanes of 4% to 12% Bis-Tris Gels (Life Technologies), then blotted onto Immobilon-P membranes (Millipore, Bedford, MA, USA), and incubated with the relevant primary antibodies such as anti-Bax antibody [E63] ab32503 and anti-caspase-3 antibody [E87] ab197202 (Abcam, Cambridge CB2 0AX UK). Appropriate species-specific conjugated secondary antibody goat anti-rabbit HRP (ab205718) was commercially obtained (Abcam, Cambridge CB2 0AX UK). Proteins were detected using the ECL prime kit or the ECL kit (GE Healthcare Tokyo Japan) with an Image Quant LAS 4000 system (GE Healthcare). All protein expression levels were normalized to the levels of GPDH protein expression in each band.

2.11. RNA Extraction, cDNA Synthesis, and Real-Time PCR. The RNA was reverse-transcribed using RT-PCR kits (Applied Biosystems, Foster City, CA, United States) with an oligo d (T) 16 primer under standard conditions. Real-time PCR amplification was performed using a Light Cycler 480 (Roche, Basel, Switzerland) and 2 μl of purified cDNA product, 5 μl of sense primer (10 pmol/ml), 5 μl of antisense primer (10 pmol/ml), 1 ml of Light Cycler Fast Start DNA Master SYBR Green I (Roche), and 0.8 ml of MgCl2 (25 mmol/L). Commercial glyceraldehyde phosphate dehydrogenase (GAPDH) primer sets were used for PCR amplification under the conditions recommended by the manufacturer (Table 1). GAPDH served as an internal reference gene, and the relative change was calculated by relative quantification, applying the formula by the 2−△△Ct method.

TABLE 1: The sequences of primers.

Gene	Primer F sequence (59->39)	Primer R sequence (5,->39)	Product size
β-Actin	5$'$-CACCATTGGCAATGAGCGGTTC-3$'$	5$'$-AGGTCTTTGCGGATGTCCACGT-3	131 bp
Caspase-3	5$'$-TGTTTGTGTGCTTCTGAGCC-3$'$	5$'$-CACGCCATGTCATCATCAAC-3	123 bp
Bax	5-ATGTTTTCTGACGGCAACTTC-3$'$	5$'$-AGTCCAATGTCCAGCCCAT-3	82 bp
Bcl-2	5-ATGTGTGTGGAGACCGTCAA-3	5-GCCGTACAGTTCCACAAAGG-3$'$	142 bp
P53	5$'$-AGAGTCTATAGGCCCACCCC-3$'$	5$'$-GCTCGACGCTAGGATCTGAC-3	81 bp

2.12. Statistical Analysis. Statistical analysis was performed using SPSS software (Ver.22; SPSS Inc., Chicago, IL, USA). Data were examined using one-way ANOVA, followed by a post hoc LSD (least significant difference) test, and the results were presented as average ± SE. p value < 0.05 was considered statistically significant.

3. Results

3.1. IC$_{50}$ Value 24 h. The IC$_{50}$ was determined by the dose-response curve graph using the program (OrigenPro 8.5) (Figures 2(a) and 2(b)), and it was determined based on the MTT test result. We observed the IC$_{50}$ value of 24 h 199 μg/ml for hexane and 161 μg/ml for chloroform extracts of the *E. arvense* (Figures 2(a) and 2(b)).

3.2. Cytotoxicity. The cell viability of HuH-7 cell lines was reduced significantly in a dose-dependent manner due to hexane and chloroform extracts of the *E. arvense* exposure (Figures 3(a) and 3(b)). The viability of HuH-7 cell line was decreased to 83%,84%, 65%, 62%, 53%, and 13% for hexane plant extract and 88%, 66%, 57%, 55%, 46%, and 14% for chloroform plant extract in 24 h at all concentration (20 μg/ml, 50 μg/ml, 100 μg/ml, 150 μg/ml, 200 μg/ml, and 500 μg/ml), respectively, through MTT test (Figure 3(a)).

The viability of HuH-7 cell line was decreased in all concentrations to 86%, 78%, 73%, 61%, and 55%, respectively, for hexane plant extract, and 88%, 83%, 66%, 49%, and 46%, respectively, for chloroform plant extract in 24 h through NRU test (Figure 3(b)).

Furthermore, the results showed that plant extract reduced viability for both solvents with significant differences (Figures 3(a) and 3(b)).

The LDH test results indicate that compared to control, the loss of membrane integrity was slightly increased to 104%, 107%, and 114% for hexane plant extract and to 116%, 126%, and 132% for chloroform plant extract in 24 h (control, 25, 50, and 75% of the IC$_{50}$, respectively) (Figure 4).

3.3. Oxidative Stress. HuH-7 cell lines were exposed with *E. arvense* extract (25%, 50%, and 75% of the IC$_{50}$ value in μg/ml) for 24 h, and CAT and SOD enzyme activity was measured. The results showed that CAT activity was increased maximum at lower concentrations (25% of the IC$_{50}$ value) for chloroform *E. arvense* extract, and it was decreased at higher concentrations (50% and 75% of the

IC$_{50}$ value) for hexane and chloroform *E. arvense* extract (Figure 5(a)). SOD enzyme was increased at lower concentration (25% of the IC$_{50}$ value) and decreased at higher concentration (50% and 75% of the IC$_{50}$ value) for hexane and chloroform *E. arvense* extract (Figure 5(b)). The results showed that compared to control, the E. arvense extracts induced CAT and SOD activity in a dose-dependent manner (Figures 5(a) and 5(b)).

3.4. Immunoblotting. To confirm the apoptosis due to the effects of plant extract (25%, 50%, and 75% of the IC$_{50}$ value in μg/ml) for 24 h, on HuH-7 cells, we have determined the expression of the apoptotic protein in cells after exposure to hexane and chloroform *E. arvense* extract. In HuH-7 cell line, the result showed that caspase-3 protein expression was upregulated at all concertation to 1.3, 1.3, and 1.4, respectively, for hexane plant extract and more upregulated to 2.8, and then, it was downregulated to 2.2 and 1.7, respectively, after treating with chloroform plant extract (Figures 6(a) and 6(b)).

While the result showed that Bax protein expression was upregulated at all concentrations (1.1, 1.4, and 1.3, respectively), for hexane plant extract and upregulated at the concentration 1.1 and 1.5, then it was downregulated to 0.9 after being treated with chloroform plant extract (Figures 6(a) and 6(b)).

3.5. Apoptotic Gene Expression. To examine the expression level of the apoptotic genes in human liver cell lines, RT-PCR analysis was performed. In HuH-7 cell line, the result showed that p53, caspase-3, and Bax mRNA expression compared to control were increased at all concentrations to 5.4, 6.4, and 7.1, 3.7, 3.8, and 2.2, and 1.5, 3.0, and 2.7, respectively, for hexane plant extract and to 2.3, 3.0, and 3.6, 2.5, 3.0, and 3.4, and 1.9, 2.0, and 1.3, respectively, for chloroform plant extract. On the other hand, the Bcl-2 mRNA expression was decreased at all concertation to 0.9, 0.6, and 0.3, respectively, for hexane plant extract and to 0.8, 0.6, and 0.3, respectively, for chloroform plant extract (Figures 7(a) and 7(b)).

4. Discussion

Several reports and studies have indicated that cancer is a major cause of death worldwide, causing nearly 10 million deaths, and liver cancer was the most common cause of death with 830,000 cases (WHO, 2020). We used extracts

(a)

(b)
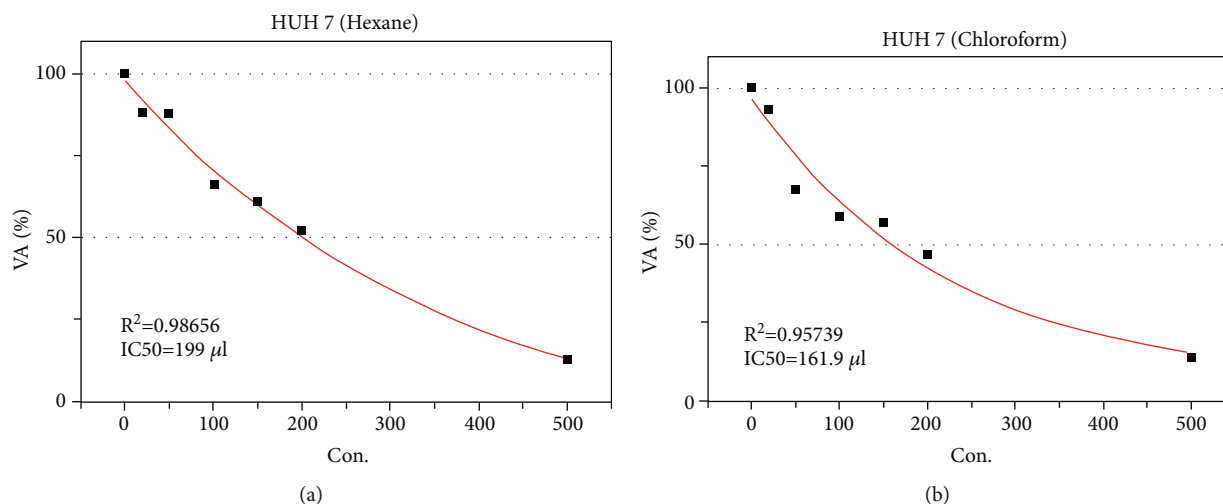
FIGURE 2: Determination of IC_{50} value-24 h of (a) hexane and (b) chloroform extracts of E. arvense for HuH-7 cells.

(a)

(b)
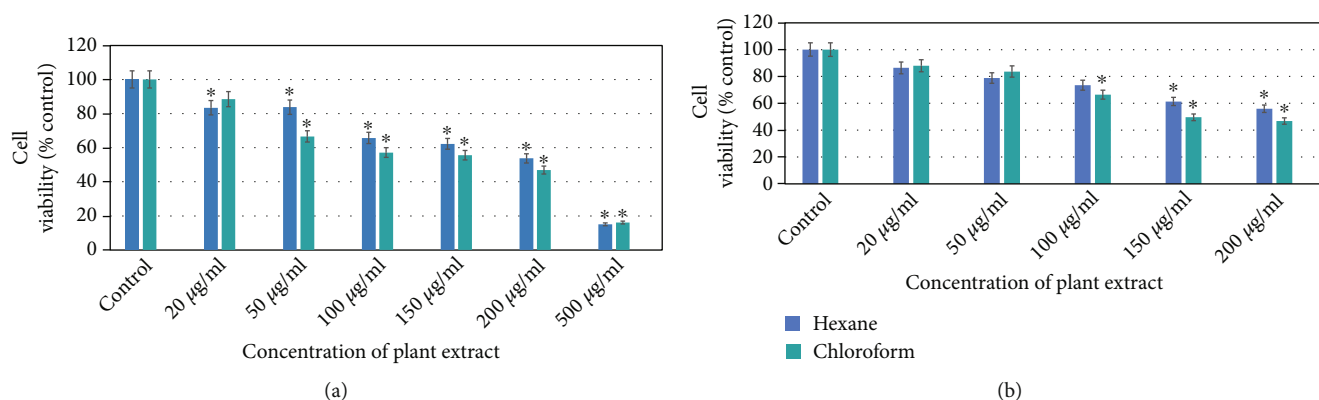
FIGURE 3: Hexane and chloroform of plant extracts of *E. arvense* induced cytotoxicity on HuH-7 cell line in a dose-dependent manner for 24 h: (a) MTT assay and (b) NRU assay. Each value represents means of three experiment. p value < 0.05 vs. control.
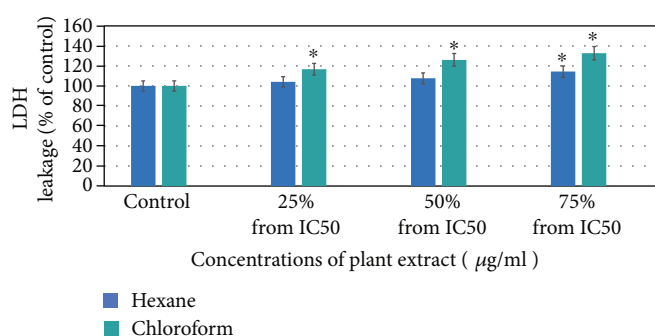
FIGURE 4: Hexane and chloroform of plant extracts of *E. arvense* induced cytotoxicity on HuH-7 cell line in a dose-dependent manner for 24 h. Each value represents means of three experiment. p value < 0.05 vs. control.

of *E. arvense*, which is considered one of the medicinal plants that current research has confirmed to have many pharmacological applications, and peer-reviewed studies showed that these pharmacological activities of medicinal plants are due to their valuable chemical components, which mainly include alkaloids, triterpenoids, flavonoids, phenols, and tannins [14]. In a previous study, *E. arvense* did not show any noticeable toxic effects; however, clinical trials are necessary (Kotwal [15]. In other studies, the extract of *E. arvense* inhibited the proliferation of cancer cells and extended the lifespan of mice [16]).

So, researchers are keen to investigate the underlying mechanism of toxicity of hexane and chloroform extracts of the E. arvense exposure on HuH-7 cells. In the present

(a)

(b)
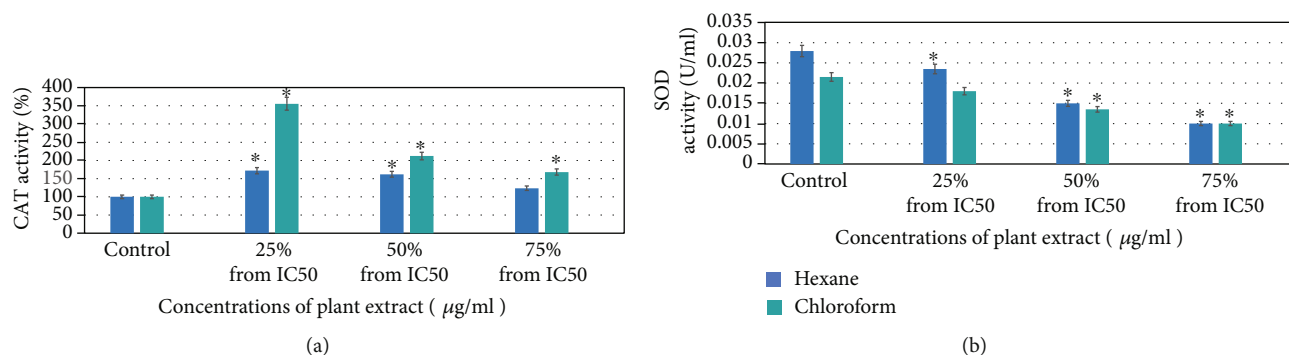
FIGURE 5: Hexane and chloroform of plant extracts of E. arvense decreased oxidative stress biomarkers in HuH-7 cell line for 24 h: (a) catalase level and (b) SOD level in cells. Each value represents means of three experiment. p value < 0.05 vs. control.

(a)

(b)
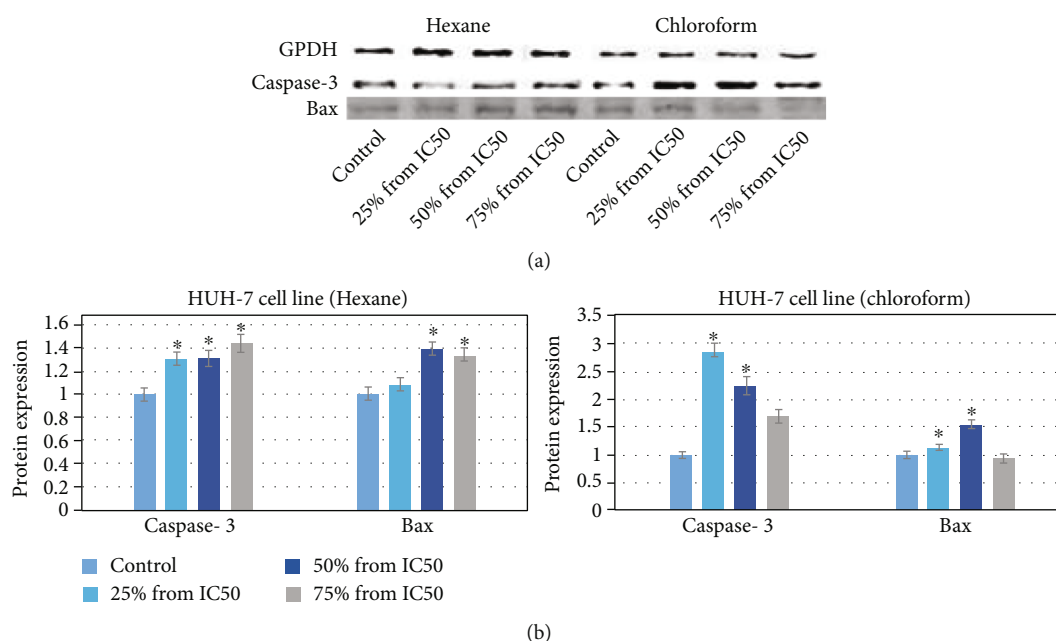
FIGURE 6: Western blotting of protein involved in apoptosis: (a) Bax and caspase-3 expression level in cells. (b) Relative quantification of protein expression level. GPDH was used as internal control to normalize the data. Each value represents means of three experiment. p value < 0.05 vs. control.

experiment, exposure of hexane and chloroform extracts of the E. arvense to cells for 24 h demonstrated significant cytotoxicity and apoptotic effects on hepatic cancer cells. In addition, a significant decrease in SOD and increase in catalase enzyme at lower concertation were observed. A recent study done by Zalewska et al. [17] showed that cancer cells mostly contain few antioxidant enzymes such as CAT, GSH-PX, and SOD, which play a dynamic role in cellular protection against ROS in normal cells. Increasing of oxidizing agents such as ROS affects cell organelles and cellular compounds, such as carbohydrates, lipids, proteins, and DNA molecules [18]), and the cells respond through protective enzymatic defense mechanisms such as CAT and SOD to reduce harmful ROS production. Moreover, it has been reported that low expression of SOD correlates with hepatocellular carcinoma mortality [19]). Also, cell death by apo-

ptosis acts as a barrier to the development of cancer [20]. The extracts of E. arvense induced apoptosis of HuH-7 cell lines in a dose-dependent manner, and we found that the gene expression level of caspase-3, Bax, and p53 were increased, in contrast to the same doses which lowered the level of bcl-2. The Bax has been shown to be regulated by p53 and to restrict tumorigenesis, and it is essential for apoptosis, while Bcl-2 binds and inhibits the activity of Bax and proapoptotic proteins, thus preventing apoptosis [21]. Taken together, upregulation of p53 leads to activation of proapoptotic members of the Bcl-2 family, such as Bax, and induces permeabilization of the outer mitochondrial membrane, which releases soluble proteins from the intermembrane space into the cytosol, where they promote caspase-9 activation and which further activates caspase-3, which lead to apoptosis [22, 23].
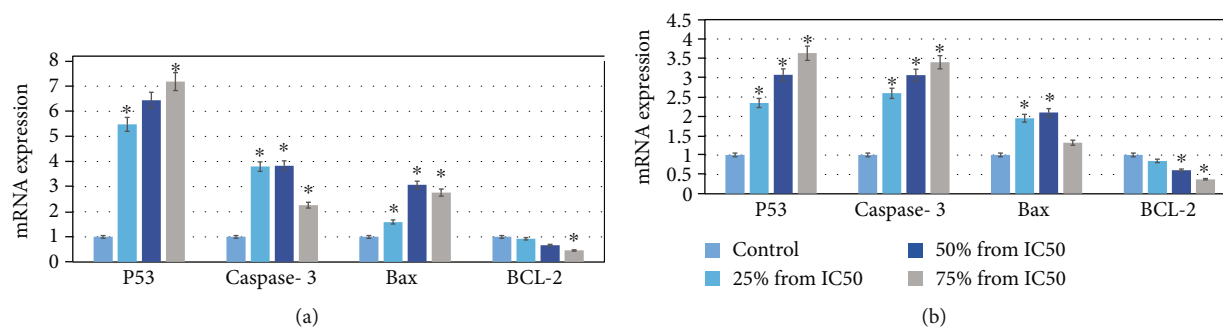
Figure 7: Expression of apoptotic gene in (a) hexane and (b) chloroform of exposure of plant extracts of *E. arvense* in HuH-7 cell line for 24 h. Each value represents means of three experiment. *p* value < 0.05 vs. control.

5. Conclusion

The current finding provides evidence for the potential efficacy of *E. arvense* extracts, and the results obtained in this work indicate that this extract may be useful as an anticancer drug by activating antioxidant enzymes and programmed cell death pathways. However, there is a need for further investigation using different molecular tests *in vivo* models.

Data Availability

The original contributions presented in the study are included in the article; further inquiries can be directed to the corresponding author.

Conflicts of Interest

The authors declare that they have no conflicts of interest.

Authors' Contributions

DA, RA, and SuA conceptualized the study; DA and HAA were responsible for the data curation; HAA, DA, BA, and HA were responsible for the formal analysis; SuA was responsible for the funding acquisition; DA, BA, SaA, NuA, and NrA were responsible for the investigation; HAA, NrA, BA, DA, KY, NuA, and HA were responsible for the methodology; SuA, RA, and DA were responsible for the project administration; HAA, DA, KY, HA, and BA were responsible for the software; DA, RA, and SuA supervised the study; DA and SaA were responsible for the validation; DA wrote the original draft; and DA, HAA, SuA, RA, and SaA wrote, reviewed, and edited the manuscript.

Acknowledgments

References

[1] C. Hegedűs, M. Muresan, A. Badale et al., "SIRT1 activation by Equisetum arvense L. (horsetail) modulates insulin sensitivity in streptozotocin induced diabetic rats," *Molecules*, vol. 25, no. 11, p. 2541, 2020.

[2] M. D'Agostino, A. Dini, C. Pizza, F. Senatore, and R. Aquino, "Sterols from Equisetum arvense," *Bollettino della Società Italiana di Biologia Sperimentale*, vol. 60, pp. 2241–2245, 1984.

[3] J. Xu, J. Zhang, and J. Wang, "The application of traditional Chinese medicine against the tumor immune escape," *Journal of Translational Internal Medicine*, vol. 8, no. 4, pp. 203-204, 2020.

[4] J. G. Dos Santos, M. M. Blanco, F. H. M. Monte et al., "Sedative and anticonvulsant effects of hydroalcoholic extract of Equisetum arvense," *Fitoterapia*, vol. 76, no. 6, pp. 508–513, 2005.

[5] N. H. Aljarba, H. Ali, and S. Alkahtani, "Synergistic dose permutation of isolated alkaloid and sterol for anticancer effect on young Swiss albino mice," *Drug Design, Development and Therapy*, vol. 15, pp. 4043–4052, 2021.

[6] M. B. Burg, J. D. Ferraris, and N. I. Dmitriev, "Cellular response to hyperosmotic stresses," *Physiological Reviews*, vol. 87, no. 4, pp. 1441–1474, 2007.

[7] D. A. Bader Almutairi, K. N. Yaseen, N. S. Alothman et al., "Mechanisms of apoptotic cell death by stainless steel nanoparticle through reactive oxygen species and caspase-3 activities on human liver cells," *Frontiers In Molecular Biosciences*, vol. 8, p. 729590, 2021.

[8] S. De Prins, E. Dons, M. Van Poppel et al., "Surface plasmon resonance scattering and absorption of anti-EGFR antibody conjugated gold nanoparticles in cancer diagnostics: applications in oral cancer," *Nano Letters*, vol. 5, no. 5, pp. 829–834, 2005.

[9] S. Muthusami, K. Senthilkumar, C. Vignesh et al., "Effects of Cissus quadrangularis on the proliferation, differentiation and matrix mineralization of human osteoblast like SaOS-2 cells," *Journal of Cellular Biochemistry*, vol. 112, no. 4, pp. 1035–1045, 2011.

[10] K. A. Reynertson, M. E. Charlson, and L. J. Gudas, "Induction of murine embryonic stem cell differentiation by medicinal plant extracts," *Experimental Cell Research*, vol. 317, no. 1, pp. 82–93, 2011.

[11] S. Alarifi, D. Ali, and S. Alkahtani, "Nanoalumina induces apoptosis by impairing antioxidant enzyme systems in human hepato carcinoma cells," *International Journal of Nanomedicine*, vol. 10, no. 1, pp. 3751–3760, 2015.

[12] E. Borenfreund and J. A. Puerner, "A simple quantitative procedure using monolayer cultures for cytotoxicity assays (HTD/

NR-90)," *Journal of Tissue Culture Methods*, vol. 9, no. 1, pp. 7–9, 1985.

[13] A. Monks, D. Scudeiro, P. Skehan et al., "Feasibility of a high-flux anticancer drug screen using a diverse panel of cultured human tumor cell lines," *Journal of the National Cancer Institute*, vol. 83, no. 11, pp. 757–766, 1991.

[14] M. Masłowski, J. Miedzianowska, A. Czylkowska, and K. Strzelec, "Horsetail (Equisetum arvense) as a functional filler for natural rubber biocomposites," *Materials (Basel)*, vol. 13, no. 11, p. 2526, 2020.

[15] S. D. Kotwal and S. R. Badole, "Anabolic therapy with Equisetum arvense along with bone mineralising nutrients in ovariectomized rat model of osteoporosis," *Indian Journal of Pharmacology*, vol. 48, no. 3, pp. 312–315, 2016.

[16] P. D. A. E. Al-Snafi, "The pharmacology of Equisetum arvense- A review," *IOSR Journal of Pharmacy (IOSRPHR)*, vol. 7, no. 2, pp. 31–42, 2017.

[17] M. Zalewska-Ziob, B. Adamek, J. Kasperczyk et al., "Activity of antioxidant enzymes in the tumor and adjacent noncancerous tissues of non-small-cell lung cancer," *Oxidative Medicine and Cellular Longevity*, vol. 2019, Article ID 2901840, 2019.

[18] L. He, T. He, S. Farrar, L. Ji, T. Liu, and X. Ma, "Antioxidants maintain cellular redox homeostasis by elimination of reactive oxygen species," *Cellular Physiology and Biochemistry*, vol. 44, no. 2, pp. 532–553, 2017.

[19] C. Zhuang, Y. Wang, Y. Zhang, and N. Xu, "Oxidative stress in osteoarthritis and antioxidant effect of polysaccharide from Angelica sinensis," *International Journal of Biological Macromolecules*, vol. 115, pp. 281–286, 2018.

[20] A. Basu, "The interplay between apoptosis and cellular senescence: Bcl-2 family proteins as targets for cancer therapy," *Pharmacology & Therapeutics*, vol. 230, p. 107943, 2022.

[21] S. Dadsena, L. E. King, and A. J. García-Sáez, "Apoptosis regulation at the mitochondria membrane level," *Biochimica et Biophysica Acta (BBA)-Biomembranes*, vol. 1863, no. 12, p. 183716, 2021.

[22] S. Alarifi, D. Ali, and S. Alkahtani, "Oxidative stress-induced DNA damage by manganese dioxide nanoparticles in human neuronal cells," *BioMed Research International*, vol. 2017, Article ID 5478790, 10 pages, 2017.

[23] L. E. Araya, I. V. Soni, J. A. Hardy, and O. Julien, "Deorphanizing caspase-3 and caspase-9 substrates in and out of apoptosis with deep substrate profiling," *ACS Chemical Biology*, vol. 16, no. 11, pp. 2280–2296, 2021.

Retraction

Retracted: lncRNA FOXD2-AS1 Promotes the Retinoblastoma Cell Viability and Migration by Sponging miR-31

BioMed Research International

This article has been retracted by Hindawi following an investigation undertaken by the publisher [1]. This investigation has uncovered evidence of one or more of the following indicators of systematic manipulation of the publication process:

(1) Discrepancies in scope

(2) Discrepancies in the description of the research reported

(3) Discrepancies between the availability of data and the research described

(4) Inappropriate citations

(5) Incoherent, meaningless and/or irrelevant content included in the article

(6) Peer-review manipulation

The presence of these indicators undermines our confidence in the integrity of the article's content and we cannot, therefore, vouch for its reliability. Please note that this notice is intended solely to alert readers that the content of this article is unreliable. We have not investigated whether authors were aware of or involved in the systematic manipulation of the publication process.

In addition, our investigation has also shown that one or more of the following human-subject reporting requirements has not been met in this article: ethical approval by an Institutional Review Board (IRB) committee or equivalent, patient/participant consent to participate, and/or agreement to publish patient/participant details (where relevant).

Wiley and Hindawi regrets that the usual quality checks did not identify these issues before publication and have since put additional measures in place to safeguard research integrity.

We wish to credit our own Research Integrity and Research Publishing teams and anonymous and named external researchers and research integrity experts for contributing to this investigation.

The corresponding author, as the representative of all authors, has been given the opportunity to register their agreement or disagreement to this retraction. We have kept a record of any response received.

References

[1] Y. Liang, H. Wang, R. Song, and X. Yin, "lncRNA FOXD2-AS1 Promotes the Retinoblastoma Cell Viability and Migration by Sponging miR-31," *BioMed Research International*, vol. 2022, Article ID 7723425, 11 pages, 2022.

Research Article

lncRNA FOXD2-AS1 Promotes the Retinoblastoma Cell Viability and Migration by Sponging miR-31

Yan Liang, Hong Wang, Ruiying Song, and Xiuyan Yin [ID]

Department of Ophthalmology, The Affiliated Yantai Yuhuangding Hospital of Qingdao University, Yantai, 264000 Shandong Province, China

Correspondence should be addressed to Xiuyan Yin; yinxiuyan@ytyhdyy.com.cn

Background. The purpose of this study was to explore the functions of FOXD2-AS1 and miR-31 in retinoblastoma. *Material and Methods.* An RT-qPCR assay was applied to calculate the mRNA levels of FOXD2-AS1, miR-31, and PAX9. A dual-luciferase reporter gene assay was employed to verify the connection between FOXD2-AS1, miR-31, and PAX9 expression. *Results.* FOXD2-AS1 was upregulated, and miR-31 was lowly expressed in retinoblastoma. Low expression of FOXD2-AS1 promoted cell proliferation and migration, and upregulation of FOXD2-AS1 inhibited proliferative and migratory abilities. lncRNA FOXD2-AS1 directly bound to miR-31 and regulated miR-31 expression in SO-RB50 cells. Cell proliferation and migration were inhibited by the miR-31 mimic. miR-31 mediated PAX9 expression via directly binding to PAX9 mRNA. A miR-31 inhibitor partially reversed the effect of FOXD2-AS1 knockdown on the proliferation and migration in SO-RB50 cells. FOXD2-AS1 knockdown reduced PAX9 expression in SO-RB50 cells. PAX9 had negative connection with miR-31, and it had positive relationship with FOXD2-AS1. *Conclusion.* lncRNA FOXD2-AS1 inhibited cell proliferation and migration via the miRNA-31/PAX9 axis in retinoblastoma.

1. Introduction

Retinoblastoma (RB) is the most frequent intraocular malignancy in childhood caused by the mutation of the RB1 gene [1]. Approximately 8000 cases of retinoblastoma are diagnosed worldwide each year, and the mortality rate in developing countries is about 70% [2, 3]. Retinoblastoma is usually observed with choroidal infiltration of the eye pathologically. The tumor begins to spread from the retina to the sclera and laminar posterior optic nerve and even metastasize to the central nervous system of advanced retinoblastoma [4]. The overall survival rate of patients after metastasis will decrease significantly. Thus, it is urgent to explore the molecular mechanism of retinoblastoma treatment to enhance clinical treatment effect.

Long noncoding RNAs (lncRNAs), longer than 200-nucleotide RNAs, acted as key regulators in eukaryotic transduction [5, 6]. Increasing evidence indicates that lncRNAs have broad prospects as a novel biomarker and therapeutic target for cancer, including retinoblastoma [7]. For instance, lncRNA SNHG16 enhanced cell proliferation and colony formation and inhibited cell apoptosis in retinoblastoma [8]. Upregulation of FOXD2-AS1 was associated with tumor progression and metastasis in papillary thyroid cancer [9]. Long noncoding RNA FOXD2-AS1 functioned as a competitive endogenous RNA by sponging miRNAs in several cancers, including hepatocellular carcinoma, thyroid cancer, esophageal squamous cell carcinoma, and glioma [10–13]. lncRNAs acted as miRNAs' competing endogenous RNA (ceRNA) or "RNA sponges" and were related to the progression of multiple tumors including cell growth, metastasis, and cell apoptosis [14].

MicroRNAs (miRNAs) are short noncoding RNA molecules that contain 19-25 nucleotides [15, 16]. miRNAs can
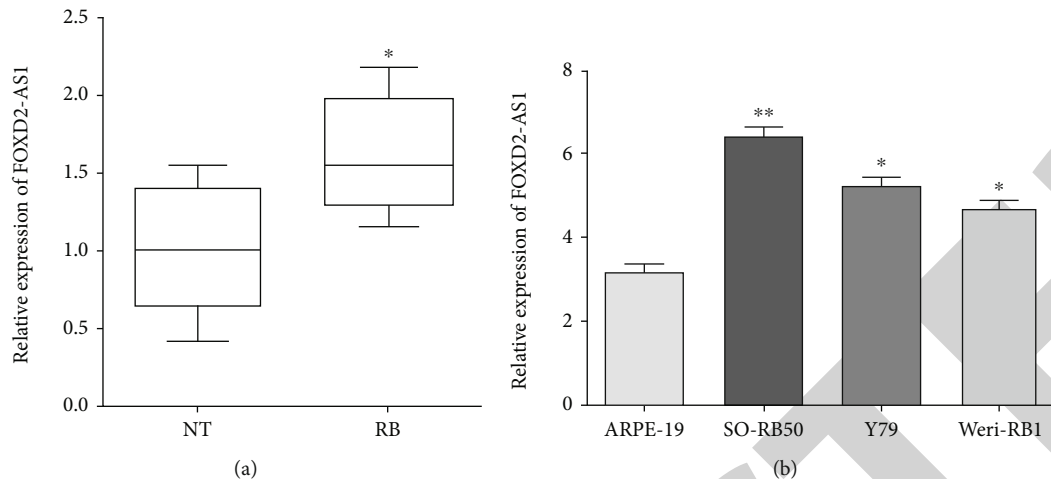
FIGURE 1: Upregulation of FOXD2-AS1 in retinoblastoma tissues and cells: (a) FOXD2-AS1 was upregulated in retinoblastoma tissues compared with normal retina samples; (b) FOXD2-AS1 was also overexpressed in RB cells.

mediate gene expression by binding to the $3'$-untranslated region ($3'$-UTR) complementary sequence of the target mRNAs, eventually leading to mRNA degradation or reduced translation [17]. As tumor-suppressive miRNAs, miR-31 suppressed cell viability, metastasis, and cell cycle in renal cell carcinoma [18]. Downregulation of miR-31 suppressed cell proliferation and invasion via Wnt/β-catenin signaling in osteosarcoma [19]. Moreover, miR-31 was lowly expressed and played great roles in gastric cancer, nasopharyngeal carcinoma, and oral cancer, while it was overexpressed in colorectal cancer [20–23]. In this study, we found that FOXD2-AS1 inhibited cell proliferation and migration via the miRNA-31/PAX9 axis in retinoblastoma.

2. Material and Methods

2.1. Patients and Specimens. We collected 38 freshly frozen retinoblastoma tissue specimens from patients who received surgery at Affiliated Yantai Yuhuangding Hospital of Qingdao University between January 2015 and June 2019. The mean age of the retinoblastoma patients was 3.6 years ranging from 2 months to 11 years. And 12 normal retina samples were obtained from patients with globe rupture. All tumor tissues were examined by two independent histopathologists and graded according to guideline issues by the 7th edition of the American Joint Committee on Cancer.

2.2. Cell Culture. Tree human retinoblastoma cells (SO-RB50, Y79, and Weri-RB1) and a normal retinal pigmented epithelial cell line ARPE-19 were obtained from ATCC. All cells were cultured in DMEM containing 10% fetal bovine serum at 37°C in a humidified incubator supplied with 5% CO_2.

2.3. Cell Transfection. The sh-FOXD2-AS1, miR-613 mimic, and miR-613 inhibitor together with their control sequences were all purchased from GenePharma (Shanghai, China). FOXD2-AS1 was inserted into a pcDNA3.1 vector (Sangon, Shanghai, China) to construct a FOXD2-AS1 overexpression vector. SO-RB50 cells were cultured overnight to achieve

TABLE 1: The expression of FOXD2-AS1 and clinicopathological features in 38 paired retinoblastoma.

Clinicopathological features	Cases ($n = 38$)	FOXD2-AS1 expression 15 high (%)	23 low (%)	P value*
Gender				0.944
Male	18	7 (38.9)	11 (61.1)	
Female	20	8 (40.0)	12 (60.0)	
Lymph node metastasis				0.017*
No	14	9 (64.3)	5 (35.7)	
Yes	24	6 (25.0)	18 (75.0)	
IIRC stage				0.036*
Group A-B	15	9 (60.0)	6 (40.0)	
Group C-E	23	6 (26.1)	17 (73.9)	

*Statistically significant difference ($P < 0.05$).

70–80% confluence prior to transfection. Thereafter, the transfection was performed in SO-RB50 cells using Lipofectamine 2000 (Invitrogen).

2.4. qRT-PCR. Ribozol was used to extract total RNAs from RB tissues and cells. In brief, the reverse transcription was performed to synthesize the first-strand cDNA chain using AMV Reverse Transcriptase XL (Clontech, USA). To detect the expression of FOXD2-AS1, qPCR was carried out using SYBR Green Master Mix (Bio-Rad, USA) on an ABI 7500 System. All experiments were performed 3 times, and the data were processed using the $2^{-\Delta\Delta CT}$ method. qRT-PCR primers were as follows: FOXD2-AS1 forward: $5'$-TGGACCTAGCTGCAGCTCCA-$3'$ and reverse: $5'$-AGTTGAAGGTGCACACACTG-$3'$; PAX9 forward: $5'$-ACCACATTTACTCATATCCCAGTCCCA-3 and reverse: $5'$-GGCTCCCTTCTCCAATCCATTCA-$3'$; GAPDH forward: $5'$-

(a)

(b)

(c)
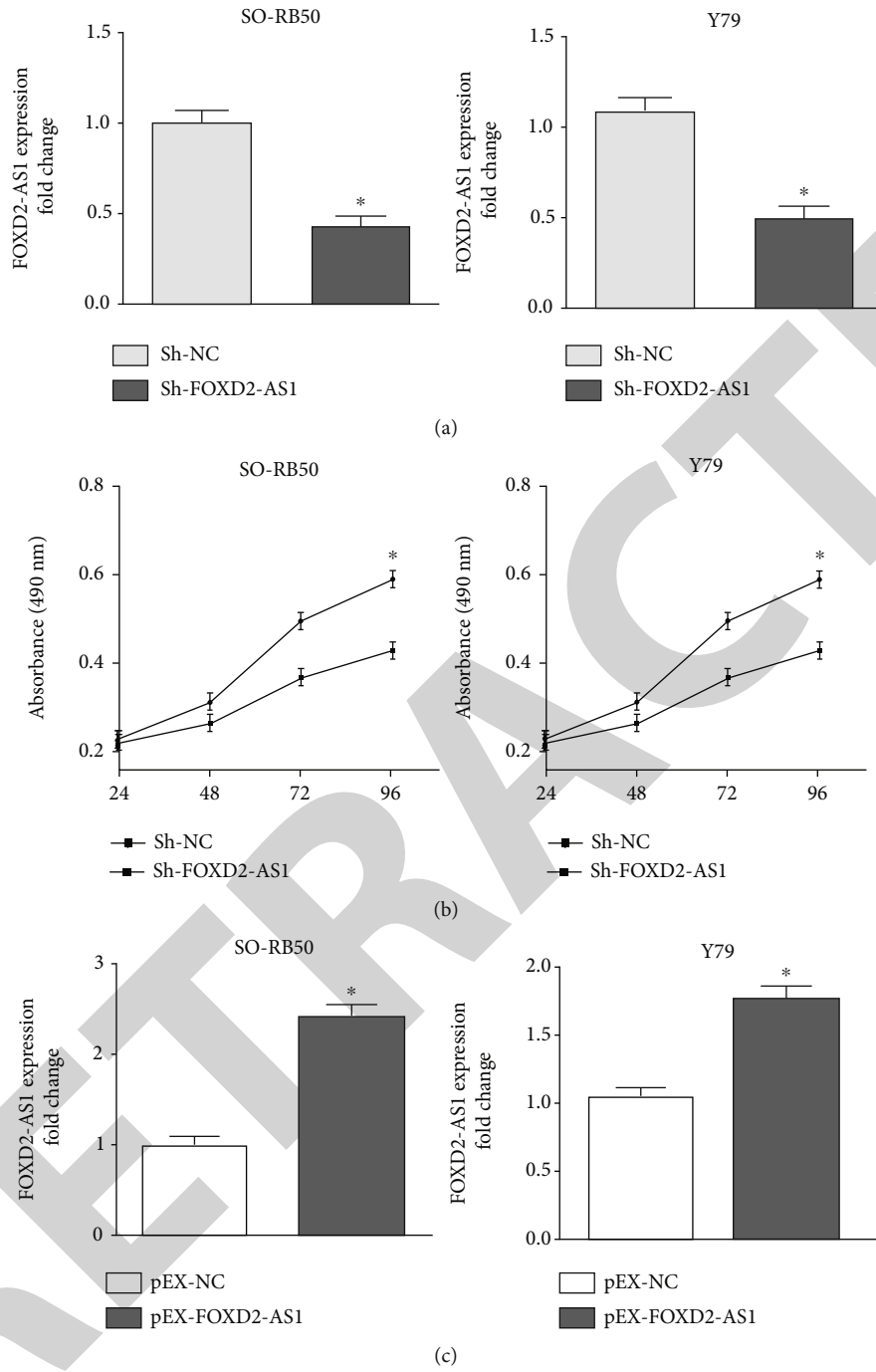
FIGURE 2: Continued.

(d)
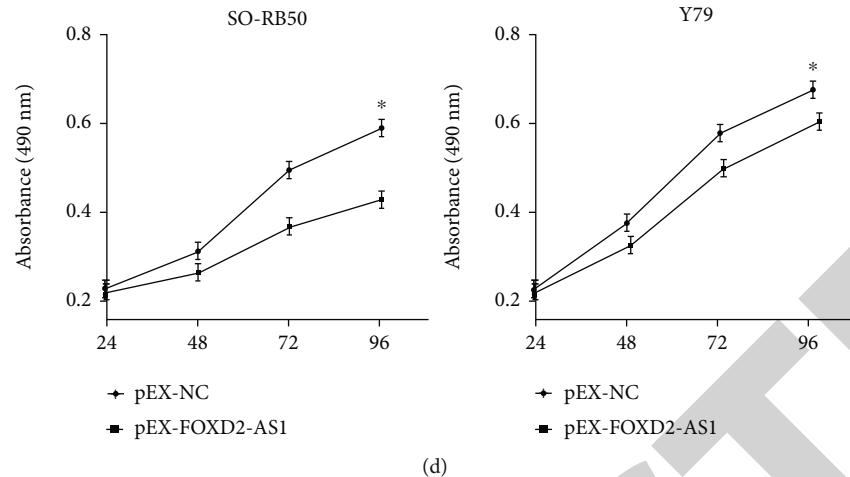
Figure 2: FOXD2-AS1 promoted cell proliferative ability in SO-RB50 and Y79 cells: (a) the transfection efficiency of FOXD2-AS1 knockdown in SO-RB50 and Y79 cells using RT-qPCR; (b) silencing of FOXD2-AS1 reduced cell proliferation in SO-RB50 and Y79 cells; (c) overexpressed FOXD2-AS1 was calculated using RT-qPCR; (d) cell proliferation was enhanced after pEX-FOXD2-AS1 transfection in SO-RB50 and Y79 cells.

TATGATGATATCAAGAGGGTAGT-3′ and reverse: 5′-TGTATCCAAACTCATTGTCATAC-3′; miR-31 forward: 5′-ACGCGGCAAGATGCTGGCA-3′ and reverse: 5′-CAGTGCTGGGTCCGAGTGA-3′; and U6 forward: 5′-CTCGCTTCGGCAGCACA-3′ and reverse: 5′-AACGCT TCACGAATTTGCGT-3′.

2.5. Proliferation Assay. For the detection of cell proliferation, the CCK-8 assay (Beyotime, Jiangsu, China) was performed. SO-RB50 cells were seeded into 96-well plates and incubated for 1, 2, 3, or 4 days. Subsequently, each well was added with the CCK-8 reagent followed by incubation of the cells for an additional 4 h. The absorbance at 450 nm was evaluated on a microplate reader.

2.6. Scratch Test. After 48 hours of transfection, cells were cultured at 5×10^5 cells per well in 6-well plates. After complete adherence to the wall, the cells were scratched with a cell scraper in the middle of each well and then cultured for 24 hours. Photographs were taken at 0 h and 24 h after scratching, and the scratch distance was computed with Image-Pro Plus 6.0. The experiments were repeated three times at least.

2.7. Transwell Assay. Cell migration was assessed by using a transwell chamber in a 24-well plate. In brief, the upper chamber was seeded with 200 μl cells suspended with medium without FBS, whereas the bottom chamber was filled with complete medium with 20% FBS. After incubation for 24 h, cells still on the upper chamber were removed using cotton swabs. Meanwhile, the migrated cells were fixed using paraformaldehyde for 15 min and then stained using crystal violet. The migrated cells were counted in five randomly selected fields under light microscopy (Olympus, Tokyo, Japan).

2.8. Dual-Luciferase Reporter Assay. Starbase was used to predict FOXD2-AS1 binding to miR-31. TargetScan predicted the potential targets of miR-31, and finally, the puta-

tive complementary sequence of which was identified in the 3′-UTR of PAX9 mRNA. SO-RB50 cells were cotransfected with the miR-31 mimic and wild-type or mutated PAX9 or FOXD2-AS1. The Lipofectamine 2000 reagent (Invitrogen) was employed to carry out the transfection. After transfection for 48 h, the dual-luciferase reporter assay system was utilized to calculate the luciferase activity. The firefly luciferase activity was evaluated and normalized by Renilla luciferase activity.

2.9. Statistical Analysis. Data were expressed as mean ± standard deviation (SD). The SPSS 20.0 software package (SPSS, Chicago, IL, USA) was employed to carry out the statistical analysis. The differences between two groups were analyzed using the Student t-test and Fisher's exact tests. One-way analysis of variance (ANOVA) and Bonferroni post hoc tests were used to compare three or more groups. Pearson correlation between FOXD2-AS1, miR-31, and PAX9 was assessed in RB tissues.

3. Results

3.1. Upregulation of FOXD2-AS1 in Retinoblastoma. To detect the functions of FOXD2-AS1 in retinoblastoma, the expression of FOXD2-AS1 was calculated using RT-qPCR. As expected, FOXD2-AS1 was upregulated in 38 retinoblastoma tissues versus 12 normal retina samples ($P < 0.05$) (Figure 1(a)). Similarly, the RT-qPCR assay demonstrated that FOXD2-AS1 was also overexpressed in RB cells SO-RB50, Y79, and WERI-RB1 versus normal cell ARPE-19 ($P < 0.05$) (Figure 1(b)). We also explored evidence for a correlation between FOXD2-AS1 expression and clinicopathological status in glioma patients. The results indicated that significant correlations were detected between FOXD2-AS1 expression and certain clinicopathological features, including lymph node metastasis and IIRC stage ($P < 0.05$) (Table 1).

(a)

(b)
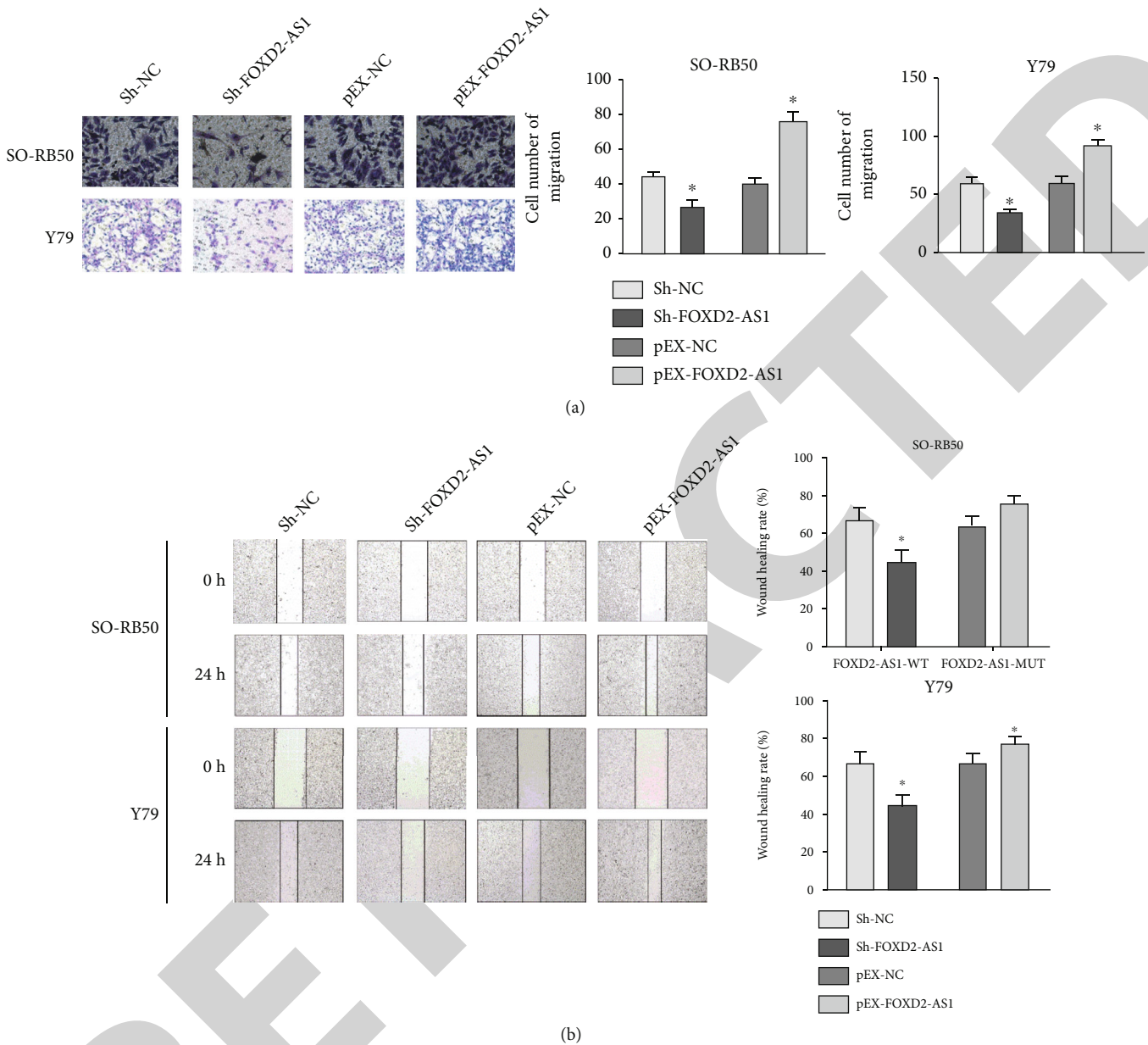
FIGURE 3: FOXD2-AS1 enhanced cell migratory ability in SO-RB50 and Y79 cells: (a) transwell assay was used to measure cell migration in SO-RB50 and Y79 cells; (b) scratch test was applied to calculate cell migratory ability in SO-RB50 and Y79 cells.

3.2. FOXD2-AS1 Promotes the Proliferative Ability in SO-RB50 and Y79 Cells. To detect the biological effects of FOXD2-AS1 in SO-RB50 and Y79 cells, sh-FOXD2-AS1 and pEX-FOXD2-AS1 were constructed. The transfection efficiency of FOXD2-AS1 knockdown ($P < 0.05$) or overexpressed FOXD2-AS1 ($P < 0.05$) was calculated using RT-qPCR (Figures 2(a) and 2(c)). The CCK-8 assay was conducted to measure the cell proliferation after transfecting sh-FOXD2-AS1 or pEX-FOXD2-AS1 in SO-RB50 and Y79 cells. As we discovered, silencing of FOXD2-AS1 reduced cell proliferation in SO-RB50 and Y79 cells ($P < 0.05$) (Figure 2(b)). In contrast, cell proliferation was enhanced after transfecting pEX-FOXD2-AS1 in SO-RB50 cells compared with control groups ($P < 0.05$) (Figure 2(d)).

3.3. FOXD2-AS1 Enhances Cell Migratory Ability in SO-RB50 and Y79 Cells. In addition, the transwell assay was employed to evaluate the cell migration after transfecting sh-FOXD2-AS1 or pEX-FOXD2-AS1 in SO-RB50 and Y79 cells. Similarly, cell migration was reduced when FOXD2-AS1 is knocked down ($P < 0.05$). On the contrary, upregulation of FOXD2-AS1 enhanced cell migratory ability in SO-RB50 and Y79 cells ($P < 0.05$) (Figure 3(a)). In addition, the scratch test was used to further measure the migratory ability in SO-RB50 and Y79 cells. The results indicated that in comparison with the sh-NC group, the migration of cells in the sh-FOXD2-AS1 group was distinctly lessened. On the contrary, overexpression of FOXD2-AS1 promoted cell migratory ability in SO-RB50 and Y79 cells (Figure 3(b)).

FOXD2–AS1 WT   5'–...CCUGUUCGGCGUCUUGCAG...3'

                                           ||||||

hsa–miR–31   3'–...UCGAUACGGUCGUAGAACGGA...5'

FOXD2–AS1 MUT   5'–...CCUGUUCGGCGUGAACCAG...3'

(a)

(b)

(c)

(d)
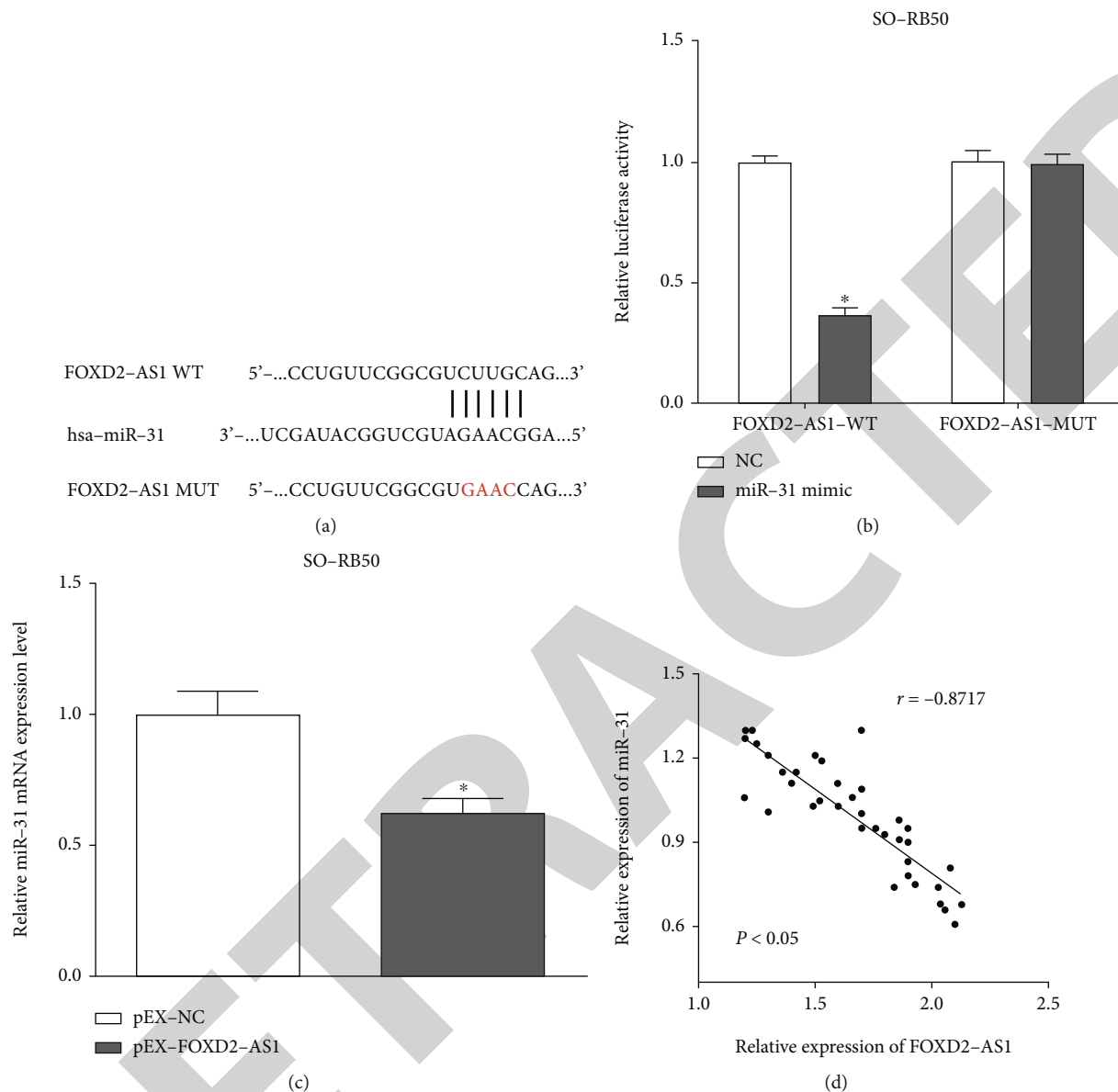
Figure 4: FOXD2-AS1 targets miR-31 in retinoblastoma: (a) miR-31 was predicted to target miRNA of FOXD2-AS1; (b) luciferase activity was reduced when the miR-31 mimic and wild-type FOXD2-AS1 were cotransfected in SO-RB50 cells; (c) miR-31 mRNA level was calculated after FOXD2-AS1 up- or downregulation in SO-RB50 cells; (d) the expression of miR-31 has a negative connection with FOXD2-AS1 in retinoblastoma tissues.

3.4. FOXD2-AS1 Targets miR-31 in Retinoblastoma.

Starbase was utilized to predict the potential target miRNAs of FOXD2-AS1, and we selected miR-31 as the research object. To test whether FOXD2-AS1 binds to miR-31, the potential binding sequences were mutated from UCUUGC to UGAA CC, and both the wild-type or the mutant FOXD2-AS1 was inserted in the psiCHECK-2 plasmid (Promega, Madison, WI, USA) (Figure 4(a)). The luciferase assay revealed that luciferase activity was reduced when the miR-31 mimic and wild-type FOXD2-AS1 were cotransfected in SO-RB50 cells ($P < 0.05$). Meanwhile, the luciferase activity has no alteration after cotransfection with the miR-31 mimic and mutant FOXD2-AS1 (Figure 4(b)). In addition, miR-31 mRNA level was calculated after up- or downregulation of

FOXD2-AS1 in SO-RB50 cells. Not unfortunately, miR-31 was reduced by overexpression of FOXD2-AS1 ($P < 0.05$) (Figure 4(c)). In addition, the expression of miR-31 has a negative connection with FOXD2-AS1 in retinoblastoma tissues ($P < 0.05$) (Figure 4(d)).

3.5. miR-31 Inhibits Cell Viability and Migration in SO-RB50 Cells.

To explore the roles of miR-31 in retinoblastoma, the expression of miR-31 was measured using RT-qPCR. Contrary to the level of FOXD2-AS1, miR-31 was lowly expressed in retinoblastoma tissues in comparison with normal retina samples ($P < 0.05$) (Figure 5(a)). Also, miR-31 was downregulated in RB cells SO-RB50, Y79, and WERI-RB1 versus normal cell ARPE-19 ($P < 0.05$) (Figure 5(b)).
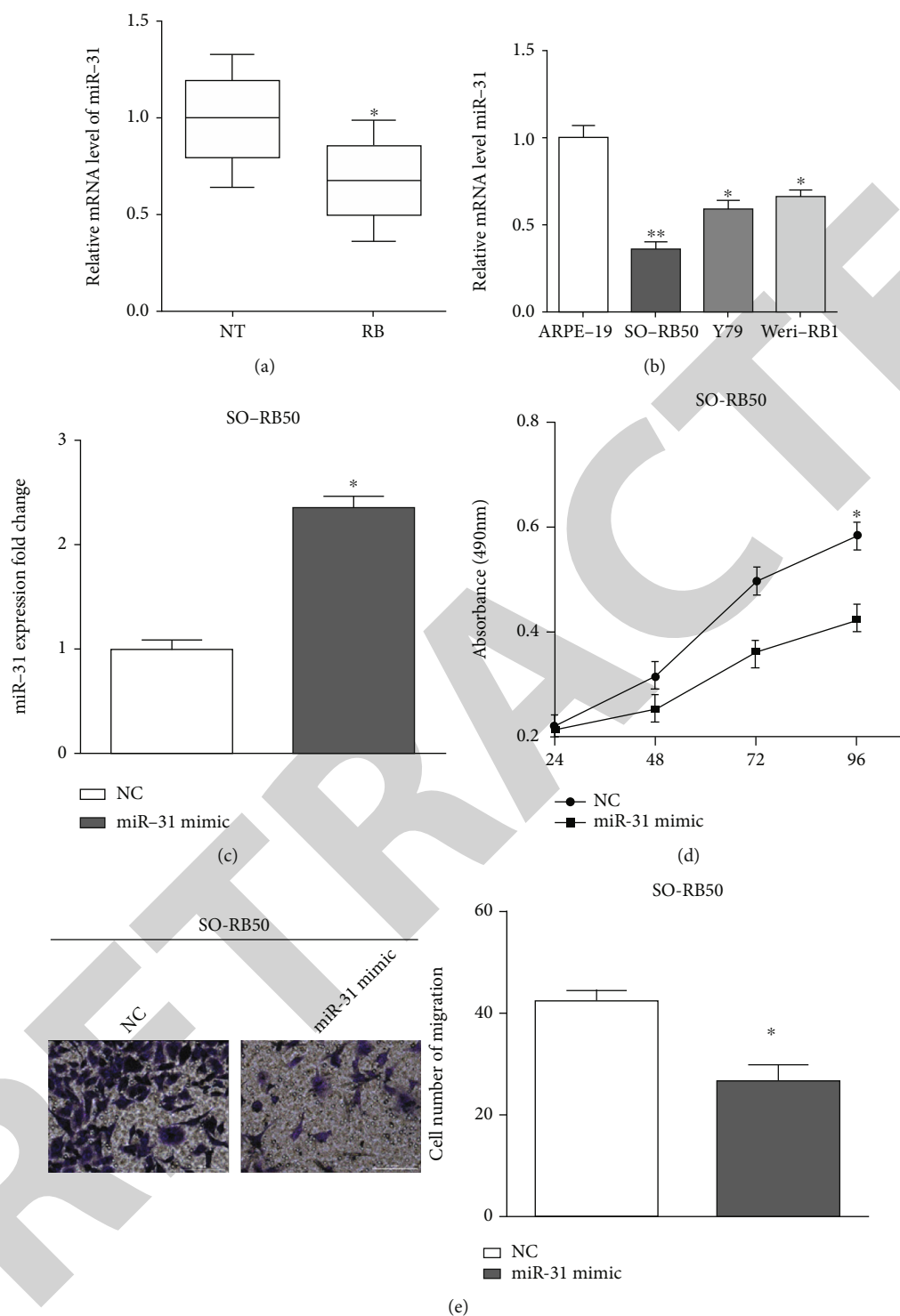
FIGURE 5: miR-31 inhibited cell viability and migration in SO-RB50 cells: (a) miR-31 was lowly expressed in retinoblastoma tissues in comparison with normal retina samples; (b) miR-31 was downregulated in RB cells; (c) the transfection efficiency of transfecting the miR-31 mimic in SO-RB50 cells using RT-qPCR; (d) miR-31 mimic impaired SO-RB50 cell proliferation; (e) cell migration was suppressed by the miR-31 mimic through the transwell assay.

To investigate the functions of miR-31, the miR-31 mimic was used to overexpress miR-31 in SO-RB50 cells, and the transfection efficiency was calculated using RT-qPCR ($P < 0.05$) (Figure 5(c)). CCK-8 results indicated that the miR-31 mimic impaired SO-RB50 cell proliferation ($P < 0.05$) (Figure 5(d)).

Moreover, cell migration was suppressed by the miR-31 mimic through the transwell assay ($P < 0.05$) (Figure 5(e)).

3.6. miR-31 Targets PAX9 in Retinoblastoma. TargetScan was utilized to predict the potential target genes of miR-31,

PAX9 WT   5'...UGACACUUACAUAUUUCUUGCCA...3'

                              | | | | | | |

hsa-miR-31   3'...UCGAUACGGUCGUAGAACGGA...5'

PAX9 MUT   5'...UGACACUUACAUAUUAGAACGGA...3'

(a)

(b)

(c)

(d)
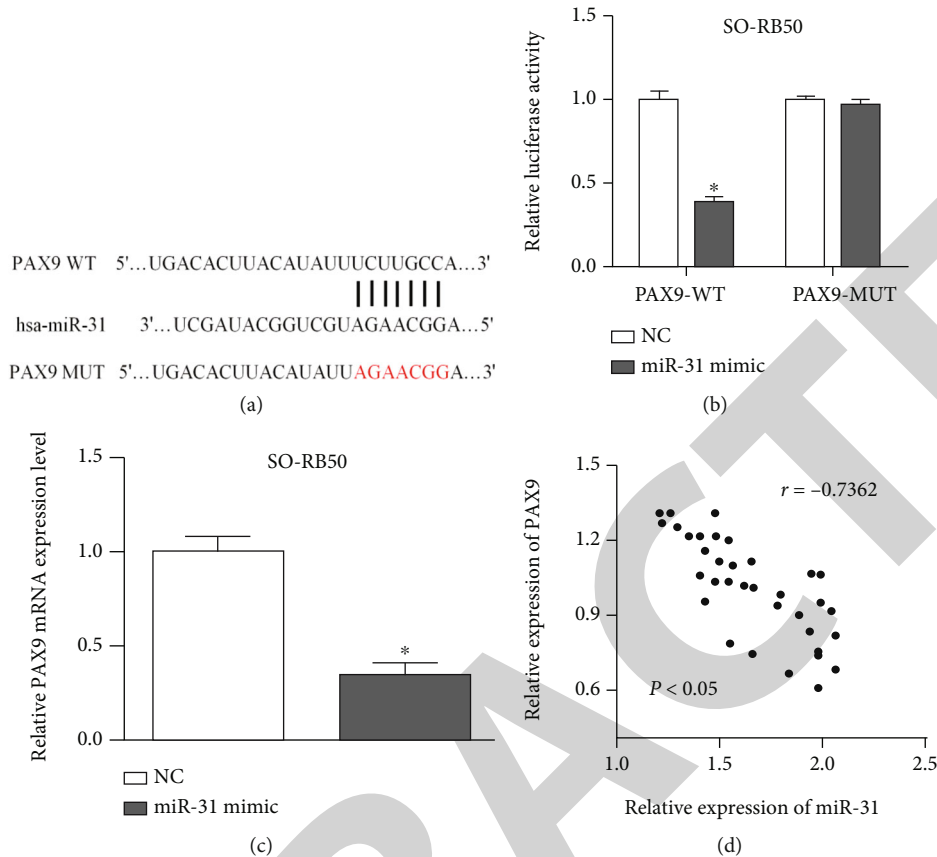
Figure 6: miR-31 targets PAX9 in retinoblastoma: (a) TargetScan predicted that PAX9 was a target of miR-31; (b) luciferase assay was performed to verify miR-31 binding to PAX9; (c) PAX9 expression was reduced by the miR-31 mimic; (d) it had a negative correlation between PAX9 and miR-31 in SO-RB50 cells.

and we selected PAX9 as a target of miR-31. To explore the functions of miR-31 in mediating retinoblastoma cells, the predicted binding sequences on PAX9 were mutated (Figure 6(a)). After that, both the wild-type and the mutant PAX9 together the with miR-31 mimic were cotransfected in SO-RB50 cells. The luciferase reporter assay indicated that the miR-31 mimic reduced the luciferase activity of wild-type PAX9 ($P < 0.05$), and the miR-31 mimic has no effect on the mutant PAX9 ($P < 0.05$) (Figure 6(b)). PAX9 expression was calculated after overexpression of miR-31 in SO-RB50 cells, and we discovered that PAX9 expression was reduced by the miR-31 mimic ($P < 0.05$) (Figure 6(c)). Pearson correlation was used to evaluate the relationship between PAX9 and miR-31 in SO-RB50 cells, and we found that it had a negative correlation between them (Figure 6(d)).

3.7. FOXD2-AS1 Regulates Cell Proliferation and Migration via the miR-31/PAX9 Axis. To investigate the molecular mechanism of FOXD2-AS1 in retinoblastoma, the miR-31 inhibitor was transfected in FOXD2-AS1-silenced SO-RB50 cells ($P < 0.05$) (Figure 7(a)). The function experiment revealed that the miR-31 inhibitor partially reversed the proliferation ($P < 0.05$) and migration ($P < 0.05$) of FOXD2-AS1 in SO-RB50 cells (Figures 7(b) and 7(c)). Moreover, PAX9 expression was calculated when transfecting sh-FOXD2-AS1,

and we found that it was decreased in SO-RB50 cells ($P < 0.05$) (Figure 7(d)). In addition, there is connection between PAX9 and FOXD2-AS1 in retinoblastoma tissues, and we found that it had a positive relationship between PAX9 and FOXD2-AS1 ($P < 0.05$) (Figure 7(e)).

4. Discussion

Retinoblastoma occurs in the retina and is a rare tumor of childhood with an incidence of 1/15,000-20,000 [1]. Specifically, retinoblastoma has the highest prevalence in Asia and Africa, with a mortality rates of about 40-70% [24]. Therefore, a new biomarker is urgently needed to treat retinoblastoma.

lncRNAs are noncoding RNAs larger than 200 nucleotides [25]. Accumulating evidence indicated that lncRNAs played great functions in retinoblastoma. For instance, lncRNA SNHG16 enhanced metastasis by LASP1 in retinoblastoma [26]. FOXD2-AS1 knockdown inhibited cell viability and motility and promoted their apoptosis [27]. Similarly, FOXD2-AS1 acted as an oncogene in hepatocellular carcinoma by accelerating cell cycle, cell colony formation, and cell proliferation [28]. In this study, we discovered that FOXD2-AS1 was overexpressed in retinoblastoma cells and tissues. Consistent with the above studies, we found that interference of FOXD2-AS1 promoted retinoblastoma cell proliferation
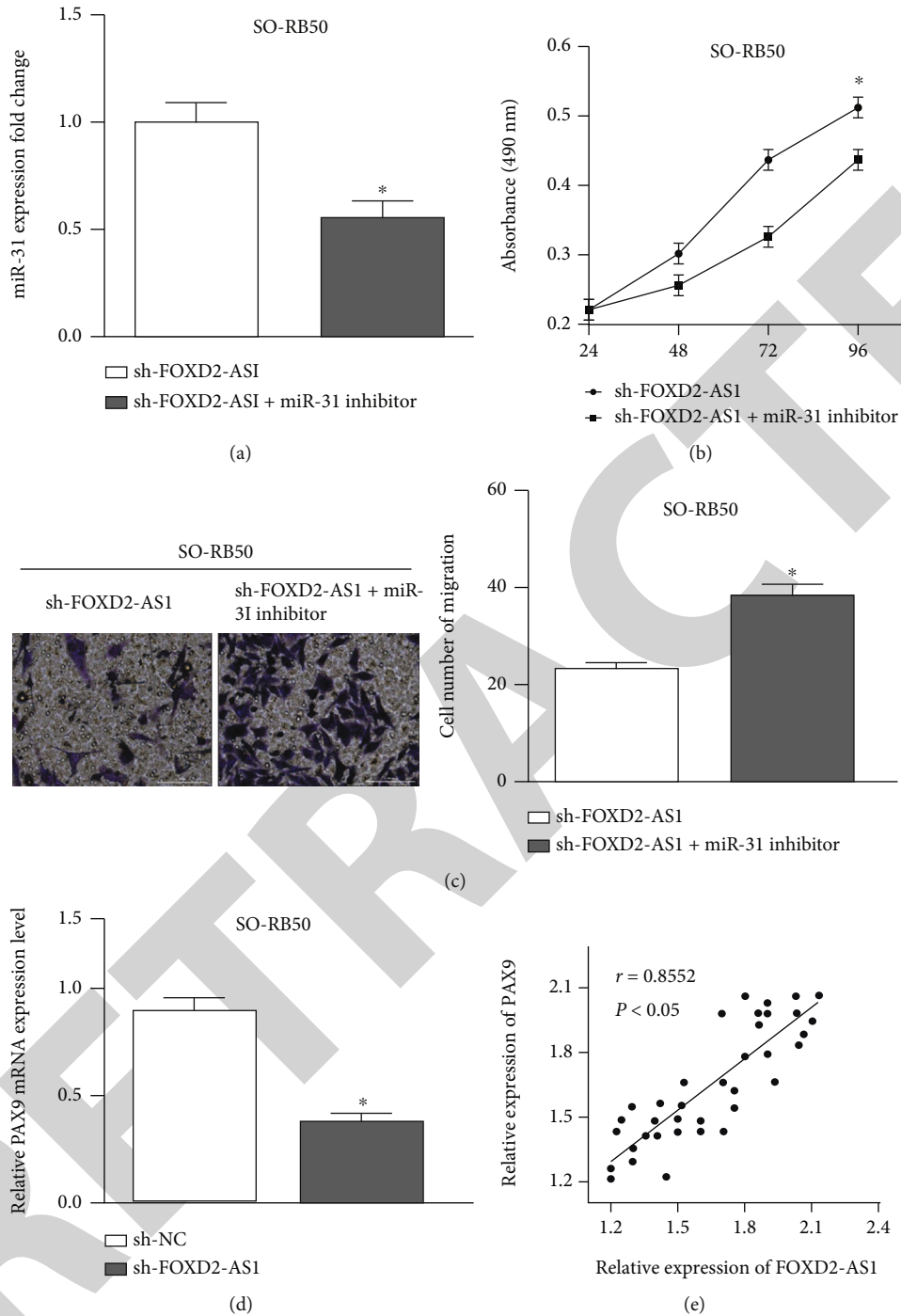
Figure 7: FOXD2-AS1 regulates cell proliferation and migration via the miR-31/PAX9 axis: (a) miR-31 inhibitor was transfected in FOXD2-AS1-silenced SO-RB50 cells; (b) miR-31 inhibitor partially reversed the proliferation of FOXD2-AS1; (c) miR-31 inhibitors can partially reverse the effect of FOXD2-AS1 on motility in SO-RB50 cells; (d) PAX9 expression was decreased in SO-RB50 cells; (e) it had a positive relationship between PAX9 and FOXD2-AS1.

and migration, and cell proliferation and migration were inhibited by overexpressing FOXD2-AS1.

lncRNAs often played roles in promoting or inhibiting tumor development via sponging miRNA. For example, lncRNA LOC554202 enhanced acquired gefitinib resistance through sponging miR-31 in NSCLC [29]. UCA1 promoted cell proliferation and multidrug resistance of retinoblastoma cells through sponging miR-513a [30]. In our study, FOXD2-AS1 was used as a ceRNA to adsorb miR-31. The expression of miR-31 was reduced after overexpression of FOXD2-AS1, and it was increased by FOXD2-AS1 knockdown. MicroRNAs (miRNAs) are small noncoding RNAs by binding to target genes to mediate gene expression [31, 32]. miR-31 inhibited cell proliferation, migration, and invasion

via targeting PIK3C2A [33]. Moreover, miR-31 regulated chemosensitivity through preventing the nuclear location of PARP1 in HCC [34]. Our findings were consistent with the previous studies; miR-31 was lowly expressed in retinoblastoma tissues and cells. Since miR-31 was lowly expressed in retinoblastoma cells, we used the miR-31 mimic to overexpress miR-31 in SO-RB50 cells. Moreover, the miR-31 mimic inhibited cell proliferation and migration in SO-RB50 cells. Thus, we proposed that FOXD2-AS1 enhanced retinoblastoma cell proliferation and invasion via regulating miR-31. In addition, the results of this current study indicated that PAX9 expression was regulated by miR-31, and PAX9 was determined to be a target gene of miR-31. Except that, silencing of FOXD2-AS1 could inhibit the expression of PAX9, indicating that FOXD2-AS1 suppresses miR-31 expression, thereby promoting PAX9 expression.

5. Conclusion

FOXD2-AS1 was used as a ceRNA to adsorb miR-31 for suppressing its expression, thereby promoting PAX9 expression. Our study provided a new insight into how FOXD2-AS1 can be an effective target for retinoblastoma diagnosis. However, we only studied the functions of FOXD2-AS1 on retinoblastoma in vitro, so in vivo experiments are needed, which is the limitation of this article.

Data Availability

Data to support the findings of this study is available on reasonable request from the corresponding author.

Conflicts of Interest

The authors have no conflicts of interest to declare.

References

[1] H. Dimaras, K. Kimani, E. A. Dimba et al., "Retinoblastoma," *Lancet*, vol. 379, no. 9824, pp. 1436–1446, 2012.

[2] R. L. Siegel, K. D. Miller, and A. Jemal, "Cancer statistics, 2018," *CA: a Cancer Journal for Clinicians*, vol. 68, no. 1, pp. 7–30, 2018.

[3] B. L. Theriault, H. Dimaras, B. L. Gallie, and T. W. Corson, "The genomic landscape of retinoblastoma: a review," *Clinical & Experimental Ophthalmology*, vol. 42, no. 1, pp. 33–52, 2014.

[4] K. Gunduz, O. Muftuoglu, I. Gunalp, E. Unal, and N. Tacyildiz, "Metastatic retinoblastoma: clinical features, treatment, and prognosis," *Ophthalmology*, vol. 113, no. 9, pp. 1558–1566, 2006.

[5] T. Nagano and P. Fraser, "No-nonsense functions for long noncoding RNAs," *Cell*, vol. 145, no. 2, pp. 178–181, 2011.

[6] M. Huarte, "The emerging role of lncRNAs in cancer," *Nature Medicine*, vol. 21, no. 11, pp. 1253–1261, 2015.

[7] A. Bhan, M. Soleimani, and S. S. Mandal, "Long noncoding RNA and cancer: a new paradigm," *Cancer Research*, vol. 77, no. 15, pp. 3965–3981, 2017.

[8] C. Xu, C. Hu, Y. Wang, and S. Liu, "Long noncoding RNA SNHG16 promotes human retinoblastoma progression via sponging miR-140-5p," *Biomedicine & Pharmacotherapy*, vol. 117, article 109153, 2019.

[9] H. Li, Q. Han, Y. Chen et al., "Upregulation of the long noncoding RNA FOXD2-AS1 is correlated with tumor progression and metastasis in papillary thyroid cancer," *American Journal of Translational Research*, vol. 11, no. 9, pp. 5457–5471, 2019.

[10] C. Sui, Z. Dong, C. Yang et al., "LncRNA FOXD2-AS1 as a competitive endogenous RNA against miR-150-5p reverses resistance to sorafenib in hepatocellular carcinoma," *Journal of Cellular and Molecular Medicine*, vol. 23, no. 9, pp. 6024–6033, 2019.

[11] X. Liu, Q. Fu, S. Li et al., "LncRNA FOXD2-AS1 functions as a competing endogenous RNA to regulate TERT expression by sponging miR-7-5p in thyroid cancer," *Frontiers in Endocrinology*, vol. 10, p. 207, 2019.

[12] H. Liu, J. Zhang, X. Luo et al., "Overexpression of the long non-coding RNA FOXD2-AS1 promotes cisplatin resistance in esophageal squamous cell carcinoma through the miR-195-Akt-mTOR axis," *Oncology Research*, vol. 28, no. 1, pp. 65–73, 2020.

[13] J. Wang, B. Li, C. Wang, Y. Luo, M. Zhao, and P. Chen, "Long noncoding RNA FOXD2-AS1 promotes glioma cell cycle progression and proliferation through the FOXD2-AS1/miR-31/CDK1 pathway," *Journal of Cellular Biochemistry*, vol. 120, no. 12, pp. 19784–19795, 2019.

[14] Y. Tay, J. Rinn, and P. P. Pandolfi, "The multilayered complexity of ceRNA crosstalk and competition," *Nature*, vol. 505, no. 7483, pp. 344–352, 2014.

[15] S. Lin and R. I. Gregory, "MicroRNA biogenesis pathways in cancer," *Nature Reviews. Cancer*, vol. 15, no. 6, pp. 321–333, 2015.

[16] H. Guo, N. T. Ingolia, J. S. Weissman, and D. P. Bartel, "Mammalian microRNAs predominantly act to decrease target mRNA levels," *Nature*, vol. 466, no. 7308, pp. 835–840, 2010.

[17] T. V. Bagnyukova, I. P. Pogribny, and V. F. Chekhun, "MicroRNAs in normal and cancer cells: a new class of gene expression regulators," *Experimental Oncology*, vol. 28, no. 4, pp. 263–269, 2006.

[18] Y. Li, J. Quan, F. Chen et al., "MiR-31-5p acts as a tumor suppressor in renal cell carcinoma by targeting cyclin-dependent kinase 1 (CDK1)," *Biomedicine & Pharmacotherapy*, vol. 111, pp. 517–526, 2019.

[19] X. Chen, L. Zhong, X. Li, W. Liu, Y. Zhao, and J. Li, "Downregulation of microRNA-31-5p inhibits proliferation and invasion of osteosarcoma cells through Wnt/β-catenin signaling pathway by enhancing AXIN1," *Experimental and Molecular Pathology*, vol. 108, pp. 32–41, 2019.

[20] K. K. Sun, X. J. Shen, D. Yang et al., "MicroRNA-31 triggers G_2/M cell cycle arrest, enhances the chemosensitivity and inhibits migration and invasion of human gastric cancer cells by downregulating the expression of zeste homolog 2 (ZH2)," *Archives of Biochemistry and Biophysics*, vol. 663, pp. 269–275, 2019.

[21] S. J. Yi, P. Liu, B. L. Chen, L. Ou-Yang, W. M. Xiong, and J. P. Su, "Circulating miR-31-5p may be a potential diagnostic biomarker in nasopharyngeal carcinoma," *Neoplasma*, vol. 66, no. 5, pp. 825–829, 2019.

[22] Z. Lu, Q. He, J. Liang et al., "miR-31-5p is a potential circulating biomarker and therapeutic target for oral cancer," *Molecular Therapy-Nucleic Acids*, vol. 16, pp. 471–480, 2019.

[23] H. Peng, L. Wang, Q. Su, K. Yi, J. Du, and Z. Wang, "MiR-31-5p promotes the cell growth, migration and invasion of

Research Article

miR-338-3p Plays a Significant Role in Casticin-Induced Suppression of Acute Myeloid Leukemia via Targeting PI3K/ Akt Pathway

Kewei Yu [iD],[1] **Juan Wang** [iD],[2] **Junhui Hou** [iD],[3] **Lei Zhang** [iD],[4] **and Hui Liang** [iD][4]

[1]*Department of Pharmacy, Jinan Central Hospital, Cheeloo College of Medicine, Shandong University, Jinan, 250013 Shandong, China*
[2]*Department of Gynaecology, Jiyang People's Hospital, Jinan 251400, China*
[3]*Department of Tumor Radiotherapy (III), The Affiliated Qingdao Central Hospital of Qingdao University, The Second Affiliated Hospital of Medical College of Qingdao University, Qingdao 266042, China*
[4]*Department of Hematology, Qingdao Women and Children's Hospital, Qingdao 266034, China*

Correspondence should be addressed to Lei Zhang; zhanglei@qdfuer.com.cn

Objective. Casticin is generally used in traditional herbal medicine for its anti-inflammatory and anticarcinogenic pharmacological properties. Also, microRNAs are indispensable oncogenes or cancer suppressors being dysregulated in various diseases. In this study, we aimed to elucidate the mechanisms underlying effects of casticin on the progression of acute myeloid leukemia (AML). *Methods*. CCK-8 and flow cytometry were utilized to measure the proliferation and apoptosis of AML cell lines, respectively, after treatment with different concentrations of casticin. The alteration of several microRNA expressions in response to casticin treatment was detected by performing qRT-PCR, and the activity of PI3K/Akt pathways was evaluated through immunoblotting. Afterwards, the potential target gene of miR-338-3p was investigated by dual-luciferase reporter assay. In order to evaluate the role of miR-338-3p in the casticin-induced cellular phenotype changes, AML cells were transfected with miR-338-3p mimics or inhibitor and then subjected to proliferation and apoptosis analysis. Finally, a mouse xenograft model system was employed to investigate the role of casticin in AML progression in vivo. *Results*. Suppressed cellular proliferation and enhanced apoptosis were observed in HL-60 and THP-1 cells after exposure to casticin, accompanied by remarkable upregulation of the miR-338-3p expression as well as a decline in the phosphorylation of PI3K and Akt proteins. RUNX2 was identified as a direct target molecular of miR-338-3p, which might account for the findings that miR-338-3p knockdown enhanced the PI3K/Akt pathway activity, whereas the miR-338-3p overexpression inactivated this signaling pathway. In addition, the inhibition of the miR-338-3p expression attenuated severe cell apoptosis and suppressions of PI3K/Akt pathway induced by casticin. Furthermore, casticin treatment retarded tumor growth rate in mouse models, whilst elevating miR-338 expression and repressing the activity of PI3K/Akt pathway in vivo. However, miR-338-3p depletion could also abolish the phenotypic alterations caused by casticin treatment. *Conclusion*. Casticin promotes AML cell apoptosis but inhibits AML cell proliferation in vitro and tumor growth in vivo by upregulating miR-338-3p, which targets RUNX2 and thereafter inactivates PI3K-Akt signaling pathway. Our results provide insights into the mechanisms underlying the action of casticin in the control of AML progression.

1. Introduction

Acute myeloid leukemia (AML) is an aggressive clonal disorder of the hematopoietic system characterized by cytogenetic heterogeneity, which manifests as malignant proliferation of immature myeloid progenitor cells and impaired generation of normal hematopoietic stromal cells [1]. AML occurs in ~80% of adult patients with acute leukemia [2]. It progresses rapidly, and most patients will have relatively poor clinical outcomes. Typically, patients with AML initially receive intensive

induction therapy, followed by additional chemotherapy, targeted therapy, or stem-cell transplantation for postremission consolidation [3]. Less than half of these patients achieve long-time survival, and the others will die of this disease owing to the occurrence of relapse [4]. Therefore, it is of great realistic significance to develop novel effective therapeutic methods to treat the refractory AML.

Accumulating evidence have demonstrated that chemicals derived from traditional Chinese medicine can be used for treatment of human aliments [5–9]. Casticin, a bioactive ingredient isolated from the plant *Vitex rotundifolia*, is well known for its anti-inflammatory bioactivity and has been extensively applied in traditional Chinese medicine for a long time [10]. Increasing number of studies have reported that casticin can induce cell cycle arrest and apoptosis of cancerous cells in various kinds of carcinomas including melanoma [11], bladder cancer [12], cervical cancer [13], breast cancer [14], and colon cancer [15], and this may probably account for its anticarcinogenic actions. It has been observed that casticin exerts its synergistic effects when used in accompany with other chemotherapeutic drugs [16]. Apart from anti-inflammatory and anticarcinogenic activities, casticin possesses diverse functions such as immunoregulation, neuro-protection, and antihyperprolactinemia, as well as analgesia [17]. In particular, the apoptosis-promoting activity of casticin has been also found in leukemic cells [18, 19], but the detailed molecular mechanisms underlying how casticin plays its role in the suppression of leukemia development are still incompletely understood. Previous study proposed that casticin effectively promotes cell apoptosis in K562 cells by blocking PI3K/Akt pathway that is implicated in the regulation of cell survival [18]. In fact, suppression of Akt phosphorylation can enhance cellular apoptosis in AML [20], and a variety of antileukemia drugs may act, at least in part, by inactivating Akt protein [21].

MicroRNAs are defined as a class of noncoding and small RNA molecules (encompassing approximately 22 nucleotides) that can inhibit gene expression at posttranscriptional level by interacting with $3'$-UTR of the target gene, contributing to either degradation or translational suppression of mRNAs [22]. An increasing number of studies have revealed that miRNAs are indispensable oncogenes or cancer suppressors being dysregulated in AML development [23–25], suggesting that miRNAs may serve as potential pharmaceutical targets for AML therapy.

In this context, we presently evaluated the biological behaviors in HL60 cell and xenograft tumor growth after exposure to casticin treatment and also investigated the potential involved microRNAs and intracellular pathway. Our results will further improve our understanding about how casticin affects cell growth in the AML pathogenesis.

2. Materials and Methods

2.1. Cell Culture.
Human promyelocytic leukemia cell line HL-60 and normal bone marrow cell line (HS-5) were kindly given by the Oncology Center of Shandong University (Jinan, Shandong, China). The gifted cell line was approved by the Ethics Committee of Qianfoshan Hospital, affiliated to Shandong University. Another AML cell line THP-1 was purchased from American Type Culture Collection (ATCC). Cells were grown in RMPI 1640 medium (Gibco, Gaithersburg, MD, USA) supplemented with 10% fetal bovine serum (FBS, Gibco) and 1% penicillin-streptomycin and maintained at 37°C in a humidified atmosphere of 5% CO_2.

2.2. Preparation of Casticin Reagent.
Casticin was provided by the laboratory of medical engineering, Hunan Normal University (Changsha, Hunan, China), and the purity achieved 99%. Casticin was then dissolved in 10% dimethyl-sulfoxide (DMSO) in PBS and added into RMPI 1640 medium at the final concentrations of 1, 2, 4, and 8 g/mL. Cells were starved for 16 h before casticin treatment.

2.3. CCK8 Assay.
Cell proliferation was assessed using the Cell Counting Kit-8 (Dojindo Laboratories, Gaithersburg, MD, USA) according to the manufacturer's protocols. In brief, cells (5×10^4 cells/well) were plated into 96-well plates and were incubated at 37°C before they were exposed to escalating concentrations of casticin (1, 2, 4, 8 mg/mL) stepwise. At the indicated time points, $10\,\mu L$ of CCK-8 solution was added to each well, and the cells were incubated for another $2 \sim 4\,h$. The absorbance of samples was measured at 495 nm using a micro-plate reader (Bio-Rad, Hercules, CA, USA).

2.4. Cell Apoptosis Analysis.
Annexin V-fluorescein isothiocyanate (FITC) apoptosis detection kit (BD Biosciences, San Jose, CA, USA) was used to assess the apoptosis rate of HL-60 cells. Cells were washed twice with prechilled PBS, centrifugated and resuspended in binding buffer, and then incubated with $5\,\mu L$ of annexin V-FITC for 30 min in dark. Next, cells were incubated with $5\,\mu L$ of PI for 5 min in dark before they were subjected to analysis with a flow cytometer (FACScan, BD Biosciences).

2.5. Quantitative RT-PCR.
Total RNA was extracted from AML cells using TRIzo Reagent (TaKaRa, Dalian, China). Afterwards, cDNA was generated from $1\,\mu g$ RNA as template by performing reverse transcription PCR. miR-338-3p was quantified by virtue of a TaqMan miRNA Reverse-Transcription Kit (Life Technologies, Carlsbad, CA, USA), and U6 snRNA acted as the internal control. The gene expression of *RUNX2* was assessed by using One Step Prime Script miRNA cDNA Synthesis Kit (Qiagen, Valencia, CA, USA) and a SYBR™ PrimeScript RT-PCR Kit (TaKaRa), according to the manufacturer's instructions. Primer sequences were shown in Table 1. The comparative 2$_{-}{}^{\Delta\Delta Ct}$ method was used for relative quantification and statistical analysis.

2.6. TUNEL Staining.
Apoptotic cells were detected using the in situ cell death detection kit (Roche, Mannheim, Germany) following the manufacturer's protocol. TUNEL staining–positive cells in the cartilage area were visualized under a fluorescence microscope.

2.7. Cell Transfection.
The miR-338-3p mimic, inhibitor, and corresponding negative control (NC) were purchased from GenePharma (Shanghai, China). 50 nM miR-338-3p/NC

TABLE 1: Primers for reverse transcription (RT) and real-time PCR.

Gene		Sequences
miR-338-3p	Forward	ATCCAGTGCGTGTCGTG
	Reverse	TGCTTCCAGCATCAGTGAT
(for RT)		GTCGTATCCAGTGCGTGTCGTGGAG TCGGCAATTGCACTGGATACGACCAACAAA
U6	Forward	GCTTCGGCAGCACATATACTAAAAT
	Reverse	CGCTTCACGAATTTGCGTGTCAT
(for RT)		CGCTTCACGAATTTGCGTGTCAT
RUNX2	Forward	CTAGGCGCATTTCAGGTGCT
	Reverse	TGGCAGGTAGGTGTGGTAGT
GAPDH	Forward	GCCAAAAGGGTCATCATCTC
	Reverse	GTAGAGGCAGGGATGATGTTC

mimics or inhibitor was transfected into cells (2×10^5/well) seeded in a 6-well plate, using Lipofectamine 3000 reagent (Invitrogen, Grand Island, NY, USA) according to the manufacturer's protocol. Cells were incubated at 37°C with 5% CO_2 and harvested at least 48 h later for the subsequent study.

2.8. Dual Luciferase Reporter Assay. The human RUNX2 $3'$-UTR fragment containing the wild-type or mutant miR-338-3p binding site was synthesized by Invitrogen and amplified before cloned into pmirGLO Vector (Promega, Madison, WI, USA) between the SacI and XhoI sites. Cells were subsequently cotransfected with miR-338-3p (or miR-NC) and the reconstructed vector and subjected to luciferase activity analysis using the dual-luciferase assay system (Promega) after 48 h transfection. Renilla-luciferase activity was used for normalization.

2.9. Western Blotting. Primary antibodies against RUNX2, β-actin, p-Akt, Akt, p-PI3K, PI3K, and HRP-conjugated goat anti-rabbit IgG were purchased from Cell Signaling Technology (Beverly, MA, USA). Proteins were extracted from cell lysates with RIPA lysis buffer (Beyotime Biotech, Shanghai, China) following the manufacturer's instructions. The total proteins were resolved by SDS-PAGE (10% acrylamide) before being transferred to PVDF membrane, which were blocked with 5% silk milk for at least 1 h and incubated overnight at 4°C with specific primary antibodies. After rinsing with TBST, the membrane was then incubated for 1 h at room temperature with goat anti-rabbit IgG. Finally, the labeled proteins were visualized with ECL substrates (Millipore, MA, USA) before quantifying the band intensity using Image Lab TM software (Bio-Rad, Shanghai, China).

2.10. Animal Experiment. 4 ~ 6-week-old BALB/c nude mice were purchased from the Provincial Laboratory Animal Center (Jinan, Shandong, China) and maintained on a 12-h light–dark cycle and were allowed free access to standard rodent chow and water ad libitum. All the mice were randomly divided into groups: (1) AML model (as the control group), (2) casticin, (3) miR-338 inhibitor, and (4) casticin + miR-338 inhibitor, $n = 5$ in each group. 5×10^6 HL-60 cells were subcutaneously injected into mice to obtain AML mouse models, and for groups (3) ~ (4), HL-60 cells transfected with miR-338 were used. Additionally, mice were administrated with casticin (40 mg/kg/d) to evaluate its antitumor role in vivo, while the control mice received only normal saline vehicle. The width and length of tumor xenografts were detected at different time points to calculate tumor volumes: volume = width^2 × length/2. After 4 weeks, the mice were sacrificed, and tumor xenografts were weighed and analyzed for gene and protein expression. This experiment was approved by the Ethics Committee of Qianfoshan Hospital, in accordance with the guidelines of our hospital regarding the welfare and ethic for experimental animals.

2.11. Statistical Analysis. Data are presented as means ± SD. All experiments included at least 3 replicates per group. Groups were compared using the two-tailed Student's t-test for parametric data. All statistical analyses were carried out using the SPSS 19.0 software (SPSS, Inc., Chicago, IL). A value of $P < 0.05$ was considered statistically significant.

3. Results

3.1. Casticin Induces the Apoptosis of HL-60 Cells. After human promyelocytic leukemia HL-60 cells were treated with casticin, there was a significant decline in cell viability (Figure 1(a)), and the impact of casticin on cell viability was in a dose- and time-dependent manner. Subsequently, flow cytometry was performed to analyze the apoptosis rate of HL-60 in response to casticin treatment, which demonstrated a dramatic increase in the proportion of apoptotic cells in parallel with the augmented casticin concentration (Figure 1(b)).

Additionally, we found that the number of TUNEL-stained HL-60 cells was increased when cells were treated with higher concentration of casticin (Figure 1(c)), consistent with results in Figure 1(b). These all indicate that casticin inhibits the proliferation and enhances apoptosis in HL-60 cells in a dose-dependent manner. In order to confirm these results, another AML cell line THP-1 was subjected to casticin treatment. We observed that casticin not only mitigated THP-1 cell proliferation but also induced cells to undergo apoptosis in a dose- and time-dependent manner (Figure S1).

(a)

(b)

FIGURE 1: Continued.

(c)
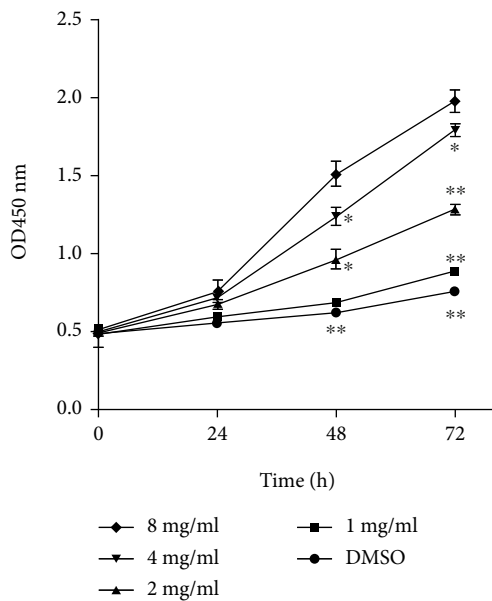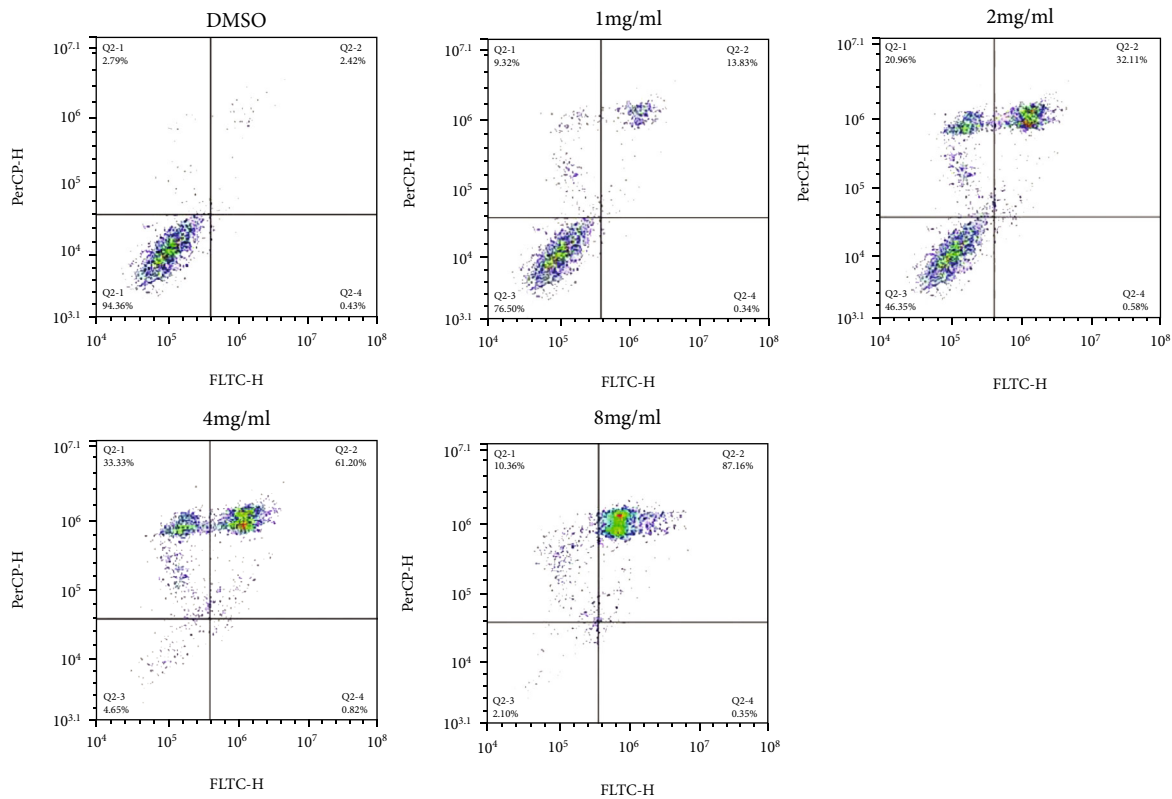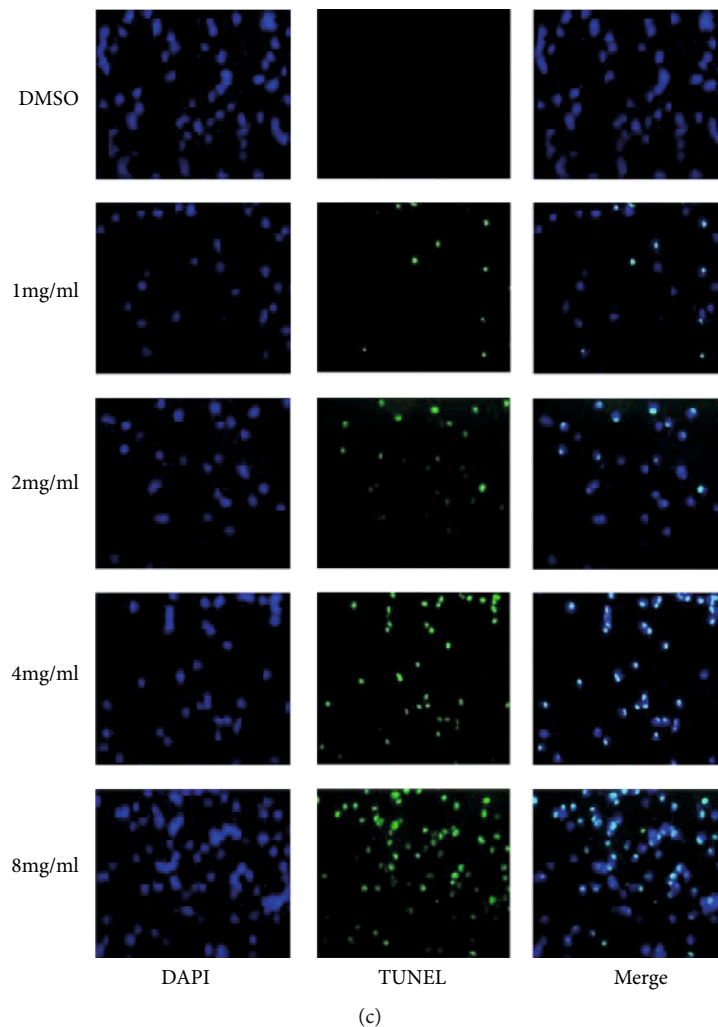
FIGURE 1: Casticin inhibits HL-60 cell proliferation and promotes apoptosis. (a) HL-60 cells were treated with different concentrations of casticin (1, 2, 4, 8 mg/mL) and subjected to CCK8 analysis at the indicated time intervals. After treatment with casticin for 72 h, cell apoptosis was analyzed by performing flow cytometry (b) and TUNEL assay (c). Compared with the DMSO control group, $*$ indicates $P < 0.05$; $**$ indicates $P < 0.01$.

3.2. miR-338-3p Is Upregulated after Casticin Treatment.

In order to further determine how casticin affects the phenotype of AML cells, we next detected the expression alteration of several microRNAs in HL60 and THP-1 cells after exposure to casticin. These microRNAs were previously reported to show aberrant expression in AML patients, which is associated with different prognoses of this disease [23–25], including miR-29, miR-338, miR-125, miR-142, miR-146, and miR-155 (data not shown), but among them, only miR-338 was sensitive to casticin treatment. As shown in Figure 2(a) and Figure S1-S2, miR-338-3p was suppressed in both HL60 and THP-1 compared with the normal bone marrow cells but obviously upregulated after exposure to casticin ($P < 0.01$), which was dose-dependent.

3.3. miR-338-3p Depletion Attenuates the Casticin-Induced Apoptosis in HL60 Cells.

In order to confirm the role of miR-338-3p in casticin-mediated cell apoptosis in AML, we introduced miR-338-3p mimics or inhibitor into HL-60 cells

in prior to casticin treatment. In fact, miR-338-3p has been extensively reported to inhibit the cell proliferation and promote cell apoptosis in various cancers [26–29]. Our results indicated that exogenous miR-338-3p suppressed cell viability and promoted apoptosis of HL-60 cells, whereas the transfection of miR-338-3p inhibitor caused the opposite results (Figures 2(b) and 2(c)). Although casticin dramatically changed cell phenotype as mentioned above, the miR-338-3p inhibitor transfected into HL-60 cells caused an increase in cell viability but impaired apoptosis rate, which seems to abrogate the function of casticin.

3.4. Inhibition of miR-338-3p Mitigates the Effect of Casticin on PI3K/Akt Activity.

Casticin was demonstrated to inactivate PI3K/Akt signaling pathway thereby enhancing apoptosis in K562, another AML cell line [13]. We therefore evaluated the PI3K/Akt activity in HL60 cells and found that this pathway was distinctly prohibited in the presence of casticin (Figure 2(d)). In addition, aberrant activation of

(a)

(b)

(c)
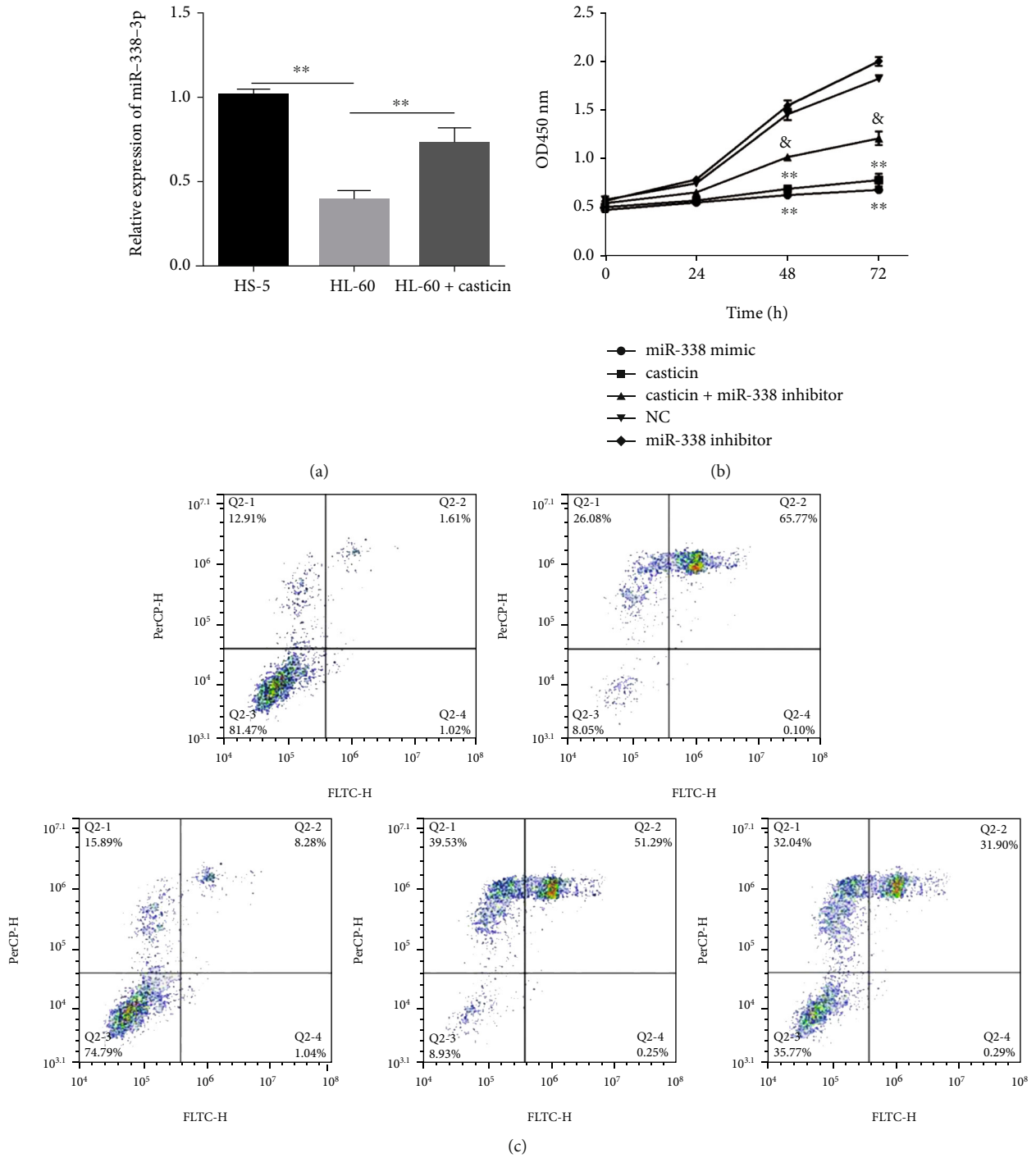
Figure 2: Continued.
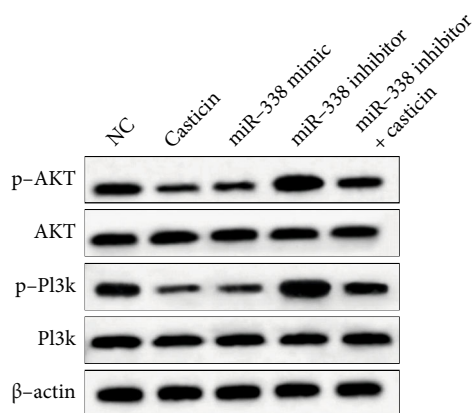
(d)

FIGURE 2: miR-338-3p is upregulated after casticin treatment, and miR-338-3p silencing mitigates the effect of casticin on PI3K/Akt activity. HL-60 cells were treated with 8 mg/mL casticin for 72 h. (a) The miR-338-3p expression was measured by qRT-PCR. **$P < 0.01$. (b) CCK8 was used to assess the viability of HL-60 cells transfected with miR-338-3p mimics or inhibitor. (c) Flow cytometry was carried out to test the apoptosis of HL-60 cells. *$P < 0.05$ and **$P < 0.01$ compared with the NC group, and "&" indicates $P < 0.05$ compared to untransfected cells treated with casticin. (d) Expression of the major components in PI3K/Akt pathway and the phosphorylated forms of them were determined using immunoblotting. NC: untransfected cells used as the negative control.

PI3K/Akt pathway was observed in HL60 cells where miR-338-3p was silenced, while it was inactivated in cells with the miR-338-3p overexpression. Intriguingly, when those casticin-treated HL60 cells were subjected to miR-338-3p knockdown, the casticin treatment seemed noneffective.

3.5. miR-338-3p Directly Targets RUNX2 in AML Cells. The putative target genes of miR-338-3p were predicted by scanning TargetScan and RegRNA as public miRNA databases. Among numerous candidate genes, RUNX2 harboring a highly conserved binding site in the 3′-UTR for miR-338-3p (Figure 3(a)) was particularly concerned due to its involvement in PI3K/Akt signaling [23]. We next performed luciferase reporter assay to verify the relationship between miR-338-3p and RUNX2. A luciferase reporter plasmid containing the 3′-UTR-binding site of RUNX2 was cotransfected with miR-338-3p response element into HL-60 cells. As shown in Figure 3(b), miR-338-3p mimics impaired the luciferase activity of reporter plasmid carrying wild-type (WT) RUNX2 3′-UTR but had no effect on the mutant (MUT) RUNX2 3′-UTR.

Afterwards, we determined whether miR-338-3p has an impact on the endogenous expression of RUNX2 in HL-60 cells by conducting RT-qPCR and Western blot assay. The results showed that the enhanced expression of miR-338-3p significantly suppressed the RUNX2 expression at both mRNA and protein levels, whereas restriction of miR-338-3p led to an increase in the RUNX2 expression (Figures 3 (c) and 3(d)). Taken together, these data demonstrate that miR-338-3p decreases the RUNX2 expression by directly targeting its 3′-UTR in AML cells.

3.6. Casticin Controls Tumor Growth In Vivo by Promoting miR-338-3p Expression. The effect of casticin on AML progression in vivo was also investigated in mice. Firstly, HL-60 cells were subcutaneously inoculated into the mice,

administrated with casticin, and the expression level of miR-338-3p was detected. Of note, according to RT-qPCR analysis, miR-338-3p was upregulated in tumor xenografts derived from casticin-treated HL-60 cells (Figure 4(a), $P < 0.05$). Next, the tumor weight and volume of xenografts were tested to evaluate the effect of casticin on tumor growth in vivo. As illustrated in Figure 4(b), the weight of tumor xenografts in the casticin group was substantially reduced in comparison with the xenografts derived from untreated HL-60 cells. Also, the tumor volume was decreased in the casticin group compared to the NC group (Figure 4(c)).

To confirm that miR-338-3p upregulation was responsible for the inhibitory role of casticin in tumor growth, cells were transfected with miR-338-3p inhibitor before they were subjected to casticin exposure. As shown in Figures 4(b) and 4(c), although the tumor formation was hindered when HL-60 cells were stimulated with casticin, miR-338-3p inhibition could accelerate the process of tumorigenesis in spite of the preceding casticin treatment, suggesting the role of miR-338-3p in the casticin-mediated tumor suppression.

The expression of RUNX2 at the protein level and the activity of PI3K/Akt pathway were analyzed. Compared with the control group, both RUNX2 expression and the phosphorylation of Akt and PI3K proteins were enhanced in the miR-338-3p group. Furthermore, remarkable decrease in the protein levels of RUNX2, p-Akt, and p-PI3K was observed in the xenografts treated with casticin, but these decreased expression profiles were abolished by the addition of miR-338 inhibitor (Figure 4(d)). The results manifest that casticin inhibits AML progression in vivo by upregulating miR-338-3p via RUNX2/PI3K/Akt axis.

4. Discussion

Nowadays, the mainstream therapeutic regimens for patients with AML are presented by stem-cell transplantation, chemotherapy, and targeted therapy. Given that

(a)

(b)

(c)

(d)
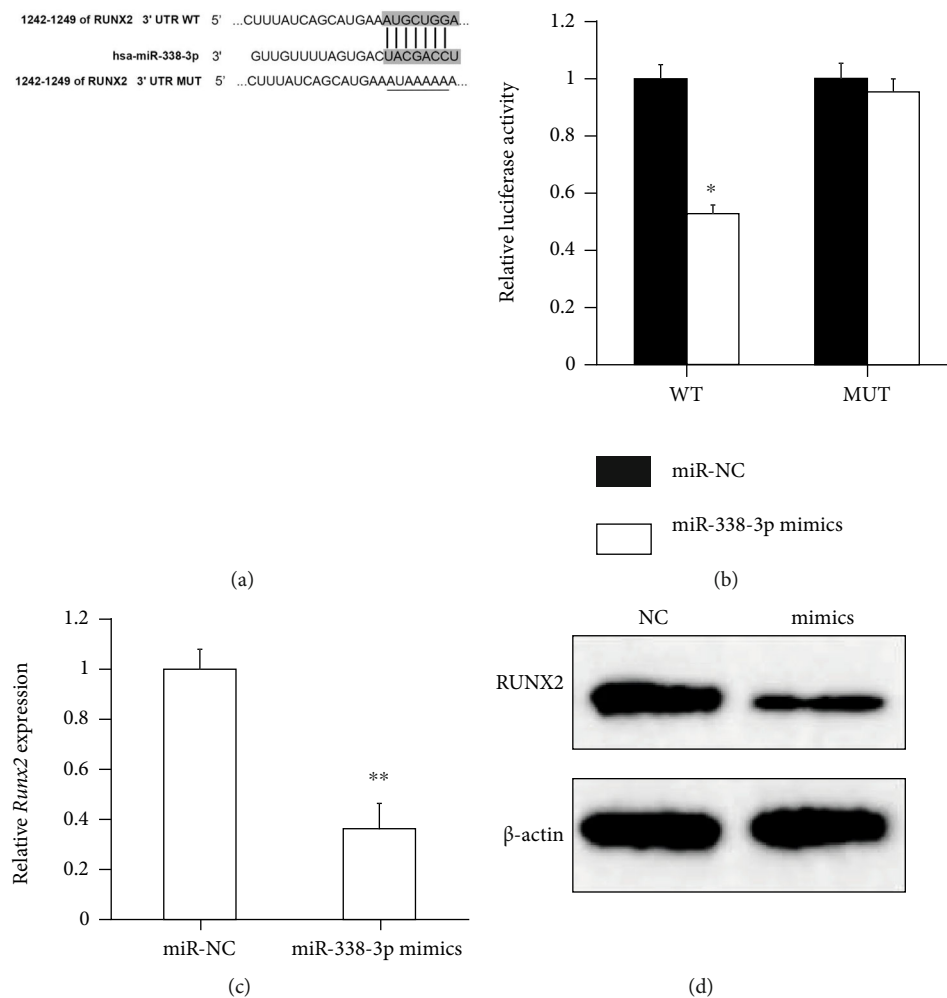
FIGURE 3: miR-338-3p directly targets RUNX2 in HL-60 cells. (a) The putative binding sites for miR-338-3p in the RUNX2 3′-UTR. WT: wild-type; MUT: mutant sequence. (b) The luciferase activity was detected using the dual luciferase reporter assay, after HL-60 cells were cotransfected with a luciferase plasmid harboring RUNX2 3′-UTR (WT or MUT) and miR-338 mimics or miR-NC. (c, d) The endogenous expression of RUNX2 was evaluated at mRNA and protein levels by conducting RT-qPCR and Western blot assay, respectively. * indicates $P < 0.05$; ** indicates $P < 0.01$.

chemotherapy cannot cure a majority of AML patients, stem-cell transplantation acts as an alternative treatment strategy in most cases. However, allogeneic stem-cell transplantation is not always feasible for those patients who have developed high-risk leukemia, and therefore, the recurrent and mortality rates in AML patients are still very high. Casticin has been reported to induce the apoptosis of several leukemic cell lines [18, 19], thereafter emerging as promising treatment that may improve the outcomes of AML patients. In this study, after human promyelocytic leukemia HL-60 cells treated with casticin, there was a significant decline in cell viability, and the impact of casticin on cell viability was in a dose- and time-dependent manner. Subsequently, flow cytometry demonstrated a dramatic increase in the proportion of apoptotic cells in parallel with the augmented casticin concentration.

Aberrant alterations in miRNA expression level are tightly related to the initiation and/or progression of diverse malignancies including AML [23–25], which suggests that

miRNAs may function as potential targets for AML treatment. miR-338-3p functions as a tumor suppressor in multiple carcinomas by targeting diverse genes and certain pathways. For example, miR-338-3p targets PREX2a, a protein that activates PI3K/Akt signaling by confronting PTEN in cancerous cells, and thus suppresses gastric cancer and neuroblastoma [26, 27]. In our present study, the expression pattern of miR-338-3p was changed upon casticin incitement. Casticin inhibited the proliferation and induced apoptosis in HL-60 cells; therefore, we attempt that casticin affects the phenotype of AML cell through regulating miR-338-3p expression level. ATF2 was also identified as a target gene of miR-338-3p, and it could inhibit the proliferation of cervical cancer cells via targeting the PI3K/Akt/mTOR signaling cascade [28].

Actually, casticin has been reported to enhance apoptosis in K562 cell line by inactivating PI3K/Akt signaling pathway [18], a critical axis modulating cancer cell survival and metastasis. We evaluated the activity of PI3K/Akt pathway

(a)

(b)

(c)

(d)
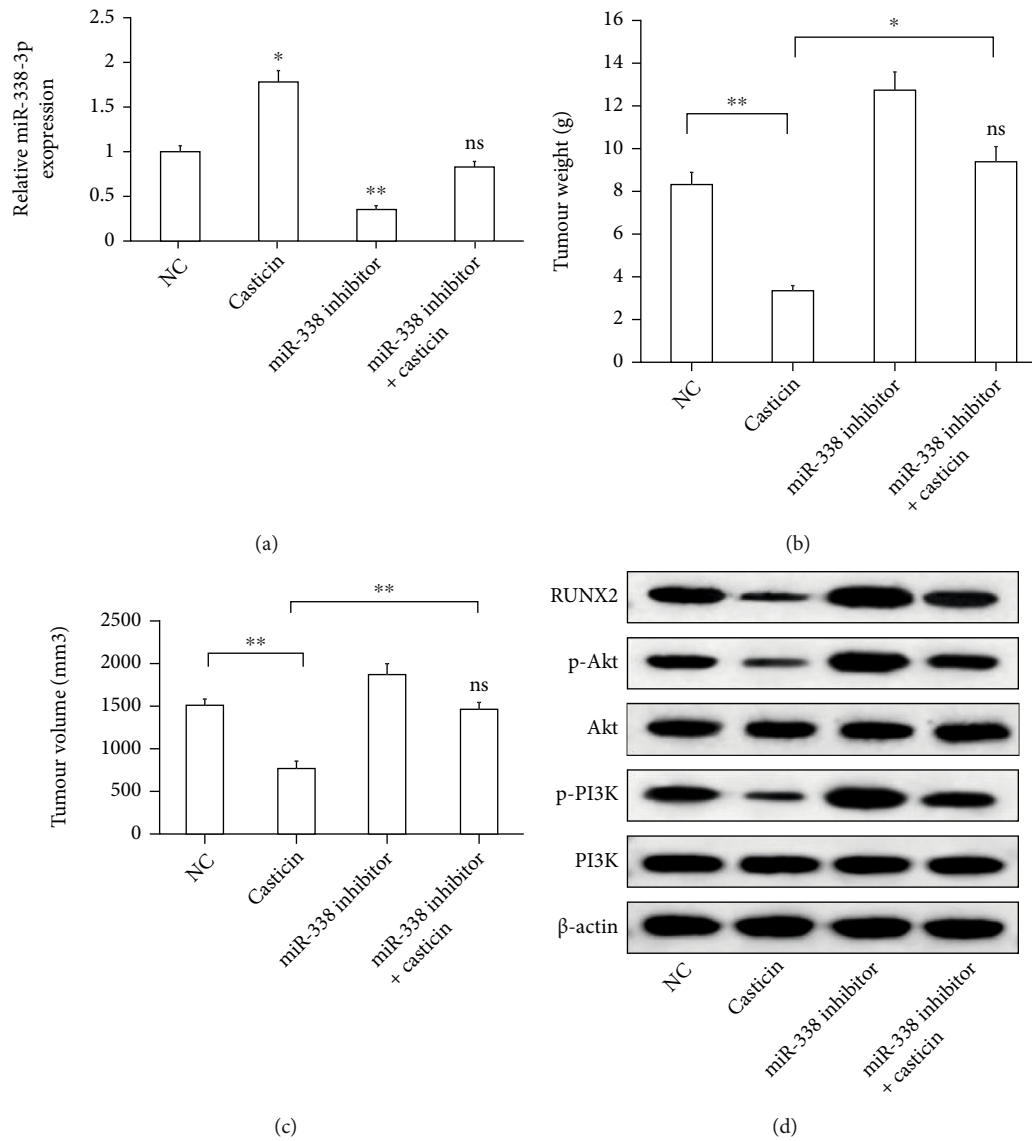
FIGURE 4: Casticin controls tumor growth in vivo by promoting miR-338-3p expression. HL-60 cells were transfected with miR-338 inhibitor, in the presence or absence of casticin. (a) The expression of miR-338-3p in HL-60 cells undergoing different treatment was assessed by qRT-PCR. Compared to untreated cells, $^*P < 0.05$; $^{**}P < 0.01$; ns means the difference is not significant. The xenograft tumors formed were excised after 4 weeks. (b) The tumor was massed in each group. $^*P < 0.05$; $^{**}P < 0.01$ between two groups; "ns" indicates not significant vs. control group. (c) The width and length of tumor were measured, and tumor volume was determined according to them: volume = width^2 × length/2. $^*P < 0.05$; $^{**}P < 0.01$ between two groups; "ns": not significant vs. control group. (d) The expression level of proteins in the tumor xenografts was detected by western blot assay. Beta-actin was used for the normalization.

in HL-60 cells after casticin treatment and found that the phosphorylated PI3K and Akt proteins were decreased in response to casticin, which is consistent with previous study. Moreover, miR-338-3p knockdown enhanced PI3K/Akt signaling pathway and abrogated the casticin-mediated inactivation of this pathway, whereas the overexpression of miR-338-3p further suppressed PI3K/Akt activity.

On the other hand, we also confirmed that RUNX2 was directly targeted by miR-338-3p in HL-60 cells. RUNX2 is a pivotal regulator for skeletal development but abnormally expressed during carcinogenesis and, in particular, its function as the direct target of miR-338-3p has been previously proved in the ovarian epithelial carcinoma [29].

There is a mutual interaction between RUNX2 and PI3K/Akt pathway: Akt can directly or indirectly enforce RUNX2 expression level and/or transcriptional activity, which will reciprocally contribute to the activation of PI3K/Akt signaling [30]. Therefore, we propose that miR-338-3p may regulate AML cell proliferation and apoptosis in vitro by targeting RUNX2-PI3K/Akt axis.

Additionally, in order to investigate the role of casticin in AML progression in vivo, we employed a mouse xenograft model system, where there was an observation that inhibition of the miR-338-3p expression remarkably accelerated tumorigenesis and abolished the inhibitory effect of casticin on tumor growth.

5. Conclusion

In aggregate, our results demonstrate that the miR-338 expression in HL-60 cells was significantly upregulated in response to casticin treatment, companied by enhanced cell apoptosis and PI3K/Akt inactivation. RUNX2 was also identified as the direct target of miR-338 in HL-60 cells. Furthermore, the enhanced miR-338 expression could mimic the inhibitory effect of casticin on cell proliferation and PI3K/Akt pathway activation, whereas miR-338 inhibition mitigated the function of casticin both in vitro and in vivo, suggesting that casticin might suppress AML development and/or progression by increasing the miR-338 expression and targeting RUNX2-PI3K/Akt signaling pathway.

Data Availability

The datasets during the current study are available from the corresponding author on reasonable request.

Conflicts of Interest

The authors declare that they do not have any commercial or associative interest that represents a conflict of interest in connection with the work submitted.

Supplementary Materials

Supplementary 1. Figure S1: casticin inhibits THP-1 cell proliferation and promotes apoptosis. (a) THP-1 cells were treated with different concentrations of casticin (1, 2, 4, 8 mg/mL) and subjected to CCK-8 analysis at the indicated time intervals. Compared with the DMSO control group, * indicates $P < 0.05$; ** indicates $P < 0.01$. (b) After treatment with casticin for 72 h, cell apoptosis was analyzed by performing flow cytometry. (c) Verification of the flow cytometry results by TUNEL assay. * $P < 0.05$; ** $P < 0.01$. (d) The miR-338-3p expression was measured by qRT-PCR in THP-1 cell. ** $P < 0.01$.

Supplementary 2. Figure S2: casticin increases the miR-338-3p expression in HL-60 (a) and THP-1 (b) cells in a dose-dependent manner. As shown in Figure S1, THP-1 cells were treated with different concentrations of casticin (1, 2, 4, 8 mg/mL), and the results showed that there was a significant decline in cell viability (Figure S1A), and the impact of casticin on cell viability was in a dose- and time-dependent manner. Subsequently, flow cytometry was performed to analyze the apoptosis rate of THP-1 in response to casticin treatment, which demonstrated a dramatic increase in the proportion of apoptotic cells in parallel with the augmented casticin concentration (Figure S1B). Additionally, we found that the number of TUNEL-stained THP-1 cells was increased when cells were treated with higher concentration of casticin (Figure S1C), consistent with results in Figure S1B. As shown in Figure S1D, miR-338-3p was suppressed in THP-1 cell compared with the normal bone marrow cells but obviously upregulated after exposure to casticin. As shown in Figure S2, miR-338-3p was obviously upregulated after exposure to casticin in HL-60 and THP-1 cells ($P < 0.01$), which was dose-dependent.

References

[1] N. J. Short and F. Ravandi, "Acute myeloid leukemia: past, present, and prospects for the future," *Clinical Lymphoma, Myeloma & Leukemia*, vol. 16, Suppl, pp. S25–S29, 2016.

[2] N. J. Short, M. E. Rytting, and J. E. Cortes, "Acute myeloid leukaemia," *The Lancet*, vol. 392, no. 10147, pp. 593–606, 2018.

[3] H. Döhner, D. J. Weisdorf, and C. D. Bloomfield, "Acute myeloid leukemia," *The New England Journal of Medicine*, vol. 373, no. 12, pp. 1136–1152, 2015.

[4] C. A. Schiffer, "Hematopoietic growth factors and the future of therapeutic research on acute myeloid leukemia," *The New England Journal of Medicine*, vol. 349, no. 8, pp. 727–729, 2003.

[5] L. Song, X. Li, X. X. Bai, J. Gao, and C. Y. Wang, "Calycosin improves cognitive function in a transgenic mouse model of Alzheimer's disease by activating the protein kinase C pathway," *Neural Regeneration Research*, vol. 12, no. 11, pp. 1870–1876, 2017.

[6] Z. Wen, W. Hou, W. Wu et al., "6-O-Galloylpaeoniflorin attenuates cerebral ischemia reperfusion-induced neuroinflammation and oxidative stress via PI3K/Akt/Nrf2 activation," *Oxidative Medicine and Cellular Longevity*, vol. 2018, Article ID 8678267, 14 pages, 2018.

[7] J. Gao, L. Song, H. Xia, L. Peng, and Z. Wen, "6'-O-galloyl-paeoniflorin regulates proliferation and metastasis of non-small cell lung cancer through AMPK/miR-299-5p/ATF2 axis," *Respiratory Research*, vol. 21, no. 1, p. 39, 2020.

[8] Y. Zhu, C. Wang, J. Luo et al., "The protective role of Zingerone in a murine asthma model via activation of the AMPK/Nrf2/HO-1 pathway," *Food & Function*, vol. 12, no. 7, pp. 3120–3131, 2021.

[9] C. Wang, J. Luo, X. Bai et al., "Calycosin alleviates injury in airway epithelial cells caused by PM 2.5 exposure via activation of AMPK signalling," *Evidence-based Complementary and Alternative Medicine*, vol. 2021, Article ID 8885716, 9 pages, 2021.

[10] S. Lin, H. Zhang, T. Han, J. Z. Wu, K. Rahman, and L. P. Qin, "In vivo effect of casticin on acute inflammation," *Zhong Xi Yi Jie He Xue Bao*, vol. 5, no. 5, pp. 573–576, 2007.

[11] Y. W. Shiue, C. C. Lu, Y. P. Hsiao et al., "Casticin induced apoptosis in A375.S2 human melanoma cells through the inhibition of NF-κB and mitochondria-dependent pathwaysin vitroand inhibited human melanoma xenografts in a mouse modelin vivo," *The American Journal of Chinese Medicine*, vol. 44, no. 3, pp. 637–661, 2016.

[12] A. Rasul, R. Bao, M. Malhi et al., "Induction of apoptosis by costunolide in bladder cancer cells is mediated through ros generation and mitochondrial dysfunction," *Molecules*, vol. 18, no. 2, pp. 1418–1433, 2013.

[13] F. Zeng, L. Tian, F. Liu, J. Cao, M. Quan, and X. Sheng, "Induction of apoptosis by casticin in cervical cancer cells: reactive oxygen species-dependent sustained activation of Jun N-terminal kinase," *Acta Biochimica et Biophysica Sinica*, vol. 44, no. 5, pp. 442–449, 2012.

[14] K. Haidara, L. Zamir, Q. W. Shi, and G. Batist, "The flavonoid casticin has multiple mechanisms of tumor cytotoxicity action," *Cancer Letters*, vol. 242, no. 2, pp. 180–190, 2006.

[15] S. Y. Tang, M. Z. Zhong, G. J. Yuan et al., "Casticin, a flavonoid, potentiates TRAIL-induced apoptosis through modulation of anti-apoptotic proteins and death receptor 5 in colon cancer cells," *Oncology Reports*, vol. 29, no. 2, pp. 474–480, 2013.

[16] J. Xia, J. Gao, Y. Inagaki, N. Kokudo, M. Nakata, and W. Tang, "Flavonoids as potential anti-hepatocellular carcinoma agents: recent approaches using HepG2 cell line," *Drug Discoveries & Therapeutics*, vol. 7, no. 1, pp. 1–8, 2013.

[17] Y. Ling, J. Zhu, M. Fan, B. Wu, L. Qin, and C. Huang, "Metabolism studies of casticin in rats using HPLC-ESI-MSn," *Biomedical Chromatography*, vol. 26, no. 12, pp. 1502–1508, 2012.

[18] J. K. Shen, Y. M. Du HP, Y. G. Wang, and J. Jin, "Casticin induces leukemic cell death through apoptosis and mitotic catastrophe," *Annals of Hematology*, vol. 88, no. 8, pp. 743–752, 2009.

[19] H. Y. Wang, B. Cai, C. B. Cui, D. Y. Zhang, and B. F. Yang, "Vitexicarpin, a flavonoid from Vitex trifolia L., induces apoptosis in K562 cells via mitochondria-controlled apoptotic pathway," *Yao Xue Xue Bao*, vol. 40, no. 1, pp. 27–31, 2005.

[20] V. Papa, P. L. Tazzari, F. Chiarini et al., "Proapoptotic activity and chemosensitizing effect of the novel Akt inhibitor perifosine in acute myelogenous leukemia cells," *Leukemia*, vol. 22, no. 1, pp. 147–160, 2008.

[21] S. Loges, H. Tinnefeld, A. Metzner et al., "Downregulation of VEGF-A, STAT5 and AKT in acute myeloid leukemia blasts of patients treated with SU5416," *Leukemia & Lymphoma*, vol. 47, no. 12, pp. 2601–2609, 2006.

[22] L. He and G. J. Hannon, "MicroRNAs: small RNAs with a big role in gene regulation," *Nature Reviews. Genetics*, vol. 5, no. 7, pp. 522–531, 2004.

[23] M. Khalaj, M. Tavakkoli, A. W. Stranahan, and C. Y. Park, "Pathogenic microRNA's in myeloid malignancies," *Frontiers in Genetics*, vol. 5, p. 361, 2014.

[24] C. H. Yeh, R. Moles, and C. Nicot, "Clinical significance of microRNAs in chronic and acute human leukemia," *Molecular Cancer*, vol. 15, no. 1, p. 37, 2016.

[25] L. Fu, J. Qi, X. Gao et al., "High expression of miR-338 is associated with poor prognosis in acute myeloid leukemia undergoing chemotherapy," *Journal of Cellular Physiology*, vol. 234, no. 11, pp. 20704–20712, 2019.

[26] X. Chen, M. Pan, L. Han, H. Lu, X. Hao, and Q. Dong, "miR-338-3p suppresses neuroblastoma proliferation, invasion and migration through targeting PREX2a," *FEBS Letters*, vol. 587, no. 22, pp. 3729–3737, 2013.

[27] B. Guo, L. Liu, J. Yao et al., "miR-338-3p suppresses gastric cancer progression through a PTEN-AKT axis by targeting P-REX2a," *Molecular Cancer Research*, vol. 12, no. 3, pp. 313–321, 2014.

[28] R. Lu, Z. Yang, G. Xu, and S. Yu, "miR-338 modulates proliferation and autophagy by PI3K/AKT/mTOR signaling pathway in cervical cancer," *Biomedicine & Pharmacotherapy*, vol. 105, pp. 633–644, 2018.

[29] C. Wen, X. Liu, H. Ma, W. Zhang, and H. Li, "miR-338-3p suppresses tumor growth of ovarian epithelial carcinoma by targeting Runx2," *International Journal of Oncology*, vol. 46, no. 5, pp. 2277–2285, 2015.

[30] K. A. Cohen-Solal, R. K. Boregowda, and A. Lasfar, "RUNX2 and the PI3K/AKT axis reciprocal activation as a driving force for tumor progression," *Molecular Cancer*, vol. 14, no. 1, p. 137, 2015.

Retraction

Retracted: The Value of m5C-Related lncRNAs in the Prognostic Assessment and Immunotherapy of Stomach Adenocarcinoma

BioMed Research International

This article has been retracted by Hindawi following an investigation undertaken by the publisher [1]. This investigation has uncovered evidence of one or more of the following indicators of systematic manipulation of the publication process:

(1) Discrepancies in scope

(2) Discrepancies in the description of the research reported

(3) Discrepancies between the availability of data and the research described

(4) Inappropriate citations

(5) Incoherent, meaningless and/or irrelevant content included in the article

(6) Peer-review manipulation

The presence of these indicators undermines our confidence in the integrity of the article's content and we cannot, therefore, vouch for its reliability. Please note that this notice is intended solely to alert readers that the content of this article is unreliable. We have not investigated whether authors were aware of or involved in the systematic manipulation of the publication process.

Wiley and Hindawi regrets that the usual quality checks did not identify these issues before publication and have since put additional measures in place to safeguard research integrity.

We wish to credit our own Research Integrity and Research Publishing teams and anonymous and named external researchers and research integrity experts for contributing to this investigation.

The corresponding author, as the representative of all authors, has been given the opportunity to register their agreement or disagreement to this retraction. We have kept a record of any response received.

References

[1] C. He, X. Zhu, F. Kong et al., "The Value of m5C-Related lncRNAs in the Prognostic Assessment and Immunotherapy of Stomach Adenocarcinoma," *BioMed Research International*, vol. 2022, Article ID 2747799, 26 pages, 2022.

Research Article

The Value of m5C-Related lncRNAs in the Prognostic Assessment and Immunotherapy of Stomach Adenocarcinoma

Chenxi He,[1,2] Xinying Zhu,[3] Fanting Kong,[2] Xiaochong Zhang,[2] Xiukun Chai,[1] Chunyan Zou,[1] and Dongqiang Zhao ⬭[1]

[1]*Department of Gastroenterology, The Second Hospital of Hebei Medical University, Shijiazhuang, 050000 Hebei Province, China*
[2]*Department of Gastroenterology, Xingtai People's Hospital, Xingtai, 054000 Hebei Province, China*
[3]*Department of Gastroenterology, The Third Hospital of Hebei Medical University, Shijiazhuang, 050000 Hebei Province, China*

Correspondence should be addressed to Dongqiang Zhao; hbzdq_1998@163.com

Long noncoding RNAs (lncRNAs) are closely associated with a variety of tumors, including stomach adenocarcinoma (STAD). However, the role of 5-methylcytosine- (m5C-) related lncRNAs in STAD is still uncertain. This study investigated the value of m5C-related lncRNAs in prognostic evaluation and immunotherapy of STAD. STAD transcriptome sequencing data were downloaded from The Cancer Genome Atlas (TCGA) database, and m5C-related lncRNAs were screened by Pearson correlation analysis. A prognostic m5C-related lncRNA signature (m5CRLSig) associated with STAD was established using univariate and multivariate Cox regression analysis. We constructed a prognostic risk model for STAD with six m5C-related lncRNAs. The receiver operating characteristic (ROC) curve was used to examine the predictive efficacy. Univariate and multifactorial Cox regression analysis and principal component analysis (PCA) validated m5CRLSig as an independent factor of STAD prognosis. The clinicopathological characteristics of the model showed higher risk scores for stages II-IV, grade 3, N1-3, and death status. The calibration curve of a nomogram revealed that the nomogram had an excellent predictive function for survival risk. Furthermore, the expression of six m5C-related lncRNAs in STAD and paracancerous tissues was detected by quantitative real-time PCR (qRT-PCR), which verified the feasibility of the m5CRLSig as a prognostic marker for STAD. m5C-related lncRNAs were linked to multiple immune-associated pathways, according to gene set enrichment analysis (GSEA). CIBERSORT analysis indicated that m5CRLSig was involved in immune cell infiltration. Risk score was associated with immune checkpoint gene expression, immune function scores, and chemotherapeutic drug sensitivity. Therefore, m5CRLSig can efficiently assess the prognosis of STAD patients and can be used as a biological marker for immunotherapy.

1. Introduction

Gastric cancer ranks fifth in cancer incidence and fourth in mortality, and with the number of new cases exceeding one million per year, the disease seriously affects human life and health [1, 2]. The most frequent gastric cancer is STAD, which originates from the glandular epithelium of the gastric mucosa. The pathogenesis of STAD is very insidious, and the early clinical symptoms are atypical. Most patients present local or distant metastases at the time of diagnosis and are already in the progressive stage of STAD, losing the opportunity for radical surgical treatment [3]. In addition, tumor recurrence after surgery is also one reason for the

high mortality rate among patients with STAD. Despite the development and progress in neoadjuvant chemotherapy, targeted therapeutic, and immunotherapy, the treatment effectiveness and prognosis of STAD are still unsatisfactory [4]. Due to the limitations of STAD treatment options, further research is critical for the identification of innovative prognostic indicators and potential therapeutic targets for STAD.

N6-Methyladenosine (m6A), N1-methyladenosine (m1A), m5C, N7-methylguanosine (m7G), and 5-hydroxymethylcytosine (hm5C) are common types of RNA methylation modifications [5]. RNA m5C methylation indicates that the fifth C position of RNA cytosine is modified by

(a)

(b)

Figure 1: Continued.

(c)
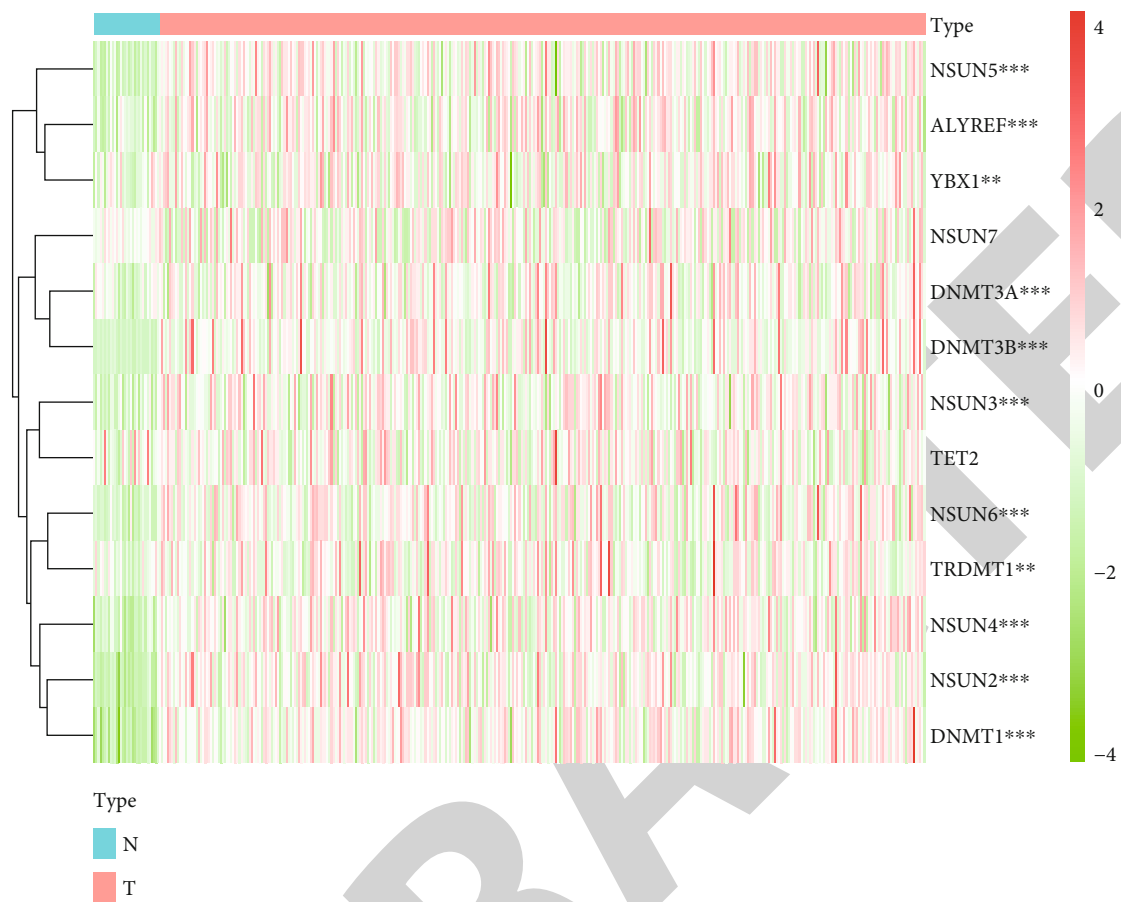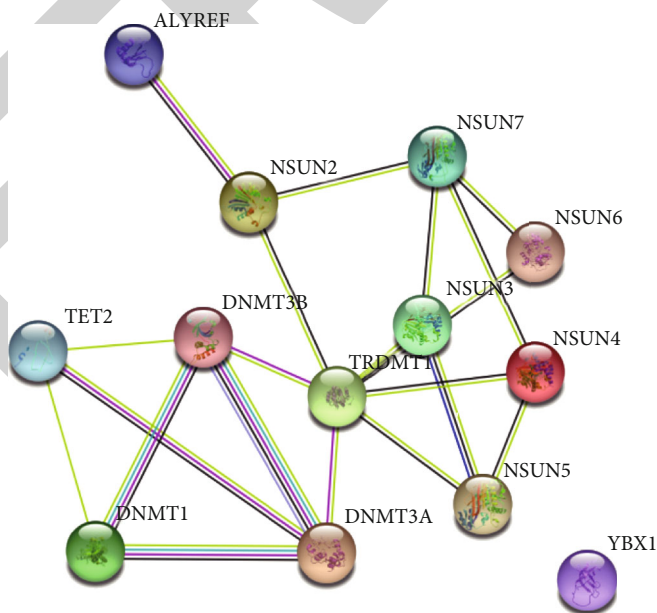
(d)
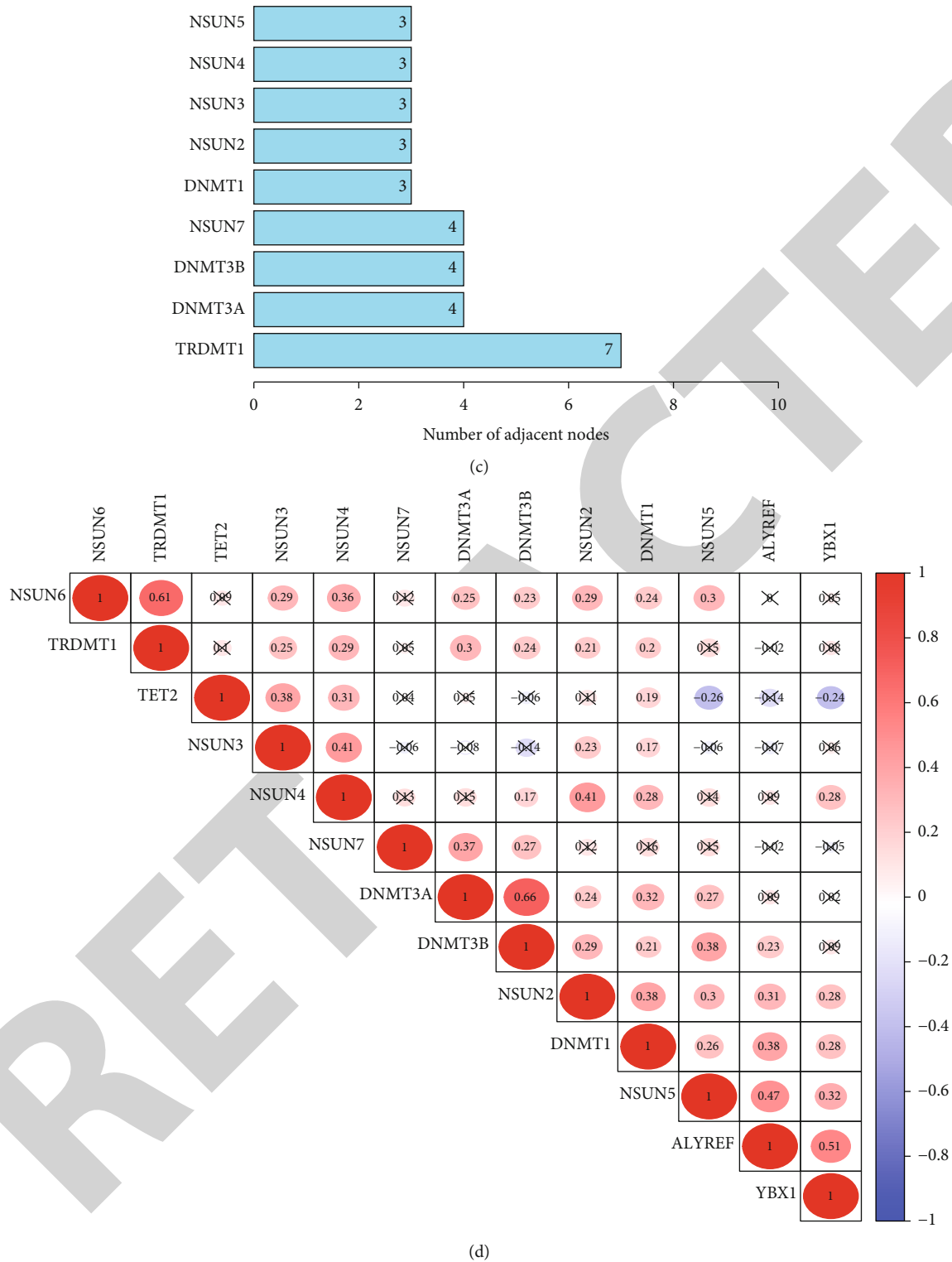
FIGURE 1: Differential expression and interactions of m5C methylation-regulated genes. (a) Heatmap of m5C methylation-regulated gene expression in STAD samples versus normal samples. The horizontal coordinates represent samples, and the vertical coordinates stand for m5C methylation-regulated genes. (b) PPI network of m5C methylation-regulated genes. (c) Number of nodes of m5C methylation-regulated genes. (d) Correlation analysis of the 13 m5C methylation-regulated genes. $^{**}p < 0.01$ and $^{***}p < 0.001$.

TABLE 1: Six prognostic m5C-related lncRNAs.

Gene ID	HR	HR.95L	HR.95H	p value
HAGLR	1.14919788	1.080942112	1.221763638	$8.53E - 06$
AC009948.1	1.202244387	0.997015744	1.449717894	0.03577198
AC005586.1	0.806843905	0.662135526	0.983178007	0.033321578
AL590666.2	0.967176382	0.94215051	0.992867004	0.012590168
AP001271.1	0.747753238	0.578011142	0.967342779	0.026918065
IPO5P1	0.750897622	0.594871707	0.94784679	0.015923186

methylation, which is a major posttranscriptional modification of RNA [6]. RNA m5C methylation plays an essential role in the regulation of RNA translation, stability, exiting the nucleus, and other biological processes [7]. Neurovascular, cardiovascular, and autoimmune diseases are closely related to m5C methylation regulation [8–10]. Furthermore, abnormal m5C methylation is linked to the onset and progression of some cancers. Upregulation of the m5C methyltransferase NSUN2 has been shown to contribute to the malignant advancement of gastric cancer cells [11]. Bioinformatics studies illustrated that the levels of m5C genes correlated with the prognosis of patients with breast cancer and colon carcinoma [12, 13]. Currently, there is a lack of comprehensive understanding of the value of m5C-related lncRNAs in the prognostic assessment of STAD.

lncRNAs have multiple roles in regulating gene expression at the transcriptional and translational levels, and they have been reported to act as biomarkers for tumor diagnosis, metastasis, and immunotherapy [14]. A study showed that lncRNA ZNRD1-AS1 and its variants contribute more to the development of lung cancer from different approaches, including in vivo and epidemiological investigations [15]. Moreover, lncRNAs can regulate target genes by methylation and influence cancer progression. For example, the lncRNA UBA6-AS1 inhibits the decay of UBA6 mRNA by modifying the methylation status of m6A, thus suppressing ovarian cancer cell malignancy [16]. The m6A demethylase ALKBH5 mediates the modification of the methylation of the lncRNA KCNQ1OT1, thus upregulating the expression of the HOXA9 gene and promoting the development of laryngeal squamous cell carcinoma [17]. Nevertheless, previous studies have focused primarily on m6A methylation. m5C modifications have been confirmed to be widely present in a variety of RNAs. Abundant m5C methylation sites have been identified in ncRNAs by high-throughput techniques [18, 19]. This suggests that m5C modifications are also prevalent in ncRNAs. However, the function of m5C in lncRNAs has not been extensively studied. Therefore, an in-depth investigation of the link between m5C methylation and lncRNA is necessary to explore its potential biological functions.

The tumor microenvironment (TME) is the local ecological environment on which tumor cells depend, and it includes immune cells, endothelial cells, microvasculature, and cytokines [20]. The interaction between the tumor and the immune cells undergoes a remodelling of the immune system, and eventually, tumor cells use a series of mecha-

nisms to undergo immune escape or tumor dormancy. lncRNAs regulate differentiation, proliferation, secretion factors, and other biological processes of immune cells in the TME, which influence tumorigenesis and development [21]. For instance, in oral squamous cell carcinoma, the lncRNA CRNDE is upregulated, and its knockdown suppresses the production of T cell immunoglobulin, thus activating the antitumor effects of CD8+ T cells [22]. Zhang et al. [23] reported that the lncRNA GATA3-AS1 promotes immune evasion of breast cancer cells by mediating effector T cell trafficking, stabilising the PD-L1 protein, and degrading the GATA3 protein. Furthermore, lncRNAs also participate in the regulation of the TME in hepatocellular carcinoma and prostate cancer [24, 25]. However, the impact of m5C-related lncRNAs for TME and immunotherapy in STAD has not been reported.

The search for novel immunological markers to improve the prognosis of STAD patients is particularly essential. Our study integrated clinical data from TCGA database for STAD samples. We used bioinformatics and statistical analysis to screen and validate six m5C-related lncRNAs with prognostic value for STAD. The association of risk scores with immune cell infiltration, immune checkpoint genes, immune cell function score, and chemotherapeutic drug sensitivity was then further investigated. This study is aimed at developing accurate biological indicators for the prognostic assessment and precise treatment of STAD.

2. Materials and Methods

2.1. Data Acquisition. We downloaded the transcriptome sequencing data and clinical data of STAD from TCGA database official website (https://portal. http://gdc.cancer .gov). Clinical data included age, gender, stage, grade, TNM stages, and survival status. Data with complete clinical information were further sorted after data download. Ultimately, RNA sequencing data was obtained for 375 STAD samples and 32 normal samples. The lncRNA annotation information was downloaded from the GENCODE database (https://www.gencodegenes.org).

2.2. Differential Expression and Interaction Identification of m5C Methylation-Regulated Genes. Thirteen m5C methylation-regulated genes have been described in the published study, namely, YBX1, ALYREF, DNMT1, NSUN4, TRDMT1, TET2, NSUN7, NSUN6, NSUN5, NSUN3, NSUN2, DNMT3A, and DNMT3B [26]. The expression
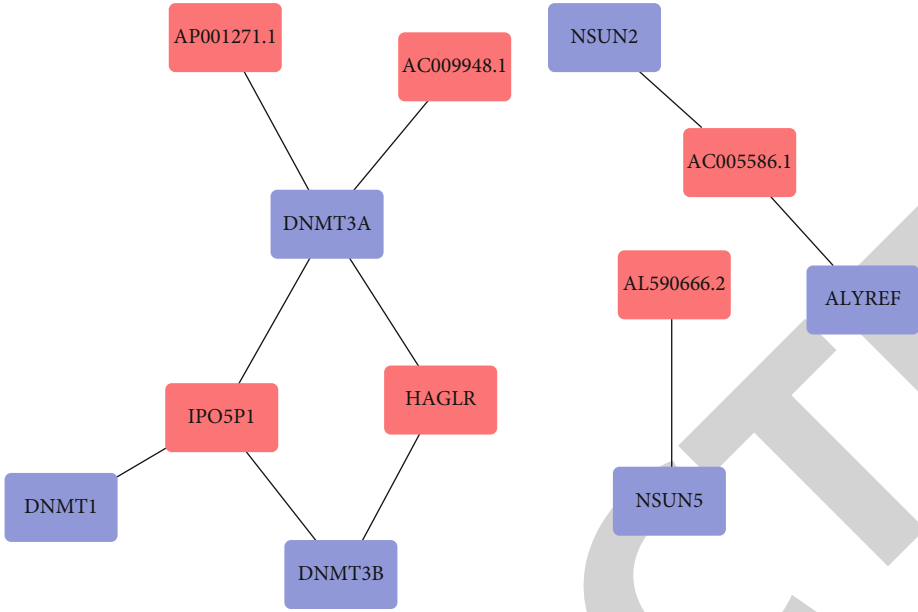
(a)
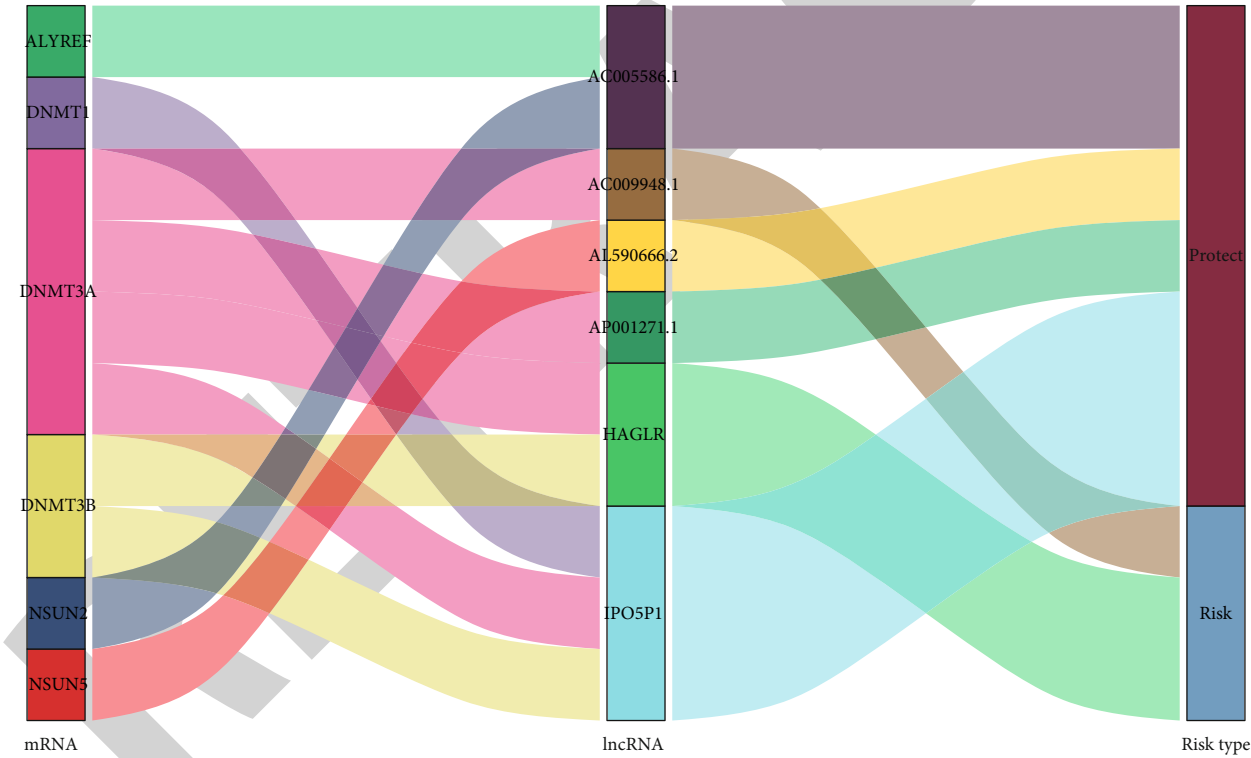
(b)

FIGURE 2: Continued.
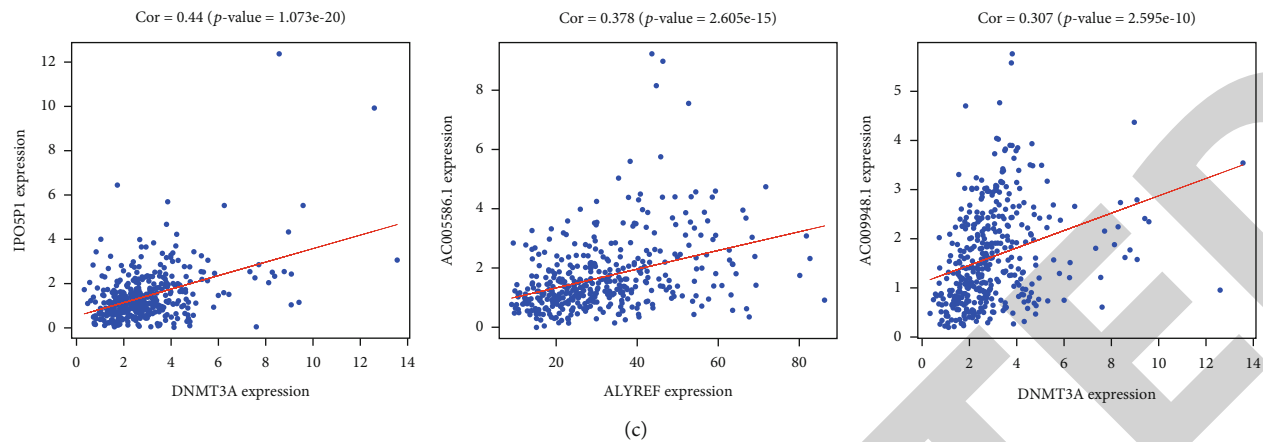
Figure 2: Correlation between prognostic m5C-related lncRNAs and m5C genes. (a) Application of Cytoscape to visualize the coexpression network of m5C genes and m5C-related lncRNAs. (b) Sankey plots showing the association between m5C genes, m5C-related lncRNAs, and risk types. (c) The m5C-related lncRNAs were positively correlated with the m5C genes ($p < 0.05$).

matrix of the 13 m5C methylation-regulated genes was obtained from RNA-seq transcriptome data. The R software "limma" was utilized to evaluate discrepancies in m5C methylation-regulated genes. The screening criteria were | $\log_2$ fold change| > 1 and a false discovery rate (FDR) < 0.05. The STRING database (https://www.string-db.org) was used to build a protein-protein interaction (PPI) network including the 13 m5C methylation-regulated genes, and the correlations were analyzed using the "corrplot" function in R software.

2.3. Acquisition of m5C-Related lncRNAs and Construction of a Prognostic Risk Model. The lncRNA profiles were obtained from the RNA-seq dataset. Subsequently, Pearson correlation analysis of m5C genes with the lncRNA expression matrix was performed to obtain m5C-related lncRNAs for STAD (|correlation coefficient| > 0.3, $p < 0.001$). The m5C-related lncRNA expression data were combined with clinical prognostic information from STAD patients. The "survival" and "survminer" packages in the R language were used to conduct the survival analysis. The m5C-related lncRNAs associated with prognostic significance were identified by univariate Cox regression and Kaplan–Meier analysis using $p < 0.05$ as the threshold. Next, they were included in multivariate Cox regression analysis to obtain regression coefficients for key lncRNAs and construct a multigene risk model. The coexpression network was visualized using Cytoscape software.

2.4. Evaluation of the Prognostic Model of m5C-Related lncRNAs. The ROC curve was used to examine the predictive efficacy of the model. The m5C-related lncRNA prognostic model was verified as an independent element of STAD prognosis using univariate and multivariate Cox regression analysis. PCA plots were generated using the R package scatterplot3D.

2.5. Construction of Nomogram and Enrichment Analysis. The R language "rms" package was adopted to create the prognostic nomogram model. We plotted calibration curves

to evaluate the consistency of the nomogram model. GSEA software (GSEA_4.1.0) was used for the enrichment analysis of multiple genes in this study.

2.6. Expression of m5C-Related lncRNAs in Tissues by qRT-PCR. We collected 20 matched STAD and paracancerous tissues from Xingtai People's Hospital. Pathologists histopathologically confirmed the diagnosis of all tissues. All patients had not received chemotherapy, radiotherapy, targeted drugs, immunotherapy, or Chinese herbal medicine. Patients were not diagnosed with malignancy at other sites or with other serious underlying diseases. The Ethics Committee of the Xingtai People's Hospital authorised this research. All patients signed the informed consent form before surgery. The specimens were removed and rapidly frozen in liquid nitrogen and stored in a low-temperature refrigerator at -80°C for subsequent studies. Then, the qRT-PCR experiment was carried out using the thermal cycler (Shanghai Qiqian Electronic Technology Co., Ltd., model: Q2000A). β-Actin was selected as the internal reference.

2.7. Immunocorrelation Analysis and Drug Sensitivity Analysis of Prognostic Features. We filtered with the Perl programming language to obtain the matrix of immune infiltrating cells and used CIBERSORT for immune infiltration analysis. Immunocorrelation analysis was visualized with the R packages "barplot," "corrplot," and "ggplot2." Enrichment scoring of immune cells and immune function was performed by applying the single sample gene set enrichment analysis (ssGSEA). We compared the difference in the half inhibitory concentration (IC50) values of chemotherapeutic agents used for STAD treatment using "pRRophetic" in the R package.

2.8. Statistical Analysis. The R software (version 4.0.3) and the Perl software (version 5.3) were mainly applied for statistical analysis of the data. In this study, univariate and multifactorial Cox regression, Kaplan–Meier method, PCA, and ROC analysis were used. The Kruskal-Wallis test was used

(a)

(b)

Figure 3: Continued.

(c)
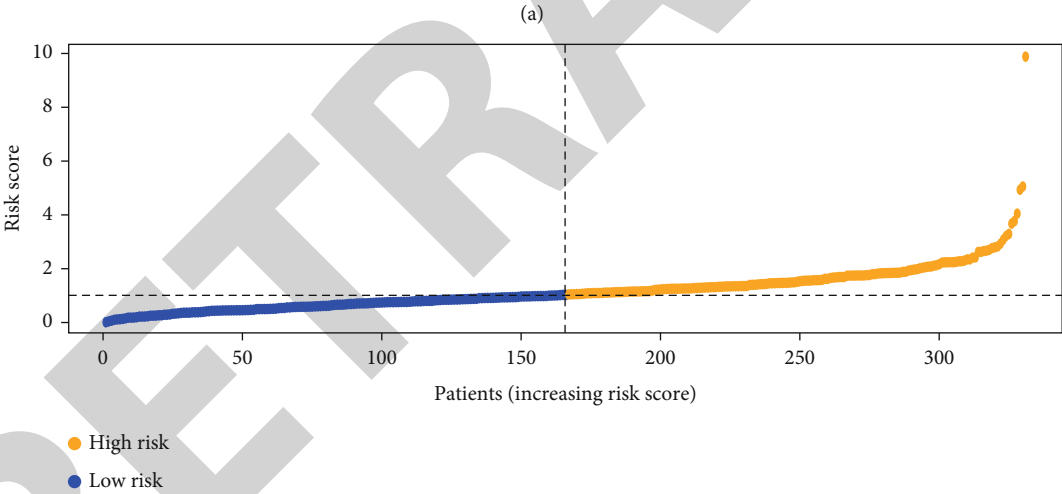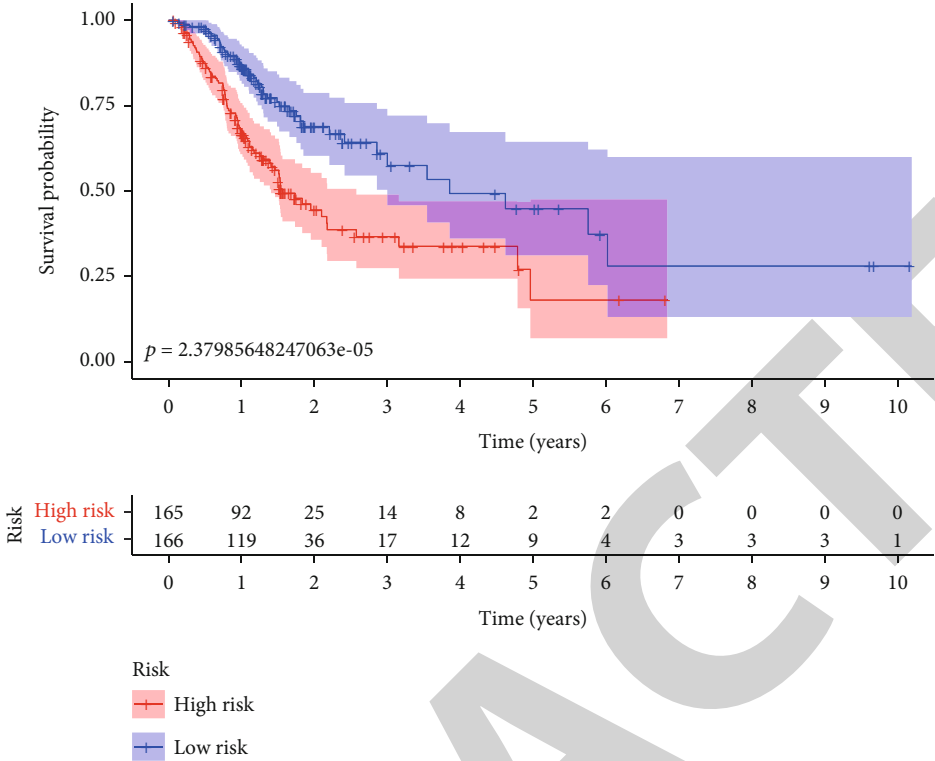
(d)
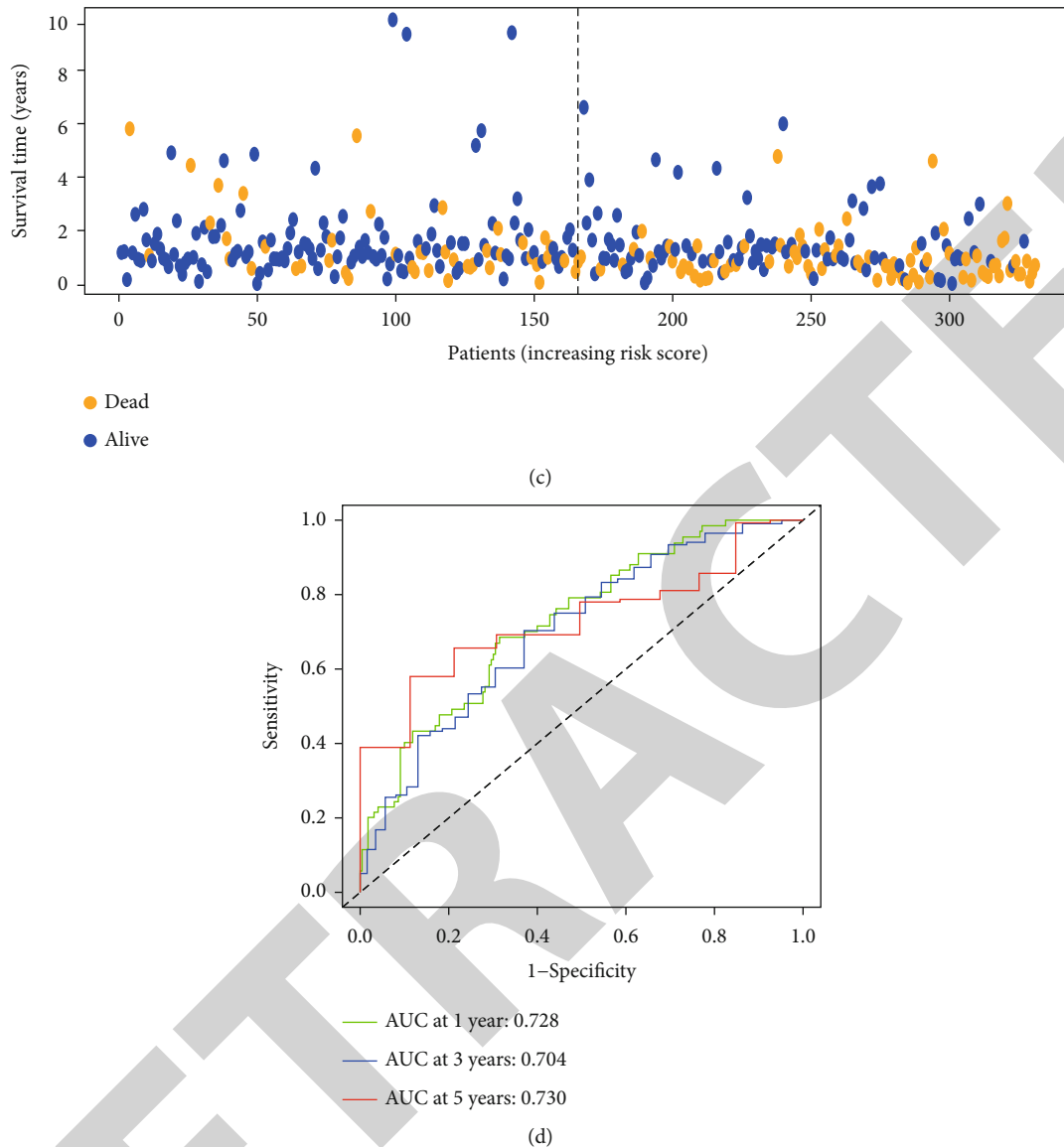
Figure 3: The prognostic value of six m5C-related lncRNAs for STAD patients. (a) Kaplan–Meier survival curves for both groups of patients ($p < 0.001$). (b, c) Risk curves and survival status scatter plots of STAD patients. (d) ROC curves to assess the predictive efficacy of the risk model (AUC > 0.7).

to compare differences between groups. The remaining analysis was performed as previously described. Two-tailed $p < 0.05$ was the threshold for statistical significance.

3. Results

3.1. Differential Expression and Interactions of m5C Methylation-Regulated Genes.
The expression of 13 m5C methylation-regulated genes was analyzed in 375 STAD samples and 32 normal samples from TCGA database. The outcomes revealed that NSUN2, NSUN3, NSUN4, NSUN5, NSUN6, DNMT3A, DNMT3B, ALYREF, DNMT1, TRDMT1, and YBX1 were expressed at high levels in STAD samples ($p < 0.05$). Nevertheless, no significant differences were observed in the expression levels of NSUN7 and TET2 in the two types of samples ($p > 0.05$, Figure 1(a)).

We constructed a PPI network of m5C methylation-regulated genes in STAD. Except for YBX1, there was a close interrelationship between the regulatory genes (Figure 1(b)). The node count showed that TRDMT1 interacted with the other seven m5C methylation-regulated genes and was a key factor in the relationship network (Figure 1(c)). DNMT3A and DNMT3B had the strongest connection, among the correlation analysis of 13 m5C methylation-regulated genes (Figure 1(d)). This indicates that the expression levels of m5C methylation-regulated genes in STAD samples and normal samples are different, and there is a certain interconnection between them.

3.2. Identification of a Prognostic m5C-Related lncRNA Signature.
Based on the data of STAD patients in TCGA database, we applied coexpression analysis to obtain 565

(a)

(b)

(c)
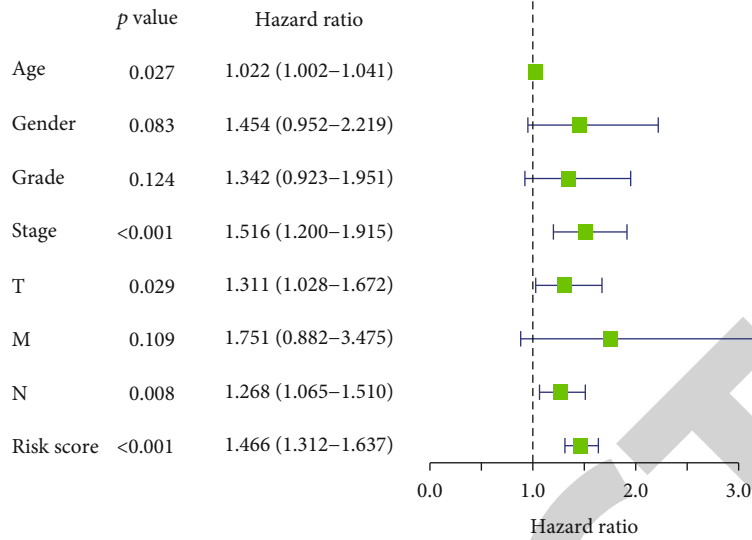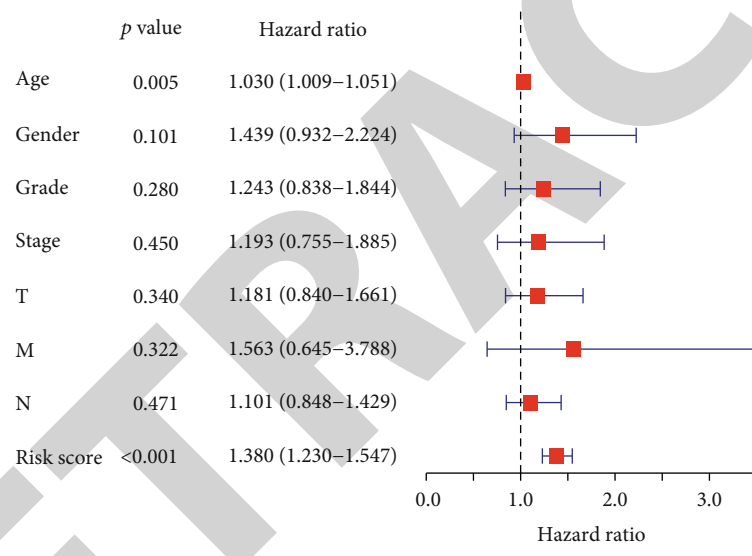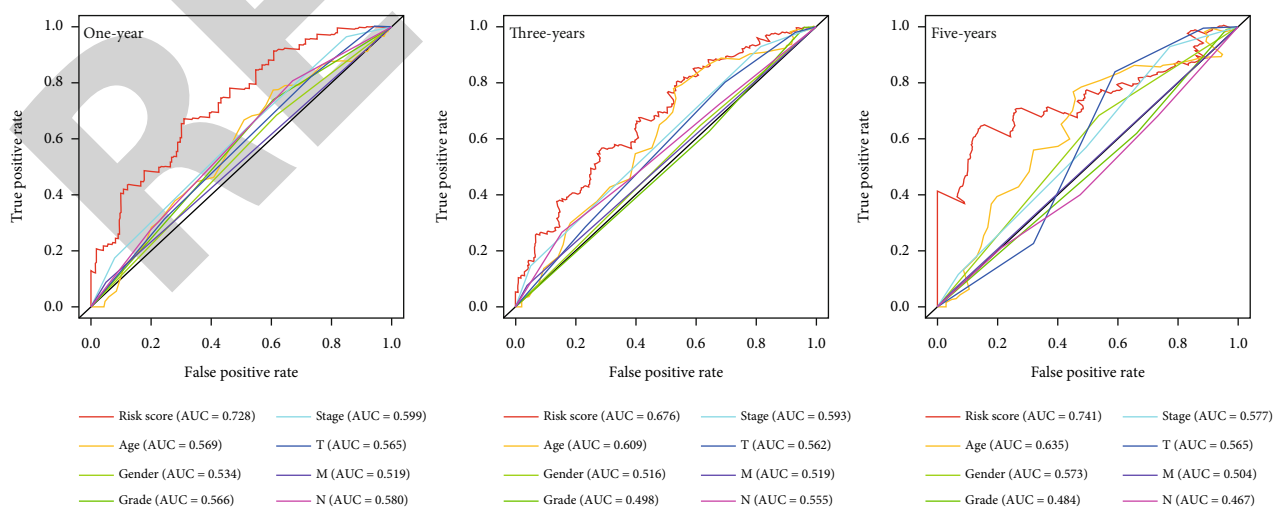
Figure 4: Continued.
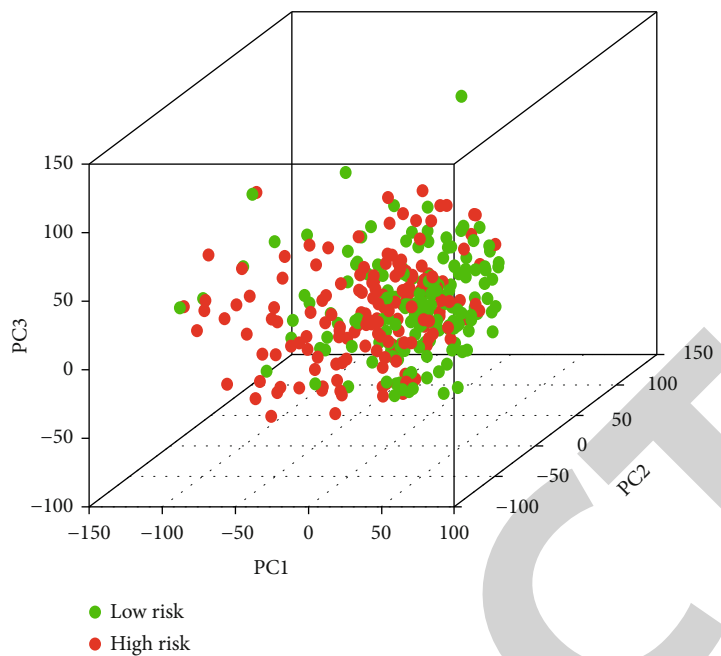
(d)
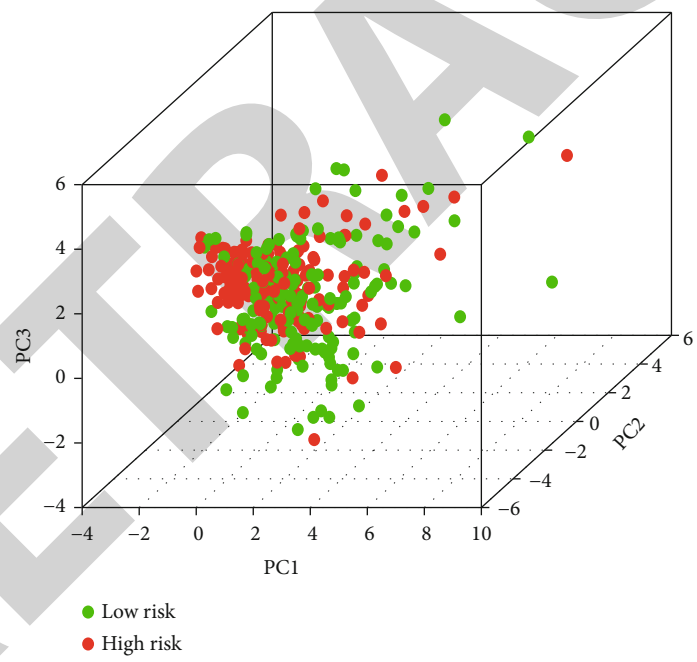
(e)

Figure 4: Continued.

(f)

(g)
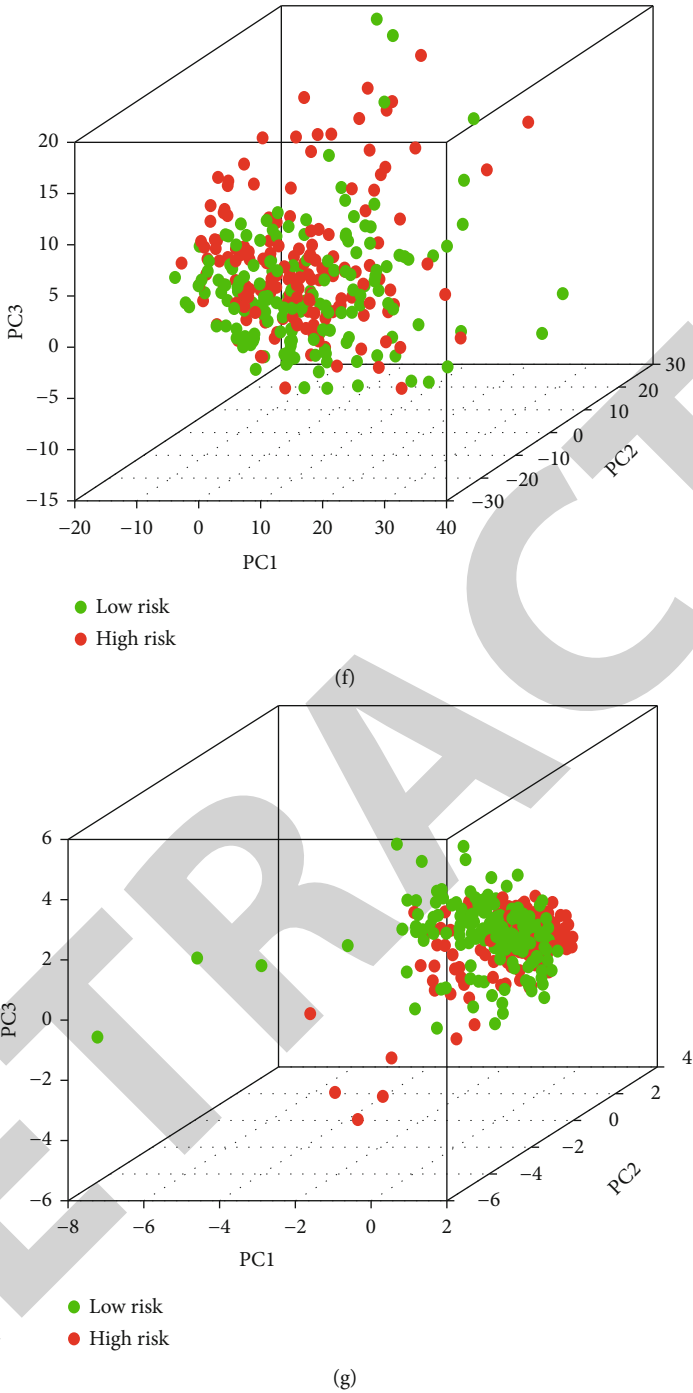
Figure 4: Verifying the independence of m5CRLSig. (a) Univariate and (b) multivariate Cox regression analyses of the relationship between multiple clinical variables (including risk scores) and OS. (c) ROC curves for clinicopathological factors and risk scores at 1, 3, and 5 years. PCA of the (d) genome-wide, (e) m5C genes, (f) m5C-related lncRNAs, and (g) six prognostic m5C-related lncRNAs.

Figure 5: Continued.

Survival curve ($p = 2.532e\text{-}02$)

— AP001271.1 high expression
— AP001271.1 low expression

(e)

Survival curve ($p = 4.704e\text{-}02$)

— IPO5P1 high expression
— IPO5P1 low expression

(f)
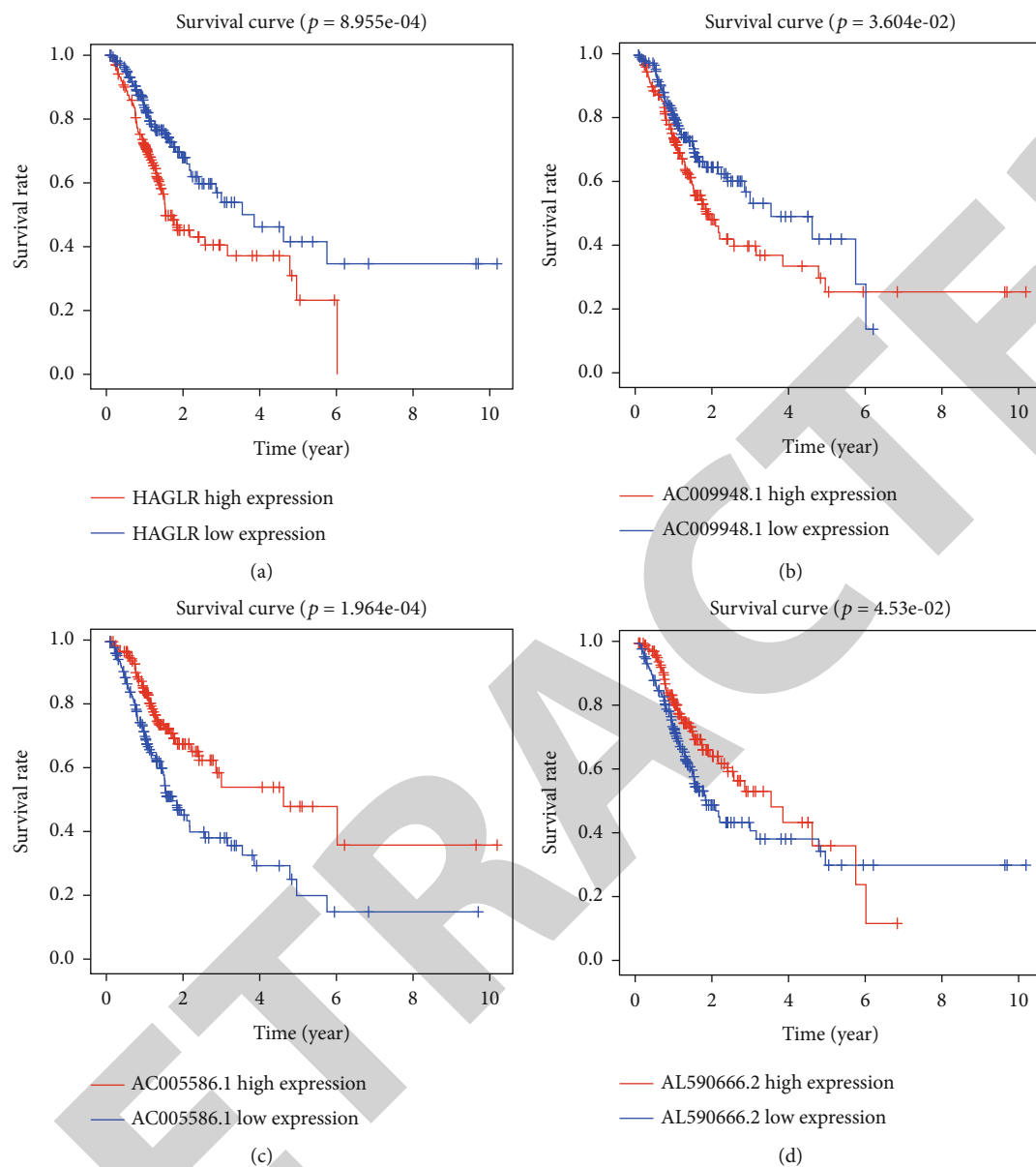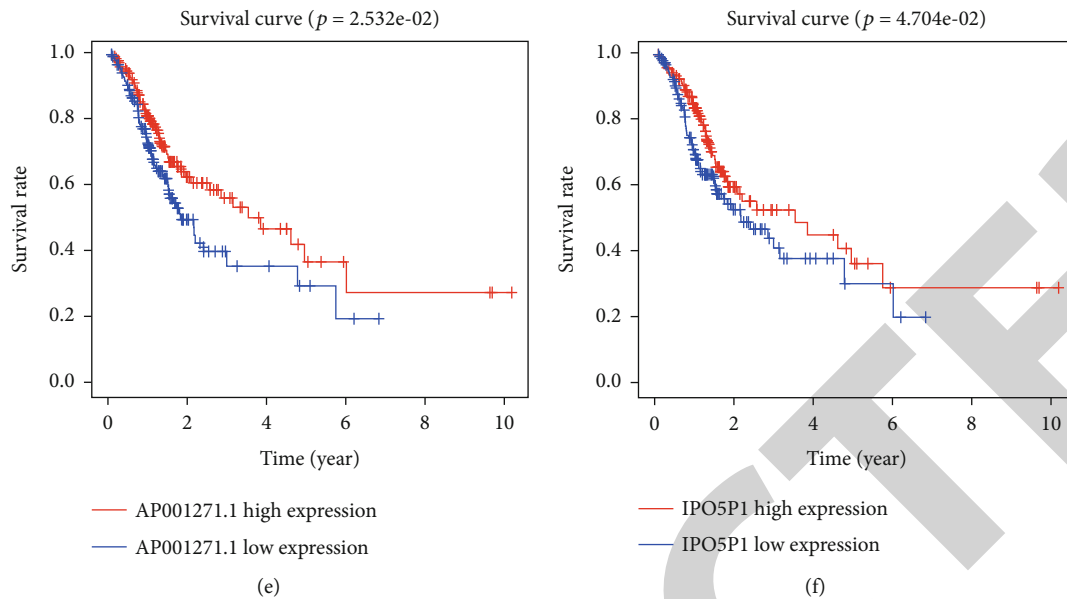
FIGURE 5: Relationship between the expression levels of six m5C-related lncRNAs and OS in STAD patients. (a, b) Kaplan–Meier survival curves displaying shorter OS in patients in the HAGLR and AC009948.1 high-expression group ($p < 0.05$). (c–f) OS was longer in patients in the AC005586.1, AL590666.2, AP001271.1, and IPO5P1 high-expression groups ($p < 0.05$).

m5C-related lncRNAs. Univariate Cox regression and Kaplan–Meier analysis identified 10 m5C-related lncRNAs with prognostic value, which were AC009948.1, IPO5P1, AP001528.2, HAGLR, BOLA3-AS1, AC005586.1, SREBF2-AS1, AL590666.2, AP001271.1, and AL365181.3 ($p < 0.05$, Supplementary Table 1). Subsequently, the six prognostic m5C-related lncRNAs necessary to create the risk model were determined using multivariate Cox regression analysis ($p < 0.05$, Table 1). The correlations of these six lncRNAs with the m5C genes are presented in Figures 2(a) and 2(b). Of these, AC005586.1, AL590666.2, AP001271.1, and IPO5P1 were considered protective effectors (HR < 1, $p < 0.05$). HAGLR and AC009948.1 were considered risk effectors (HR > 1, $p < 0.05$). The expression correlations of m5C genes and m5C-related lncRNAs were compared in this study, and they were all positively correlated ($p < 0.05$, Figure 2(c), Supplementary Figure 1). Among them, DNMT3A and IPO5P1 correlated the strongest (Cor = 0.44, $p = 1.073e - 20$).

The risk score for STAD patients was calculated on the basis of the following formula. Risk score = (EXP HAGLR × 0.139064203280377) + (EXP AC009948.1 × 0.184190132013409) + (EXP AC005586.1 × − 0.21462505604275) + (EXP AL590666.2 × − 0.0333743988485729) + (EXP AP001271.1 × − 0.29068225147328) + (EXP IPO5P1 × −0.286485959190337). EXP indicates the expression level of m5C-related lncRNAs. Patients with STAD were divided into high- and low-risk groups according to the median risk score. The Kaplan–Meier survival curves revealed that overall survival (OS) was markedly shorter in the high-risk group ($p < 0.001$, Figure 3(a)). Patients in the high-risk group had a worse survival status, according to the risk curves and the survival status scatter plots (Figures 3(b) and 3(c)). The

ROC curves were then used to assess the predictor capacity of this risk model for 1-, 2-, and 3-year OS of STAD patients. The areas under the curve (AUC) were 0.728, 0.704, and 0.730, respectively (Figure 3(d)). This implies that the use of m5CRLSig to predict the prognosis of STAD has a certain accuracy.

3.3. m5CRLSig as an Independent Prognostic Factor for STAD. To explore whether m5CRLSig is an independent predictive factor for OS in STAD patients, we conducted univariate and multivariate Cox regression analyses (HR: 1.466, 95% CI: 1.312–1.637, $p < 0.001$, Figure 4(a); HR: 1.380, 95% CI: 1.230–1.547, $p < 0.001$, Figure 4(b)). The risk score remained an independent risk factor for prognosis in STAD patients after excluding clinical confounders. Time-dependent ROC curves were also used to examine the accuracy of model prediction at 1, 3, and 5 years, with AUC values of 0.728, 0.676, and 0.741, respectively (Figure 4(c)). The accuracy of risk score was considerably higher than other clinicopathological factors. Next, we performed PCA for STAD patients according to the genome-wide (Figure 4 (d)), m5C genes (Figure 4(e)), m5C-related lncRNAs (Figure 4(f)), and six prognostic m5C-related lncRNAs (Figure 4(g)). PCA according to the first three methods was ineffective in distinguishing high- and low-risk groups. However, the PCA could clearly separate the two groups of patients according to six prognostic m5C-related lncRNAs. These results demonstrate that m5CRLSig is an independent predictor of the prognosis in STAD.

3.4. Correlation of m5CRLSig with the Clinicopathological Characteristics of Patients. We examined the impact of six m5C-related lncRNAs' expression levels on OS in STAD patients. Based on the expression levels of lncRNAs, we
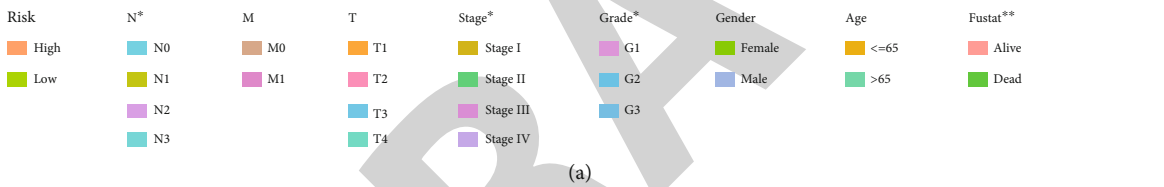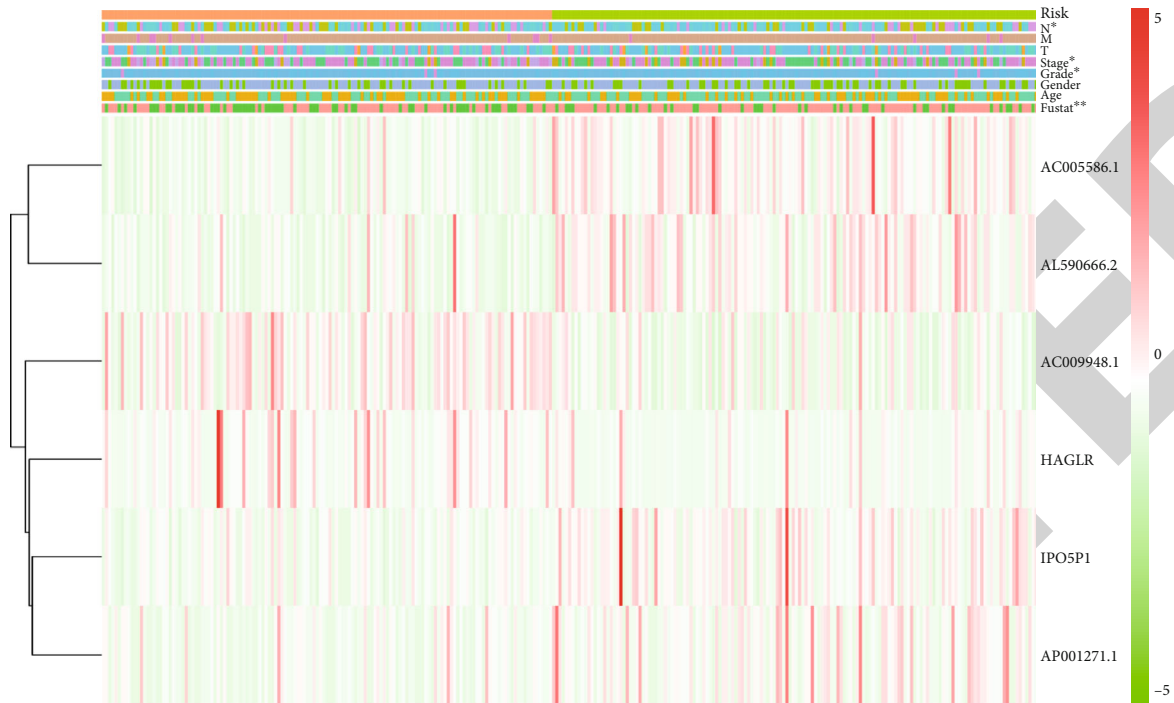
(a)
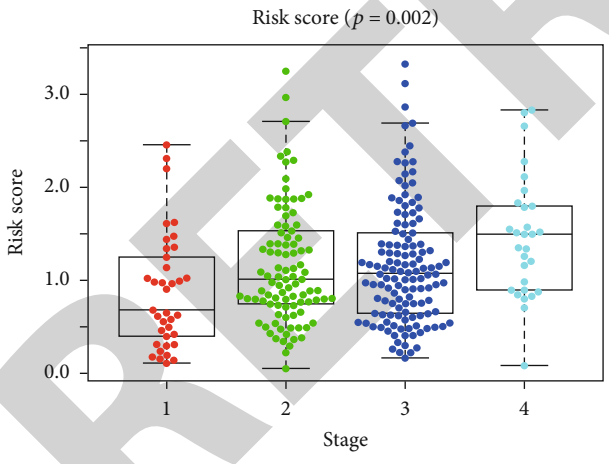
(b)
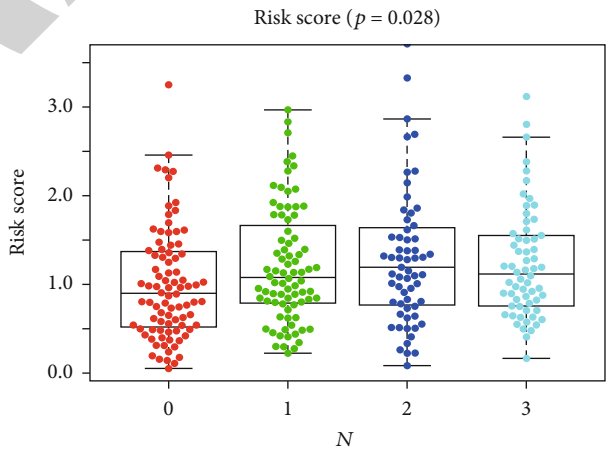
(c)

Figure 6: Continued.
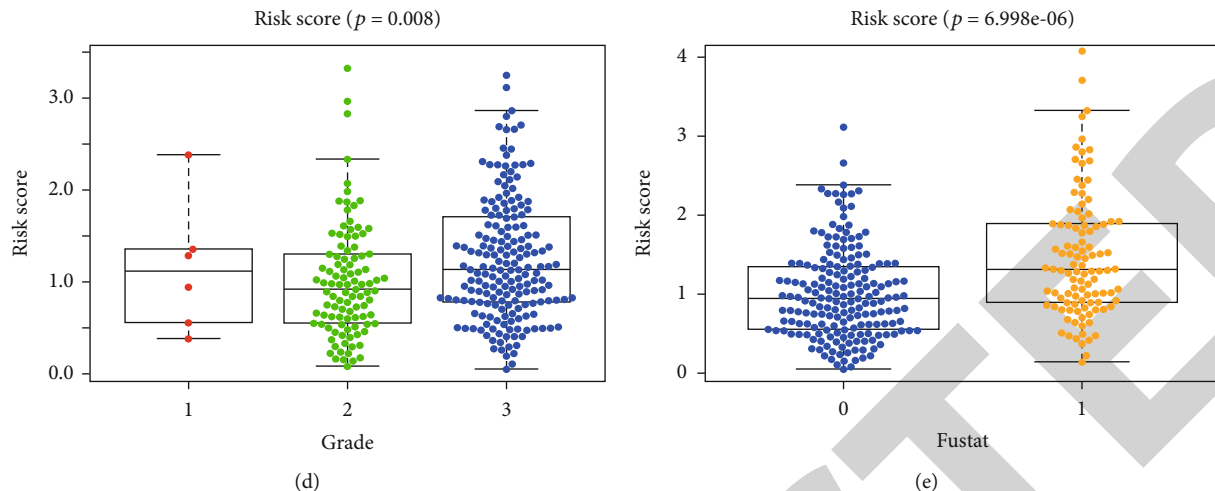
FIGURE 6: Relationship between risk score and clinicopathological characteristics. (a) Heatmap illustrating the clinicopathological characteristics and expression of six m5C-related lncRNAs in the high- and low-risk groups. Association of the risk score with the (b) stage, (c) lymph node metastasis status, (d) grade, and (e) survival status. $^*p < 0.05$ and $^{**}p < 0.01$.

divided STAD patients into high- and low-expression groups, as shown in Figure 5. The risk effector HAGLR and AC009948.1 high expression groups had shorter OS ($p < 0.05$, Figures 5(a) and 5(b)). The protective effector AC005586.1, AL590666.2, AP001271.1, and IPO5P1 high-expression groups had longer OS ($p < 0.05$, Figures 5(c)–5(f)).

We investigated the relationships between the risk score and clinicopathological characteristics and evaluated whether m5CRLSig influenced STAD development. Risk scores were significantly correlated with stage, grade, N stage, and survival status ($p < 0.05$, Figure 6(a)). Further studies determined that stages II-IV, N1-3, and grade 3 had higher risk scores ($p < 0.05$, Figures 6(b)–6(d)). Patients with high-risk scores had a worse survival status ($p < 0.001$, Figure 6(e)). This implied that patients having high-risk scores were predisposed to present with advanced clinicopathological characteristics.

3.5. Clinical Prognostic Nomogram. To predict the survival risk for patients with STAD, a clinical prognostic nomogram was also designed (Figure 7(a)). We plotted the calibration curves to estimate the agreement with the model predictions and the actual observations (Figure 7(b)). The results displayed that the calibration curve was close to the diagonal, indicating a favourable agreement between the projected and real observed values. Thus, the nomogram designed using m5CRLSig has an excellent predictive capacity for the prognosis of STAD patients.

3.6. Expression of m5C-Related lncRNAs in Tissues by qRT-PCR. The information from TCGA database revealed that AC005586.1, AL590666.2, AP001271.1, and IPO5P1 had low expression, while HAGLR and AC009948.1 were highly expressed in STAD samples. To verify the feasibility of the prognostic model, we measured the expression of lncRNAs in STAD tissues and paired normal paracancerous tissues by qRT-PCR. The primers utilized are presented in

Table 2. The expression levels of HAGLR and AC009948.1 were markedly elevated in STAD tissues compared to para-cancerous tissues ($p < 0.001$). This indicates that HAGLR and AC009948.1 may be oncogenic factors in STAD. The expression of AC005586.1, AL590666.2, AP001271.1, and IPO5P1 was significantly reduced in STAD tissues ($p < 0.01$, Figure 8). We validated the reliability of m5C-related lncRNAs as prognostic markers for STAD using qRT-PCR experiments.

3.7. GSEA Situation. We then utilized functional enrichment analysis to probe potential signalling pathways of m5C-related lncRNAs. We visualized two groups of the top 5 signalling pathways based on GSEA software. Gene Ontology (GO) pathway analysis illustrated that immunoglobulin binding, extracellular matrix structural constituent conferring compression resistance, sialyltransferase activity, collagen trimer, and the collagen-containing extracellular matrix signalling pathway were enriched in the high-risk group. Acetyltransferase activity, endonuclease activity, lysine N-methyltransferase activity, catalytic activity acting on DNA, and DNA synthesis involved in DNA repair were enriched in the low-risk group (Figure 9(a)). Kyoto Encyclopedia of Genes and Genomes (KEGG) pathway analysis revealed that glycosphingolipid biosynthesis-ganglio series, hematopoietic cell lineage, cytokine–cytokine receptor interaction, asthma, and neuroactive ligand-receptor interaction signalling pathways were enriched in the high-risk group. The low-risk group had higher levels of RNA degradation, glycosylphosphatidylinositol (GPI) anchor production, cell cycle, base excision repair, and homologous recombination (Figure 9(b)). This implies that m5CRLSig may influence STAD development through immune-related pathways.

3.8. Correlation between m5CRLSig and Immune Cell Infiltration. To investigate the value of m5CRLSig in the TME, we analyzed 22 tumor immune cells using CIBER-SORT and the output was visualized with a heatmap
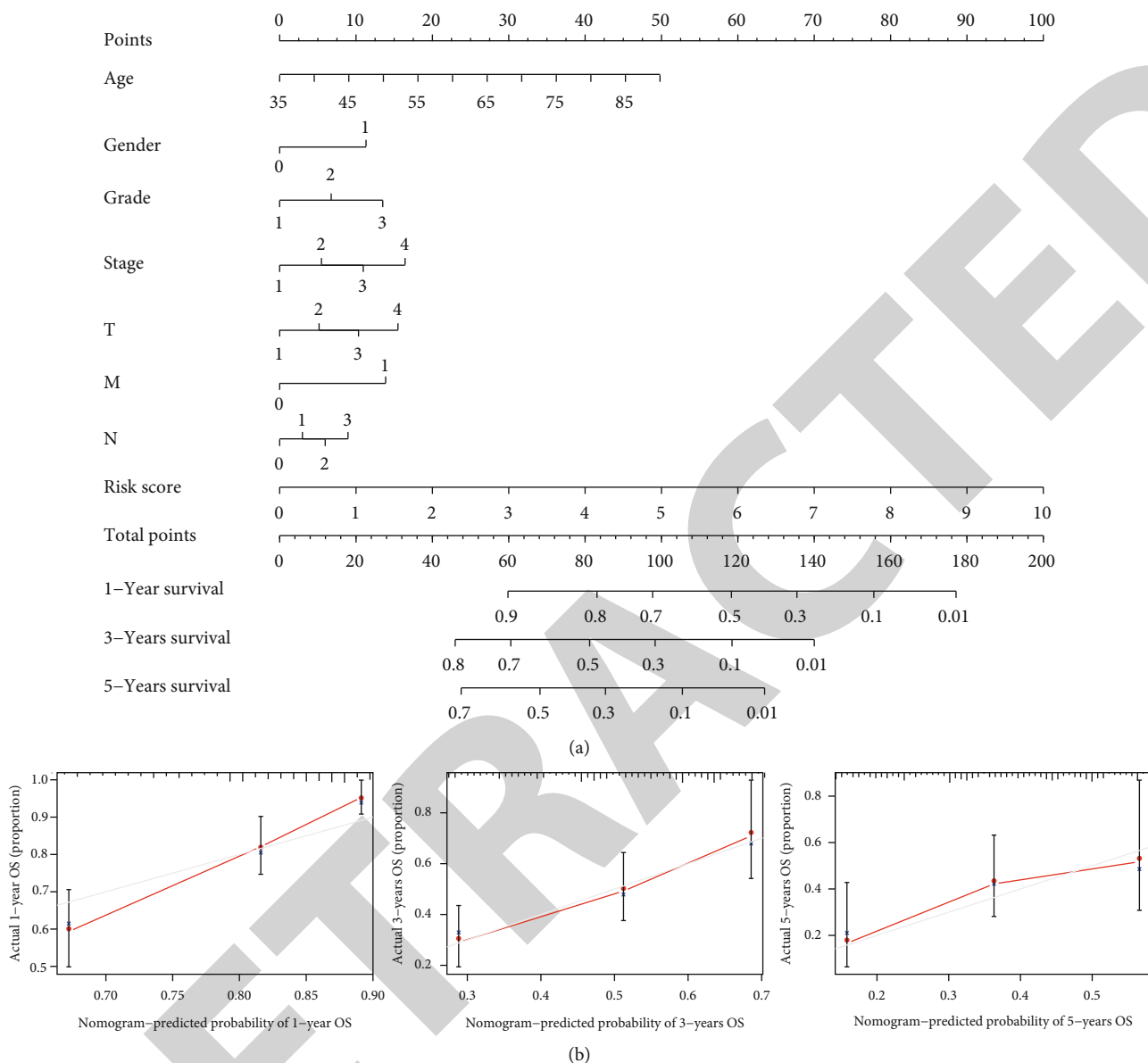
Figure 7: Clinical nomogram. (a) Clinical prognostic nomogram predicting patient survival risk. (b) Calibration curves of the clinical prognosis nomogram.

(Figure 10(a)). The violin plot illustrated that immune cell infiltration differed in the two groups (Figure 10(b)). Patients with STAD in the high-risk group had a higher infiltration abundance of NK cells activated, dendritic cells resting, and mast cells resting ($p < 0.05$). Conversely, the infiltration abundance of NK cells resting was decreased in the high-risk group ($p < 0.05$). This evidences that immune cell infiltration in STAD patients was involved in tumor risk stratification. This study described the relationship between the risk score and the immune cells. The risk score was positively associated with the level of NK cells activated ($R = 0.16$, $p < 0.05$), dendritic cells resting ($R = 0.26$, $p < 0.001$), and mast cells resting infiltration ($R = 0.18$, $p < 0.05$, Figure 10(c)). The above three types of immune cells may be linked to the poor prognosis. Fur-

thermore, we presented the proportions of 22 immune cell infiltration in STAD patients and visualized the results with a barplot (Supplementary Figure 2). m5CRLSig can distinguish immune cells in STAD with diverse features. We then evaluated the role of m5CRLSig in enrichment scoring of immune cells and immune function by ssGSEA. The results revealed that the enrichment scores of multiple immune cell (aDCs, B cells, DCs, iDCs, macrophages, mast cells, neutrophils, pDCs, T helper cells, TIL, and Treg) were elevated in the high-risk group ($p < 0.05$, Figure 10(d)). Furthermore, immune function scores such as APC costimulation, CCR, HLA, parainflammation, T cell costimulation, type I IFN response, and type II IFN response were also significantly elevated in the high-risk group ($p < 0.05$,

Table 2: Primer information for qRT-PCR.

Primer	Sequence	Primer length	Tm	Product size
AC009948.1-F	CTTTTGGAACTTGATGGCACCTTA	24	59.72	236 bp
AC009948.1-R	CCTGGAAACTCTGCTCTGTAACT	23	59.99	
IPO5P1-F	TCCACAATGGTGTTGGAGGG	20	59.89	77 bp
IPO5P1-R	CTCAGGACCACGGACTCTCA	20	60.61	
HAGLR-F	CGCCCTTTCTGACCTGCTTA	20	60.04	284 bp
HAGLR-R	TGGCAGTCGTCTGGACATTC	20	60.04	
AC005586.1-F	CCACCTGCTGTAACTTCCTCTTTAG	25	61.08	90 bp
AC005586.1-R	CCTTTGCCACTCATTTTCTTTCTGC	25	61.53	
AL590666.2-F	GCTGGAACTTAACGCTGTCG	20	59.56	267 bp
AL590666.2-R	GAATTTTGGAGAGGAAGTGGAAGAC	25	59.82	
AP001271.1-F	GAAAGTAATGACGCTGGTGAGTATG	25	59.99	124 bp
AP001271.1-R	TCTGTGTTTAAGGTTTTGAGGAGCA	25	60.86	
β-Actin-F	GGCTGTATTCCCCTCCATCG	20	61.80	154 bp
β-Actin-R	CCAGTTGGTAACAATGCCATGT	22	61.10	
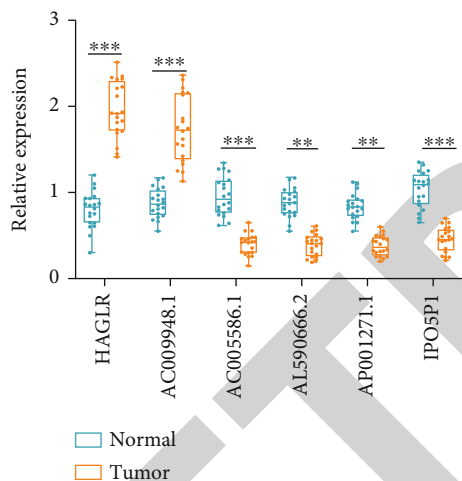
Figure 8: The expression of six m5C-related lncRNAs in STAD tissues and paracancerous tissues was measured by qRT-PCR. $^{**}p < 0.01$ and $^{***}p < 0.001$.

Figure 10(e)). These results imply that m5C-related lncRNAs are involved in the regulation of immune cell function.

3.9. The Value of m5CRLSig in Immunotherapy and Chemotherapy. Immune checkpoint inhibitors (ICI) act on immune checkpoints to enhance the immune response or relieve immune suppression. To evaluate the connection between the risk score and ICI, we examined the expression of immune checkpoint genes in the two groups (Figure 11 (a)). The results displayed that 18 immune checkpoint genes (CD40, CD200R1, TNFSF4, TNFRSF8, CD48, LAIR1, CD86, NRP1, PDCD1LG2, CD28, TNFRSF4, BTLA, TNFSF18, CD200, CD27, CD40LG, TNFSF14, and HAVCR2) were more expressed in the high-risk group ($p < 0.05$). However, two immune checkpoint genes, TNFRSF14 and TNFRSF25, were expressed at higher levels

in the low-risk group ($p < 0.05$). The findings suggest that m5CRLSig may be a predictor of ICI treatment. We applied risk scores to assess the sensitivity of STAD patients to commonly used chemotherapeutic agents. Patients with low-risk scores were significantly more sensitive to cisplatin and paclitaxel ($p < 0.05$, Figures 11(b) and 11(c)). This implies that patients in the low-risk group would respond more effective to chemotherapy and would have a favourable prognosis.

4. Discussion

Research on the pathogenesis of gastrointestinal tumors has made impressive achievements in recent years, and methods for effective prognostic assessment are being explored [27, 28]. Using bioinformatics research methods, we can analyze genes and their internal relations from the system level. In-depth mining of key regulatory molecules in STAD is important for finding effective and reliable therapeutic targets for STAD. The m5C modification of RNA has a wide range of functions, including cell signalling, tissue development and differentiation, and cancer regulation [29]. In the prognosis of many diseases, such as gastric cancer, lncRNAs play a key role [30]. However, the study of m5C methylation in lncRNAs is still in its infancy [31]. We used TCGA database to download details of transcriptome sequencing and clinical information from STAD patients to filter out m5C-related lncRNAs that are closely associated with patient prognosis. Combined with bioinformatics database resources, we constructed a prognostic risk model for m5C-related lncRNAs in STAD. To our knowledge, this is the first study on the feasibility and accuracy of m5CRLSig in STAD.

Methylation modifications and lncRNAs affect tumorigenesis and progression through a complex regulatory network. A study revealed that the m6A reader YTHDC1 blocked ubiquitination between lncRNA LSG1 and ESRP2 and inhibited the advancement of renal cell carcinoma [32]. By altering the stability of lncRNA ZFAS1, the m6A methyltransferase METTL3 influenced autophagy and the

High expression<----------->Low expression

— GOBP_DNA_SYNTHESIS_INVOLVED_IN_DNA_REPAIR
— GOCC_COLLAGEN_CONTAINING_EXTRACELLULAR_MATRIX
— GOCC_COLLAGEN_TRIMER
— GOMF_ACETYLTRANSFERASE_ACTIVITY
— GOMF_CATALYTIC_ACTIVITY_ACTING_ON_DNA
— GOMF_ENDONUCLEASE_ACTIVITY
— GOMF_EXTRACELLULAR_MATRIX_STRUCTURAL_CONSTITUENT_CONFERRING_COMPRESSION_RESISTANCE
— GOMF_IMMUNOGLOBULIN_BINDING
— GOMF_LYSINE_N_METHYLTRANSFERASE_ACTIVITY
— GOMF_SIALYLTRANSFERASE_ACTIVITY

(a)

Figure 9: Continued.

High expression<----------->Low expression

—— KEGG_ASTHMA

—— KEGG_BASE_EXCISION_REPAIR

—— KEGG_CELL_CYCLE

—— KEGG_CYTOKINE_CYTOKINE_RECEPTOR_INTERACTION

—— KEGG_GLYCOSPHINGOLIPID_BIOSYNTHESIS_GANGLIO_SERIES

—— KEGG_GLYCOSYLPHOSPHATIDYLINOSITOL_GPI_ANCHOR_BIOSYNTHESIS

—— KEGG_HEMATOPOIETIC_CELL_LINEAGE

—— KEGG_HOMOLOGOUS_RECOMBINATION

—— KEGG_NEUROACTIVE_LIGAND_RECEPTOR_INTERACTION

—— KEGG_RNA_DEGRADATION

(b)

FIGURE 9: GSEA situation. Top 5 (a) GO and (b) KEGG signalling pathways in the two groups.

development of nasopharyngeal cancer cells [33]. Bioinformatics studies have also indicated the prognostic characteristics of m6A-related lncRNAs in gastric cancer [34, 35]. At present, the mechanism and function of m5C methylation modifications in lncRNAs remain to be elucidated. Yan et al. [36] demonstrated that NSUN2 methyltransferase catalyses m5C methylation of the lncRNA FOXC2-AS1 and inhibits FOXC2 mRNA degradation, thus promoting gastric cancer cell malignancy. Therefore, systematically establishing the molecular regulatory network of m5C-related lncRNAs in STAD is essential to uncover reliable therapeutic targets.

We observed the expression of m5C methylation-regulated genes in STAD samples and normal control samples based on gene transcript data and understood their interactions in this investigation. Among the 13 m5C methylation-regulated genes, 11 had markedly elevated expression in STAD samples. It is indicated that m5C

methylation-regulated genes may be associated with the pathogenesis of STAD. Through a comprehensive analysis, we detected m5CRLSig with important prognostic value. In addition, the risk score was discovered to be an independent risk factor for the prognosis of STAD patients. The qRT-PCR results further confirmed the reliability of m5CRLSig as a prognostic marker for STAD. Patients with high-risk scores were prone to develop advanced clinicopathological characteristics. These findings imply that six m5C-related lncRNAs may play a role in the progression and prognosis of STAD and had potential clinical value.

Among the six m5C-related lncRNAs obtained from the data analysis of this study, HAGLR and AC009948.1 were risk genes, while AC005586.1, AL590666.2, AP001271.1, and IPO5P1 were protected genes. We reviewed the research related to these six lncRNAs in tumors and especially in gastric cancer. HAGLR has been studied in tumors and has been found to act as a procarcinogenic factor in multiple

(a)

(b)

Figure 10: Continued.

(c)
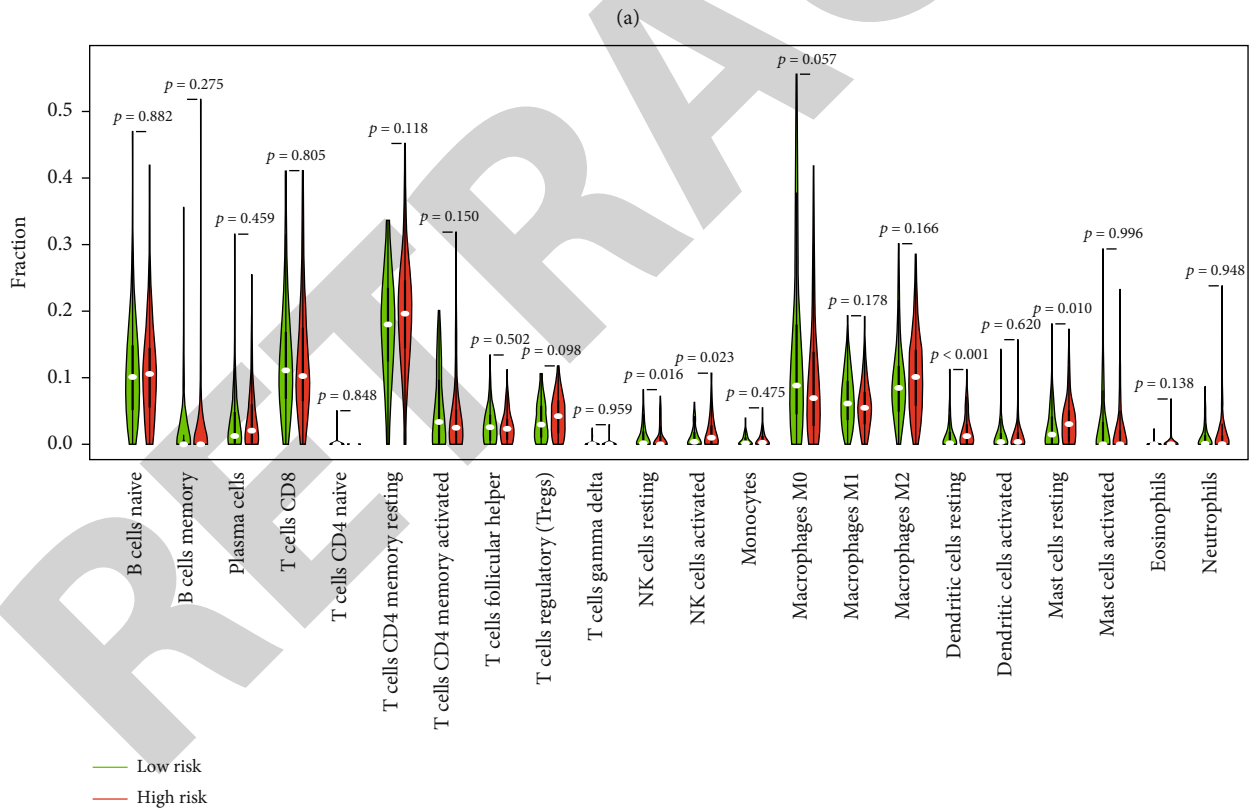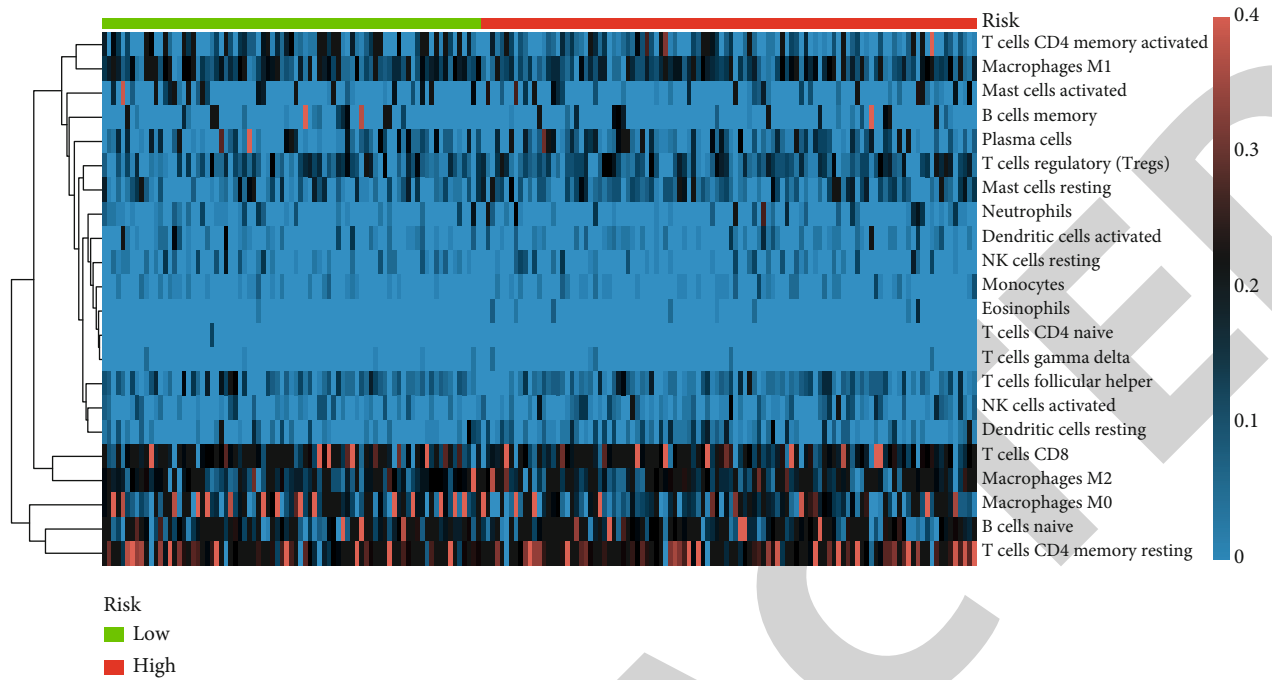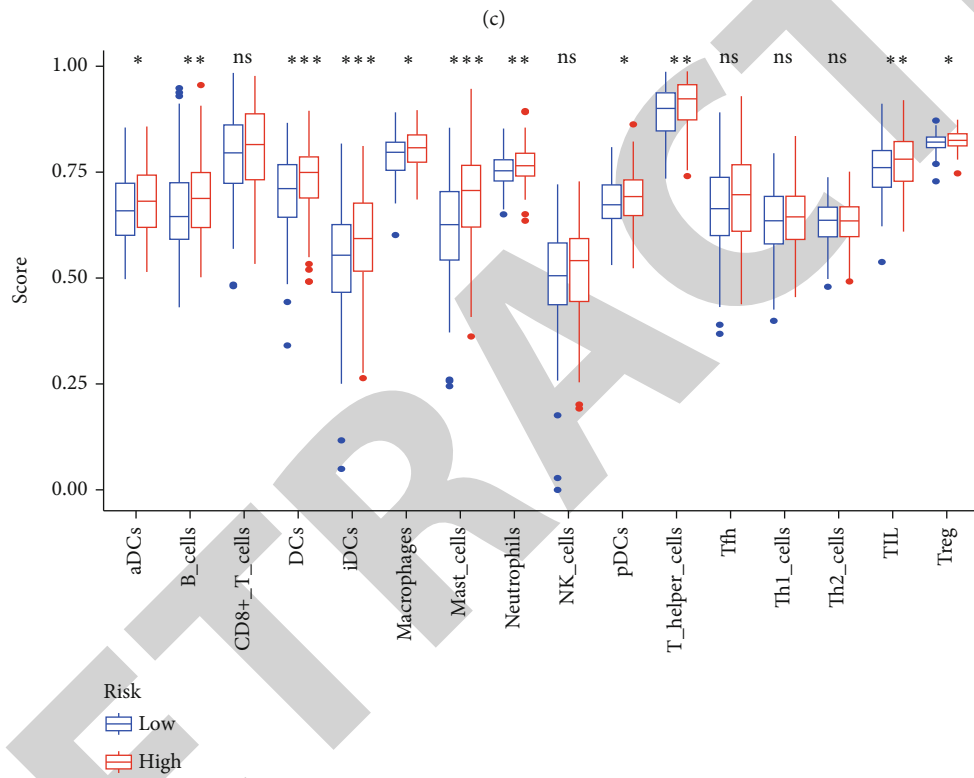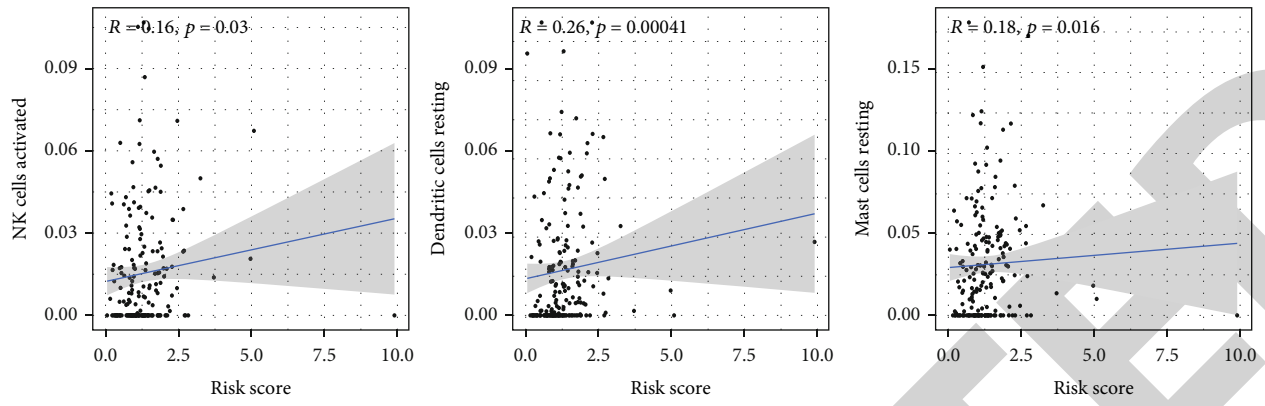
(d)

Figure 10: Continued.

(e)
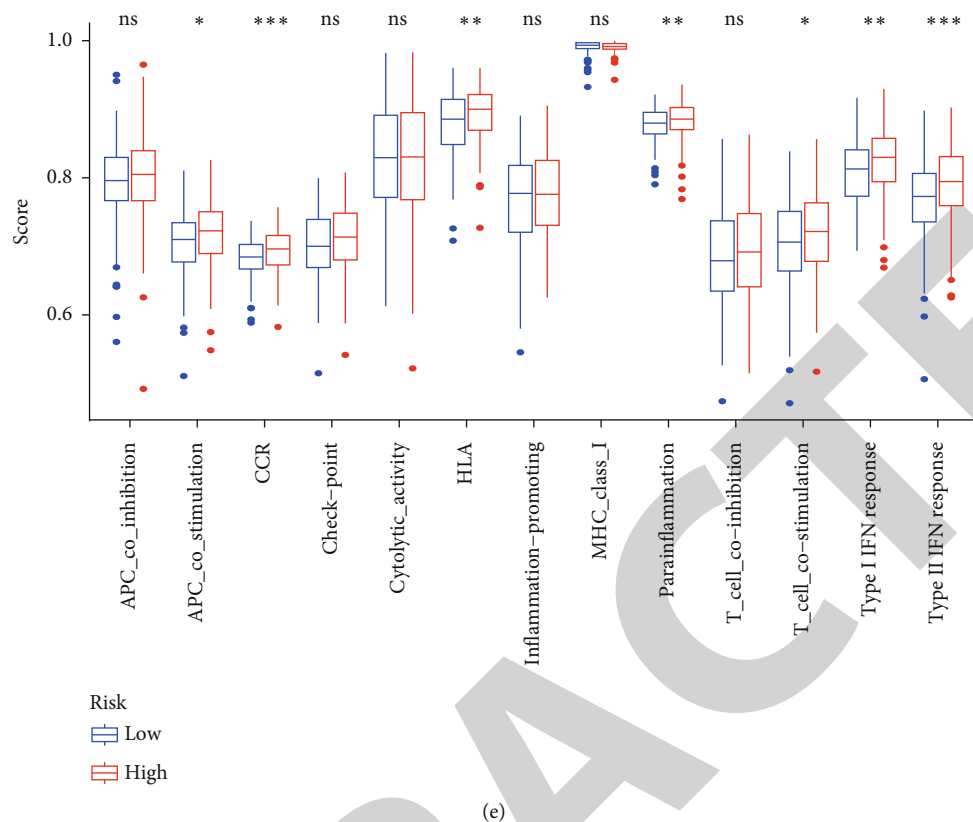
Figure 10: m5CRLSig is related to immune cell infiltration. (a, b) Heatmap and violin map of immune cell infiltration. (c) Relevance of the risk score to three types of immune cells. Enrichment scores of (d) immune cells and (e) immune function.

tumors, including gastric cancer and breast cancer [37, 38]. Hu et al. [37] proved that HAGLR accelerated gastric cancer cell proliferation and promoted gastric cancer cell resistance to 5-Fu by regulating the miR-338-3p/lactate dehydrogenase-A (LDHA) axis. In triple-negative breast cancer, HAGLR was found to be closely associated with tumor growth, and HAGLR knockdown restrained the aggressive proliferation of breast cancer cells [38]. Further animal experiments also showed that upregulation of HAGLR significantly accelerated tumor growth [38]. Wei et al. [39] exhibited that AP001271.1 could be used as a ferroptosis-related lncRNA, and it constituted a model with three other lncRNAs to evaluate the prognosis of patients with gastric cancer, which is similar to our experimental results. IPO5P1 has not been reported in gastric cancer, but bioinformatics studies imply that IPO5P1 is a prognostic factor in bladder cancer and correlates with the effects of immunotherapy [40]. Currently, studies of AL590666.2, AC009948.1, and AC005586.1 in the tumor field have not been covered, which provide new molecular targets for relevant studies in the future.

The identification of tumor immune characteristics can be of great benefit for precise immunotherapy and vaccine development [41]. lncRNAs have an important role in immune recognition and immune evasion of tumor cells [42]. For instance, lncRNA HOTTIP maintains high levels of PD-L1 on the surface of neutrophils, inhibiting T cell proliferation through cumulative immune depletion, leading to

tumor cell evasion of immune surveillance [43]. Furthermore, m5C methylation can also participate in the regulation of the TME. Gao et al. [44] revealed that patients with oral squamous cell carcinoma with high m5C methylation scores had lower immune activity and a poor prognosis. What roles do m5C-related lncRNAs play in the TME? In pancreatic ductal adenocarcinoma, m5C-related lncRNAs have been reported to induce polarisation or infiltration of M2 phenotype macrophages [26]. In this research, we investigated the relationship between m5C-related lncRNAs and tumor immune cell infiltration in STAD. We discovered that the risk score was positively associated with the level of NK cells activated, dendritic cells resting, and mast cells resting infiltration. The above three types of immune cells may be linked to a poor prognosis in STAD. However, the infiltration abundance of NK cells resting was decreased in the high-risk group. Dynamic interactions between m5CRLSig and the tumor immune microenvironment can produce different clinical outcomes. The regulatory function of m5C-related lncRNAs in STAD immune cell infiltration may be dual and may be significant players in the process of tumor immune escape or immune dormancy. The prognostic role of m5CRLSig in STAD is to a certain degree related to tumor immune cell infiltration.

According to GO and KEGG enrichment analyses, m5C-related lncRNAs are linked to multiple immunological-associated pathways, such as immunoglobulin binding. This study also investigated the impact of m5CRLSig on the

(a)
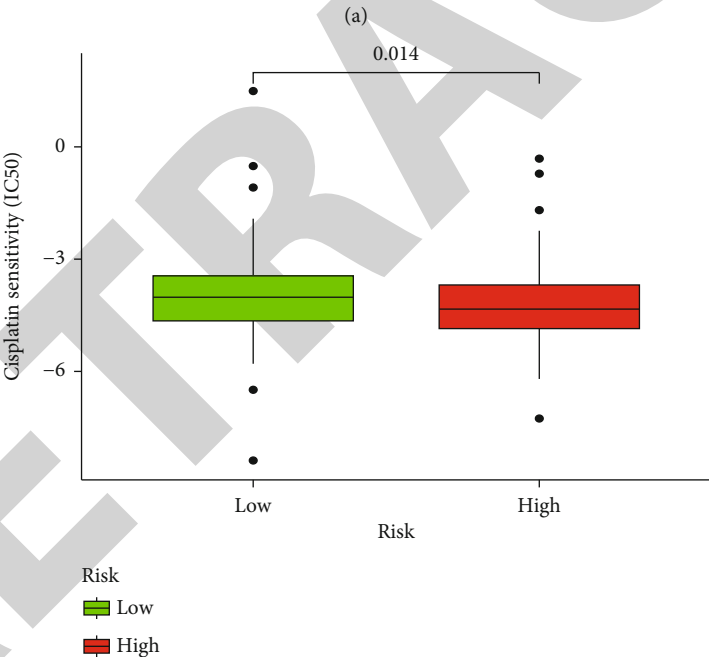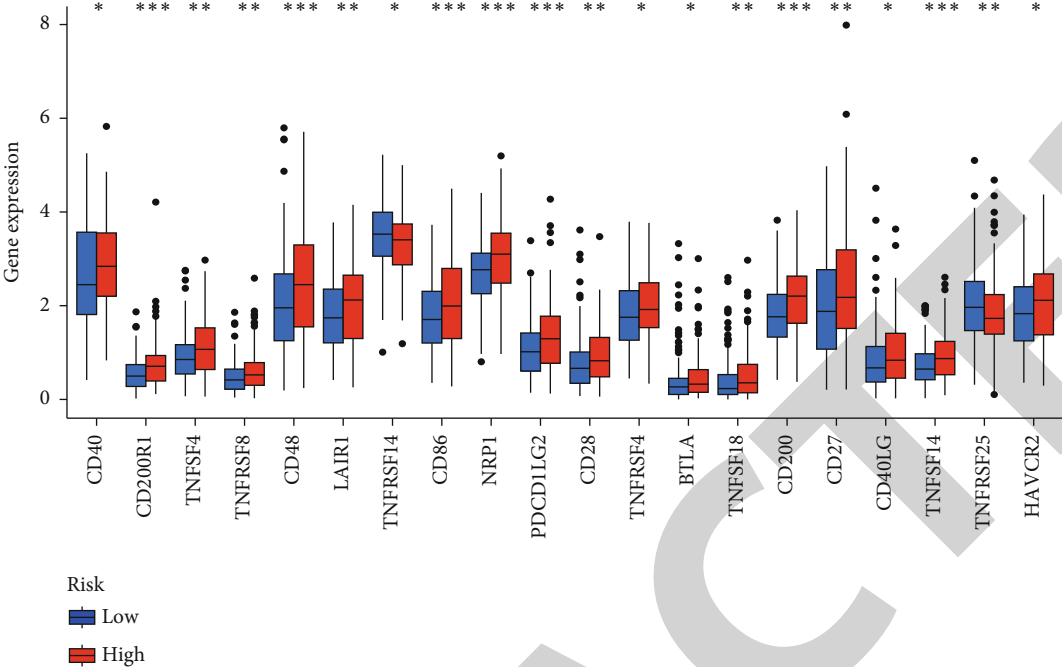
(b)

Figure 11: Continued.
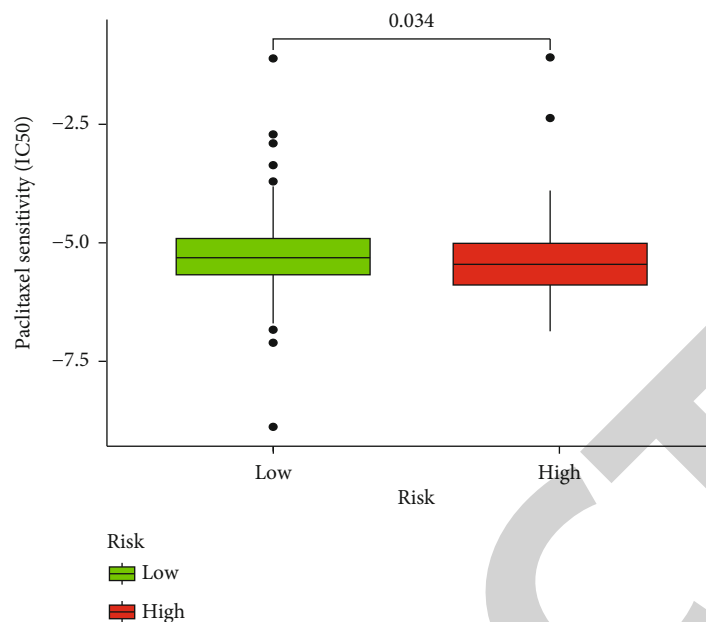
(c)

FIGURE 11: Relevance of m5CRLSig to immunotherapy and chemotherapy. (a) Differences in the expression of immune checkpoint genes in the two groups. (b, c) Sensitivity of the two groups to cisplatin and paclitaxel. $^*p < 0.05$, $^{**}p < 0.01$, and $^{***}p < 0.001$.

enrichment score of immune cells and immune function. The enrichment scores of multiple immune cell were higher in the high-risk group, such as aDCs, iDCs, and macrophages. Importantly, several immune function scores, such as CCR, HLA, and parainflammation, were also significantly higher in the high-risk group. The findings suggest that m5C-related lncRNAs participate in the adjustment of multiple immune cell functions. This may also be one reason for the discrepancy in the effectiveness of immunotherapy in patients with different risk scores. ICI can prevent cancer cells from undergoing immune escape and has become an important treatment for malignancies [45]. In this study, 18 immune checkpoint genes were highly expressed in the high-risk group of patients. m5CRLSig could provide some reference for ICI treatment in STAD patients. Next, we assessed the sensitivity of STAD patients to conventional chemotherapeutic drugs. Patients in the high-risk group were poorly sensitive to cisplatin and paclitaxel, which may also be a reason for the adverse prognosis in this group. These results suggest that m5CRLSig could be a potential predictive marker for immunotherapy and chemotherapy.

This research has certain limitations. The model we created was not tested in additional datasets outside of TCGA. Most of the study population was Caucasian; thus, the results may not be universally applicable to all races. The mechanism of action of AL590666.2, AC009948.1, and AC005586.1 in tumors was unclear. The outcome of bioinformatics analysis still needs to be confirmed by a large amount of sequencing data and clinical trials.

5. Conclusions

Based on TCGA database, we selected six m5C-related lncRNAs that were highly related to the prognosis of STAD

patients. Importantly, m5CRLSig participate in the modulation of tumor immune cell infiltration and are closely associated with both the expression of immune checkpoint genes and the sensitivity of chemotherapeutic agents. The present study provides new potential biological markers for immune treatment of STAD.

Data Availability

This study analyzed data from The Cancer Genome Atlas (TCGA) (https://http://portal.gdc.cancer.gov/). These data are free and publicly available.

Conflicts of Interest

The authors report no conflicts of interest for this work.

Authors' Contributions

DZ and CH designed the study. CZ and XZ collected the data. CH, XC, and XZ wrote the manuscript. CH and FK were responsible for the collection of tissue specimens and testing. All authors contributed to manuscript revision and read and approved the submitted manuscript.

Acknowledgments

Thanks are due to TCGA database; it provides free data for our research.

Supplementary Materials

Table 1: univariate Cox regression and Kaplan–Meier analysis of m5C-related lncRNAs in STAD. Supplementary Figure 1: correlation between prognostic m5C-related lncRNAs and

m5C genes. Supplementary Figure 2: barplot of the proportion of immune cell infiltration in the high- and low-risk groups. The 22 immune cells were labelled with various colours in the legend. *(Supplementary Materials)*

References

[1] H. Sung, J. Ferlay, R. L. Siegel et al., "Global cancer statistics 2020: GLOBOCAN estimates of incidence and mortality worldwide for 36 cancers in 185 countries," *Ca-a Cancer Journal for Clinicians*, vol. 71, no. 3, pp. 209–249, 2021.

[2] A. P. Thrift and H. B. El-Serag, "Burden of gastric cancer," *Clinical Gastroenterology and Hepatology*, vol. 18, no. 3, pp. 534–542, 2020.

[3] Z. D. Chen, P. F. Zhang, H. Q. Xi, B. Wei, L. Chen, and Y. Tang, "Recent advances in the diagnosis, staging, treatment, and prognosis of advanced gastric cancer: a literature review," *Frontiers in Medicine*, vol. 8, p. 12, 2021.

[4] E. C. Smyth, M. Nilsson, H. I. Grabsch, N. C. T. van Grieken, and F. Lordick, "Gastric cancer," *The Lancet*, vol. 396, no. 10251, pp. 635–648, 2020.

[5] D. W. Rong, G. S. Sun, F. Wu et al., "Epigenetics: roles and therapeutic implications of non-coding RNA modifications in human cancers," *Molecular Therapy-Nucleic Acids*, vol. 25, pp. 67–82, 2021.

[6] Q. Zhang, F. Liu, W. Chen et al., "The role of RNA m5C modification in cancer metastasis," *International Journal of Biological Sciences*, vol. 17, no. 13, pp. 3369–3380, 2021.

[7] G. Guo, K. Pan, S. Fang et al., "Advances in mRNA 5-methylcytosine modifications: detection, effectors, biological functions, and clinical relevance," *Molecular Therapy-Nucleic Acids*, vol. 26, pp. 575–593, 2021.

[8] X. Lu, Y. Fan, S. Kang, B. Xiao, and M. Zhang, "RNA methylation and neurovascular unit remodeling," *Yi xue ban= Journal of Central South University. Medical Sciences*, vol. 46, no. 5, pp. 536–544, 2021.

[9] W. Zhou, C. Wang, J. Chang et al., "RNA methylations in cardiovascular diseases, molecular structure, biological functions and regulatory roles in cardiovascular diseases," *Frontiers in Pharmacology*, vol. 12, 2021.

[10] W. Zhou, X. Wang, J. Chang, C. Cheng, and C. Miao, "The molecular structure and biological functions of RNA methylation, with special emphasis on the roles of RNA methylation in autoimmune diseases," *Critical Reviews in Clinical Laboratory Sciences*, vol. 59, no. 3, pp. 203–218, 2022.

[11] Y. Hu, C. Chen, X. Tong et al., "NSUN2 modified by SUMO-2/3 promotes gastric cancer progression and regulates mRNA m5C methylation," *Cell Death & Disease*, vol. 12, no. 9, p. 842, 2021.

[12] Z. Huang, J. Li, J. Chen, and D. Chen, "Construction of prognostic risk model of 5-methylcytosine-related long noncoding RNAs and evaluation of the characteristics of tumor-infiltrating immune cells in breast cancer," *Frontiers in Genetics*, vol. 12, 2021.

[13] Q. Geng, Q. Wei, Z. Shen et al., "Comprehensive analysis of the prognostic value and immune infiltrates of the three-m5C signature in colon carcinoma," *Cancer Management and Research*, vol. 13, pp. 7989–8002, 2021.

[14] M. C. Jiang, J. J. Ni, W. Y. Cui, B. Y. Wang, and W. Zhuo, "Emerging roles of lncRNA in cancer and therapeutic opportunities," *American Journal of Cancer Research*, vol. 9, no. 7, pp. 1354–1366, 2019.

[15] D. Li, L. Song, Z. M. Wen et al., "Strong evidence for LncRNA ZNRD1-AS1, and its functional cis- eQTL locus contributing more to the susceptibility of lung cancer," *Oncotarget*, vol. 7, no. 24, pp. 35813–35817, 2016.

[16] Y. Wang and Z. Chen, "Long noncoding RNA UBA6-AS1 inhibits the malignancy of ovarian cancer cells via suppressing the decay of UBA6 mRNA," *Bioengineered*, vol. 13, no. 1, pp. 178–189, 2022.

[17] Y. Li, B. Yan, X. Wang et al., "ALKBH5-mediated m6A modification of lncRNA KCNQ1OT1 triggers the development of LSCC via upregulation of HOXA9," *Journal of Cellular and Molecular Medicine*, vol. 26, no. 2, pp. 385–398, 2022.

[18] C. Carissimi, I. Laudadio, E. Lorefice, G. Azzalin, V. de Paolis, and V. Fulci, "Bisulphite miRNA-seq reveals widespread CpG and non-CpG 5-(hydroxy)methyl-cytosine in human micro-RNAs," *RNA Biology*, vol. 18, no. 12, pp. 2226–2235, 2021.

[19] J. E. Squires, H. R. Patel, M. Nousch et al., "Widespread occurrence of 5-methylcytosine in human coding and non-coding RNA," *Nucleic Acids Research*, vol. 40, no. 11, pp. 5023–5033, 2012.

[20] K. Pansy, B. Uhl, J. Krstic et al., "Immune regulatory processes of the tumor microenvironment under malignant conditions," *International Journal of Molecular Sciences*, vol. 22, no. 24, p. 13311, 2021.

[21] G. C. Eptaminitaki, N. Wolff, D. Stellas, K. Sifakis, and S. Baritaki, "Long non-coding RNAs (lncRNAs) in response and resistance to cancer immunosurveillance and immunotherapy," *Cell*, vol. 10, no. 12, p. 3313, 2021.

[22] Y. L. Ai, S. Y. Wu, H. Gao et al., "Repression of CRNDE enhances the anti-tumour activity of CD8 + T cells against oral squamous cell carcinoma through regulating miR-545-5p and TIM-3," *Journal of Cellular and Molecular Medicine*, vol. 25, no. 23, pp. 10857–10868, 2021.

[23] M. Zhang, N. Wang, P. Song et al., "LncRNA GATA3-AS1 facilitates tumour progression and immune escape in triple-negative breast cancer through destabilization of GATA3 but stabilization of PD-L1," *Cell Proliferation*, vol. 53, no. 9, p. 13, 2020.

[24] D. Chen, X. T. Li, H. Li, K. Wang, and X. Tian, "Identification of immune-related prognostic mRNA and lncRNA in patients with hepatocellular carcinoma," *Journal of Oncology*, vol. 2022, Article ID 5313149, 16 pages, 2022.

[25] Y. Yan, J. Liu, Z. Xu, M. Ye, and J. Li, "lncRNA PCAT14 is a diagnostic marker for prostate cancer and is associated with immune cell infiltration," *Disease Markers*, vol. 2021, Article ID 9494619, 9 pages, 2021.

[26] H. Yuan, J. Liu, L. Zhao et al., "Prognostic risk model and tumor immune environment modulation of m5C-related LncRNAs in pancreatic ductal adenocarcinoma," *Frontiers in Immunology*, vol. 12, 2021.

[27] H. L. Feng, Z. J. Lyu, J. B. Zheng et al., "Association of tumor size with prognosis in colon cancer: a Surveillance, Epidemiology, and End Results (SEER) database analysis," *Surgery*, vol. 169, no. 5, pp. 1116–1123, 2021.

[28] H. L. Feng, Z. J. Lyu, W. J. Liang et al., "Optimal examined lymph node count in node-negative colon cancer should be determined," *Future Oncology*, vol. 17, no. 29, pp. 3865–3872, 2021.

Retraction

Retracted: Gene Differential Expression and Interaction Networks Illustrate the Biomarkers and Molecular Biological Mechanisms of Unsaponifiable Matter in Kanglaite Injection for Pancreatic Ductal Adenocarcinoma

BioMed Research International

This article has been retracted by Hindawi following an investigation undertaken by the publisher [1]. This investigation has uncovered evidence of one or more of the following indicators of systematic manipulation of the publication process:

(1) Discrepancies in scope

(2) Discrepancies in the description of the research reported

(3) Discrepancies between the availability of data and the research described

(4) Inappropriate citations

(5) Incoherent, meaningless and/or irrelevant content included in the article

(6) Manipulated or compromised peer review

The presence of these indicators undermines our confidence in the integrity of the article's content and we cannot, therefore, vouch for its reliability. Please note that this notice is intended solely to alert readers that the content of this article is unreliable. We have not investigated whether authors were aware of or involved in the systematic manipulation of the publication process.

Wiley and Hindawi regrets that the usual quality checks did not identify these issues before publication and have since put additional measures in place to safeguard research integrity.

We wish to credit our own Research Integrity and Research Publishing teams and anonymous and named external researchers and research integrity experts for contributing to this investigation.

The corresponding author, as the representative of all authors, has been given the opportunity to register their agreement or disagreement to this retraction. We have kept a record of any response received.

References

[1] B. Xu, W. Dan, X. Zhang et al., "Gene Differential Expression and Interaction Networks Illustrate the Biomarkers and Molecular Biological Mechanisms of Unsaponifiable Matter in Kanglaite Injection for Pancreatic Ductal Adenocarcinoma," *BioMed Research International*, vol. 2022, Article ID 6229462, 19 pages, 2022.

Research Article

Gene Differential Expression and Interaction Networks Illustrate the Biomarkers and Molecular Biological Mechanisms of Unsaponifiable Matter in Kanglaite Injection for Pancreatic Ductal Adenocarcinoma

Bowen Xu [ID],[1,2] Wenchao Dan [ID],[3] Xiaoxiao Zhang [ID],[1] Heping Wang [ID],[1] Luchang Cao [ID],[1] Shixin Li [ID],[1,2] and Jie Li [ID][1]

[1]*Department of Oncology, Guang'anmen Hospital, China Academy of Chinese Medical Sciences, Beijing 100053, China*
[2]*Beijing University of Chinese Medicine, Beijing 100029, China*
[3]*Department of Dermatological, Beijing Hospital of Traditional Chinese Medicine, Capital Medical University, Beijing 100010, China*

Correspondence should be addressed to Jie Li; qfm2020jieli@yeah.net

Background. Kanglaite injection (KLTi) has shown good clinical efficacy in the treatment of pancreatic ductal adenocarcinoma (PDAC). While previous studies have demonstrated the antitumor effects of the oil compounds in KLTi, it is unclear whether the unsaponifiable matter (USM) also has antitumor effects. This study used network pharmacology, molecular docking, and database verification methods to investigate the molecular biological mechanisms of USM. *Methods.* Compounds of USM were obtained from GC-MS, and targets from DrugBank. Next, the GEO database was searched for differentially expressed genes in cancerous tissues and healthy tissues of PDAC to identify targets. Subsequently, the protein-protein interaction of USM and PDAC targets was constructed by BisoGenet to extract candidate genes. The candidate genes were enriched using GO and KEGG by Metascape, and the gene-pathway network was constructed to screen the key genes. Molecular docking and molecular dynamic simulations of core compound targets were finally performed and to explore the diagnostic, survival, and prognosis value of targets. *Results.* A total of 10 active compounds and 36 drug targets were screened for USM, 919 genes associated with PDAC, and 139 USM candidate genes against PDAC were excavated. The enrichment predicted USM by acting on *RELA*, *NFKB1*, *IKBKG*, *JUN*, *MAPK1*, *TP53*, and *AKT1*. Molecular docking and dynamic simulations confirmed the screened core targets had good affinity and stability with the corresponding compounds. In diagnostic ROC validation, the above targets have certain accuracy for diagnosing PDAC, and the combined diagnosis is more advantageous. As the most diagnostic value of *RELA*, it is equally significant in predicting disease-specific survival and progression-free interval. *Conclusions.* USM in KLTi plays an anti-PDAC role by intervening in the cell cycle, inducing apoptosis, and downregulating the NF-κB, MAPK, and PI3K-Akt pathways. It might participate in the pancreatic cancer pathway, and core target groups have diagnostic, survival, and prognosis value biomarker significance.

1. Introduction

Pancreatic ductal adenocarcinoma (PDAC) is a malignant tumor of the digestive tract and accounts for about 90% of all pancreatic cancers (PC). The five-year relative survival rate for PDAC is only 9% [1]. At present, the incidence and case

fatality rates of PDAC continue to rise, and it is expected to become the second leading cause of cancer-related deaths in 2030 [2]. About 90% of the patients with PDAC are diagnosed at an advanced stage, and only 20% of the patients receive surgical treatment. Moreover, the surgical resection rate of PDAC is low, and the five-year survival rate of patients with complete

resection is 27% [3]. PDAC is highly metastatic and develops drug resistance easily. Due to the low efficacy and high toxicity associated with chemoradiotherapy [4], the conventional treatment modalities for PDAC have run into a bottleneck. Therefore, it is of great clinical significance and practical value to seek a safe and efficacious adjuvant therapy for PDAC.

Numerous studies have indicated that traditional Chinese medicine (TCM) has been shown to play an active role in the adjuvant treatment of PDAC by reducing the toxic effects and side effects associated with modern medical treatment [5], improving the quality of life, and prolonging the survival of patients [6]. Kanglaite injection (KLTi) is a neutral oil extracted and isolated from the seeds of the Chinese herbal medicine, *Coix lacryma-jobi* L.. It has been widely used in China as adjuvant therapy for the treatment of various advanced malignant tumors and has shown anticachexia and analgesic effects.

In mechanism research [7], KLTi has shown antitumor activity in mouse models of PDAC by inhibiting proliferation and metastasis and inducing apoptosis and necrosis. A phase II clinical trial showed that the combination of KLTi and gemcitabine in PDAC presented a difference in progression-free survival (114 days versus 57.7 days, $P = 0.0080$) and objective response rate [8], but it was fully sponsored by KLT company and may lead to the existence of conflicts of interest. To further confirm the ability of KLTi in improving the efficacy of PDAC, a meta-analysis showed that the combination of KLTi and chemoradiotherapy is more effective than chemoradiotherapy alone in the treatment of advanced PDAC. The combination treatment not only improved the 1-year overall survival rate, overall response, and disease control rate but also enhanced the quality of life, relieving pain, and alleviated adverse reactions [9]. In addition, a network meta-analysis was performed to assess the effectiveness and safety of Chinese herbal injections combined with chemotherapy for the treatment of PC. The results demonstrated that Kanglaite injection combined with chemotherapy yielded a significantly higher probability of improving performance status [10].

Further exploration of KLTi is expected to provide benefit in improving the comprehensive treatment of PDAC. A total of 12 triglycerides were identified as the main compounds in KLTi by high-performance liquid chromatography-atmospheric pressure chemical ionization-mass spectrometry (HPLC-MS) [11]. While the oily compounds in KLTi have been studied well, there are few studies on the unsaponifiable matter (USM) in KLTi. Whether these USM also have antitumor effects need further investigation.

Network pharmacology is based on various types of biological information databases. Through the network analysis of drugs, genes, compounds, and diseases and thoroughly examining the key nodes in the network [12], it is possible to systematically explain the material basis and mechanism of action of TCM [13]. Network pharmacology also emphasizes the study of multitarget pathways, which is consistent with the overall concept of TCM. Hence, it is currently used to investigate the mechanism of action and new drug development of TCM and its compound prescriptions, especially in cancer treatment [14]. Therefore, in this study, the net-

work pharmacology and molecular docking method were used to elucidate the specific molecular biological mechanisms of USM in KLTi intervention in PDAC. And The Cancer Genome Atlas (TCGA) database was used to analyze the diagnostic effect of core targets on PDAC and the predictive effect on long-term survival.

2. Materials and Methods

2.1. Screening of Active Compounds and Targets in Unsaponifiable Matter.
The USM in KLTi was separated, and their main compounds were identified by gas chromatography-mass spectrometric (GC-MS) [15]. Next, we identified the total chemical composition of *Coix lacryma-jobi* L. from the Traditional Chinese Medicine Database and Analysis Platform (TCMSP) [16] and HERB. According to the ADME (absorption, distribution, metabolism, and excretion) screening principle, there are two core indicators, oral bioavailability (OB) and drug-likeness (DL), used for screening compounds. Since KLTi is administered intravenously, it did not require screening of OB, which is specific to orally administered drugs. The screening condition for DL was set as ≥0.18. Compounds related to *Coix lacryma-jobi* L. that demonstrated antitumor activity, as confirmed from previous studies, were collected to supplement and improve the results and obtain candidate compounds.

Candidate compounds were then matched to drug targets in the DrugBank database [17] and corrected to standard gene names, using the Uniprot database [18]. Cytoscape 3.7.2 was employed to construct a compound-target network of KLTi for the selected compounds and targets [19]. The network was analyzed to analyze the relationship between the important compounds and targets in KLTi, with the help of Cytoscape's built-in network analyzer tool, focusing on the degree of connectivity. The more connected the degree, the higher importance involved in biological functions. The workflow of the network pharmacology analysis performed in this study is depicted in Figure 1.

2.2. Identification of PDAC-Related Targets.
The differential expressed genes in cancerous tissues and healthy tissues of PDAC patients were obtained from the Gene Expression Omnibus (GEO) [20] series (GSE15471, samples: GSM388115-GSM388153 and GSM388076-GSM388114). Disease targets of PDAC were screened under the conditions of adjusted P value < 0.05 and |logFC| > 1, and the gene markers with significant differentially expressed genes corresponded to gene names.

2.3. Construction of Protein-Protein Interaction.
Based on the built-in function of BisoGenet in Cytoscape 3.7.2, the protein-protein interaction (PPI) network between KLTi USM and PDAC was constructed and visualized. The intersection network of two PPI networks was extracted by the merge function, and the attribute values of each node in the intersection network were analyzed using CytoNCA [21]. The median $k1$ of the connectivity degree was calculated, and all nodes with a connectivity degree greater than 2 times $k1$ were selected and termed as "Hit hubs." The
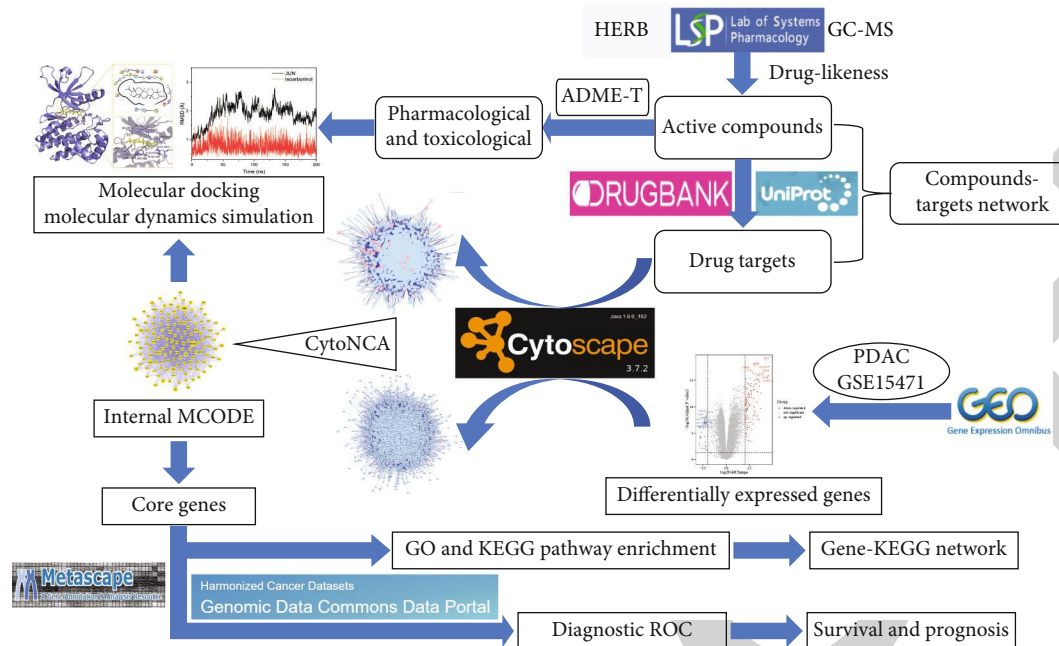
Figure 1: Workflow of network pharmacology analysis.

properties of each node of the Hit hubs network were calculated to obtain three medians $k2$, $l2$, and $m2$ for connectivity degree centrality (DC), closeness centrality (CC), and betweenness centrality (BC), respectively. All nodes whose node properties were simultaneously greater than $k2$, $l2$, and $m2$ were screened as candidate targets.

2.4. Pathway Enrichment Analysis.

The Metascape platform integrates several reliable databases such as gene ontology (GO) and Kyoto Encyclopedia of Genes and Genomes (KEGG) for pathway enrichment analysis of gene targets and is updated monthly to ensure data accuracy [22]. GO utilizes three parameters; namely, molecular function, biological process, and cellular component to interpret the antitumor biological process of candidate genes. KEGG analysis examines the main antitumor signaling pathways involved in candidate genes. The 20 GO and KEGG processes, with significant differences, were screened, and the results were visualized and analyzed with R software. Based on the relevant targets mapped by KEGG results, a gene-pathway network was constructed to further screen key target genes for KLTi treatment of PDAC.

2.5. Molecular Docking

2.5.1. Preparation of Protein.
The crystal structure of the protein was downloaded from RCSB PDB (Protein Data Bank) [23]. GUI-based "Auto-Dock Tools" was used to prepare and execute the docking studies. Kollman atom charges, solvation parameters, and polar hydrogens were added to the protein and proceeded for docking studies. As the ligands used are not peptides, Gasteiger charges were assigned only to the protein, and the nonpolar hydrogens were merged. Based on the reference ligand, literature, and predicted active regions, a grid box was assigned around the active sites using the AutoGrid application.

2.5.2. Preparation of Ligand.
The 3D structures of the main compounds were retrieved from the PubChem database. Minimize the energy of the downloaded compound through Chem3D and convert it into mol2 format. Import the small molecular compound into Auto-Dock Tools software, add atomic charge, and assign an atomic type [21]. All flexible keys are rotatable by default. Finally, the best conformation was retained in pdbqt format for utilization in further docking studies.

2.6. Molecular Dynamic Simulation.
MD simulations of protein complexes with compounds were performed using Desmond (version 2020). Here, the molecular force field for MD simulations was chosen as OPLS3e, and the system was solvated using the TIP3 water model. Neutralize system charge by adding ions. The energy minimization of the whole system is achieved using the OPLS3e force field (all-atom type force field). The geometry of water molecules, bond lengths, and bond angles of heavy atoms are all constrained by the SHAKE algorithm. The continuous system is simulated by applying periodic boundary conditions, and long-range electrostatics are maintained by the particle mesh Ewald method. The system was equilibrated using an NPT ensemble with a temperature of 300 k and a pressure of 1.0 bar. The Berendsen coupling algorithm was used for the coupling of temperature-pressure parameters. At the time of late preparation of the system, 200 ns runs were performed at a time step of 1.2 fs, and trajectory recording was performed every 100 ps for a total of 20,00 frames. The RMSD (root mean square deviation) of the main chain atoms was calculated and graphically analyzed to understand the nature of protein-ligand interactions.

2.7. Diagnostic, Survival, and Prognosis Value Analysis of Key Targets.
ROC curves were made using key target genes

Name	PubChem ID	Formula	MW(g/mol)	Hdon	Hacc	Rbon	LogP
Stigmasterol	5280794	$C_{29}H_{48}O$	412.7	1	1	5	8.6
Mandenol	5282184	$C_{20}H_{36}O_2$	308.5	0	2	16	7.3
Sitosterol alpha1	9548595	$C_{30}H_{50}O$	426.7	1	1	5	9
Isoarborinol	12305182	$C_{30}H_{50}O$	426.7	1	1	1	9
CLR	5997	$C_{27}H_{46}O$	386.7	1	1	5	8.7
Omaine	220401	$C_{21}H_{25}NO_5$	371.4	1	6	5	1.4
Ergosterol	444679	$C_{28}H_{44}O$	396.6	1	1	4	7.4
Sitosterol	222284	$C_{29}H_{50}O$	414.7	1	1	6	9.3
Campesterol	173183	$C_{28}H_{48}O$	400.7	1	1	5	8.8
2-Monoolein	5319879	$C_{21}H_{40}O_4$	356.5	2	4	19	6.3

(a)

(b)

(c)
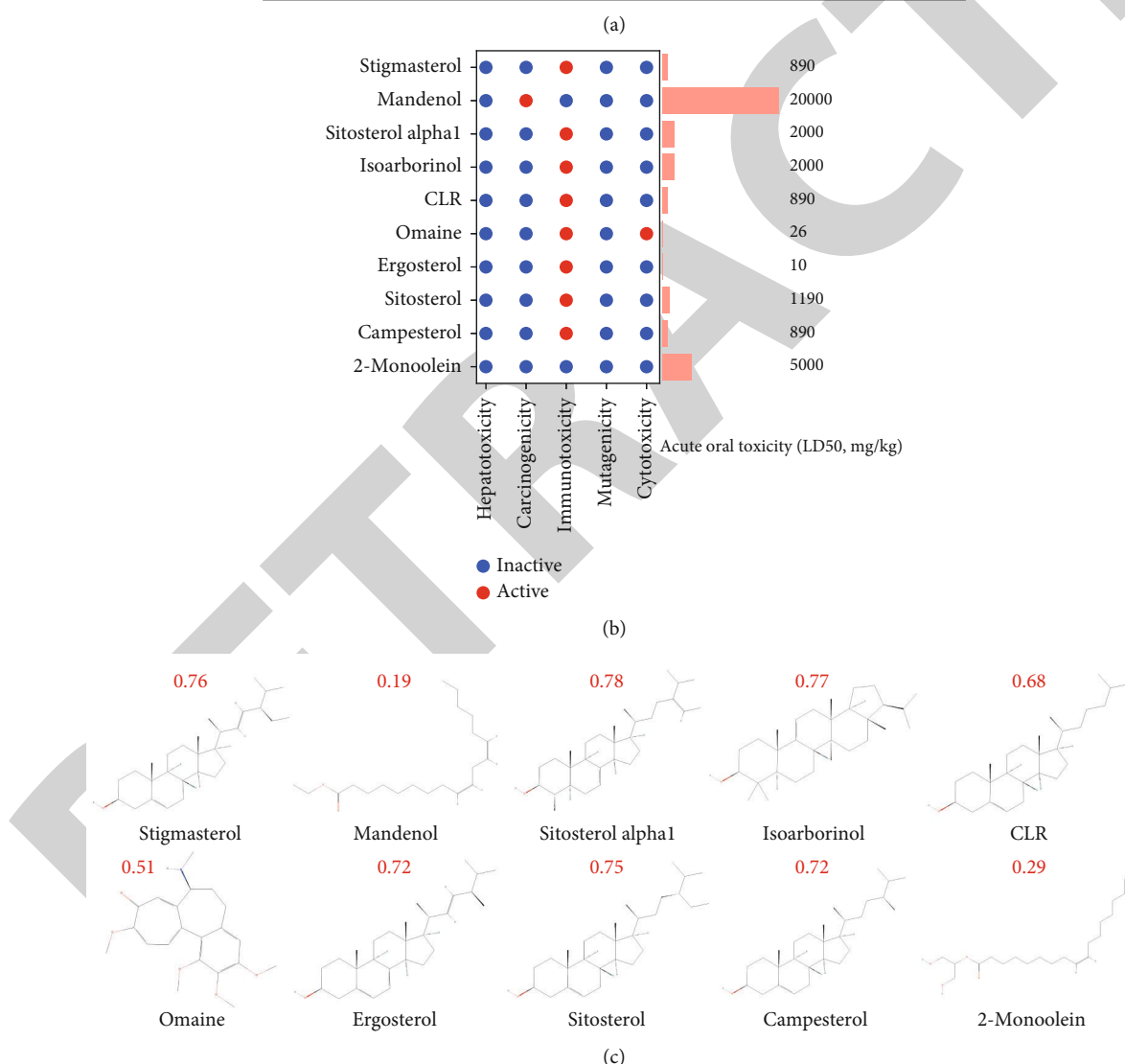
Figure 2: Evaluation of pharmacological and toxicological parameters of main compounds from unsaponifiable matter (USM). ((a) Pharmacological and molecular properties of the main compounds in USM. (b) The toxicological parameters include hepatotoxicity, carcinogenicity, immunotoxicity, mutagenicity, cytotoxicity, and acute oral toxicity of the main compounds in USM. (c) The chemical structure and drug-likeness parameters of the main compounds extracted from USM. Red numbers represent drug-likeness values. MW: molecular weight; Hdon: hydrogen bond donor count; Hacc: hydrogen bond acceptor count; Rbon: rotatable bond count; LoaP: lipid-water partition coefficient).

(a)

(b)

FIGURE 3: Continued.

(c)
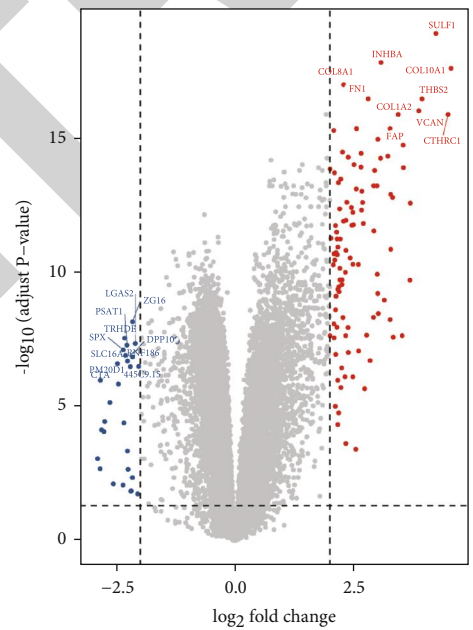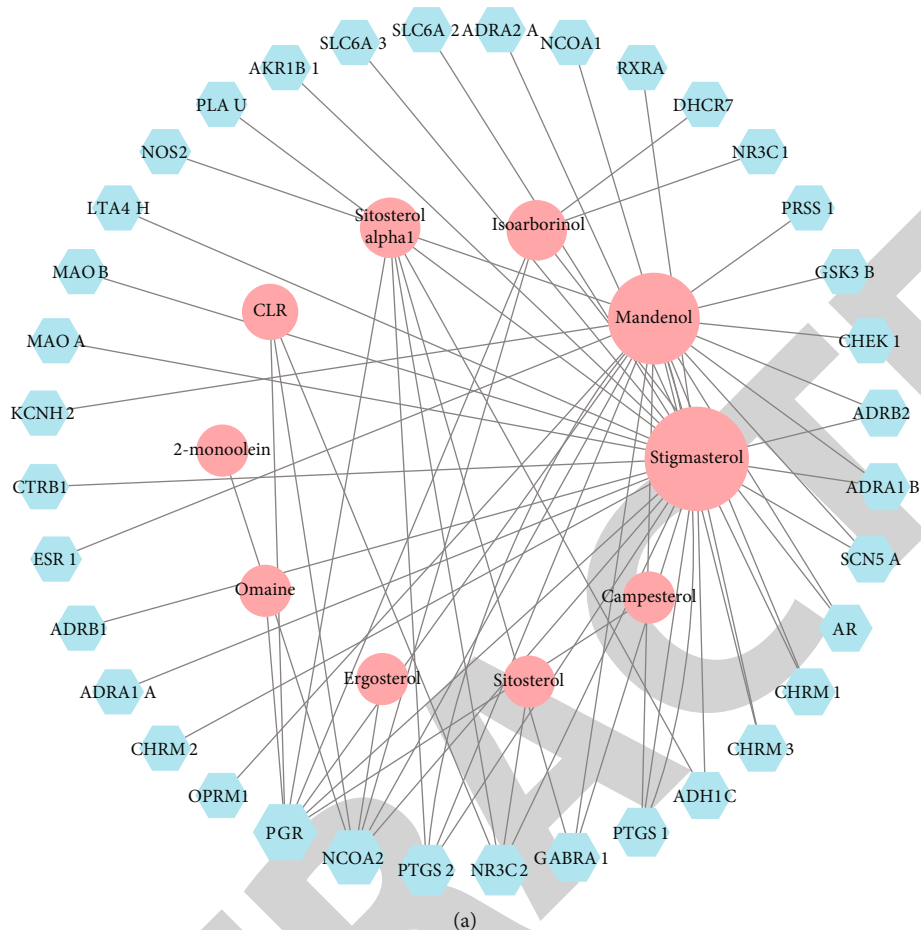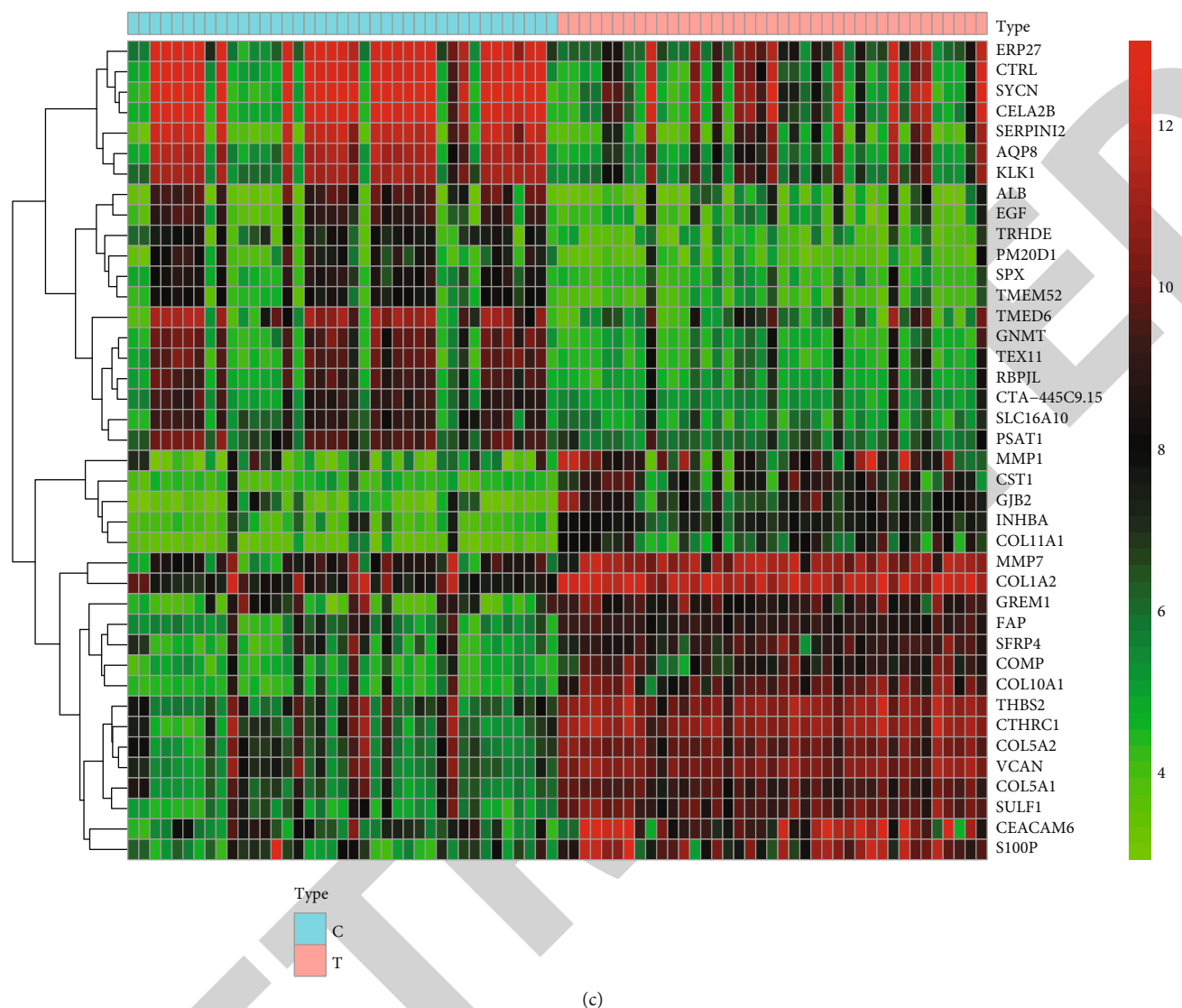
Figure 3: Related targets in unsaponifiable matter (USM) and pancreatic ductal adenocarcinoma (PDAC). ((a) Compound-target network of USM. Blue hexagons represent targets; pink circles represent compounds. (b) Volcano plot of differentially expressed genes in PDAC. The abscissa represents the fold changes in gene expression, and the ordinate represents the statistical significance of the variations in gene expression. The red dots represent significantly differentially expressed genes. (c) Heat map of differentially expressed genes in PDAC).

in combination with the data set to determine the diagnostic value for PDAC. Then, combined with the data of the GEO and TCGA database and RNAseq data from the PAAD (pancreatic cancer) project. Log-rank test with Cox regression was used. Suppose $P < 0.05$, the difference in the survival time distribution of the groups was statistically significant. Thus, the survival and prognosis analyses of the core targets obtained by the screening are carried out.

3. Results

3.1. Active Compounds of Unsaponifiable Matter. According to the GC-MS results of USM in KLTi, 10 compounds were included and queried for their DL values. A total of 38 compounds were identified in TCMSP and HERB, based on the chemical composition of *Coix lacryma-jobi* L.. Candidate compounds with DL ≥ 0.18 (18 active com-

pounds) were included in the study. Two compounds, olein and mboa, which had demonstrated antitumor activity in previous studies [24], were excluded since their DL < 0.18. A total of 36 drug targets were matched in the DrugBank database. Of these, 10 active compounds were mapped to the corresponding targets, while 8 compounds did not match any target (Figure 2(a)). Pharmacotoxicology is commonly used to evaluate the safety profile of compounds. The protox II webserver was used to predict toxicological parameters such as hepatotoxicity, carcinogenicity, immunotoxicity, mutagenicity, cytotoxicity, and acute oral toxicity (LD50, mg/kg). None of the compounds in USM showed hepatotoxicity and mutagenicity, and 2-monoolein also presented inactive in toxicological parameters. Meanwhile, stigmasterol, sitosterol alpha1, isoarborinol, CLR, omaine, ergosterol, sitosterol, campesterol, and 2-monoolein have the risk of immunotoxicity. Mandenol

1558 nodes and 40405 edges   382 nodes and 14158 edges   139 nodes and 3593 edges
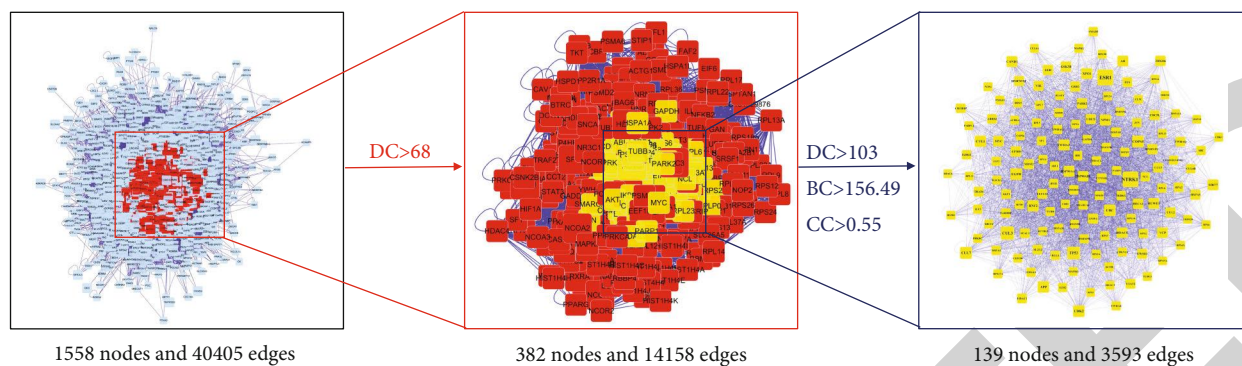
Figure 4: The protein-protein interaction (PPI) network of unsaponifiable matter candidate genes against pancreatic ductal adenocarcinoma (PDAC). ((a) The interactive PPI network of unsaponifiable matter putative targets and PDAC-related targets. (b) PPI network of significant proteins extracted from (a). (c) PPI network of candidate unsaponifiable matter targets for PDAC therapy extracted from (b). DC: degree centrality; BC: betweenness centrality; CC: closeness centrality).
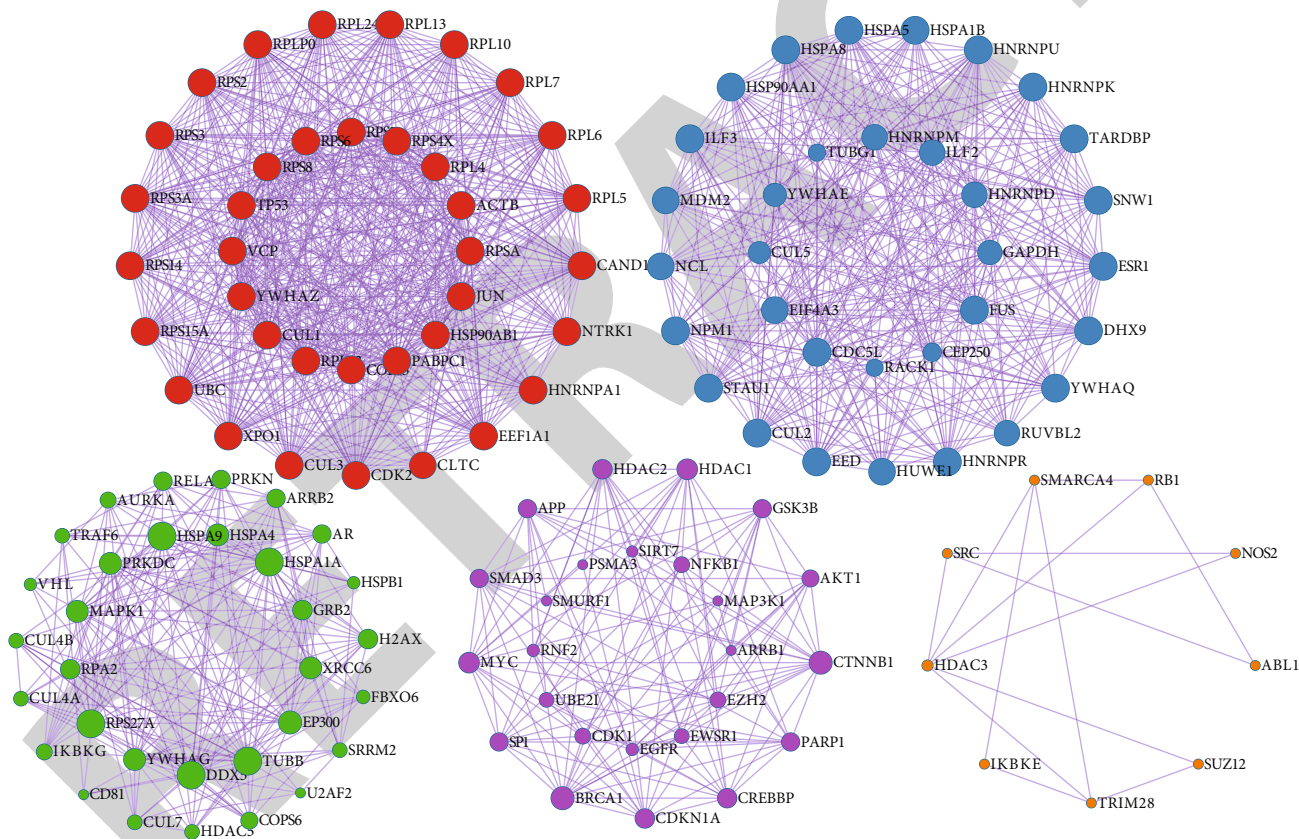
Figure 5: Unsaponifiable matter treatment of pancreatic ductal adenocarcinoma core protein-protein interaction network internal potential module network.

has the risk of carcinogenicity, while omaine has cytotoxicity. Moreover, ergosterol and omaine showed the lowest LD50 values (10 mg/kg, 26 mg/kg) (Figure 2(b)). The chemical structure and DL of 10 compounds from USM are shown in Figure 2(c). All the compounds displayed favorable DL parameters (shown in red font). These results indicate that these 10 compounds showed good pharmacological parameters and molecular properties,

which could be used as active compounds for follow-up analysis.

3.2. Unsaponifiable Matter and PDAC-Related Targets. A compound-target network was constructed for USM (Figure 3(a)), the nodes represented compounds or targets, and the edges represented the relationship of interactions. This network contained 46 nodes (10 compounds and 36

Table 1: Description of potential module functions within protein-protein interaction network for unsaponifiable matter treatment of pancreatic ductal adenocarcinoma (top 3).

Color	GO	Description	Log10P
Red	GO:0003735	Structural constituent of ribosome	-29.7
	GO:0005198	Structural molecule activity	-21.6
	GO:0019843	rRNA binding	-11.2
Blue	GO:0019904	Protein domain-specific binding	-11.5
	GO:0043021	Ribonucleoprotein complex binding	-9.3
	GO:0031625	Ubiquitin protein ligase binding	-8.4
Green	GO:0031625	Ubiquitin protein ligase binding	-18.4
	GO:0044389	Ubiquitin-like protein ligase binding	-18.1
	GO:0019904	Protein domain-specific binding	-11.7
Purple	GO:0008134	Transcription factor binding	-13.8
	GO:0003682	Chromatin binding	-11.6
	GO:0001085	RNA polymerase II transcription factor binding	-9.8
Orange	GO:0003712	Transcription coregulator activity	-6.1
	GO:0031625	Ubiquitin protein ligase binding	-5.6
	GO:0044389	Ubiquitin-like protein ligase binding	-5.5

targets) and 64 edges. The top four key active compounds in USM were stigmasterol, mandenol, sitosterol alpha1, and isoarborinol, and their respective degrees were 26, 20, 5, and 5.

A total of 919 PDAC-related targets were identified from the GEO database. Among these, 709 were upregulated genes, and 210 were downregulated genes. A volcano plot was created to show the distribution of differentially expressed genes (Figure 3(b)), and a heat map of expression for these differential genes is shown in Figure 3(c).

3.3. Candidate Genes for Unsaponifiable Matter Treatment of PDAC. The PPI networks found that the drug targets of USM had a relationship with 1,966 targets, and 45,343 interrelationships existed among these targets. The PPI network of PDAC was found to contain 7,983 targets (nodes) and 17,6870 interrelationships (edges). The above two PPI networks were merged to reveal the specific targets of USM intervention in PDAC. This network, consisting of 1,558 nodes and 40,405 edges, is presented in Figure 4(a). According to data statistics, the median degree of all nodes was 37, which was filtered with DC > 68 to obtain Figure 4(b). The final candidate genes were screened and 139 targets, with DC > 103, BC > 156.4916701, and CC > 0.547414, were identified, as shown in Figure 4(c).

Since the roles of proteins in PPI networks are reciprocal, they are usually classified as undirected graphs. The presence of regions with high partial density in complex networks of PPI is referred to as a module. The network inside the module is the potential subnetwork of the PPI network, which has a higher density of subnetwork connections and fewer regional partial connections. Thus, the module can be considered a biologically meaningful set, which has two components. First is the protein complex, consisting of multiple proteins to form a complex, which subsequently plays a

biological role. The other is the functional module, comprising proteins located in the same pathway but with closer interactions. Therefore, to analyze the mechanism of USM in the treatment of PDAC more precisely, it was necessary to further identify its module after obtaining the core PPI network. The module was obtained by analyzing the interaction relationship through the molecular complex detection algorithm, as shown in Figure 5. Based on the Log10P value, the biological processes of the top three scores in the module were retained and functionally described, as shown in Table 1.

3.4. GO and KEGG Pathway Enrichment. Metascape platform was used to perform GO and KEGG pathway analysis of the 139 identified candidate genes. The GO results of candidate genes showed that a total of 1,762 GO terms were significantly enriched, including 1,520 in biological processes, 133 in cellular compositions, and 109 in molecular functions. KEGG results for candidate genes revealed 119 significantly enriched pathways. According to the log10 (false discovery ratio (FDR)) value ranking, the 20 genes or pathways were selected (Figure 6).

3.5. Gene-Pathway Network. The gene-pathway network was constructed based on the significant difference in KEGG pathways and genes that regulated these pathways. It included 20 pathways, 57 genes, and 253 relationships (Figure 7). From the network, it was observed that *RELA* and *NFKB1* had the largest degree (19). The other genes with large degrees were *IKBKG, JUN, MAPK1, AKT1,* and *TP53* (17, 16, 15, 12, and 10, respectively).

3.6. Molecular Docking and Molecular Dynamic Simulation Analysis of Compound-Targets. Docking calculations were performed between *JUN, MAPK1, TP53, RELA* (PDB ID:
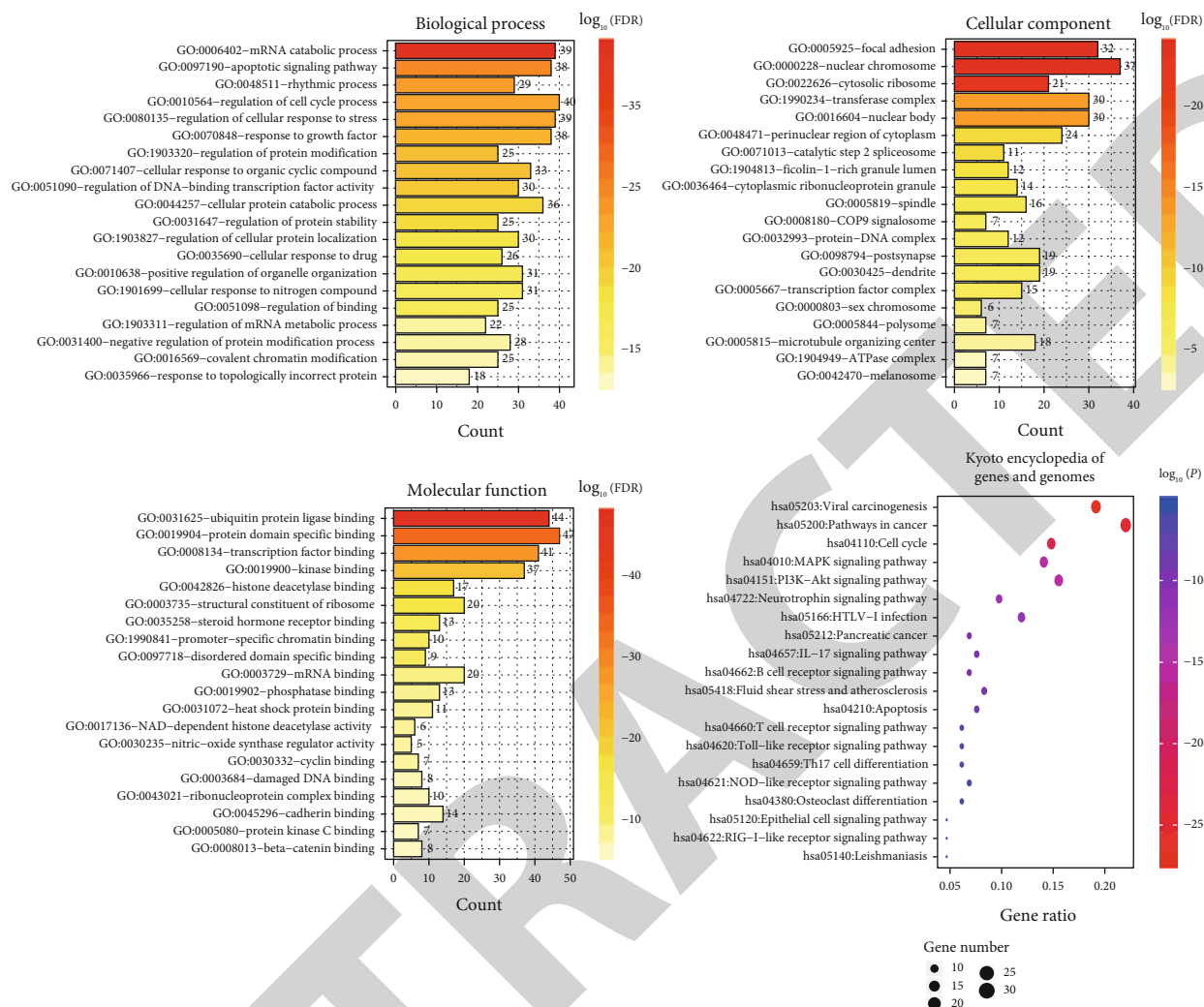
Figure 6: Gene ontology (GO) terms and KEGG pathway enrichment of candidate genes of unsaponifiable matter against pancreatic ductal adenocarcinoma. (The left side of the graph is the top GO name, the colors of the bars from orange to red represent the log10 (FDR) values (from small to large), and the longer bar represents the gene count of this GO. The size of the bubble represents the number of genes in the pathway, the colors from blue to red represent log10*P* values (from small to large), the vertical axis represents the top pathway name, and the horizontal axis represents the ratio of the overall input genes in the pathway).

5AEP, 2OJG, 5BUA, and 1VJ7) and stigmasterol, isoarborinol using AutoDock4.2 to compute the free energy of binding on protein model. Essential hydrogen atoms, Kollman united atom type charges, and solvation parameters were added with the aid of AutoDock tools. Affinity (grid) maps of $60 \times 60 \times 60$ Å grid points and 0.375 Å spacing were generated using the AutoGrid program. AutoDock parameter set and distance-dependent dielectric functions were used in the calculation of the Van der Waals and the electrostatic terms, respectively. Docking simulations were performed using the Lamarckian genetic algorithm (LGA) and the Solis and Wets local search method. The initial position, orientation, and torsions of the ligand molecules were set randomly, and all rotatable torsions were released during docking. Each docking experiment was derived from 100 different runs that were set to terminate after a maximum of 250000 energy evaluations. The population size was set to 150. During the

search, a translational step of 0.2 Å and quaternion and torsion steps of 5 was applied. Then, we used an RMSD plot during molecular dynamic simulations of core compound targets, as shown in Table 2 and Figures 8 and 9.

3.7. Diagnostic ROC Analysis of Key Targets. In predicting the outcomes of cancerous tissues and healthy tissues, the predictive ability of *RELA* and *TP53* had certain accuracy (AUC = 0.811, CI = 0.713 – 0.910; AUC = 0.723, CI = 0.607 – 0.839), the remaining 5 were low accuracy. Unlike before, the predictive ability of the 7-genes combination also had certain accuracy, and their values were higher than those of single-gene prediction (AUC = 0.892, CI = 0.820 – 0.964), which had certain clinical predictive value (Figure 10).

3.8. Survival and Prognosis Analysis of Key Target. In predicting the outcomes of survival and prognosis in PDAC,
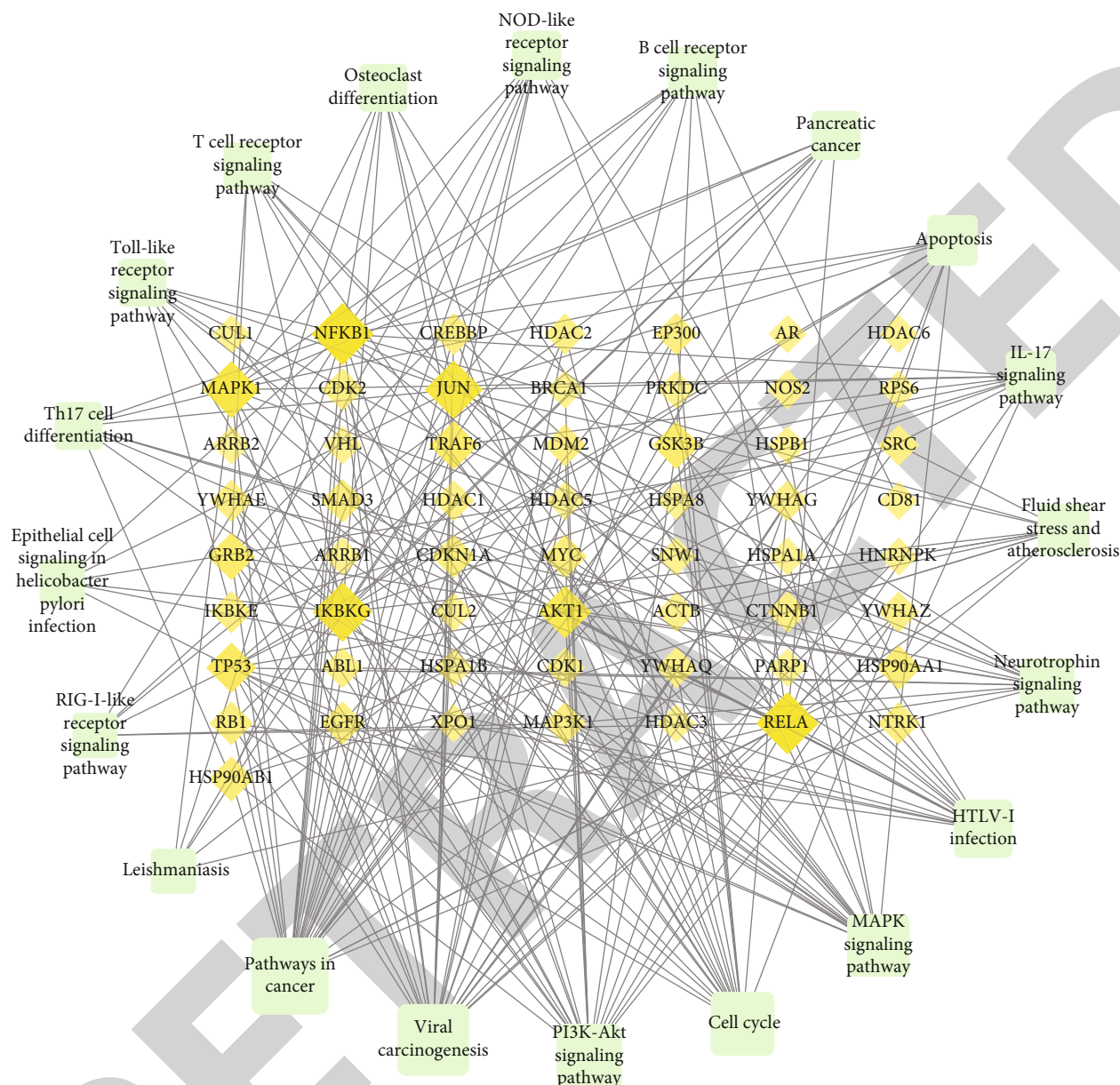
FIGURE 7: Gene-pathway network of unsaponifiable matter against pancreatic ductal adenocarcinoma. (Yellow diamonds represent target genes, light blue squares represent pathways, and a bigger size represents a larger degree).

TABLE 2: Molecular docking results of compound-target.

Number	Compounds	Targets	Binding affinity (kcal/mol)
A	Stigmasterol	JUN	-9.4
B	Stigmasterol	MAPK1	-9.3
D	Stigmasterol	RELA	-7.61
C	Stigmasterol	TP53	-6.5
E	Isoarborinol	JUN	-7.4
F	Isoarborinol	MAPK1	-7.6
H	Isoarborinol	RELA	-7.25
G	Isoarborinol	TP53	-7.2

the predictive ability of *RELA* had high accuracy (AUC = 0.926, CI = 0.897 – 0.955). In disease-specific survival and progress free interval, low expression of *RELA* has a higher predictive value than high expression of patient viability ($P = 0.027$, HR: 1.98 (1.08–3.62); $P = 0.003$, HR: 2.25 (1.32–3.81)), especially in progress free interval. However, there was no significant difference in overall survival between high and low *RELA* expression ($P = 0.087$, HR: 1.55 (0.94–2.55)), but there was a trend towards larger spacing (Figure 11).

4. Discussion

In this research, we found that USM achieved a synergistic effect through multiple compounds, targets, and pathways.

(a)

(b)

(c)

(d)

(e)

(f)
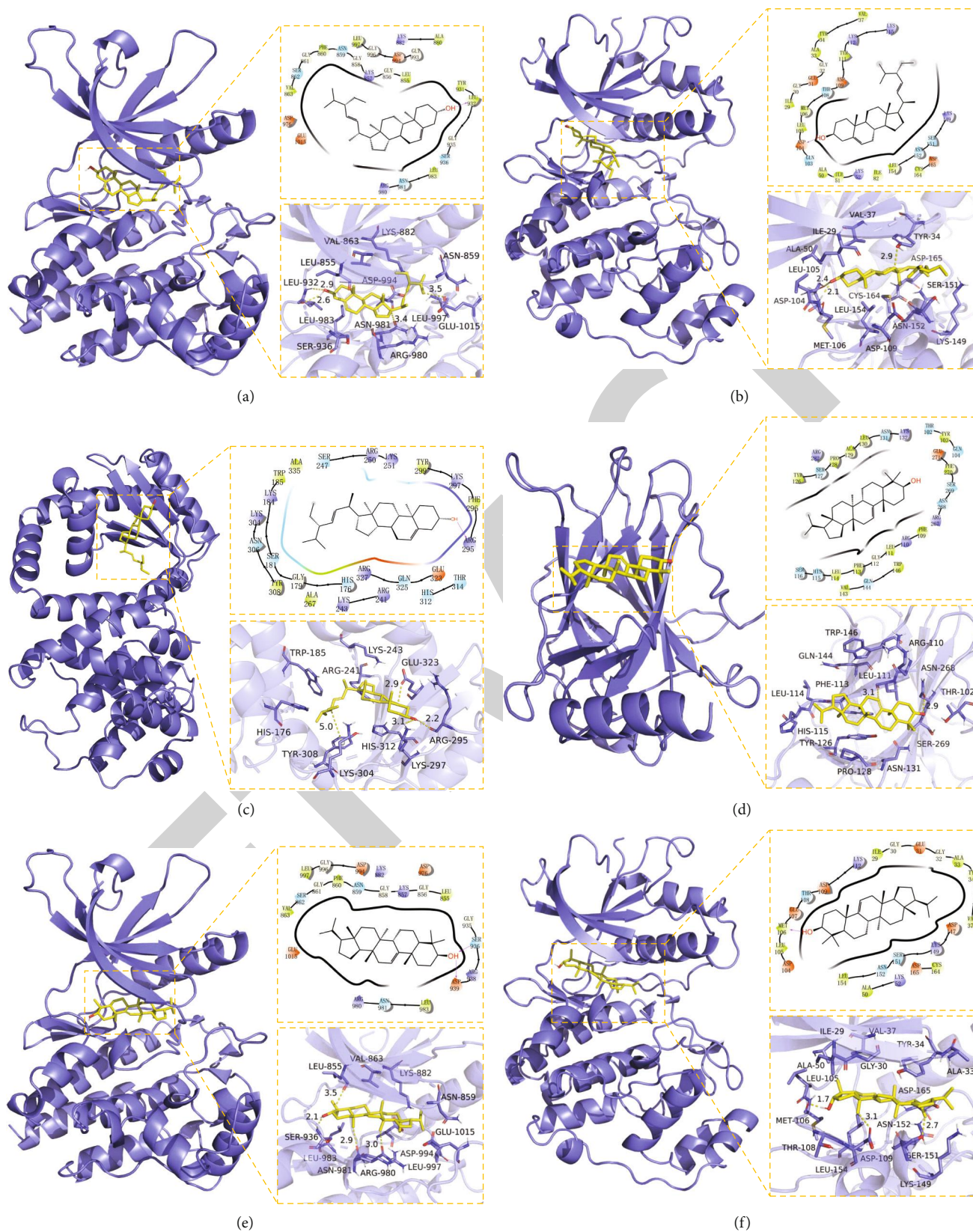
FIGURE 8: Continued.

(g)   (h)
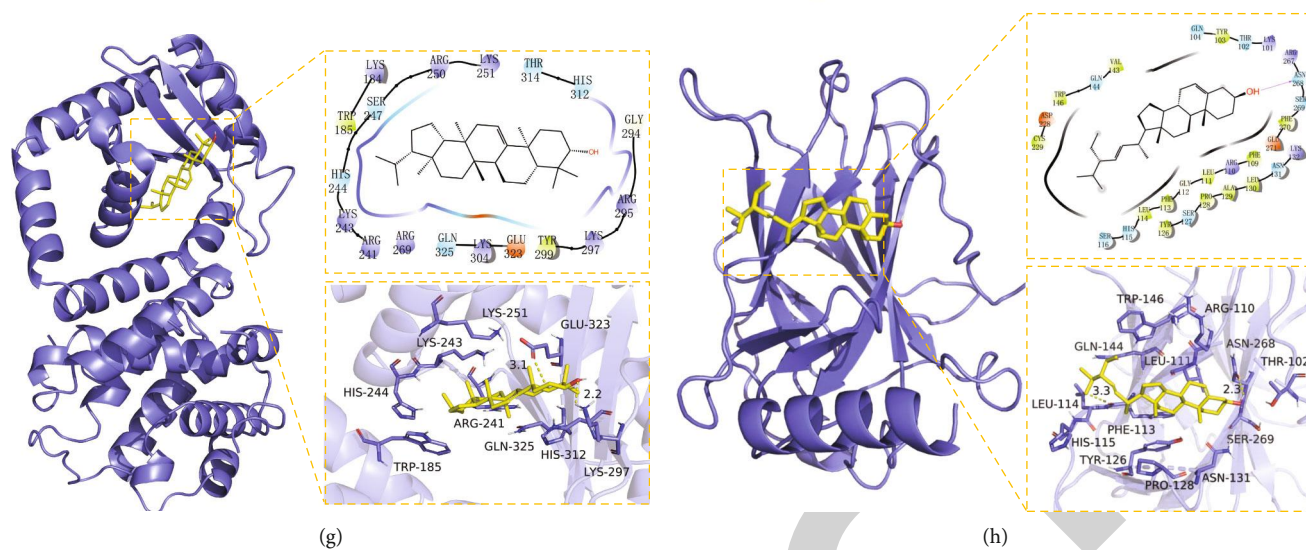
FIGURE 8: Molecular docking of compounds with targets.

Molecular docking and molecular dynamic simulations showed good affinity and stability of core compound targets. The diagnostic ROC results confirmed that *RELA* and *TP53* had some accuracy in the diagnostic prediction of PDAC, and the diagnosis of combined key gene groups had more advantages, providing a basis for screening new biomarkers. We also found that *RELA* expression differed most in cancerous tissues and healthy tissues. It has also been similarly found in survival prognosis analysis that *RELA* is significant in predicting disease-specific survival and progress-free interval and can be considered as the prognostic predictors of PDAC in the future.

4.1. Potential Active Compounds with Antitumor Effects. The top four compounds obtained from the compound-target network of USM were stigmasterol, mandenol, sitosterol α1, and isoarborinol. Stigmasterol and sitosterol α1 belong to the class of phytosterols as anticancer dietary components [25]. Stigmasterol inhibited lipopolysaccharide- (LPS-) induced innate immune responses in murine models [26], significantly reduced the transcription level of TNF-α, destroyed tumor angiogenesis, and reduced the chance of metastasis [27]. Although there is insufficient data on sitosterol α1, related subclasses such as β-sitosterol and γ-sitosterol have demonstrated obvious anticancer effects [28, 29], and the level changes of β-sitosterol can significantly distinguish PC patients from healthy controls[30]. Modern pharmacological studies have confirmed that isoarborinol can be used to improve anxiety, depression, and pain. Moreover, it has an auxiliary effect on the clinical symptoms, which are prone to occur during the development of cancer treatment [31]. In the case of mandenol, there is currently no relevant clinical or experimental research data available, which can be used as a potential antitumor compound for further study.

4.2. Potential Gene Targets with Molecular Docking, Survival, and Prognosis Analysis. From the gene-pathway network, it was found that *RELA*, *NFKB1*, *IKBKG*, *JUN*, *MAPK1*,

TP53, and *AKT1* were the genes with the highest interactions and were identified as potential gene targets for USM intervention in PDAC. The screened core targets were found to have good affinity and stability to the corresponding compounds, suggesting that the screening results have some reliability. Among these genes, *RELA*, *NFKB1*, and *IKBKG* are all components of the NF-κB signaling pathway. The NF-κB signaling pathway is one of the major signaling pathways linking cancer to inflammation. This classical pathway is activated when the cells are exposed to inflammatory cytokines, such as TNFα and IL-1, or in response to inflammatory signals, such as LPS [32]. In addition to inhibiting tumor cell proliferation and metastasis, NF-κB also interferes with inflammation [33]. Specifically, for PDAC with pancreatitis, intervention with the NF-κB signaling pathway can simultaneously result in tumor and tumor-related inflammation [34]. NF-κB also helps TNF-α to induce epithelial-mesenchymal transition (EMT) and complete angiogenesis and metastasis. Thus, KLTi could curb tumor progression by inhibiting the NF-κB signaling pathway.

RELA can promote PDAC progression by activating proliferation or migration-related gene expression. The binding of miR-302a-3p to *RELA* inhibited *RELA* expression as well as PDAC cell proliferation and migration [35]. This suggests that the overexpression of *RELA* promotes proliferation and metastasis of PDAC cells. Tumor suppression, mediated by oncogene-induced senescence (OIS), is thought to play a protective role in the development of PDAC. In the Kras-driven PDAC mouse model, Lesina et al. demonstrated that *RELA* reinforced OIS to inhibit carcinogenesis [36]. However, genetically disabling OIS can cause *RELA* to promote tumor proliferation; thus, revealing a dual role of *RELA* in PDAC carcinogenesis.

NFKB1 and *IKBKG* are part of the NF-κB signaling pathway. As a transcription factor, *NFKB1* is closely related to the risk of PDAC occurrence and prognosis [37]. Low expression of MUC4 inhibited the expression of *NFKB1*, thereby downregulating the NF-κB signaling pathway to
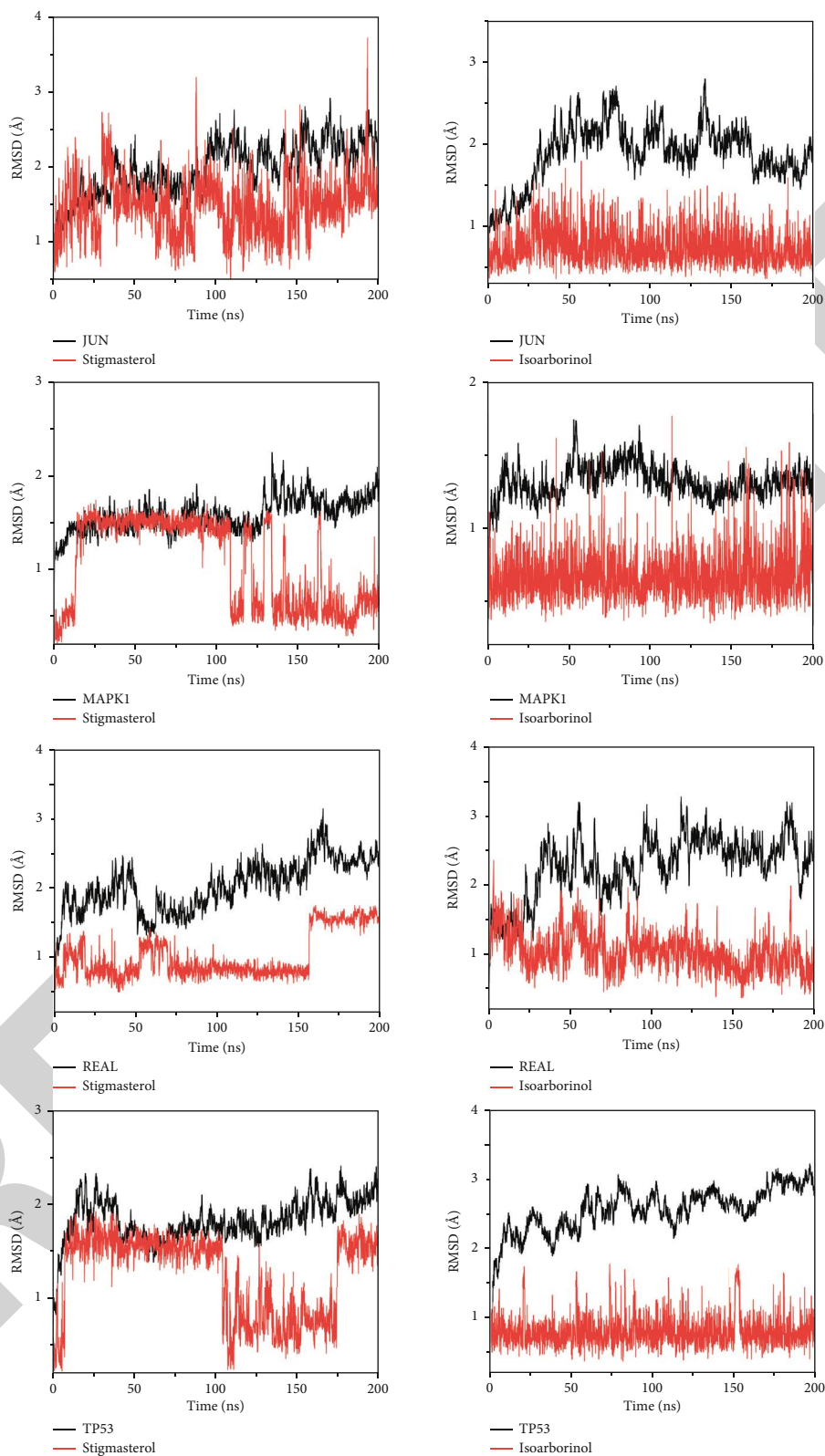
Figure 9: RMSD plot during molecular dynamic simulations of compounds with targets.

inhibit the migration and invasion of PDAC cells along the nerve [38]. The polymorphisms of *NFKB1* also significantly increase susceptibility to cancer in Asians [39], and several researchers have pointed out the important role of *NFKB1*

as an inhibitor of PDAC [40]. *IKBKG* binds and regulates IκB kinase (IKK), which inhibits NF-κB activation and increases the cleavage of PARP and Caspase 3 in the apoptotic pathway to promote apoptosis in PDAC cells. It has also
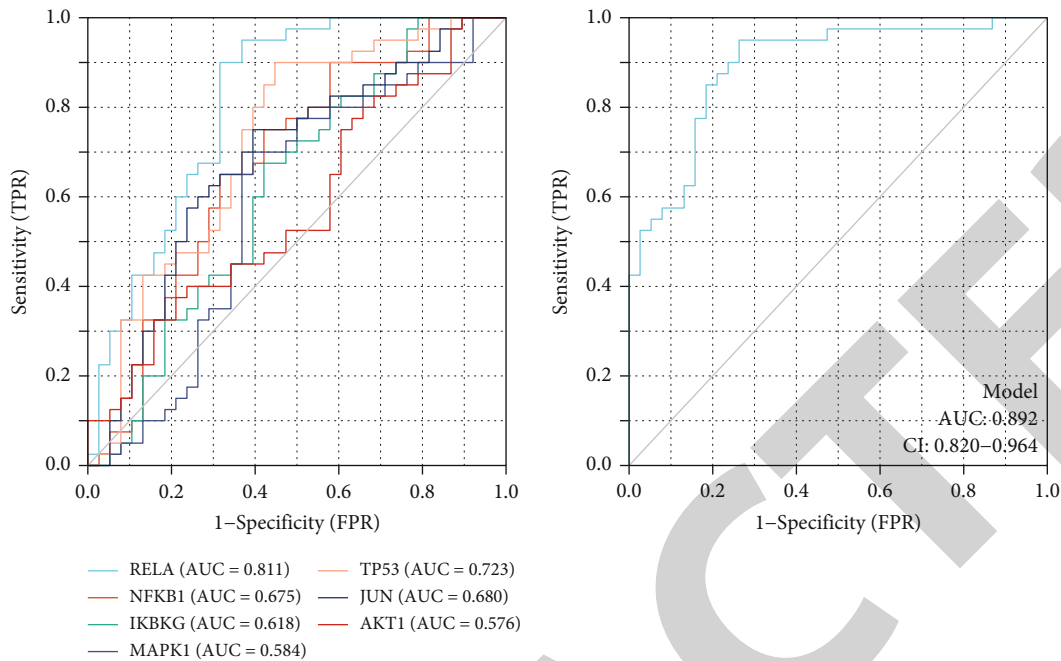
FIGURE 10: Diagnostic ROC with targets. (The area value under the ROC curve is between 0.5 and 1. The closer the AUC is to 1, the better the diagnostic effect. Low accuracy of AUC between 0.5 and 0.7, certain accuracy of AUC between 0.7 and 0.9, and high accuracy of AUC above 0.9).

been reported that regulating the activity of *IKBKG* is used to promote the sensitivity of PDAC to gemcitabine [41]. The NF-κB signaling pathway and TGF-β have a role in delaying the progression of pancreatic fibrosis [42], thereby inhibiting PDAC progression.

JUN may be involved in the growth of PDAC cells. It plays an important role in regulating the K-Ras and p38MAPKpathway by interfering with *JUN* and exerting anti-inflammatory activity and inhibiting PDAC metastasis [43]. *MAPK1* is an important regulatory factor in the MAPK signaling pathway, which greatly enhances the migration and invasion of PDAC cells for inducing EMT [44]. Therefore, inhibition of *MAPK1* expression is also a potential target for future oncological research. *AKT1* has been identified as an oncogene in a variety of cancers, including PDAC, which confirmed that activated *AKT1* accelerates the occurrence and development of PDAC and induces apoptosis of PDAC cells by inhibiting *AKT1* expression [45]. Phosphorylation of *AKT1* also increases the risk of cachexia in the PDAC population, which is strongly associated with disease prognosis [46].

TP53 mutations occur in more than 75% of PC patients, and mutated *TP53* promotes EMT and tumor cell invasion [47]. *TP53* is a driver gene that is essential for the proliferation and metastasis of PDAC, and the expression of *TP53* results in shorter disease-free survival (HR: 1.33; 95% CI, 1.02-1.75; $P = 0.04$) [48]. In addition, some studies have found that the mutation of *TP53* is closely related to the occurrence of malignant intraductal papillary mucinous neoplasm (IPMN) [49]. Therefore, silencing or inactivation of *TP53* will prevent the further development of IPMN to PDAC and improve the prognosis of patients.

For the diagnostic value of the above genes in PDAC, we found that *RELA* had the highest value, which is consistent with previous findings. And the predictive value of the combined group was much higher than that of a single gene. However, this study failed to select more effective combined predictive markers because the predictive value of *AKT1* and *JUN* in the results is low, which may reduce the predictive value of the combined group, which is the direction we need to study in the future.

Similarly, in prognostic and survival analyses, we selected *RELA*, which has the highest diagnostic value, for prediction, and excitedly, it has a high value in predicting disease-specific survival and progress-free interval, even if it is not meaningful in overall survival. However, the derivation of the above predictive markers still needs to be further confirmed by experimental or clinical studies, which is also one of the limitations of this study.

4.3. Gene Ontology Interprets the Multifaceted Nature of USM. There are many transcription factors in the gene targets of USM for the treatment of PDAC, as well as in the binding processes of enzyme, transcription factor, and receptor protein. For example, myc-associated zinc-finger protein (MAZ) is the transcription factor involved in the transcription initiation and termination. Deregulation of MAZ expression is associated with the progression of PDAC and increases the CRAF-ERK signal. It is mediated through p21-activated protein kinase and protein kinase B (AKT) signaling cascades to enhance the invasion of PDAC cells [50].

USM inhibited the proliferation and induced apoptosis in human PC xenografts through various mechanisms, such
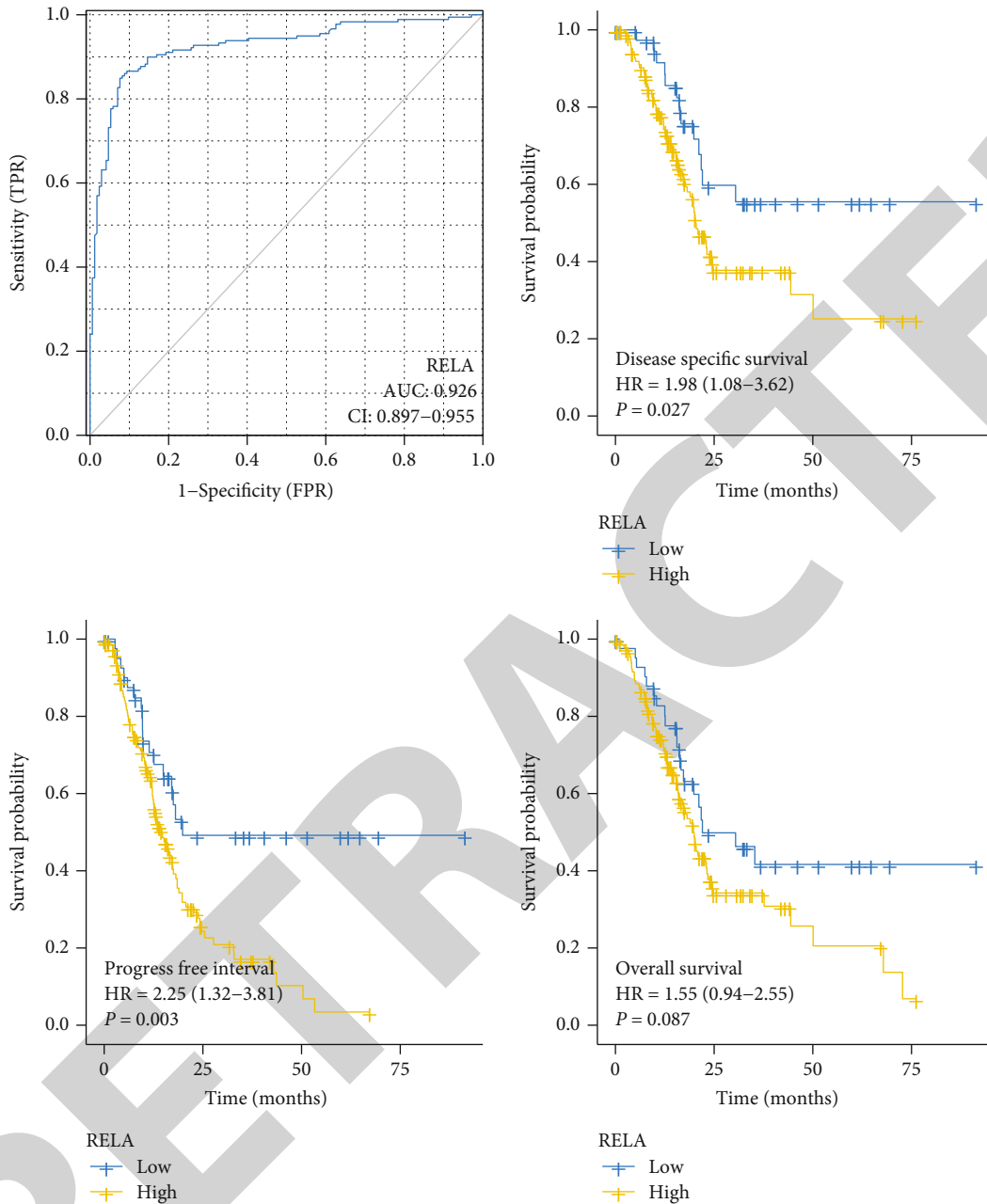
Figure 11: Survival and prognosis value of *RELA*.

as cell cycle arrest in the G2/M phase, downregulating the expression of phosphorylated Akt and mTOR, and regulating the PI3K/Akt/mTOR signaling pathway [7]. Previous studies have shown that KLTi reduces NF-κB levels in the nucleus. Additionally, it reduces the expression of IκBα, IKK, and EGFR in tumor cells and the overall cytoplasm. This corresponds to the role of KLTi at the nuclear and cytoplasmic levels [51]. Thus, the intervention of the binding of factors might have some interference effects on PDAC.

4.4. USM through Multiple Pathway Regulation for PDAC. Results from KEGG analysis showed that USM can act directly on PC, in addition to intervening in pathways that

affect tumor development. This observation indirectly illustrates the important value of KLTi in the treatment of PDAC.

It has been proven that many malignant tumors are associated with virus infection. Studies have shown a correlation between hepatitis-B virus (HBV) infection and the occurrence of PC and poor prognosis. The X protein released by HBV significantly enhances cell proliferation and migration, induces EMT, upregulates PI3K-Akt and MAPK signaling pathways, renders PDAC malignant, and promotes disease progression [52].

Regulating the cell cycle also plays a role in the development of PDAC. A variety of genes and proteins are involved

in this process. Usami et al. [53] observed that the class IIa HDACi could inhibit the activation of FOXO3, thus inhibiting the growth of PC cells. The combination of class IIa HDACi with the proteasome inhibitor carfilzomib could have a synergistic effect on the FOXO3 activation, thus, resulting in G1/S arrest in AsPC-1 cells.

Peripancreatic nerve invasion is an important oncological feature of PDAC and is closely related to disease prognosis. USM can also act on the neurotrophin signaling pathway to intervene in nerve invasion. Perineural invasion is associated with a variety of neurotrophic factors produced by neural tissue inside and outside the pancreas, which bind to specific receptors resulting in autophosphorylation and activation of multiple signaling pathways, such as MAPK PI3K-Akt and NF-κB [54]. The nerve growth factor promotes the spread of PC cells by autocrine and/or paracrine mechanisms through MAPK-mediated phosphorylation [55]. It also activates the ERK/CD133 signaling cascade, resulting in enhanced tumor cell invasion, and plays a key role in the perineural invasion of PC [56]. Studies have confirmed that regulating the NF-κB signaling pathway through activating IKK plays an important role in mediating EMT and inducing neural invasion [57].

The activation of the MAPK signaling pathway is crucial for PDAC proliferation and metastasis. This pathway is involved in the regulation of various biological activities through three major proteins, ERK1/2, p38MAPK, and MKK4 [58]. Yan et al. [59] compared the expression of p-ERK1/2 between cancerous pancreatic tissues and normal cells. They found that the expression of p-ERK1/2 in pancreatic tissues was significantly increased. In vivo and in vitro experiments confirmed that the inhibition of ERK1/2 expression reduced EMT, activated cancer-related autophagy, and decreased cell proliferation and migration in human PC cells. In another study [60], it was shown that the p38MAPK inhibitor, VCP979, could regulate the MAPK/NF-κB signaling pathway, reduce inflammation, and inhibit EMT to exert an antitumor effect. Further, MKK4 was associated with the high proliferation of tumor cells and promoted the rapid proliferation of PDAC cells.

The PI3K-Akt signaling pathway is a key pathway that promotes tumor cell proliferation, invasion, metastasis, and drug resistance. As one of the substrates of Akt, Girdin enhanced phosphorylation of Akt and induced activation. Wang et al. [61] found that Girdin showed high expression in PDAC and was involved in the regulation of tumor cell metastasis, angiogenesis, and autophagy. Silencing of the Girdin gene resulted in decreased levels of p-Akt and p-PI3K and inhibition of the PI3K-Akt signaling pathway, thereby increasing apoptosis and inducing cell cycle arrest in tumor cells. PI3K-Akt signaling pathway is closely related to the abnormal expression of lncRNA. Studies [62] have shown that the expression of lncRNA small nucleolar RNA host gene1 elevates the expression of PI3K and phosphorylated Akt, which in turn activates the PI3K-Akt signaling pathway to promote cell proliferation, inhibits apoptosis, and enhances invasion in PDAC. The expression of lncRNA AB209630 inhibited the PI3K-Akt signaling pathway in gemcitabine-resistant PDAC cells and reduced the proliferation of resistant cells to improve the sensitivity to chemotherapy [63].

It is worth noting that both MAPK and PI3K-Akt are important signaling pathways for the transduction of membrane receptor signals into cells, and there exists an interaction of receptor signals in the two pathways [64]. Ras, an upstream molecule of MAPK, can induce the activation of Akt, and p38MAPK can act between PI3K and Akt and thus play an important role in Akt phosphorylation. Similarly, the activity of PI3K has an important induction effect on the activity of the Ras/MAPK pathway, and Akt can also negatively regulate the Ras/MAPK pathway by phosphorylating Raf [65]. PI3K-Akt and NF-κB signaling pathways also have an interaction effect. Akt activates Ikk, by phosphorylation, then releases NF-κB from the cytoplasm for nuclear translocation, activates downstream gene expression, and participates in the regulation of the NF-κB pathway [66].

5. Conclusions

Through the network pharmacology, molecular docking, and database verification (GEO, TCGA, diagnostic ROC, and survival prognosis analysis), our study found that the USM in KLTi for PDAC could regulate the pancreatic cancer pathway and provide new diagnostic and predicted molecules for *RELA*, thus, providing scientific evidence for the rational application of KLTi for PDAC in clinical practice.

Data Availability

All datasets presented in this study are available from the corresponding author upon request.

Disclosure

A preprint has previously been published at Research Square (Xu et al. 2020); this version has been updated. The results shown here are in whole or part based upon data generated by the TCGA Research Network: https://www.cancer.gov/tcga.

Conflicts of Interest

The authors declare that the research was conducted in the absence of any commercial or financial relationships that could be construed as a potential conflict of interest.

Authors' Contributions

BX and WD came up with the idea and designed the study with JL. BX and WD performed the main analysis, drafted the manuscript. XZ assisted discussion and analysis. HW, LC, and SL assisted in preparing the manuscript. All authors wrote, read, and approved the final manuscript. Bowen Xu, Wenchao Dan and Xiaoxiao Zhang contributed equally to this work.

Acknowledgments

References

[1] H. Sung, J. Ferlay, R. L. Siegel et al., "Global cancer statistics 2020: GLOBOCAN estimates of incidence and mortality worldwide for 36 cancers in 185 countries," *CA: a Cancer Journal for Clinicians*, vol. 71, no. 3, pp. 209–249, 2021.

[2] L. Rahib, B. D. Smith, R. Aizenberg, A. B. Rosenzweig, J. M. Fleshman, and L. M. Matrisian, "Projecting cancer incidence and deaths to 2030: the unexpected burden of thyroid, liver, and pancreas cancers in the United States," *Cancer Research*, vol. 74, no. 11, pp. 2913–2921, 2014.

[3] A. McGuigan, P. Kelly, R. C. Turkington, C. Jones, H. G. Coleman, and R. S. McCain, "Pancreatic cancer: a review of clinical diagnosis, epidemiology, treatment and outcomes," *World Journal of Gastroenterology*, vol. 24, no. 43, pp. 4846–4861, 2018.

[4] H. X. Zhan, J. W. Xu, D. Wu et al., "Neoadjuvant therapy in pancreatic cancer: a systematic review and meta- analysis of prospective studies," *Cancer Medicine*, vol. 6, no. 6, pp. 1201–1219, 2017.

[5] X. Yang, J. Hao, C. H. Zhu et al., "Survival benefits of Western and traditional Chinese medicine treatment for patients with pancreatic cancer," *Medicine (Baltimore)*, vol. 94, no. 26, p. e1008, 2015.

[6] L. Wang, F. Wang, L. Na et al., "lncRNA AB209630 inhibits gemcitabine resistance cell proliferation by regulating PI3K/AKT signaling in pancreatic ductal adenocarcinoma," *Cancer Biomarkers*, vol. 22, no. 1, pp. 169–174, 2018.

[7] Y. Liu, W. Zhang, X. J. Wang, and S. Liu, "Antitumor effect of Kanglaite® injection in human pancreatic cancer xenografts," *BMC Complementary and Alternative Medicine*, vol. 14, no. 1, p. 228, 2014.

[8] L. S. Schwartzberg, F. P. Arena, B. J. Bienvenu et al., "A randomized, open-label, safety and exploratory efficacy study of Kanglaite injection (KLTi) plus gemcitabine versus gemcitabine in patients with advanced pancreatic cancer," *Journal of Cancer*, vol. 8, no. 10, pp. 1872–1883, 2017.

[9] J. Liu, L. Yu, and W. Ding, "Efficacy and safety of Kanglaite injection combined with radiochemotherapy in the treatment of advanced pancreatic cancer: a PRISMA-compliant meta-analysis," *Medicine (Baltimore)*, vol. 98, no. 32, article e16656, 2019.

[10] D. Zhang, W. Jiarui, S. Liu, X. Zhang, and B. Zhang, "Network meta-analysis of Chinese herbal injections combined with the chemotherapy for the treatment of pancreatic cancer," *Medicine*, vol. 96, no. 21, p. e7005, 2017.

[11] Z. M. Xiang, M. Zhu, B. L. Chen, and Y. Chen, "Identification of triacylglycerols in coix oil by high performance liquid chromatography–atmospheric pressure chemical ionization–mass spectrometry," *China Journal of Chinese Materia Medica*, vol. 30, no. 18, pp. 1436–1438, 2005.

[12] S. Li and B. Zhang, "Traditional Chinese medicine network pharmacology: theory, methodology and application," *Chinese Journal of Natural Medicines*, vol. 11, no. 2, pp. 110–120, 2013.

[13] H. Li, L. Zhao, B. Zhang et al., "A network pharmacology approach to determine active compounds and action mechanisms of ge-gen-qin-lian decoction for treatment of type 2 diabetes," *Evidence-Based Complementary and Alternative Medicine : eCAM*, vol. 2014, article 495840, 12 pages, 2014.

[14] J. Zheng, M. Wu, H. Wang et al., "Network pharmacology to unveil the biological basis of health-strengthening herbal medicine in cancer treatment," *Cancers*, vol. 10, no. 11, p. 461, 2018.

[15] B. L. Chen, M. Zhu, Y. Chen, and Y. Z. He, "Analysis of main compounds of unsaponifiable matter in coix seed oil by gas chromatography-mass spectrometric," *Chinese Patent Medicines*, vol. 31, no. 6, pp. 953-954, 2009.

[16] J. Ru, P. Li, J. Wang et al., "TCMSP: a database of systems pharmacology for drug discovery from herbal medicines," *Journal of Cheminformatics*, vol. 6, no. 1, p. 13, 2014.

[17] D. S. Wishart, Y. D. Feunang, A. C. Guo et al., "DrugBank 5.0: a major update to the DrugBank database for 2018," *Nucleic Acids Research*, vol. 46, no. D1, pp. 1074–1082, 2018.

[18] UniProt Consortium, "UniProt: the universal protein knowledgebase in 2021," *Nucleic Acids Research*, vol. 49, no. D1, pp. D480–d489, 2021.

[19] P. Shannon, A. Markiel, O. Ozier et al., "Cytoscape: a software environment for integrated models of biomolecular interaction networks," *Genome Research*, vol. 13, no. 11, pp. 2498–2504, 2003.

[20] E. Clough and T. Barrett, "The gene expression omnibus database," *Methods in Molecular Biology*, vol. 1418, pp. 93–110, 2016.

[21] Y. Tang, M. Li, J. Wang, Y. Pan, and F. X. Wu, "CytoNCA: a cytoscape plugin for centrality analysis and evaluation of protein interaction networks," *Biosystems*, vol. 127, pp. 67–72, 2015.

[22] Y. Zhou, B. Zhou, L. Pache et al., "Metascape provides a biologist-oriented resource for the analysis of systems-level datasets," *Nature Communications*, vol. 10, no. 1, p. 1523, 2019.

[23] S. K. Burley, C. Bhikadiya, C. Bi et al., "RCSB Protein Data Bank: powerful new tools for exploring 3D structures of biological macromolecules for basic and applied research and education in fundamental biology, biomedicine, biotechnology, bioengineering and energy sciences," *Nucleic Acids Research*, vol. 49, no. 1, pp. 437–451, 2021.

[24] B. L. Wang, "Network pharmacology study of anticancer mechanism of three main components in Kanglaite injection," *Journal of Modern Applied Pharmacy*, vol. 36, no. 1, pp. 58–63, 2019.

[25] E. Nattagh-Eshtivani, H. Barghchi, N. Pahlavani et al., "Biological and pharmacological effects and nutritional impact of phytosterols: a comprehensive review," *Phytotherapy Research : PTR*, vol. 36, no. 1, pp. 299–322, 2022.

[26] A. O. Antwi, D. D. Obiri, N. Osafo, A. D. Forkuo, and L. B. Essel, "Stigmasterol inhibits lipopolysaccharide-induced innate immune responses in murine models," *International Immunopharmacology*, vol. 53, pp. 105–113, 2017.

[27] T. Kangsamaksin, S. Chaithongyot, C. Wootthichairangsan, R. Hanchaina, C. Tangshewinsirikul, and J. Svasti, "Lupeol and stigmasterol suppress tumor angiogenesis and inhibit cholangiocarcinoma growth in mice via downregulation of tumor necrosis factor-α," *PLoS One*, vol. 12, no. 12, p. e0189628, 2017.

[28] Z. Q. Cao, X. X. Wang, L. Lu et al., "β-Sitosterol and gemcitabine exhibit synergistic anti-pancreatic cancer activity by modulating apoptosis and inhibiting epithelial-mesenchymal transition by deactivating Akt/GSK-3β signaling," *Frontiers in Pharmacology*, vol. 9, p. 1525, 2018.

[29] S. Sundarraj, R. Thangam, V. Sreevani et al., "γ-Sitosterol from Acacia nilotica L. induces G2/M cell cycle arrest and apoptosis through c-Myc suppression in MCF-7 and A549 cells," *Journal of Ethnopharmacology*, vol. 141, no. 3, pp. 803–809, 2012.

[30] X. Luo, J. Liu, H. Wang, and L. Haitao, "Metabolomics identified new biomarkers for the precise diagnosis of pancreatic cancer and associated tissue metastasis," *Pharmacological Research*, vol. 156, p. 104805, 2020.

[31] D. A. Luz, A. M. Pinheiro, M. L. Silva et al., "Ethnobotany, phytochemistry and neuropharmacological effects of Petiveria alliacea L. (Phytolaccaceae): a review," *Journal of Ethnopharmacology*, vol. 185, pp. 182–201, 2016.

[32] D. Kabacaoglu, D. A. Ruess, J. Ai, and H. Algul, "NF-κB/Rel transcription factors in pancreatic cancer: focusing on RelA, c-Rel, and RelB," *Cancers (Basel)*, vol. 11, no. 7, p. 937, 2019.

[33] Y. Ben-Neriah and M. Karin, "Inflammation meets cancer, with NF-κB as the matchmaker," *Nature Immunology*, vol. 12, no. 8, pp. 715–723, 2011.

[34] Y. Guo, Q. Nie, A. L. MacLean, Y. Li, J. Lei, and S. Li, "Multiscale modeling of inflammation-induced tumorigenesis reveals competing oncogenic and oncoprotective roles for inflammation," *Cancer Research*, vol. 77, no. 22, pp. 6429–6441, 2017.

[35] Z. Luo, Z. J. Yi, Z. L. Ou et al., "RELA/NEAT1/miR-302a-3p/RELA feedback loop modulates pancreatic ductal adenocarcinoma cell proliferation and migration," *Journal of Cellular Physiology*, vol. 234, no. 4, pp. 3583–3597, 2019.

[36] M. Lesina, S. M. Wormann, J. Morton et al., "RelA regulates CXCL1/CXCR2-dependent oncogene-induced senescence in murine Kras-driven pancreatic carcinogenesis," *The Journal of Clinical Investigation*, vol. 126, no. 8, pp. 2919–2932, 2016.

[37] D. Pectasides, V. Kotoula, G. Papaxoinis et al., "Expression patterns of growth and survival genes with prognostic implications in advanced pancreatic cancer," *Anticancer Research*, vol. 36, no. 12, pp. 6347–6356, 2016.

[38] L. Wang, X. Zhi, Y. Zhu et al., "MUC4-promoted neural invasion is mediated by the axon guidance factor Netrin-1 in PDAC," *Oncotarget*, vol. 6, no. 32, pp. 33805–33822, 2015.

[39] Y. Q. Luo, D. Wang, T. Gong, and J. Zhu, "An updated meta-analysis of 37 case-control studies on the association between NFKB1 -94ins/del ATTG promoter polymorphism and cancer susceptibility," *Oncotarget*, vol. 7, no. 36, pp. 58659–58670, 2016.

[40] T. Cartwright, N. D. Perkins, and C. L. Wilson, "NFKB1: a suppressor of inflammation, ageing and cancer," *The FEBS Journal*, vol. 283, no. 10, pp. 1812–1822, 2016.

[41] Z. Zhuang, H. Li, H. Lee et al., "NEMO peptide inhibits the growth of pancreatic ductal adenocarcinoma by blocking NF-κB activation," *Cancer Letters*, vol. 411, pp. 44–56, 2017.

[42] X. Ze, W. Zou, and Z. Li, "Translational research in antipancreatic fibrosis drug discovery and development," *Journal of Translational Internal Medicine*, vol. 9, no. 4, pp. 225–227, 2021.

[43] V. Tjomsland, L. Bojmar, P. Sandstrom et al., "IL-1α expression in pancreatic ductal adenocarcinoma affects the tumor cell migration and is regulated by the p38MAPK signaling pathway," *PLoS One*, vol. 8, no. 8, p. e70874, 2013.

[44] J. Hu, L. Li, H. Chen et al., "miR-361-3p regulates ERK1/2-induced EMT via DUSP2 mRNA degradation in pancreatic ductal adenocarcinoma," *Cell Death & Disease*, vol. 9, no. 8, p. 807, 2018.

[45] R. L. Xu, W. He, J. Tang et al., "Primate-specific miRNA-637 inhibited tumorigenesis in human pancreatic ductal adenocarcinoma cells by suppressing Akt1 expression," *Experimental Cell Research*, vol. 363, no. 2, pp. 310–314, 2018.

[46] A. Avan, A. Avan, T. Y. Le Large et al., "AKT1 and SELP polymorphisms predict the risk of developing cachexia in pancreatic cancer patients," *PLoS One*, vol. 9, no. 9, p. e108057, 2014.

[47] H. K. Schofield, J. Zeller, C. Espinoza et al., "Mutant p53R270H drives altered metabolism and increased invasion in pancreatic ductal adenocarcinoma," *Insight*, vol. 3, no. 2, 2018.

[48] Z. R. Qian, D. A. Rubinson, J. A. Nowak et al., "Association of alterations in main driver genes with outcomes of patients with resected pancreatic ductal adenocarcinoma," *JAMA Oncology*, vol. 4, no. 3, p. e173420, 2018.

[49] S. Takano, M. Fukasawa, M. Kadokura et al., "Next-generation sequencing revealed TP53 mutations to be malignant marker for intraductal papillary mucinous neoplasms that could be detected using pancreatic juice," *Pancreas*, vol. 46, no. 10, pp. 1281–1287, 2017.

[50] G. Maity, I. Haque, A. Ghosh et al., "The MAZ transcription factor is a downstream target of the oncoprotein Cyr61/CCN1 and promotes pancreatic cancer cell invasion via CRAF-ERK signaling," *The Journal of Biological Chemistry*, vol. 293, no. 12, pp. 4334–4349, 2018.

[51] P. Pan, Y. Wu, Z. Y. Guo, R. Wang, Y. J. Wang, and Y. F. Yuan, "Antitumor activity and immunomodulatory effects of the intraperitoneal administration of Kanglaite in vivo in Lewis lung carcinoma," *Journal of Ethnopharmacology*, vol. 143, no. 2, pp. 680–685, 2012.

[52] Y. Chen, X. Bai, Q. Zhang et al., "The hepatitis B virus X protein promotes pancreatic cancer through modulation of the PI3K/AKT signaling pathway," *Cancer Letters*, vol. 380, no. 1, pp. 98–105, 2016.

[53] M. Usami, S. Kikuchi, K. Takada et al., "FOXO3a activation by HDAC class IIa inhibition induces cell cycle arrest in pancreatic cancer cells," *Pancreas*, vol. 49, no. 1, pp. 135–142, 2020.

[54] G. Gasparini, M. Pellegatta, S. Crippa et al., "Nerves and pancreatic cancer: new insights into a dangerous relationship," *Cancers (Basel)*, vol. 11, no. 7, 2019.

[55] Z. W. Zhu, H. Friess, L. Wang et al., "Nerve growth factor exerts differential effects on the growth of human pancreatic cancer cells," *Clinical Cancer Research*, vol. 7, no. 1, pp. 105–112, 2001.

[56] B. Xin, X. He, J. Wang et al., "Nerve growth factor regulates CD133 function to promote tumor cell migration and invasion via activating ERK1/2 signaling in pancreatic cancer," *Pancreatology*, vol. 16, no. 6, pp. 1005–1014, 2016.

[57] A. Nomura, K. Majumder, B. Giri et al., "Inhibition of NF-kappa B pathway leads to deregulation of epithelial- mesenchymal transition and neural invasion in pancreatic cancer," *Laboratory Investigation*, vol. 96, no. 12, pp. 1268–1278, 2016.

[58] A. Handra-Luca, C. Lesty, P. Hammel et al., "Biological and prognostic relevance of mitogen-activated protein kinases in pancreatic adenocarcinoma," *Pancreas*, vol. 41, no. 3, pp. 416–421, 2012.

[59] Z. Yan, K. Ohuchida, S. Fei et al., "Inhibition of ERK1/2 in cancer-associated pancreatic stellate cells suppresses cancer-stromal interaction and metastasis," *Journal of Experimental & Clinical Cancer Research*, vol. 38, no. 1, p. 221, 2019.

[60] T. Xu, J. Ding, H. Ge et al., "Effects of VCP979 novel p38 mitogen activated protein kinase inhibitor on progression of pancreatic cancer in mouse model with diabetic conditions," *Journal of Biomedical Nanotechnology*, vol. 15, no. 6, pp. 1325–1333, 2019.

Hindawi

Research Article

6′-O-Galloylpaeoniflorin Exerts Inhibitory Bioactivities in Human Neuroblastoma Cells via Modulating AMPK/miR-489/XIAP Pathway

Lijun Zhou (ID)**, Aiwu Li** (ID)**, and Qiangye Zhang** (ID)

Department of Pediatric Surgery, Qilu Hospital of Shandong University, Jinan 250012, China

Correspondence should be addressed to Aiwu Li; liaiwu@qiluhospital.com and Qiangye Zhang; zhangqiangye@qiluhospital.com

Although therapies against neuroblastoma (NBM) have advanced, the patients still suffer from poor prognoses due to distal metastasis or the occurrence of multidrug resistance. Accumulating evidence has proved that chemicals derived from natural products possess potent anti-NBM properties or can be used as adjuvants for chemotherapy. In the present study, we demonstrated that 6′-O-galloylpaeoniflorin (GPF), a galloylated derivative of paeoniflorin isolated from the roots of *Paeonia lactiflora Pall*, exerted significant inhibitory effects on proliferation and invasion of SH-SY5Y cells (an NBM cell line) and enhanced the sensitivity of SH-SY5Y cells to cisplatin in vitro. Further studies showed that GPF treatment upregulated miR-489 in NBM cells via activating AMP-activated protein kinase (AMPK). We also demonstrated that similar to GPF treatment, miR-489 exhibited a significant anti-NBM capacity. Further studies showed that miR-489 directly targeted the X-linked inhibitor of apoptosis protein (XIAP). Overall, our results indicated that GPF possessed an evident anti-NBM capacity dependent on AMPK/miR-489/XIAP pathway, providing an emerging strategy for clinical treatment of NBM.

1. Introduction

As one of the most frequent malignancies in infants and young children, neuroblastoma (NBM) accounts for about 15% of cancer-related mortality in the pediatric population [1]. Therapeutic approaches for NBM include surgery, chemotherapy, radiotherapy, and/or stem cell transplantation [2]. Unfortunately, although modest improvements have yielded in the prognosis of NBM patients with common treatments, the median overall survival (OS) in drug-resistant NBM remains poor [3]. Recently, more and more attention has been paid to the precise molecular regulatory mechanisms in the tumorigenesis of NBM, aiming at developing novel effective diagnostic and therapeutic strategies [4–6].

Since ancient times, natural compounds have been applied to cure disorders [7]. Accumulating evidence has proved the efficiency of natural compound-based strategies in the treatment of human diseases, such as asthma [8, 9], infection [10], diabetes mellitus, neurological disease [11,

12], and various types of tumors [13, 14]. These compounds present as chemotherapeutic agents independently and can be used as adjuvants for chemotherapy or radiotherapy [13]. For example, isatin has been reported to arrest the proliferation and promote apoptosis in NBM cell line SH-SY5Y cells [15]. Gallic acid, epigallocatechin-3-gallate, and curcumin enhance cisplatin-induced apoptosis in non-small-cell lung cancer (NSCLC) cells via activating proapoptotic signaling and antagonism of the antiapoptotic proteins [16–18]. Oleanolic acid, as well as ursolic acid and micheliolide, enhance the radiosensitivity of NSCLC cells via accelerating the degradation of HIF-1α [19–21]. Therefore, natural compounds are expected to become potential anti-NBM chemicals [22].

As a family of endogenous short RNAs (18-25 nt), microRNAs (miRNAs) regulate the expressions of their cellular targets through binding to the 3′-untranslated region (3′-UTR) of mRNA [23, 24]. Studies have identified that miRNAs are implicated in regulating over 60% of human coding genes [25]. miRNAs function extensively in a wide
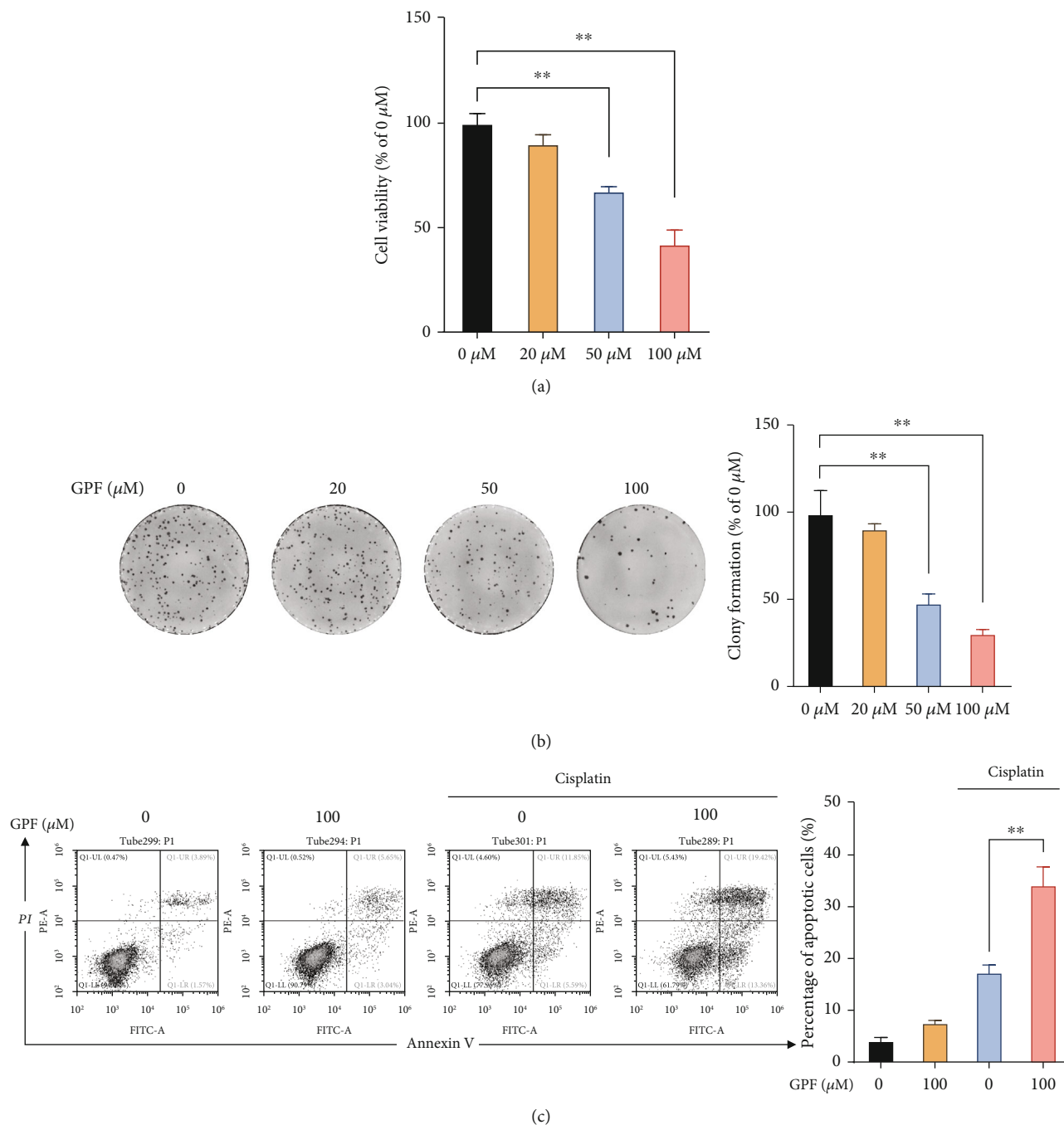
Figure 1: GPF treatment inhibits the proliferation and survival of NBM cells. SH-SY5Y cells were treated with indicated doses of GPF. (a) At 24 h posttreatment, the CCK-8 assay was conducted to evaluate the proliferation of SH-SY5Y cells. (b) At 10 days post-GPF treatment, SH-SY5Y cells were stained with crystal violet, and the number of cell colonies was calculated. (c) At 24 h after treatment, SH-SY5Y cells were treated with cisplatin (5 μM) or the vehicle for another 24 h, followed by apoptosis assay. p values: $^*p < 0.05$; $^{**}p < 0.01$ (versus the control group without any treatment).

range of cellular biological and pathophysiological processes, such as embryonic development [26], differentiation [27], inflammation [28], and carcinogenesis [29]. In addition, accumulating evidence has emphasized the critical role of miRNAs in various malignant neoplasms, including NBM [6]. Intriguingly, some natural compounds have been demonstrated to exert their pharmacological effects by regulating the expressions of miRNAs [30]. For instance, osthole inhibits the expression of miRNA-22-3p in pulmonary artery smooth muscle cells, restoring the dysregulated lipid metabolism, which alleviates pulmonary vascular remodeling in pulmonary arterial hypertension [31]. 6′-O-Galloylpaeoniflorin

(a)

(b)

(c)
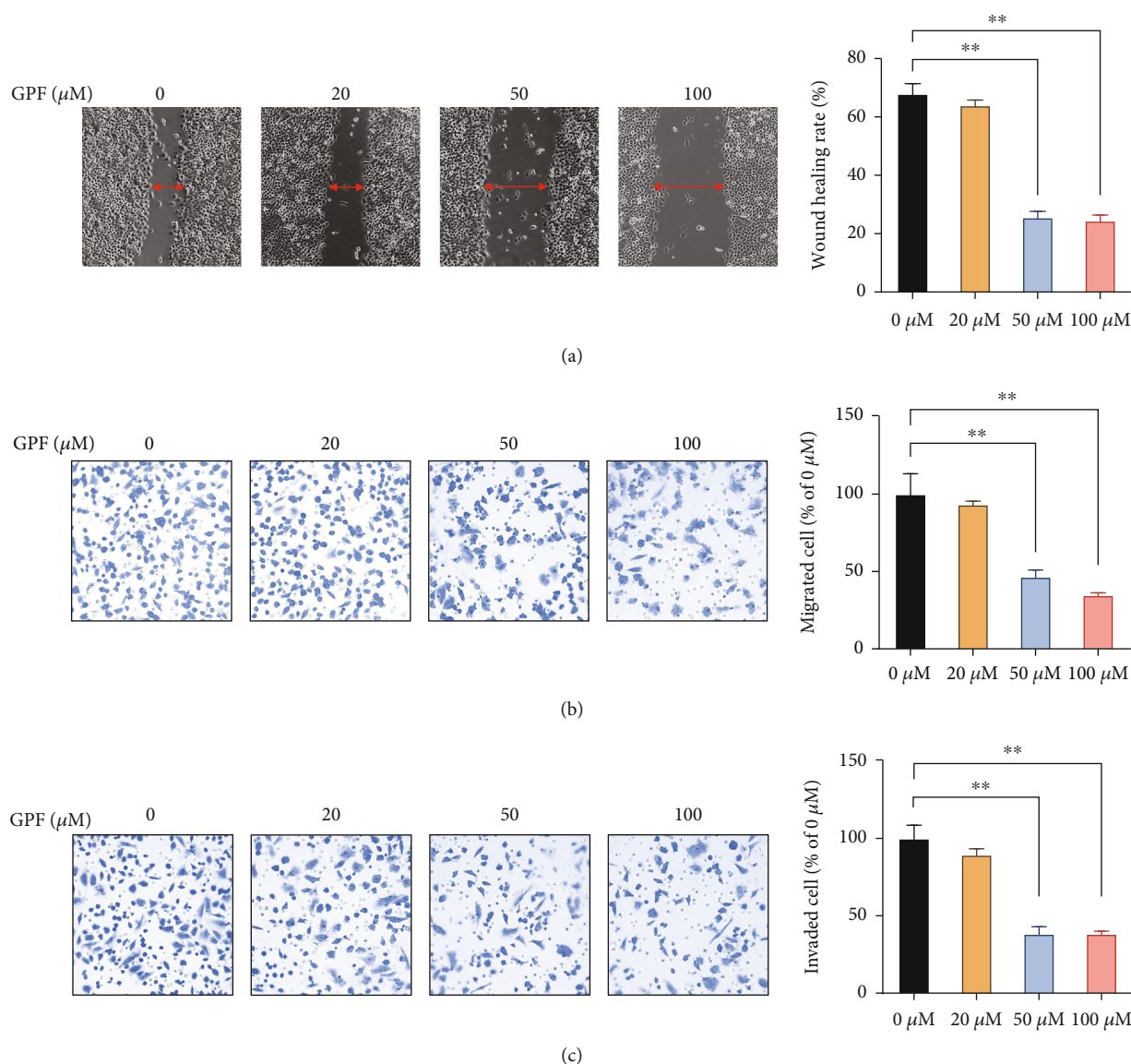
FIGURE 2: GPF treatment inhibits the migratory and invasive ability of NBM cells. SH-SY5Y cells were treated with the indicated concentrations of GPF for 24 h. (a) The migratory ability of SH-SY5Y cells was evaluated by a cell scratch test. The migratory and invasive abilities of SH-SY5Y cells were evaluated by transwell migration (b) and invasion (c) assays. $^*p < 0.05$; $^{**}p < 0.01$.

(GPF) is a galloylated derivative of paeoniflorin isolated from the roots of *Paeonia lactiflora Pall*, which possesses therapeutic effects in treating cerebral infarct [11], osteoporosis [32], and lung cancer [33]. GPF can upregulate miR-299-5p via activating the AMP-activated protein kinase (AMPK) pathway and downregulate ATF2, resulting in the suppressed proliferation and invasion in NSCLC cell lines, A549, and H1299 cells [33]. However, whether GPF possesses an anti-NBM capacity remains largely unexplored.

Based on the abovementioned evidence, we aimed to clarify the role of GPF in treating NBM in the present study. Our findings showed that GPF treatment remarkably restrained the proliferation and invasion of NBM cell line SH-SY5Y cells and enhanced the chemosensitivities of SH-SY5Y cells to cisplatin. The results also demonstrated that the expression of a tumor-suppressive miRNA, miR-489,

was increased in response to treatment of GPF, which was primed by AMPK activation. Further studies identified that the agonism of miR-489 could reduce proliferation and enhance cisplatin-induced apoptosis in NBM cells. Additionally, we revealed that the X-linked inhibitor of apoptosis protein (XIAP), a critical oncogene, was a cellular target of miR-489 in SH-SY5Y cells. Collectively, our findings provided valuable insights into the pharmacological effects of GPF, highlighting its therapeutic potential in the treatment of NBM by regulating the expression of XIAP.

2. Materials and Methods

2.1. Cell Culture. The human NBM cell line SH-SY5Y was kindly gifted by Dr. Hao at Jilin University. Cells were maintained in Dulbecco's Modified Eagle Medium (DMEM, Gibco)

(a)

(b)

(c)
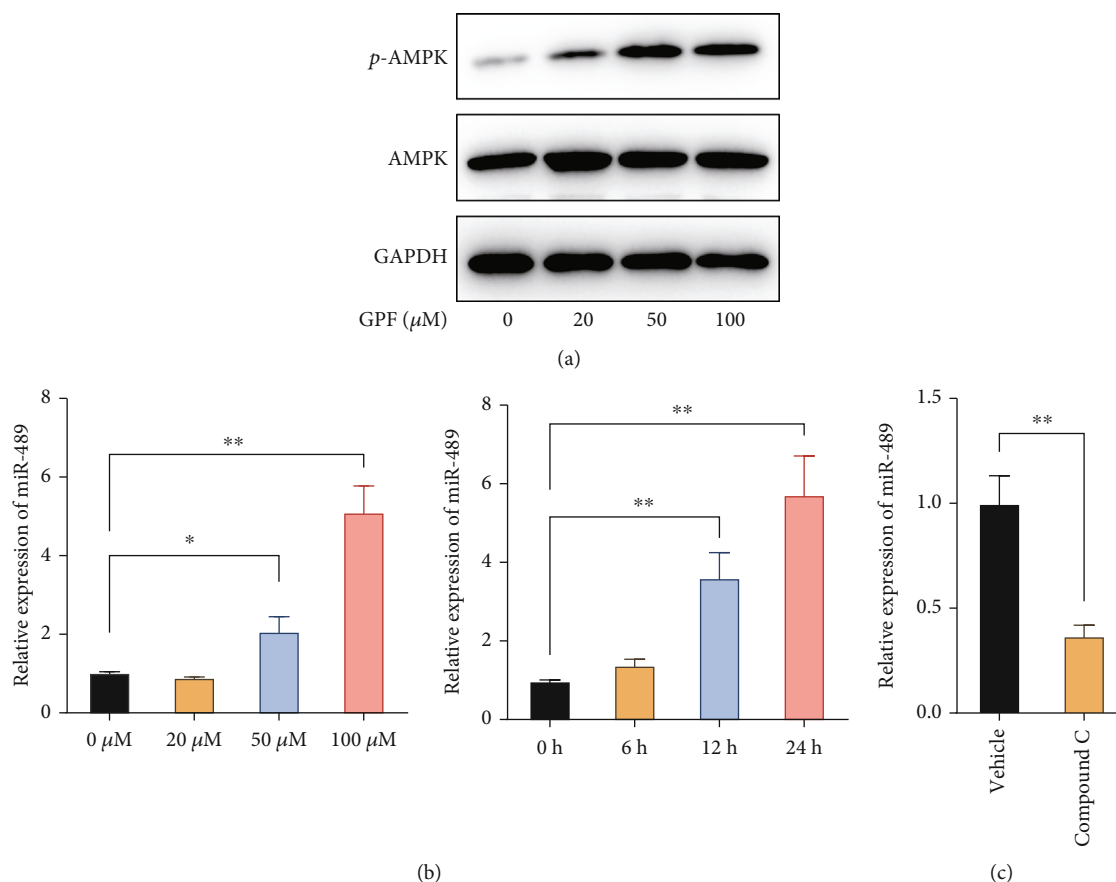
Figure 3: GPF treatment increases the expression of miR-489 in NBM cells. (a) SH-SY5Y cells were treated with the indicated concentrations of GPF. At 6 h after GFP treatment, phosphorylated AMPK in cells was detected by immunoblotting. (b) SH-SY5Y cells were treated with the indicated concentrations of GPF for 24 h or 100 μM GPF for different durations. The expression of miR-489 was determined by qPCR. (c) After pretreatment with or without compound C for 6 h, SH-SY5Y cells were exposed to GPF treatment for another 18 h, and the expression of miR-489 was determined by qPCR. $^*p < 0.05$; $^{**}p < 0.01$.

supplemented with 10% fetal bovine serum (FBS, Sigma) at 37°C in a humidified atmosphere containing 5% CO_2.

2.2. miRNA Transfection. The miR-489 and negative control were purchased from RiboBio Co. (Guangzhou, China) and transfected into SH-SY5Y cells as previously described [34]. Briefly, digested cells were prepared as a single-cell suspension and then plated at appropriate densities. When a confluence of 80% was achieved, miR-489 or the negative miRNA was added to each well at a final concentration of 50 nM.

2.3. Cell Proliferation Test. Cell Counting Kit-8 (CCK-8; Sigma-Aldrich) assay was performed to assess the proliferation rate of SH-SY5Y cells in vitro. Briefly, after transfection with miR-489 or scramble control, cells (3×10^3 cells/mL) were seeded into 96-well plates. After 24, 48, and 72 h of incubation, 10 μL CCK-8 solution was added to each well, followed by incubation for another 90 min. The OD at a wavelength of 450 nm was determined using a BioTek Synergy H1 microplate reader.

2.4. Colony Formation Assay. The colony formation assay was performed to evaluate the cell survival in vitro as previ-

ously described [34]. Briefly, SH-SY5Y cells were seeded into 6-well plates (300 cells/well) and cultured at 37°C in a humidified atmosphere containing 5% CO_2 for 10 days. Subsequently, the culture medium was discarded, and 0.1% crystal violet (Beyotime, Haimen, China) was used to stain the cells. Colonies of greater than 64 cells were counted.

2.5. Cell Apoptosis Assay. Cell apoptosis was assessed using an Annexin V/propidium iodide (PI) kit (Beyotime, Haimen, China) according to the manufacturer's instructions. After miR-489 or the scramble miRNA transfection, SH-SY5Y cells were digested using 0.25% Trypsin (Invitrogen) and washed three times. Subsequently, the cells were resuspended in provided staining buffer, followed by incubation with Annexin V for about 1 h. Then, the cells were incubated with PI for another 5 min. The proportion of apoptotic cells was determined by flow cytometry (Beckman CytoFLEX).

2.6. Cell Scratch Assay. Cell scratch assay was conducted to determine the migratory ability of SH-SY5Y cells as previously described [35]. Briefly, cells were prepared as a single-cell suspension and then seeded into 6-well plates. When a confluence of approximately 80% was achieved, the cell monolayer was scratched to create a "wound." Next,

(a)

(b)

(c)
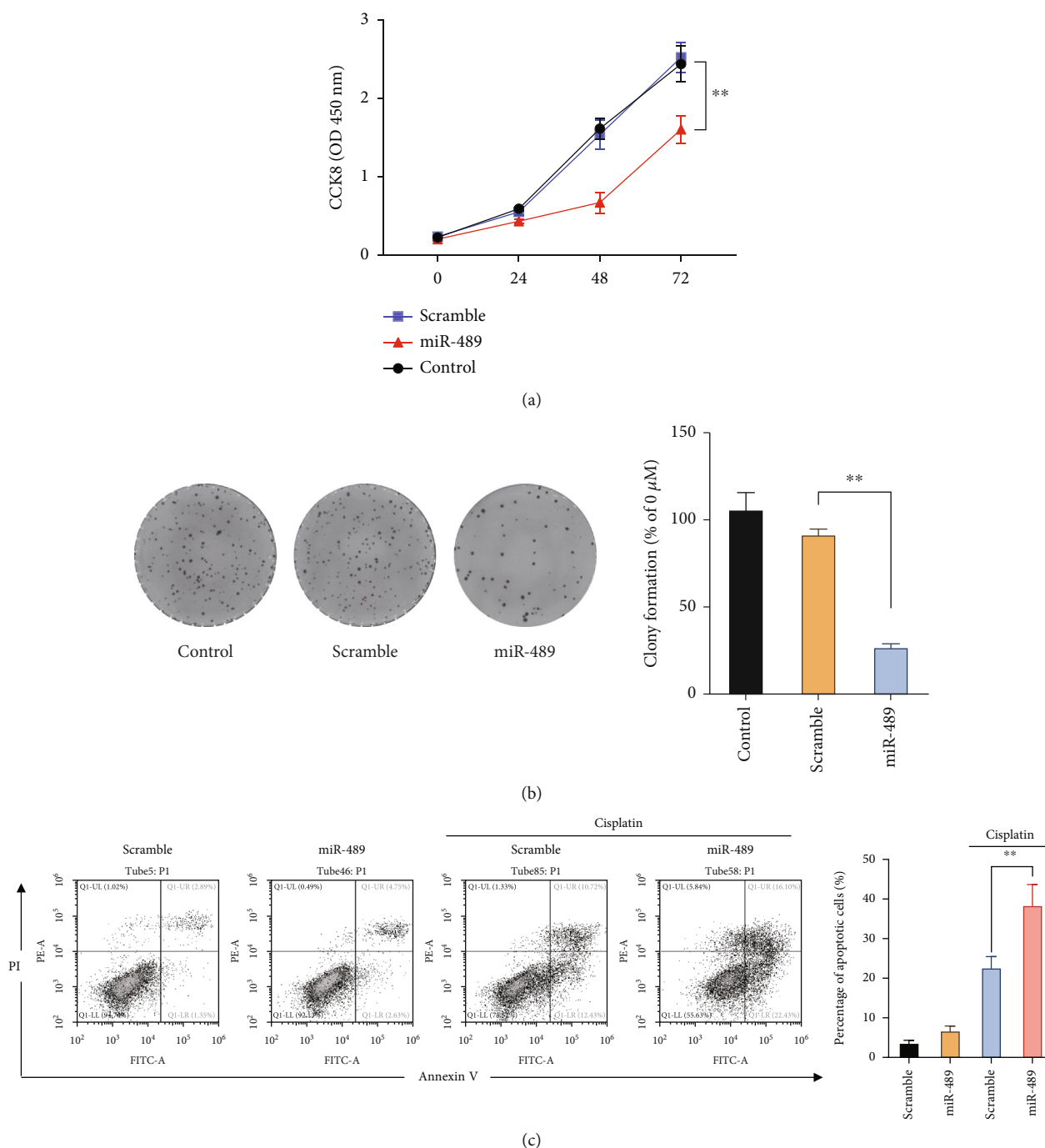
FIGURE 4: Transfection with miR-489 inhibits the proliferation and survival of NBM cells. Either miR-489 or scramble miRNA was transfected into SH-SY5Y cells. (a) At 24 h, 48 h, and 72 h post-miR-489 transfection, the CCK-8 assay was conducted to evaluate SH-SY5Y proliferation. (b) At 10 days post-GPF treatment, SH-SY5Y cells were stained with crystal violet, and the number of cell colonies was calculated. (c) At 48 h after transfection, SH-SY5Y cells were treated with cisplatin ($5\,\mu$M) or the vehicle for another 24 h, followed by an apoptosis assay. $^{*}p < 0.05$, $^{**}p < 0.01$.

the cells were cultured with a culture medium supplemented with 1% FBS at 37°C in a humidified atmosphere containing 5% CO_2 for 2 and 24 h. Subsequently, the width of the wound was examined using an inverted microscope (Olympus).

2.7. Transwell Assay. A transwell assay was conducted to evaluate the migratory capacity of SH-SY5Y cells as previ-

ously reported [36]. Briefly, cells were seeded into a Millicell cell culture insert (Millipore) containing $100\,\mu$L serum-free medium at a density of 10^5 cells/mL. Then, the insert was added to a 24-well plate containing $100\,\mu$L DMEM (10% FBS) in each well. Then, the plate was incubated at 37°C. After 1 day, the medium was discarded, and the membrane of the chamber was removed, followed by staining using

(a)

(b)

(c)
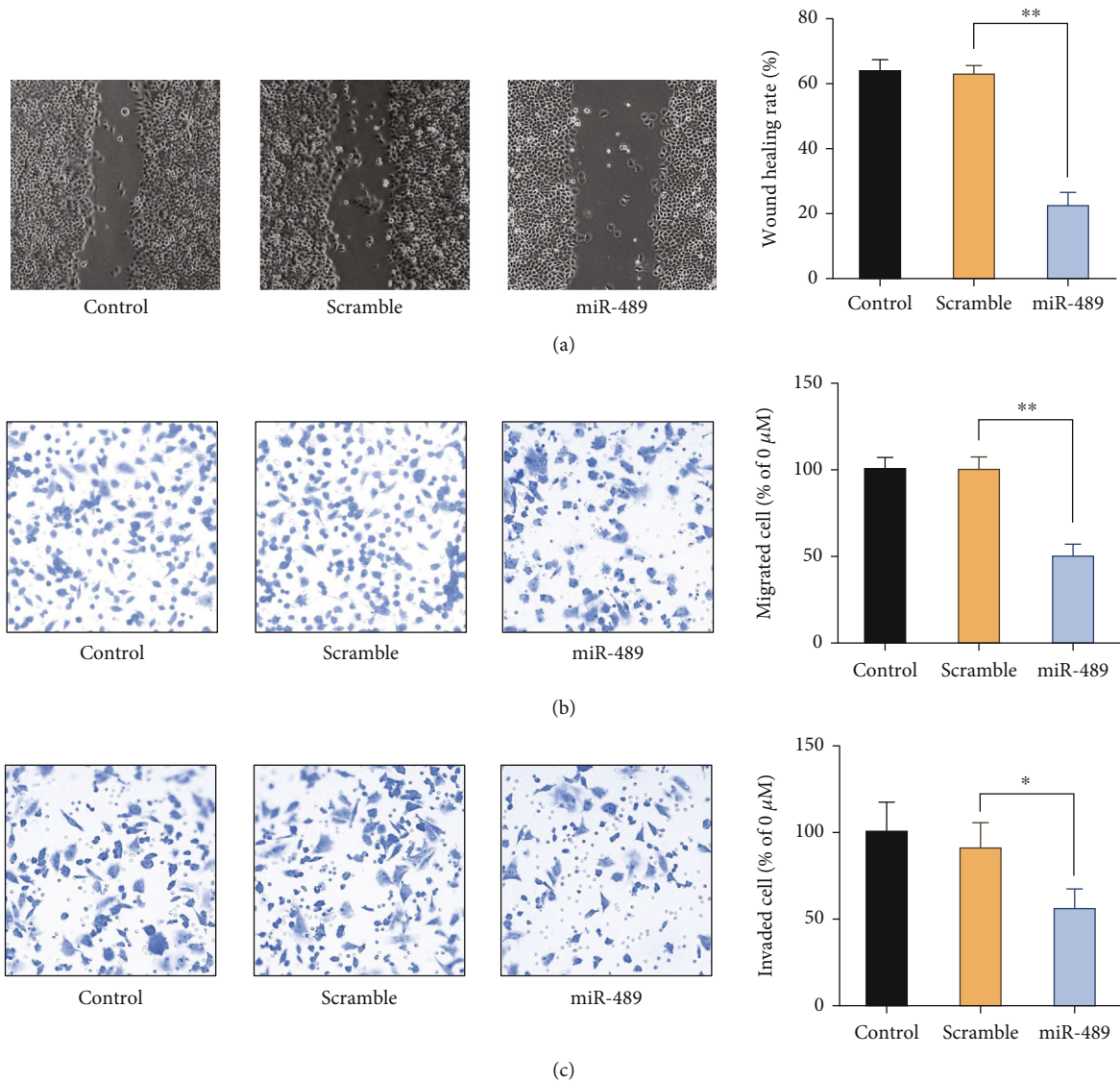
FIGURE 5: miR-489 inhibits the migratory and invasive ability of NBM cells. Either miR-489 or scramble miRNA was transfected into SH-SY5Y cells. (a) The migratory ability of SH-SY5Y cells was evaluated by a cell scratch test. The migratory and invasive abilities of SH-SY5Y cells were evaluated by transwell migration (b) and invasion (c) assays. $^*p < 0.05$; $^{**}p < 0.01$.

0.5% crystal violet solution. The migrated cells were photographed using an Olympus MX40 inverted microscope and quantified by counting six randomly selected fields. To assess the cell invasive ability, the bottom of the cell culture insert was coated with Matrigel (Corning) prior to the migration assay.

2.8. Quantitative PCR (qPCR). Total RNA was extracted from SH-SY5Y cells using Biomarker total RNA isolation kit. Purified RNA was reversely transcribed to cDNA with MonScript™ RTIII Super Mix with dsDNase (Monald, Wuhan, China) according to the manufacturer's instructions. qPCR assay was performed to determine the expressions of mRNAs and miRNAs using MonAmp™ Fast SYBR® Green qPCR Mix (Monald) on a Bio-Rad CFX Connect PCR System. The primers of XIAP and housekeeping gene GAPDH were listed as follows:

XIAP-forward: $5'$-AAGAGAAGATGACTTTTAACAG-$3'$, XIAP-reverse: $5'$-TGCTGAGTCTCCATATTGCC-$3'$; GAPDH-forward: $5'$-GCGAGATCGCACTCATCATCT-$3'$, GAPDH-reverse: $5'$-TCAGTGGTGGACCTGACC-$3'$.

The relative expressions of the target mRNA and miRNA were calculated using the $2^{-\Delta\Delta Ct}$ method [37].

2.9. Immunoblotting Analysis. Total protein was isolated from SH-SY5Y cells using Tris-NaCl buffer (50 mM Tris, 150 mM NaCl) containing 1% Triton. The expression of XIAP at the protein level was semiquantitated by the Western blotting analysis as previously described [38]. Briefly, equal amounts of proteins were subjected to sodium dodecyl sulfate-polyacrylamide gel electrophoresis (SDS-PAGE) on 10% gels and then electrotransferred onto the polyvinylidene difluoride membranes. The blots were blocked in PBS

(a)

(b)

(c)

(d)
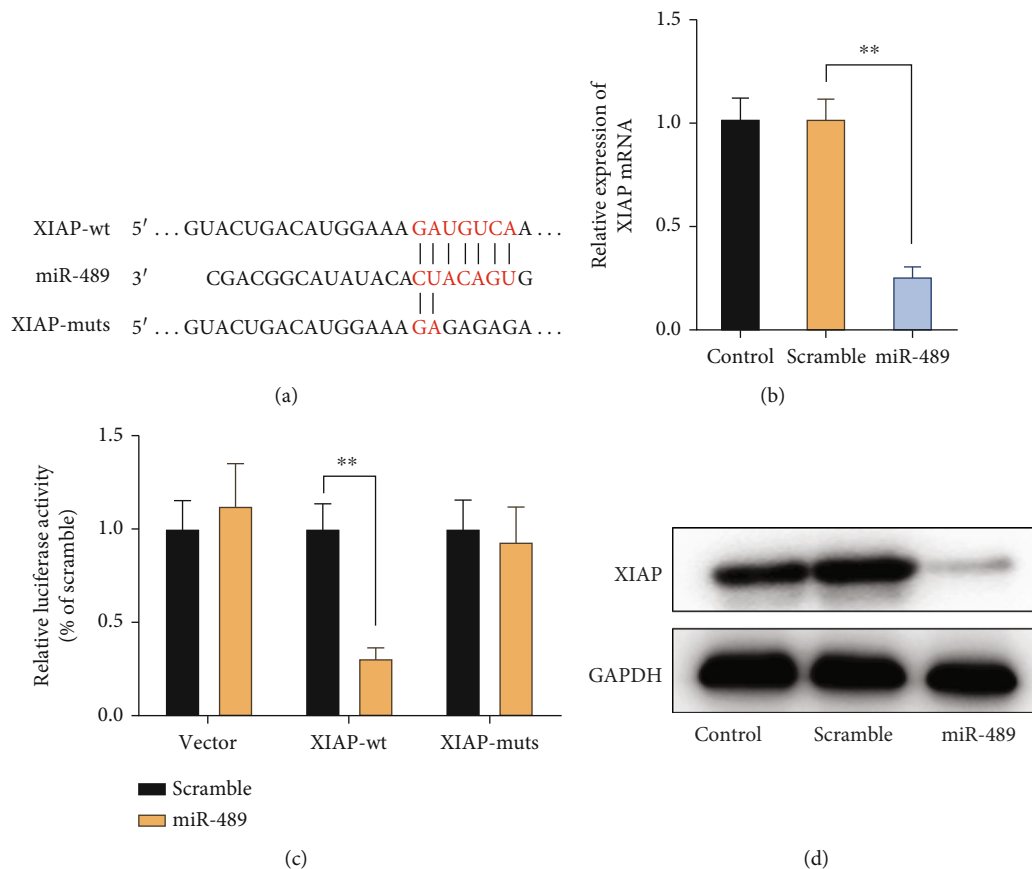
FIGURE 6: miR-489 targets XIAP 3′UTR. (a) The binding site of miR-489 and its mutants within the XIAP mRNA 3′UTR were shown. (b) miR-489 or scramble miRNA was cotransfected into NBM cells with pMIR-REPORT (vector), recombinant pMIR-REPORT expressing 3′UTR-wt, or the mutants, respectively. The luciferase activity in cells was determined at 48 h after transfection. Either miR-489 or scramble miRNA was transfected into SH-SY5Y cells. The expression of XIAP at the mRNA (c) and protein (d) levels was determined at 48 h after transfection by qPCR and immunoblotting, respectively. $^*p < 0.05$; $^{**}p < 0.01$.

containing Tween-20 (PBST) supplemented with 1% bovine serum albumin, followed by incubation with primary antibodies against α-XIAP (Abcam, ab229050, 1 : 3,000) and α-GAPDH (Abcam, ab8245, 1 : 5,000) overnight at 4℃. Subsequently, the blots were washed with PBST and incubated with horseradish peroxidase-labeled secondary antibodies (1 : 5,000) at room temperature for 2 h. The immunoreactive bands were visualized using the Bio-Rad ChemiDoc Touch System.

2.10. Luciferase Assay. Luciferase assay was conducted to validate the interaction between miR-489 and 3′UTR of XIAP as previously reported [39]. Briefly, the 3′UTR of XIAP was cloned into the pmirGLO vector, termed XIAP 3′UTR-wt. Mutation in the predicted miR-489 binding site was introduced using the Quikchange kit (Agilent, cat.# 600670), which was set as a negative control (XIAP 3′UTR-mut). Either miR-489 or the scramble control was cotransfected with the reporter plasmids (Invitrogen) into SH-SY5Y cells. After 48 h of transfection, the cell luciferase activity was determined using a BioTek Synergy H1 microplate reader.

2.11. Statistical Analysis. Statistical analysis was performed using GraphPad Prism 8.0. A $p < 0.05$ was considered statistically different.

3. Results

3.1. GPF Treatment Inhibits Proliferation and Restores Chemosensitivity in SH-SY5Y Cells. The pharmacological effects of GPF on the proliferation of NBM were determined using a CCK-8 assay. The results indicated that GPF treatment dose-dependently decreased the proliferation of SH-SY5Y cells in vitro (Figure 1(a)). Consistently, the colony formation assay showed that GPF treatment dose-dependently inhibited the colony formation of SH-SY5Y cells (Figure 1(b)). To determine the effects of GPF on chemosensitivity in NBM, SH-SY5Y cells stimulated with or without GPF were subjected to cisplatin treatment, and then the proportion of apoptotic SH-SY5Y cells was determined by Annexin V-FITC/PI staining. Fewer apoptotic cells were detected in untreated or GPF-treated cells, whereas about 17% of apoptotic cells were detected in the cisplatin treatment (Figure 1(c)). Intriguingly, as shown in Figure 1(c), pretreatment with GPF significantly enhanced
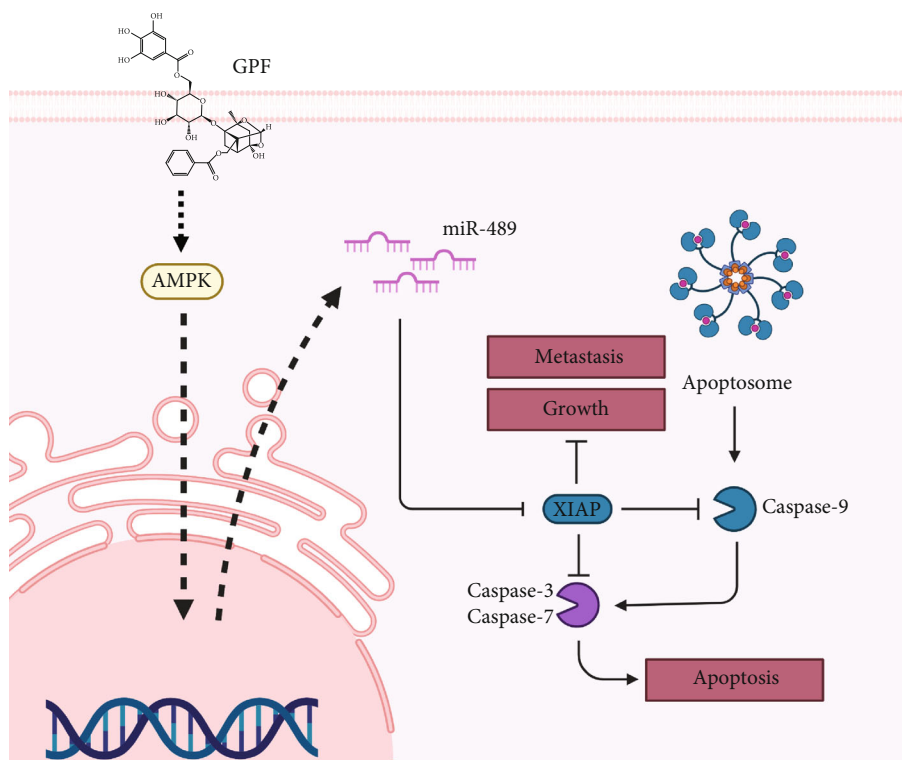
Figure 7: Schematic diagram depicting the anti-NBM effects of GPF.

the cisplatin-induced apoptosis. These results indicated that GPF exerted antiproliferation and proapoptotic capacity in NBM cells.

3.2. Treatment with GPF Restrains the Migratory and Invasive Ability of SH-SY5Y Cells.

The pharmacological effects of GPF treatment on the migratory and invasive ability of NBM cells were evaluated by cell scratch and transwell assays in SH-SY5Y cells. Figure 2(a) shows that the wound healing rate of SH-SY5Y cells treated with GPF was significantly lower compared with untreated cells (Figure 2(a)). In addition, the transwell assay demonstrated that GPF treatment significantly reduced the migratory and invasive capacity of SH-SY5Y cells (Figures 2(b) and 2(c)) in a dose-dependent manner. These results indicated that GPF possessed suppressive effects on the migratory and invasive ability of NBM cells in vitro.

3.3. GPF Treatment Upregulates the Expressions of miR-489 Dependent on AMPK Activation.

A previous study has demonstrated that GPF treatment induces AMPK activation in NSCLC A549 and H460 cells. Consistently, we found that GPF treatment also activated AMPK in SH-SY5Y cells in a dose-dependent manner, which could be retarded by AMPK antagonist compound C (Figure 3(a)). Intriguingly, we also found that treatment with GPF remarkably enhanced the expression of a tumor suppressor, miR-489, in SH-SY5Y cells in a dose- and time-dependent manner (Figure 3(b)). Besides, the upregulation of miR-489 induced by GPF treatment was markedly blocked by compound C (Figure 3(c)).

These results suggested that GPF induced an AMPK-dependent upregulation of miR-489 in NBM cells.

3.4. miR-489 Induces Proliferation Arrest and Apoptosis in NBM Cells.

The role of miR-489 in the proliferation of NBM cells was determined using a CCK-8 assay. The results indicated that the proliferation of SH-SY5Y cells transfected with miR-489 was decreased compared with those transfected with scramble miRNAs (Figure 4(a)). Furthermore, the colony formation assay suggested that enforced expression of miR-489 decreased the number of cell colonies compared with the scramble miRNA (Figure 4(b)). Additionally, the apoptosis assay demonstrated that SH-SY5Y cells transfected with miR-489 displayed higher apoptotic rates compared with those transfected with the scramble miRNA in response to cisplatin treatment (Figure 4(c)). These findings manifested that miR-489 played a regulatory role in the proliferation, survival, and apoptosis of NBM cells.

3.5. miR-489 Restrains the Migratory and Invasive Ability of SH-SY5Y Cells.

The role of miR-489 in the migratory and invasive ability of NBM cells was evaluated by cell scratch and transwell assays in SH-SY5Y cells. The enhanced expression of miR-489 remarkably reduced the wound healing rate compared with scramble miRNA-treated cells (Figure 5(a)). Additionally, the transwell assay demonstrated that miR-489 transfection reduced the migratory (Figure 5(b)) and invasive (Figure 5(c)) capacity of SH-SY5Y cells. These findings indicated that miR-489 functioned as a suppressor in regulating migration and invasion of NBM cells in vitro.

3.6. miR-489 Targets XIAP and Decreases Its Expression in NBM Cells. Bioinformatic analysis using two predictive algorithms, TargetScan and http://microRNA.org, was performed to further explore the genes targeted by miR-489 in NBM cells. The results revealed a potential miR-489 binding site within the 3'UTR of XIAP, a potent antiapoptotic adaptor (Figure 6(a)). The luciferase assay indicated that miR-489 transfection inhibited the activities of luciferase in SH-SY5Y cells transfected with plasmids expressing 3′UTR of XIAP, but not the 3′UTR mutants (Figure 6(b)). Furthermore, the overexpression of miR-489 downregulated the expression of XIAP at the mRNA level in SH-SY5Y cells (Figure 6(c)). Consistently, miR-489 transfection downregulated the expression of XIAP at the protein level in NBM cells (Figure 6(d)). Taken together, these findings suggested that miR-489 bound to 3′UTR of XIAP mRNA for degradation, thus regulating its expression.

4. Discussion

Up to date, the most well-documented pharmacological effect of GPF is its antioxidant capacities. In vitro, GPF exerts a practical radical scavenging effect due to its multiple phenolic hydroxyl groups [40] and rescues human keratinocyte cell line HaCaT cells from ultraviolet-induced apoptosis via scavenging reactive oxygen species (ROS) [41]. Besides the intrinsic capacity to eliminate free radicals, GPF treatment significantly attenuates oxidative stress induced by cerebral ischemia-reperfusion through the nuclear factor erythroid 2-related factor 2 (NRF2) pathway [11]. However, the pharmacological effects of GPF on cancer remain largely unexplored. In the present study, we aimed to reveal a novel function of GPF. We found that treatment with GPF remarkably arrested the proliferation, suppressed the invasion, and enhanced chemosensitivity in NBM cells at a dosage that was not toxic to normal cells.

A previous study has reported that GPF treatment upregulates the expression of miR-299-5p to downregulate activating transcription factor 2 (ATF2), thus leading to inhibited progression of NSCLC cells [33]. Intriguingly, we demonstrated that upregulation of miR-489 induced by GPF was implicated in its anti-NBM capacity. Furthermore, it has been reported that GPF remarkably induces the phosphorylation of AMPK, resulting in Nrf2/HO-1 pathway activation [11]. We also observed that GPF treatment induced phosphorylation of AMPK in NBM cells. Intriguingly, pretreatment with compound C, an AMPK antagonist, significantly reduced the upregulation of miR-489 induced by GPF, indicating that this effect of GPF was AMPK dependent.

Accumulating evidence indicates that dysregulation of miR-489 is a common event in tumorigenesis, and it functions as a potent suppressor in growth and metastasis in various malignancies, including breast cancer [42], glioma [43], hepatoma [44], and bladder cancer [45]. In addition, Chen et al. have reported that miR-489 modulates chemosensitivity in human breast cancer cells [46], and upregulation of miR-489 restores the cisplatin chemosensitivity in ovarian cancer cells via directly targeting Akt3 for degradation [47].

To date, very few studies have explored the role of miR-489 in NBM. As complementary information, we provided dramatic biological evidence that miR-489 could arrest the proliferation and promote apoptosis of NBM cells, indicating the antioncogenic property of miR-489 in the NBM.

It has been reported that miR-489 can promote apoptosis in glioma cells via inhibiting the SPIN1-priming PI3K/AKT pathway [43]. Similarly, our findings revealed that the overexpression of miR-489 could also induce compelling apoptosis in NBM cells in vitro. To further explore the mechanism underlying the antiapoptotic effects of miR-489, we first identified XIAP as a bona fide target of miR-489. XIAP, also known as an inhibitor of apoptosis protein 3 (IAP3), is one of the most potent members of the human inhibitor of apoptosis protein (IAP) family, which consists of eight members [48]. Dysregulation of XIAP has been found in several malignancies, including thyroid carcinoma [49], lymphoma [50], and glioma [51]. Furthermore, XIAP hyperexpression accelerates the tumor growth and induces blockage of apoptosis, leading to the development and progression of cancer [52]. XIAP exerts its antiapoptotic function through inhibiting caspases 3, 7, and 9 [53, 54], accounting for the proapoptotic effects of miR-489 indicated in our study.

There are still limitations in this study. First, the precise mechanism underlying the GPF-induced expression of miR-489 is still elusive, though our results indicated that the AMPK pathway was involved in this process. AMPK can interact with diverse signaling pathways, such as the Nrf2 pathway, autophagy, PI3K/Akt pathway, and the mitogen-activated protein kinase (MAPK) pathway. The direct downstream pathway of AMPK mediating miR-489 upregulation needs to be further elucidated. Finally, although miR-489 exerted anti-NBM effects, its contributions to the tumor-suppressive capabilities of GPF are not well documented. Therefore, additional experiments, such as the usage of miR-489 inhibitors, should be carried out to determine the role of miR-489 in the anti-NBM properties of GPF.

In conclusion, our findings presented that GPF was a novel AMPK agonist, which regulated miR-489/XIAP. Through this mechanism, GPF exhibited significant capacity in suppressing the progression of NBM in vitro (Figure 7). These results indicated that GPF could be used as an alternative to the current treatment of NBM and highlighted the potential value of targeting the AMPK/miR-489/XIAP axis in the development of new approaches against NBM.

Data Availability

All data used to support the findings of this study are included within the article.

Conflicts of Interest

The authors declare that they have no conflicts of interest.

References

[1] N. C. Colon and D. H. Chung, "Neuroblastoma," *Adv Pediatr*, vol. 58, no. 1, pp. 297–311, 2011.

[2] P. Bhoopathi, P. Mannangatti, L. Emdad, S. K. Das, and P. B. Fisher, "The quest to develop an effective therapy for neuroblastoma," *Journal of Cellular Physiology*, vol. 236, no. 11, pp. 7775–7791, 2021.

[3] A. S. Abdelmeguid, D. Bell, D. Roberts et al., "Long-term outcomes of olfactory neuroblastoma: MD Anderson Cancer Center Experience and Review of the Literature," *Laryngoscope*, vol. 132, no. 2, pp. 290–297, 2022.

[4] S. Huang, N. Gong, J. Li et al., "The role of ncRNAs in neuroblastoma: mechanisms, biomarkers and therapeutic targets," *Biomarker Research*, vol. 10, no. 1, p. 18, 2022.

[5] S. A. Stainczyk and F. Westermann, "Neuroblastoma—Telomere maintenance, deregulated signaling transduction and beyond," *International Journal of Cancer*, vol. 150, no. 6, pp. 903–915, 2022.

[6] V. P. Veeraraghavan, S. Jayaraman, G. Rengasamy, U. Mony, and D. M. Ganapathy, "Deciphering the role of microRNAs in neuroblastoma," *Molecules*, vol. 27, no. 1, 2022.

[7] B. Chopra and A. K. Dhingra, "Natural products: a lead for drug discovery and development," *Phytotherapy Research*, vol. 35, no. 9, pp. 4660–4702, 2021.

[8] Y. Zhu, D. Sun, H. Liu et al., "Bixin protects mice against bronchial asthma though modulating PI3K/Akt pathway," *International Immunopharmacology*, vol. 101, article 108266, 2021.

[9] Y. Zhu, C. Wang, J. Luo et al., "The protective role of Zingerone in a murine asthma model via activation of the AMPK/Nrf2/HO-1 pathway," *Food & Function*, vol. 12, no. 7, pp. 3120–3131, 2021.

[10] Y. Zhang, Y. Liu, J. Luo, J. Jie, X. Deng, and L. Song, "The herbal compound thymol targets multiple salmonella typhimurium virulence factors for Lon protease degradation," *Frontiers in Pharmacology*, vol. 12, article 674955, 2021.

[11] Z. Wen, W. Hou, W. Wu et al., "6'-O-Galloylpaeoniflorin attenuates cerebral ischemia reperfusion-induced Neuroinflammation and oxidative stress via PI3K/Akt/Nrf2 activation," *Oxidative Medicine and Cellular Longevity*, vol. 2018, Article ID 8678267, 14 pages, 2018.

[12] L. Song, X. Li, X. X. Bai, J. Gao, and C. Y. Wang, "Calycosin improves cognitive function in a transgenic mouse model of Alzheimer's disease by activating the protein kinase C pathway," *Neural Regeneration Research*, vol. 12, no. 11, pp. 1870–1876, 2017.

[13] T. Wen, L. Song, and S. Hua, "Perspectives and controversies regarding the use of natural products for the treatment of lung cancer," *Cancer Medicine*, vol. 10, no. 7, pp. 2396–2422, 2021.

[14] A. Lichota and K. Gwozdzinski, "Anticancer activity of natural compounds from plant and marine environment," *International Journal of Molecular Sciences*, vol. 19, no. 11, p. 3533, 2018.

[15] P. Xu, L. Hou, C. Ju et al., "Isatin inhibits the proliferation and invasion of SH-SY5Y neuroblastoma cells," *Molecular Medicine Reports*, vol. 13, no. 3, pp. 2757–2762, 2016.

[16] P. Chanvorachote, V. Pongrakhananon, S. Wannachaiyasit, S. Luanpitpong, Y. Rojanasakul, and U. Nimmannit, "Curcumin sensitizes lung cancer cells to cisplatin-induced apoptosis through superoxide anion-mediated Bcl-2 degradation," *Cancer Investigation*, vol. 27, no. 6, pp. 624–635, 2009.

[17] R. Wang, L. Ma, D. Weng, J. Yao, X. Liu, and F. Jin, "Gallic acid induces apoptosis and enhances the anticancer effects of cisplatin in human small cell lung cancer H446 cell line via the ROS-dependent mitochondrial apoptotic pathway," *Oncology Reports*, vol. 35, no. 5, pp. 3075–3083, 2016.

[18] Y. Zhang, X. Wang, L. Han, Y. Zhou, and S. Sun, "Green tea polyphenol EGCG reverse cisplatin resistance of A549/DDP cell line through candidate genes demethylation," *Biomedicine & Pharmacotherapy*, vol. 69, pp. 285–290, 2015.

[19] R. Qi, W. Jin, J. Wang et al., "Oleanolic acid enhances the radiosensitivity of tumor cells under mimetic hypoxia through the reduction in intracellular GSH content and HIF-1α expression," *Oncology Reports*, vol. 31, no. 5, pp. 2399–2406, 2014.

[20] B. Song, Q. Zhang, M. Yu et al., "Ursolic acid sensitizes radioresistant NSCLC cells expressing HIF-1α through reducing endogenous GSH and inhibiting HIF-1α," *Oncology Letters*, vol. 13, no. 2, pp. 754–762, 2017.

[21] P. Kong, K. N. Yu, M. Yang et al., "Micheliolide enhances radiosensitivities of p53-deficient non-small-cell lung cancer via promoting HIF-1α degradation," *International Journal of Molecular Sciences*, vol. 21, no. 9, p. 3392, 2020.

[22] C. C. Patiño-Morales, R. Jaime-Cruz, C. Sánchez-Gómez et al., "Antitumor effects of natural compounds derived from Allium sativum on neuroblastoma: an overview," *Antioxidants (Basel)*, vol. 11, no. 1, 2022.

[23] H. Seok, J. Ham, E. S. Jang, and S. W. Chi, "MicroRNA target recognition: insights from transcriptome-wide non-canonical interactions," *Molecules and Cells*, vol. 39, no. 5, pp. 375–381, 2016.

[24] K. Chaudhuri and R. Chatterjee, "MicroRNA detection and target prediction: integration of computational and experimental approaches," *DNA and Cell Biology*, vol. 26, no. 5, pp. 321–337, 2007.

[25] M. Leclercq, A. B. Diallo, and M. Blanchette, "Prediction of human miRNA target genes using computationally reconstructed ancestral mammalian sequences," *Nucleic Acids Research*, vol. 45, no. 2, pp. 556–566, 2017.

[26] D. M. Kasper, A. Moro, E. Ristori et al., "MicroRNAs establish uniform traits during the architecture of vertebrate embryos," *Developmental Cell*, vol. 40, no. 6, pp. 552–565.e5, 2017.

[27] Y. Gu, L. Ma, L. Song, X. Li, D. Chen, and X. Bai, "miR-155 inhibits mouse osteoblast differentiation by suppressing SMAD5 expression," *BioMed Research International*, vol. 2017, Article ID 1893520, 7 pages, 2017.

[28] L. Xiao, L. Jiang, Q. Hu, and Y. Li, "MicroRNA-133b ameliorates allergic inflammation and symptom in murine model of allergic rhinitis by targeting Nlrp3," *Cellular Physiology and Biochemistry*, vol. 42, no. 3, pp. 901–912, 2017.

[29] J. T. Powers, K. M. Tsanov, D. S. Pearson et al., "Multiple mechanisms disrupt the _let-7_ microRNA family in neuroblastoma," *Nature*, vol. 535, no. 7611, pp. 246–251, 2016.

[30] A. Shakeri, M. Ghanbari, A. Tasbandi, and A. Sahebkar, "Regulation of microRNA-21 expression by natural products in cancer," *Phytotherapy Research*, vol. 35, no. 7, pp. 3732–3746, 2021.

[31] Z. Niu, M. Fu, Y. Li, H. Ren, X. Zhang, and L. Yao, "Osthole alleviates pulmonary vascular remodeling by modulating microRNA-22-3p mediated lipid metabolic reprogramming," *Phytomedicine*, vol. 96, article 153840, 2022.

[32] W. Liu, G. Xie, G. Yuan et al., "6'-O-Galloylpaeoniflorin attenuates Osteoclasto-genesis and relieves Ovariectomy-induced osteoporosis by inhibiting reactive oxygen species and MAPKs/c-Fos/NFATc1 signaling pathway," *Frontiers in Pharmacology*, vol. 12, article 641277, 2021.

[33] J. Gao, L. Song, H. Xia, L. Peng, and Z. Wen, "6'-O-galloylpaeoniflorin regulates proliferation and metastasis of non-

small cell lung cancer through AMPK/miR-299-5p/ATF2 axis," *Respiratory Research*, vol. 21, no. 1, p. 39, 2020.

[34] L. Song, L. Peng, S. Hua et al., "miR-144-5p enhances the radiosensitivity of non-small-cell lung cancer cells via targeting ATF2," *BioMed Research International*, vol. 2018, Article ID 5109497, 10 pages, 2018.

[35] L. Song, J. Luo, H. Wang et al., "Legionella pneumophila regulates host cell motility by targeting Phldb2 with a 14-3-3ζ-dependent protease effector," *eLife*, vol. 11, 2022.

[36] L. Song, D. Li, Y. Gu et al., "MicroRNA-126 targeting _PIK3R2_ inhibits NSCLC A549 cell proliferation, migration, and invasion by regulation of PTEN/PI3K/AKT pathway," *Clinical Lung Cancer*, vol. 17, no. 5, pp. e65–e75, 2016.

[37] L. Song, D. Li, X. Li et al., "Exposure to PM2.5 induces aberrant activation of NF-κB in human airway epithelial cells by downregulating miR-331 expression," *Environmental Toxicology and Pharmacology*, vol. 50, pp. 192–199, 2017.

[38] L. Song, Y. Xie, C. Li et al., "TheLegionellaeffector SdjA is a bifunctional enzyme that distinctly regulates phosphoribosyl ubiquitination," *MBio*, vol. 12, no. 5, article e0231621, 2021.

[39] L. Song, D. Li, Y. Gu, X. Li, and L. Peng, "Let-7a modulates particulate matter (</=2.5 mum)-induced oxidative stress and injury in human airway epithelial cells by targeting arginase 2," *Journal of Applied Toxicology*, vol. 36, no. 10, pp. 1302–1310, 2016.

[40] R. Furuya, H. Hu, Z. Zhang, and H. Shigemori, "Suffruyabiosides a and B, two new monoterpene diglycosides from moutan cortex," *Molecules*, vol. 17, no. 5, pp. 4915–4923, 2012.

[41] C. W. Yao, M. J. Piao, K. C. Kim et al., "Cytoprotective effects of 6'-O-galloylpaeoniflorin against ultraviolet B radiation-induced cell damage in human keratinocytes," *In Vitro Cellular & Developmental Biology. Animal*, vol. 50, no. 7, pp. 664–674, 2014.

[42] P. Chai, J. Tian, D. Zhao et al., "GSE1 negative regulation by miR-489-5p promotes breast cancer cell proliferation and invasion," *Biochemical and Biophysical Research Communications*, vol. 471, no. 1, pp. 123–128, 2016.

[43] Y. Li, X. Ma, Y. Wang, and G. Li, "miR-489 inhibits proliferation, cell cycle progression and induces apoptosis of glioma cells via targeting SPIN1-mediated PI3K/AKT pathway," *Biomedicine & Pharmacotherapy*, vol. 93, pp. 435–443, 2017.

[44] Y. Lin, J. Liu, Y. Huang, D. Liu, G. Zhang, and H. Kan, "microRNA-489 plays an anti-metastatic role in human hepatocellular carcinoma by targeting matrix Metalloproteinase-7," *Translational Oncology*, vol. 10, no. 2, pp. 211–220, 2017.

[45] J. Li, W. Qu, Y. Jiang et al., "miR-489 suppresses proliferation and invasion of human bladder cancer cells," *Oncology Research*, vol. 24, no. 6, pp. 391–398, 2016.

[46] X. Chen, Y. W. Wang, A. Y. Xing et al., "Suppression of SPIN1-mediated PI3K–Akt pathway by miR-489 increases chemosensitivity in breast cancer," *The Journal of Pathology*, vol. 239, no. 4, pp. 459–472, 2016.

[47] H. Wu, Z. Xiao, H. Zhang, K. Wang, W. Liu, and Q. Hao, "MiR-489 modulates cisplatin resistance in human ovarian cancer cells by targeting Akt3," *Anti-Cancer Drugs*, vol. 25, no. 7, pp. 799–809, 2014.

[48] J. Silke and D. Vucic, "IAP family of cell death and signaling regulators," *Methods in Enzymology*, vol. 545, pp. 35–65, 2014.

[49] T. A. Werner, Y. Tamkan-Ölcek, L. Dizdar et al., "Survivin and XIAP: two valuable biomarkers in medullary thyroid carcinoma," *British Journal of Cancer*, vol. 114, no. 4, pp. 427–434, 2016.

[50] F. Lin, G. Ghislat, S. Luo, M. Renna, F. Siddiqi, and D. C. Rubinsztein, "XIAP and cIAP1 amplifications induce Beclin 1-dependent autophagy through NFκB activation," *Human Molecular Genetics*, vol. 24, no. 10, pp. 2899–2913, 2015.

[51] I. F. Emery, A. Gopalan, S. Wood et al., "Expression and function of ABCG2 and XIAP in glioblastomas," *Journal of Neuro-Oncology*, vol. 133, no. 1, pp. 47–57, 2017.

[52] P. Obexer and M. J. Ausserlechner, "X-linked inhibitor of apoptosis protein - a critical death resistance regulator and therapeutic target for personalized cancer therapy," *Frontiers in Oncology*, vol. 4, p. 197, 2014.

[53] Q. L. Deveraux, R. Takahashi, G. S. Salvesen, and J. C. Reed, "X-linked IAP is a direct inhibitor of cell-death proteases," *Nature*, vol. 388, no. 6639, pp. 300–304, 1997.

[54] Q. L. Deveraux and J. C. Reed, "IAP family proteins–suppressors of apoptosis," *Genes & Development*, vol. 13, no. 3, pp. 239–252, 1999.

Hindawi

Research Article

Antitumor Activity of Royal Jelly and Its Cellular Mechanisms against Ehrlich Solid Tumor in Mice

Aishah E. Albalawi [1], **Norah A. Althobaiti** [2], **Salma S. Alrdahe** [1],
Reem Hasaballah Alhasani [3], **Fatima S. Alaryani** [4], **and Mona N. BinMowyna** [5]

[1]*Department of Biology, Faculty of Science, University of Tabuk, Tabuk, Saudi Arabia*
[2]*Biology Department, College of Science and Humanities-Al Quwaiiyah, Shaqra University, Al Quwaiiyah 19257, Saudi Arabia*
[3]*Department of Biology, Faculty of Applied Science, Umm Al-Qura University, Makkah, Saudi Arabia*
[4]*Biology Department, Faculty of Sciences, University of Jeddah, Jeddah, Saudi Arabia*
[5]*College of Applied Medical Sciences, Shaqra University, Shaqra, Saudi Arabia*

Correspondence should be addressed to Aishah E. Albalawi; ae.albalawi@ut.edu.sa

Objective. The present study was aimed at evaluating the antitumor effects of royal jelly (RJ) obtained from *Apis mellifera* compared with cyclophosphamide against the Ehrlich solid tumors (EST) in mice. *Methods.* Tumor growth inhibition, body weight, the serum level of alpha-fetoprotein (AFP) and carcinoembryonic antigen tumor (CAE), liver and kidney enzymes, tumor lipid peroxidation (LPO), nitric oxide (NO), antioxidant enzymes (glutathione peroxidase (GPx), catalase enzyme (CAT), and superoxide dismutase enzyme activity (SOD)), tumor necrosis factor alpha level (TNF-α), and the apoptosis-regulatory genes expression were assessed in EST mice treated with RJ (200 and 400 mg/kg orally once a day for 2 weeks). *Results.* The results showed that treatment of EST-suffering mice with RJ at the doses of 200 and 400 mg/kg causes significant reduction in tumor volume and inhibition rate, body weight, tumor markers (AFP and CEA), serum level of liver and kidney, LPO and NO, TNF-α level, as well as the expression level of Bcl-2 in comparison with the EST mice receiving the normal saline; whereas RJ at the doses of 200 and 400 mg/kg/day significantly increased ($p < 0.05$) the level of antioxidant enzymes of GPx, CAT, and SOD and the expression level of caspase-3 and Bax genes. *Conclusion.* The findings revealed that oral administration of royal jelly especially at the doses of 200 and 400 mg/kg exhibited promising antitumor effects against EST in mice through induction of apoptosis as well as its antioxidant and anti-inflammatory effects, which suggest it as a novel anticancer agent against tumor; however, additional surveys especially in clinical setting are necessary to approve these findings.

1. Introduction

Cancer as one of the main concerns in public health is described by unregulated cell growth, invasion and spread of cells from the original site, or the unusual site in other parts of the body [1]. Cancer also is a main cause for death involving more than 7.5 million people around the world each year [2]. Previous reports have demonstrated the six main issues in the occurrence of cancer including the ability to produce messages of autonomic growth, escape growth

inhibition messages, avoid apoptotic cell death, unlimited replication, angiogenesis, invasion, and metastasis [3, 4].

At present, a number of approaches are applied for the diagnosis and treatment of several types of cancer, the most significant of which are chemotherapy with chemical agents, radiotherapy, surgery, etc. [5]. By chemotherapy, there are several synthetic agents for cancer therapy including antimetabolites drugs (e.g., methotrexate), passive compounds of DNA (e.g., doxorubicin and cisplatin), antitubulin drugs (e.g., taxis), etc. [6, 7]. Recent reports have revealed some

limitations and adverse side effects in the use of the synthetic agents, such as hair loss, nausea, vomiting, gastrointestinal and kidney disorders, bone marrow suppression, and fatigue, as well as the resistance of cancer cells to common therapies; these reasons encourage the researchers to search new agents especially in natural products with greater effectiveness and less toxicity [6, 7]

Natural products are well known as a valuable resource of appropriate new agents with great chemical diversity observed in millions species of herbs, animal, marine, and microbes [8]. In the recent decades, rising interest has observed on the part of consumers and the food industry into useful food materials and the habits in which it can help keep human health; whereas the key role of diet broadly has been reported for treatment and prevention of a large number of diseases such as cancers [9]. Between foods that have health-promoting properties are products deriving from the beehive, such as royal jelly, honey, and propolis [10].

Royal jelly (RJ) is one of the most noteworthy nutritious substance which is secreted from the hypopharyngeal and mandibular salivary glands of young nurse honey bees [11]. RJ due to having different bioactive compounds, such as polyphenols, protein, lipids, carbohydrates, and mineral salt, has various biological and pharmacological properties such as antioxidant, neurotrophic, anticancer, anti-inflammatory, antidiabetic, antilipidemic, and antimicrobial [11, 12]. Clinical trials, in vitro and in vivo studies, demonstrated that RJ displayed its anticancer effects through induction of apoptosis, thereby increasing the activities of antioxidant factors, inhibiting elevated serum markers and histological alterations, and regulating the inflammatory factors, etc [13]; therefore, the present study was aimed at evaluating the antitumor effects of royal jelly obtained from *Apis mellifera* compared with cyclophosphamide (CP), as an alkylating agent which widely used for the treatment of neoplastic cancers, against the Ehrlich solid tumors (EST) in mice.

2. Materials and Methods

2.1. Royal Jelly. To ensure the relative purity and authenticity of botanical sources, the royal jelly materials were obtained from May 2021 from Langstroth hives containing colonies of the *A. mellifera* grown at the Shaqra University, Saudi Arabia. RJ samples were dissolved with normal saline and filtered under a vacuum by means of filter paper (Whatman membrane, England) to reach the doses of 200 and 400 mg/kg. The selection of these concentrations was based on the previous study that showed promising biological effects with minimum toxicity [14–16].

2.2. Secondary Metabolites Contents

2.2.1. Total Phenol Content. The total phenol content in RJ sample was assessed based on the technique explained previously. To do this, $50 \mu L$ of RJ solution (50 mg/mL) was add to $250 \mu L$ of Folin-Ciocalteu's reagent (0.2 N) for 6 minutes; then, 0.2 mL of sodium carbonate (7.5%) was put into the tested tubes. After 120 min incubation in room temperature,

the absorbance of suspension was determined at 760 nm. Distilled water was also used as the blank solution [17].

Total phenol content was exhibited as mg gallic acid equivalents (GAE)/g. The determination of flavonoid content was performed according to the method explained by El-Guendouz et al. In this way, $200 \mu L$ of RJ solution was poured into the tubes containing $200 \mu L$ aluminum chloride (20%). The mixture was incubated at room temperature for 60 min, and the absorbance of it was determined at 420 nm [18].

2.2.2. Total Flavonoid Contents. The total flavonoid contents were reported as milligram of quercetin equivalents per gram of RJ (mg QE/g RJ) by means of a standard curve. Here, we used the Bradford technique which also called Bio-Rad assay to determine the protein content. In brief, 200 mg RJ sample was added in a tube containing 10 mL methanol/water (50/50; v/v); the suspension was sonicated for 1 h. in the next step, the pH of suspension was adjusted to 2.5 with phosphoric acid and was then diluted 10 times. Next, 5 mL of Bio-Rad reagent was mixed with $250 \mu L$ of RJ solutions. Lastly, the absorbance of mixture was determined at 595 nm. The total protein content was reported as percentage (%) by means of the bovine serum albumin standard curve [19].

2.3. The Ehrlich Ascites Tumor (EAT) Cell Line. Ehrlich ascites tumor (EAT) cell line were prepared from the American Type Tissue Culture Collection (Manassas, USA). EAT cells were then adjusted into 2×10^6 cells/mL in sterile saline solution by means of a Neubauer hemocytometer.

2.4. Animals. A total of 56 female Swiss albino mice with weight of 20-25 g and 6–8 weeks' old were applied to induce the animal model of EST. Animals were kept in the animal house at 22–24°C with condition of 12 h light/12 h dark cycle. Animals also were provided with food for rodents and water ad libitum. This in vivo study was accomplished in consistent with the guidelines of the Guide for Care and Use of Laboratory Animals of the National Institutes of Health. However, the study was permitted by the ethical committee of Shaqra University, Saudi Arabia (214-2020).

2.5. Study Design. EST in mice were established by intramuscularly injection of $200 \mu L$ of cell suspension in the right thigh of mice. On 7th day after induction of the EAT, the mice were randomly divided into 7 groups (8 mice/group) including

(i) Non-EST and nontreated mice (C1)

(ii) EST mice receiving the normal saline (C2)

(iii) EST mice treated with CP (50 mg/kg) intraperitoneally once a day for 3 days (C3)

(iv) Non-EST mice treated with RJ 200 mg/kg orally once a day for 2 weeks (C4)

(v) Non-EST mice treated with RJ 400 mg/kg orally once a day for 2 weeks (C5)

(vi) EST mice treated with RJ 200 mg/kg orally once a day for 2 weeks (Ex1)

(vii) EST mice treated with RJ 400 mg/kg orally once a day for 2 weeks (Ex2)

2.6. Blood and Tumor Sampling. On the 15th after treatment, animals were anesthetized with ketamine (100 mg/kg) xylazine (10 mg/kg) by opening their abdomen cavities, and blood specimens were obtained from the animal's heart. Blood specimens were then centrifuged at 6000 rpm for 10 min and the acquired sera were separated and stored at −80°C until examining. Tumors were also aseptically collected and weighed, and their dimensions were recorded.

After that, they were equally divided into two parts: one part was kept in −80°C for molecular examinations, and the other part was stored at −20°C for other examinations.

2.7. Tumor Growth Inhibition. In this survey, by calculating the tumor volume (TV) and tumor growth inhibition rate, we assessed the in vivo antitumor activity of RJ. TV was determined by the Vernier caliper after the 7th day of the treatment through the equation TV (mm^3) = $4\pi(A/2)^2 \times (B/2)$; whereas A and B are the minor and major tumor axes. Tumor growth inhibition rate (TGIR) also was determined according to the technique elucidated elsewhere with the below formula [20]:

$$TGIR\,(\%) = \frac{(\text{The } mean \, tumor \, weight \text{ of } control \, group - \text{the } mean \, tumor \, weight \text{ of } treated \, group)}{(\text{The } mean \, tumor \, weight \text{ of } control \, group)} \times 100. \tag{1}$$

2.8. Body Weight (BW) Changes. Mice in all studied groups were weighed on day 7 and day 21. The percentage weight gain was determined using the following equation [18]:

$$\%\text{weight gain} = \left[\frac{\text{Mice weight on 19th day}}{\text{Mice weight on day 0}}\right] - 1 \times 100. \tag{2}$$

2.9. Assessing the Tumor Markers. The alpha-fetoprotein (AFP) level in sera was evaluated by means of an automated quantitative enzyme-linked fluorescent assay (ELFA) using mini-VIDAS® AFP (bioMérieux, Marcyl'Etoile, France) according to the guidelines of the manufacturer. On the other hand, carcinoembryonic antigen tumor (CAE) level in mice sera was assessed by using quantitative sandwich immunoassay, MyBio-Source Mouse Carcinoembryonic Antigen Elisa Kit (MyBio-Source, San Diego, USA).

2.10. Evaluation of Serum Levels of Liver Enzymes. Liver function following treatment with RJ was assessed by measuring the serum level of alanine aminotransferase (ALT) and aspartate aminotransferase (AST) using the commercial diagnostic kits (Roche, Germany) [21].

2.11. Evaluation of Serum Levels of Kidney Enzymes. Kidney function following treatment with RJ was also determined by measuring the serum level of creatinine (Cr) and blood urea nitrogen (BUN) using the commercial diagnostic kits (Roche, Germany) [21].

2.12. Evaluation of the Oxidative Stress Markers. The level of oxidative stress (lipid peroxidation (LPO) and nitric oxide (NO)) in tumor homogenates was evaluated by a biodiagnostic analyze kits based on the malondialdehyde (MDA) creation through the thiobarbituric acid (TBA) procedure defined by of Ohkawa et al. [22]. No production was also evaluated in the tumor homogenates based on the method explained by Green et al. [23].

2.13. Evaluation of the Antioxidant Enzymes. The antioxidant activities were assessed through the evaluation of some enzymes such as glutathione reductase (GR), glutathione peroxidase (GPx), catalase enzyme (CAT), and superoxide dismutase enzyme activity (SOD) by means of the commercial kits and according to the technique defined by Weydert and Cullen [24], Luck [25], and Sun et al., [26], respectively.

2.14. Measuring the Tumor Necrosis Factor Alpha Level (TNF-α). Here, we evaluated the level of TNF-α in tumor homogenates by means of mice TNFα ELISA kit (ab100747; Abcam) based on the guidelines of the manufacturer.

2.15. Assessing the Expression Level of Apoptosis-Regulatory Genes. The expression level of some apoptosis-regulatory genes such as caspase-3, Bcl2, and Bax was evaluated by quantitative real-time PCR. Briefly, a total RNA of tumor tissue was extracted by an RNeasy tissue kit (Qiagen, Germany) in line with the protocols of manufacturer. Then, cDNA synthesis was produced using random primers through the complementary DNA (cDNA) synthesis based on the manufacture's recommendations. In the next step, cDNA was utilized for conventional PCR reaction analysis or real-time PCR through SYBR green. The thermal profile of reaction was 95°C for 8 min, 40 cycles of 95°C for 10 s, and 56°C for 30 s, respectively. Finally, the ΔCt was calculated by means of iQTM5 optical system software (Bio-Rad, Hercules, CA). β-Actin was applied as a housekeeping gene and normalization control. Table 1 displayed oligonucleotide primers which were used for real-time PCR [27].

2.16. Statistical Analysis. All obtained results were presented as the means ± standard deviation. SPSS statistical software version, 22.0 (SPSS Inc., Chicago, IL, USA) was applied for data analysis. One-way ANOVA with Turkey's potshot test was used to assess the differences between the experimental groups.

TABLE 1: Sequence of primers of used for real-time PCR.

Amplicon	Primers	Sequence (5′–3′)
Bax	FR	GGCTGGACACTGGACTTCCTGGTGAGGACTCCAGCCACAA
Bcl-2	FR	CATGCCAAGAGGGAAACACCAGAA GTGCTTTGCATTCTTGGA TGAGGG
Caspase-3	FR	TTCATTATTCAGGCCTGCCGAGGTTCTGACAGGCCATGTCATCCTCA
β-Actin	FR	GTGACGTTGACATCCGTAAAGAGCCGGACTCATCGTACTCC

TABLE 2: The results of measurement of the secondary metabolites contents of RJ.

Total content	Test	Amount
Phenolic	Folin–Ciocalteau's reagent colorimetric	96.3 ± 0.31 mg GEA/g DW
Flavonoids	Aluminum chloride ($AlCl_3$ 2%) colorimetric	2.85 ± 0.026 mg QE/g DW
Protein	Bradford method	11.3%

3. Results and Discussion

Cancer as a main concern of public problem is one of the most serious causes of death among humans [2]. In recent years, studies have demonstrated some limitations and adverse side effects of existing drugs in the treatment of cancer; these reasons promote the researchers to search for substitute anticancer agents with relevant efficacy and fewer toxicity [5].

RJ, a viscous secretion of A. mellifera worker bees, is considered an important functional natural product with a wide range of commercial, cosmetic and medical applications [10]. Moreover, in modern medicine, RJ has been demonstrated various pharmacological properties such as antioxidant, anti-inflammatory, immunomodulatory, nephroprotective, wound-healing, and antimicrobial effects [11–14]. The present study was aimed at evaluating the antitumor effects of royal jelly obtained from A. mellifera compared with cyclophosphamide (CP), as an alkylating agent which is widely used for the treatment of neoplastic cancers, against the Ehrlich solid tumors (EST) in mice.

The findings of the secondary metabolites analysis of RJ displayed that total phenolic and flavonoid content was 96.3 ± 0.31 (mg GEA/g DW) and 2.85 ± 0.026 (mg QE/g DW), respectively; the results also showed that the total protein content of RJ sample was 11.3% (Table 2).

As shown in Table 3, treatment of EST-suffering mice with RJ meaningfully reduced the tumor volume in a dose-dependent response; RJ at the doses of 200 and 400 mg/kg decreased the tumor weight by 1.54 ± 0.04 g and 0.86 ± 0.022 g, respectively. The findings also revealed tumor inhibition rate was 50.6 and 72.4% after treatment of EST-suffering mice by RJ at the dose of 200 and 400 mg/kg, respectively. By the body weight evaluation, as shown in Figure 1, EST-suffering mice treated with RJ (200 and 400 mg/kg) displayed a significant ($p < 0.05$) decrease in BW when compared with that of untreated EST mice in the C2 control.

In regard to anticancer effects of royal jelly, Nakaya et al. have shown that RJ has anticancer effects by suppression of the estradiol-induced cell proliferation of MCF-7 breast cancer cells [28]. Mohammadi Abandansari et al. have reported

TABLE 3: Effect of various doses of royal jelly (RJ) of tumor volume and tumor inhibition rate.

Group	Tumor volume (g)	% of inhibition
RJ 200 mg/kg	1.54 ± 0.04	50.6
RJ 400 mg/kg	0.86 ± 0.22	72.4
C2	3.12 ± 0.12	—
C3	0.96 ± 0.03	69.2

C2: EST mice receiving the normal saline; C3: EST mice treated with CP (50 mg/kg) intraperitoneally once a day for 3 days (C3). Data are expressed as the *mean* ± *SD* ($n = 3$).

that RJ especially at the concentrations of 50 and 100 mg/mL significantly showed the cytotoxic activity against the prostate cancer cell line [29]. Recently, in a randomized double-blind clinical trial, Miyata et al. have revealed that oral administration of capsules having 900 mg royal jelly considerably reduces the tumor size and some adverse side effects such as fatigue and anorexia in patients with renal carcinoma [30]. In the other study conducted by Zhang et al., the results exhibited that RJ at the doses of 0.5 and 1.5 g/kg meaningfully decreased the tumor weight in the 4 T1 (breast tumor)-suffering mice [31]. In addition, previous clinical trials, in vitro and in vivo studies, demonstrated that RJ displayed its anticancer effects through induction of apoptosis, thereby increasing the activities of antioxidant factors, inhibition of elevated serum markers and histological alterations and regulation the inflammatory factors, etc [13].

It has been previously proven that RJ contains several bioactive compounds such as peptides, proteins, fatty acids (e.g., 10-hydroxydecanoic acid), polyphenols, and flavonoids (e.g., pinocembrin, quercetin, and galangin) [32]; while in other studies, the anticancer effects and possible mechanisms of these compounds have been proven. For example, Bhosale et al. have demonstrated that the polyphenols compounds display their anticancer activity through several mode of actions such as elimination of cell via signaling pathways alteration, suppression of cell cycle actions, and apoptosis stimulation as well as their antimetastasis, antiangiogenic, etc [33]. Kopustinskiene et al. also have shown that flavonoids exhibit their anticancer effects through a number
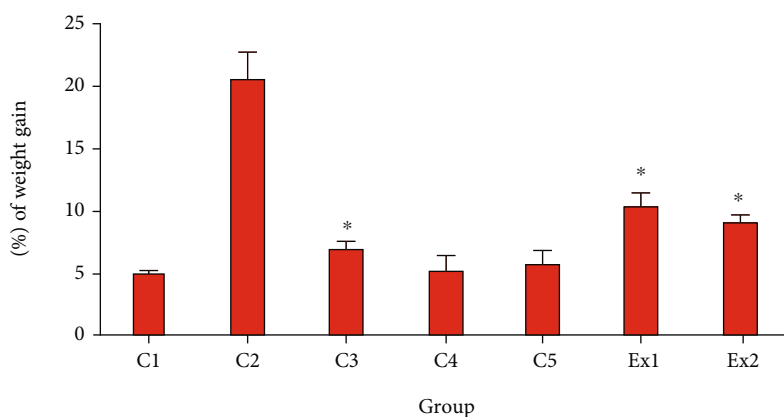
Figure 1: The mean of % of weight gains in EST-bearing mice treated with royal jelly (RJ). Non-EST and nontreated mice (C1); EST mice receiving the normal saline (C2); EST mice treated with CP (50 mg/kg) intraperitoneally once a day for 3 days (C3); non-EST mice treated with RJ 200 mg/kg orally once a day for 2 weeks (C4); non-EST mice treated with RJ 400 mg/kg orally once a day for 2 weeks (C5); EST mice treated with RJ 200 mg/kg orally once a day for 2 weeks (Ex1); EST mice treated with RJ 200 mg/kg orally once a day for 2 weeks (Ex2). Data are expressed as the mean $\pm$ SD ($n = 8$). $^*p < 0.001$ significant difference compared with C2 group.
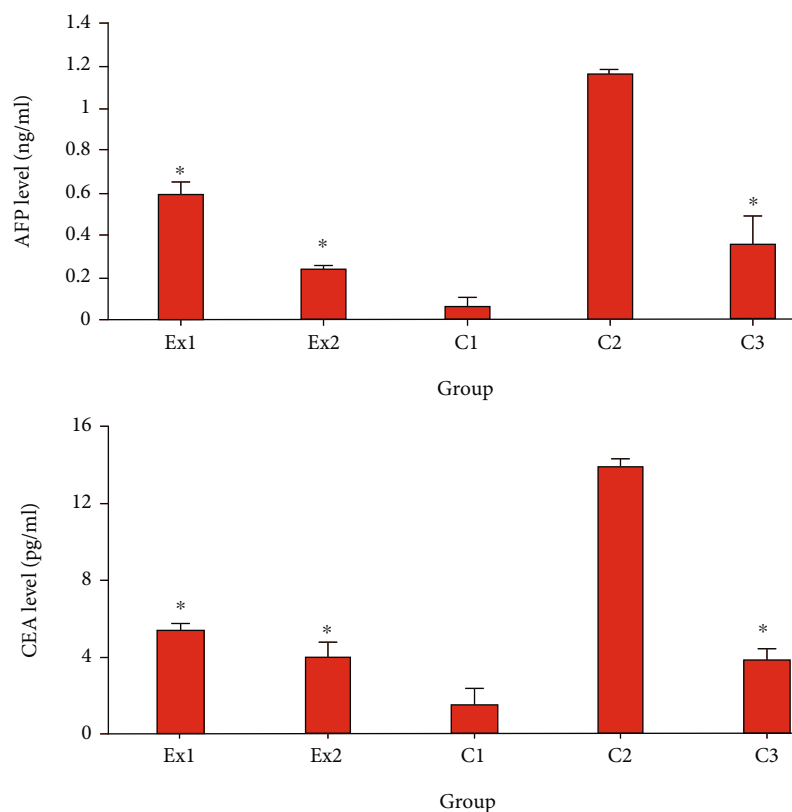
Figure 2: The serum level of alpha-fetoprotein(AFP) and carcinoembryonic antigen tumor (CEA) in EST-bearing mice treated with royal jelly (RJ) at the doses of 200 (Ex1) and 400 (Ex2) mg/kg when compared with (i) non-EST and nontreated mice (C1); (ii) EST mice receiving the normal saline (C2); (iii) EST mice treated with CP (50 mg/kg) (C3). Data are expressed as the mean $\pm$ SD ($n = 8$). $^*p < 0.001$ significant difference compared with C2 group.

of mechanisms such as autophagy, controlling of reactive oxygen species- (ROS-) scavenging enzyme activities, suppressing the cell cycle, and promoting the apoptosis and inhibition of proliferation of cancer cells [34]. Recently, Albalawi et al. have reported that queen bee acid (10-hydroxy-2-decenoic acid, 10-HDA), a main fatty acid in royal jelly, at the doses of 2.5 and 5 mg/kg mainly in combi-

nation with cyclophosphamide, displayed favorable antitumor activity against EST in mice through induction of apoptosis and increasing the antioxidant activities and be able to be suggested as novel substitute anticancer agent [35].

Today, it has been proven that the elevated serum level of AFP and CEA indicate liver and renal tissue damage
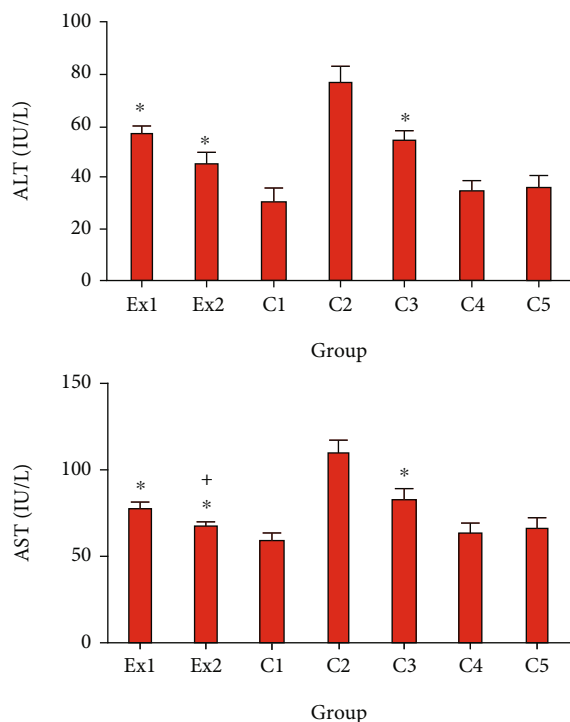
FIGURE 3: The serum level of alanine aminotransferase (ALT) and aspartate aminotransferase (AST) in EST-bearing mice treated with royal jelly (RJ). Non-EST and nontreated mice (C1); EST mice receiving the normal saline (C2); EST mice treated with CP (50 mg/kg) intraperitoneally once a day for 3 days (C3); non-EST mice treated with RJ 200 mg/kg orally once a day for 2 weeks (C4); non-EST mice treated with RJ 400 mg/kg orally once a day for 2 weeks (C5); EST mice treated with RJ 200 mg/kg orally once a day for 2 weeks (E1); EST mice treated with RJ 400 mg/kg orally once a day for 2 weeks (E2) ($n = 8$). $*p < 0.001$ significant difference compared with C2 group; $+$ $p < 0.001$ significant difference compared with C3 group.

FIGURE 4: The serum level of blood urea nitrogen (BUN) and creatinine (Cr) in EST-suffering mice treated with royal jelly (RJ). Non-EST and nontreated mice (C1); EST mice receiving the normal saline (C2); EST mice treated with CP (50 mg/kg) intraperitoneally once a day for 3 days (C3); non-EST mice treated with RJ 200 mg/kg orally once a day for 2 weeks (C4); non-EST mice treated with RJ 400 mg/kg orally once a day for 2 weeks (C5); EST mice treated with RJ 200 mg/kg orally once a day for 2 weeks (Ex1); EST mice treated with RJ 400 mg/kg orally once a day for 2 weeks (Ex2) ($n = 8$). $*p < 0.001$ significant difference compared with C2 group; $+$ $p < 0.001$ significant difference compared with C3 group.

during cancer [36]. The obtained results revealed that in the mice of control group of C2, the serum level of CEA and AFP was significantly elevated in comparison with the mice of C1 group. Nevertheless, the level of CEA and AFP was significantly ($p < 0.001$) decreased in the EST-suffering mice treated with RJ at the doses of 200 and 400 mg/kg when compared with the mice of C1 group (Figure 2).

Due to the potential effect of cancer cells on the metabolism and function of liver cells and subsequently increased serum level of liver enzymes [37], we decided to measure the serum level of AST in the EST-bearing mice after treatment with RJ. Similar to the previous studies [38, 39], our findings revealed that the serum level of AST and ALT remarkably elevated in the mice of C2 group; representing that EST triggered severe hepatocellular damage. Whereas, in the EST-suffering mice treating with the RJ at the doses of 200 and 400 mg/kg the level of ALT and AST was meaningfully ($p < 0.001$) collapsed compared with the mice of C2 group (Figure 3). With respect to the toxicity profile of RJ, our results exhibited that there was no significant difference between the serum level liver and kidney enzymes in healthy

mice and EST mice treated with RJ at the doses 200 and 400 mg/kg for two weeks.

As previously reported, the EST impairs the renal function and results in increasing the blood BUN and Cr [40, 41]. In consistent with previous investigations, Figure 4 indicated that the serum level of BUN and Cr considerably raised in in the EST-suffering mice in control group of C2; conversely, treatment of the EST-suffering mice with RJ at the doses of 200 and 400 mg/kg the level of BUN and Cr was meaningfully ($p < 0.001$) declined compared with the mice of C2 group.

Oxidative stress is one of the most important factors in the initiation and progression of cancer through increasing mutations and damage in DNA, genome variation, and inhibition of cell multiplying, etc. [42]. Studies shows that antioxidants agents especially those extracted from natural products are potentially able to interfere with carcinogenesis and preserve human beings from damages of oxidative stress [43–47].

Considering the effects of royal jelly on anticancer agentinduced toxicities, Amirshahi et al. have demonstrated the protective effect of royal jelly by improving the serum levels of testosterone and sperm parameters in bleomycin-induced male rats [48]. Karadeniz et al. reported that royal jelly modulates oxidative stress, apoptosis, and histological alterations
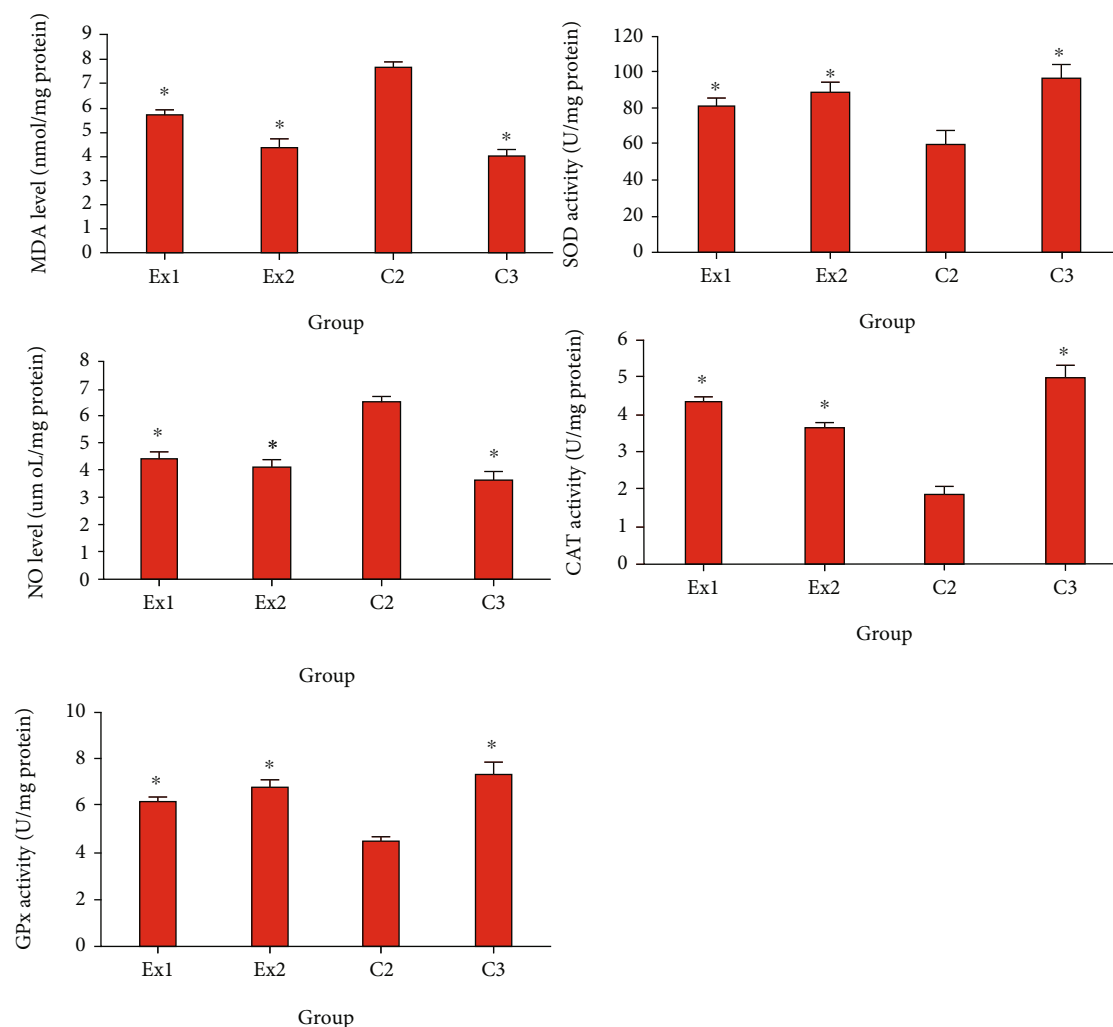
FIGURE 5: The tumor level of the malondialdehyde (MDA), nitric oxide (NO), glutathione reductase (GR), glutathione peroxidase (GPx), catalase enzyme (CAT), and superoxide dismutase enzyme activity (SOD) in EST-suffering mice treated with royal jelly (RJ). EST mice receiving the normal saline (C2); EST mice treated with CP (50 mg/kg) intraperitoneally once a day for 3 days (C3); EST mice treated with RJ 200 mg/kg orally once a day for 2 weeks (Ex1); EST mice treated with RJ 400 mg/kg orally once a day for 2 weeks (Ex2). $^*p < 0.001$ significant difference compared with C2 group. Data are expressed as the mean ± SD ($n = 8$).

in the liver and kidneys of rats treated with cisplatin [49]. In the study consucted by Malekinejad et al., the results showed the cardioprotective effect of royal jelly on paclitaxel-induced cardiotoxicity in rats by conferred protection against histopathological and biochemical alterations [50]. Another study conducted by Kaynar et al. revealed that royal jelly suppressed methotrexate-induced systemic oxidative stress and damage to small intestine in rats through an increase in the activities of antioxidant factors [51].

As shown in Figure 5, the obtained findings exhibited that the tumor level of MDA and NO was meaningfully raised; but the level of GPx, CAT, and SOD was considerably reduced in the mice of C2 group. Conversely, RJ at the doses of 200 and 400 mg/kg/day considerably ($p < 0.01$) declined the expansion in the LPO and NO as well as raised ($p < 0.05$) the level of GPx, CAT, and SOD. Similarly, Zhang et al. demonstrated that RJ at the doses of 0.5 and 1.5 g/kg meaningfully increased the SOD and total antioxidant

capacity (T-AOC) in the 4 T1-suffering mice [31]. Moreover, previous studies have revealed the antioxidant effects of RJ by DPPH-based radical scavenging with IC_{50} value ranging 150 to 219 μg/g for various royal jelly samples [32]. In line with our results, Abdel-Hafez et al. have demonstrated the protective effect of royal jelly against cyclophosphamide induced prostatic damage in male albino rats through the reducing of NO and MDA as well as increasing of GPx, GST, and SOD [52].

Based on previous studies, cancer cells can damage normal tissues and result in hypoxia via two main methods including (i) mechanical injury of the tumor and (ii) stimulating the secretion of some proinflammatory cytokines [53]. As shown in Figure 6, the obtained results confirmed that the level of TNF-α in the EST-suffering mice in C2 group was considerably ($p < 0.001$) raised; nevertheless, treatment of the EST-suffering mice with RJ at the doses of 200 and 400 mg/kg/day meaningfully ($p < 0.05$) declined the level of
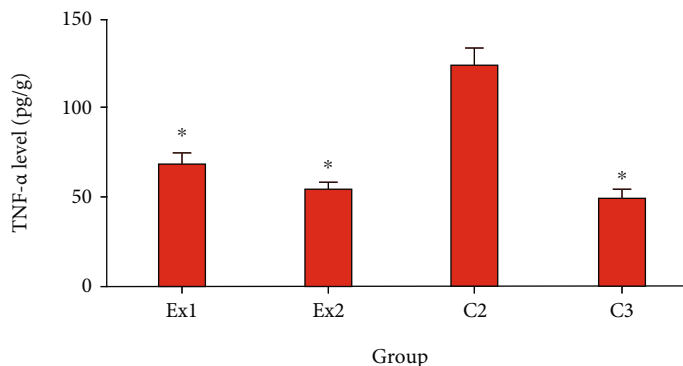
FIGURE 6: The tumor level of the TNF-α in EST-bearing mice treated with royal jelly (RJ) EST mice receiving the normal saline (C2); EST mice treated with CP (50 mg/kg) intraperitoneally once a day for 3 days (C3); EST mice treated with RJ 200 mg/kg orally once a day for 2 weeks (Ex1); EST mice treated with RJ 400 mg/kg orally once a day for 2 weeks (Ex2). $^*p < 0.001$ significant difference compared with C2 group. Data are expressed as the mean $\pm$ SD ($n = 8$).
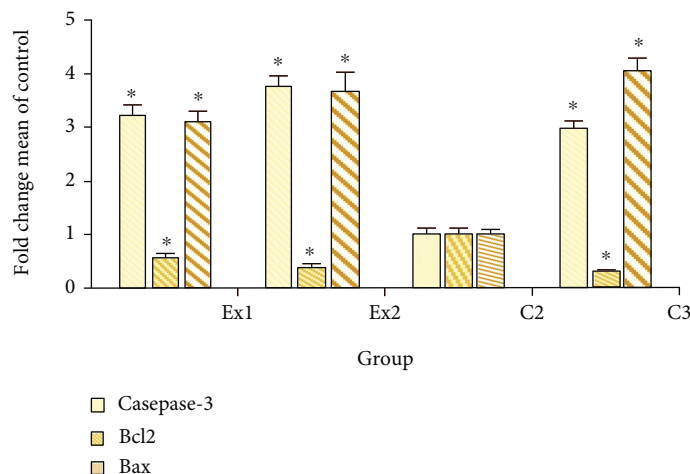
FIGURE 7: The expression level of the caspase-3, Bcl-2, and Bax genes in EST-bearing mice treated with royal jelly (RJ). EST mice receiving the normal saline (C2); EST mice treated with CP (50 mg/kg) intraperitoneally once a day for 3 days (C3); EST mice treated with RJ 200 mg/kg orally once a day for 2 weeks (Ex1); EST mice treated with RJ 400 mg/kg orally once a day for 2 weeks (Ex2). $^*p < 0.001$ significant difference compared with C2 group. Data are expressed as the mean $\pm$ SD ($n = 8$).

TNF-α in mice. In line with our results, Miyata et al. have exhibited that oral administration of capsules having 900 mg royal jelly significantly decreased the serum levels of TNF-α in patients receiving capsules having 900 mg royal jelly [30].

Apoptosis or programmed cell death is well known as one of the key factors in various phases of a living organism's biological evolution and which in case of irregular and abnormal activity, it results in various serious diseases [54]. Apoptosis inhibition is one of the main routes in tumorigenesis and cancers which is essential for cancer cells to continue their uncontrollable proliferating. Hence, induction and elevation of apoptosis is a standard target to discover new anticancer agents [55]. Figure 7 exhibited that the expression level of caspase-3 gene was significantly ($p < 0.001$) upregulated in tumor tissues, with 3.22 and 3.76 fold after treatment of the EST-suffering mice with RJ at the at the doses of 200 and 400 mg/kg, respectively. Likewise, the expression level of Bax gene was meaningfully

($p < 0.001$) upregulated in tumor tissues, by 3.11 and 3.98 fold after treatment of the EST-bearing mice with RJ at the doses of 200 and 400 mg/kg, respectively. The findings of quantitative real-time PCR displayed that the expression level of Bcl2 was considerably ($p < 0.05$) downregulated in the tumor after treatment of the EST-suffering mice with RJ at the doses of 200 and 400 mg/kg, respectively. Similarly, Aslan et al. and Ali et al., have demonstrated that royal jelly elevates the caspase and Bcl-2 expression level and subsequently declined the muscle tissue injury induced with fluoride in rats [56, 57].

4. Conclusion

The findings of the current study revealed that oral administration of royal jelly especially at the doses of 200 and 400 mg/kg exhibited promising antitumor effects against EST in mice and might be proposed as a novel anticancer

agent against tumor; however, additional surveys especially in clinical setting are necessary to approve these findings.

Abbreviations

EST: Ehrlich solid tumors
AFP: Alpha-fetoprotein
CAE: Carcinoembryonic antigen tumor
LPO: Lipid peroxidation
NO: Nitric oxide
Gpx: Glutathione peroxidase
CAT: Catalase enzyme
SOD: Superoxide dismutase enzyme activity
TNF-α: Tumor necrosis factor alpha level
ALT: Alanine aminotransferase
AST: Aspartate aminotransferase
Cr: Creatinine
BUN: Blood urea nitrogen.

Data Availability

All data generated or analyzed during this study are included in this published article.

Conflicts of Interest

All authors declare that they have no competing interests.

Authors' Contributions

AEA contributed to the study's conception or design; AEA and MNB contributed to data analyzation and draft manuscript preparation; NA A, SS A, RH A, FS A, and MN B contributed to the critical revision of the paper; AE A supervised the research.

Acknowledgments

References

[1] D. Hanahan and R. A. Weinberg, "The hallmarks of cancer," *Cell*, vol. 100, no. 1, pp. 57–70, 2000.

[2] C. Mattiuzzi and G. Lippi, "Current cancer epidemiology," *Journal of Epidemiology and Global Health*, vol. 9, no. 4, p. 217, 2019.

[3] E. A. Golemis, P. Scheet, T. N. Beck et al., "Molecular mechanisms of the preventable causes of cancer in the United States," *Genes & Development*, vol. 32, no. 13-14, pp. 868–902, 2018.

[4] T. Yaguchi, H. Sumimoto, C. Kudo-Saito et al., "The mechanisms of cancer immunoescape and development of overcoming strategies," *International Journal of Hematology*, vol. 93, no. 3, pp. 294–300, 2011.

[5] B. A. Chabner and T. G. Roberts, "Chemotherapy and the war on cancer," *Nature Reviews Cancer*, vol. 5, no. 1, pp. 65–72, 2005.

[6] V. Diaby, R. Tawk, V. Sanogo, H. Xiao, and A. J. Montero, "A review of systematic reviews of the cost-effectiveness of hormone therapy, chemotherapy, and targeted therapy for breast cancer," *Breast Cancer Research and Treatment*, vol. 151, no. 1, pp. 27–40, 2015.

[7] R. B. Valenti, "Chemotherapy education for patients with cancer: a literature review," *Clinical Journal of Oncology Nursing*, vol. 18, no. 6, pp. 637–640, 2014.

[8] G. M. Cragg and D. J. Newman, "Natural products: a continuing source of novel drug leads," *Biochimica et BiophysicaActa (BBA)-General Subjects*, vol. 1830, no. 6, pp. 3670–3695, 2013.

[9] W. J. Craig, "Health-promoting properties of common herbs," *The American Journal of Clinical Nutrition*, vol. 70, no. 3, pp. 491s–499s, 1999.

[10] V. R. Pasupuleti, L. Sammugam, N. Ramesh, and S. H. Gan, "Honey, propolis, and royal jelly: a comprehensive review of their biological actions and health benefits," *Oxidative Medicine and Cellular Longevity*, vol. 2017, 21 pages, 2017.

[11] C. I. Pavel, L. A. Mărghitaş, O. Bobiş et al., "Biological activities of royal jelly-review," *Scientific Papers Animal Science and Biotechnologies*, vol. 44, no. 2, pp. 108–118, 2011.

[12] M. F. Ramadan and A. Al-Ghamdi, "Bioactive compounds and health-promoting properties of royal jelly: a review," *Journal of Functional Foods*, vol. 4, no. 1, pp. 39–52, 2012.

[13] Y. Miyata and H. Sakai, "Anti-cancer and protective effects of royal jelly for therapy-induced toxicities in malignancies," *International Journal of Molecular Sciences*, vol. 19, no. 10, p. 3270, 2018.

[14] J. B. Suleiman, A. B. Bakar, and M. Mohamed, "Review on bee products as potential protective and therapeutic agents in male reproductive impairment," *Molecules*, vol. 26, no. 11, p. 3421, 2021.

[15] E. Ghanbari, M. R. Khazaei, M. Khazaei, and V. Nejati, "Royal jelly promotes ovarian follicles growth and increases steroid hormones in immature rats," *International Journal of Fertility & Sterility*, vol. 11, no. 4, pp. 263–269, 2018.

[16] M. Kanbur, G. Eraslan, L. Beyaz et al., "The effects of royal jelly on liver damage induced by paracetamol in mice," *Experimental and Toxicologic Pathology*, vol. 61, no. 2, pp. 123–132, 2009.

[17] V. L. Singleton, R. Orthofer, and M. Lamuela-Raventós, "[14] Analysis of total phenols and other oxidation substrates and antioxidants by means of Folin-Ciocalteu reagent," *Methods in Enzymology*, vol. 299, pp. 152–178, 1999.

[18] S. El-Guendouz, S. Aazza, B. Lyoussi, M. D. Antunes, M. L. Faleiro, and M. G. Miguel, "Anti-acetylcholinesterase, antidiabetic, anti-inflammatory, antityrosinase and antixanthine oxidase activities of Moroccan propolis," *International Journal of Food Science and Technology*, vol. 51, no. 8, pp. 1762–1773, 2016.

[19] K. Hartfelder, M. M. G. Bitondi, C. S. Brent et al., "Standard methods for physiology and biochemistry research inApis mellifera," *Journal of Apicultural Research*, vol. 52, no. 1, pp. 1–48, 2013.

[20] Z. W. Sharawi, "Therapeutic effect of Arthrocnemum machrostachyum methanolic extract on Ehrlich solid tumor in mice," *BMC Complementary Medicine and Therapies*, vol. 20, no. 1, p. 1, 2020.

[21] M. Shakibaie, A. R. Shahverdi, M. A. Faramarzi, G. R. Hassanzadeh, H. R. Rahimi, and O. Sabzevari, "Acute and subacute toxicity of novel biogenic selenium nanoparticles in mice," *Pharmaceutical Biology*, vol. 51, no. 1, pp. 58–63, 2013.

[22] H. Ohkawa, N. Ohishi, and K. Yagi, "Assay for lipid peroxides in animal tissues by thiobarbituric acid reaction," *Analytical Biochemistry*, vol. 95, no. 2, pp. 351–358, 1979.

[23] L. C. Green, D. A. Wagner, J. Glogowski, P. L. Skipper, J. S. Wishnok, and S. R. Tannenbaum, "Analysis of nitrate, nitrite, and [15N]nitrate in biological fluids," *Analytical Biochemistry*, vol. 126, no. 1, pp. 131–138, 1982.

[24] C. J. Weydert and J. J. Cullen, "Measurement of superoxide dismutase, catalase and glutathione peroxidase in cultured cells and tissue," *Nature Protocols*, vol. 5, no. 1, pp. 51–66, 2010.

[25] L. H. Catalase, *Methods of enzymatic analysis*, H. U. Bergmeyer, Ed., Academic Press, New York, 1965.

[26] Y. Sun, L. W. Oberley, and Y. Li, "A simple method for clinical assay of superoxide dismutase," *Clinical Chemistry*, vol. 34, no. 3, pp. 497–500, 1988.

[27] N. M. Selim, A. A. Elgazar, N. M. Abdel-Hamid et al., "Chrysophanol, physcion, hesperidin and curcumin modulate the gene expression of pro-inflammatory mediators induced by lps in hepg2: in silico and molecular studies," *Antioxidants*, vol. 8, no. 9, p. 371, 2019.

[28] M. Nakaya, H. Onda, K. Sasaki, A. Yukiyoshi, H. Tachibana, and K. Yamada, "Effect of royal jelly on bisphenol A-induced proliferation of human breast cancer cells," *Bioscience, Biotechnology, and Biochemistry*, vol. 71, no. 1, pp. 253–255, 2007, Epub 2007 Jan 7.

[29] R. Mohammadi Abandansari, H. Parsian, F. Kazerouni, R. Porbagher, E. Zabihi, and A. Rahimipour, "Effect of simultaneous treatment with royal jelly and doxorubicin on the survival of the prostate cancer cell line (pc3): an in vitro study," *International Journal of Cancer Management*, vol. 11, no. 4, p. 11(4), 2018.

[30] Y. Miyata, K. Araki, K. Ohba et al., "Oral intake of royal jelly improves anti-cancer effects and suppresses adverse events of molecular targeted therapy by regulating TNF-α and TGF-β in renal cell carcinoma: a preliminary study based on a randomized double-blind clinical trial," *Molecular and Clinical Oncology*, vol. 13, no. 4, p. 1, 2020.

[31] S. Zhang, Q. Shao, H. Geng, and S. Su, "The effect of royal jelly on the growth of breast cancer in mice," *Oncology Letters*, vol. 14, no. 6, pp. 7615–7621, 2017.

[32] M. Martinello and F. Mutinelli, "Antioxidant activity in bee products: a review," *Antioxidants*, vol. 10, no. 1, p. 71, 2021.

[33] P. B. Bhosale, S. E. Ha, P. Vetrivel, H. H. Kim, S. M. Kim, and G. S. Kim, "Functions of polyphenols and its anticancer properties in biomedical research: a narrative review," *Translational Cancer Research*, vol. 9, no. 12, pp. 7619–7631, 2020.

[34] D. M. Kopustinskiene, V. Jakstas, A. Savickas, and J. Bernatoniene, "Flavonoids as Anticancer Agents," *Nutrients*, vol. 12, no. 2, p. 457, 2020.

[35] A. E. Albalawi, N. A. Althobaiti, S. S. Alrdahe, R. H. Alhasani, F. S. Alaryani, and M. N. BinMowyna, "Anti-tumor effects of queen bee acid (10-hydroxy-2-decenoic acid) alone and in combination with cyclophosphamide and its cellular mechanisms against Ehrlich solid tumor in mice," *Molecules*, vol. 26, no. 22, p. 7021, 2021.

[36] M. I. A. Edoo, V. K. Chutturghoon, G. K. Wusu-Ansah et al., "Serum Biomarkers AFP, CEA and CA19-9 combined detection for early diagnosis of hepatocellular carcinoma," *Iranian Journal of Public Health*, vol. 48, no. 2, pp. 314–322, 2019.

[37] S. K. Kim and F. Karadeniz, "Biological importance and applications of squalene and squalane," *Advances in Food and Nutrition Research*, vol. 65, pp. 223–233, 2012.

[38] R. Saravanan, P. Viswanathan, and K. V. Pugalendi, "Protective effect of ursolic acid on ethanol-mediated experimental liver damage in rats," *Life Sciences*, vol. 78, no. 7, pp. 713–718, 2006.

[39] M. Gupta, U. K. Mazumder, R. S. Kumar, T. Sivakumar, and M. L. Vamsi, "Antitumor activity and antioxidant status of Caesalpinia bonducella against Ehrlich ascites carcinoma in Swiss albino mice," *Journal of Pharmacological Sciences*, vol. 94, no. 2, pp. 177–184, 2004.

[40] S. A. Hussein and M. E. Azab, "Effect of insulin treatment on some metabolic changes on experimentally induced tumor in female mice," *Egyptian Journal of Biochemistry and Molecular Biology*, vol. 15, pp. 61–80, 1997.

[41] O. A. Abou Zaid, M. R. Hassanein, Y. A. EL-Senosi, and M. F. EL-Shiekha, "Biochemical effect of some antioxidant on metabolic changes in experimentally induced tumor in female mice," *Benha Veterinary Medical Journal*, vol. 1, no. 1, pp. 52–60, 2011.

[42] R. Visconti and D. Grieco, "New insights on oxidative stress in cancer," *Current Opinion in Drug Discovery & Development*, vol. 12, no. 2, pp. 240–245, 2009.

[43] W. Chen, Z. Jia, M. H. Pan, and P. V. AnandhBabu, "Natural products for the prevention of oxidative stress-related diseases: mechanisms and strategies," *Oxidative Medicine and Cellular Longevity*, vol. 2016, 2 pages, 2016.

[44] D. Ali and H. Ali, "Assessment of DNA damage and cytotoxicity of palmatine on human skin epithelial carcinoma cells," *Toxicological & Environmental Chemistry*, vol. 96, no. 6, pp. 941–950, 2014.

[45] D. Ali, "Evaluation of environmental stress by comet assay on freshwater snail Lymnea luteola L. exposed to titanium dioxide nanoparticles," *Toxicological & Environmental Chemistry*, vol. 96, no. 8, pp. 1185–1194, 2014.

[46] S. Alarifi, D. Ali, S. Alkahtani, and M. S. Alhader, "Iron oxide nanoparticles induce oxidative stress, DNA damage, and caspase activation in the human breast cancer cell line," *Biological Trace Element Research*, vol. 159, no. 1-3, pp. 416–424, 2014.

[47] D. A. Bader Almutairi, K. N. Yaseen, N. S. Alothman et al., "Mechanisms of apoptotic cell death by stainless steel nanoparticle through reactive oxygen species and caspase-3 activities on human liver cells," *Frontiers in Molecular Biosciences*, vol. 8, 2021.

[48] T. Amirshahi, G. Najafi, and V. Nejati, "Protective effect of royal jelly on fertility and biochemical parameters in bleomycin-induced male rats," *Iranian Journal of Reproductive Medicine*, vol. 12, no. 3, pp. 209–216, 2014.

[49] A. Karadeniz, N. Simsek, E. Karakus et al., "Royal jelly modulates oxidative stress and apoptosis in liver and kidneys of rats treated with cisplatin," *Oxidative Medicine and Cellular Longevity*, vol. 2011, 10 pages, 2011.

[50] H. Malekinejad, S. Ahsan, F. Delkhosh-Kasmaie, H. Cheraghi, A. Rezaei-Golmisheh, and H. Janbaz-Acyabar, "Cardioprotective effect of royal jelly on paclitaxel-induced cardio-toxicity in rats," *Iranian Journal of Basic Medical Sciences*, vol. 19, no. 2, pp. 221–227, 2016.

[51] L. Kaynar, A. Cetin, S. K. Hacioglu et al., "Efficacy of royal jelly on methotrexate-induced systemic oxidative stress and damage to small intestine in rats," *African Journal of Traditional,*

Complementary and Alternative Medicines, vol. 9, no. 3, pp. 412–417, 2012.

[52] S. M. N. Abdel-Hafez, R. A. Rifaai, and W. Y. Abdelzaher, "Possible protective effect of royal jelly against cyclophosphamide induced prostatic damage in male albino rats; a biochemical, histological and immuno-histo-chemical study," *Biomedicine & Pharmacotherapy*, vol. 90, pp. 15–23, 2017.

[53] F. Balkwill, "TNF-α in promotion and progression of cancer," *Cancer and Metastasis Reviews*, vol. 25, no. 3, pp. 409–416, 2006.

[54] S. L. Sankari, K. M. Masthan, N. A. Babu, T. Bhattacharjee, and M. Elumalai, "Apoptosis in cancer-an update," *Asian Pacific Journal of Cancer Prevention*, vol. 13, no. 10, pp. 4873–4878, 2012.

[55] J. L. Koff, S. Ramachandiran, and L. Bernal-Mizrachi, "A time to kill: targeting apoptosis in cancer," *International Journal of Molecular Sciences*, vol. 16, no. 2, pp. 2942–2955, 2015.

[56] A. Aslan, M. I. Can, O. Gok, S. Beyaz, G. Parlak, and I. H. Ozercan, "The inducing of caspase and bcl-2 pathway with royal jelly decreases the muscle tissue damage exposed with fluoride in rats," *Environmental Science and Pollution Research*, vol. 29, no. 7, pp. 10547–10557, 2022.

[57] D. Ali, P. G. Yadav, S. Kumar, H. Ali, S. Alarifi, and A. H. Harrath, "Sensitivity of freshwater pulmonate snail Lymnaea luteola L., to silver nanoparticles," *Chemosphere*, vol. 104, pp. 134–140, 2014.

Research Article

Effects of Traditional Chinese Medicine Anticancer Decoction Combined with Basic Chemotherapy and Nursing Intervention on Oral Cancer Patients after Surgery and Its Effect on Tumor Markers and Immune Function

Dan Jiang [iD],[1] **Fengying Xiao** [iD],[2] **Lihua Liu** [iD],[3] **Zhen Meng** [iD],[4] **and Chengwei Zhang** [iD][5]

[1]*Department of Stomatology, Yantaishan Hospital, Yantai 264000, China*
[2]*Operation Room, Jiyang People's Hospital, Jinan 251400, China*
[3]*Department of ICU, The Affiliated Qingdao Central Hospital of Qingdao University, The Second Affiliated Hospital of Medical College of Qingdao University, Qingdao 266042, China*
[4]*Department of Ultrasound, Zhangqiu District People's Hospital, Jinan 250200, China*
[5]*Medical Laboratory and Diagnostic Center, Jinan Central Hospital, Jinan 250013, China*

Correspondence should be addressed to Chengwei Zhang; zhangchengwei@jnzxhospital.cn

Objective. To prospectively study the application effect of traditional Chinese medicine (TCM) anticancer decoction with basic chemotherapy and nursing intervention on oral cancer patients after surgery and the effect on tumor markers and immune function. *Methods*. Eighty-four postoperative oral cancer patients in our hospital from May 2017 to February 2019 were selected and divided into observation group (42 cases) and control group (42 cases). The control group was treated with basic chemotherapy combined with basic nursing care, and the observation group was treated with TCM anticancer decoction and comprehensive nursing intervention on the basis of the control group. The clinical efficacy, the occurrence of adverse reactions, the satisfaction of nursing care, and the two-year cumulative survival rate of the two groups were compared. The immune function, tumor marker level, VAS score, QoR40 score, and survival quality score of the two groups were compared before and after nursing care. *Results*. The total clinical treatment efficiency of the observation group (88.10%) was significantly higher than that of the control group (69.05%), and the differences between the two groups in oral cleanliness, aspiration frequency, and oral comfort were statistically significant ($P < 0.05$). The differences in the occurrence of halitosis, oral fungal infection, leukopenia, gastrointestinal reaction, and fever in the observation group were statistically significant compared with the control group ($P < 0.05$). The nursing satisfaction rate in the observation group (95.24%) was significantly higher than that in the control group (78.57%). The two-year cumulative survival rate of the observation group (92.86%) was significantly higher than that of the control group (73.81%). After nursing care, CD4+, CD4+/CD8+, VAS scores, QoR40 scores, and quality of survival scores in both groups all increased, and CD8+, CD56+, CEA level, NSE level, and CA19-9 level all decreased (all $P < 0.05$). *Conclusion*. The clinical efficacy of TCM anticancer decoction with basic chemotherapy and nursing interventions in the treatment of postoperative oral cancer patients was remarkable, which could significantly improve patients' oral cleanliness and comfort, reduce the frequency of sputum aspiration, improve patients' immunity, reduce tumor marker levels, inhibit tumor activity, improve patients' nursing satisfaction, further improve patients' treatment compliance, reduce patients' pain level, improve patients' survival quality, and prolong patients' survival time with high safety. It could be used as a theoretical basis for subsequent clinical research.

1. Introduction

Oral cancer, as a common malignant tumor of the head and neck, accounts for 0.58% to 1.3% of all malignant tumors in the body and is most common in people aged 40 to 70 years, with the incidence increasing year by year and mostly squamous epithelial cell carcinoma [1]. According to relevant data [2–4], about 270,000 people are diagnosed with oral cancer each year, and 2/3 of these patients are found in developing countries. Oral cancer occurs in the oral cavity and any anatomical parts adjacent to it, which can seriously affect patients' normal diet, speech, and other functions, thus affecting their survival quality and even threatening their life safety. Surgical resection is the first choice of treatment for oral cancer, but there are risks such as incomplete surgical resection, easy recurrence after surgery plus possible combination with other serious complications, the prognosis is poor, and the survival rate is extremely low [5].

Some studies have shown that comprehensive treatment such as chemotherapy and Chinese medicine treatment after oral cancer surgery can improve the therapeutic effect of patients after surgery [6, 7]. Although chemotherapy has obvious antitumor effects, long-term treatment can also cause serious adverse effects such as bone marrow suppression and gastrointestinal reactions [8]. Traditional Chinese medicine (TCM) has been wildly used in treatment of various human ailments including cancer [9, 10], neurological disease [11, 12], lung disease [13–15], and infectious disease [16]. Given obvious antitumor effects and good safety, TCM can play a role in increasing the effectiveness and reducing toxicity [17]. However, there are few studies on anticancer soup for the treatment of patients with intermediate and advanced oral cancer after surgery.

Relevant studies have confirmed that pathogenic bacteria can easily colonize and multiply in the oral cavity of the organism, and normal people can effectively remove oral pathogenic bacteria due to their own cleansing function, which makes the incidence of serious infection low [18, 19]. However, postoperative oral cancer patients have surgical trauma in the oral cavity, and the daily secretion of blood and saliva is significantly reduced. Moreover, long-term postoperative fasting makes the self-cleaning function of the patient's oral cavity significantly weakened, and the rapid reproduction of pathogenic bacteria leads to serious infection of the trauma, which in turn affects the effect of surgical treatment. Therefore, a systematic understanding of oral cancer patients' needs, including physical, psychological, and interpersonal communication needs, is very important for postoperative oral cancer patients to adopt effective oral care measures and improve their survival quality. Therefore, this study is aimed at investigating the effects of anticancer soup combined with basic chemotherapy and nursing intervention on tumor markers and immune function of postoperative oral cancer patients.

2. Materials and Methods

2.1. General Data. Eighty-four cases of postoperative oral cancer patients admitted to our hospital from May 2017 to February 2019 were selected and divided into observation and control groups, 42 cases each.

Inclusion criteria were as follows: (i) patients who met the relevant diagnostic criteria for oral cancer [20]; (ii) patients who were 44-71 years old; (iii) patients who were diagnosed with oral squamous cell carcinoma by postoperative pathological examination and had typical symptoms such as dysphagia, unexplained bleeding, nodules, masses, and white smooth squamous plaques [21]; (iv) patients who underwent tumor resection; (v) patients who had no allergic reactions to the drugs used in this study; (vi) patients with an ASA classification of I to III; and (vii) patients and their families agreed to participate in this study and signed the informed consent form.

Exclusion criteria were as follows: (i) patients who had received antitumor treatment before admission, (ii) patients who combined with primary tumors of nose and throat, (iii) patients with severe organ dysfunction, (iv) patients who were accompanied by serious systemic diseases, (v) patients who combined with malignant tumors of other organs, (vi) patients with poor compliance and active withdrawal from the study, and (vii) treatment plan had to be terminated due to serious adverse reactions during the treatment period. The differences between the two groups were not statistically significant ($P > 0.05$) when comparing baseline data, such as gender, age, and disease type, and were comparable (Table 1). This study was approved by the Medical Ethics Committee of our hospital (LLBH20170316), and all patients gave their informed consent and signed the informed consent form.

2.2. Treatment and Nursing Methods. Patients in the control group were treated with basic chemotherapy combined with basic nursing care. The basic chemotherapy regimen was as follows: 1 mg vincristine (National Drug Approval H20068151, Luyi Furen Oncology Drug Co., Ltd., 1 mg) and 30 ml 0.9% sodium chloride solution were intravenously injected in the morning of every Tuesday and Friday. In the afternoon of the same day, 16 mg pingyangmycin (national drug approval no. H20123357, Jilin Adodong Pharmaceutical Group Yanji Co., Ltd., 8 mg) and 5 mg dexamethasone (national drug approval no. H20044139, Tianjin Jinjin Pharmaceutical Co., Ltd.) were intravenously injected. One treatment cycle was 8 weeks. The basic nursing care included daily saline solution rinsing of patients' mouths, health guidance and nutritional guidance, observation of patients' condition changes, and providing patients with a neat and clean ward environment. In the observation group, patients were treated with TCM anticancer decoction and comprehensive nursing intervention on the basis of the control group. In this study, we reviewed a large amount of literature related to Chinese medicine [22–27], and through the joint research and selection of authoritative Chinese medicine practitioners in our hospital, the prescription of TCM anticancer decoction was 15 g of raw milkvetch root, 15 g of dried fresh ginseng, 15 g of largehead atractylodes rhizome, 15 g of Indian bread, 15 g of pinellia tuber, 15 g of Coix seeds, 15 g of Hedyotis, 15 g of barbated skullcup herb, 10 g of giant knotweed rhizome, 10 g of official magnolia bark, 10 g of

TABLE 1: Comparison of general data between the two groups.

	Observation group ($n = 42$)	Control group ($n = 42$)	χ^2	P value
Gender			0.449	>0.05
Male	27	24		
Female	15	18		
Age (years)			0.194	>0.05
>60	23	25		
≤60	19	17		
Degree of education			0.192	>0.05
High school and below	22	24		
College and above	20	18		
Betel nut			0.094	>0.05
Yes	28	30		
No	14	13		
Cigarettes			0.283	>0.05
Yes	34	32		
No	8	10		
Alcohol			0.664	>0.05
Yes	35	32		
No	7	10		
Disease type			0.501	>0.05
Tongue cancer	21	20		
Gingival carcinoma	13	15		
Palate cancer	6	6		
Cheilocarcinoma	2	1		
ASA			0.297	>0.05
I	11	13		
II	26	25		
III	5	4		

zedoary rhizome, 10 g of cablin patchouli herb, 6 g of Chinese date, 6 g of fresh ginger, 6 g of golden thread, and 6 g of liquorice root. Add or subtract medicine according to the patient's actual condition. One dose per day, decocted to 200 ml with water, is to be taken warm in the morning and evening.

Oral care: the patient's oral care was rinsed with 0.5% povidone-iodine solution [28], and the patient's head was raised 20° with the head to the side during rinsing, and the patient's teeth, cheek, tongue, pharynx, and hard palate were rinsed slowly in turn, and the fluid in the oral cavity was aspirated with a suction tube during the rinsing process, and the negative pressure of the suction tube was controlled at 0.04 to 0.06 mPa. A long cotton swab could be used to gently wipe the blood crust and oral secretion attachment site until the aspirate became clear. Psychological care: the nursing staff should establish good communication with the patients, actively answer their questions, encourage their family members and friends to give them comprehensive care, support

them in life and emotion, enhance their self-worth, and improve their will and self-confidence in facing oral cancer.

2.3. Observational Index. Oral cleanliness evaluation standard [29]: grade III referred to ideal oral cleanliness, with a small number of oral bacterial colonies and no foreign bodies on the gums and teeth and no odor; grade II was ideal oral cleanliness, with less oral bacterial colonies, foreign bodies on gums and teeth, and no odor. Grade I referred to poor oral cleanliness, with a large number of oral bacterial colonies, foreign bodies on gums and teeth, and odor. The evaluation standard of sputum aspiration frequency [30]: according to the records of medical staff on the number of sputum aspiration times of patients every day, the minimum sputum was less than 2 min per sputum aspiration time and less than 10 times per day. The moderate sputum volume was 2-5 min for each sputum aspiration and 10-20 times of sputum aspiration per day. Excessive sputum was more than 5 minutes per time of sputum aspiration and more than 20 times per day. Oral comfort evaluation criteria were as follows: nursing staff to understand the feelings of patients by asking patients, according to the real oral cleanliness and comfort of patients into good, good, general three grades. The nursing staff understood the patient's feeling by asking the patient, and according to the actual oral cleanliness and comfort of patients, the oral comfort degree was divided into three grades: good, better, and average.

The immune function of the two groups was compared: 3 ml of peripheral blood of the two groups was collected 2 days before nursing and 8 weeks after nursing, respectively. The levels of T lymphocyte subsets (CD4+, CD8+, and CD56+ cells) in serum of the patients were detected by flow cytometry, and the ratio of CD4+/CD8+ was calculated.

To compare the levels of tumor markers in the two groups: enzyme-linked immunosorbent assay (ELISA) was used to measure the expression levels of carcinoembryonic antigen (CEA), neuron specific enolase (NSE), and carbohydrate antigen 19-9 (CA19-9) in the serum of patients before and after care.

To compare the two-year cumulative survival rates and recurrence rate of the two groups: after care, all patients were followed up regularly for 2 years, with outpatient or telephone follow-up every 3 months, and the two-year cumulative survival rates and recurrence of the two groups were counted and compared.

To compare the degree of pain, recovery, and quality of survival between the two groups: the VAS [31], QoR40 [32], and UW-QOL scale [33] scores were used to assess the degree of pain, quality of recovery, and quality of survival in the two groups, with total scores of 0-10, 40-200, and 0-100, respectively. The quality of recovery and quality of survival gradually improved as the score increased.

The incidence of adverse reactions during care was compared between the two groups, and CTCAE evaluation criteria [34] were used to evaluate reactions including halitosis, oral fungal infections, fever, leukopenia, and gastrointestinal reactions.

To compare the nursing satisfaction of the two groups: a homemade questionnaire was filled out at the time of patient

discharge with a total score of 100 points and three levels (very satisfied: >90 points, satisfied: >70 points, and unsatisfied: ≤70 points), with higher scores representing better patient satisfaction.

2.4. Statistical Analysis. The SPSS 20.0 software was used for statistical analysis of the data. Measurement data were expressed as mean ± standard deviation ($x \pm s$), independent sample t test was used for inter-group comparison, and paired t test was used for intragroup comparison. The count data were expressed as the number of cases and rate (%), and χ^2 test was used for comparison between groups. GraphPad5 was used to draw the survival curve, and log-rank test was used for comparison between groups. $P < 0.05$ was considered as statistically significant difference.

3. Results

3.1. Comparison of Clinical Efficacy between the Two Groups. The differences between the two groups in oral care effects including oral cleanliness, suction frequency, and oral comfort were statistically significant ($P < 0.05$, Table 2).

3.2. Comparison of Immune Function between Two Groups before and after Care. Before care, the differences in CD4+, CD8+, CD56+, and CD4+/CD8+ levels between the two groups were not statistically significant ($P > 0.05$); after care, CD4+ and CD4+/CD8+ levels increased and CD8+ and CD56+ levels decreased in both groups, and the differences were statistically significant ($P < 0.05$, Figure 1).

3.3. Comparison of Adverse Reactions between the Two Groups after Nursing. There were statistically significant differences in halitosis, oral fungal infection, leukopenia, gastrointestinal reaction, and fever between the two groups ($P < 0.05$, Table 3).

3.4. Comparison of Nursing Satisfaction between the Two Groups. The nursing satisfaction of the observation group was 95.24%, and that of the control group was 78.57%. The difference between the two groups was statistically significant ($\chi^2 = 8.333$, $P = 0.016$) (Table 4).

3.5. The Levels of Tumor Markers Were Compared between the Two Groups before and after Nursing. Before nursing, there were no significant differences in CEA, NSE, and CA19-9 levels between 2 groups ($P > 0.05$). After nursing, the levels of tumor markers in both groups were decreased, and the decrease in the observation group was more obvious than that in the control group ($P < 0.05$, Figure 2).

3.6. VAS Score, QoR40 Score, and Quality of Life Score Were Compared between the Two Groups before and after Nursing. Before nursing, there were no significant differences in VAS score, QoR40 score, and quality of life between the two groups ($P > 0.05$). After nursing, VAS score, QoR40 score and quality of life score increased in both groups, and the scores of the observation group increased more significantly ($P < 0.05$, Tables 5 and 6).

3.7. Comparison of Two-Year Cumulative Survival Rates and Recurrence Rate between the Two Groups. The two-year cumulative survival rate was 92.86% in the observation group and 73.81% in the control group ($P < 0.05$, Figure 3). The recurrence rate was 31.0% (13/42) in the control group and 11.9% (5/42) in the observation group. The difference between the two groups was statistically significant.

4. Discussion

Oral cancer is a general term for a group of malignant tumors that occur mainly in the oral cavity, mostly squamous epithelial cell carcinoma. At the present stage, patients with oral cancer in China mainly have a high prevalence in the middle-aged and elderly population, but in the late 1970s and especially since the 1980s, there has been a significant ageing trend in oral cancer patients worldwide [35]. According to relevant data [36], patients aged 60 years or older account for about 30% of the total number of patients. In recent years, with the rapid development of oral cancer treatments, the quality of survival of oral cancer patients has been greatly improved and the mortality rate has decreased, but the absolute number of patients is still large because of the large population in China. The goal of tumor treatment is not only to eliminate lesions and reduce recurrence but also to maximize the quality of life of patients and preserve the function of the organism as the goal to be pursued, following the principle that survival rate and quality of survival are equally important [37]. Currently, the use of a single means to treat oral cancer is prone to postoperative recurrence and metastasis, and the long-term efficacy is not ideal, and conducting a comprehensive sequence of various protocols to improve clinical efficacy has been a hot spot of research in recent years. In this study, we used TCM anticancer decoction with nursing intervention to treat postoperative patients with oral cancer.

In this study, raw milkvetch root, dried fresh ginseng, and largehead atractylodes rhizome could strengthen the body and nourish the spleen and kidney. Indian bread could regulate blood and nourish qi, support healthy energy to eliminate evils; zedoary rhizome had the effect of promoting blood circulation and dispersing knot. Hedyotis had the effect of replenishing vital essence to strengthen the kidneys; giant knotweed rhizome could detoxify and fight cancer, soothe liver, and promote blood circulation; Coix seed, pinellia tuber, barbated skullcup herb, cablin patchouli herb, officinal magnolia bark, and golden thread had the functions of expelling phlegm and resolving turbidity, clearing away heat and detoxifying; Chinese date, fresh ginger can spleen stomach, blood tonic; liquorice root played a role in harmonizing various herbs [38–42]. The whole formula played the effect of invigorating the spleen and benefiting the kidney, detoxifying and removing blood stasis.

In this study, after nursing care, the expression levels of tumor markers in the serum of patients in both groups were lower than those before treatment in this group ($P < 0.05$), and the expression levels of tumor markers in the serum of patients in the observation group were significantly lower than those of patients in the control group ($P < 0.05$). CEA, NSE, and CA199 are commonly used serum tumor

TABLE 2: Comparison of oral nursing effect between the two groups.

Grade	Observation group ($n = 42$)	Control group ($n = 42$)	χ^2	P value
Cleanliness of oral cavity			7.863	<0.05
I	2	11		
II	16	15		
III	24	16		
Frequency of sputum suction			6.992	<0.05
More	7	17		
Medium	16	15		
Less	19	10		
Oral comfort			6.424	<0.05
Good	22	11		
Better	14	19		
Average	6	12		

(a)

(b)

(c)

(d)
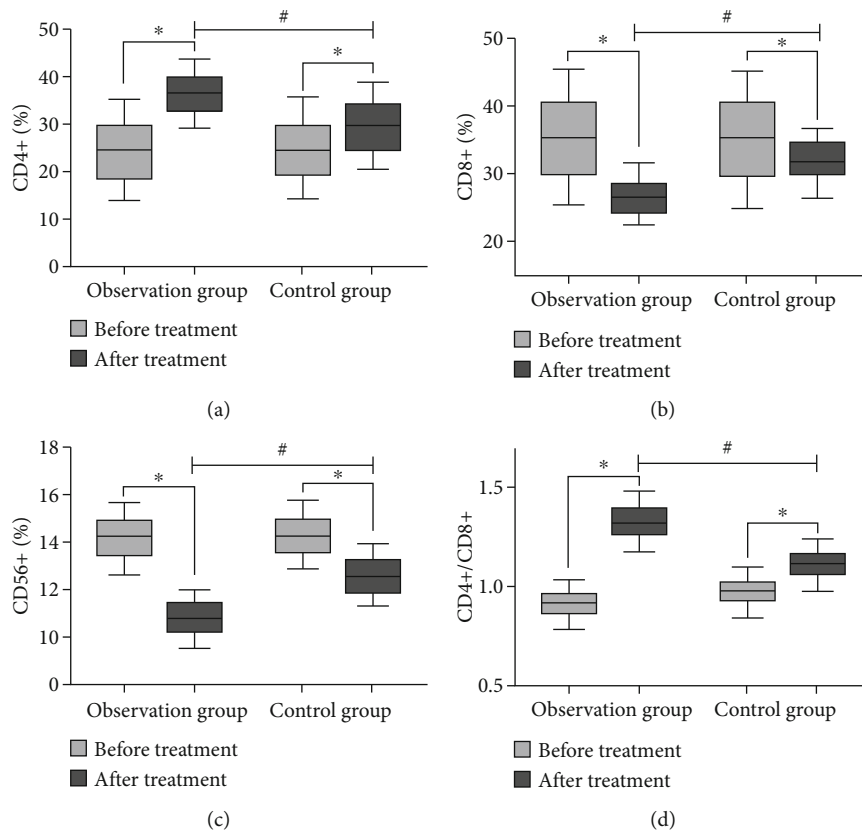
FIGURE 1: Comparison of immune function between the two groups before and after nursing (*compared with before nursing, $P < 0.05$; #compared with the control group, $P < 0.05$). (a) The comparison of CD4+ level between the two groups before and after nursing. (b) The comparison of CD8+ levels between the two groups before and after nursing. (c) The comparison of CD56+ level between the two groups before and after nursing. (d) The comparison of CD4+/CD8+ between the two groups before and after nursing.

TABLE 3: Comparison of adverse reactions between the two groups.

Group	n	Halitosis	Oral fungal infections	Leukopenia	Gastrointestinal reactions	Fever
Observation group	42	3 (7.14)	3 (7.14)	2 (4.76)	4 (8.52)	3 (7.14)
Control group	42	11 (26.19)	9 (21.43)	8 (19.05)	11 (26.19)	6 (14.29)
χ^2		6.903	6.134	5.773	7.624	5.714
P value		<0.05	<0.05	<0.05	<0.05	<0.05

TABLE 4: Comparison of nursing satisfaction between the two groups.

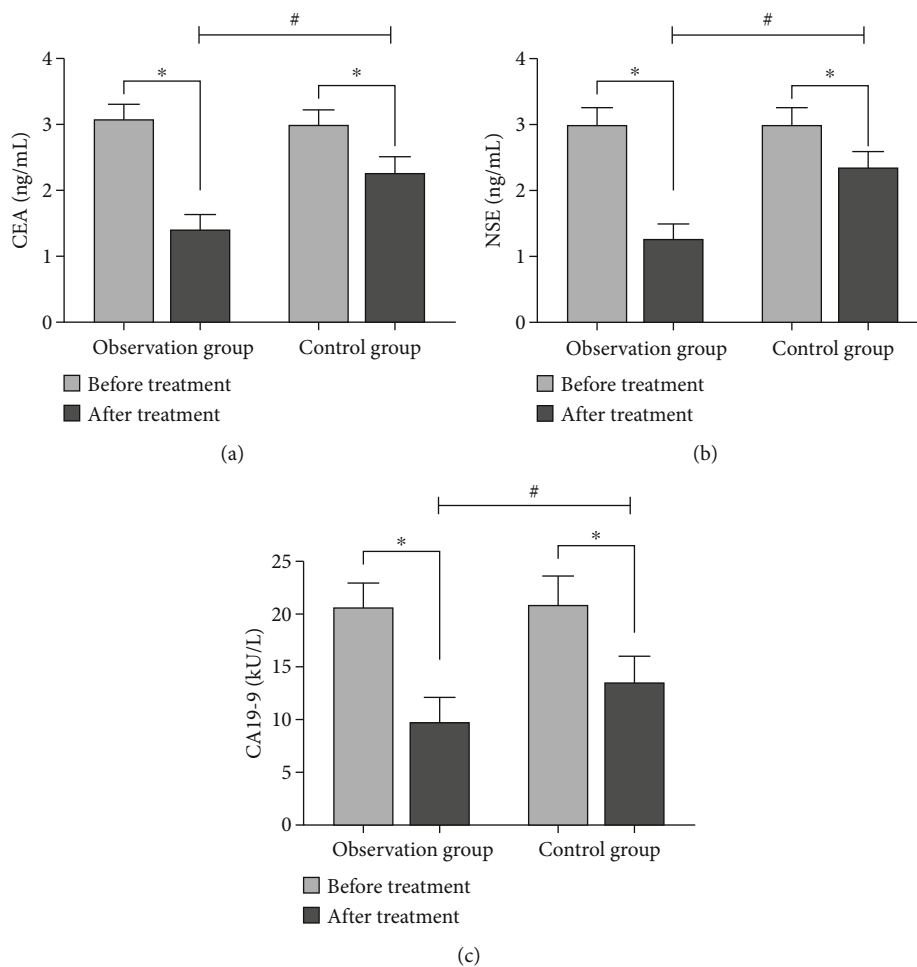| Group	n	Very satisfied	Satisfied	Unsatisfied	Degree of satisfaction
Observation group	42	23	17	2	42 (95.24)
Control group	42	12	21	9	33 (78.57)

(a)

(b)

(c)

FIGURE 2: Comparison of tumor marker levels between the two groups before and after nursing (*compared with before nursing, $P < 0.05$; $^\#$compared with the control group, $P < 0.05$). (a) The comparison of CEA levels between the two groups before and after nursing. (b) The comparison of NSE levels between the two groups before and after nursing. (c) The comparison of CA19-9 levels between the two groups before and after nursing.

TABLE 5: Comparison of postoperative VAS and QoR40 scores between the two groups of patients ($x \pm s$).

Group	VAS score		QoR40 score	
	Before nursing	After nursing	Before nursing	After nursing
Observation group ($n = 42$)	4.64 ± 1.37	8.41 ± 0.76	91.27 ± 23.55	173.14 ± 18.52
Control group ($n = 42$)	4.58 ± 1.42	6.34 ± 1.03	93.46 ± 22.63	132.68 ± 20.04
t	1.623	5.798	2.152	11.663
P	>0.05	<0.05	>0.05	<0.05

markers in clinical practice. Studies have shown that the blood levels of tumor markers are significantly higher in patients with malignant tumors than in healthy individuals [43]. CEA is a glycoprotein located on the cell surface and is synthesized in early fetal life by the gastrointestinal tract, liver, and pancreas, and in adults, the epithelial tissue of the gastrointestinal tract and the liver and pancreas can also synthesize small amounts of CEA and secrete it into the digestive tract at low levels under normal conditions [44]. There have been many studies on CEA as a marker of oral

TABLE 6: Comparison of quality of life between the two groups ($x \pm s$).

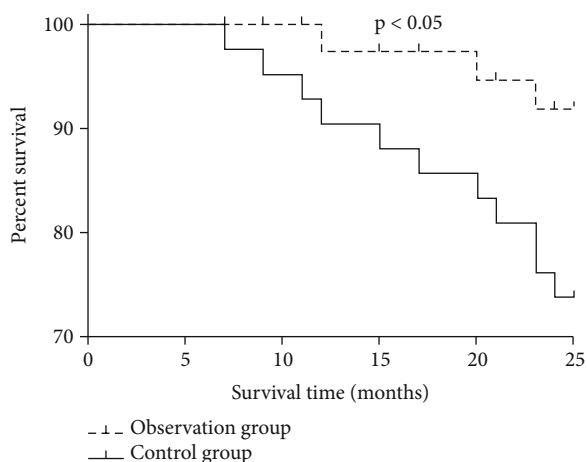| Group	Material state	Social function	Mental function	Physical function
Observation group ($n = 42$)	57.83 ± 6.71	61.58 ± 5.42	59.26 ± 7.92	64.14 ± 5.73
	84.22 ± 6.29	88.65 ± 6.77	87.97 ± 6.49	86.36 ± 5.67
Control group ($n = 42$)	58.26 ± 6.57	62.14 ± 5.83	59.64 ± 7.58	64.82 ± 5.42
	71.45 ± 6.32	73.48 ± 6.53	72.87 ± 6.62	72.86 ± 5.27
t	7.633	8.842	7.964	9.721
P	<0.05	<0.05	<0.05	<0.05

FIGURE 3: Comparison of two-year cumulative survival rates between the two groups.

and maxillofacial malignancies [45, 46]. CEA has been found to be highly expressed in tumor tissues of patients with squamous cell carcinoma of the head and neck [47]. NSE is a glycolytic enzyme present in neuroendocrine cells, neurons, and neurogenic tumors, and its expression is increased in squamous carcinoma tissues with high sensitivity and specificity [48]. CA19-9 is an oligosaccharide tumor-associated antigen first found in gallbladder and pancreatic cancer tissues. Nowadays, its expression has been found to be increased in lung cancer, breast cancer, and other tumor tissues [49–51].

Results of current study indicated that postoperative treatment combined with basic chemotherapy and anticancer decoction together with nursing intervention could effectively eliminate malignant lesion tissues of oral cancer patients. Zedoary rhizome, barbated skullcup herb, and Hedyotis in TCM anticancer decoction had obvious antitumor effects, which could more effectively reduce the expression levels of tumor markers in serum of oral cancer patients after surgery.

The results of this study showed that the oral cleanliness, suction frequency, and comfort of patients in the observation group were significantly higher than those in the control group after care, and the occurrence of adverse reactions was significantly lower than those in the control group. It showed that the combination of TCM anticancer decoction, basic chemotherapy, and comprehensive nursing intervention could improve the therapeutic effect of oral cancer

patients. 0.5% povidone-iodine solution could oxidize bacterial active genes and denature proteins after the slow release of active iodine components in oral mucosal tissue rinsing, which could finally achieve the purpose of sterilization. Moreover, it was an effective oral care solution because of its small stimulating effect, long-lasting and strong bactericidal ability, and clear flavor to eliminate oral odor [52]. The abnormal immune function of oral cancer patients, coupled with surgical stress, further reduced the immune capacity. Studies have reported that cellular immunity among the antitumor immune effects of the body can significantly remove tumor cells from the body, among which T lymphocyte subsets and NK cells play a major role, and their concentration changes can objectively reflect the degree of tumor cell suppression [53]. Another study has also been claimed that the kidney is an important organ of reproductive immunity of the body and plays a stabilizing and regulating role in immune function; the spleen also has a significant enhancing effect on immune function [54, 55]. The results of this study showed that the immune capacity of the observation group was significantly higher than that of the control group after the care. This indicated that the combination of TCM anticancer decoction, basic chemotherapy, and nursing intervention could effectively mobilize the immune function of the body and had the effects of strengthening the spleen and stomach, nourishing the liver, and tonifying the kidney. The results of this study showed that the nursing satisfaction, quality of survival, and two-year cumulative survival rate of the observation group were significantly higher than those of the control group, and the recurrence rate was significantly lower than the control group. The control group was only given basic oral rinsing, nutritional guidance, and health guidance, while the observation group was given professional oral rinsing and psychological care on the basis of the control group, since patients would have psychological fear and irritability after diagnosis, and the torture of the disease would make them more overwhelmed. Thanks to the professional guidance and care of nursing staff, the oral condition of patients would be improved, making them feel comfortable and further improving their treatment compliance and nursing satisfaction and the clinical treatment effect. It indicated that the combination of nursing intervention, basic chemotherapy, and TCM anticancer decoction could improve nursing satisfaction and patients' survival quality, effectively kill tumor cells, and significantly improve patients' survival time with higher safety.

In conclusion, TCM anticancer decoction combined with basic chemotherapy and nursing intervention could effectively improve the immune function of postoperative oral cancer patients, reduce tumor cell activity and the occurrence of adverse reactions, improve their clinical efficacy, enhance the survival quality, and prolong the survival time of patients. However, the sample size of this study was small, and the observation period was short, so further clinical research is needed to verify.

Data Availability

The data used to support the findings of this study are available from the corresponding author upon request.

Conflicts of Interest

The authors declare that they have no conflicts of interest.

References

[1] P. H. Montero and S. G. Patel, "Cancer of the oral cavity," *Surgical Oncology Clinics of North America*, vol. 24, no. 3, pp. 491–508, 2015.

[2] C. U. Hübbers and B. Akgül, "HPV and cancer of the oral cavity," *Virulence*, vol. 6, no. 3, pp. 244–248, 2015.

[3] C. Kerawala, T. Roques, J. P. Jeannon, and B. Bisase, "Oral cavity and lip cancer: United Kingdom National Multidisciplinary Guidelines," *The Journal of Laryngology and Otology*, vol. 130, no. S2, pp. S83–S89, 2016.

[4] M. Kumar, R. Nanavati, T. G. Modi, and C. Dobariya, "Oral cancer: etiology and risk factors: a review," *Journal of Cancer Research and Therapeutics*, vol. 12, no. 2, pp. 458–463, 2016.

[5] C. C. Hsiang, A. W. Chen, C. H. Chen, and M. K. Chen, "Early postoperative oral exercise improves swallowing function among patients with oral cavity cancer: a randomized controlled trial," *Ear, Nose, & Throat Journal*, vol. 98, no. 6, pp. E73–E80, 2019.

[6] C. Y. Yang, C. C. Hsieh, C. K. Lin et al., "Danshen extract circumvents drug resistance and represses cell growth in human oral cancer cells," *BMC Complementary and Alternative Medicine*, vol. 17, no. 1, p. 555, 2017.

[7] H. Chen, C. Wang, M. Qi et al., "Anti-tumor effect of Rhaponticum uniflorum ethyl acetate extract by regulation of peroxiredoxin 1 and epithelial-to-mesenchymal transition in oral cancer," *Frontiers in Pharmacology*, vol. 8, no. 8, p. 870, 2017.

[8] J. N. Carneiro-Neto, "Protocols for management of oral complications of chemotherapy and/or radiotherapy for oral cancer: systematic review and meta-analysis current," *Medicina Oral, Patología Oral y Cirugía Bucal*, vol. 22, no. 1, pp. e15–e23, 2017.

[9] J. Gao, L. Song, H. Xia, L. Peng, and Z. Wen, "6'-O-galloylpaeoniflorin regulates proliferation and metastasis of non-small cell lung cancer through AMPK/mi R-299-5p/ATF2 axis," *Respiratory Research*, vol. 21, no. 1, p. 39, 2020.

[10] T. Wen, L. Song, and S. Hua, "Perspectives and controversies regarding the use of natural products for the treatment of lung cancer," *Cancer Medicine*, vol. 10, no. 7, pp. 2396–2422, 2021.

[11] L. Song, X. Li, X. X. Bai, J. Gao, and C. Y. Wang, "Calycosin improves cognitive function in a transgenic mouse model of Alzheimer's disease by activating the protein kinase C pathway," *Neural Regeneration Research*, vol. 12, no. 11, pp. 1870–1876, 2017.

[12] Z. Wen, W. Hou, W. Wu et al., "6-O-Galloylpaeoniflorin attenuates cerebral ischemia reperfusion-induced neuroinflammation and oxidative stress via PI3K/Akt/Nrf 2 activation," *Oxidative Medicine and Cellular Longevity*, vol. 2018, Article ID 8678267, 14 pages, 2018.

[13] Y. Zhu, C. Wang, J. Luo et al., "The protective role of Zingerone in a murine asthma model via activation of the AMPK/Nrf 2/HO-1 pathway," *Food & Function*, vol. 12, no. 7, pp. 3120–3131, 2021.

[14] C. Wang, J. Luo, X. Bai et al., "Calycosin alleviates injury in airway epithelial cells caused by PM 2.5 exposure via activation of AMPK signalling," *Evidence-based Complementary and Alternative Medicine*, vol. 2021, Article ID 8885716, 9 pages, 2021.

[15] Y. Zhu, D. Sun, H. Liu et al., "Bixin protects mice against bronchial asthma though modulating PI3K/Akt pathway," *International Immunopharmacology*, vol. 101, article 108266, 2021.

[16] Y. Zhang, Y. Liu, J. Luo, J. Jie, X. Deng, and L. Song, "The herbal compound thymol targets multiple salmonella typhimurium virulence factors for Lon protease degradation," *Frontiers in Pharmacology*, vol. 12, article 674955, 2021.

[17] D. Wang, X. Duan, Y. Zhang, Z. Meng, and J. Wang, "Traditional Chinese medicine for oral squamous cell carcinoma: a Bayesian network meta-analysis protocol," *Medicine (Baltimore)*, vol. 99, no. 43, article e22955, 2020.

[18] M. Iwamoto, T. Morikawa, M. Narita, T. Shibahara, and A. Katakura, "Investigation of surgical site infections and bacteria detected following neck dissection in patients with oral cancer," *The Bulletin of Tokyo Dental College*, vol. 61, no. 1, pp. 1–7, 2020.

[19] Z. Saidak, C. Lailler, S. Testelin, B. Chauffert, F. Clatot, and A. Galmiche, "Contribution of genomics to the surgical management and study of oral cancer," *Annals of Surgical Oncology*, vol. 28, no. 11, pp. 5842–5854, 2021.

[20] F. Inchingolo, L. Santacroce, A. Ballini et al., "Oral cancer: a historical review," *International Journal of Environmental Research and Public Health*, vol. 17, no. 9, p. 3168, 2020.

[21] T. Sasahira and T. Kirita, "Hallmarks of cancer-related newly prognostic factors of oral squamous cell carcinoma," *International Journal of Molecular Sciences*, vol. 19, no. 8, p. 2413, 2018.

[22] X. Liu, W. Hou, and D. Dou, "The mealiness and quality of herbal medicine: licorice for example," *Pharmacognosy Research*, vol. 9, no. 2, pp. 151–155, 2017.

[23] Y. Zhang, Y. Liang, and C. He, "Anticancer activities and mechanisms of heat-clearing and detoxicating traditional Chinese herbal medicine," *Chinese Medicine*, vol. 12, no. 1, p. 20, 2017.

[24] S. Takayama and K. Iwasaki, "Systematic review of traditional Chinese medicine for geriatrics," *Geriatrics & Gerontology International*, vol. 17, no. 5, pp. 679–688, 2017.

[25] J. T. Azietaku, H. Ma, X. A. Yu et al., "A review of the ethnopharmacology, phytochemistry and pharmacology of Notopterygium incisum," *Journal of Ethnopharmacology*, vol. 202, no. 202, pp. 241–255, 2017.

[26] S. Li, X. Cheng, and C. Wang, "A review on traditional uses, phytochemistry, pharmacology, pharmacokinetics and toxicology of the genus Peganum," *Journal of Ethnopharmacology*, vol. 203, no. 203, pp. 127–162, 2017.

[27] D. Liu and X. C. Liang, "New developments in the pharmacodynamics and pharmacokinetics of combination of Chinese

medicine and Western medicine," *Chinese Journal of Integrative Medicine*, vol. 23, no. 4, pp. 312–319, 2017.

[28] P. L. Bigliardi, S. A. L. Alsagoff, H. Y. El-Kafrawi, J. K. Pyon, C. T. C. Wa, and M. A. Villa, "Povidone iodine in wound healing: a review of current concepts and practices," *International Journal of Surgery*, vol. 44, pp. 260–268, 2017.

[29] T. Y. Wu, H. Y. Liu, C. Y. Wu, H. C. Chen, S. T. Huang, and P. H. Chen, "Professional oral care in end-of-life patients with advanced cancers in a hospice ward: improvement of oral conditions," *BMC Palliative Care*, vol. 19, no. 1, p. 181, 2020.

[30] T. Manabe, S. Teramoto, N. Tamiya, J. Okochi, and N. Hizawa, "Risk factors for aspiration pneumonia in older adults," *PLoS One*, vol. 10, no. 10, p. e0140060, 2015.

[31] Y. T. Sung and J. S. Wu, "The visual analogue scale for rating, ranking and paired-comparison VAS-RRP: a new technique for psychological measurement," *Behavior Research Methods*, vol. 50, no. 4, pp. 1694–1715, 2018.

[32] J. Kim, D. Choi, M. S. Yeo, G. E. Yoo, S. J. Kim, and S. Na, "Effects of patient-directed interactive music therapy on sleep quality in postoperative elderly patients: a randomized-controlled trial," *Nature and Science of Sleep*, vol. 12, no. 12, pp. 791–800, 2020.

[33] R. Kazi, C. Johnson, V. Prasad et al., "Quality of life outcome measures following partial glossectomy: assessment using the UW-QOL scale," *Journal of Cancer Research and Therapeutics*, vol. 4, no. 3, pp. 116–120, 2008.

[34] A. K. LeBlanc, M. Atherton, R. T. Bentley et al., "Veterinary Cooperative Oncology Group-Common Terminology Criteria for Adverse Events VCOG-CTCAE v2 following investigational therapy in dogs and cats," *Veterinary and Comparative Oncology*, vol. 19, no. 2, pp. 311–352, 2021.

[35] I. Chattopadhyay, M. Verma, and M. Panda, "Role of oral microbiome signatures in diagnosis and prognosis of oral cancer," *Technology in Cancer Research & Treatment*, vol. 18, no. 18, article 153303381986735, 2019.

[36] S. Abati, C. Bramati, S. Bondi, A. Lissoni, and M. Trimarchi, "Oral cancer and precancer: a narrative review on the relevance of early diagnosis," *International Journal of Environmental Research and Public Health*, vol. 17, no. 24, p. 9160, 2020.

[37] T. F. Wang, Y. J. Li, L. C. Chen, C. Chou, and S. C. Yang, "Correlation between postoperative health-related quality of life and care needs of oral cancer patients," *Cancer Nursing*, vol. 43, no. 1, pp. 12–21, 2020.

[38] Y. G. Tao, X. F. Huang, J. Y. Wang, M. R. Kang, L. J. Wang, and S. X. Xian, "Exploring molecular mechanism of Huangqi in treating heart failure using network pharmacology," *Evidence-based Complementary and Alternative Medicine*, vol. 2020, Article ID 6473745, 17 pages, 2020.

[39] J. Xia, L. Zhang, X. Zhang et al., "Effect of large dosage of Fuling on urinary protein of diabetic nephropathy: a protocol of systematic review and meta-analysis of randomized clinical trials," *Medicine (Baltimore)*, vol. 99, no. 40, article e22377, 2020.

[40] C. Xu, Y. Wang, J. Feng, R. Xu, and Y. Dou, "Extracts from Huangqi Radix Astragali Mongoliciplus and Ezhu Rhizoma Curcumae Phaeocaulis inhibit Lewis lung carcinoma cell growth in a xenograft mouse model by impairing mitogen-activated protein kinase signaling, vascular endothelial growth factor production, and angiogenesis," *Journal of Traditional Chinese Medicine*, vol. 39, no. 4, pp. 559–565, 2019.

[41] P. Y. Yang and C. J. Tai, "Chinese medicine treatment for afatinib-induced paronychia," *Case Reports in Oncological Medicine*, vol. 2017, 7327356 pages, 2017.

[42] Y. Zhang, L. Zheng, Y. Zheng et al., "Assembly and annotation of a draft genome of the medicinal plant Polygonum cuspidatum," *Frontiers in Plant Science*, vol. 18, p. 1274, 2019.

[43] W. Sauerbrei, S. E. Taube, L. M. McShane, M. M. Cavenagh, and D. G. Altman, "Reporting recommendations for tumor marker prognostic studies REMARK: an abridged explanation and elaboration," *Journal of the National Cancer Institute*, vol. 110, no. 8, pp. 803–811, 2018.

[44] C. Hao, G. Zhang, and L. Zhang, "Serum CEA levels in 49 different types of cancer and noncancer diseases," *Progress in Molecular Biology and Translational Science*, vol. 162, pp. 213–227, 2019.

[45] Y. H. Wu, P. Y. Lin, J. H. Yang, Y. S. Kuo, and Y. C. Wu, "Serum levels and positive rates of tumor biomarkers in oral precancer patients," *Journal of the Formosan Medical Association*, vol. 120, no. 6, pp. 1324–1331, 2021.

[46] Y. H. Wu, P. Y. Lin, J. H. Yang, Y. S. Kuo, Y. C. Wu, and C. P. Chiang, "Significantly higher serum tumor marker levels in patients with oral submucous fibrosis," *Journal of Dental Sciences*, vol. 16, no. 3, pp. 846–853, 2021.

[47] J. Zheng, L. Sun, W. Yuan et al., "Clinical value of Naa 10p and CEA levels in saliva and serum for diagnosis of oral squamous cell carcinoma," *Journal of Oral Pathology & Medicine*, vol. 47, no. 9, pp. 830–835, 2018.

[48] M. Ju, X. Ge, X. Di, Y. Zhang, L. Liang, and Y. Shi, "Diagnostic, prognostic, and recurrence monitoring value of plasma CYFRA21-1 and NSE levels in patients with esophageal squamous cell carcinoma," *Frontiers in Oncology*, vol. 11, no. 11, article 789312, 2022.

[49] J. F. Fahrmann, C. M. Schmidt, X. Mao et al., "Lead-time trajectory of CA19-9 as an anchor marker for pancreatic cancer early detection," *Gastroenterology*, vol. 160, no. 4, pp. 1373–1383, 2021.

[50] P. Zeng, H. Li, Y. Chen, H. Pei, and L. Zhang, "Serum CA199 levels are significantly increased in patients suffering from liver, lung, and other diseases," *Progress in Molecular Biology and Translational Science*, vol. 162, pp. 253–264, 2019.

[51] J. Zhang, Y. Huang, J. Chen, X. Wang, and H. Ma, "Potential of combination of DCE-MRI and DWI with serum CA125 and CA199 in evaluating effectiveness of neoadjuvant chemotherapy in breast cancer," *World Journal of Surgical Oncology*, vol. 19, no. 1, p. 284, 2021.

[52] D. Lepelletier, J. Y. Maillard, B. Pozzetto, and A. Simon, "Povidone iodine: properties, mechanisms of action, and role in infection control and Staphylococcus aureus decolonization," *Antimicrobial Agents and Chemotherapy*, vol. 64, no. 9, pp. e00682–e00720, 2020.

[53] Y. Yang, Y. Shi, H. Wang, Y. Zhou, and Q. Liao, "The cancer metabolic reprogramming and immune response," *Molecular Cancer*, vol. 20, no. 1, p. 28, 2021.

[54] N. Petejova and A. Martinek, "Renal cell carcinoma: review of etiology, pathophysiology and risk factors," *Biomedical Papers of the Medical Faculty of the University Palacky, Olomouc, Czech Republic*, vol. 160, no. 2, pp. 183–194, 2016.

[55] S. M. Lewis, A. Williams, and S. C. Eisenbarth, "Structure and function of the immune system in the spleen," *Science Immunology*, vol. 4, no. 33, p. eaau6085, 2019.

Research Article

Bixin Prevents Colorectal Cancer Development through AMPK-Activated Endoplasmic Reticulum Stress

Yunfeng Qiu [ID], Changfeng Li [ID], and Bin Zhang [ID]

Department of Endoscopy Center, China-Japan Union Hospital of Jilin University, China

Correspondence should be addressed to Bin Zhang; z_bin@jlu.edu.cn

Chemicals isolated from natural products have been broadly applied in the treatment of colorectal cancer (CRC). Bixin, an apocarotenoid from the seeds of *Bixa orellana*, exerts multiple pharmacological properties, including neuroprotective, anti-inflammatory, cardioprotective, and antitumor effects; yet, the therapeutic effects of Bixin on CRC are still unknown. Here, we described that Bixin treatment significantly inhibited the proliferation and motility of two CRC cell lines (CaCO2 and SW480) in vitro and in vivo. In addition, Bixin administration has sensitized CRC cells to TNF-related apoptosis-inducing ligand- (TRAIL-) induced cell apoptosis. Moreover, we showed that Bixin treatment initiated the activation of PERK/eIF-2α signal in CaCO2 and SW480 cells, leading to endoplasmic reticulum stress-associated apoptosis. Pharmacological inhibition of AMP-activated protein kinase (AMPK) abrogated the Bixin-induced activation of protein kinase RNA-like endoplasmic reticulum kinase (PERK)/eukaryotic initiation factor 2 alpha (eIF-2α) pathway, as well as reversed the inhibitory effects of Bixin on CRC development. In conclusion, this study indicated that Bixin treatment inhibits the progression of CRC through activating the AMPK/PERK/eIF-2α pathway, providing a novel potential strategy for clinical prevention of CRC.

1. Introduction

Colorectal cancer (CRC) is one of the most common and life-threatening malignant tumors worldwide, contributing to 11% of all new cancer diagnoses and 52,980 deaths in 2021 [1, 2]. According to the histological types, colorectal cancer (CRC) can be classified into adenocarcinomas, signet ring cell carcinomas, squamous cell carcinomas, and some other rare variants [3]. Adenocarcinoma accounts for approximately 90% of all colorectal cancer (CRC) cases, and many patients have advanced-stage disease at diagnosis [3]. In addition to traditional approaches including chemotherapy, radiotherapy, and surgery, targeted therapy and immunotherapy have developed rapidly for the treatment of CRC in recent times. Despite these advances, only 63% of CRC patients will survive 5 years or more after diagnosis, due to the development of drug resistance and obvious systemic side effects [2]. Therefore, new strategies are urgently needed to prevent progression and reduce mortality from this disease.

Accumulating evidence has shown that phytochemical compounds from natural sources are remarkably effective in treating malignancies and other diseases [4–7]. The most successful example is paclitaxel, a diterpenoid isolated from the *Taxus brevifolia* bark for the first time in 1971 [8]. It is widely used in the treatment of malignant tumors such as lung cancer, esophageal cancer, breast cancer, and pancreatic cancer [9]. Doxorubicin, a product derived from the soil fungus *Streptomyces peucetius*, has been commonly applied in the clinical treatment of various solid tumors [10]. Other well-known natural product-derived anticancer drugs are camptothecin, podophyllotoxin, anhydrovinblastine, and vinorelbine [11]. However, CRC is proven to be resistant to these chemotherapeutic agents. Clinical trials have shown that phytochemicals including curcumin, resveratrol, artesunate, and Ginkgo biloba have great potential in the treatment of CRC patients. Novel drugs derived from natural chemicals remain to be further excavated and developed.

Bixin is a liposoluble diapocarotenoid isolated from *Bixa orellana*, which has been widely explored as a herbal medicine by local communities in America. Bixin has been demonstrated to have multiple pharmaceutical properties, such as antiasthma [12], antioxidant [13], anti-inflammatory [14],
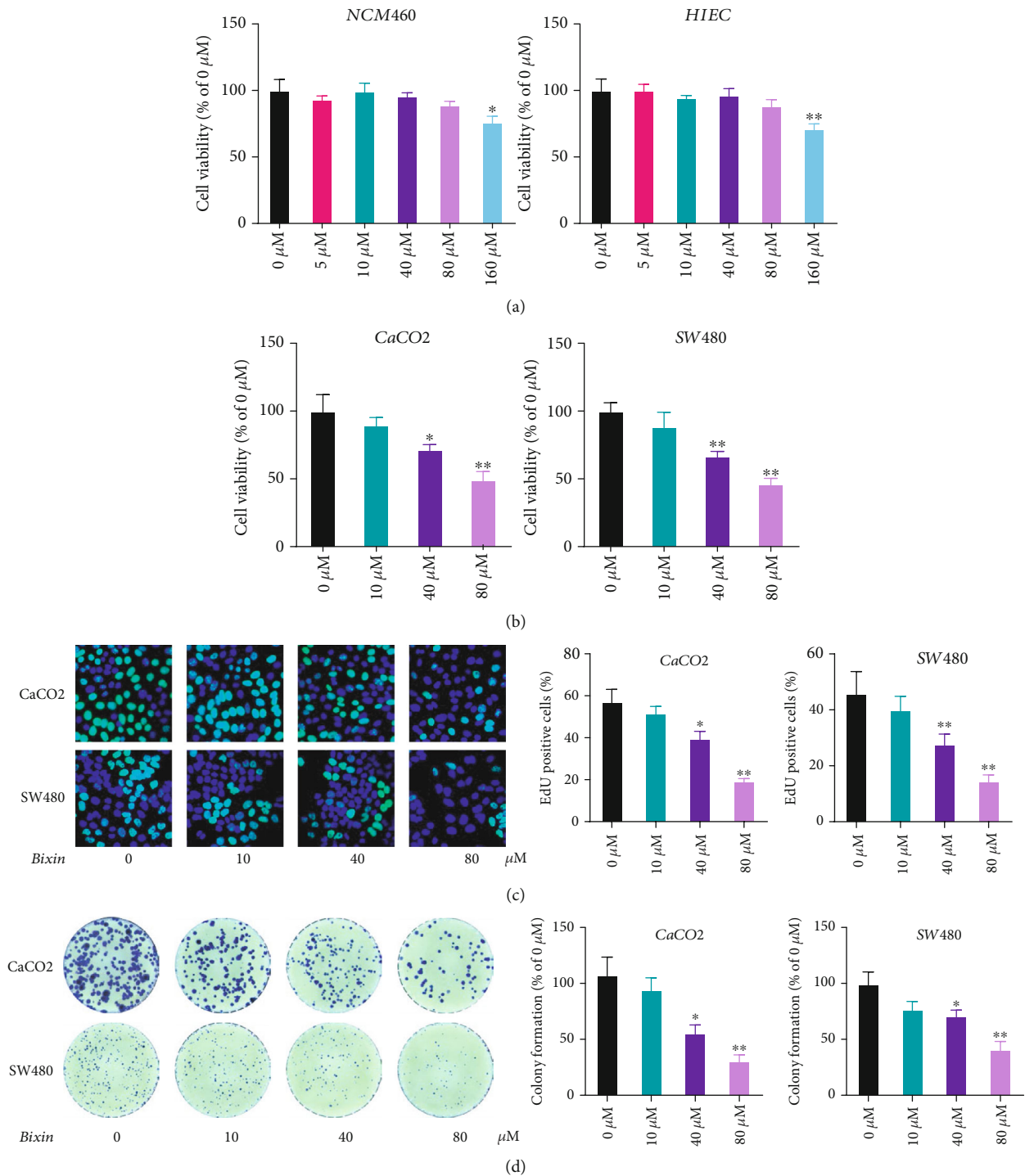
(a)

(b)

(c)

(d)

FIGURE 1: Bixin treatment inhibits the proliferation of CRC cells in vitro. After treatment with indicated doses of Bixin *in vitro*, HIEC and NCM460 cells (a), as well as $CaCO_2$ and SW480 cells (b), were used for cell viability determination by the CCK-8 assay. (c) EdU staining was performed in $CaCO_2$ and SW480 cells after the Bixin treatment. (d) The cell colony formation was analyzed by crystal violet staining. P values: $^*P \leq 0.05$; $^{**}P \leq 0.01$ (versus the control group without any treatment).
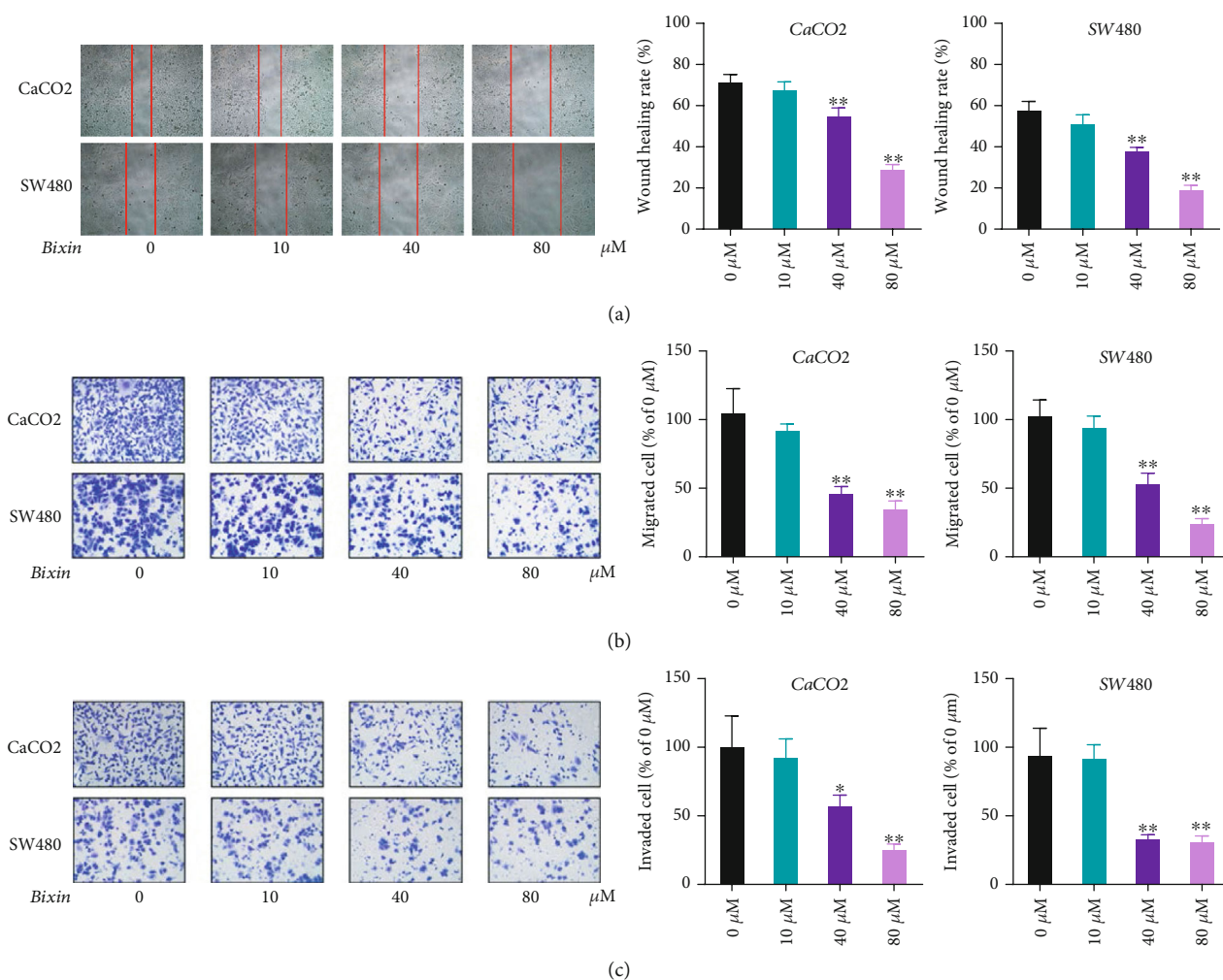
(a)

(b)

(c)

FIGURE 2: Bixin treatment suppresses the migration and invasion of CRC cells. CaCO$_2$ and SW480 cells were incubated with Bixin (0-80 μM) for 24 h. (a) Effects of Bixin treatment on colorectal cancer (CRC) cell migration evaluated by wound healing analysis. Effects of Bixin on colorectal cancer (CRC) (b) cell migration and (c) invasion were evaluated by transwell assays. P values: $^{*}P \leq 0.05$; $^{**}P \leq 0.01$ (versus the control group without any treatment).

and neuroprotective effects [15]. Besides, Bixin also exhibits antitumor activities in blood and solid tumor cancers. In vitro studies indicated that cis-Bixin induced cytotoxicity in several tumor cell types, especially in patient myeloma cells and highly drug-resistant myeloma cell lines [16]. Zhang et al. reported that Bixin significantly inhibited proliferation and induced apoptosis in K562 leukemic cells by interfering with cell cycle progression [17]. Moreover, Bixin plays a suppressive role in melanoma and hepatocellular carcinoma cells [18, 19]. Despite these diverse antitumor effects, the therapeutic effects of Bixin on CRC are still unknown.

The present study investigated the anticancer effects of Bixin on CRC cells, and the results showed that Bixin has tumor-suppressive properties in vitro and in vivo. We also revealed that AMP-activated protein kinase- (AMPK-) induced activation of protein kinase RNA-like endoplasmic reticulum kinase (PERK)/eukaryotic initiation factor 2 alpha (eIF-2α) signaling is involved in the inhibitory role of Bixin in CRC cells. These results are expected to provide a new therapeutic strategy for CRC chemotherapy.

2. Materials and Methods

2.1. Chemicals and Antibodies. Bixin (>97% purity) was purchased from Acmec Biochemical Co., Ltd. (Shanghai, China). According to experiment purposes, Bixin was dissolved in DMSO or coin oil, respectively. TNF-related apoptosis-inducing ligand (TRAIL) from human source (R&D Systems, MN, USA) was prepared in saline solution containing 0.1% bovine serum albumin (BSA). Compound C (Selleck Chemicals, TX, USA) was used for AMPK inhibition following the manufacturer's instruction. Primary antibodies for p-AMPK, p-PERK, p-eIF2α, B-cell lymphoma 2 (Bcl-2), activating transcription factor 4 (ATF4), GAPDH, C/EBP homologous protein (CHOP), and Bcl-2-associated X (Bax) were purchased from ProteinTech Group (Rosemont, IL, USA).

2.2. Cell Cultures. Human CRC CaCO2 and SW480 cell lines, as well as the normal human colon epithelial HIEC and NCM460 cell lines, were purchased from the China Cell
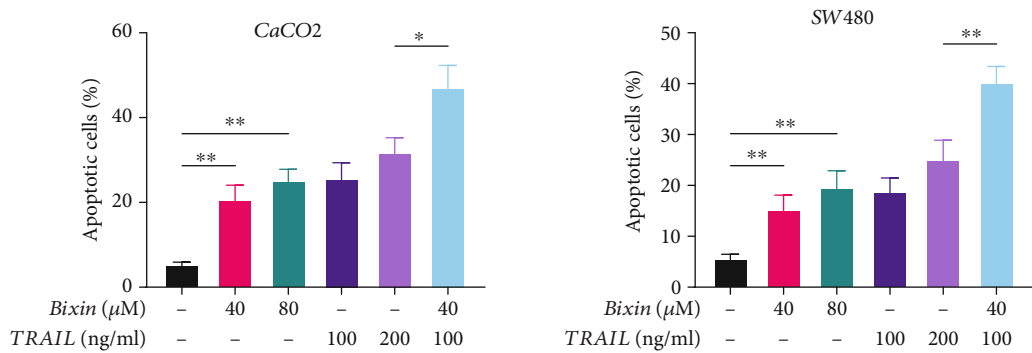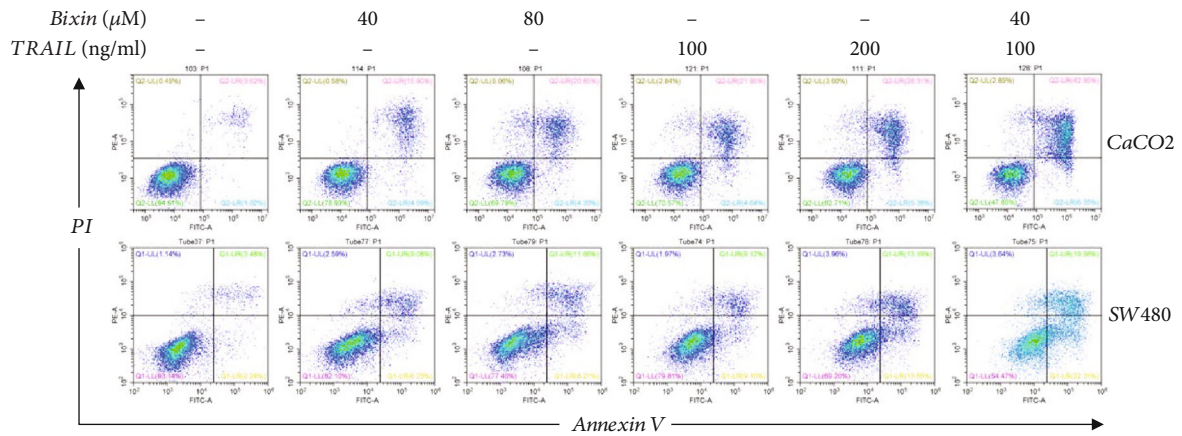
(a)
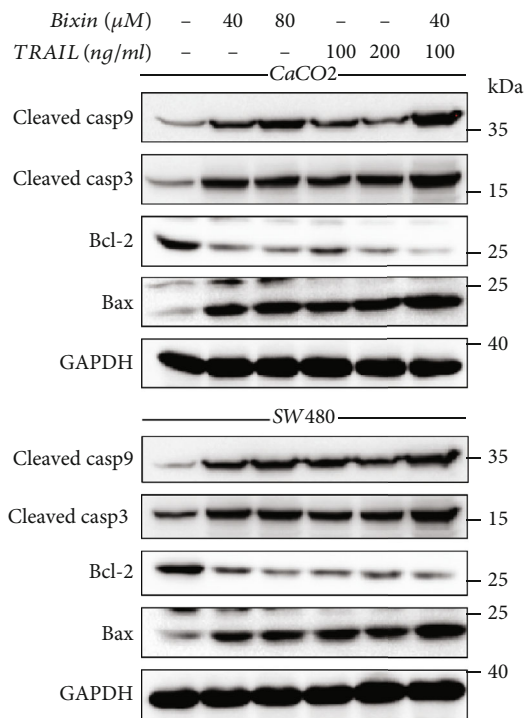
(b)

FIGURE 3: Bixin treatment sensitizes CRC cells to TRAIL-induced apoptosis. CaCO2 and SW480 cells were treated with Bixin at different doses for 24 h, either individually or combined with TRAIL. (a) Cells were stained with Annexin V and PI, and the cell apoptosis was examined by a flow cytometer. (b) Immunoblotting was performed to determine caspase 3 and caspase 9 cleavage levels, as well as Bcl-2 and Bax protein expression levels. P values: $^{*}P \leq 0.05$; $^{**}P \leq 0.01$.
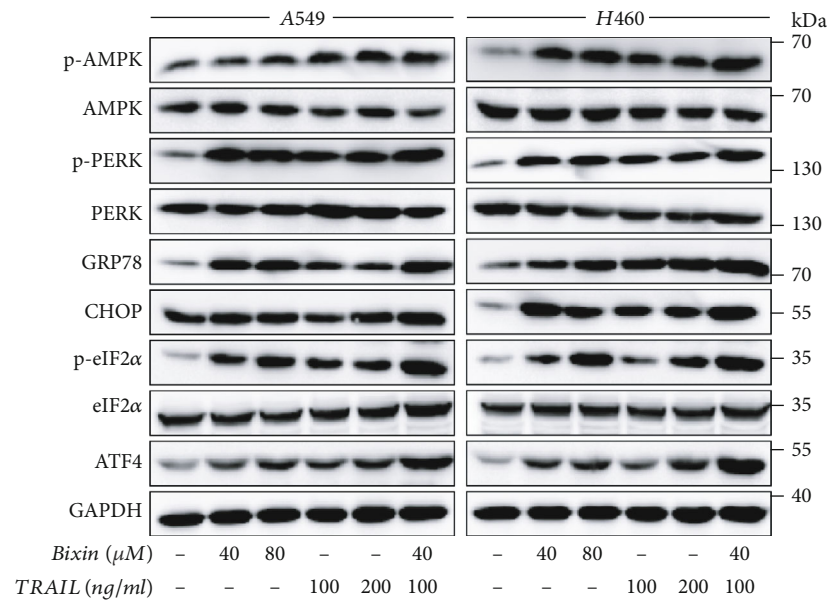
(a)
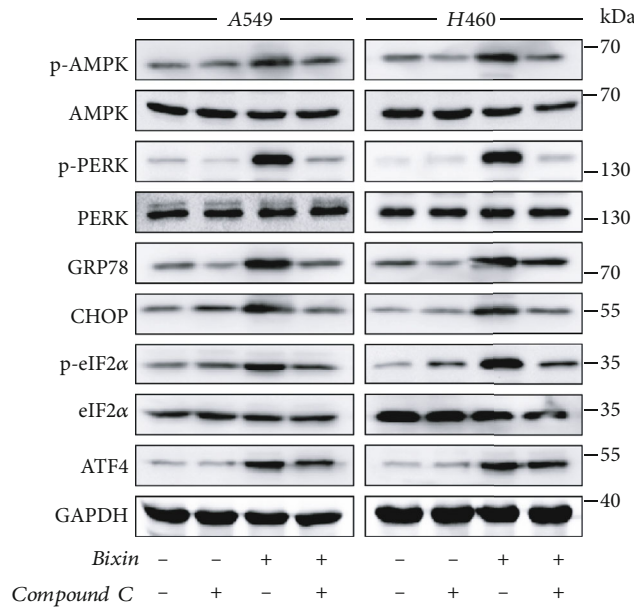
(b)

Figure 4: Bixin induces ER stress in CRC cells via AMPK activation. Western blotting analysis was performed to evaluate the expression levels of p-AMPK, p-PERK, CHOP, GRP78, p-eIF2α, and ATF4. (a) CaCO2 and SW480 cells were treated with Bixin at different doses for 24 h, either individually or combined with TRAIL. (b) Bixin and TRAIL combined treatment in CaCO2 and SW480 cells in the absence or presence of 1 μM Compound C (Comp) for 24 h. Each graph represents one of three independently performed experiments.

Collection Center (Beijing, China). Cells were cultured in Dulbecco's Modified Eagle's Medium (DMEM, HyClone™, Carlsbad, CA, USA) containing 10% fetal bovine serum (Sigma-Aldrich, St. Louis, MO, USA) and were incubated at 37°C in a humidified atmosphere of 5% CO_2. The culture medium was replenished every three days.

2.3. Assay of Cell Viability. The cell viability was determined using a CCK-8 kit (Sigma-Aldrich) according to the manufacturer's instruction. Briefly, cells were suspended and seeded into 96-well plates at a density of 2,000 cells per well.

24 h after incubation with or without Bixin treatment, 10 μL of CCK-8 reagent was added into each well, and then, the cells were cultured at 37°C for another 2 h. The absorbance of each well was recorded at 450 nm using a microplate reader (BioTek, Winooski, VT, USA).

2.4. EdU (5-Ethynyl-2′-Deoxyuridine) Assay. CRC cells were seeded on coverslips overnight. Upon reaching 60-80% confluence, the cells were treated with indicated doses of Bixin for 24 h. After replacement of cell culture medium, EdU was added into the plate at 10 μM final concentration. Cells
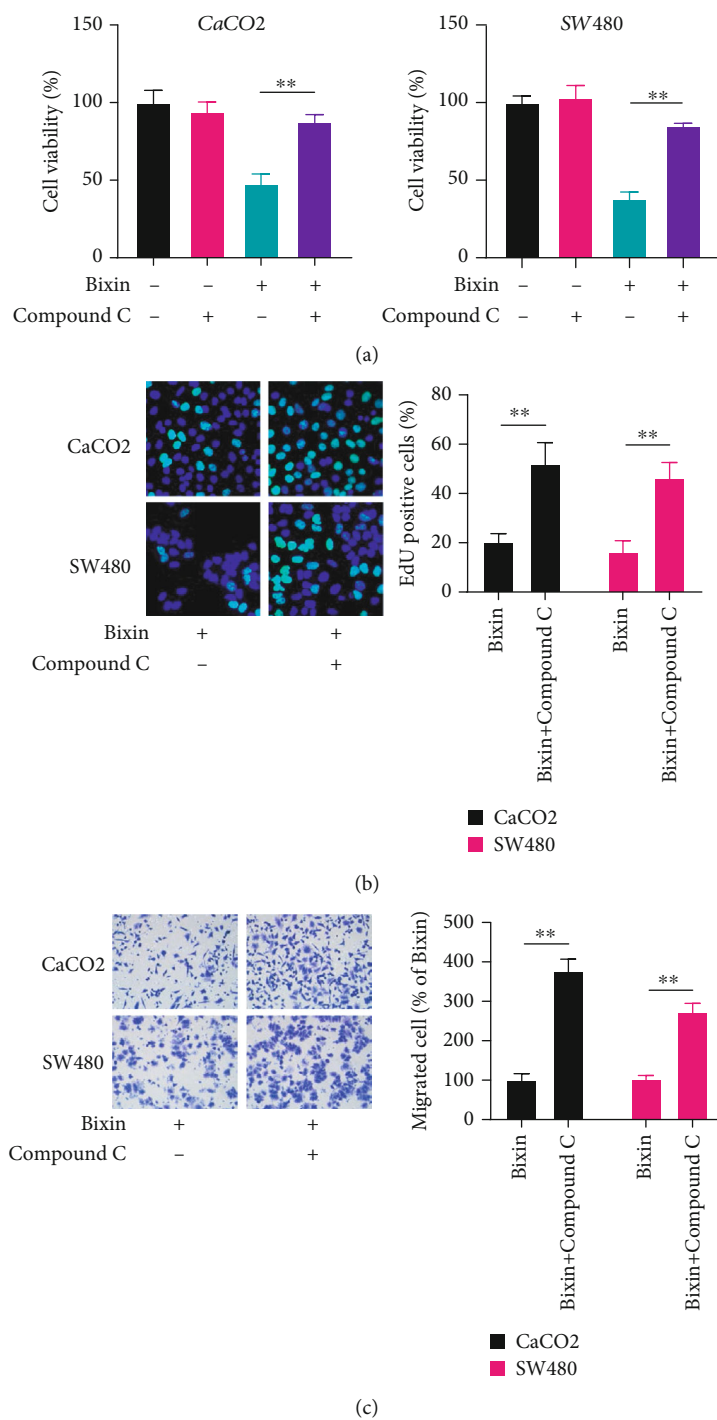
(a)
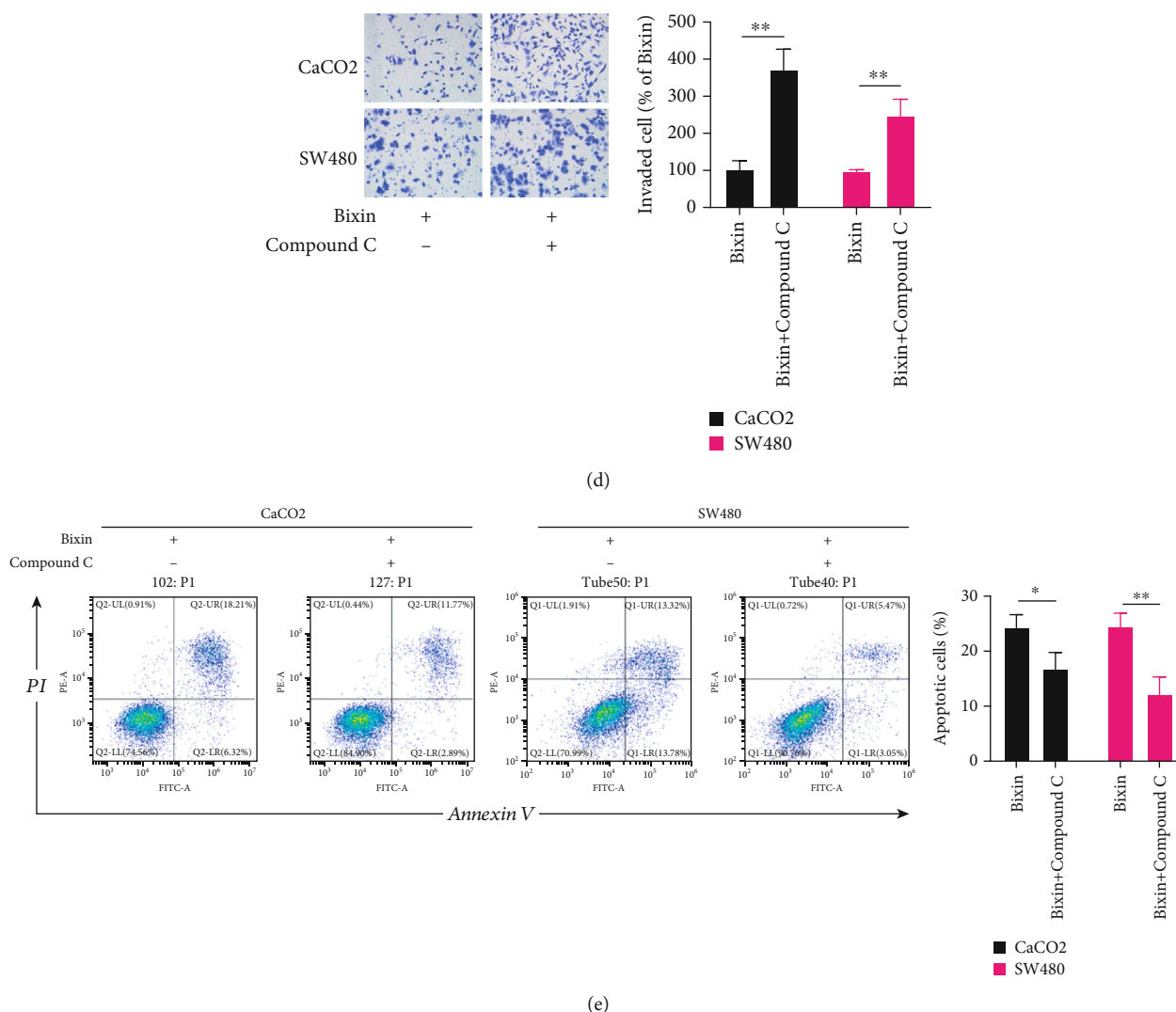

(b)

(c)

Figure 5: Continued.

(d)

(e)

FIGURE 5: AMPK inhibition abrogates the Bixin antitumor effects. CaCO2 and SW480 cells were administered with Bixin for 24 h in the absence or presence of 1 μM Compound C, a specific AMPK inhibitor, to assess (a) cell viability, (b) EdU staining, (c) transwell migration, (d) invasion, and (e) apoptosis. P values: $^*P \leq 0.05$; $^{**}P \leq 0.01$.

were placed back into the incubator for another 2 h. The cells were washed with PBS twice, followed by fixation with 4% paraformaldehyde. Subsequently, the cells were subjected to Hoechst 33342 staining. After being washed twice with PBS, the images of cells were captured under a fluorescence microscope (Olympus, Tokyo, Japan).

2.5. Colony Formation Assays. CaCO2 and SW480 cells were, respectively, seeded into 6-well plates (200 cells/each well) and treated with different doses of Bixin. The culture was terminated after the appearance of visible colonies on the Petri dish. The cells were washed twice with PBS, and then, 5 mL of pure methanol or acetic acid/methanol 1 : 3 was added for fixation for 15 minutes. Then, the fixation solution was removed and an appropriate amount of crystal violet solution (0.1%) was used for cell staining at room temperature for 30 minutes. Finally, the staining solution was discarded and the cells were washed with PBS for three times. The images were captured using an inverted microscope

(Olympus), and colonies (>60 cells) of each well were counted.

2.6. Wound Healing Analysis. CaCO2 and SW480 cells were seeded into 6-well plates (5×10^5 cells/well) and incubated until the confluency reached 90% approximately. Then, the cell monolayer was scratched in a straight line using a p200 pipette tip. PBS was used to wash cell debris, and the cells were placed back into a 37°C incubator for another 24 h to allow cell migration. Representative images 0, 24 h after the injury were acquired by an inverted microscope (Olympus).

2.7. Flow Cytometry. For apoptosis assay, cells were collected and washed with PBS for two times. Then, the cells were resuspended in binding buffer at a final concentration of 1 $\times 10^6$ cells/mL, followed by staining using Annexin V/PI cell apoptosis detection kit (Beyotime, Beijing, China) according to the manufacturer's instructions. The percentage of

(a)

(b)

(c)

(d)

(e)
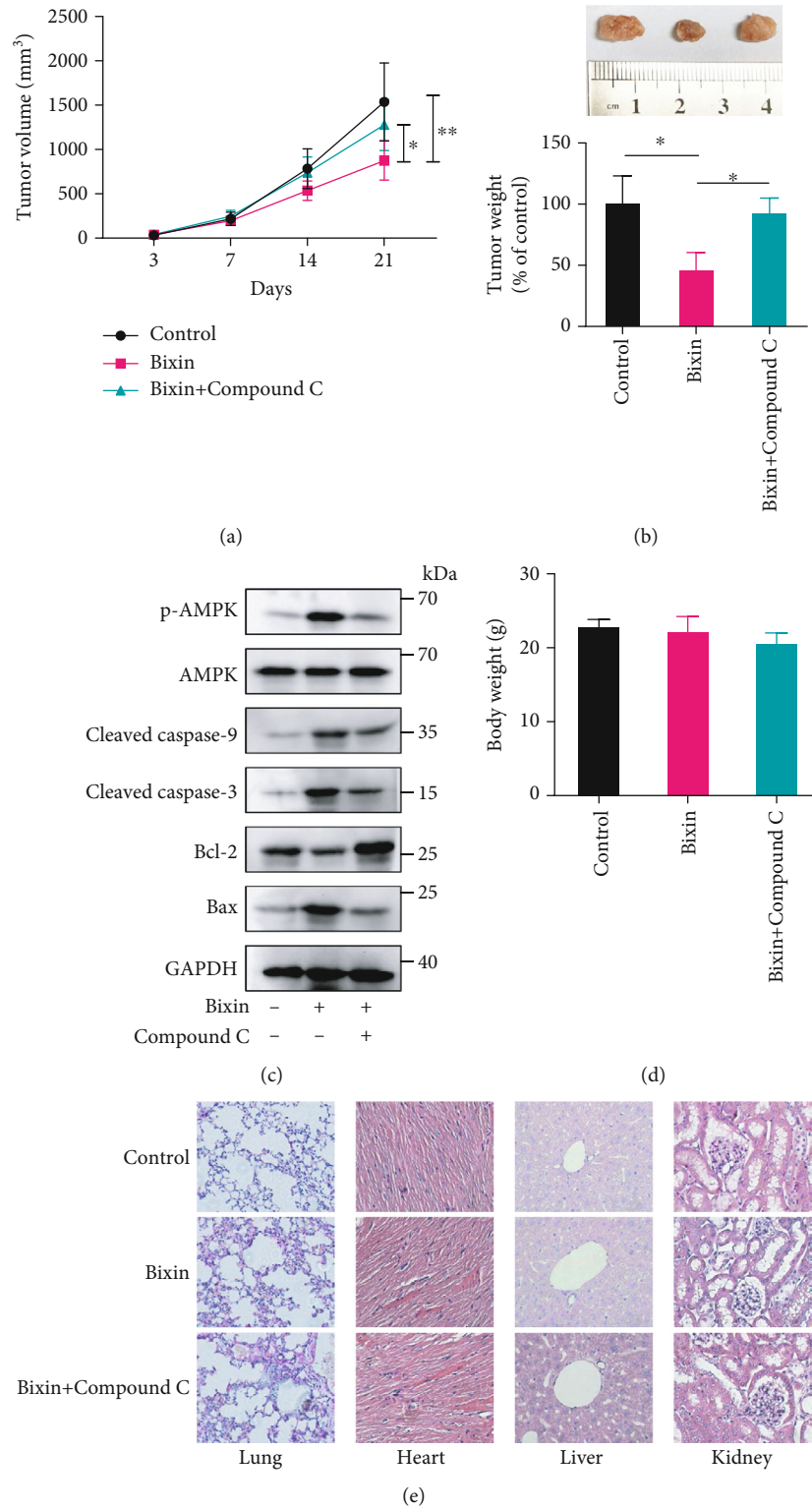
FIGURE 6: Bixin suppresses CRC development in vivo through AMPK activation. Seven days after the xenograft, Bixin (100 mg/kg) was administrated by intraperitoneal (i.p.) injection every 3 days for four times. For AMPK inhibition, Compound C (10 mg/kg) was administered through i.p. injection every day after Bixin administration until sacrifice. 24 d after the xenograft, all mice were euthanized and the tumor (a) volume and (b) weight were measured. (c) p-AMPK, caspase 3, caspase 9, Bcl-2, and Bax expression levels in tumor tissue were determined using immunoblotting. (d) Mice body weight was measured at the end of the treatments. (e) Histological data of H&E staining of the heart, kidney, and liver from different experimental groups. P values: $^{*}P \leq 0.05$; $^{**}P \leq 0.01$.

apoptotic cells was analyzed using a flow cytometer (Becton Dickinson; San Jose, CA, USA).

2.8. Western Blot. Total cellular protein was prepared using RIPA buffer (Cell Signaling Technology), according to the manufacturer's instruction. Protein concentration was determined using a protein quantitative kit (Sigma-Aldrich). After boiling with 5x loading buffer, a proper volume of each sample was loaded onto a discontinuous sodium dodecyl sulfate-polyacrylamide gel (SDS-PAGE) and then the proteins were transferred to PVDF membranes (Millipore, Bedford, MA, USA). 5% nonfat dry milk prepared in PBS-Tween-20 (PBST) was used for membrane blocking for 1 hour, and then, the membranes were washed with PBST for 3 times, followed by incubation with primary (1 : 2000) or monoclonal anti-GAPDH (1 : 5000) antibodies at 4°C overnight. After being washed with PBST, the membranes were incubated with the horseradish peroxidase-linked secondary antibody (1 : 5000) at room temperature for another 2 h. Finally, the chemical signals were detected using the Bio-Rad ChemiDoc MP Image System.

2.9. Xenograft Mouse Models. Four-week-old male athymic nude mice were supplied by Charles River Laboratories and maintained in animal facilities (20-25°C, 50-60% humidity, and 12 h light/12 h dark cycle). The mice were maintained with free access to sterilized food and water, and the procedures of animal experiments were approved by the Animal Care and Use Committee of the China-Japan Union Hospital of Jilin University (Changchun, China). Briefly, CaCO2 cells suspended in PBS with Matrigel and 1×10^6 cells with a total volume of 0.2 mL were injected subcutaneously into the mice's left flank. For the treatment, 7 days after the xenograft, Bixin (100 mg/kg, dissolved in corn oil) was administrated through intraperitoneal (i.p.) injection every 3 days for four times. For in vivo AMPK inhibition, Compound C (10 mg/kg) was administered once every day by i.p. injection following Bixin administration until sacrifice. Tumor volume was measured with a vernier caliper every 3 days after injection and was calculated as tumor volume $(\mathrm{mm}^3) = \text{maximal length (mm)} \times [\text{perpendicular width (mm)}]^2/2$. The tumors were dissected and photographed on day 24 after injection.

2.10. Histology Analysis. Hematoxylin and eosin (H&E) stain was performed to evaluate organ injury according to a standard protocol. Briefly, an adequate amount of hematoxylin was added to the tissue section, followed by incubation for 5 min. Then, the slides were washed twice with distilled water. Subsequently, the tissue section was incubated with bluing reagent for 10 s. After rinsing, the slides were covered with eosin Y reagent and incubated for 2 min. Then, the slides were dehydrated with absolute alcohol. After being sealed with resin, the slides were observed under a microscope and photographed.

2.11. Statistical Analysis. GraphPad Prism 8 software was applied for statistical analysis, and all data were presented as means ± standard deviation (SD). The results were ana-lyzed by one-way analysis of variance (ANOVA) with post hoc multiple comparisons, and Student's t-test was applied for pairwise comparisons. P value of <0.05 was set as statistically significant.

3. Results

3.1. Bixin Treatment Suppresses the Proliferation of CRC Cells In Vitro. To evaluate the cytotoxicity of Bixin in normal airway epithelial cells, the viability of HIEC and NCM460 cells treated with indicated doses of Bixin was determined using the CCK-8 assay. Bixin treatment at a dosage below 80 μM did not show detectable toxic effects on HIEC and NCM460 cells (Figure 1(a)). Nevertheless, Bixin treatment with doses of 40 μM or 80 μM significantly inhibited the proliferation of CaCO2 and SW480 cell lines in vitro (Figure 1(b)).

EdU staining was also applied to evaluate the effects of Bixin on the CRC cell proliferation. The results showed that Bixin treatment triggered a decrease in the percentage of staining positive cells in a dose-dependent manner (Figure 1(c)). In addition, Bixin treatment can significantly inhibit the formation of CaCO2 and SW480 cell colonies (Figure 1(d)). Therefore, these results demonstrated that Bixin treatment efficiently suppressed the proliferation of CRC cells in vitro.

3.2. Bixin Treatment Suppresses the Migration and Invasion of CRC Cells. The effects of Bixin treatment on migration and invasion of CRC cells were assessed by wound healing, transwell migration, and invasion assays in CaCO2 and SW480 cells. The scratch repair rate of Bixin-treated CaCO2 and SW480 cells was lower compared to vehicle-treated cells (Figure 2(a)). Moreover, the results of transwell assay revealed that Bixin treatment remarkably decreased the number of migrated (Figure 2(b)) and invaded cells (Figure 2(c)) in a dose-dependent manner. These results showed that Bixin significantly restricted the migration and invasion of CRC cells in vitro.

3.3. Bixin Treatment Sensitizes CRC Cells to TRAIL-Induced Apoptosis. TRAIL has been indicated as a potent anticancer agent because of its specific induction of apoptosis in several cancer cell lines instead of normal cells [20]. To identify whether Bixin can increase TRAIL-induced apoptosis in CRC cells, CaCO2 and SW480 cell lines were stimulated with Bixin and TRAIL individually or in combination. CRC cells treated with TRAIL, Bixin, or both were staining with Annexin V and PI reagents, followed by cytometry analysis. As shown in Figure 3(a), both TRAIL and Bixin could induce remarkable increases in Annexin V/PI-positive cells in a dose-dependent manner, whereas the combined treatment with Bixin, even in a lower dose, enhanced the proapoptotic ability of TRAIL on CRC cells. In addition, immunoblotting assays suggested that combined treatment increased caspase-dependent apoptosis, as it induced higher levels of cleaved-caspase 3, cleaved-caspase 9, and Bax compared to individual treatments (Figure 3(b)). Taken together,

these results demonstrate that Bixin treatment sensitized CRC cells to TRAIL-induced apoptosis.

3.4. Bixin Induces ER Stress in an AMPK-Dependent Way.
Endoplasmic reticulum (ER) stress plays a crucial regulatory role in the cancer cell proliferation and apoptosis [21]. Thus, levels of ER stress markers in CaCO2 and SW480 cells treated with Bixin and/or TRAIL were determined to explore the association between ER stress and antitumor effects of Bixin. The data showed that individual treatment with TRAIL or Bixin increased the levels of phosphorylated PERK (p-PERK) and phosphorylated eIF2α (p-eIF2α), as well as the protein levels of GRP78, CHOP, and ATF4 (Figure 4(a)). Remarkably, this effect was enhanced by the combined treatment with Bixin and TRAIL (Figure 4(a)).

Bixin also induced AMPK activation in CRC cells, which was increased by combined treatment with TRAIL (Figure 4(a)). Pretreatment with Compound C, a specific AMPK inhibitor, significantly attenuated Bixin or/and TRAIL-induced upregulation of p-AMPK, p-PERK, p-eIF2α, GRP78, ATF4, and CHOP (Figure 4(b)). These results reveal that the Bixin-induced ER stress in CaCO2 and SW480 cells depends on AMPK activation.

3.5. AMPK Inhibition Abrogates the Bixin Antitumor Effects In Vitro.
To validate the role of the AMPK pathway in the antitumor effects of Bixin, the AMPK activation in CRC cells was suppressed using Compound C. Compound C treatment was able to attenuate the inhibitory effect of Bixin on the CaCO2 and SW480 cell proliferation in vitro (Figure 5(a)), as well as reversed the Bixin-induced downregulation in numbers of EdU-positive cells (Figure 5(b)). In addition, Compound C treatment abolished the inhibitory effects of Bixin on CRC cell migration and invasion abilities (Figures 5(c) and 5(d)). As expected, Compound C also suppressed the Bixin-induced apoptosis in CaCO2 and SW480 cells (Figure 5(e)). Therefore, these data indicate that AMPK inhibition restrained the antitumor effects of Bixin.

3.6. Bixin Administration Inhibits CRC Development In Vivo by Activating AMPK.
Antitumor effects of Bixin were also evaluated in vivo, and the results showed that Bixin treatment significantly inhibited tumor growth in mice bearing CaCO2 tumor xenografts, whereas Compound C treatment reduced the antitumor capability of Bixin (Figures 6(a) and 6(b)). Bixin treatment activated AMPK and promoted apoptosis in vivo, which was inhibited by Compound C treatment (Figure 6(c)). The treatment with Bixin and/or Compound C did not significantly affect the mouse weight (Figure 6(d)). In addition, histology analysis data indicated that the treatments with Bixin and/or Compound C did not cause toxicity to the major organs of mice, including the lung, heart, liver, and kidney (Figure 6(e)).

4. Discussion

A previous study has demonstrated that Bixin can induce in vitro cytotoxicity in a variety of cancer cell lines [16]. In the present study, we confirmed that Bixin treatment is able to inhibit the CRC cell proliferation and survival in vitro

and, at the same time, does not present toxicity to normal colon epithelial cells. We also found that Bixin can suppress CRC cell invasion and tumor growth in vivo. TRAIL, an endogenous cytokine belonging to the tumor necrosis factor superfamily, induces a caspase 8-dependent process of apoptosis in malignant cells, rather than in normal cells [22]. However, many tumor types present resistance to TRAIL-mediated apoptosis, which restricts its clinical application [23, 24]. The combination of Bixin with TRAIL showed a stronger proapoptotic effect than Bixin or TRAIL administered individually, indicating the Bixin ability to increase sensitivity to TRAIL of CRC cells. Collectively, these results indicate that Bixin has an effective role in the treatment of CRC.

The mechanism involved in the Bixin antitumor effects has not been clearly elucidated. Physiological or pathological stresses can lead to disturbances in the normal protein folding ER functions, thereby causing ER stress [25]. It can induce the expression of the glucose-regulated proteins GRP78, GRP94, and other endoplasmic reticulum chaperones to produce a protective effect [25, 26]. In addition, ER stress can also independently induce cell cycle arrest and endogenous apoptosis [27, 28]. There is accumulating evidence suggesting that ER stress in cancer cells may be an effective strategy to induce cancer cell death [21, 29]. Therefore, we hypothesized that ER stress would be involved in the Bixin inhibitory effects on colorectal cancer (CRC) cells. There are at least three signal transduction pathways to detect and respond to ER stress, including inositol-requiring protein 1 (IRE1), PKR-like endoplasmic reticulum kinase (PERK), and activating transcription factor- (ATF-) 6 signaling [30]. Our results showed that Bixin administration, either individually or combined with TRAIL, significantly increased the PERK and eIF-2α phosphorylation levels, as well as the ATF4 and CHOP expression levels. These data indicate that Bixin induced apoptosis in CaCO2 and SW480 cells via the PERK-mediated apoptosis pathway.

Previous studies have shown that the CHOP overexpression promotes Bax transfer from the cytoplasm to the mitochondria and suppresses Bcl-2 expression [31]. Bcl-2 is an antiapoptotic protein that plays an important role in inhibiting cellular apoptosis, whereas BAX, also known as bcl-2-like protein 4, is a proapoptotic regulator [32]. We noted here that CaCO2 or SW480 cells treated with Bixin and TRAIL combination exhibited substantial increases in phosphorylated caspase 9, phosphorylated caspase 3, and Bax levels and decreases in Bcl-2 expression.

AMPK is a key molecule in the energy metabolism regulation and has been pointed out as a new target for cancer treatment due to its key role in the regulation of growth and death in mammalian cells [33, 34]. Here, we demonstrate that Bixin is a potent activator of AMPK and that AMPK is required for the activation of the PERK/eIF-2α/ATF4 pathway induced by Bixin or by its combination with TRAIL in CRC cells. The mechanism underlying the interaction of AMPK with the PERK pathway is not fully understood. A previous study identified PERK as an upstream activator of AMPK phosphorylation, leading to mTOR inhibition and initiation of autophagy [35]. In turn, AMPK can

directly phosphorylate PERK at least two conserved residues. Thus, AMPK can activate the PERK/eIF2α signaling cascade, resulting in apoptosis in acute myeloid leukemia cells [36]. We demonstrated in this study that AMPK inhibition abrogated the Bixin antitumor effects in vitro and in vivo. These data indicate that an AMPK-priming activation of PERK/eIF2α/ATF4 appears to be a major, if not the only, pathway involved in Bixin-induced cell growth inhibition and apoptosis.

In conclusion, our results showed that Bixin inhibited CRC progression depending on AMPK/PERK/eIF-2α signaling pathway activation without presenting toxicity to normal cells or organs. Based on these observations, we provide evidence indicating that Bixin can be used as a chemotherapy agent for CRC treatment, by effectively inhibiting proliferation and invasion, as well as inducing apoptosis in CRC cells.

Data Availability

All data generated or analyzed during this study are included in this published article.

Conflicts of Interest

The authors declare that they have no conflicts of interest.

References

[1] F. Bray, J. Ferlay, I. Soerjomataram, R. L. Siegel, L. A. Torre, and A. Jemal, "Global cancer statistics 2018: GLOBOCAN estimates of incidence and mortality worldwide for 36 cancers in 185 countries," *CA: a Cancer Journal for Clinicians*, vol. 68, no. 6, pp. 394–424, 2018.

[2] R. L. Siegel, K. D. Miller, H. E. Fuchs, and A. Jemal, "Cancer statistics, 2021," *CA: a Cancer Journal for Clinicians*, vol. 71, no. 1, pp. 7–33, 2021.

[3] C. Li, H. Zheng, H. Jia et al., "Prognosis of three histological subtypes of colorectal adenocarcinoma: a retrospective analysis of 8005 Chinese patients," *Cancer Medicine*, vol. 8, no. 7, pp. 3411–3419, 2019.

[4] Z. Wen, W. Hou, W. Wu et al., "6'-O-Galloylpaeoniflorin attenuates cerebral ischemia reperfusion-induced neuroinflammation and oxidative stress via PI3K/Akt/Nrf2 activation," *Oxidative Medicine and Cellular Longevity*, vol. 2018, 2018.

[5] L. Song, X. Li, X. X. Bai, J. Gao, and C. Y. Wang, "Calycosin improves cognitive function in a transgenic mouse model of Alzheimer's disease by activating the protein kinase C pathway," *Neural Regeneration Research*, vol. 12, no. 11, pp. 1870–1876, 2017.

[6] J. Gao, L. Song, H. Xia, L. Peng, and Z. Wen, "6'-O-Galloylpaeoniflorin regulates proliferation and metastasis of non-small cell lung cancer through AMPK/miR-299-5p/ATF2 axis," *Respiratory Research*, vol. 21, no. 1, p. 39, 2020.

[7] T. Wen, L. Song, and S. Hua, "Perspectives and controversies regarding the use of natural products for the treatment of lung cancer," *Cancer Medicine*, vol. 10, no. 7, pp. 2396–2422, 2021.

[8] M. E. Wall and M. C. Wani, "Camptothecin and taxol: discovery to clinic–thirteenth Bruce F. Cain Memorial Award Lecture," *Cancer Res*, vol. 55, no. 4, pp. 753–760, 1995.

[9] S. Novello and T. Le Chevalier, "European perspectives on paclitaxel/platinum-based therapy for advanced non- Small cell lung cancer," *Seminars in Oncology*, vol. 28, no. 4, pp. 3–9, 2001.

[10] S. Rivankar, "An overview of doxorubicin formulations in cancer therapy," *Journal of Cancer Research and Therapeutics*, vol. 10, no. 4, pp. 853–858, 2014.

[11] A. Lichota and K. Gwozdzinski, "Anticancer activity of natural compounds from plant and marine environment," *International Journal of Molecular Sciences*, vol. 19, no. 11, p. 3533, 2018.

[12] Y. Zhu, D. Sun, H. Liu et al., "Bixin protects mice against bronchial asthma though modulating PI3K/Akt pathway," *International Immunopharmacology*, vol. 101, article 108266, 2021.

[13] Z. Xu and X. Q. Kong, "Bixin ameliorates high fat diet-induced cardiac injury in mice through inflammation and oxidative stress suppression," *Biomedicine & Pharmacotherapy*, vol. 89, pp. 991–1004, 2017.

[14] H. Zhang, L. Xue, B. Li, H. Tian, Z. Zhang, and S. Tao, "Therapeutic potential of bixin in PM2.5 particles-induced lung injury in an Nrf2-dependent manner," *Free Radical Biology & Medicine*, vol. 126, pp. 166–176, 2018.

[15] J. Lakey-Beitia, D. J. Kumar, M. Hegde, and K. S. Rao, "Carotenoids as novel therapeutic molecules against neurodegenerative disorders: chemistry and molecular docking analysis," *International Journal of Molecular Sciences*, vol. 20, no. 22, p. 5553, 2019.

[16] J. D. Tibodeau, C. R. Isham, and K. C. Bible, "Annatto constituent cis-bixin has selective antimyeloma effects mediated by oxidative stress and associated with inhibition of thioredoxin and thioredoxin reductase," *Antioxidants & Redox Signaling*, vol. 13, no. 7, pp. 987–997, 2010.

[17] X. Zhang, W. E. Zhao, L. Hu, L. Zhao, and J. Huang, "Carotenoids inhibit proliferation and regulate expression of peroxisome proliferators-activated receptor gamma (PPARγ) in K562 cancer cells," *Archives of Biochemistry and Biophysics*, vol. 512, no. 1, pp. 96–106, 2011.

[18] R. G. de Oliveira Júnior, A. Bonnet, E. Braconnier et al., "Bixin, an apocarotenoid isolated from _Bixa orellana_ L., sensitizes human melanoma cells to dacarbazine-induced apoptosis through ROS-mediated cytotoxicity," *Food and Chemical Toxicology*, vol. 125, pp. 549–561, 2019.

[19] Y. Kumar, A. Phaniendra, and L. Periyasamy, "Bixin triggers apoptosis of human Hep3B hepatocellular carcinoma cells: an insight to molecular and in silico approach," *Nutrition and Cancer*, vol. 70, no. 6, pp. 971–983, 2018.

[20] D. Mahalingam, E. Szegezdi, M. Keane, S. . Jong, and A. Samali, "TRAIL receptor signalling and modulation: are we on the right TRAIL?," *Cancer Treatment Reviews*, vol. 35, no. 3, pp. 280–288, 2009.

[21] E. P. McGrath, F. G. Centonze, E. Chevet, T. Avril, and E. Lafont, "Death sentence: the tale of a fallen endoplasmic reticulum," *Biochim Biophys Acta Mol Cell Res*, vol. 1868, no. 6, article 119001, 2021.

[22] R. W. Johnstone, A. J. Frew, and M. J. Smyth, "The TRAIL apoptotic pathway in cancer onset, progression and therapy," *Nature Reviews. Cancer*, vol. 8, no. 10, pp. 782–798, 2008.

[23] Y. Cao, S. Kong, Y. Xin, Y. Meng, S. Shang, and Y. Qi, "Lestaurtinib potentiates TRAIL-induced apoptosis in glioma via CHOP-dependent DR5 induction," *Journal of Cellular and Molecular Medicine*, vol. 24, no. 14, pp. 7829–7840, 2020.

[24] D. Stöhr, J. O. Schmid, T. B. Beigl et al., "Stress-induced TRAILR2 expression overcomes TRAIL resistance in cancer cell spheroids," *Cell Death and Differentiation*, vol. 27, no. 11, pp. 3037–3052, 2020.

[25] S. Mustapha, M. Mohammed, A. K. Azemi et al., "Current status of endoplasmic reticulum stress in type II diabetes," *Molecules*, vol. 26, no. 14, p. 4362, 2021.

[26] G. Zhu and A. S. Lee, "Role of the unfolded protein response, GRP78 and GRP94 in organ homeostasis," *Journal of Cellular Physiology*, vol. 230, no. 7, pp. 1413–1420, 2015.

[27] K. Bourougaa, N. Naski, C. Boularan et al., "Endoplasmic reticulum stress induces G2 cell-cycle arrest via mRNA translation of the p53 isoform p53/47," *Molecular Cell*, vol. 38, no. 1, pp. 78–88, 2010.

[28] S. S. Lin, H. P. Huang, J. S. Yang et al., "DNA damage and endoplasmic reticulum stress mediated curcumin-induced cell cycle arrest and apoptosis in human lung carcinoma A-549 cells through the activation caspases cascade- and mitochondrial-dependent pathway," *Cancer Letters*, vol. 272, no. 1, pp. 77–90, 2008.

[29] P. Limonta, R. Moretti, M. Marzagalli, F. Fontana, M. Raimondi, and M. Montagnani Marelli, "Role of endoplasmic reticulum stress in the anticancer activity of natural compounds," *International Journal of Molecular Sciences*, vol. 20, no. 4, p. 961, 2019.

[30] B. M. Gardner, D. Pincus, K. Gotthardt, C. M. Gallagher, and P. Walter, "Endoplasmic reticulum stress sensing in the unfolded protein response," *Cold Spring Harbor Perspectives in Biology*, vol. 5, no. 3, article a013169, 2013.

[31] Y. Li, Y. Guo, J. Tang, J. Jiang, and Z. Chen, "New insights into the roles of CHOP-induced apoptosis in ER stress," *Acta Biochim Biophys Sin (Shanghai)*, vol. 46, no. 8, pp. 629–640, 2014.

[32] J. Kale, E. J. Osterlund, and D. W. Andrews, "BCL-2 family proteins: changing partners in the dance towards death," *Cell Death and Differentiation*, vol. 25, no. 1, pp. 65–80, 2018.

[33] S. Herzig and R. J. Shaw, "AMPK: guardian of metabolism and mitochondrial homeostasis," *Nature Reviews. Molecular Cell Biology*, vol. 19, no. 2, pp. 121–135, 2018.

[34] C. Wang, J. Luo, X. Bai et al., "Calycosin alleviates injury in airway epithelial cells caused by PM 2.5 exposure via activation of AMPK signalling," *Evidence-based Complementary and Alternative Medicine*, vol. 2021, 2021.

[35] A. Avivar-Valderas, E. Bobrovnikova-Marjon, J. Alan Diehl, N. Bardeesy, J. Debnath, and J. A. Aguirre-Ghiso, "Regulation of autophagy during ECM detachment is linked to a selective inhibition of mTORC1 by PERK," *Oncogene*, vol. 32, no. 41, pp. 4932–4940, 2013.

[36] L. Poulain, A. Grenier, J. Mondesir et al., "PKR-like endoplasmic reticulum kinase mediates apoptosis induced by pharmacological AMP-activated protein kinase activation in acute myeloid leukemia," *Blood*, vol. 134, Supplement_1, pp. 2552–2552, 2019.